NUREG/CP-0072
Vol. 3

Proceedings of the U.S. Nuclear Regulatory Commission

Thirteenth Water Reactor Safety Research Information Meeting

Volume 3
- Mechanical and Structural Research
- Seismic Research
- Equipment Qualification
- Nuclear Plant Aging
- Process Control

Held at
National Bureau of Standards
Gaithersburg, Maryland
October 22-25, 1985

U.S. Nuclear Regulatory Commission

Office of Nuclear Regulatory Research

Proceedings prepared by
Brookhaven National Laboratory

NOTICE

These proceedings have been authored by a contractor of the United States Government. Neither the United States Government nor any agency thereof, or any of their employees, makes any warranty, expressed or implied, or assumes any legal liability or responsibility for any third party's use, or the results of such use, of any information, apparatus, product or process disclosed in these proceedings, or represents that its use by such third party would not infringe privately owned rights. The views expressed in these proceedings are not necessarily those of the U.S. Nuclear Regulatory Commission.

Available from

Superintendent of Documents
U.S. Government Printing Office
P.O. Box 37082
Washington D.C. 20013-7082

and

National Technical Information Service
Springfield , VA 22161

NUREG/CP-0072
Vol. 3
RD, RM, RV

Proceedings of the U.S. Nuclear Regulatory Commission

Thirteenth Water Reactor Safety Research Information Meeting

Volume 3
- Mechanical and Structural Research
- Seismic Research
- Equipment Qualification
- Nuclear Plant Aging
- Process Control

Held at
National Bureau of Standards
Gaithersburg, Maryland
October 22-25, 1985

Date Published: February 1986

Compiled by: Allen J. Weiss

Office of Nuclear Regulatory Research
U.S. Nuclear Regulatory Commission
Washington, D.C. 20555

Proceedings prepared by
Brookhaven National Laboratory

ABSTRACT

This six-volume report contains 151 papers out of the 178 that were presented at the Thirteenth Water Reactor Safety Research Information Meeting held at the National Bureau of Standards, Gaithersburg, Maryland, during the week of October 22-25, 1985. The papers are printed in the order of their presentation in each session and describe progress and results of programs in nuclear safety research conducted in this country and abroad. Foreign participation in the meeting included thirty-one different papers presented by researchers from Japan, Canada and eight European countries. The titles of the papers and the names of the authors have been updated and may differ from those that appeared in the final program of the meeting.

PROCEEDINGS OF THE
THIRTEENTH WATER REACTOR SAFETY RESEARCH
INFORMATION MEETING

October 22-25, 1985

Published in Six Volumes

GENERAL INDEX

VOLUME 1
- Plenary Session
- Risk Analysis/PRA Application
- Severe Accident Sequence Analysis
- Risk Analysis/Dependent Failure Analysis
- Industry Safety Research

VOLUME 2
- Materials Engineering Research/Pressure Vessel Research
- Materials Engineering Research/Piping Research & Fracture Mechanics
- Environmental Effects in Piping
- Surry Steam Generator/Examination and Evaluation
- Materials Engineering Research/Non-Destructive Evaluation

VOLUME 3
- Mechanical and Structural Research
- Seismic Research
- Equipment Qualification
- Nuclear Plant Aging
- Process Control

VOLUME 4
- Integral Systems Tests
- 2D/3D Research
- Separate Effects/Experiments and Analyses

VOLUME 5
- International Code Assessment Program
- Code Assessment and Improvement
- Nuclear Plant Analyzer

VOLUME 6
- Fission Product Release and Transport in Containment
- Containment Systems Research/Containment Loads Analysis
- Severe Accident Source Term

REGISTERED ATTENDEES
13th WRSR INFORMATION MEETING

Abe, Y.
Japan Atomic Energy Research Institute
3000 Trinity Dr. #23
Los Alamos, NM 87544

Acker, D.
Centre d'Etudes Nucleaires de Saclay
DEMT/SMTS/RDMS
GIF S/YVETTE
FRANCE 91191

Adamantiades, A.
MITRE Corp.
1820 Dolly Madison Blvd.
McLean, Virginia 22102

Adams, R.E.
Oak Ridge National Laboratory
P.O. Box Y, Bldg. 9108, MS-2
Oak Ridge, Tennessee 37831

Agarwal, B.K.
Foster Wheeler
#1503, 20N., Clark Street
Chicago, Illinois 60602

Ahlfeld, C.E.
E.I. duPont de Nemours-Savannah River Lab.
Building 773-A/A-235
Aiken, SC 29808

Ahmad, J.
Battelle Columbus Laboratory
505 King Avenue
Columbus, Ohio 43201

Akimoto, H.
Japan Atomic Energy Research Institute
Tokai-mura, Ibaraki-ken
Japan

Almenas, K.
University of Maryland
College Park, Maryland 20740

Amico, P.
Applied Risk Technology Corp.
P.O. Box 175
Columbia, Maryland 21045

Andersen, J.G.
General Electric
175 Curtner Avenue
San Jose, California 95125

Andersen, P.
DYNATREK, Inc.
2115 E. Jefferson St.
Rockville, Maryland 20852

Anderson, J.L.
EG&G Idaho, Inc.
P.O. Box 1625
Idaho Falls, Idaho 83401

Andrews, B.
Battelle - Pacific Northwest Laboratory
P.O. Box 999
Richland, Washington 99336

Anoda, Y.
Japan Atomic Energy Research Institute
197 Dale #8
Idaho Falls, Idaho 83402

Araya, F.
Japan Institute of Nuclear Safety
Mita Kokusai Bldg., Mita 1-4-28
Minato-ku, Tokyo
Japan

Aro, I.M.
Finnish Centre for Radiation & Nuc. Safety
P.O. Box 268
SF-00101 Helsinki 10. FINLAND

Atkinson, J.D.
CERL, CEGB
Kelvin Avenue
Leatherhead, Surrey KT22 7SE
United Kingdom

Bailey, G.F.
UNC Nuclear Industries
19815 Bazzellton Place
Gaithersburg, Maryland 20879

Ball, D.G.
Oak Ridge National Laboratory
P.O. Box P
Oak Ridge, Tennessee 37831

Bandyopadhyay, K.K.
Brookhaven National Laboratory
Building 129
Upton, New York 11973

Bari, R.A.
Brookhaven National Laboratory
Building 130
Upton, New York 11973

Bass, B.R.
Martin Marietta Energy Systems, Inc.
P.O. Box P
Oak Ridge, Tennessee 37831

Basselier, J.E.
Belgonucleaire
36, Teniersdreef
Overijse, Belgium 1900
Belgium

Bell, C.R.
Los Alamos National Laboratory
P.O. Box 1663
Los Alamos, NM 87545

Bennett, J.G.
Los Alamos National Laboratory
P.O. Box 1663, MS J576
Los Alamos, NM 87545

Bergeron, K.D.
Sandia National Laboratory
Division 6449
Albuquerque, New Mexico 87185

Berman, M.
Sandia National Laboratory
Division 6427
Albuquerque, New Mexico 87111

Berry, D.L.
Sandia National Laboratory
Division 6447
Albuquerque, NM 87111

Bezler, P.
Brookhaven National Laboratory
Building 129
Upton, New York 11973

Bingham, B.E.
Babcock & Wilcox
3315 Old Forest Road
Lynchburg, Virginia 24506

Binner, W.
Austrian Research Center Seibersdorf
Lenaugasse 10
Vienna A-1082
Austria

Bloomfield, W.L.
GPU Nuclear
P.O. Box 480
Middletown, PA 17057

Board, S.J.
CEGB - Berkeley Nuclear Laboratory
Berkeley, Gloucestershire, England

Boccio, J.L.
Brookhaven National Laboratory
Bldg. 130
Upton, New York 11973

Boehnert, P.A.
U.S. Nuclear Regulatory Commission
Washington, D. C. 20555

Bonzon, L. L.
Sandia National Laboratory
Division 6446
Albuquerque, NM 87185

Borsum, R.B
Babcock & Wilcox
7910 Woodmont Avenue, Suite 220
Bethesda, MD 20814

Boucher, T.J.
EG&G Idaho, Inc.
P.O. Box 1625
Idaho Falls, Idaho 83402

Boyack, B.E.
Los Alamos National Laboratory
P.O. Box 1663
Los Alamos, NM 87545

Bradley, D.R.
Sandia National Laboratory
P.O. Bo 5800
Albuquerque, New Mexico 87185

Bratby, P.A.
National Nuclear Corporation
Cambridge Road, Whetstone
Leicester, LE83LH ENGLAND

Brittain, I.
United Kingdom Atomic Energy Authority
AEE Winfrith
Dorchester, Dorset DT28DH
United Kingdom

Bruemmer, S.M.
Battelle - Pacific Northwest Laboratory
P.O. Box 999
Richland, Washington 99352

Brust, B.
Battelle - Pacific Northwest Laboratory
505 King Avenue
Columbus, Ohio 43214

Bryan, R. H.
Oak Ridge National Laboratory
P.O. Box Y
Oak Ridge, Tennessee 37831

Budnitz, R.J.
Future Resources Associates Inc.
2000 Center Street--Suite 418
Berkeley, California 94704

Burda, A.J.
Nuclear Regulatory Commission
Mail Stop 1130SS
Washington, D. C. 20555

Burns, N. L.
Westinghouse Electric Corp.
P.O. Box 355
Pittsburgh, Pennsylvania 15230 5230

Butland, A.T.
United Kingdom Atomic Energy Authority
AEE Winfrith
Dorchester, Dorset DT28DH
United Kingdom

Butler, C.N.
Baltimore Gas & Electric
P.O. Box 1475
Baltimore, Maryland 21203

Butler, J.
UKAEA Winfrith
Barr Road Broadstone
Dorset BH18 8NT

Butler, T.A.
Los Alamos National Laboratory
P.O. Box 1663, MS J576
Los Alamos, NM 87545

Buxbaum, S.R.
Baltimore Gas & Electirc
P.O. Box 1475
Baltimore, Maryland 21203

Buxton, L.D.
Sandia National Laboratory
Division 6444
P.O. Box 5800
Albuquerque, New Mexico 87185

Byrne, S.T.
Combustion Engineering
1000 Prospect Hill Road
Windsor, CT 06095

Cadek, F.F.
Westinghouse
P.O. Box 355
Pittsburgh, Pennsylvania 15230

Cadwallader, L.C.
Idaho National Engineering Lab/EG&G Idaho
P.O. Box 1625
Idaho Falls, Idaho 83415

Campbell, D.J.
JBF Associates
1000 Technology Park Center
Knoxville, Tennessee 37932

Cardinal, J. W.
Southwest Research Institute
6220 Culebra Road
P.O. Drawer 28510
San Antonio, Texas 78284

Carey, C.
Tennessee Valley Authority
400 W. Summit Hill Drive, W100181
Knoxville, TN 37902

Carroll, D.E.
Sandia National Laboratory
Division 6449
Albuquerque, New Mexico 87185

Carter, H.R.
Babcock & Wilcox
1562 Beeson Street
Alliance, Ohio 44601

Casper, H.F.
Gesellschaft fur Reaktorsicherheit
5 Koln 1, Schwertnergasse 1
FRG

Catton, I.
UCLA
5731 Boelter Hall
Los Angeles, California 90024

Cazzoli, E.G.
Brookhaven National Labortory
Building 130
Upton, New York 11973

Charlton, T.R.
EG&G Idaho, Inc
5374 Township Road
Idaho Falls, Idaho 83401

Chen, J.C.
Lehigh University
Department of Chemical Engineering
Bethlehem, PA 18015

Chen, Y.
Institute of Nuclear Energy Research
P.O. Box 3-3
Lung-Tan, Taiwan 325
Republic of China

Cheng, H-S
Brookhaven National Laboratory
Building 130
Upton, New York 11973

Cheng, T.C.
EG&G Idaho, Inc.
P.O. Box 1625
Idaho Falls, Idaho 83415

Cheverton, R.D.
Oak Ridge National Laboratory
P.O. Box Y
Oak Ridge, Tennessee 37831

Chien, T.
Argonne National Laboratory
9700 South Cass Avenue
Argonne, Illinois 60439

Chiou, J-S.
Westinghouse
178 Penn Lear Drive
Monroeville, Pennsylvania 15146

Choi, Y.S.
Korea Electric Power Corporation R & D
52, Cheongdam-Dong, Kangnam-Ku
Seoul
Korea

Chopra, O.K.
Argonne National Laboratory
9700 S. Cass Avenue
Argonne, Illinois 60439

Chow, S.K.
Westinghouse
178 Penn Lear Drive
Monroeville, Pennsylvania 15146

Cirilli, J.J.
Northwest Utilities
P.O. Box 270
Hartford, Connecticut 06141-0270

Clark, R.A.
Battelle-Pacific Northwest Laboratory
Box 999
Richland, WA 99352

Cleary, J. M.
Combustion Engineering
1000 Prospect Hill Road
Windsor, CT 06095

Cleveland, J.W.
SEA Consultants, Inc.
1625 The Alameda Ste303
San Jose, California 95126

Cliquet, J.
Brussels University
AV. F.D. Roosevelt, 50
Bruxelles 1050
Belgium

Colagrossi, M.
ENEA/Rome
V.V. Brancati 48
Rome, Italy 00144

Cole, R.K.
Sandia National Laboratory
Division 6444
P.O. Box 5800
Albuquerque, New Mexico 87185

Condie, K.G.
EG&G Idaho, Inc.
P. O. Box 1625
Idaho Falls, Idaho 83415

Cook, T.L.
Baltimore Gas & Electric
P.O. Box 1475
Room 720, G&E Bldg.
Baltimore, Maryland 21203

Corwin, W.R.
Oak Ridge National Laboratory
Building 4500S, Room D61
P.O. Box X
Oak Ridge, TN 37831

Courtaud, M.
C.E.A/CENG/STT
85X -38041 Grenoble CEDEX
Grenoble, FRANCE

Coward, R.N.
MPR Associates
1050 Conn. Avenue, N.W.
Washington, D. C. 20036

Cowne, S.R.
Baltimore Gas & Electric
P.O. Box 1535
Calvert Cliffs
Luby Maryland 20657

Cramblitt, K.L.
Baltimore Gas & Electric
P.O. Box 1475
Baltimore, Maryland 21203

Crawford, T.J.
American Electric Power
1 Riverside Plaza
Columbus, Ohio 43215

Creswell, S. L.
HM Nuclear Installations Inspectorate
Thames House North
Millbank
London SWIP 4QJ, U.K.

Cummings, G.E.
Lawrence Livermore National Laboratory
L-198, P.O. Box 808
Livermore, CA 94526

Dahlgren, D.A.
Sandia National Laboratory
Dept. 6440
P.O. Box 5800
Albuquerque, NM 87185

Dai, A.
Shanghai Rekeleau, Eng. of Research Inst.
Shanghai
China

Dallman, R.J.
EG&G Idaho, Inc.
P.O. Box 1625
Idaho Falls, Idaho 83415

Damerell, P.
MPR Associates
1050 Connecticut Avenue, N.W. 20036

Dankosky, J.D.
Westinghouse - Bettis
P.O. Box 79
West Mifflin, Pennsylvania 15122

Darling, W.R.
Duke Power Company
P.O. Box 33189
Charlotte, NC 28242

Davis, R.E.
Brookhaven National Laboratory
Bldg. 703M
Upton, New York 11973

De, N.K.
U.S. Nuclear Regulatory Commission
9451 Lee Highway, #1016
Fairfax, VA 22031

DeAgostino, E.
ENEA/Rome
V.V. Brancati 48
Rome, Italy 00144

Deem, R.E.
New York Power Authority
123 Main Street
White Plains, New York 10601

Della Loggia, E.
CEC - DG XII
Rue De La Loi, 200 Sdm 2/77
Brussels B-1049
BELGIUM

Denning, R.S.
Battelle - Pacific Northwest Laboratory
505 King Avenue
Columbus, Ohio 43201

DeVault, R.M.
Tennessee Valley Authority
400 West Summit Hill Drive, W10D210
Knoxville, TN 37902

deWit, R.
National Bureau of Standards
Room B113, Materials Building
Gaithersburg, MD 20899

Dietershagen, H.P.
Knolls Atomic Power Laboratory
P.O. Box 1072
Schenectady, New York 12301

Dingman, S.E.
Sandia National Laboratory
P.O. Box 5800
Division 6415
Albuquerque, New Mexico 87185

Dluzniewski, E.J.
GRS Representative in U.S.A.
CLOCUENGASSE 1
5000 KOLN 1
West Germany

Dobbe, C.A.
EG&G Idaho, Inc.
P.O. Box 1625
Idaho Falls, Idaho 83415

Doctor, P.G.
Battelle - Pacific Northwest Laboratory
Box 999
Richland, WA 99352

Doctor, S.R.
Battelle - Pacific Northwest Laboratory
Battelle Blvd.
Richland, Washington 99352

Dodd, C.V.
Oak Ridge National Laboratory
P.O. Box X
Oak Ridge, Tennessee 37831

Dougherty, E.M.
Science Applications International Corp.
3400 Middlebrook Park C-1
Knoxville, Tennessee 37923

Duco, J.J.
CEA/FRANCE
IPSN/CEN/FAR
92265 Fontenay aux Roses
France

Duffey, R.B.
Electric Power Research Institute
3412 Hillview Avenue
Palo Alto, California 94303

Eiji, T.
Japan Institute of Nuclear Safety
Mita 1-4-28 Minato-ku
Tokyo 108
Japan

El-Zeftawy, M.M.
U.S. Nuclear Regulatory Commission
11621 Flints Grove
Gaithersburg, Maryland 20878

Emilio, V.E.
University of PISA
Via Diotisalvi, 2
Pisa, Italy 56100

English, W.F.
General Electric Company
175 Curtner Avenue
San Jose, California 95125

Esenwine, R.C.
Baltimore Gas & Electric
P.O. Box 1475
Baltimore, Maryland 21203

Espefalt, R.G.
Swedish State Power Board
Vaellingby, Sweden S-16287

Fabry, A.M.
SCK-CEN
270 Boeretang
2400 Mol
Belgium

Farber, S.A.
Radiation Controls, Inc.
114 Airport Road
Warren, VT 05674

Farrant, D.R.
British Nuclear Fuels PLC
Springfields Work, Salwick, Preston
Lancashire PR4 0XJ
U.K.

Fell, J.
United Kingdom Atomic Energy Authority
AEE Winfrith
Dorchester, Dorset DT28DH
United Kingdom

Fernandez, R.T.
YAEC
1671 Worcester Road
Framingham, MA 01701

Ferris, R.H.
Battelle - Pacific Northwest Laboratory
Box 999
Richland, WA 99352

Fiege, A.W.
Kernforschungszentrum Karlsruhe GmbH
P.O. Box 3640
D-7500 Karlsruhe, FRG 7500

Fields, R.J.
National Bureau of Standards
A113/223
Gaithersburg, Maryland 20855

Figlhuber, D.
Utility Power Corporation
Atlanta, Georgia

Filacchione, H.E.
NUS Corporation
910 Clopper Road
Gaithersburg, Maryland 20878

Finley, M.T.
Baltimore Gas & Electric
Calvert Cliffs
Lusby, Maryland 20632

Fiorino, E.
Ente Nazionale Energia Elettrica
V.G.B. Martini 3
Rome 00100
ITALY

Flanagan, G.F.
Oak Ridge National Laboratory
P.O. Box X
Building 6025
Oak Ridge, TN 37831

Fox, J.R.
Combustion Engineering
1000 Prospect Hill Road
Windsor, CT 06095

Freed, D.A.
MPR Associates
1050 Connecticut Avenue, N.W. 20036

Freund, G.A.
Science Applications International Corp.
P.O. Box 696
Idaho Falls, Idaho 83402

Friderichs, T.
MPR Associates
1050 Connecticut Avenue, N.W. 20036

Fujimoto, H.
Mitsubishi Atomic Power Industries, Inc.
No. 4-1, Shibakouen 2-chome, Minato-ku
Tokyo 105
Japan

Fujishiro, T.
Japan Atomic Energy Research Institute
Tokai-mura, Nakagun, Ibaraki-ken
Japan

Gabetta, G.
CISE
Via Reggio emilia, 39
Segrate (MI), Italy 20090

Gallerly, R.T.
UKAEA, SRD
Wigshaw Lane, Culcheth
Warrington, Cheshire
U.K.

Gasparl, G.
SIET
N. Bixio 21 P
Piacenza, Italy

Gasparini, M.
ENEA-Disp
Via Vitaliano Brancati 48
Rome, Italy 00144

Gast, P.
Kernforschungszentrum Karlsruhe GmbH
Postfach 3640
D-7500 Karlsruhe
FRG 7500

George, P.R.
CEGB-PMT
Booths Hall
Knutsford, Cheshire WA168QG
ENGLAND

Ghosh, S.
Central Electricity Generating Board
Boothshall, Chelsford Road
Knutsford, Cheshire, England
UK

Gieseke, J.A.
Battelle - Columbus Laboratories
505 King Avenue
Columbus, Ohio 43201

Gilman, J.D.
Electric Power Research Institute
P.O. Box 10412
Palo Alto, California 95120

Ginsberg, T.
Brookhaven National Laboratory
Building 820
Upton, New York 11973

Girrens, S.P.
Los Alamos National Laboratory
P.O. Box 1663
Los Alamos, NM 87545

Gitnick, B.J.
ENSA, Inc.
15825 Shady Grove Road
Rockville, Maryland 20850

Gloudemens, J. R.
Babcock & Wilcox
Old Forrest Road
Lynchburg, Virginia 24501

Gold, R.
Hanford Engineering Development Laboratory
P.O. Box 1970
Richland, WA 99301

Gonzalez, E.G.
Consejo De Seguridad Nuclear
Sor Angela de la Cruz
Madrid, Spain 28020

Goodwin, E.F.
Stone & Webster
P.O. Box 5200
Cherry Hill, NJ 08034

Gordon, B.M.
General Electric Company
175 Curtner Avenue, MC 785
San Jose, California 95125

Grant, S.P.
Carolina Power & Light Co.
P.O. Box 1551
Raleigh, North Carolina 27602

Greenblatt, M.
Materials Engineering Associates
9700 B Palmer Highway
Lanham, Maryland 20706

Greene, G.A.
Brookhaven National Laboratory
Building 820
Upton, New York 11973

Griffith, P.
Massachusetts Inst. of Technology
77 Massachusetts Avenue
Cambridge, Massachusetts 02139

Grotenhuis, M.
U.S. Nuclear Regulatory Commission
7920 Norfolk Avenue
Bethesda, Maryland 20014

Guppy, J.G.
Brookhaven National Laboratory
Building 130
Upton, New York 11973

Hall, R.E.
Brookhaven National Laboratory
Bldg. 130
Upton, New York 11973

Hampel, G.
Battelle-Institut e.V.
Am Roemerhof 35
6000 Frankfurt 90
Germany

Hawley, J. T.
MPR Associates
1050 Connecticut Ave., N.W.
Washington, D. C. 20036

Hawthorne, J.R.
Materials Engineering Associates
9700 B Palmer Highway
Lanham, Maryland 20706

Hazzan, M.J.
Stone & Webster
3 Executive Campus
Cherry Hill, NJ 08034

Heck, C. L.
Westinghouse Electric Corp.
P.O. Box 355
Pittsburgh, Pennsylvania 15230

Hepper, P.J.
Central Electricity Generating Board
Berkeley Nuclear Lab
Berkeley, England

Herter, K.H.
MPA-Stuttgart/W. Germany
505 King Avenue
Columbus, Ohio 43201

Hewitt, G. F.
AERE Harwell
Oxfordshire OX11 ORA
United Kingdom

Hidinger, D.E.
Knolls Atomic Power Laboratory
P.O. Box 1072
Schenectady, New York 12301

Hill, P.R.
Pennsylvania Power & Light Co.
2N 9th Street
Allentown, Pennsylvania 18101

Hill, R.C.
EG&G Idaho, Inc.
P.O. Box 1625
Idaho Falls, Idaho 83415

Hiser, Jr., A. L.
Materials Engineering Associates
9700-B George Palmer Highway
Lanham, Maryland 20801

Hitchcock, J.T.
Sandia National Laboratories
P.O. Box 5800
Albuquerque, NM 87185

Hodge, S.A.
Oak Ridge National Laboratory
P.O. Box Y
Building 9104-1
Oak Ridge, Tennessee 37831

Hofmann, K.R.
GRS (Gesellschaft fuer Reaktorsicherheit)
Schwertnergasse 1
5000 Koeln 1
West Germany

Hofmayer, C.H.
Brookhaven National Laboratory
Building 129
Upton, New York 11973

Holian, B.E.
Baltimore Gas & Electric
CCNPP
Lusby, Maryland 20657

Holler, P.J.
Fraunhofer-Institut fur zerstorungsfreie
Universitat, Gebsude 37
D-6600 Saarbrucken 11
West Germany

Holman, G.S.
Lawrence Livermore National Laboratory
P.O. Box 808
Livermore, CA 94550

Holmstrom, H. L.
Technical Research Centre of Finland (VTT)
P.O. Box 169, SF-00181 Helsinki, Finland

Holtzclaw, K.W.
General Electric
175 Curtner Avenue, M/C 682
San Jose, California 95125

Hoppe, R.G.
Westinghouse - Bettis
P.O. Box 79
West Mifflin, Pennsylvania 15122

Hosemann, P.J.
Kernforschungszentrum Karlsruhe GmbH
Postfach 3640
D-7500 Karlsruhe
Federal Republic of Germany

House, R.K.
Intermountain Technologies Inc.
P.O. Box 1604
Idaho Falls, Idaho 83403-1604

Hsia, D.Y.
Atomic Energy Council of Republic of China
67.Lane 144 Keelung Road Sec. 4
Taipei, Taiwan
Rep. of China

Hsu, T.W.
Virginia Power
P.O. Box 26666
Richmond, Virginia 23113

Hsu, Y-Y.
University of Maryland
College Park, Maryland 20742

Hu, T.K.
Bechtel Power Corporation
15740 Shady Grove Road
Gaithersburg, Maryland 20878

Hull, A.P.
Brookhaven National Laboratory
Building 535A
Upton, New York 11973

Hutton, P.H.
Battelle - Pacific Northwest Laboratory
Box 999
Richland, Washington 99352

Hwang, H.H.
Brookhaven National Laboratory
Building 129
Upton, New York 11973

Hyman, C.R.
Oak Ridge National Laboratory
P.O. Box Y
Building 9104-1
Oak Ridge, TN 37831

Iguchi, T.
Japan Atomic Energy Research Institute
Tokai-mura
Ibaraki-ken
Japan 319-11

Imai, T.
JEPIC
1726 M Street, N.W., S. 603
Washington, D. C. 20036

Irby, R.G.
Tennessee Valley Authority
400 West Summit Hill Drive, W10D205
Knoxville, TN 37902

Irwin, G.R.
University of Maryland
College Park, Maryland 20742

Ishigami, T.
Japan Atomic Energy Research Institute
Naka-Ibaraki 319-11
Japan

Ishii, M.
Argonne National Laboratory
9700 South Cass Avenue
Argonne, Illinois 60439

Iskander, S.K.
USNRC/ORNL/MPA
MPA, Pfaffenwaldring 32
7000 Stuttgart 80
FRG (West Germany)

Iwamura, T.
Japan Atomic Energy Research Institute
Tokai-mura Naka-gun
Ibaraki-ken, Japan 319-11

Izquierdo, J.M.
Consejo Seguirdad Nuclear
Sor Angela de la Cruz 3
Madrid, Spain

Jacobs, P.J.
EG&G Idaho, Inc.
P.O. Box 1625
Idaho Falls, Idaho 83415

Janssen, L.G.
Netherlands Energy Research Foundation
Westerduinweg 3, P.O. Box 1
Petten 1755 ZG
The Netherlands

Jeanmougin, N.M.
Energy Technology Engineering Center
P.O. Box 1449
Canoga Park, California 91304

Jegu, J.A.
FRAMATOME
Tour Fiat Cedex 16
Paris La Defense 92084
FRANCE

Jenks, R.
Los Alamos National Laboratory
P.O. Box 1663
Los Alamos, New Mexico 87545

Jo, J.H.
Brookhaven National Laboratory
Building 130
Upton, New York 11973

Johnsen, G.W.
EG&G Idaho, Inc.
P.O. Box 1625
Idaho Falls, Idaho 83415

Jones, D.
AEC SA
Private Bag X256
Pretoria, Transvaal 0001
South Africa

Jun, H.R.
KAERI/DaeJeon
DaeJeon, Korea

Kalra, S.P.
Electric Power Research Institute
3412 Hillview Avenue
Palo Alto, California 94303

Kam, F.B.
Oak Ridge National Laboratory
P.O. Box X, Bldg. 3001
Oak Ridge, Tennessee 37831

Kannberg, L.D.
Battelle - Pacific Northwest Laboratory
P.O. Box 999
Richland, Washington 99352

Kanninen, M.F.
Southwest Research Institute
6220 Culebra Road (P.O. Drawer 28510)
San Antonia, TX 78284

Kanzleiter, T.F.
Battelle-Institut e.V.
Am Roemerhof 35
D-6000 Frankfurt, FR Germany D-6000
FRG

Kao, L.
MIT
60 Wadsworth Street, Apt. 3/
Cambridge, MA 02142

Karwat, H.
Techn. Univ. Munich-FRG
Forschungsgelaende
D8046 Garching
Bavaria 8046
FRG

Kashima, K
Central Res. Inst. of Elec. Power Inst.
11-1, Iwato Kita 2-Chome
Komae-Shi, Tokyo 201
Japan

Kasprzak, S.
Rensselaer Polytechnic Institute
NES Bldg., Tibbits Avenue
Troy, New York 12180-3590

Kato, W.Y.
Brookhaven National Laboratory
Building 197C
Upton, New York 11973

Kawaji, M.
Japan Atomic Energy Research Institute
2-4, Shirane, Shirakata, Naka-gun, Ibaraki-ken
Japan

Kawasaki, M.
NIPPON Energy Incorporated
1-16-5 Nishishinbashi
Minato-ku, Tokyo 105
Japan

Kayser, W.V.
Exxon Nuclear Company, Inc.
P.O. Box 130
Richland, Washington 99352

Kazimi, M.S.
MIT
77 Mass Avenue
Cambridge, MA 02139

Kelly, J.E.
Sandia National Laboratory
Division 6425
P.O. Box 5800
Albuquerque, New Mexico 87185

Khatib-Rahbar, M.
Brookhaven National Laboratory
Building 130
Upton, New York 11973

Kikuta, M.
Mitsubishi Atomic Power Industries, Inc.
No. 4-1, Shibakouen 2-chome, Minato-ku
Tokyo 105
Japan

Kim, J.
Korea Power Eng. Co.
3785-D Logans Ferry Road
Pittsburgh, PA 15239

Kimmins, A.D.
ORNL/Nuclear Safety Journal
P.O. Box Y - Bldg. 9201-3, M/S-5
Oak Ridge, TN 37831

Kiyoshi, K.
Japan Atomic Energy Research Institute
Tokai-mura
Ibaraki-ken
Japan 319-11

Klansnitzer, E.N.
KWN
Hammerbacher Street
Erlangen, FRG

Kleimola, F.W.
NUCLEDYNE Engineering Corporation
728 W. Michigan Avenue
Jackson, Michigan 49201

Klorig, W.N.
Aptech Eng. Services
101 1/2 S. Union Street
Alexandria, VA 22314

Kmetyk, L.N.
Sandia National Laboratory
Division 6444
P.O. Box 5800
Albuquerque, New Mexico 87185

Knight, T.D.
Los Alamos National Laboratory
P.O. Box 1663
Los Alamos, New Mexico 87545

Knipe, A.D.
UKAEA (EG & G Idaho, Inc.)
Building TSA
P.O. Box 1625
Idaho Falls, Idaho 83415

Koch, D.A.
Gilbert/Commonwealth
P.O. Box 1498
Reading, PA 19603

Kogan, V.
Battelle - Pacific Northwest Laboratory
505 King Avenue
Columbus, Ohio 43201

Koizumi, Y.
Japan Atomic Energy Research Institute
Tokai-mura, Naka-gun
Ibaraki-ken, Japan 319-11

Koski, S.J.
TVO Power Company
SF-27160 Olkiluoto
FINLAND

Kot, C.A.
Argonne National Laboratory
9700 S. Cass Avenue
Building 335
Argonne, Illinois 60439

Koziol, J.J.
Combustion Engineering Inc.
1000 Prospect Hill Road
Windsor, CT 06095-0500

Kress, T.S.
Oak Ridge National Laboratory
102 Daniel Lane
Oak Ridge, TN 37830

Kumamaru, H.
Japan Atomic Energy Research Institute
2-4, Shirane, Shirakata, Naka-gun, Ibaraki
Japan

Kupperman, D.S.
Argonne National Laboratory
9700 S. Cass Avenue
Building 212
Argonne, Illinois 60439

Kurtz, R.J.
Battelle - Pacific Northwest Laboratory
P.O. Box 999
Richland, WA 99352

Kussmaul, K.F.
MPA Stuttgart
32 Pfaffenwaldring
Stuttgart, FRG 07000

Laats, T.
EG&G Idaho, Inc.
P.O. Box 1625
Idaho Falls, Idaho 83415

Laguardia, T.S.
TLG Engineering, Inc.
640 Federal Road
Brookfield, CT 06804

Lain, P.J.
Westinghouse Electric Power Systems
P.O. Box 355
Pittsburgh, PA 15230

Lang, R.E.
U.S. Department of Energy
9800 S. Cass Avenue
Argonne, Illinois 60439

Lareau, J.P.
Combustion Engineering
1000 Prospect Hill Road
Windsor, CT 06095

Larson, T.K.
EG&G Idaho, Inc
P.O. Box 1625
Idaho Falls, Idaho 83415

Lee, C.T.
Ontario Hydro
700 University Avenue, (H9)
Toronto, Ontario M5G 1X6
Canada

Lee, G.
KAERI
Holiday Inn
Seoul, Korea

Lau, J.H.
Ontario Hydro
700 University Avenue, (H9)
Toronto, Ontario M5G 1X6
Canada

Lee, N.
Westinghouse
Monroeville Nuclear Center
Monroeville, PA 15146

Leven, D. W.
Gesellschaft fur Reaktorsicherheit
Schwertnergasse
Koln, FRG

Leve, C.K.
NUS Corporation
910 Clopper Road
Gaithersburgh, Maryland 20878

Liesch, K.
Gesellschaft fuer Reaktorsicherheit
Bernheimersh. 4
Munchen, W. Germany

Lindeman, E.D.
McGraw Hill
1120 Vermont Avenue, N.W.
Washington, D. C. 20005

Lippincott, E.P.
Westinghouse
P.O. Box 355
Pittsburgh, PA 15230

Lloyd, G. J.
United Kingdom Atomic Energy Authority
Risley, Cheshire WA36AT
England

Loewenstein, W.B.
Electric Power Research Institute
3412 Hillview Avenue
P.O. Box 10412
Palo Alto, CA 94303

Loss, F.V.
Materials Engineering Associates
9700-B George Palmer Highway
Lanham, Maryland 20706

Lowe, A.L.
Babcock & Wilcox
2708 Evergreen Road
Lynchburg, VA 24503

Majumdar, D.
U.S. Department of Energy
785 DOE Place
Idaho Falls, Idaho 83402

Malinauskas, A.P.
Oak Ridge National Laboratory
P.O. Box X
Building 4500S, Rm. A174
Oak Ridge, TN 37831

Mallen, A.N.
Brookhaven National Laboratory
Building 130
Upton, New York 11973

Malliakos, A.
Combustion Engineering, Inc.
1000 Prospect Hill Rt.
Windsor, CT 06095

Mancuso, V.
ENEA-Rome
Dipartimento Reattori Termici
Roma, Italia 00060

Mandl, R.M.
Kraftwerk Union Aktiengesellschaft
Hammerbacherstr. 12+14
8520 Erlangen
West Germany

Martinell, J.S.
EG&G Idaho, Inc.
Foote Drive
Idaho Falls, Idaho 83401

Marx, K.D.
Sandia National Laboratory
P.O. Box 969
Livermore, California 94550

Maskewitz, B.F.
Oak Ridge National Laboratory
P.O. Box X
Oak Ridge, Tennessee 37831

Masuda, F.
Toshiba
9-3-104, 5 chome, Isogo
Yokahama, Japan

Matsumoto, K.
Japan Atomic Energy Research Institute
q3220 Wyoming N.E. Apt. B
Albuquerque, NM 87111

Mattson, J.S.
Swedish Nuclear Power Inspectorate
Box 27106
S-102 52 Stockholm
Sweden

McCabe, D.E.
Materials Engineering Associates, Inc.
9700B Palmer Highway
Lanham, Maryland 20706

McElroy, W.N.
Hanford Engineering Development Laboratory
P.O. Box 1970
Richland, Washington 99352

McHarry, E.D.
National Bureau of Standards
Gaithersburg, Maryland 20855

McLean, J.
Robert L. Cloud Associates
20 Main Street
Cotuit, Massachusetts 02635

McMillan, R.N.
UKAEA, SRD
Wigshaw Lane, Culcheth
Warrington, England

McPherson, G.D.
U.S. Department of Energy
6636 Kirby Court
Falls Church, VA 22043

Mebich, C.
SIET
Via Nino Bixio 27
Piacenza 29100
Italy

Mercier, O. M.
Swiss Federal Institute for Reactor Res.
Wuerenlingen, Switzerland 5430

Meyer, P.E.
Westinghouse
P.O Box 355
Pittsburgh, PA 15230

Micaelli, J.
CEA/CENG/STT
85X-38041 Grenoble Cedex
Grenoble
FRANCE

Milella, P.P.
ENEA
Via V. Brancati 48
Roma, Italy 00144

Miller, C.D.
CBI Industries
1501 N. Division St.
Naperville, IL 60544

Miller, R.L.
UNC Nuclear Industries
P.O. Box 490 J1
Richland, Washington 99352

Mitake, S.
EG&G Idaho/JAERI
P.O. Box 1625
Idaho Falls, Idaho 83415

Modro, S.M.
FZS-Austria
c/o EG&G Idaho, Inc.
P.O. Box 1625
Idaho Falls, Idaho 83415

Moody, J.H.
YAECO
1671 Worcester Road
Framingham, MA 01701

Mukherjee, B.
Ontario Hydro Research
800 Kipling Avenue
Toronto, Ontario M8Z 554

Muramoto, T.
Chupu Electric Power Co., Inc.
900 17th St., N.W., Suite 714
Washington, D. C. 20006

Murao, Y.
Japan Atomic Energy Research Institute
Tokai-mura, Ibaraki-ken, Japan 319-11

Murase, M.
Hitachi, Ltd.
1168 Moriyama-cho
Hitachi, Ibaraki 316
Japan

Naff, S.A.
EG&G Idaho, Inc.
Esperstr 19
8525 Uttenreuth, W. Germany

Nair, P.K.
Southwest Research Institute
P.O. Drawer 28510
6220 Culebra Road
San Antonio, TX 78284

Nakagawa, S.
Kansai Electric Power
1100 17th St., N.W.
Washington, D. C. 20036

Nakajima, H.
Century Research Center Corporation
2,3-chome, Hon-Cho, Nihonbashi, Chuo-ku
Tokyo 103
JAPAN

Nakajima, H.
Japan Atomic Energy Research Institute
Tokai-mura, Ibaraki-ken, Japan 319-11

Nanstad, R.K.
Oak Ridge National Laboratory
Bldg. 4500-S, Mail Stop D-61
P.O. Box X
Oak Ridge, TN 37831

Nelson, B.M.
Knolls Atomic Power Laboratory
P.O. Box 1072
Schenectady, New York 12301

Nelson, L.S.
Sandia National Laboratory
P.O. Box 5800
Albuquerque, New Mexico 87185

Nelson, R. A.
Los Alamos National Laboratory
MS-K553
Los Alamos, NM 87545

Neuvonen, A.
Imatran Voima Oy
P.O. Box 138
Helsinki, Finland

Neymotin, L.
Brookhaven National Laboratory
Bldg. 130
Upton, New York 11973

Ni, M.S.
Atomic Energy Council of Republic of China
67.Lane 144 Keelung Road Sec. 4
Taipei, Taiwan
Rep. of China

Niemczyk, S.J.
Gull Associates
1545 18th St., N.W.
Washington, D. C. 20036

Nithianandan, C.K.
Babcock & Wilcox
3315 Old Forest Road
Lynchburg, VA 24506

North, P.
LOFT - TAN 602
P.O. Box 1625
Idaho Falls, Idaho 83415

O'Neill, L.A.
Stone & Webster
50 Summer Street
Boston, MA 02146

Oddo, J.M.
Stone & Webster Eng. Corp.
P.O. Box 2325
Boston, MA 02107

Ogata, Y.
Mitsubishi Heavy Industries, Ltd.
4-1 Shibakoen 2-Chome
Minato Ku, Tokyo 105 JAPAN

Ohno, T.
Nuclear Power Engineering Test Center
No. 2 Akiyama Bldg., 6-2,3-chome
Toranomon Minato
Tokyo, Japan

Ohnuki, A.
Japan Atomic Energy Research Institute
Tokai-mura
Ibaraki-ken, Japan 319-11

Ohtsubo, A.
Nuclear Power Engineering Test Center
1-4-28, Mita, Minato-ku
Tokyo 108, Japan

Okada, S.
Japan Atomic Energy Research Institute
1233 Watanuki-machi, Takasaki, Gunma-ken JAPAN

Okano, Y.
EG&G Idaho
1361 S. Woodruff
Idaho Falls, Idaho 83401

Oldfield, G.V.
Washington Public Power Supply System
P.O. Box 968
Richland, WA 99352

Olsen, C.S.
EG&G Idaho, Inc.
P.O. Box 1625
Idaho Falls, Idaho 83415

Omar, A. M.
Atomic Energy Control Board
270 Albert Street
Ottawa, Ontario K1P5S9, Canada

Onesto, A.T.
ETEC/Rockwell
P.O. Box 1449
Canoga Park, CA 91304

Ott, L.J.
Oak Ridge National Laboratory
P.O. Box Y
Building 9104-1
Oak Ridge, TN 37831

Pan, J.
The University of Michigan
Ann Arbor, Michigan 48109

Parece, M.V.
Babcock & Wilcox
206 Shadwell Drive
Lynchburg, VA 24503

Parish, H. G.
Atomic Energy Corp. of South Africa
Private Box X256
Pretoria 0001
South Africa

Pearson, K.G.
United Kingdom Atomic Energy Authority
AEE Winfrith
Dorchester, Dorset DT28DH
United Kingdom

Pence, J.H.
Baltimore Gas & Electric
P.O. Box 1475
Baltimore, Maryland 21203

Perkins, K.
Brookhaven National Laboratory
Bldg. 130
Upton, New York 11973

Peterson, A.C.
Sandia National Laboratories
P.O. Box 5800
Albuquerque, NM 87185

Petrangeli, G.
ENEA/Disp
Via Vitaliano Brancati, 48
Rome, Italy 00144

Philippacopoulos, A.J.
Brookhaven National Laboratory
Building 129
Upton, New York 11973

Piciulo, P.L.
Brookhaven National Laboratory
Building 830
Upton, New York 11973

Pilch, M.
Sandia National Laboratory
Division 6425
P.O. Box 5800
Albuquerque, New Mexico 87185

Pino, G.
ENEA/Disp
Via Vitaliano Brancati, 48
Rome, Italy 00144

Podowski, M. Z.
Rensselaer Polytechnic Institute
NES Bldg., Tibbits Avenue
Troy, New York 12810-3590

Posakony, G.J.
Battelle - Pacific Northwest Laboratory
P.O. Box 999
Richland, WA 99352

Potter, C.
HM Nuclear Installations Inspectorate
Thames House North
Millbank
London SWIP 4QJ, U.K.

Powers, D.A.
Sandia National Laboratory
P.O. Box 5800
Albuquerque, New Mexico 87185

Prelewicz, D.A.
ENSA, Inc.
15825 Shady Grove Road, Suite 170
Rockville, Maryland 20850

Pugh, C.E.
Oak Ridge National Laboratory
P.O. Box Y
Oak Ridge, Tennessee 37831

Pugh, M. C.
UKAEA
Wigshaw Lane
Culcheth, Cheshire
Wa34NE, England

Rahn, F.
Electric Power Research Institute
P.O. Box 10412
Palo Alto, California 94301

Rainey, P.
Rolls Royce Associates
P.O. Box 31
Raynesway
Derby, England

Reich, M.
Brookhaven National Laboratory
Bldg. 129
Upton, New York 11973

Reimann, M.
Kernforschungszentrum KarlsruheGmbH
Postfach 3640
Karlsruhe, W. Germany D-7500

Renner, H.
NUS Corporation
910 Clopper Road
Gaithersburg, Maryland 20878

Reocreux, M. L.
CEA/France
CEN Fontenay aux Roses BP n° 6
Fontenay aux Roses, France 92265

Reuland, W.B.
Electric Power Research Institute
P.O. Box 10412
Palo Alto, California 94304

Reynen, J.
EEC
2100 M SW NW
Washington, D. C. 20037

Rhoads, J.E.
Washington Public Power Supply System
3000 George Washington Way
Richland, Washington 99352

Rib, L.N.
LNR Associates
8605 Grimsby Court
Potomac, Maryland 20854

Robinson, D.
IIT Res. Institute
10 W. 35th
Chicago, Illinois 60616

Robinson, G.E.
Penn State University
1101 Oak Ridge Avenue
State College
PA 16801

Roh, E.R.
Korea Electric Power Corporation R & D
52, Cheongdam-Dong, Kangnam-Ku
Seoul
Korea

Rohatgi, U.S.
Brookhaven National Laboratory
Building 130
Upton, New York 11973

Rohde, J.
Gesellschaft fur Reaktorsicherheit (GRS)
Schwertnergasse 1
5000 koln 1
FRG
West Germany

Romano, A.J.
Brookhaven National Laboratory
Building 197C
Upton, New York 11973

Ross, C.P.
DuPont
10024-203 Stedwick Road
Gaithersburg, Maryland 20879

Rouhani, S.Z.
EG&G Idaho, Inc.
P.O. Box 1625
Idaho Falls, Idaho 83415

Rupprecht, S.D.
Westinghouse
P.O. Box 355
Pittsburgh, PA 15146

Saluja, J.K.
Viking Energy Corp.
121 N. Highland Avenue
Suite 203
Pittsburgh, PA 15206

Samanta, P.K.
Brookhaven National Laboratory
Bldg. 130
Upton, New York 11973

Sandervag, O.S.
Studsvik Energiteknik Ab
S-61182
Nykoping, Sweden

Satoshi, M.
Hitachi, Ltd.
Hitachi, Ibaraki 316
Japan

Scarbrough, T.G.
U.S. Nuclear Regulatory Commission
Washington, D. C. 20555

Schelling, F.J.
Sandia National Laboratory
Division 6449
Albuquerque, New Mexico 87185

Schikarski, W.O.
Kernforschungszentrum Karlsruhe GmbH
P.O. Box 36 40
Karlsruhe, Baden-Wuerttemberg D-7500
FRG

Schleifer, F.
GRS (Gesellschaft fur Reaktorsicherheit)
Schwertuergasse 1
Koln (Cologn) 1 5000
FRG

Schlotthauer, U.C.
FRAMATOME
Tour Fiat Cedex 16
Paris La Defense 92084
FRANCE

Schmidt, E.R.
NUS
910 Clopper Road
Gaithersburgh, Maryland 20874

Schmitt, A.P.
Commissariat A L'Energie Atomique
CEN-FAR-BPu-692260
Fontenay.Aux.Roses
France

Schnurstein, R.E.
EG&G
P.O. Box 1449
Canoga Park, California 91304

Schoech, W.
Kernforschungszentrum Karlsruhe GmbH
Weberstr. 5
Karlsruhe, FRG 7500

Schrock, V.E.
University of California, Berkeley
Berkeley, California 94720

Schwarzer, W.J.
Kerntechnischer Ausschuss (KTA)
c/o GRS mbH, Schwertnergasse 1
5000 Koeln
F.R. of Germany

Schweitzer, G.J.
Sargent & Lundy Engineers
55 E. Monroe Street
MC/31V30
Chicago, Illinois 60603

Scott, P.M.
UK Atomic Energy
Aere
Harwell, Oxon OX11 ORA, U.K.

Seihiro, I.
Nippon Atomic Industry Group Co.
4-1, Ukishima-cho, Kawasaki-ku
Kawasaki, Kanagawa 210
Japan

Sestak, P.F.
Stone & Webster Eng. Corp.
3 Executive Campus
Cherry Hill, New Jersey

Seth, S.S.
MITRE Corp.
1820 Dolley Madison
McLean, VA 22102

Sgalambro, G.
ENEA/Disp
Via V. Brancati, 48
Roma, Italy 00144

Shack, W.J.
Argonne National Laboratory
Bldg. 212
Argonne, Illinois 60439

Shah, N.H.
Babcock & Wilcox
Lynchburg, Virginia 24502

Sharma, R.S.
American Electric Power
One Riverside Plaza
Columbus, Ohio 43215

Sharp, D.A.
Savannah River Laboratory, E.I. duPont
Aiken, SC 29801

Sherman, M.
Sandia National Laboratory
P.O. Box 5800
Albuquerque, NM 87185

Sherry, R.R.
NUS
910 Clopper Road
Gaithersburg, Maryland 20878

Shigero, K.
Tokyo Electric Power Co.
No. 1-3.1-chome Uchisaiwai-cho
Chiyodako/Tokyo 100
Japan

Shimeck, D.J.
WestinghouseElectric Corp.
P.O. Box 355
Pittsburgh, PA 15146

Shipsky, W.E.
WestinghouseElectric Corp.
Expomart
Monroeville, PA

Shiralkar, B.S.
General Electric
175 Curtner Avenue
San Jose, California 95125

Shoji, T.
Res. Inst. for Strength and Fracture of...
Aramaki Aoba Sendai/980, Japan
SENDAI, MIYAGI
JAPAN

Shunro, N.
Tokotestack Co. Ltd.
21-10 6Chome Sagamidai
Sagamihara, Kanagawa
Japan

Sigal, G.B.
Burns & Roe
800 Kinderkamack Road
Oradell, New Jersey 07649

Simonen, F.A.
Battelle - Pacific Northwest Laboratory
P.O. Box 999
Richland, WA 99352

Slaughter, G.M.
Oak Ridge National Laboratory
Oak Ridge, Tennessee 37831

Slegers, L.
KWU
605 Offenbach
Berlinerstr, W. Germany

Slovik, G.C.
Brookhaven National Laboratory
Building 130
Upton, New York 11973

Smith, D.L.
Wyle Laboratories
1841 Hillside Avenue
Norco, California 91760

Snyder, A.W.
Sandia National Laboratory
P.O. Box 5800
Albuquerque, NM 87185

Soda, K.
Japan Atomic Energy Research Institute
Tokaimura
Nakagun, Ibarakiken 319-11
Japan

Somers, W.S.
Dept. of Energy-Idaho Operations Office
785 DOE Place
Idaho Falls, Idaho 83402

Soong, D.Y.
Bechtel Power Corp.
Gaithersburg, Maryland 20877

Sozer, A.
Oak Ridge National Laboratory
P.O. Box Y, Building 9104-1
Oak Ridge, TN 37831

Spatz, R.
Institut fur Verfahrenstechnik
Universitat Hannover
Callinstr. 36
Hannover D-3000

Spencer, B.W.
Argonne National Laboratory
Argonne, Illinois 60439

Squarer, D.
Westinghouse
P.O. Box 355
Pittsburgh, PA 15230

St. John, K.E.
Yankee Atomic Electric Company
1671 Worcester Road
Framingham, Massachusetts 01701

Stadtke, H.
EURATOM - Joint Research Centre, Ispra
I-21020 Ispra (Varese), Italy
Ispra, ITALY

Stallmann, F.W.
Oak Ridge National Laboratory
P.O. Box X
Building 3001
Oak Ridge, Tennessee 37831

Stepnewski, D.D.
Westinghouse, Hanford Co.
P.O. Box 1970
Richland, Washington 99352

Strawson, D.
MPR Associates
1050 Connecticut Avenue, N.W. 20036

Stubbe, E.J.
Tractionel/Belgium
31 Rue De La Science
Brussels, Belgium 1040
Belgium

Sullivan, H.L.
Los Alamos National Laboratory
Mail Stop K552
Los Alamos, New Mexico 87545

Suo-Anttila, A.J.
Sandia National Laboratory
Division 6425
P.O. Box 5800
Albuquerque, New Mexico 87185

Sutherland, W.A.
General Electric Co.
175 Curtner Avenue
Mail Code 186
San Jose, California 95125

Swan, D.I.
Rolls Royce & Associates, Ltd.
P.O. Box 31
Derby
De2 8BJ, U.K.

Syouichi, S.
Japan Institute of Nuclear Safety
Mita Kokusai, Bldg. 4-28
Minato-ku, Tokyo, Japan 108

Tajbakhsh, A.
Westinghouse Electric Co.
Northern Pike
Monroeville, PA 15146

Takeda, M.
SHIMIZU Construction Co., Ltd.
13-16, Mita 3-chome, Minato-ku
Tokyo 108
JAPAN

Tang, H.
Electric Power Research Institute
3412 Hillview Avenue
P.O. Box 10412
Palo Alto, CA 94303

Tasaka, K.
Japan Atomic Energy Research Institute
2-4, Shirane, Shirakata, Naka-gun, Ibaraki-ken
Japan

Taylor, J.H.
Brookhaven National Labortory
Building 130
Upton, New York 11973

Taylor, L.G.
National Nuclear Corp.
Booths Hall
Chelford Road
Knutsford, England

Tazawa, K.
Japan NUS Co., Ltd.
7-1 Nishi-shinjuku 2-chome shinjukuku
Tokyo, Japan

Thiess, P.E.
American Env. Central Systems Inc.
P.O. Box 1189
Washington, D. C. 20013

Thomas, A.F.
Rolls Royce & Associates
P.O. Box 31 Raynesway
Derby, U.K. DEZ

Thomas, G.R.
Electric Power Research Institute
P.O. Box 10412
Palo Alto, California 94306

Thorne, L.R.
Sandia National Laboratory
P.O. Box 969
Livermore, California 94550

Tieszen, S. R.
Sandia National Laboratory
P.O. Box 5800
Albuquerque, New Mexico 87185

Tkach, R.J.
PSE&G
P.O. Box 570
80 Park Plaza
Newark, New Jersey 07101

Toman, G.J.
Franklin Research
20th & Race Streets
Philadelphia, Pennsylvania 19103

Tong, L.S.
Tong and Associates, Inc.
9733 Lookout Place
Gaithersburg, Maryland 20879

Torronen, K.J.
Technical Research Centre of Finland
Metals Lab.
Metallimiehenkuja 6
SF-02150 Espoo
Finland

Toshiyuki, Y.
Japan Atomic Energy Research Institute
100 Sanford Lane
Oak Ridge, Tennessee 37830

Trammell, H.E.
Oak Ridge National Laboratory
P.O. Box Y
Oak Ridge, Tennessee 37831

Tsai, C-K.
Westinghouse Electric Corp.
P.O. Box 355
Pittsburgh, Pennsylvania 15230

Tsai, S-f.
Westinghouse Electric Corp.
P.O. Box 355
Pittsburgh, Pennsylvania 15230

Tsai, Z.
Institute of Nuclear Energy Research
P.O. Box 3-6
Lung-tan, Taiwan 325
Taiwan, Republic of China

Tunon-Sanjur, L.J.
Westinghouse
100 Penn Center
Wilkins Twp., Pennsylvania 15239

Turland, B.D.
UKAEA Culham Laboratory
Culham Laboratory, Abingdon
Oxon, England OX 143DB
England

Ueda, S.
Japan Atomic Energy Research Institute
Tokai-mura, Ibaraki-ken
Japan

Unger, H.E.
University Stuttgart
Pfaffenwaldring 31
Stuttgart-80, W. Germany D-7000

Utton, D.B.
National Nuclear Corporation
Cambridge Road, Whetstone
Leicester, LE83LH ENGLAND

Van Kuijk, R.M.
KEMA
Utrechtseweg 310
Arnhem, The Netherlands

Varrin, R.
MPR Associates
1050 Connecticut Avenue, N.W.
Washington, D. C. 20036

Vasudevan, N.
Babcock & Wilcox
P.O. Box 1260
Old Forest Road
Lynchburg, VA 24503

Versteegh, A.M.
Netherlands Energy Research Foundation
Westerduinweg 3, P.O. Box 1
Petten 1755 ZG
The Netherlands

Vesely, W.E.
Battelle - Columbus Laboratories
505 King Avenue
Columbus, Ohio 43201

Vinjamuri, K.
EG&G Idaho, Inc.
P.O. Box 1625
Idaho Falls, Idaho 83415

Vogel, R.C.
Electric Power Research Institute
3412 Hillview Avenue
Palo Alto, California 94303

von Riesemann, W. A.
Sandia National Laboratory
Division 6442
Albuquerque, New Mexico 87185

Vorees, J.
Arizona Nuclear Power Project
P.O. Box 52034, MS 4082
Phoenix, Arizona 85072-2034

Walker, L.I.
Westinghouse
Pittsburgh, PA 15542

Wang, W.Y.
Stone & Webster Eng.
P.O. Box 5200, 3, Executive Campus
Cherry Hill, NJ 08054

Ward, D.T.
Baltimore Gas & Electric
P.O. Box 1475
Baltimore, Maryland 21203

Ward, G.N.
Exxon Nuclear
2101 Horn Rapids Road
Richland, Washington 99352

Ware, A.G.
EG&G Idaho, Inc.
P.O. Box 1625
Idaho Falls, Idaho 83415

Watkins, J.C.
EG&G, Idaho
P.O. Box 1625
Idaho Falls, Idaho 83415

Webb, S.W.
Sandia National Laboratory
Division 6444
P.O. Box 5800
Albuquerque, New Mexico 87185

Weber, C.F.
Oak Ridge National Laboratory
P.O. Box X
Bldg. 6025
Oak Ridge, TN 37831

Weber, G.
Gesellschaft fur Reaktorsicherheit
Forschungsgelande
D-8046
Garching, Germany

Weeks, J.R.
Brookhaven National Laboratory
Building 703
Upton, New York 11973

Weiss, A. J.
Brookhaven National Laboratory
Building 197-C
Upton, New York 11973

Weiss, F. A.
Kraftwerk Union R 315
Hammerbacherstrasse 12+14
Erlangen 8520, FRG

Welch, E.C.
EG&G, Idaho
P.O. Box 1625
Idaho Falls, Idaho 83415

Wells, J.E.
Lawrence Livermore National Laboratory
740 Hanover Street
Livermore, California 94550

Wessel, E.T.
Consultant to ORNL
3570 Meadowgate Drive
Murrysville, Pennsylvania 15668

Wheatley, P.D.
EG&G Idaho, Inc.
P.O. Box 1625
Idaho Falls, Idaho 83415

Whipple, R.C.
Combustion Engineering
1000 Prospect Hill Road
Windsor, CT 06095

White, J.R.
J.R. White Consulting
2100 Belmont Avenue
Idaho Falls, Idaho 83401

Whitehead, T.J.
Science Applications International Corp.
101 S. Park Avenue
Idaho Falls, Idaho 83402

Wilkowski, G.M.
Battelle Columbus Laboratory
505 King Avenue
Columbus, Ohio 43201

Williams, K.A.
Science Applications International Corp.
Suite 1200
Albuquerque, New Mexico 87102

Winegardner, W.K.
Battelle - Pacific Northwest Laboratory
P.O. Box 999
Richland, Washington 99352

Winkler, F. J.
Kraftwerk Union Aktiengesellschaft
Hammerbacherstrasse 12+14
P.O. Box 3220
D-8520 Erlangen, FRG

Winslow, S.G.
Oak Ridge National Laboratory
P.O. Box X
Oak Ridge, TN 37831

Wolf, J.R.
EG&G Idaho, Inc.
P.O. Box 1625
Idaho Falls, Idaho 83401

Wolf, L.
Project HDR-Sicherheitsprogramm
Kernforschungszentrum Karlsruhe GMBH
Postfach 3640,7600

Woodruff, S.B.
Los Alamos National Laboratory
Q-9/MS K553
Los Alamos, New Mexico 87544

Wolfert, K.
Gesellschaft fur Reaktorsicherheit
Forschungsgelande
D-8046 Garching, Germany

Wong, C.C.
Sandia National Laboratory
P.O. Box 5800
Albuquerque, NM 87185

Worner, J.
Konig & Heunisch
Gerhurt Hauptmann str. 12
6100 Darmstadt, W. Germany

Wos, S.
Westinghouse - Bettis
P.O. Box 79
West Mifflin, Pennsylvania 15122

Wright, D.A.
Baltimore Gas & Electric
9612 Quarry Bridge Ct.
Columbia, Maryland 21046

Wu, D.
Suzhou Nuclear Power Research Institute
Jinmen Road
Suzhou, Jiangsu Province
Peoples Rep. of China

Wulff, W.
Brookhaven National Laboratory
Building 130
Upton, New York 11973

Yagawa, G.
University of Tokyo
Hongo, Bunkyoku
Tokyo 113
Japan

Yang, C.
Nuclear Industry Ministry of PRC
Beijing, China

Yaremy, E.M.
International Atomic Energy Agency
Wagrammerstrasse 5
Vienna, A-1400 Austria

Ybarrondo, L.J.
SCIENTECH, Inc.
P.O. Box 1406
Idaho Falls, Idaho 83403-1406

Young, M.Y.
Westinghouse
P.O. Box 355
Pittsburgh, Pennsylvania 15230

Young, R.L.
UKAEA/SRD
Wigshaw Lane
Culcheth, Cheshire
U.K.

Zbarek, J.
Czechoslovakian Embassy
3900 Linnean Avenue
Washington, D.C. 20008

Zhong, W.
National Nuclear Safety Administration
54 Sanlihe Road
Beijing
Peoples Republic of China

Zinnari, R.
Ansaldo Divisione Impianti/Italy
ViaG. D'Annunzio, 113
Genova 16100
Italy

PROCEEDINGS OF THE
THIRTEENTH WATER REACTOR SAFETY RESEARCH
INFORMATION MEETING

October 22-25, 1985

TABLE OF CONTENTS - VOLUME 3

	Page
ABSTRACT	iii
GENERAL INDEX	v
REGISTERED ATTENDEES	vii

MECHANICAL AND STRUCTURAL RESEARCH
Chairman: J. J. Burns (NRC)

Structural Load Combinations H. Hwang and M. Reich (BNL), B. Ellingwood (NBS) and M. Shinozuka (Columbia Univ.)	1
Standard Problems for Structural Computer Codes A. J. Philippacopoulos, C. A. Miller and C. J. Costantino (BNL)	27
Steel Containment Buckling T. A. Butler and W. E. Baker (LANL)	37
Piping Research Overview D. Guzy (NRC)	63
Pipe Damping A. G. Ware (EG&G)	73
BNL Piping Research P. Bezler et al. (BNL)	83
Pipe Ruptures in BWR Plants G. Holman, T. Lo and C. K. Chou (LLNL)	99
Valve Performance Testing N. M. Jeanmougin (ETEC)	117

SEISMIC RESEARCH
Chairman: J. J. Burns (NRC)

The Seismic Category I Structures Program J. G. Bennett, W. E. Dunwoody and C. R. Farrar (LANL)	127

SEISMIC RESEARCH
(Cont'd)

Page

Component Fragilities - Data Collection, Analysis and Interpretation. 139
K. K. Bandyopadhyay and C. H. Hofmayer (BNL)

Heissdampfreaktor Phase II Vibration Tests. 159
L. Malcher (KfK), H. Steinhilber (LBF) and C. Kot (ANL)

BWR Risk Assessment 179
T. Y. Chuang et al. (LLNL)

EQUIPMENT QUALIFICATION
Chairman: W. S. Farmer (NRC)

Progress on Qualification Testing Methodology Study of Electric Cables 203
S. Okada et al. (JAERI)

Equipment Qualification and Survivability Research at Sandia National Laboratories 235
L. L. Bonzon (SNL)

Fire Protection and Hydrogen Burn Equipment Survival Research 251
D. L. Berry (SNL)

Environmental and Dynamic Qualification of Equipment Research at the Idaho National Engineering Laboratory. 277
R. C. Hill (EG&G)

NUCLEAR PLANT AGING
Chairman: J. P. Vora (NRC)

Materials Aspects of BWR Plant Life Extension 293
B. M. Gordon and G. M. Gordon (GE)

The Measurement of Equipment Degradation. 319
G. J. Toman (FRC)

An Approach to Evaluate the Safety and Risk Implications of Aging. 331
W. E. Vesely (BCL)

PROCESS CONTROL
Chairman: F. P. Cardile (NRC)

	Page
Identification and Evaluation of Facilitation Techniques for Decommissioning Light Water Power Reactors. . . . . T. S. LaGuardia (TLG Engineering)	343
Impacts of Decontamination on Solidification and Waste Disposal . . . . P. L. Piciulo and J. W. Adams (BNL)	367
Evaluation of Nuclear Facility Decommissioning Projects Program - Status. . . . . R. L. Miller (UNC Nuclear Industries)	381
LWR Spent Fuel Rod Behavior During Long-Term Dry Fuel Storage Conditions. . . . . C. S. Olsen (EG&G)	385
Lessons Learned from a NUREG-0737 Review of High-Range Effluent Monitors and Samplers. . . . . A. P. Hull (BNL) and J. R. White (NRC)	409

Structural Load Combinations

H. Hwang and M. Reich
Brookhaven National Laboaratory

B. Ellingwood
National Bureau of Standards

M. Shinozuka
Columbia University

Abstract

This paper presents the latest results of the program entitled, "Probability Based Load Combinations For Design of Category I Structures". In FY 85, a probability-based reliability analysis method has been developed to evaluate safety of shear wall structures. The shear walls are analyzed using stick models with beam elements and may be subjected to dead load, live load and in-plane earthquake. Both shear and flexure limit states are defined analytically. The limit state probabilities can be evaluated on the basis of these limit states.

Utilizing the reliability analysis method mentioned above, load combinations for the design of shear wall structures have been established. The proposed design criteria are in the load and resistance factor design (LRFD) format. In this study, the resistance factors for shear and flexure and load factors for dead and live loads are preassigned, while the load factor for SSE is determined for a specified target limit state probability of 1.0×10^{-6} or 1.0×10^{-5} during a lifetime of 40 years.

1. INTRODUCTION

The program entitled, "Probability Based Load Combinations for Design of Category I Structures", is currently being worked on for the Office of Nuclear Regulatory Research, U.S. Nuclear Regulatory Commission. The objective of this program is to develop a probabilistic approach for evaluating safety of reactor containments and other seismic category I structures subjected to multiple static and dynamic loadings. Furthermore, based on this probabilistic approach, load combination criteria for the design of Category I structures will also be established.

This paper presents the latest results of the program. Specifically, the reliability analysis method for shear wall structures, and the probability-based load combinations for the design of shear walls recently have been de-

Work performed under the auspices of the U.S. Nuclear Regulatory Commission.

veloped. In the following sections, the shear wall structures and the limit states used in this study are described first. Then, the probabilistic models of loads and material strengths are presented. Next, the reliability analysis method for shear walls is discussed and an example is given to demonstrate the method. Finally, the probability-based design criteria are presented.

2. SHEAR WALL STRUCTURES AND LIMIT STATES

Shear walls are used in many Category I structures in nuclear power plants as the primary system for resisting lateral loads such as earthquakes. These shear walls usually have low height-to-length ratios and exist either as part of a rectangular box or as individual walls. In this study, a low-rise three-story rectangular shear wall, as shown in Fig. 1, is chosen as a representative shear wall structure. The shear wall is analyzed using a stick model with beam elements and it may be subjected to dead load, live load and in-plane horizontal earthquake during its lifetime.

The limit states of a low-rise shear wall include flexure, shear, sliding and buckling. A typical shear wall in a nuclear plant structure is massive and low. Thus, buckling failure would be very rare. Resistance to sliding is provided by aggregate interlock and dowel action of vertical reinforcement and boundary elements. For a low-rise massive shear wall with proper boundary elements, sliding failures would also be rare. In this study, therefore, sliding and buckling failures of shear walls are not considered. The shear and flexure limit states are defined below.

2.1 Flexure Limit State

The flexure limit state for shear walls is defined analytically according to ultimate strength analysis of reinforced concrete. It is described as follows: At any time during the service life of the structure, the state of structural response is considered to have reached the limit state if a maximum concrete compressive strain at the extreme fiber of the cross-section is equal to 0.003, while yielding of rebars is permitted. Based on the above definition of the limit state, a limit state surface can be constructed for a cross-section with given geometry and rebar arrangement in terms of the axial force and bending moment on a cross-section. A typical flexure limit state surface, which is approximated by a polygon, is shown in Fig. 2. In this figure, point "a" is determined from a stress state of uniform compression. Points "c" and "c'" are the so-called "balanced points", at which a concrete compression strain of 0.003 and a steel tensile strain of f_y/E_s are reached simultaneously. Points "e" and "e'" correspond to zero axial force. Lines abc and ab'c' in Fig. 2 represent compression failure and lines cde and c'd'e' represent tension failure.

The flexure limit state surface represents the flexural capacity of a shear wall. Since the flexural capacity is calculated using the ultimate strength analysis of reinforced concrete, the variability of the capacity is caused primarily by the variations of concrete compressive strength and rebar yield strength.

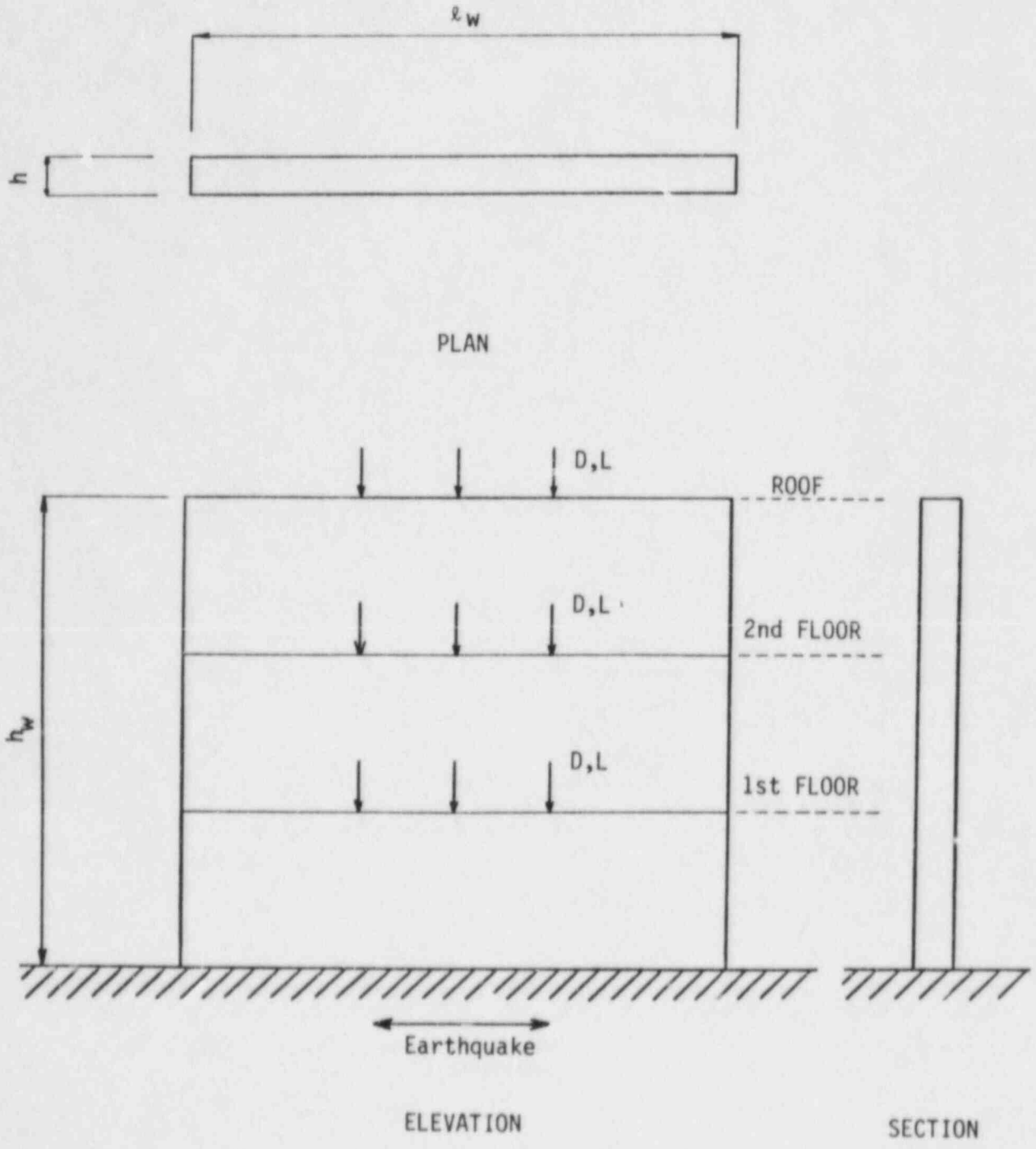

Fig. 1. Representative Shear Wall Structure.

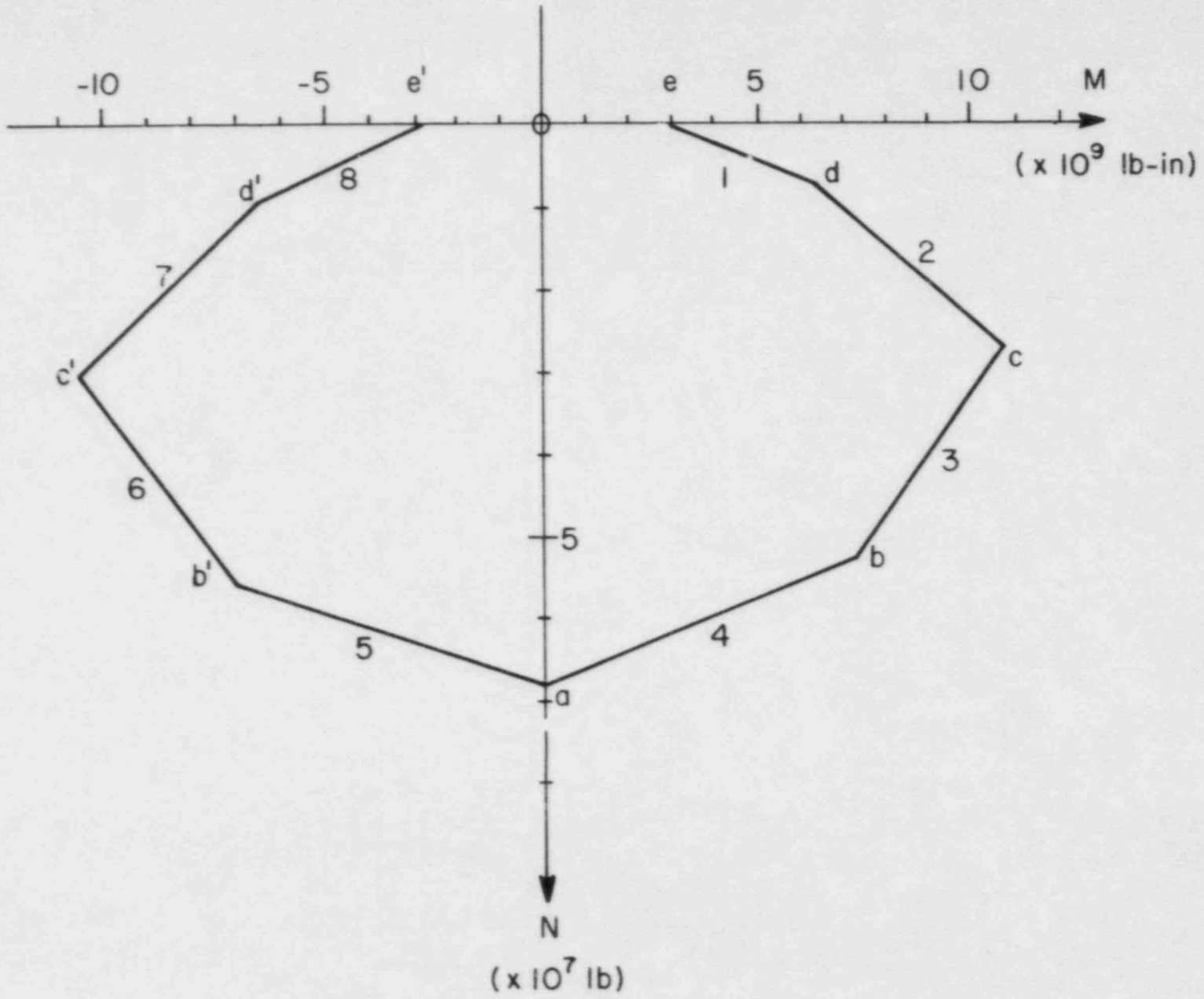

Fig. 2. Flexure Limit State Surface.

2.2 Shear Limit State

The shear limit state is reached when diagonal cracks form in two directions; following the formation of the diagonal cracks, either concrete crushes or rebars yield and fracture. The ultimate shear strength of a shear wall, v_u, expressed in units of force/area, is

$$v_u = v_c + v_s \tag{1}$$

in which v_c and v_s are the contributions of concrete and reinforcement to the unit ultimate shear strength.

Barda, et al.[2], conducted tests on eight specimens representing low-rise shear walls with boundary elements and suggested that for shear walls with height-to-length ratio h_w/ℓ_w between 1/4 and 1, v_c could be given by,

$$v_c = 8.3\sqrt{f'_c} - 3.4\sqrt{f'_c}\left(\frac{h_w}{\ell_w} - \frac{1}{2}\right) + \frac{N_u}{4\ell_w h} \quad ; \frac{1}{4} \leq \frac{h_w}{\ell_w} \leq 1.0 \tag{2}$$

in which N_u is axial force taken as positive in compression and h is the wall thickness. Barda, et al., also concluded that for shear walls with a height-to-length ratio of 1/2 and less, the horizontal wall reinforcement, which is effective for high-rise shear walls, did not contribute to shear strength. On the other hand, vertical wall reinforcement was effective as shear reinforcement in shear walls with height-to-length ratio of 1/2 and less. However, it was less effective as height-to-length ratio approached 1.

Since the effectiveness of the horizontal and vertical reinforcement varies for different height-to-length ratios, the following equation for v_s is recommended[22],

$$v_s = (a\,\rho_h + b\,\rho_n)f_y \tag{3}$$

where ρ_h and ρ_n are horizontal and vertical reinforcement ratio, respectively.The constants a and b are determined as follows:

$$b = \begin{cases} 1 & ; \quad \frac{h_w}{\ell_w} < 1/2 \\ 2\text{-}2\,\frac{h_w}{\ell_w} & ; \quad 1/2 \leq \frac{h_w}{\ell_w} \leq 1 \\ 0 & ; \quad \frac{h_w}{\ell_w} > 1 \end{cases} \tag{4}$$

and

$$a = 1 - b$$

Both horizontal and vertical rebars are partially effective outside the given limits, but Eq. 4 is not sensitive to these limits as long as horizontal and vertical rebars both are used.

Gergely[12] has suggested that a low-rise shear wall would fail by diagonal crushing of the concrete if the shear stress is larger than the following unit ultimate shear strength:

$$v_u = 0.25\, f'_c \tag{5}$$

However, Eq. 5 does not account for the effects of wall slenderness and reinforcement. In this study, the unit ultimate shear strength is taken as the smaller of those determined from Eqs. 1-4 or Eq. 5. The total ultimate shear strength V_u is computed as

$$V_u = v_u\, h\, d \tag{6}$$

where h is the wall thickness and d is the effective depth, which is taken to be 0.8 ℓ_w for rectangular walls. From Eq. 6, a shear limit state surface can be constructed for any shear wall cross-section. A typical shear limit state surface is shown in Fig. 3. In this figure, lines 9 and 12 are governed by Eqs. 1-4 and lines 10 and 11 are governed by Eq. 5.

From simulation results, Ellingwood[10] suggested that the actual shear resistance can be treated as

$$V_u = B\, \bar{V}_u \tag{7}$$

where $\bar{V}_u$ is the mean value determined from Eq. 6 using mean values of f'_c and f_y. B is a lognormal random variable with unit mean value and coefficient of variation of 0.19. In this study, the shear strength obtained from Eq. 7 is used for the reliability assessment of the shear wall.

3. PROBABILISTIC CHARACTERISTICS OF LOADS AND MATERIAL STRENGTHS

Since the loads involve random and other uncertainties, an appropriate probabilistic model for each load must be established in order to perform the reliability analysis.

3.1 Dead Load

Dead load is a static load and acts permanently on a structure. It is derived mainly from the weights of the structural system, the permanent equipment and attachments such as pipings, HVAC ducts and cable trays. Except for the attachments, the variations associated with the weights of structure or equipment are small.[11,13] Dead load is assumed to be normally distributed.[11] The mean value is equal to the design value and the coefficient of variation (CoV) is estimated to be 0.07.[11] Permanent equipment loads are treated separately in the proposed probability-based load combinations.[11,14]

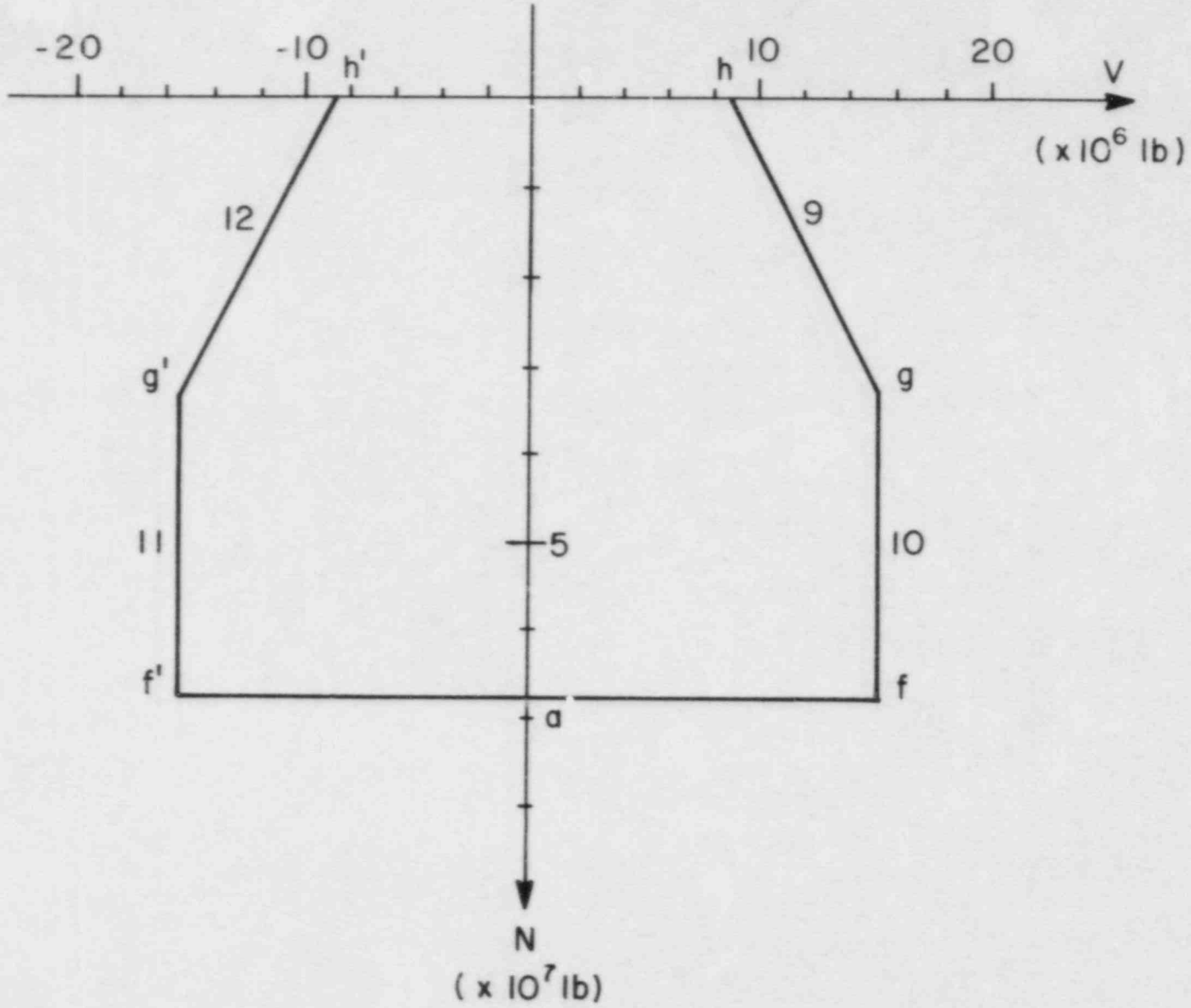

Fig. 3. Shear Limit State Surface.

3.2 Live Load

Live load in nuclear power plants denotes any temporary load resulting from human occupancy, movable equipment and other operational or maintenance conditions. Significant live load might arise from temporary equipment or materials during maintenance or repair within the plant. Thus, live load is modeled as a Poisson renewal rectangular pulse process which is defined by the occurrence rate, mean duration, and the probability distribution of the point-in-time intensity.

Measurements of live loads in nuclear power plants were unavailable. Statistical data on live loads were obtained from a limited number of responses to a questionnaire used as part of a consensus estimation survey of loads in nuclear power plants.[13] The live load data from the consensus estimation survey were analyzed in Appendix A of Ref. 11. Considering both PWR and BWR plants, the mean value of the maximum live load to occur in 40 years is 0.81 times the nominal value and its coefficient of variation is 0.37. With a mean duration of three months, several statistics for the point-in-time live load corresponding to different occurrence rates can be obtained.[11] In this study, the occurrence rate is taken to be 0.5 per year; thus, the mean value of the point-in-time live load intensity is 0.36 times the nominal design value and the coefficient of variation is 0.54. The point-in-time live load is assumed to have a gamma distribution.

3.3 Earthquake

The seismic hazard at the site of a nuclear power plant is described by a seismic hazard curve. A seismic hazard curve, is a plot of annual exceedance probability $G_A(a)$ vs. the peak ground acceleration. In this study, the probability distribution $F_A(a)$ of the annual peak ground acceleration A is assumed to be the Type II extreme value distribution[9],

$$1 - G_A(a) = F_A(a) = \exp\left[-(a/\mu)^{-\alpha}\right] \qquad (8)$$

where α and μ are two parameters to be determined. The value of α for the U.S. is estimated to be 2.7.[14] The parameter μ is computed based on this α-value and the assumption that the annual probability of exceeding the safe shutdown earthquake at the site is 4×10^{-4} per year.[19] The hazard curve used in this study compares well with six out of the eight curves with 50 percent confidence for eight specific plant sites in the Eastern United States.[3,14]

In addition to the mean duration of an earthquake, the lower and upper bounds of peak ground acceleration are required in the analysis. The lower bound, a_0, indicates the minimum peak ground acceleration for the ground shaking to be considered as an earthquake. a_0 is assumed to be 0.05 g. The upper bound, a_{max}, represents the largest earthquake possible at a site. However, the state-of-the-art in seismology can not precisely determine the value of a_{max}. The effects of different values of a_{max} on the load factors are reported in Ref. 14. In this study, a_{max} is chosen to be $2a_{SSE}$.

The ground acceleration, on the condition that an earthquake occurs, is idealized as a segment of a zero-mean stationary Gaussian process, described in the frequency domain by a Kanai-Tajimi power spectral density[19],

$$S_{gg}(\omega) = S_o \frac{1 + 4\zeta_g^2(\omega/\omega_g)^2}{[1 - (\omega/\omega_g)^2]^2 + 4\zeta_g^2(\omega/\omega_g)^2} \qquad (9)$$

where the parameter S_o is a random variable which represents the intensity of an earthquake. The distribution of S_o can be determined as shown in Ref. 20. Parameters ω_g and ζ_g are the dominant ground frequency and the critical damping, respectively, which depend on the site soil conditions. For rock and deep cohesionless soil conditions, ω_g is taken to be 8π rad/sec and 5π rad/sec, respectively. ζ_g is taken to be 0.6 for both soil conditions.[9]

3.4 Material Properties

In order to perform a reliability analysis of a shear wall structure, it is necessary to determine the actual material properties. In this study, the material strengths are random, while other properties are assumed to be deterministic.

A. Concrete

The density of concrete is taken to be 150 lb/ft^3. Young's modulus is computed according to ACI code[5] and Poisson's ratio for concrete is 0.2. The concrete compressive strength, f'_c, is assumed to be normally distributed with CoV of 0.14 and a mean value at 1 year, $\bar{f}'_c$[10],

$$\bar{f}'_c = 1219 + 1.02\, f'_{cn} \quad \text{(psi)} \qquad (10)$$

in which f'_{cn} = specified compressive strength of concrete at 28 days. For example, if f'_{cn} is specified as 4000 psi, the mean value of concrete compressive strength is 5299 psi.

B. Reinforcing Bars

The yield strength f_y of ASTM A 615 Grade 60 deformed bars is assumed to have a lognormal distribution with a mean value of 71.0 ksi and CoV of 0.11.[10,17] Young's modulus and Poisson's ratio are taken to be 29.0×10^6 psi and 0.3, respectively.

4. RELIABILITY ANALYSIS METHODOLOGY

The reliability analysis methodology for shear walls is presented in Ref. 21. It follows the same approach as described in Ref. 20. The limit state probability, $P_{f,s}$ is defined as the probability that the structural response will reach the limit state "s" during the lifetime. In this study,

the shear wall is considered to be subjected to three loads, i.e., dead load (D), live load (L) and earthquake (E). Thus, the wall is subjected to at least one of the following mutually exclusive load combinations in its lifetime: D, D+L, D+E and D+L+E. With the assumption that the limit state probability under D and D+L is zero, the limit state probability $P_{f,s}$ can be expressed as

$$P_{f,s} = P_{f,s}^{(D+E)} + P_{f,s}^{(D+L+E)} \tag{11}$$

The limit state probability for a load combination q, i.e., $P_{f,s}^{(q)}$, can be computed approximately by

$$P_{f,s}^{(q)} = T\ \lambda(q)\ P_{c,s}^{(q)} \tag{12}$$

in which T is the lifetime of the structure, taken as 40 years. $\lambda(q)$ is the occurrence rate of the load combination (q) and is determined by formulas in Ref. 20. The conditional limit state probability given the occurrence of the load combination (q), i.e., $P_{c,s}^{(q)}$, is the probability that the combined load effects exceed the structural resistance. The technique to compute $P_{c,s}^{(q)}$ is shown in Ref. 21.

The fragility, P_s, is defined as the conditional limit state probability with respect to a limit state "s", given a peak ground acceleration. The evaluation of the fragility is also shown in Ref. 21.

4.1 Illustrative Application

A rectangular shear wall, as shown in Fig. 1, is subjected to dead load and earthquake during its lifetime. The height of the shear wall is 75 feet, the width is 125 feet and the thickness is 15 inches. Three floors are supported on the wall at 25, 50 and 75 feet above the ground. It is assumed that the superimposed dead load on each floor is 16 Kip/ft and the safe shutdown earthquake (SSE) for design of the wall is taken to be 0.32 g. The specified concrete compressive strength is 5000 psi and yield strength of the reinforcing bar is 60,000 psi. The wall is designed according to the proposed Load combination criteria as shown in Section 5.5. The required horizontal and vertical reinforcement ratios are determined to be 0.00236 and 0.00523, respectively.

The probabilistic characteristics of loads and material strengths described in Section 3 are summarized in Tables 1 and 2, respectively. The limit states for flexure and shear as defined in Section 2 are reached at the base of the shear wall. In this study, the variations of structural resistance and dead load are included in the analysis using a Latin hypercube sampling technique.[14] The sample size is chosen to be ten; thus, ten values of f'_c, f_y, D and B, are chosen according to their distributions, and each value has equal probability. Table 3 gives the ten sets of the Latin hypercube samples and the corresponding conditional limit state probabilities for flexure and shear limit states i.e., $P_{c,m}^{(D+E)}$ and $P_{c,v}^{(D+E)}$. The average values of these ten conditional limit state probabilities are 2.52×10^{-11} and 4.10×10^{-10}. For a lifetime of 40 years, the flexure and shear limit state probabilities are 6.06×10^{-11} and 9.86×10^{-10}, respectively.

For the shear limit state, the fragility of the shear wall, which is defined as the conditional limit state probability given a peak ground acceleration, is also evaluated. The fragility data are tabulated in Table 4 and plotted in Fig. 4.

Table 1. Probabilistic Models for Loads.

Load	Model
Dead Load (D)	Time Invariant Normal Distribution With $\bar{D} = 1.0\ D_n$ and CoV(D) = 0.07, D_n = 16 Kip/ft per each floor
Earthquake (E)	Seismic Hazard Follows a Type II Distribution $1 - G_A(a) = \exp[-(a/\mu)^{-\alpha}]$; $\alpha = 2.7$, $\mu = 0.01765$ $S_{gg}(\omega) = S_o \dfrac{1 + 4\zeta_g^2(\omega/\omega_g)^2}{[1 - (\omega/\omega_g)^2]^2 + 4\zeta_g^2(\omega/\omega_g)^2}$ where $\omega_g = 5\pi$ rad/sec, $\zeta_g = 0.6$ $a_o = 0.05g$, $a_{max} = 0.64g$ Occurrence rate, $\lambda_E = 0.0601$ per year Mean duration, $\mu_{dE} = 20$ seconds

Table 2. Probabilistic Model for Material Strength.

Material Strength	Model
f_c'	Normal Distribution $\bar{f}_c' = 1.219 + 1.02\ f_{cn}'$ $f_{cn}' = 5000$ psi, $\bar{f}_c' = 6319$ psi CoV(f_c') = 0.14
f_y	Lognormal Distribution $\bar{f}_y = 71000$ psi ($f_{yn} = 60{,}000$ psi) CoV(f_y) = 0.11

Table 3. Conditional Limit State Probabilities With Latin Hypercube Samples.

Samples	f_c'(psi)	f_y(psi)	D(lb)	B	$P_{c,m}^{(D+E)}$	$P_{c,v}^{(D+E)}$
1	6.659 +3	7.362 +4	8.122 +6	0.808	6.016 -13	5.459 -11
2	5.978 +3	6.765 +4	7.547 +6	0.865	3.119 -11	3.602 -12
3	4.863 +3	8.452 +4	8.319 +6	1.339	7.196 -14	0
4	7.235 +3	6.297 +4	7.824 +6	0.913	3.086 -11	2.153 -13
5	6.207 +3	7.906 +4	7.965 +6	0.720	2.171 -13	4.041 -9
6	7.774 +3	7.599 +4	6.863 +6	1.115	3.670 -12	1.414 -18
7	6.915 +3	6.960 +4	7.193 +6	1.194	2.118 -11	0
8	5.722 +3	6.554 +4	7.390 +6	0.959	1.063 -10	1.961 -14
9	5.402 +3	5.892 +4	8.649 +6	1.005	5.379 -11	5.217 -16
10	6.430 +3	7.155 +4	7.688 +6	1.056	4.458 -12	4.082 -17
Average					2.52 -11	4.10 -10

NOTE: $6.659 + 3 = 6.659 \times 10^3$.

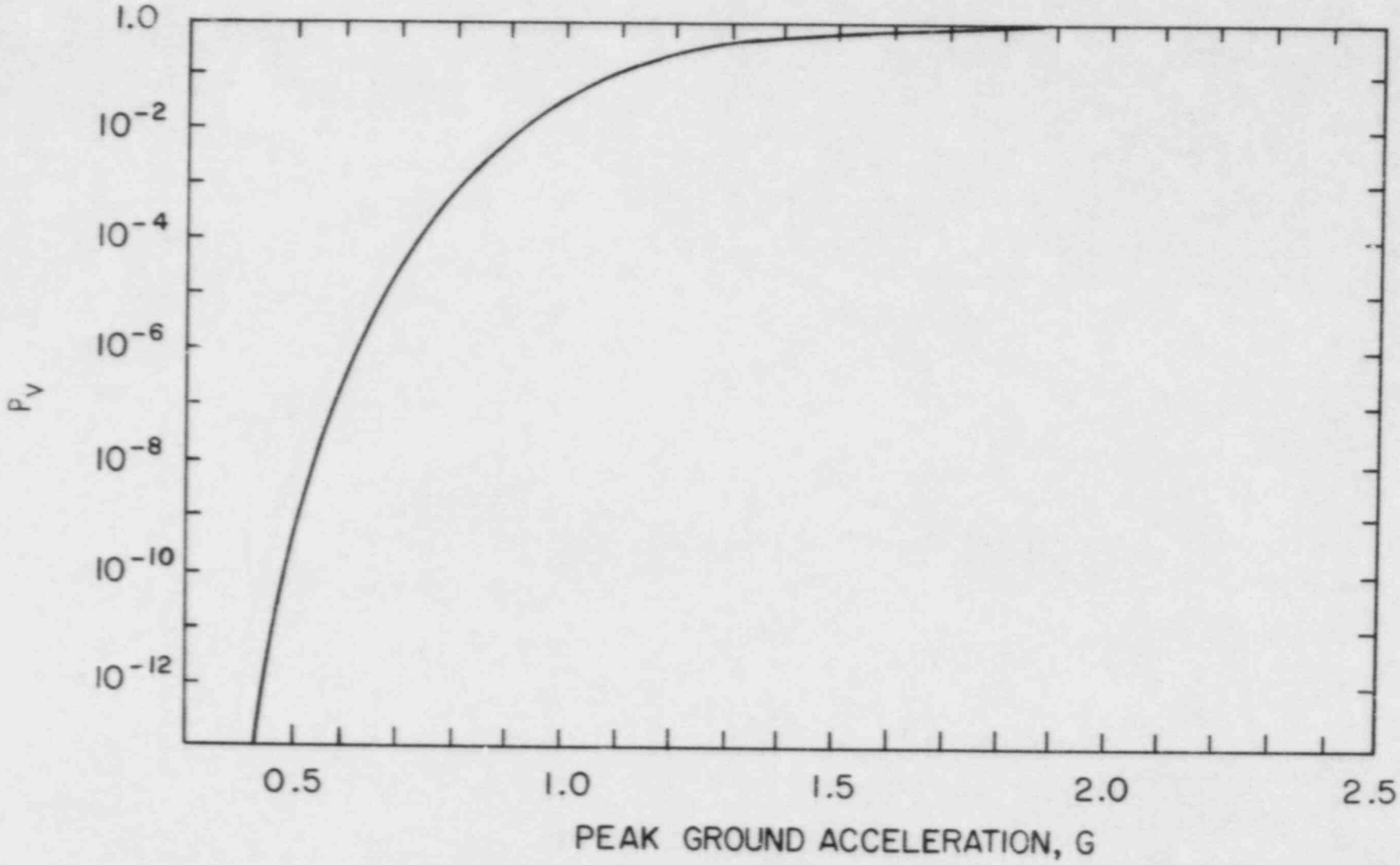

Fig. 4. Fragility Curve (Shear).

Table 4. Fragility Data (Shear).

PGA(g)	P_V
0.45	5.713 -13
0.50	2.234 -10
0.55	1.853 -08
0.60	5.359 -07
0.65	7.392 -06
0.70	5.975 -05
0.75	3.251 -04
0.80	1.310 -03
0.85	4.169 -03
0.90	1.095 -02
0.95	2.441 -02
1.00	4.714 -02
1.05	8.022 -02
1.10	0.123
1.15	0.173
1.20	0.229
1.25	0.291
1.30	0.357
1.40	0.493
1.50	0.622
1.60	0.733
1.80	0.884
2.00	0.959
2.20	0.992
2.40	0.999
2.60	1.000

5. LOAD COMBINATION CRITERIA FOR DESIGN OF SHEAR WALL STRUCTURES

A procedure for developing probability-based load combinations for the design of category I structures has been established.[11,14] Using this procedure, load factors for design of shear walls were determined.[15] The procedure is summarized as follows:

1. Select an appropriate load combination format.
2. Establish representative structures.
3. Define limit states and select a target limit state probability.
4. Assign initial values for all parameters (e.g., load and resistance factors) associated with the selected load combination format.
5. Design each representative structure.
6. Determine the limit state probability of each representative structure.
7. Compute the objective function measuring the difference between the target limit state probability and the computed limit state probability.
8. Determine a new set of parameters along the direction of maximum descent with respect to the objective function.
9. Repeat steps 5 to 8 until a set of parameters that minimizes the objective function is found.

5.1 Load Combination Format

The load and resistance factor design (LRFD) format[18] has been selected for this study. This format has been adopted in several specifications[1,4,5] and the Standard Review Plan, Section 3.8.4.[23] The LRFD format is simple enough to be used in routine design while offering sufficient flexibility to achieve consistent reliabilities in various design situations. If three loads, i.e., dead load, live load and earthquake are considered to act on the shear walls during a reference period, the load combinations in the LRFD format are:

$$1.2\ D + 1.0\ L + \gamma_{ES} E_{SS} \leq \phi_i R_i \qquad (13)$$

$$0.9\ D - \gamma_{ES} E_{SS} \leq \phi_i R_i \qquad (14)$$

where

D = load effect due to design dead load
L = load effect due to design live load
E_{SS} = load effect due to safe shutdown earthquake (SSE)
γ_{ES} = load factor for safe shutdown earthquake
ϕ_i = resistance factor for the i-th limit state under consideration
R_i = nominal structural resistance for the i-th limit state under consideration

It is assumed that design loads and nominal structural resistance are defined as in current standards. The load and resistance factors are determined so as to achieve the desired reliability. However, in this study the dead load factor, live load factor and resistance factors are preset to simplify the optimization. The mean value of the dead load is approximately equal to its nominal value and its variability is quite small. A dead load factor of 1.2 (or 0.9 when the dead load has a stablizing effect) has been found to be more than adequate to account for uncertainty in dead load.[1,8] Furthermore, experience with the treatment of live load as a companion load in conventional structures has shown that it is reasonable to preassign the live load factor of 1.0 (or zero if live load has a stabilizing effect).[8,11] The dead and live load factors in Eqs. 13 and 14 are the same as those appearing in the A58 load requirements.[1] With a few trials, it was found that if the resistance factor for shear, ϕ_v, is set to be 0.85 and the resistance factor for compression or compression with flexure, ϕ_m, is set to be 0.65, they will produce approximately the same optimum values of the load factor γ_{ES}. Hence, in this study, these resistance factors, which are similar to those specified in ACI Standard 349, are adopted.

5.2 Representative Shear Wall Structures

An important requirement for codified structural design is that all the structures designed according to a code should meet the code performance objectives which are expressed in probabilistic terms. In order to test if this requirement is satisfied, four representative (sample) structures are selected for evaluating the design criteria. In this study, representative shear wall

structures are determined from examining existing shear walls in U.S. nuclear power plants. A low-rise three-story rectangular shear wall, as shown in Fig. 1, is chosen as a representative shear wall structure. The shear wall may be subjected to dead load, live load and in-plane earthquake forces. The ranges of the design parameters such as height-to-length ratio, material strengths, and design loads are determined and one, two or four representative values are selected to represent the range of each design parameter. Then the Latin hypercube sampling technique is used to identify sample shear walls using these representative design values. Four sample shear walls thus identified are shown in Table 5. With the design parameters in Table 5 specified, the remaining design parameters, which still need to be determined, are the wall thickness and the reinforcement.

Table 5. Representative Shear Wall Structures.

Design Parameters	Sample 1	Sample 2	Sample 3	Sample 4
Height (ft)	75	75	75	75
Width (ft)	75	125	100	150
Concrete Compressive Strength (psi)	4000	5000	5000	4000
Rebar Yield Strength (psi)	60,000	60,000	60,000	60,000
Superimposed Dead Load (Kip/ft)	16	16	16	16
Live Load (Kip/ft)	12	8	12	8
SSE (g)	0.17	0.32	0.25	0.50
Soil	Rock	Deep Cohesionless	Deep Cohesionless	Rock
Earthquake Duration (sec)	10	20	10	20

5.3 Design of Shear Walls

Each representative shear wall shown in Table 5 has to be designed according to the proposed load combinations with trial load and resistance fac-

tors, specified design loads, and nominal resistance. The shear strength determmned from Eq. 6 is proportional to the wall thickness. It is known that the shear limit state probability of a shear wall with larger wall thickness is less than that of a shear wall with smaller thickness, even through both shear walls are designed according to the same criteria. Thus, for the design of shear wall structures, the wall thickness cannot be assigned arbitrarily. Utilizing the nominal shear strength expression for shear walls in the ACI code and a horizontal wall reinforcement ratio of 0.0025, the following expression is used in this study to determine the appropriate wall thickness.

$$h \geq \frac{\frac{V_u}{\phi_v d} - \frac{N_u}{4\ell_w}}{3.3\sqrt{f'_{cn}} + 0.0025 f_{yn}} \qquad (15)$$

where

h = thickness of a shear wall
V_u = factored shear force at a cross-section
N_u = factored axial force at a cross-section
ϕ_v = resistance factor for shear
ℓ_w = total length of a shear wall
d = effective length of a shear wall, $d = 0.8\ \ell_w$ for rectangular wall
f'_{cn} = nominal concrete compressive strength
f_{yn} = nominal yield strength of reinforcement

Once the wall thickness is determined, the remaining design parameter, which needs to be determined, is the required wall reinforcement. For the structural analysis of the shear wall, a beam element model is used. In this study, 3 beam elements are used to model each story; thus, a shear wall is represented by a beam model with 10 nodes. The mass used in the model is calculated from the mean values of dead and live loads, as specified in Section 3. The axial force, which results from dead load with or without live load, is obtained from static analysis. The shear and moment due to earthquake are obtained from response spectrum analysis. The horizontal response spectrum used in this study is the design spectrum specified in the Regulatory Guide (R.G.) 1.60.[6] The damping ratio is taken to be 7 percent of critical for the SSE, as specified in the R.G. 1.61.[7] The axial force, shear and moment thus obtained are combined using the proposed load combinations, i.e., Eqs. 13 and 14, with the trial load factors.

The nominal resistance of the shear wall is computed using the formula specified in the current ACI code. The minimum wall reinforcement can be determined such that the factored nominal resistance will be larger than the factored load effect. In practice, the designers usually provide reinforcement larger than the minimum requirement. In this study, however, the minimum rebar area will be used in design and reliability assessments. The representative shear walls designed by the procedure described above are shown in Table 6.

Table 6. Required Wall Thickness and Reinforcement Ratios ($D+L+E_{SS}$).

Sample	γ_{ES}	h (in)	ρ_m	ρ_h	ρ_n
1	1.1	8	0.00623	0.00148	0.00148
	1.2	8	0.00793	0.00213	0.00213
	1.3	8	0.00957	0.00278	0.00271
	1.4	9	0.00947	0.00266	0.00262
	1.5	10	0.00926	0.00257	0.00256
2	1.1	13	0.00265	0.00256	0.00256
	1.2	15	0.00284	0.00235	0.00235
	1.3	16	0.00315	0.00257	0.00256
	1.4	18	0.00331	0.00241	0.00241
	1.5	20	0.00334	0.00230	0.00230
3	1.1	10	0.00480	0.00278	0.00275
	1.2	12	0.00459	0.00232	0.00232
	1.3	13	0.00508	0.00245	0.00245
	1.4	14	0.00534	0.00256	0.00256
	1.5	15	0.00564	0.00267	0.00265
4	1.1	25	0.00230	0.00256	0.00256
	1.2	28	0.00255	0.00260	0.00260
	1.3	32	0.00270	0.00250	0.00250
	1.4	36	0.00277	0.00245	0.00245
	1.5	40	0.00284	0.00243	0.00243

NOTE: 1. ρ_m is vertical reinforcement ratio required by flexure.

2. ρ_h and ρ_n are horizontal and vertical reinforcement ratios, respectively required by shear.

5.4 Determination of Load Factors

The load and resistance factors are determined to be consistent with a specified target limit state probability for each limit state. The selection of a target limit state probability should consider many factors, e.g., the characteristics of the limit states, the consequence of failure, and the risk evaluation and damage cost. Hence, the target reliability may not necessarily be the same for different limit states. It is anticipated that the target limit state probability will be set by the regulatory authority and/or the code committee.

Once a target limit state probability $P_{f,T}$ is specified, the load and resistance factors are determined such that the limit state probabilities of the sample shear walls are sufficiently close to the target limit state probability. The closeness is measured by an objective function defined as follows:

$$\Omega(\gamma,\phi) = \sum_{i=1}^{N} w_i \, (\log P_{f,i} - \log P_{f,T})^2 \qquad (16)$$

where N is the total number of representative shear wall structures, $P_{f,i}$ is the limit state probability computed for the i-th sample structure, w_i represents a weight factor for the i-th sample structure. In the Latin hypercube sampling technique, it is assumed that each sample in Table 5 is equally representative, and thus, $w_i = 1.0$. The optimum values of the load and resistance factors are then derived by minimizing the objective function Ω.

The limit state probabilities of the shear walls shown in Table 6 under the three loads in 40 years, are shown in Table 7. It is to be noticed that the limit state probability for shear is calculated on the basis of the required shear reinforcement without including the reinforcement required for flexure. Similarly, the limit state probability for flexure is computed without considering the shear reinforcement. Using these limit state probabilities, the objective function Ω can be computed for several values of γ_{ES} and $P_{f,T}$. Figure 5 shows parabolic curves plotted through these values of the objective function. For $P_{f,T} = 1.0 \times 10^{-6}$ per 40 years, the optimum values of γ_{ES} are 1.366 and 1.411 for shear and flexure limit states, respectively. For $P_{f,T} = 1.0 \times 10^{-5}$ per 40 years, the optimum values of γ_{ES} are 1.214 and 1.267 for shear and flexure limit states, respectively. Hence, γ_{ES} is recommended as 1.4 or 1.2 corresponding to the specific target limit state probability mentioned above.

Table 7. Limit State Probabilities ($D+L+E_{SS}$).

Sample	Limit State	$\gamma_{ES}=1.1$	$\gamma_{ES}=1.2$	$\gamma_{ES}=1.3$	$\gamma_{ES}=1.4$	$\gamma_{ES}=1.5$
1	Flexure	3.349 -4	1.240 -4	4.670 -5	1.315 -5	3.930 -6
	Shear	3.312 -4	1.829 -4	9.847 -5	4.249 -5	1.681 -5
2	Flexure	5.452 -5	9.453 -6	2.041 -6	2.586 -7	4.507 -8
	Shear	2.002 -5	3.087 -6	7.162 -7	9.165 -8	1.076 -8
3	Flexure	3.483 -5	6.607 -6	9.835 -7	1.862 -7	2.779 -8
	Shear	4.302 -5	6.414 -6	1.507 -6	3.327 -7	6.842 -8
4	Flexure	7.968 -4	2.195 -4	4.635 -5	1.105 -5	2.511 -6
	Shear	1.021 -4	2.736 -5	5.466 -6	1.028 -6	1.870 -7

5.5 Proposed Load Combination Design Criteria

If the target limit state probability is selected as 1.0×10^{-6} per 40 years (equivalent to 2.5×10^{-8} per year), the proposed load combinations for design of the shear walls subjected to dead load, live load and earthquake during the service life are as follows:

$$\left.\begin{array}{l} 1.2D + 1.0L + 1.4\,E_{SS} \\ 0.9D \qquad\quad - 1.4\,E_{SS} \end{array}\right\} \leq \phi_i R_i \qquad (17)$$

The resistance factor for shear, ϕ_v, is 0.85 and the resistance factor for compression or compression with flexure, ϕ_m, is 0.65. The determination of the nominal design values for loads and nominal resistance follows current practice.

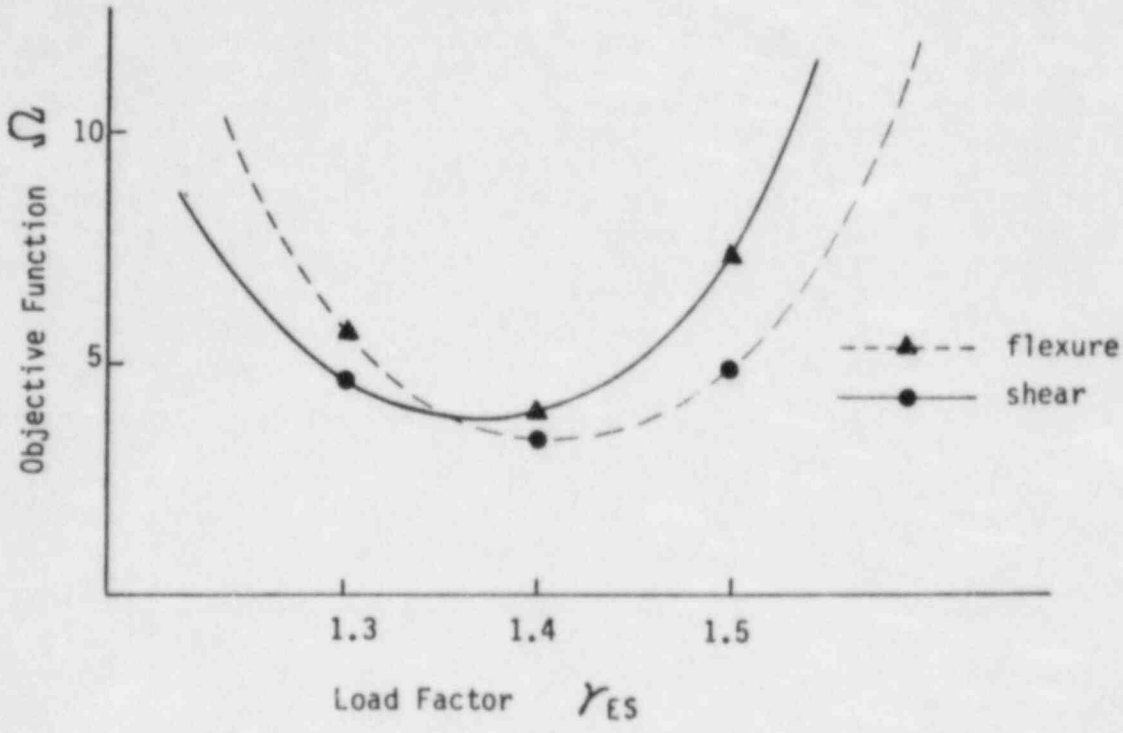

Case A ($P_{f,T} = 1.0 \times 10^{-6}$)

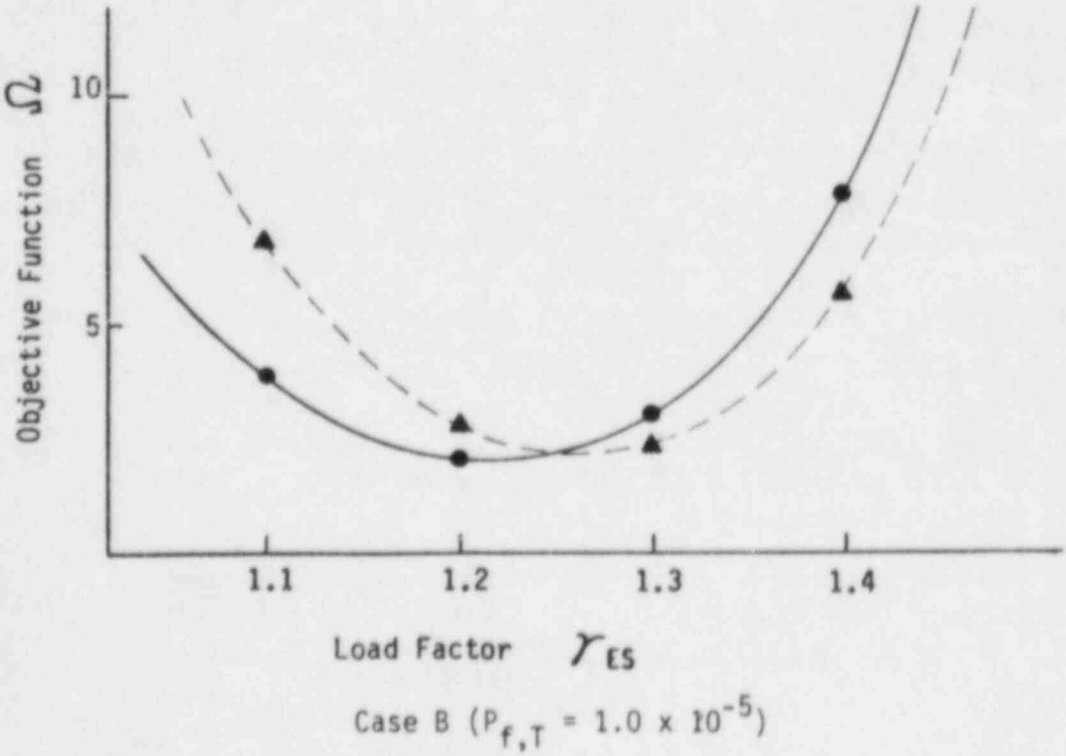

Case B ($P_{f,T} = 1.0 \times 10^{-5}$)

Fig. 5. Objective Function vs. Load Factor ($D+L+E_{SS}$).

The proposed load combinations are similar to those specified in ANSI Standard A58.1-1982.[1] The proposed load factor for earthquake in this study is 1.4 instead of 1.5 in the A58 standard. However, the definition of earthquake is quite different from the design earthquake in the A58 Standard. In general, the safe shutdown earthquake specified for nuclear structures is much stronger than that specified for conventional structures. Another difference appears in the resistance factor for shear. In this study, the resistance factor for shear is recommended to be 0.85, while 0.70 was recommended for use with the A58 load criteria.[16] In this connection, however, it should be noted that the mean shear capacity of low-rise walls, as described by Eqs. 1-4, is much higher with respect to the nominal shear capacity specified by ACI[4,5] than is the mean shear capacity of slender walls and beams.[8,10]

Reference 15 compared two shear wall structures designed using the proposed design criteria and the current ACI-349 code. The results with respect to shear limit state are shown in Tables 8 and 9. This comparison revealed that the proposed design criteria, based on the target limit state probability of 1.0×10^{-6} per 40 years, are more stringent than those specified in ACI-349.

Table 8. Shear Walls Designed With ACI and Proposed Criteria.

Sample	Design Criteria	Thickness (in)	ρ_n	ρ_h
2	ACI	9	0.00263	0.00264
	Proposed	15	0.00236	0.00236
4	ACI	18	0.00271	0.00271
	Proposed	30	0.00245	0.00245

Table 9. Reliability Assessments of Shear Walls.

Design Criteria	Limit State	Sample 2	Sample 4
ACI	Shear	1.644 -4	3.614 -4
Proposed	Shear	1.453 -7	1.385 -6

6. CONCLUDING REMARKS

A reliability analysis method for shear walls has been developed. In this method, the shear wall is modelled by beam elements. The limit state for flexure is defined according to ultimate strength analysis for combined axial forces and bending moments. The shear limit state is established from test results. At present, three loads, i.e., dead load, live load and in-plane earthquake, are considered in the reliability analysis. The randomness and other uncertainties of the structural resistance are included in the reliability analysis using a Latin hypercube sampling technique. Based on the above information, the limit state probabilities of a shear wall can be computed for flexure and shear limit states. This reliability analysis method can be used to evaluate the reliability level of existing shear walls and to derive fragility curves of shear walls for PRA studies.

Utilizing the reliability analysis method described above, load combination criteria for the design of shear wall structures have also been established. The proposed design criteria are in the load and resistance factor design (LRFD) format. The load factor for SSE is determined for a target limit state probabilities of 1.0×10^{-6} or 1.0×10^{-5} during a lifetime of 40 years. The proposed load combinations according to $P_{f,T} = 1.0 \times 10^{-6}$ per 40 years are summarized in Section 5.5. It is clear that the use of such criteria would entail no major change in the way that routine structural design calculations are performed. However, in contrast to existing design procedures, the proposed criteria are risk-consistent and have a well-established rationale.

On the basis of the data used in this study, shear walls designed by current ACI-349 for earthquake loading , but without tornado loads, may not be adequate for the reliability level specified. This may be because the target limit state probability is too small or because of other assumptions made in our analysis. However, it may be due to the fact that the code committee does not consider the whole range of seismic hazard. If the a_{max} is larger than two times the SSE value, the difference will be even greater. We believe that this problem should be given proper attention. However, this does not necessarily imply that the current shear walls used in the nuclear plants are unsafe. Since shear walls are designed to resist tornado-borne missiles, they are more massive than would be required to resist only earthquake loadings.

REFERENCES

1. American National Standard A58, "Minimum Design Loads for Building and Other Structures, (ANSI A58.1-1982)", American National Standards Institute, New York, 1982.

2. Barda, F., Hanson, J.M., and Corley, W.G., "Shear Strength of Low-Rise Walls With Boundary Element", Reinforced Concrete Structures in Seismic Zones, ACI SP-53, American Concrete Institute, Detroit, MI, 1977.

3. Bernreuter, D.L., Savy, J.F., Mensing, R.W. and Cheng,D.H., "Seismic Hazard Characterization of the Eastern United States: Methodology and Interim Results for Ten Sites", UCRL-53527, NUREG/CR-3756, April, 1984.

4. "Building Code Requirements for Reinforced Concrete (ACI 318-83)", American Concrete Institute, Detroit, Michigan, 1983.

5. "Code Requirements for Nuclear Safety Related Concrete Structures (ACI 349-76)", American Concrete Institute, Detroit, MI, 1976.

6. "Design Response Spectra for Nuclear Power Plants", Regulatory Guide 1.60, U.S. Atomic Energy Commission, Washington, D.C., 1973.

7. "Damping Values for Seismic Design of Nuclear Power Plants", Regulatory Guide 1.61, U.S. Atomic Energy Commission, Washington, D.C., 1973.

8. Ellingwood, B., et al., "Development of a Probability-Based Load Criterion for American National Standard A58", National Bureau of Standards Special Publication No. 577, Washington, D.C., June 1980.

9. Ellingwood, B. and Batts, M., "Characterization of Earthquake Forces for Probability Based Design of Nuclear Structures", NUREG/CR-2945, September 1982.

10. Ellingwood, B., "Probabilistic Descriptions of Resistance of Safety-Related Nuclear Structures", NUREG/CR-3341, May 1983.

11. Ellingwood, B., Probability Based Safety Checking of Nuclear Plant Structures", NUREG/CR-3628, BNL-NUREG-51737, Dec. 1983.

12. Gergely, P., "Seismic Fragility of Reinforced Concrete Structures and Components for Application to Nuclear Facilities", NUREG/CR-4123, December, 1984.

13. Hwang, H., Wang, P.C.,Shooman,M. and Reich, M., "A Consensus Estimation Study of Nuclear Power Plant Structural Loads", BNL-NUREG-51678, NUREG/CR-3315, May 1983.

14. Hwang, H., et al., "Probability Based Load Combination Criteria for Design of Concrete Containment Structures", BNL-NUREG-51795, NUREG/CR-3876, March 1985.

15. Hwang, H., et al., "Probability Based Load Combination Criteria for Design of Shear Wall Structures" (Draft), BNL-NUREG-51905, NUREG/CR-4238, June 1985.

16. MacGregor, J., "Load and Resistance Factors for Concrete Design", ACI Journal July-August, 1983, pp.279-287,

17. Mirza, S.A. and MacGregor, J.G., "Variability of Mechanical Properties of Reinforcing Bars", Journal of the Structural Division, ASCE, Vol. 105, No. ST5, May 1979, pp.921-937.

18. Ravindra, M.K. and Galambos, T.V., "Load and Resistance Factor Design for Steel", Journal of the Structural Division, ASCE, Vol. 104, No. ST9, September 1978, pp.1337-1353.

19. Reiter, L., "Uses of Probabilistic Estimates of Seismic Hazard and Nuclear Power Plants in the U.S.", Second CSNI Specialist Meeting on Probabilistic Methods in Seismic Risk Assessment for Nuclear Power Plants, Livermore, CA, May 16-19, 1983.

20. Shinozuka, M., Hwang, H., and Reich, M., "Reliability Assessment of Reinforced Concrete Containment Structures", Nuclear Engineering and Design, Vol. 80, pp. 247-267, 1984.

21. Wang, P.C. et al., "Reliability Analysis of Shear Wall Structures" (Draft), BNL-NUREG-51900, NUREG/CR-4293, May 1985.

22. Wesley, D.A. and Hashimoto, P.S., "Seismic Structural Fragility Investigation for the Zion Nuclear Power Plant", NUREG/CR-2320, October 1981.

23. USNRC, Standard Review Plan, Section 3.8.4, NUREG-0800, Rev. 1, 1981.

STANDARD PROBLEMS FOR STRUCTURAL COMPUTER CODES

A.J. Philippacopoulos, C.A. Miller and C.J. Costantino

Brookhaven National Laboratory
Upton, New York 11973

ABSTRACT

Various numerical approaches with different degrees of approximations have been developed and utilized for the evaluation of the structural response of nuclear containments and other Class I nuclear structures. These approaches however, inherently rely on various degrees of approximations in order to simplify the mathematical equations associated with the analysis methods. Thus, they may not necessarily represent the actual response behavior of the structure in question. This is especially true for operating or accident conditions that involve seismic and dynamic loads. Under this program BNL is investigating the ranges of validity of the analytical methods used to predict the behavior of nuclear safety related structures under accidental and extreme environmental loadings.

During FY 85, the investigations were concentrated on special problems that can significantly influence the outcome of the soil structure interaction evaluation process. Specially, limitations and applicability of the standard interaction methods when dealing with lift-off, layering and water table effects, were investigated. This paper describes the work and the results obtained during FY 85 from the studies on lift-off, layering and water-table effects in soil-structure interaction.

1. INTRODUCTION

This paper describes work performed at Brookhaven National Laboratory (BNL) on the program "Standard Problems for Structural Computer Codes" (FIN No. A-3242) during FY 85. The work reported here is concerned with three tasks related to the soil-structure interaction area. There tasks are: a) lift-off effects, b) layering effects and c) water table effects. The overall objective of these tasks is to evaluate these effects for nuclear plant structures and utilize experimental data, when available, to quantify the uncertainties which exist in the mathematical models.

In the lift-off area, the capability of the SIM code which was developed at BNL was extended in order to treat the lift-off process. Mathematical laws pertaining to the structure-foundation interface were developed to account for local nonlinearities associated with the lift-off phenomenon. The SIMQUAKE experiment was utilized to compare analytical predictions with the SIM code versus recorded data. Furthermore, the

Work performed under the auspices of the U.S. Nuclear Regulatory Commission.

conditions under which lift-off can occur in nuclear plant structures were investigated.

The influence of the foundation layering on the response of structure-foundation system was studied. Several foundation configurations were used with different geometrical and wave propagation characteristics in order to quantify the effect on the system transfer functions. Based on the numerical data generated for the system transfer functions, a method was developed which gives an approximation to the layering problem. The procedure was applied to a set of foundation configurations in order to demonstrate its applicability and limitations.

Water table effects were studied for nuclear facilities located on sites characterized by high water tables. In conventional SSI evaluations the foundation impedances are computed without taking into account the effect of the water table. The influence of the latter on the foundation impedances studied using a version of the SLAM code. A capability of treating the water phase in SSI evaluations was developed and incorporated into the SLAM computer program. Numerical results for foundation impedances were obtained with the without the presence of water in the foundation.

Details pertaining to the lift-off, layering and water table studies are described in the following sections.

2. LIFT-OFF EFFECTS

A study was performed to evaluate the extent to which lift-off (separation of foundation and soil) may be important in evaluating the seismic response of nuclear power plant structures. The standard lumped parameter analysis method was modified by representing the lumped soil/structure interaction horizontal and rocking springs and dampers with disturbed (over the foundation area) springs and dampers are then modified so that they can only transmit compressive stresses. Additional interaction damping is included to account for the impact which occurs when a portion of the foundation which has separated comes back into contact with the soil.

The validity of the model is evaluated by comparing predictions made with it to data measured during the SIMQUAKE II experiment. The predictions were found to correlate quite well with the measured data except for some discrepancies at the higher frequency (>10 cps) range. This discrepancy was attributed to the relatively crude model used impact effects.

Data is presented which identify the peak accumulation required to cause lift-off. For parameters typical of nuclear power plant structures lift-off was found to occur when the peak accelerations are in the range of 0.3 - 0.6 G's. Studies were then performed to evaluate the consequence of neglecting lift-off when it occurs. A typical result is shown as Fig. 1. Spectra were compiled for the rocking motions both including and neglecting lift-off. This was done for three inputs having peak accelerations of

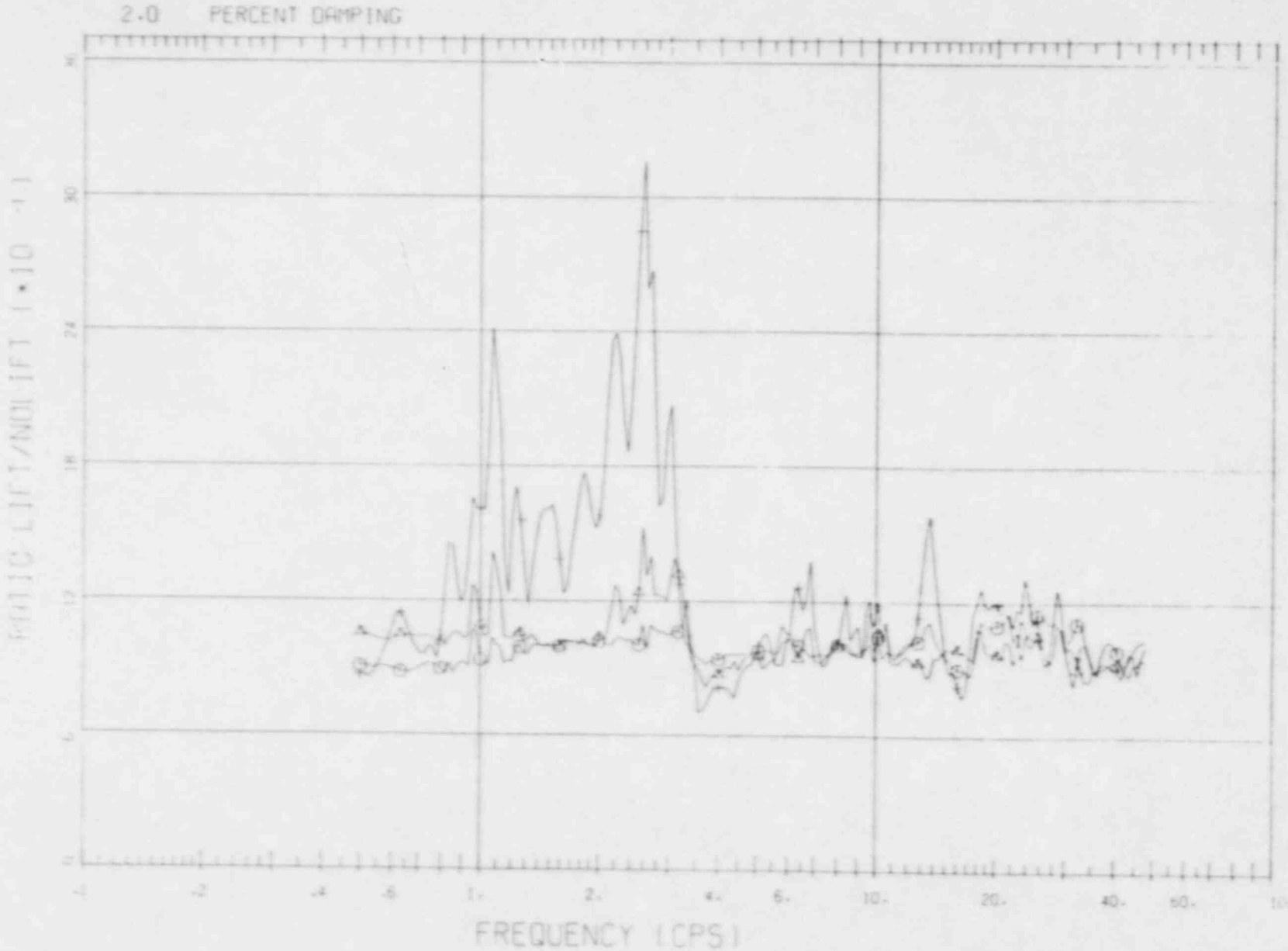

Fig. 1 Ratio Rotational Lift-off/No Liftoff Spectra

1.33, 1.67, and 2 times that required to cause lift-off. The ratio of the spectral values including lift-off to that neglecting lift-off is shown as Fig. 1. It may be seen that the spectra including lift-off effects are significantly higher (by a factor of 3 when the peak acceleration is 2 times that required to cause lift-off) than those neglecting lift-off.

3. LAYERING EFFECTS

Analytical and numerical methods are available today for the evaluation of the dynamic stiffness of foundations resting on the uniform and the layered halfspace. It is desirable, however, to have simplified methods which can give a resonable approximation to the foundation stiffness. The latter, are very important in the computation of the seismic response of building-foundation systems. Approximate methods for deriving foundation impedance functions can be used in preliminary design as well as for checking the overall results from computer codes. Such approximations have been proposed for the uniform halfspace and the case of soil stratum on rigid base. It is generally more difficult to derive simple approximations for impedance functions associated with layered profiles. This is due to the fact that the wave propagation is dispersive in this case. Thus the speed of the propagation depends on the wavelength.

Under this program, a simplified procedure to evaluate the response of structures resting on layered foundations was developed. This procedure is based on an equivalent radiation damping which was evaluated for different foundation configurations. Comprehensive data to demonstrate the applicability and accuracy of the method were generated. Response comparisons between the simplified method and a vigorous method were made for massless foundation, foundation with mass and finally for flexible structures. Fig. 2 shows typical comparison of the harmonic response of a foundation for which the radius is equal to the layer depth. The ratio of the S-wave speed between the layer material and the material of the halfspace is equal to 0.3. It can be seen, that the response obtained by the approximate method is in very good agreement with the rigorously computed response.

Furthermore, the application of the method in computing the transient response due to earthquake inputs was investigated. In these investigations the free-field motion was represented by a synthetic acceleration time history. The accuracy was examined at the floor spectra level. Fig. 3 shows a comparison between approximate and rigorously computed floor spectral curves for 2% equipment damping. The agreement is very good. Similiar results were obtained for a set of different foundation systems.

4. WATER TABLE EFFECTS

One aspect of the soil-structure interaction process which has not generally been included in the soil-structure interaction process is the impact of ground water (or pore water) on the response of typical nuclear power plant facilities located at soil sites where the ground water table

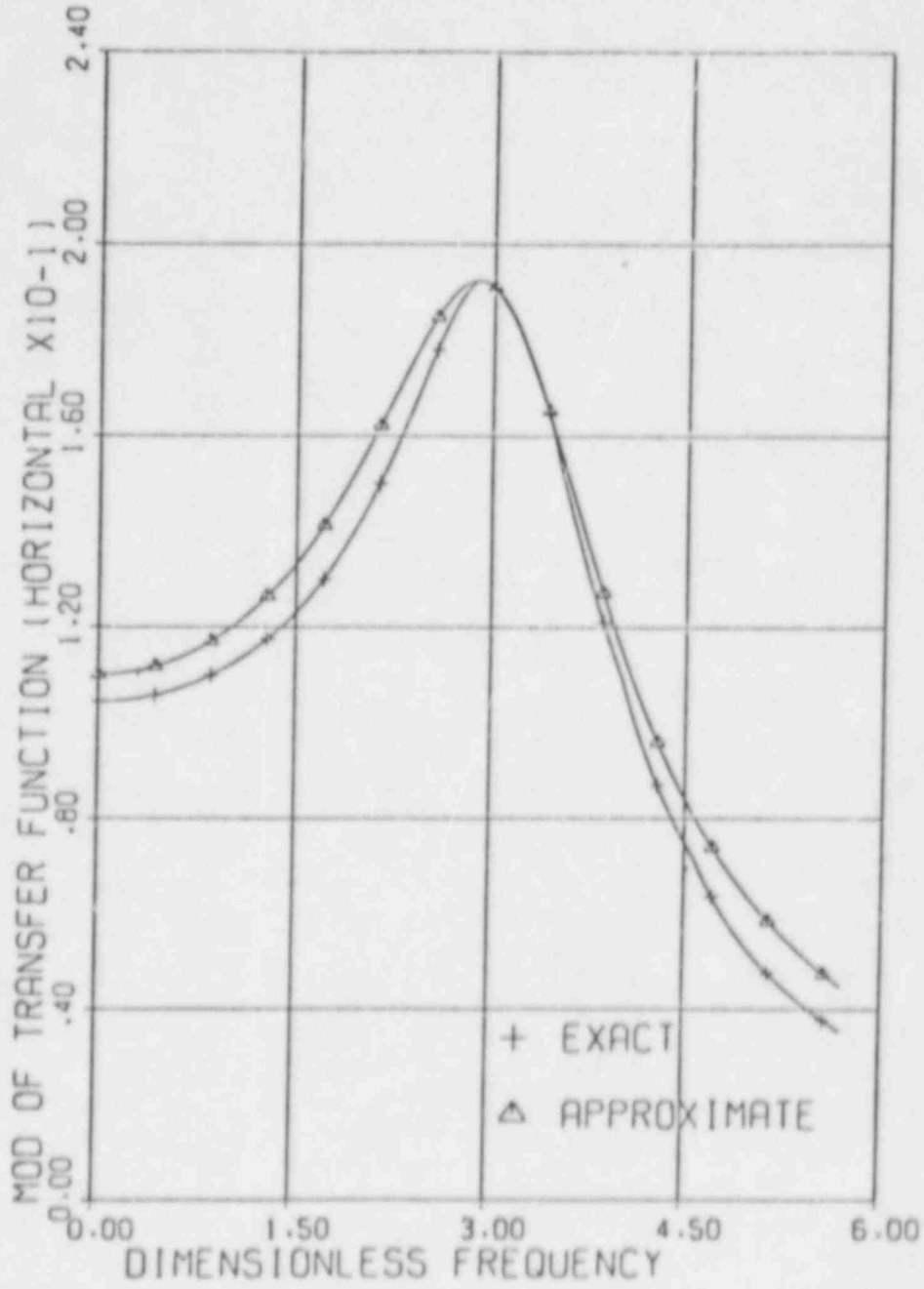

Fig. 2 Steady-State Response Comparison

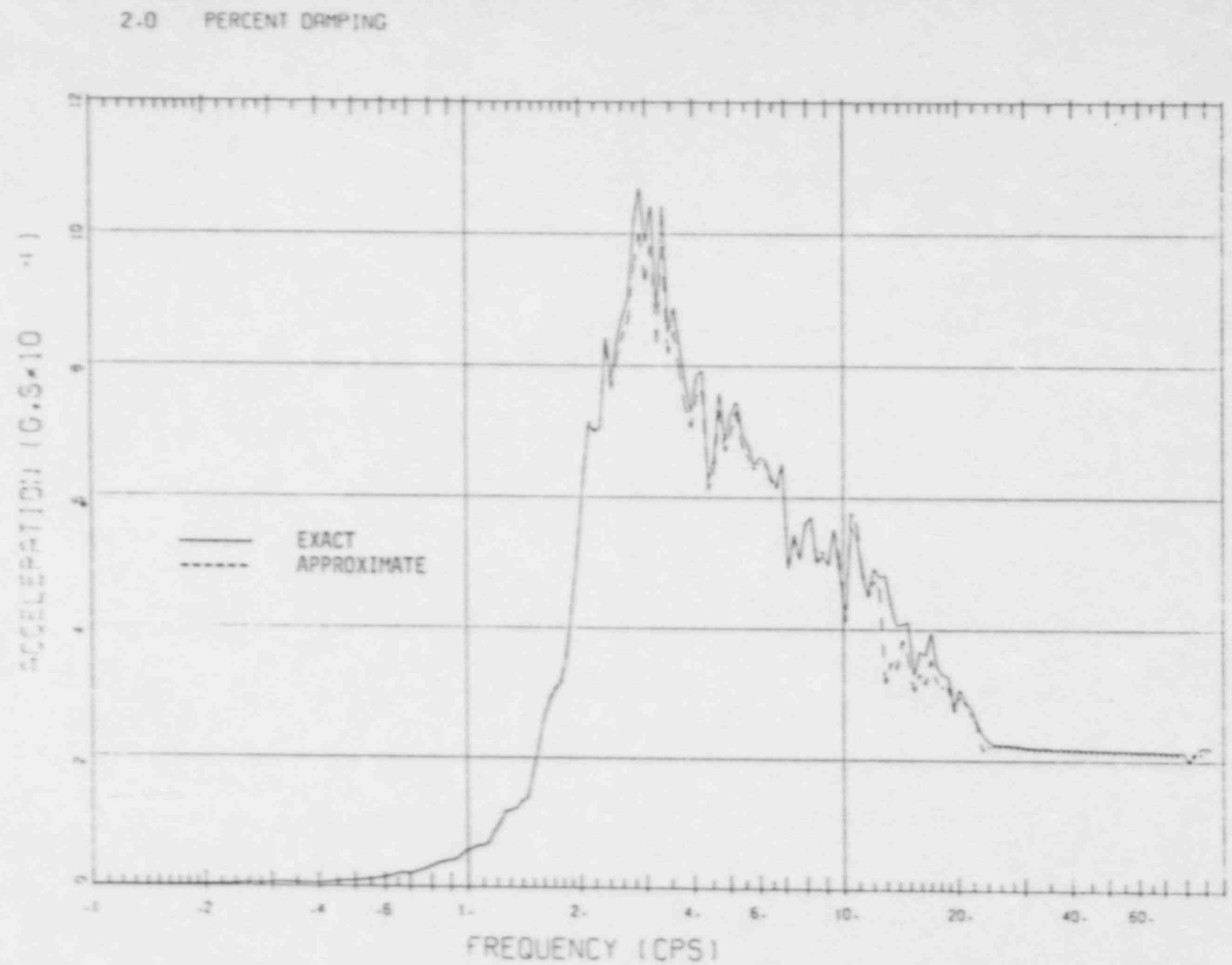

Fig. 3 Floor Spectra Comparison

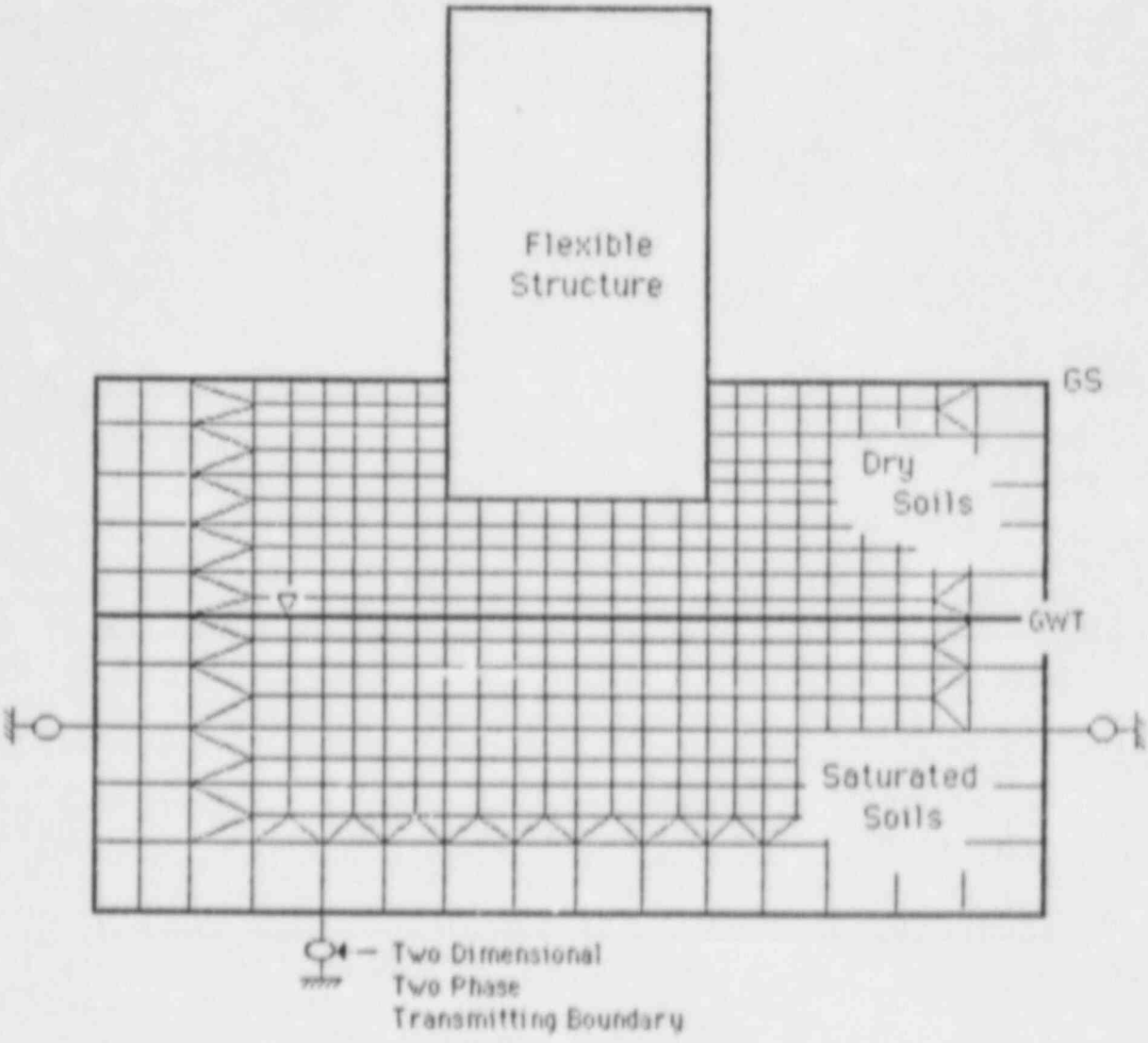

Fig. 4 Finite Element Representation

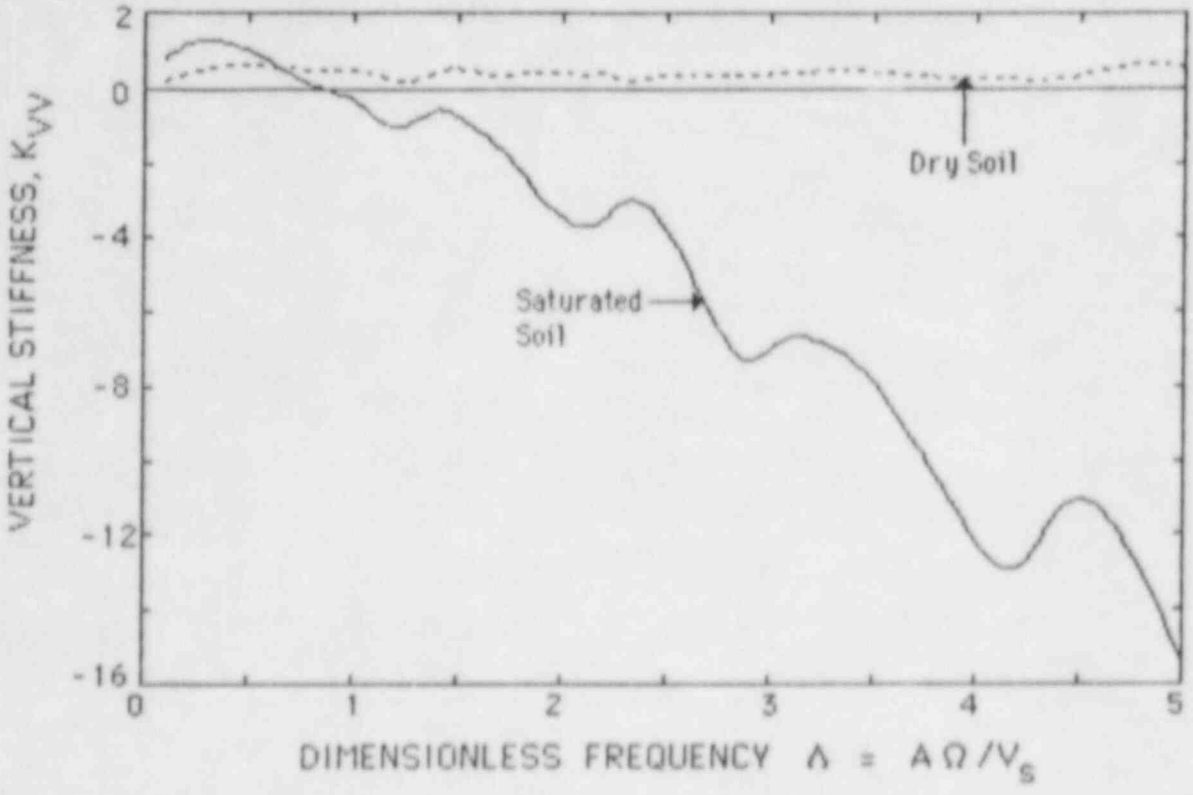

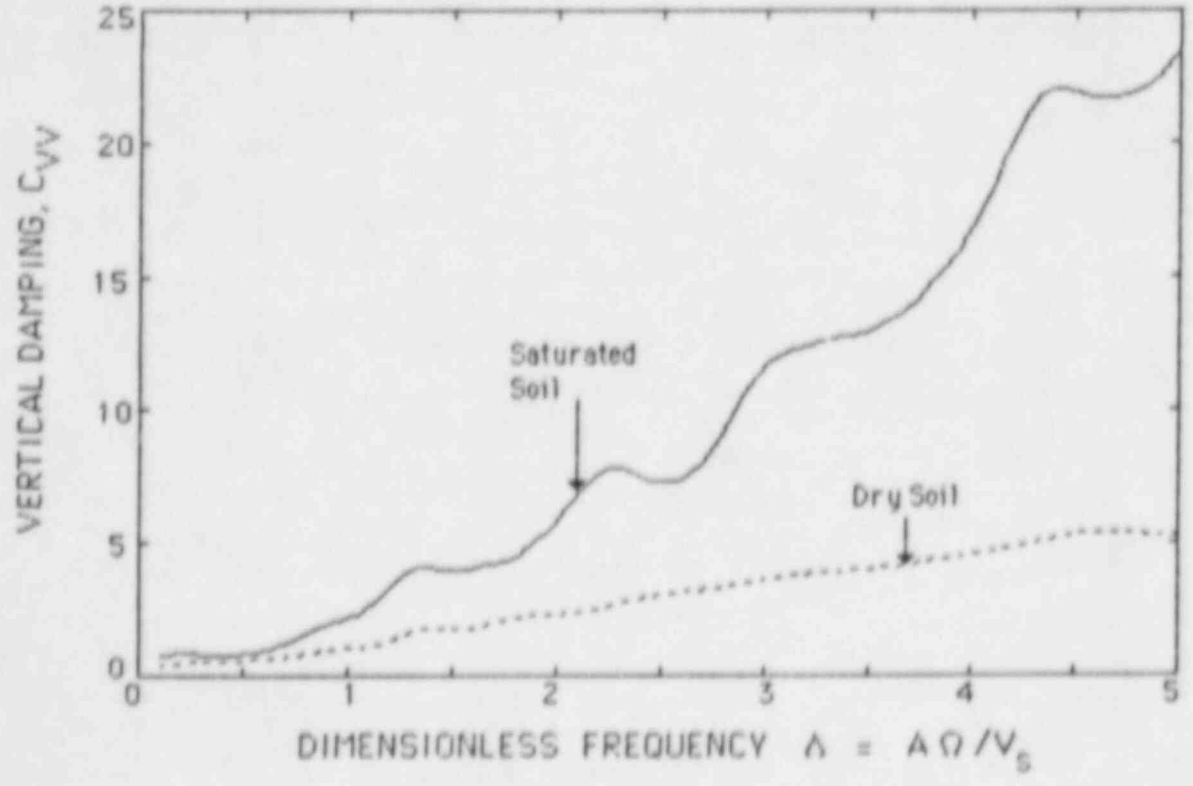

Fig. 5 Comparison of Dry and Fully Saturated Computations Using Mesh 1, k = 0.1 cm/sec

is reasonably close to the structural foundations. There are very good reasons for the current state of affairs, however, not the least of which is the difficulty of incorporating this aspect into the SSI analysis.

At one extreme of the problem at which soil strains approach the failure strain condition, the analysis typically focuses on the potential failure under the structure, and the development of liquefaction conditions in the soil. The current state of the art in this area is to a great extent based upon on empirical methods of analysis. The difficulties in this area stem primarily from a lack of knowledge of soil constitutive data at large strains.

At the small strain end of the spectrum, the analytic approaches that can be used to study the impact of pore water are more tenable, and in fact a relatively long history, extending back some 40 years, is available to guide the development. To be sure, difficulties still exist in this area, and these again are primarily associated with constitutive properties of real soils. However, with the availability of computer power, realistic problems can be investigated to allow engineers to assess the potential impact as seismic structural analysis.

The objective of this phase of the study was to generate a finite element computer program to treat the seismic response of a soil-structure system in which a typical linear structure is situated near the surface of the ground. The soil is represented as a linear medium in which all potential nonlinearities are at most lumped into an equivalent hysteretic damping modulus. However the soil pores is saturated with compressible fluid (water) to some depth close to the structure (Fig. 4). A numerical finite element model is developed to treat this two-phased linear media, this model being based upon the analytic developments extending back to the work of Biot. In keeping with typical SSI analyses, in order to make the finite element approach yield reasonable results, a comparable two-phase transmitting boundary formulation was developed to adequately take care of relative damping effects.

The code was developed and made operational with several parameter variations performed to assess impact of pore water on response. A typical result is shown in Fig. 5, in which a comparison of frequency dependent interactive coefficients (stiffness and damping) is presented for vertical motions of a rigid footing of half-width A. As may be moted, the pore water has a major impact on the character and magnitude of these coefficients, with effective radiation damping increasing from the dry to the fully satuarated case.

ACKNOWLEDGEMENT

This work is being performed under the auspices of the Division of Engineering Technology, Office of Nuclear Regulatory Research, U.S. Nuclear Regulatory Commission. The authors wish to express their special thanks to NRC Project Manager, for his continued support and guidance throughout the course of this program.

STEEL CONTAINMENT BUCKLING

T. A. Butler and W. E. Baker
Los Alamos National Laboratory
Los Alamos, New Mexico

ABSTRACT

Two aspects of buckling of a free-standing nuclear steel containment building were investigated in a combined experimental and analytical program. In the first part of the study, the response of a scale model of a containment building to dynamic base excitation is investigated. A simple harmonic signal was used for preliminary studies followed by experiments with scaled earthquake signals as the excitation source. The experiments and accompanying analyses indicate that the scale model response to earthquake-type excitations is very complex and that current analytical methods may require a dynamic capacity reduction factor to be incorporated. The second part of the study quantified the effects of framing at large penetrations on the static buckling capacity of scale model containments. Results show little effect from the framing for the scale models constructed from the polycarbonate, Lexan. However, additional studies with a model constructed of the prototypic steel material are suggested.

I. INTRODUCTION

The Steel Containment Buckling program being conducted at the Los Alamos National Laboratory is directed at investigating various aspects of reactor containment failure induced by buckling of the steel containment shell. This buckling can arise from an instability in the shell when loading conditions lead to excessive membrane stresses. Failure mechanisms that can be caused by buckling of the shell include material splitting or tearing, seal failure at penetrations, and shell puncture from nearby hard points. The program focuses upon dynamic loading conditions such as those that arise from a Loss-of-Cooling Accident (LOCA) or from an earthquake; however, the program also deals with certain static loading conditions and geometries that have been identified by the NRC as being appropriate computer code bench mark problems.

The research focus is on five areas: (1) effects of the ASME Area Replacement Method for reinforcing penetrations, (2) establishing bench mark static load experiments for computer code verification, (3) investigation of knuckle region buckling for torispherical shallow dome geometries under internal pressure, (4) evaluation of design and analysis procedures used for buckling under time-dependent loadings (dynamic buckling), and (5) evaluation of the effect

of penetration framing on shell buckling capacity. The first three of these areas have previously been investigated [1-5] and will not be reported here. This paper focuses on the research involved with dynamic buckling and the effects of penetration framing.

The study of buckling under the influence of time-dependent loadings is still in progress. A preliminary test series has been completed using a scale model Lexan cylinder excited by scaled earthquake and harmonic signals on an electrodynamic shaker. The occurrence of bucking was determined during the tests by audibility and during posttest analysis by highspeed video, strain gage signals, and accelerations of the top of the test specimen. The tests were analyzed using a freezing-in-time method with standard modal analysis techniques and an experimentally derived buckling interaction curve.

In the penetration framing study four Lexan cylinders modelling containment structures were used to study the effects of different framing designs around large penetrations on the buckling capacity of containments. Two of the cylinders had equipment hatch-type penetrations and two had personnel airlock-type penetrations. Both types of cylinders were loaded with axial loads and shear loads as framing was incrementally added. Analysis with numerical models is being used to determine how containments with prototypic containment materials would respond under the loads being studied.

II. DYNAMIC BUCKLING STUDY

The goal of this work is to assess the current (and past) design and analysis procedures for predicting buckling of steel containment vessels under time-dependent loadings. In particular, in this phase of the work the freezing-in-time method is evaluated. For this analysis method, time-dependent stresses are calculated with a structural dynamic computer code or the stresses are derived from equivalent static loads and then, in either case, are assumed to be static (frozen in time) during performance of bifurcation buckling analyses. Implicit in this procedure is the assumption that the stress field, which causes the buckling, changes little during the time that it takes the structure to deform into the buckled configuration.

A. Test Model

The cylinder used for the experimental studies was constructed from the polycarbonate, Lexan and was supported with aluminum end rings (Fig. 1). The geometry of the cylinder was designed to provide similarity of essential features with steel nuclear containment structures. The size and spacing of the ring stiffeners were based upon the requirements of ASME Code Case N-284 [6] for prevention of both ring and global buckling under typical design loadings for nuclear containments. For the tests described in this paper, additional mass was added to the top ring to separate the frequency of the fundamental response mode from the lowest shell frequencies.

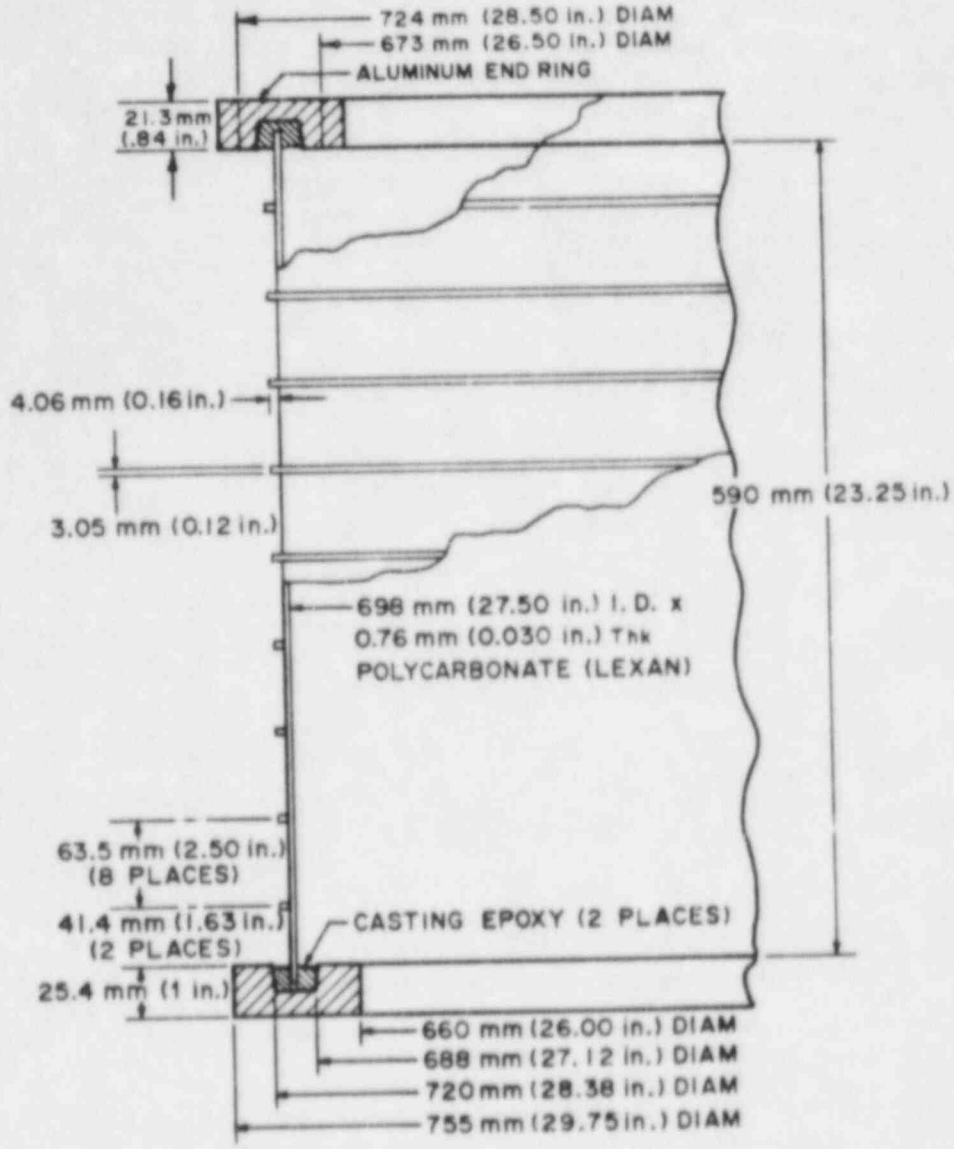

Fig. 1. Details of Lexan model used for dynamic buckling experiments.

The polycarbonate material, Lexan, used for constructing the cylinder and stiffening rings has two characteristics that make it particularly convenient for dynamic buckling tests; models may be fabricated using a convenient solvent bonding technique and the material remains elastic throughout a test involving reasonable post-buckling deformations. Therefore, the model may be subjected to buckling deformations many times without substantial change in the response of either the buckling load or the buckled mode shape.

Before the model was mounted on the shake table a modal survey was performed to determine its dynamic characteristics. During this modal survey several shell modes were identified and compared with analytical results obtained with

the BOSOR-IV computer code. As can be seen from the results shown in Fig. 2, the analytical results are quite close to the test results. Also shown on the figure are analytical frequencies for mode shapes other than pure shell modes. The fundamental beam bending/shear mode frequency is 43.6 Hz, which compares closely with the frequency indicated for this mode during the transient tests described below. The test model was purposely designed so that this mode's frequency would be well separated from the lowest shell modes. In a prototypic containment this frequency could be close to the lowest shell frequencies (see Fig. 3) and, as discussed below, more interaction between the fundamental beam bending/shear mode and the shell modes could be expected. Based upon data from the modal survey and transient tests discussed below, the damping of the cylinder structure is approximately one per cent of critical.

B. Buckling Criteria

Preliminary to the dynamic tests, a series of static tests were performed on the cylinder to establish its buckling strength. Both axial compression and bending tests were conducted. The results of these tests along with the

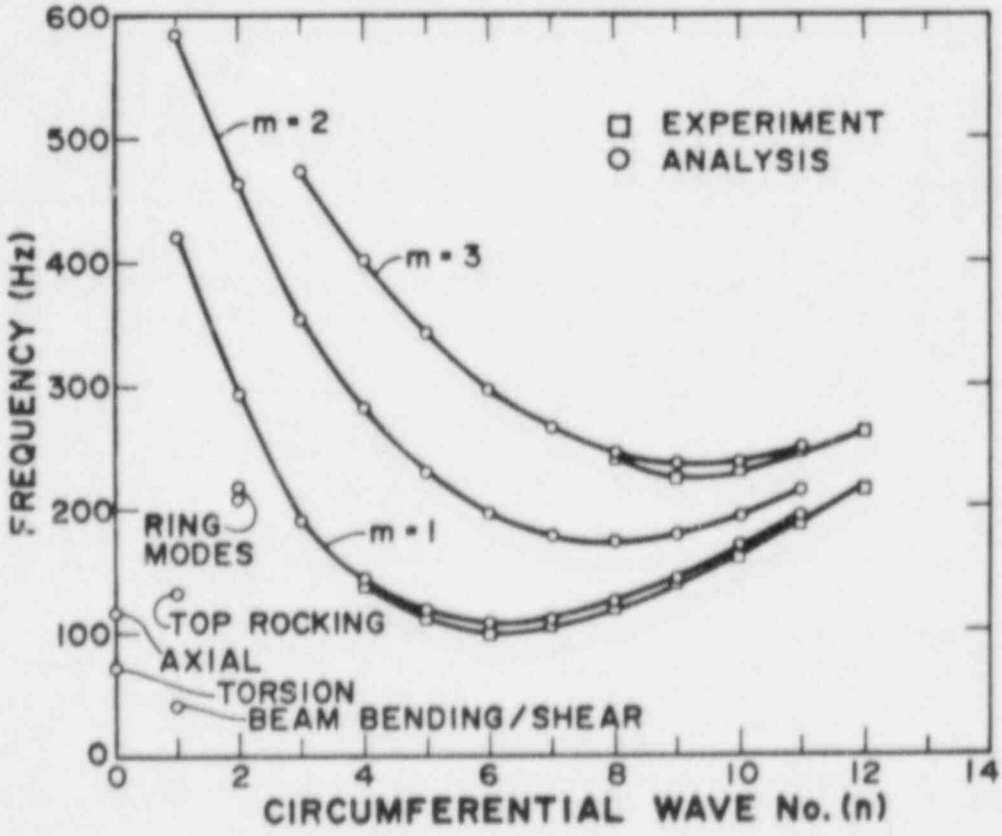

Fig. 2. Natural frequencies for vibration modes of Lexan model used for dynamic buckling experiments.

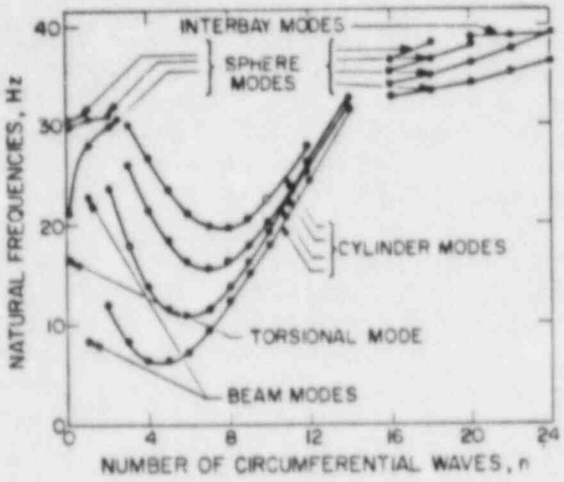

Fig. 3. Natural frequencies for vibration modes of a prototypic containment.

buckling interaction diagram that is discussed in detail in Ref. 7 were used to define the static buckling criterion for the freezing-in-time analysis.

The static axial compression tests were conducted with a 200 kN (55 kip) servo-hydraulic testing machine. Rubber cushions were placed between the thick end plates, which provided the load path from the testing machine to the cylinder, and the aluminum end rings of the cylinder to obtain a uniform load distribution around the cylinder. Axisymmetric loading was used and five tests were performed with the cylinder at different angular positions relative to the end plates. The average load at general collapse, 4092 N (920 lb), is approximately 71 percent of the classical buckling load for an unstiffened cylinder of this geometry.

The bending tests were conducted by clamping the lower end ring to a rigid test fixture and applying a load along a diameter at the top ring. In essence, the shell acted as a short cantilevered beam with a load at the end giving a constant shear distribution along the length of the shell. As with the axial tests, considerable care was given to ensure minimal deviation from an ideal stress distribution at the clamped end. During the tests, as the load was slowly applied, visible, but stable, shear buckles formed before general collapse at the peak load. For a series of nine tests the average buckling load was 1770 N (397 lb).

C. Vibration Test Results

The vibration tests were conducted on a single-axis, horizontal shake table that was controlled with a digital control system. Included in the data taken during each test were the three components of input acceleration recorded with accelerometers mounted on the lower ring of the cylinder, three components of output acceleration recorded from accelerometers mounted on the cylinder's upper ring, and four strain measurements. Two of the strain gages were oriented vertically at the "toe" of the cylinder where buckling from compressive

stresses was judged most likely to occur. These gages were centered between the lower end ring and the first ring stiffener, one being on the inside and the other on the outside. The other two strain gages were on the side of the cylinder, 90 degrees from the first set of gages and centered in the bay just below the center ring stiffener. As with the first pair, the two gages were back-to-back, one inside and the other outside. The orientation of the gages on the shell was 60 degrees from the axial direction.

In addition to recording time histories of these ten transducers, photographic coverage of each test was otained with two high-speed, video cameras. An equivalent framing speed of 1000 frames per second was used. These records permitted visual identification of when buckling occurred in the areas covered on the cylinder. One of the cameras was oriented toward the toe of the cylinder just above the bottom aluminum ring. The other was oriented to show shear buckling on the cylinder at a location approximately 45 degrees to the direction of excitation.

In the first set of tests the excitation was sinusoidal in nature. the objective of these tests was to use the simplest possible transient excitation so that the response would be relatively easy to analyze and the various buckling phenomena could be well understood before more complex earthquake-type transients are studied.

The desired acceleration transient for each test had forty cycles of a sine wave at a given frequency that increased linearly in amplitude from zero to a predetermined peak in 40 cycles. The peak acceleration was held for one additional cycle followed by ten cycles of linearly decreasing amplitude to zero acceleration. This particular transient was selected to reduce the chance of failing the cylinder by restricting the number of cycles of buckling that the cylinder could experience during any one test. For a given test, frequency and the peak acceleration were selected and then the peak acceleration was increased during successive tests until buckling was detected. The decreasing amplitude tail on the transient was necessary to avoid the introduction of a "shut-down" transient, which could cause a severe transient at the end of each test. The harmonic tests were performed at frequencies from 10 Hz to 80 Hz in increments of 10 Hz.

Several different criteria were used to determine when buckling occurred in the cylinder for each of the tests. Some of these were more effective within certain frequency ranges; however, by using all the criteria, the point at which buckling occurred for each frequency considered was reasonably well identified. Only at one frequency, 80 Hz, were we unable to buckle the cylinder because of a lack of shaker table capability. A summary of test results is shown in Fig. 4. The first, and most consistent, method for identification of buckling is labeled "top acceleration" in the figure. For this method, measured acceleration of the top ring of the cylinder in the direction of primary excitation was used along with the mass of the top ring to determine buckling with an equivalent static criterion. When this acceleration first reached a level that the equivalent static load acting on the ring was equal to the static buckling load (1770 N (397 lb)) the cylinder was considered to have buckled. The buckling acceleration was then identified it the same point

in time from the accelerometer located at the base of the cylinder and oriented in the direction of excitation. This method of identifying buckling is an experimental freezing-in-time technique.

A second criterion, based solely on the acceleration response verified the first criterion for frequencies above 43.6 Hz (the frequency of the lowest beam mode). The vertical acceleration response of the top ring of the model initially increases linearly, as would be expected from the prescribed input acceleration. Then at a particular point in time, a high frequency response component appears and the response becomes nonlinear, as indicated by the peak response for each cycle. Again, the buckling acceleration is identified from the base input at the appropriate point in time. Results using this criterion are within 5 percent of the first criterion. Another, similar, method for identifying buckling involves comparing the top acceleration in the horizontal direction with the calculated acceleration. The calculated response does not include buckling effects, so, by comparing the two signals and determining when the experimental response deviates significantly from the analytical, buckling can be identified. For certain tests, this criterion for identifying buckling again gives results close to the equivalent static criterion.

Buckling was also identified for all except the 20 and 80 Hz tests using the recorded video signals. For each of the tests, the video was analyzed frame by frame near the initiation of buckling and the time at which buckling occurred was identified. From Fig. 4 it can be seen that, except for the 70 Hz case, this criterion results in buckling accelerations that are very close to those for the other criteria already discussed. The final criterion used for

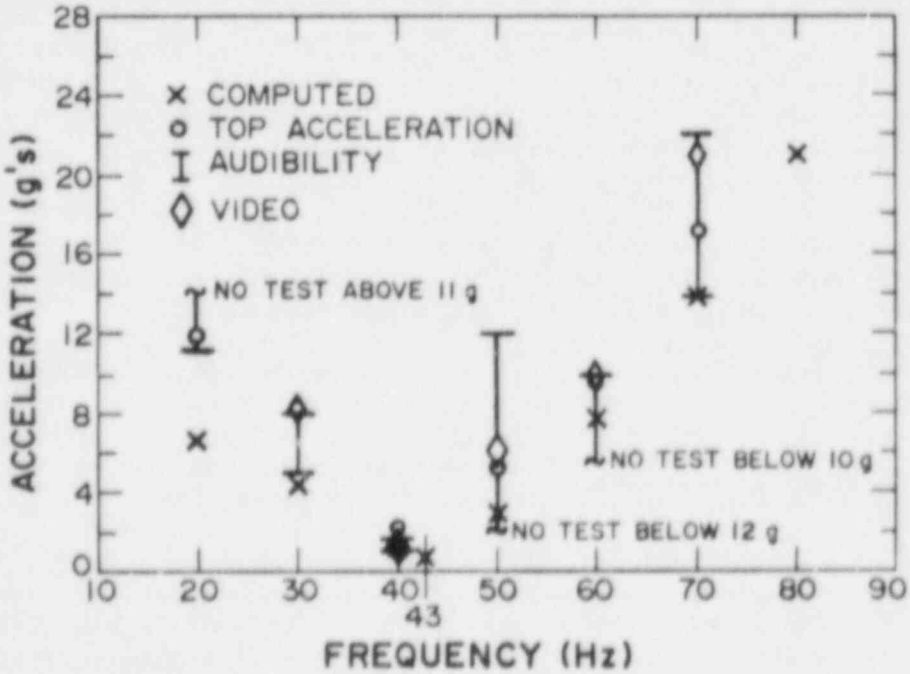

Fig. 4. Required base acceleration to buckle Lexan cylinder as a a function of frequency.

identifying buckling involved audibility. When buckling occurred the cylinder produced an audible popping sound. While each test was being performed two of the experimenters were positioned near the shake table and listened for this characteristic sound. Because the tests were short in duration, the point in time at which the sound occurred could not be identified. It could only be determined that buckling either did or did not occur for each test. Therefore, this criterion results in the wide range of results shown by the bars in Fig. 4.

The BOSOR-IV computer code was modified to calculate modal stresses and these, along with the frequencies, generalized masses, and mode shapes were used in a separate computer code that integrates the uncoupled equations of motion in modal coordinates. The modal response values are then used to predict the stress in the cylinder at each location for each point in time. These stresses are normalized with the critical buckling stress determined in the static tests discussed above. A postprocessor is then used to plot the maximum normalized stresses at specified points on the shell and these are compared with the buckling interaction curve discussed in detail in Ref. 7. When any of the computed stress values are outside of the interaction curve, buckling can be expected. The sequence described here is a freezing-in-time technique and was used to analyze all of the tests.

The numerical model was used to analyze response of the cylinder to the harmonic excitation at each frequency considered in the test series and, in addition, at the fundamental frequency of the cylinder (43.6 Hz). Results of these calculations are shown in Fig. 4, along with the experimental results. The computed buckling acceleration levels are consistently below the experimental data. The primary explanation for this difference is the fact that the computational buckling criterion when compared with the particular static buckling interaction curve used here, should probably use an integrated stress level over a characteristic area rather than point values. The characteristic area has not yet been determined but should probably be related somehow to the buckling wave length for the cylinder.

Two different signals were used to develop the earthquake-type transient excitation. These were based on normalized accelerations from the east-west motion of the 1965 Olympia, WA earthquake and the north-south motion of the 1933 Long Beach, CA earthquake. Response spectra of these two earthquake transients using 1 per cent damping are shown in Figs. 5 and 6. The signals were scaled in time and amplitude to be appropriate for excitation of the 1/50th scale model Lexan cylinder. Consecutive tests were performed with each of the transients, with each test having a higher maximum acceleration level until buckling could be definitely identified through audibility.

Table 1 presents results for several of the tests performed in this series. Before discussing the buckling of the test model, some general comments should be made concerning the response of the model to the two different earthquakes. The amplification of the input base acceleration to the model top ring is approximately 2.5 for the Olympia signal whereas the amplification is two to three times that value for the Long Beach signal. This difference in response can be explained by referring to the response spectra presented in Figs. 5 and

6 and realizing that, before buckling occurs, the top ring at the end of the very light Lexan shell responds to this type of input as a linear single-degree-of-freedom system with a natural frequency equal to the fundamental beam bending/shear modal frequency (43.6 Hz).

Buckling was identified in much the same way as for the harmonic tests described above except that we did not use video records. The primary method for determining whether buckling occurred for a given test was to analyze the bending strain measured with the strain gage pair located approximately halfway up the cylinder wall. If the shell does not buckle and there are no initial imperfections in the shell, the bending strain at this location should remain small because none of the shell modes with harmonics greater than one are theoretically excited. There are obviously small imperfections in the shell so this bending strain is expected to remain small but have a finite value throughout each of the transients. Compare, for instance, the three signals shown in Fig. 7. The top signal is the bending strain from Test 17 where buckling was indicated by every other measure, both from experimental data and by analysis. It shows significant bending strain being introduced at approximately 0.25 s into the transient. The middle signal is from Test 18

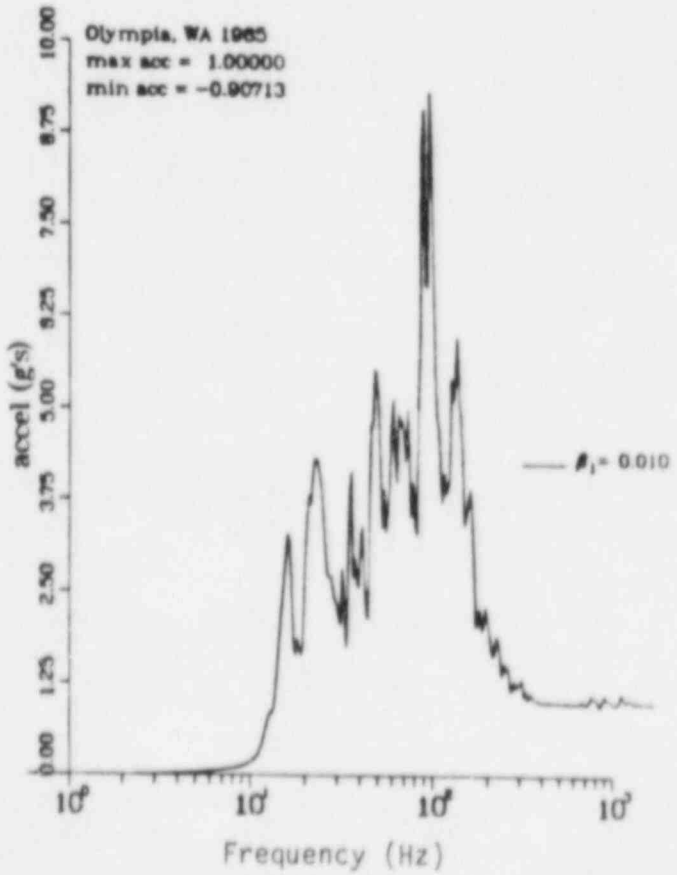

Fig. 5. Response spectrum for Olympia 1965 earthquake scaled for model study and normalized to a maximum acceleration of 1.00 g.

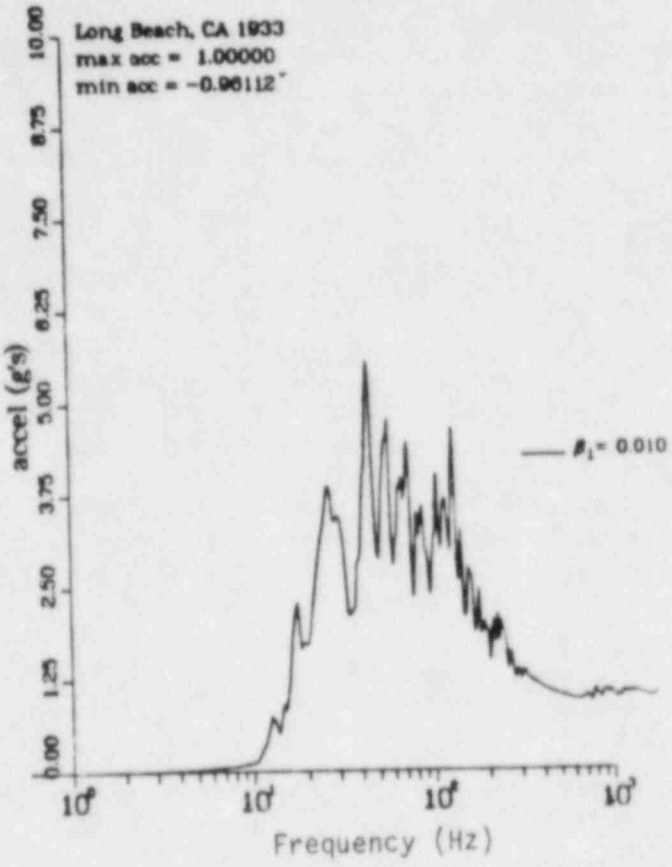

Fig. 6. Response spectrum for Long Beach 1933 earthquake scaled for model study and normalized to a maximum acceleration of 1.00 g.

where it is believed that buckling did not occur. The lower signal is from Test 19, a test for which there is no other indication that buckling did occur. Based on this comparison, however, we would say that buckling did occur for this test.

A second measure for the occurrence of buckling is to analyze the vertical acceleration of the top ring in the frequency domain. If buckling occurs, higher shell harmonics should be excited and the vertical response of the ring should show significant energy at frequencies other than the fundamental system frequency (43.6 Hz). The power spectral density of the vertical acceleration of the top ring during Test 9 is shown in Fig. 8. Note the expected peak at approximately 43.6 Hz and the larger peak at 140 Hz. The higher of the two frequecies coincides with the shell vibration frequency for n=9 (see Fig. 2). When the shell was statically buckled, it buckled into the n=9 harmonic so this is a frequency that we would expect to see excited when buckling occurs. Figure 9 shows the power spectral density for the top ring vertical acceleration for Test 18, where buckling did not occur. Using this measure, bu kling

TABLE I

SUMMARY OF RESULTS FOR DYNAMIC BUCKLING FROM EARTHQUAKE TRANSIENTS

Test No.	Earthquake	Peak Horizontal Base Acceleration (g's)	Peak Horizontal Acceleration Top Ring (g's)	Audibility	Buckling Indicated By			
					Bending Strain	Top Vertical Acceleration	Equivalent Static Load	Analysis (Freezing-in-time)
7	Olympia	4.15	10.92	No	Yes	Yes	No	Yes
8	Olympia	4.53	11.95	Possible	Yes	Yes	No	Yes
9	Olympia	5.06	12.72	Possible	Yes	Yes	No	Yes
17	Long Beach	3.67	27.60	Yes	Yes	Yes	Yes	Yes
18	Long Beach	2.23	14.74	Possible	No	No	Yes	Yes
19	Long Beach	2.36	21.90	Possible	Yes	No	Yes	Yes

did not occur for Test 19, which has a power spectral density for this acceleration signal that is very similar to the one for Test 18.

The most accurate method for experimentally identifying buckling for the harmonic tests was the equivalent static load method where buckling was assumed to occur when the acceleration of the top ring mass was high enough that its weight multiplied by its horizontal acceleration in g's exceeded the load required to buckle the cylinder during static tests. This method indicates that when the horizontal acceleration of the top ring exceeds 14.3 g's, the shell should buckle. As can be observed from the data in Table I, this measure is not appropriate for both of the earthquake transients. For the Long Beach signals the method may be acceptable. However, use of this method for the Olympia signals would be nonconservative. Here, the buckling load calculated from the measured response acceleration is approximately 75 per cent of the required static load. The reason for this lower required buckling load is probably that shell harmonics are excited and introduce what amounts to additional imperfections in the Lexan cylinder, thus lowering the required buckling load.

An important point is that the equivalent static load method being considered here is, in essence, a freezing-in-time technique. The fact that the method does not accurately predict buckling does not necessarily mean that any freezing-in-time technique is not acceptable because it is conceivable, but unlikely, that some analysis techniques could account for the excitation of higher harmonics and the imperfections that they introduce. Another important aspect of the problem is that, in the test model, the frequency of the fundamental response mode is far removed from the lowest shell frequencies.

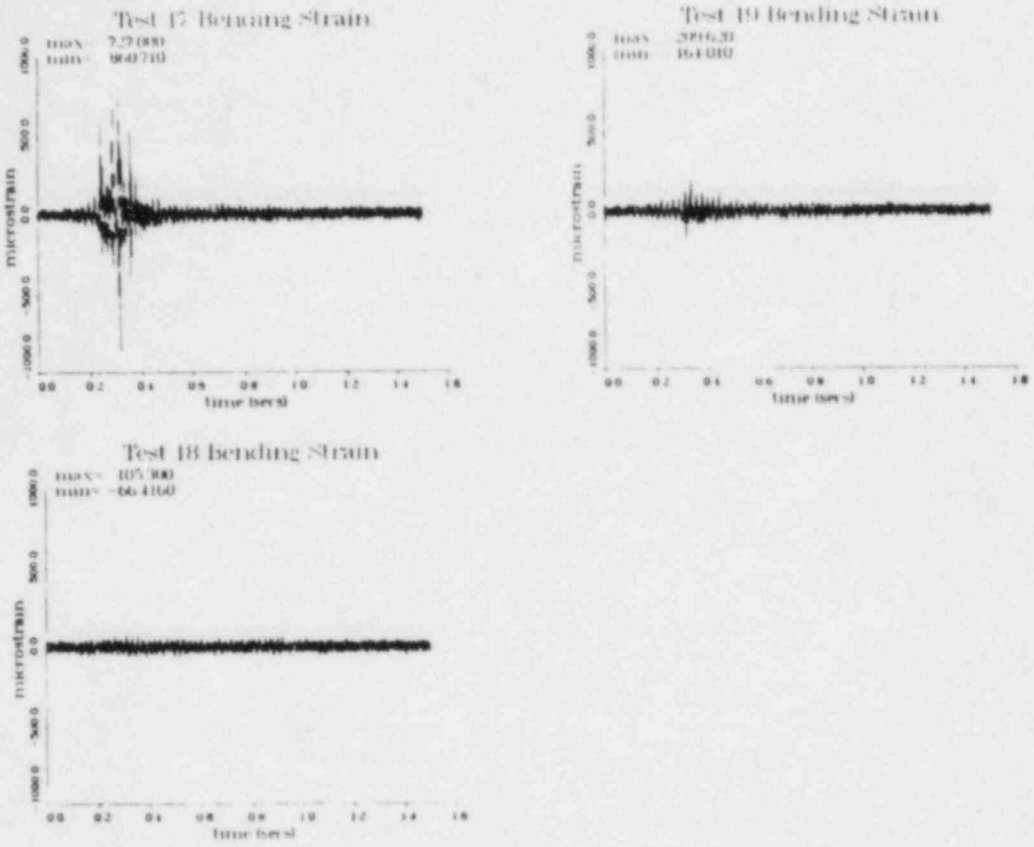

Fig. 7. Bending strain in Lexan shell at height L/2 and 90° from direction of excitation for different levels of Long Beach 1933 earthquake.

In the prototypic containment the fundamental frequency is very near to the lowest shell frequencies (see Fig. 3). In addition, the presence of a penetration structure that has significant mass, such as a personnel airlock, introduces the possibility for other important vibration modes with frequencies in the range of interest.

The analytical freezing-in-time technique being used for this study predicts that the shell buckles for all of the six cases listed in the Table I. As described above in the discussion of response to harmonic base excitation, this method is quite conservative because of the manner in which the stresses in the shell are treated when compared with the buckling interaction curve.

III. PENETRATION FRAMING EVALUATION

The objective of the penetration framing study is to develop a set of guidelines that can be used in evaluating the effect of framing on overall

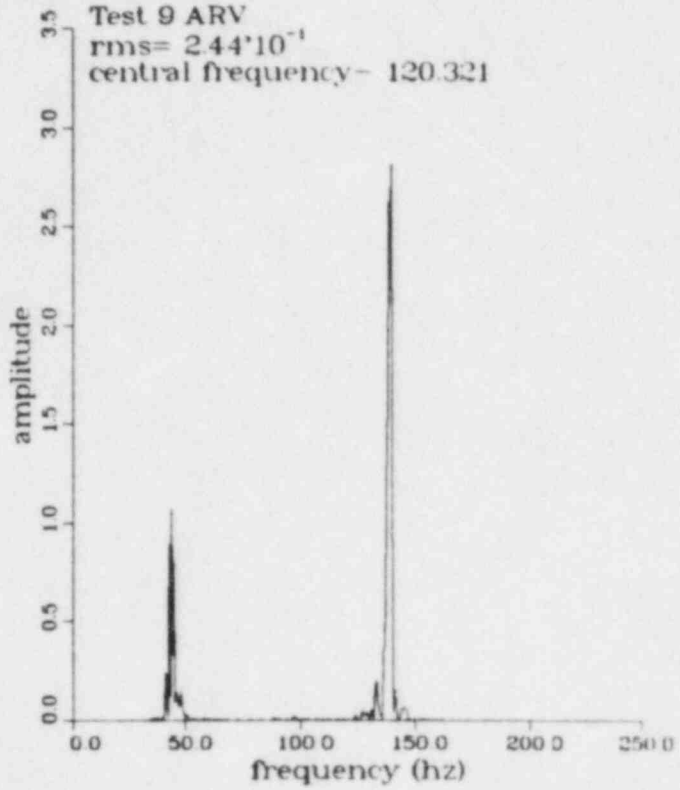

Fig. 8. Power spectral density of vertical acceleration of top ring on Lexan model for Test 9 (Olympia 1965).

containment vessel structural stability. Framing is normally added to a containment structure when one or more circumferential stiffening rings are interrupted by a large penetration such as an equipment hatch or a personnel airlock. The purpose of the framing is to carry loads in the circumferential stiffeners around the penetration with as little disturbance of the load path as possible. Presence of the framing can affect the buckling capacity of the containment for several reasons; one is that it can introduce additional stress concentrations and another is that the added mass can affect dynamic response characteristics of the containment. Results of a previous study [3] using steel models indicated that framing could possibly lower buckling capacity, particularly when the buckling is characterized by plastic collapse. Altering the dynamic response characteristics can lead to increased membrane compressive stresses under certain loading conditions and can also introduce dynamic imperfections.

In the work reported here we evaluate the effects of framing only in a static sense. Later work in our dynamic buckling program is oriented toward determining the effect of added mass associated with penetrations on the buckling response of containments loaded dynamically.

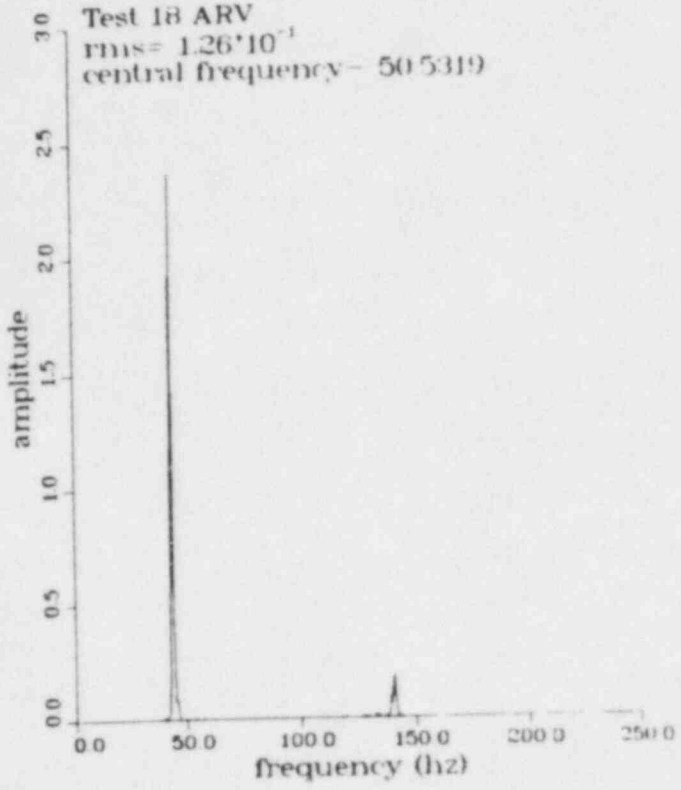

Fig. 9. Power spectral density of vertical acceleration of top ring on Lexan model for Test 18 (Long Beach 1933).

A. Test Models

For this study, four Lexan models were fabricated with large penetrations. The test models were similar to the model described above for the dynamic study (see Fig. 1) except that penetrations were introduced. Two of the models had the equipment hatch-type penetration shown in Fig. 10 and two had the personnel airlock-type hatch shown in Fig. 11. Before any framing was added, doublers and collars that satisfy the ASME Area Replacement Method were bonded to the Lexan cylinders. The design of the penetrations is nominally patterned after those described in Ref. 8 for the containments designated Units 6 and 7 in that report.

During fabrication all components that were to be bonded to the cylinder, such as doublers, stiffening rings, and framing members, were preformed to the appropriate cylindrical radius using a heat treatment process. This preforming minimized any distortion of the cylinder or introduction of prestresses that could affect the buckling capacity. The resulting models were of high quality with the required load to buckle with axisymmetric, axial loading ranging from 85 to 96 per cent of the classical value for an unpenetrated cylinder of the same diameter.

B. Test Procedure

Each of the four models were tested with three types of loads: an axial center load, an axial load eccentric to the center at one half the radius and located above the penetration, and a shear load oriented along the diameter of the cylinder acting on the top ring of the model. For each model framing was incrementally added during one of the last two load types to determine its effect on the buckling capacity. In addition, each model was tested before any framing was added and after the final framing was added for the other two load types. The method for loading the models was the same as described above for determining the buckling capacity of the model that was loaded dynamically.

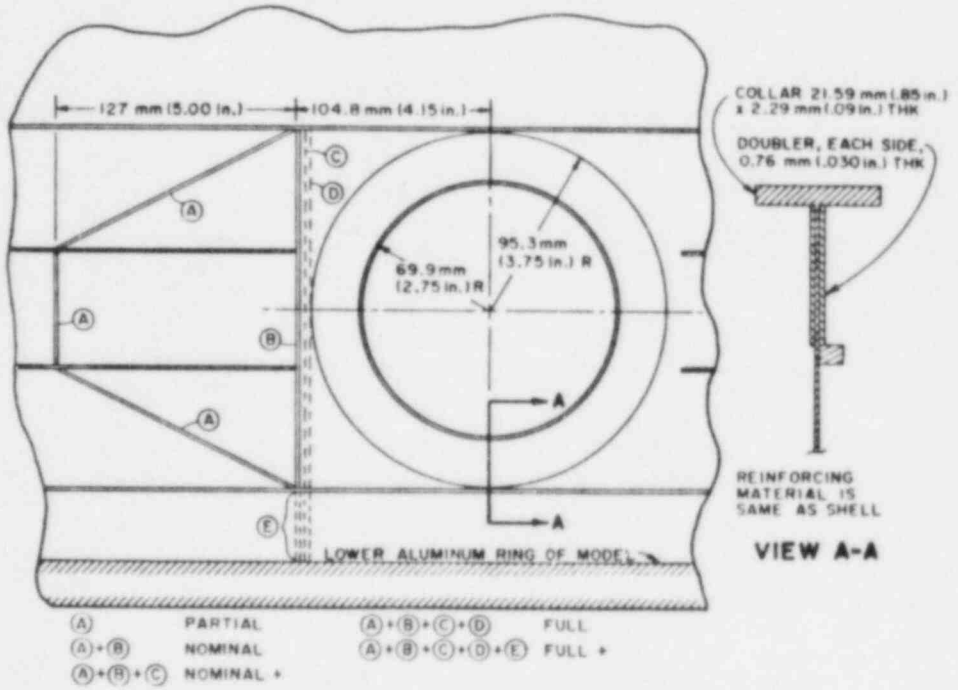

Fig. 10. Schematic of models that represent containments with equipment hatch-type penetrations.

During the test series where framing was added incrementally the sequence that it was attached to the models is shown in Figs. 10 and 11. Two of the models, designated E1 and P2, had framing added until they were in the "Full +" configuration. Additional framing beyond the nominal condition was not added for the other two models, designated E2 and P1, so that these models could be used for further dynamic buckling studies.

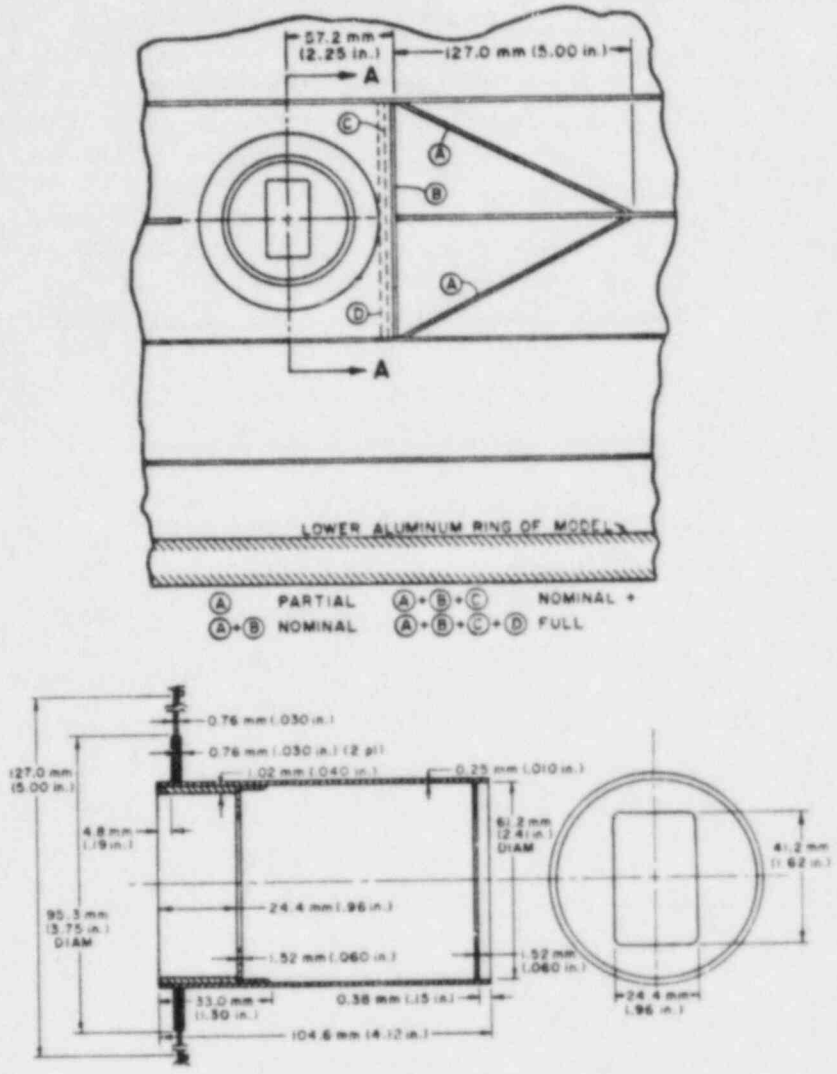

Fig. 11. Schematic of models that represent containments with personnel airlock-type penetrations.

C. Experimental Results

Results of the buckling experiments for each of the four models are shown in Figs. 12-15. The data presented in each of the plots are normalized to the results of the first buckling test for that model for the particular load case considered and, in the case of the R/2 eccentric load and the shear load, with the load applied on the side of the model opposite the penetration. For instance, for the shear load case every load on the plot is normalized to the buckling load with the shear load applied at a position 180 degrees to the penetration so that the penetration would have a minimal effect on the buckling

capacity. For both axial load cases, center and R/2 eccentric, several tests were performed with the model oriented in an inverted position, that is, with the penetration located at the top of the model. For the particular loading hardware used for these tests, buckling was more likely to occur near the penetration with the model in this orientation, making the test data more meaningful in determining the effects of the penetration and additional framing.

Data from all of the tests indicate that, for these particular models (small imperfections) and this particular material (Lexan), the addition of framing near penetrations has little effect on the models buckling capacity. The largest difference is an increase in capacity of about 10 per cent for model E2 with a shear load. Some of the observed small decreases in buckling

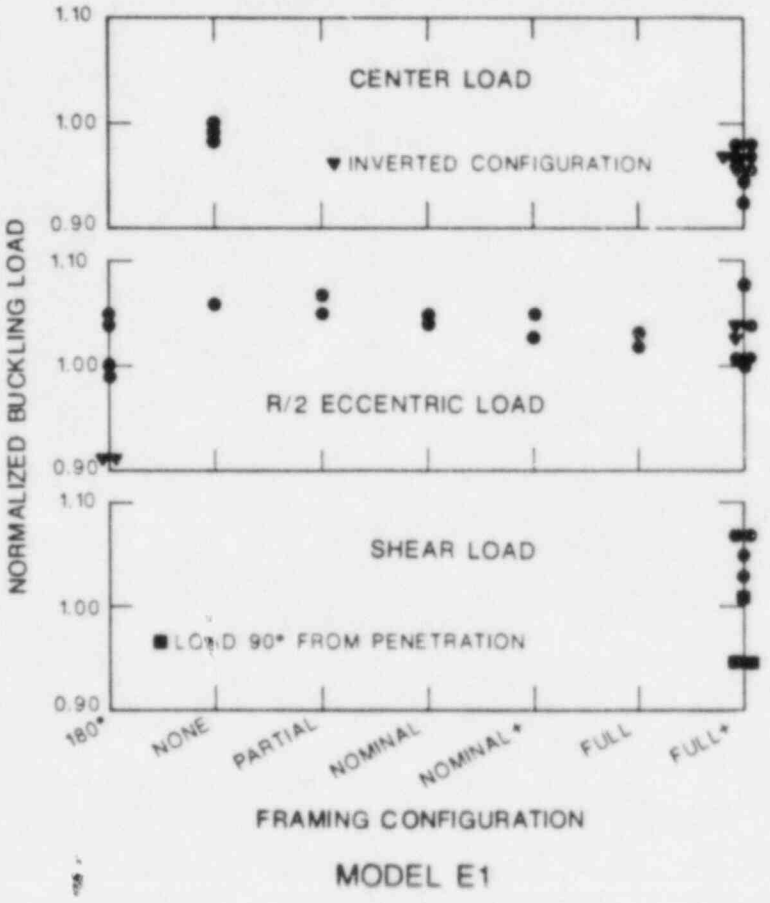

Fig. 12. Normalized buckling loads for model E1.

capacity must be viewed in light of a general trend for the buckling capacity of a given model to decrease during repeated tests with short time periods (less than an hour) between tests. Note an apparent decrease in the buckling capacity of model E1 with the addition of framing for the R/2 eccentric axial

load. In this case all of the tests from the "Partial" framed condition through the Full framed condition were performed on the same day. The lower two data points for the "Full +" condition were also obtained on the same day. The upper two points for the "Full +" framing condition, neglecting the two tests in the inverted configuration, were obtained after the model had not been tested for several days. The highest of these two points is higher than any other point for any framing condition.

Three of the four models were loaded in shear with the load located 90 degrees from the penetration. The resulting data are indicated with solid squares in the plots. This particular orientation locates the penetration in the region where stable shear buckles first form during the shear tests rather than near the toe where the axial compressive stress is the maximum. Results seem to indicate that the model orientation has little effect on the buckling load,

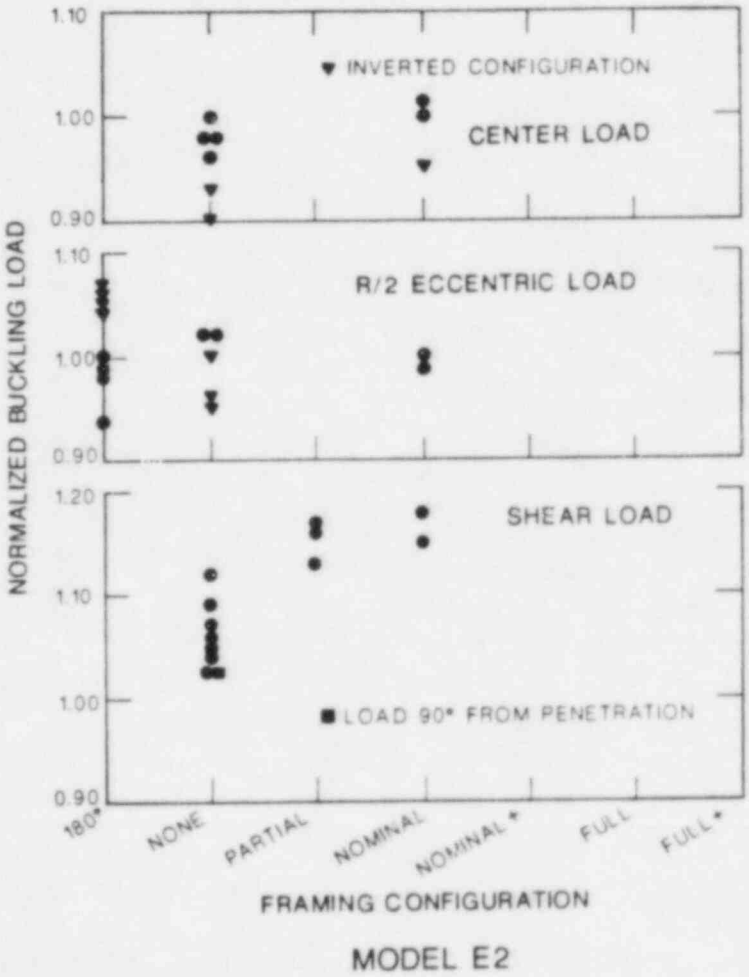

Fig. 13. Normalized buckling loads for model E-2.

which, in turn, further suggests that neither the penetration or the framing significantly affect the buckling capacity of the Lexan models.

Another point that can be made from Figs. 12-15 is that the penetrations reinforced in accordance with the ASME Area Replacement Method do not lower the buckling capacity of the models. This conclusion is in accordance with the work previously performed with steel models and reported in Refs. 1 and 2. For the central axial load case, this fact is indicated by the buckling load being near to the classical value for unpenetrated cylinders. For the other load cases it is supported by the fact that the 180 degree orientation agrees quite closely with the no framing case.

D. Analysis Results

A finite element model (FEM) of the Lexan models with the equipment hatch-type penetration was developed using the ABAQUS computer code [9]. The model was represented with 198 shell elements and 196 beam elements. The stiffening rings and framing, represented with beam elements, were offset from the center

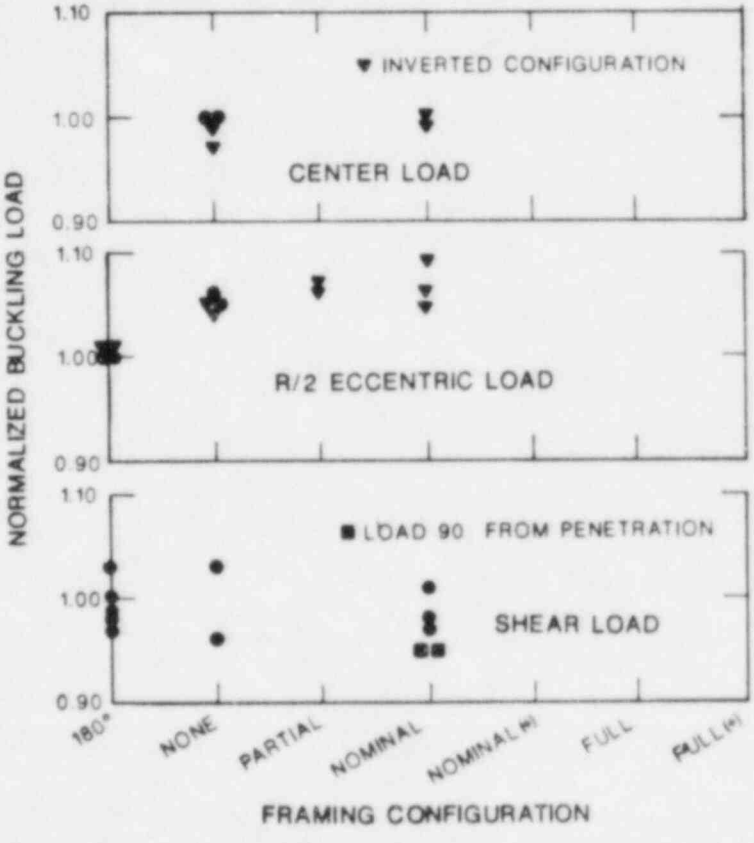

Fig. 14. Normalized buckling loads for model P1.

line of the shell elements using multipoint constraints. Linear material properties were used for the Lexan and the ends of the cylinder were fixed from rotating. The lower end was also fixed from translating and the upper end was forced to remain circular in a plane that could rotate and, in the case of the shear load, translate.

Several studies were performed with the FEM representing the different framing configurations that were studied experimentally. In all of our studies, the material was assumed to remain linear and bifurcation buckling solutions were obtained. Only the more important of the analytical studies will be reported

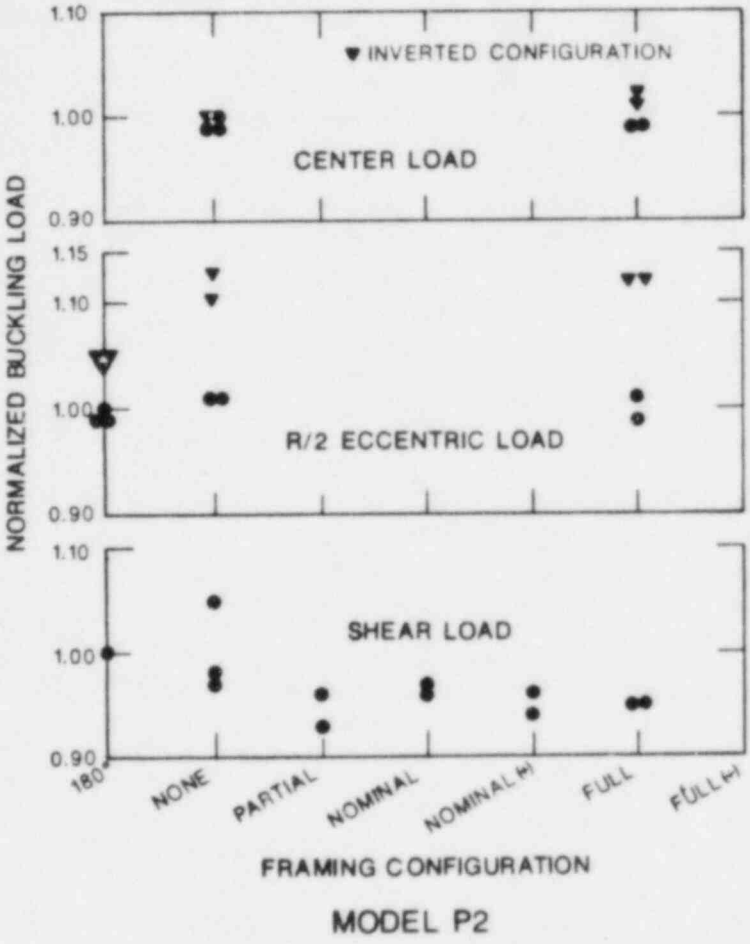

Fig. 15. Normalized buckling loads for model P2.

here. These include analysis of buckling response for the R/2 eccentric axial load and the shear load with no framing and with nominal framing. Since the top load plate was not included in the model, the load distribution for the R/2 eccentric load case was developed using strain data from the bench mark studies [3] and an assumed cos (θ) variation of the load magnitude. For the shear load cases, the FEM was loaded with a concentrated load on the top ring

above the penetration, which accurately represents the actual loading condition for the experiments.

Results of the FEM analysis are shown in Figs. 16 and 17 for the R/2 eccentric and shear load cases. For the R/2 eccentric load case the addition of framing up to the nominal framing state lowers the computed buckling load by approximately 15 per cent. The buckled shape without framing is similar to the experimental buckled shape with general buckling over the front half and lower portion of the cylinder. When the framing is added the buckling becomes localized above the penetration. For the shear load case the addition of framing raises the buckling load by approximately 15 per cent. The cylinder buckles near the base next to the penetration without framing. When framing is added the buckle is forced upward to the top of the framing and penetration.

E. Discussion

Results of the FEM analysis, in terms of buckling load are not out of line with the experimental results. Even though the experimental results do not show the magnitude of change that the FEM analysis does, the buckling load seems to decrease slightly for the R/2 eccentric case with the addition of

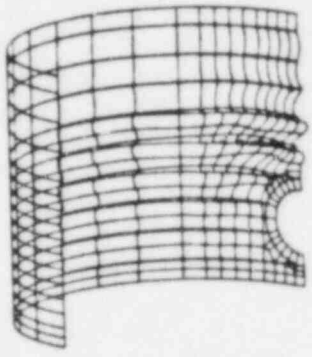

R/2 eccentric load without framing buckling load is 4604N (1035 lb)

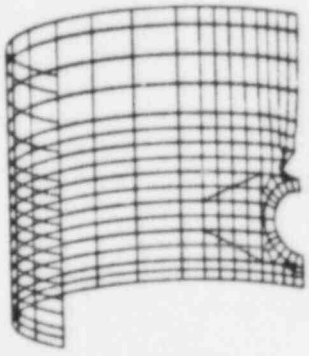

R/2 eccentric load with framing buckling load is 3959N (890 lb)

Fig. 16. Finite element model results for equipment hatch-type penetration with and without framing for R/2 eccentric load.

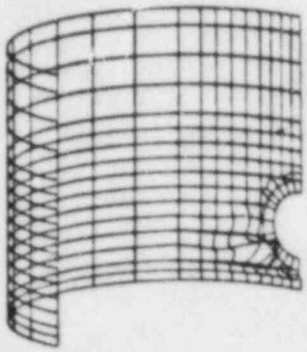

Shear load without framing buckling load is 1933N (448 lb)

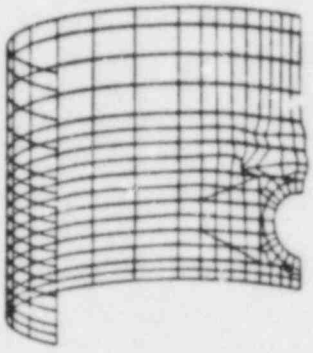

Shear load with framing buckling load is 2309N (519 lb)

Fig. 17. Finite element model results for equipment hatch-type penetration with and without framing for shear load.

framing up to nominal for both models E1 and E2 and to increase slightly for the shear load case for both models.

Some caution must be used in extapolating the results of either the experimental results or the FEM results to the prototype. First, the material Lexan used for the experiments behaves somewhat differently than the prototypic material, A516 Grade 70 steel. The Lexan remains nominally linear for all of the loads used for our buckling studies. There is, however, some question about the effect of short-term creep of the material during loading. For instance, we obtained slightly different buckling loads depending on the loading time used for the tests. The prototypic steel material, unlike the Lexan, may exceed its elastic limit for some of the loading conditions studied, depending on the capacity reduction factor for the prototype. For the R/2 eccentric load, the maximum stress in the Lexan cylinder just prior to buckling is estimated to be 3.86 MPa (560 psi). This translates [10] to a stress level of 331 Mpa (48000 psi) for the prototype, which is below the normal elastic limit of 379 MPa (55000 psi). The difference in capacity reduction factor between the Lexan models and the prototype would make the maximum expected stress level in the prototype before buckling even less. On the other hand, for the shear load, which probably gives a stress field like that which

could be expected during an actual earthquake, the maximum expected stress level when bifurcation buckling is expected in the prototype, not accounting for differences in the capacity reduction factors betweem Lexan and steel cylinders, would be approximately 1014 MPa (147000 psi). Depending on the capacity reduction factor for the prototype, the prototypic material may or may not yield before it buckles. If the material does yield significantly before buckling, the response would be expected to be similar to that seen in the bench mark studies [3] where a steel with a rather low elastic limit of approximately 193 MPa (28000 psi) was used.

Based on the Lexan model tests, the FEM analysis, and the previous bench mark experiments [3], we can reach several conclusions relative to the effect of framing on the buckling capacity of a penetrated containment. First, a penetration that does not interrupt more than two circumferential stiffeners and is reinforced according to the ASME Area Replacement Method does not significantly lower the buckling capacity of the containment. Second, if the capacity reduction factor for the containment is such that the containment material membrane stress stays in the linear range, except for local stresses, the buckling capacity should not change significantly (less than 15 per cent). Third, if the containment material does not remain in the linear range, stress limits, as defined by the ASME Code, will govern the containment design. Several questions remain, the most significant having to do with how the response of the prototype compares with that of the Lexan models, particularly in terms of the capacity reduction factor. We will learn more about the capacity reduction factor in our dynamic tests but at least one or two additional static tests need to be performed using a steel model with material properties close to the prototypic material and with imperfections representative of the prototypic containment.

IV. CONCLUSIONS

A ring stiffened, axisymmetric, Lexan cylinder was submitted to two types of dynamic excitation to provide data for evaluating current analysis methods for predicting load levels at which steel containments could buckle. One of the excitation types, a single-frequency, harmonic signal was used to study the phenomena associated with buckling of a ring-stiffened shell loaded dynamically. The other excitation type consisted of scaled earthquake signals. Tests using the harmonic-type excitation showed that, for this type of excitation, buckling can be predicted rather accurately given that an appropriate static buckling criterion exists for the types of forces with which the shell is loaded. This indicates that a freezing-in-time analysis could give an accurate prediction for the excitation levels that would cause the shell to buckle dynamically. Prediction of shell buckling with earthquake-type dynamic loads is much more difficult. Results from the tests reported here indicate that for some earthquake signals shell modes with more than one circumferential wave may be excited and become important in predicting the buckling response of the shell. Since these higher harmonics are not normally included in freezing-in-time analyses, the technique needs more evaluation before it is used without a conservative dynamic capacity reduction factor.

Another part of the Los Alamos program for evaluating buckling of steel containments involved determining the effects of framing at large penetrations in the containment shell. Two penetration types were studied experimentally with four Lexan models. Results of these experiments and a finite element analysis of one of the penetration geometries indicates that the framing has little effect on the buckling capacity of the penetrated containment. The experiments indicated a change in buckling capacity of less than 10 per cent and analysis indicated a change of less than 15 per cent. The framing increased buckling capacity for shear types of loads and decreased the loads required to buckle the models for an axial compression load type. Extrapolation of the results to the prototype indicates that for certain load combinations, the prototypic material may experience considerable plastic yielding before the bifurcation buckling loads are reached, thus causing failure through plastic collapse rather than linear bifurcation buckling. Additional tests need to be performed on a model constructed using field fabrication techniques with a steel that has material properties close to those normally used for steel containments to determine how the results reported here relate to typical steel containment buildings.

V. ACKNOWLEDGEMENT

This work is sponsored by the US Nuclear Regulatory Commission, Division of Engineering Technology, Mechanical/Structural Engineering Branch. The encouragement of Dr. Boris Browzin, Project Monitor, is gratefully acknowledged.

VI. REFERENCES

1. J. G. Bennett, R. C. Dove, and T. A. Butler, "An Investigation of Buckling of Steel Cylinders with Circular Reinforced Cutouts," Nuclear Engineering and Design 69 (1982), pp. 229-239.

2. J. G. Bennett, R. C. Dove, and T. A. Butler, "An Investigation of Buckling of Steel Cylinders with Circular Cutouts Reinforced in Accordance with ASME rules," Los Alamos Scientific Laboratory report, NUREG/CR-2165 (June 1981).

3. W. E. Baker and J. G. Bennett, "Buckling Investigation of Ring-Stiffened Cylindrical Shells with Reinforced Openings Under Unsymmetrical Axial Loads," Los Alamos National Laboratory report, NUREG/CR-3135 (February 1983).

4. W. E. Baker, J. G. Bennett, and C. D. Babcock, "Experimental Buckling Investigation of Ring-Stiffened Cylindrical Shells Under Unsymmetrical Axial Loads," Journal of Pressure Vessel Technology, Vol. 105, pp. 342-346, November 1983.

5. G. Fly, J. G. Bennett, W. E. Baker, and C. D. Babcock, "Experiments Designed to Assess the Margin-to-Failure of Steel Containments Susceptible to Knuckle Buckling," 7th International Conference on Structural Mechanics in Reactor Technology, Chicago, Illinois, August 22-26, 1983.

6. Code Case N-284, "Metal Containment Shell Buckling," ASME, Boiler and Pressure Vessel Code, Section III, Nuclear Power Plant Components, Division 1, Subsection NE, 1983 edition.

7. W. E. Baker and J. G. Bennett, "Experimental Investigation of the Buckling of Nuclear Containment-Like Cylindrical Geometries Under Combined Shear and Bending," Nuclear Engineering and Design, 79 (1984), pp. 211-216.

8. T. R. Bump, R. W. Seidensticker, M. A. Shakelford, V. K. Gambir, and G. L. McLennan, "Characterization of Nuclear Reactor Containment Penetrations--Preliminary Report," Sandia National Laboratory report, NUREG/CR-3855 (June 1984).

9. ABAQUS Computer Program Manuals (Hibbitt, Karlsson, and Sorensen, Inc., Providence, Rhode Island, 1981), Vols. 1-4.

10. C. D. Babcock, W. E. Baker, G. Fly, and J. G. Bennett, "Buckling of Steel Containment Shells Under Time-Dependent Loading," Los Alamos National Laboratory report, NUREG/CR-3742 (May 1984).

PIPING RESEARCH OVERVIEW

DAN GUZY, MSEB/DET/RES

Introduction

The USNRC Piping Review Committee was formed in 1983, at the request of the USNRC Executive Director for Operations. Its charter was to perform a comprehensive review of NRC requirements in the area of nuclear power plant piping. The Piping Review Committee completed its mission in 1985, with the publication of the five volumes of NUREG 1061 (References 1 through 5). These reports present recommendations for both regulatory changes and for needed research.

The Piping Review Committee's research recommendations are now being implemented through a combination of projects sponsored by industry and the NRC's Office of Nuclear Regulatory Research (RES). The division of tasks within RES is such that those addressing pipe cracking and pipe break will be managed by the Materials Engineering Branch and those dealing with the dynamic load design of piping will be managed by the Mechanical/Structural Engineering Branch. This paper will outline the research activities in the latter category. Recommendations from Volumes 2 and 4 of NUREG 1061 form the basis for doing the work discussed below.

Dynamic Load Capacity and Failure Modes of Piping

The Piping Review Committee recognized the potential benefits from more realistically identifying failure mechanisms and improving acceptance criteria for the dynamic loading of piping. Inertial loadings from dynamic events such as earthquakes are time-varying and have limited durations and energy content. These now, however, are evaluated like gravity and other sustained piping loads. ASME Code requirements for the dynamic load design of piping assume that plastic collapse is the dominant failure mode but, recent analytical studies (Reference 6) indicate that some combination of ratcheting and fatigue is more likely to occure. Limited testing has also shown the onset of dynamic ratcheting in piping; however, actual failure data is so scarce that appropriate design rule changes can not be made at this time. If it can be demonstrated conclusively that fatigue/ratcheting is the principal dynamic failure mode, then significant changes can be made with regards to how the ASME Code sets limits on inertial stresses. This would dramatically change the nature of piping system design and could in turn reduce the number of snubbers used in nuclear power plants.

To address this issue, the NRC and EPRI are cooperating jointly in the Piping and Fitting Reliability Research Program. The objectives of this program are to clearly determine the likely dynamic failure modes of piping systems, to identify procedures to predict failure (and margins), and to provide a basis for changing ASME Code rules, if appropriate. This program consists of dynamic capacity testing of piping at the system, component, and specimen levels, plus analyses needed in support of test planning and the development of recommendations for criteria changes. Seismic, BWR hydrodynamic, and water hammer loadings will be addressed in the program.

The joint EPRI/NRC program began in the Spring of 1985, and will take approximately 3 years to complete. General Electric of San Jose is the main

contractor and performs the overall management, coordination and integration of the program. General Electric is working with consultants and the testing sub-contractors to develop test matrices, configurations, and data acquisition procedures. EPRI and the NRC approve program planning and review results as they develop.

A matrix of forty piping component tests is being conducted at ANCO Engineers. The objective is to systematically obtain dynamic failure data for components under severe (but characteristic) seismic, hydrodynamic, and water hammer loadings. Elbows, tees, reducers, support connections, nozzles and lugs will be tested. The test specimens will consist of both carbon and stainless steel 6" NPS piping components (with various schedules) under different internal pressures. The seismic and hydrodynamic test set-ups have the components attached to shakers at one end and weights at the other end (see Figure 1).

Three different 6" piping systems will also be tested to failure under simulated earthquake, hydrodynamic, and water hammer loadings. These pressured systems will use components compatible with those above and will also have piping supports at the 4 or 5 load input points. The tests will be repeated at least once to give two (or more) tests per load-type. Piping system testing under the joint EPRI/NRC program will not begin until next year, but a related NRC-sponsored test is now underway at ETEC (FIN B3052). The objectives of this test are to demonstrate the feasibility of failing a representative piping system (see Figure 2) under a high earthquake-like load, and to provide information and insights needed in the test planning of the main EPRI/NRC program.

The basic phenomena of fatigue ratcheting will be studied at General Electric of Schenectady using laboratory specimens. Since at the present time there is no standard laboratory test specimen which addresses this failure behavior, specimen designs need to be developed. Both uniaxial and bending loads will be applied. The influence of different material and temperatures will be studied. The outcome of this task will be the basis for evaluating ratchet effects under dynamic fatigue for ASME Code pipe materials.

The results of the three types of tests discussed above will be analyzed and synthesized to form the basis of failure criteria for the combined static and dynamic loading of nuclear piping components. These criteria will be design-oriented and applicable for ASME Class 1, 2, and 3 piping. Analytical studies will be made to develop and justify the alternative piping design rules. It is intended that a strong liason be maintained with the NRC licensing staff, the PVRC, and the ASME Section III Code body which ultimately makes the rule changes.

The EPRI/NRC program outlined above is directed primarily at evaluating and improving piping design rules. Additional work will be sponsored later by the NRC to use the failure information obtained to validate or improve seismic risk piping fragility models.

The piping design rules of Section III of the ASME Code do not explicitly address pipe cracking. While the EPRI/NRC tests will not include flawed piping, the NRC Degraded Piping Program will perform seismic tests on relatively short pipe specimens with known crack sizes. The results of these two programs will be studied together later. Data about the capacity of flawed piping needs to be evaluated along with data concerning the nonlinear response behavior of piping systems at high input levels to give an integrated assessment of failure.

Pipe Damping

The newly developed PVRC pipe damping criteria (Fig. 3 and Ref. 7) will have the greatest immediate impact on seismic piping design and the reduction of snubber use. The NRC supported the PVRC effort through staff participation, and through pipe damping research at INEL (Refs. 8 and 9) and the Stiff vs. Flexible Piping Research Program at LLNL (Refs. 10 and 11). The PVRC damping criteria has been adopted by the ASME as Code Case N-411. This code case should soon be formally endorsed by the NRC through Revision 24 of Regulatory Guide 1.84.

Although being a significant departure from the pipe damping criteria of Regulatory Guide 1.61, the NRC's endorsement of Code Case N-411 carries some restrictions. Firstly, the code case provides no guidance for modal response frequencies above the seismic range (i.e., above 33 H_z). The pipe damping program at INEL (FIN A6316) is now addressing this and should provide criteria recommendations next year for modal response in the hydrodynamic load range (33 to 100 H_z) . What high frequency pipe damping data exists in INEL's world data base has been evaluated, and the ongoing test program has been extended to include high frequency input. INEL will complete testing this Fall and later provide the conclusions from their study of parameters influencing pipe damping values. Important initial findings are the general confirmation of the PVRC's criteria and the identification of support configuration as a dominant factor.

Another limitation of the NRC's endorsement of Code Case N-411 is that its use for time-history analyses has not been accepted. Since a multiple-support input time history analysis using the code case damping criteria will essentially be a "best-estimate" prediction of the piping response itself, it needs to be clearly shown that some conservatisms would remain the design process. One approach being considered would quantify the conservatisms in the Standard Review Plan's criteria for evaluating soil and building response, using piping response as a figure of measure. This would be similar to a previous LLNL/SMA study (Ref. 12), but the new pipe damping criteria would be used instead of the constant 2% value assumed before. Other ways to address the problem could account for failure margins and nonlinear effects above the SSE response level to show that best-estimate design analysis produce adequate overall conservatisms. Although further planning decisions need to be made, it is hoped that an NRC research project to evaluate damping criteria for time-history analysis will be performed within a year.

The combined use of Code Case N-411 with other proposed piping criteria changes may need to be evaluated as the new criteria is adopted. The effect of using the Independent Support Motion Method in conjunction with new damping criteria is an example of this and is discussed below.

Piping Response Predictions Methods

Through the Mechanical Piping Benchmark Project, BNL developed the basis for acceptance of the Independent Support Motion (ISM) method (Ref. 13). This method provides an alternative to enveloping spectra when more than one floor spectra is specified for a piping system. Although the ISM method was endorsed (with modification) by the Piping Review Committee, the Committee recommended that further research be conducted to better account for structural phase

correlation. Research addressing the treatment of closely spaced modes and high frequency modes in spectrum methods was also recommended.

BNL will begin research in these areas next year, following the current effort (FIN A3287) to assess the impact of PVRC damping used in conjunction with the ISM method. The present task involves redoing the spectra and time-history analyses presented in Reference 13, using the new damping criteria throughout instead of uniform damping values. Preliminary results indicate a significant loss of relative conservatism (i.e., lower ratios of spectra method response predictions to time-history predictions)when the PVRC damping criteria is used in conjunction with the ISM method.

The Piping Review Committee recommended that studies be made to develop pseudo-linear estimation methods and design procedures to account for inelastic piping response. It is hoped that the end product of this would be a methodology simple enough for routine design evaluations. The Nonlinear Piping Response Prediction Project at HEDL (FIN D1611) is now assessing nonlinear response prediction techniques having differing degrees of accuracy (and complexity). Pretest response and failure predictions of the ETEC pipe test mentioned previously will be made by HEDL using NONPIPE (a nonlinear piping code) along with candidate simpler techniques such as inelastic spectra, a "dynamic margins" approach, and seismic PRA fragility estimation methods. Post test assessments will be made of the various results with the hope that a simple design-oriented method could be endorsed.

The NRC Piping Review Committee also recommended that further studies be conducted to more completely assess the uncertainties in seismic piping response, and to evaluate the feasability of improving the way Regulatory Guide 1.122 now specifies the development of spectra used in piping design. These studies will be performed in a two-phased project at LLNL, "Assessment and Improvement of Spectrum-Broadening Procedures Used in Piping Design" (FIN A0453). Phase 1 is underway and consists of the gathering and synthesis of information on response frequency uncertainties (for both nuclear structures and piping). A state-of-the-art summary will be made concerning what has been done to date in this area. All related NRC-sponsored work be considered along with outside research. An assessment of the adequacy of the $\pm$15% peak broadening range specified by Regulatory Guide 1.122 will be made.

Phase 2 of this LLNL project will be based to some extent on the results of Phase 1. The objective of Phase 2 is to develop and justify a probabilistically-based procedure for "simple" in-structure spectra that realistically account for the maximum energy a design earthquake can transmit. A goal would be to establish the basis for "flattened and broadened" spectra that could replace those now specified by Regulatory Guide 1.122. The extreme of this would be a completely level spectrum that would facilitate the use of static analyses for piping inertial loads, and thus greatly reduce the complexity of current design practice.

Nozzle Design Guidance

The need for improved design guidance on nozzle flexibility and allowable loads was recognized by the Piping Review Committee. This improved guidance will

both help reduce the number of seismic supports used in current design practice, and will provide a more realistic basis for evaluating nozzle loads in future, more flexible, piping system designs. Both nozzle and support load criteria become limiting in piping design as seismic restraints are removed.

ORNL (FIN B0474) is developing improved design guidance for vessel nozzles and piping branch connections in typical Class 1, 2, and 3 nuclear power plant piping systems. Particular attention will be given to the interaction effects at the vessel-piping (and piping-piping) juncture, including the effects of nozzle flexibility on calculated bending and thrust loads under both static and dynamic conditions. Design methods used to prevent plastic collapse and fatigue failure will be addressed through an assessment of current primary, and secondary load stress indices and stress limits based on recently developed theoretical data (shell theory and finite element solutions) and existing experimental results. Of particular importance are the recent recommendations from WRC Bulletin 297 (Ref. 14). ORNL will develop recommendated improvements to ASME Code design rules for vessel nozzles and piping. These will be reviewed by the ASME and the NRC. This project is currently underway and should be completed in 1986.

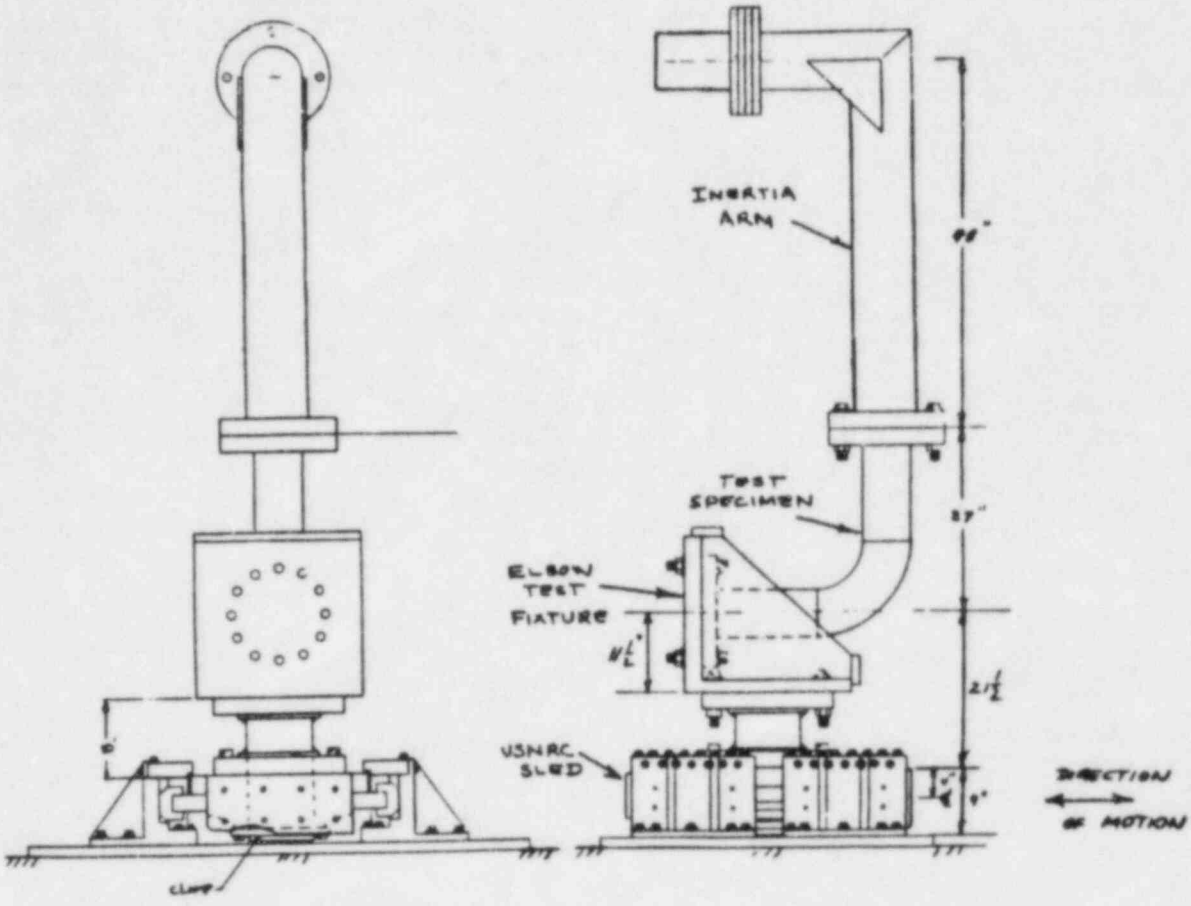

Figure 1 - Representative Set-up For EPRI/NRC Component Tests

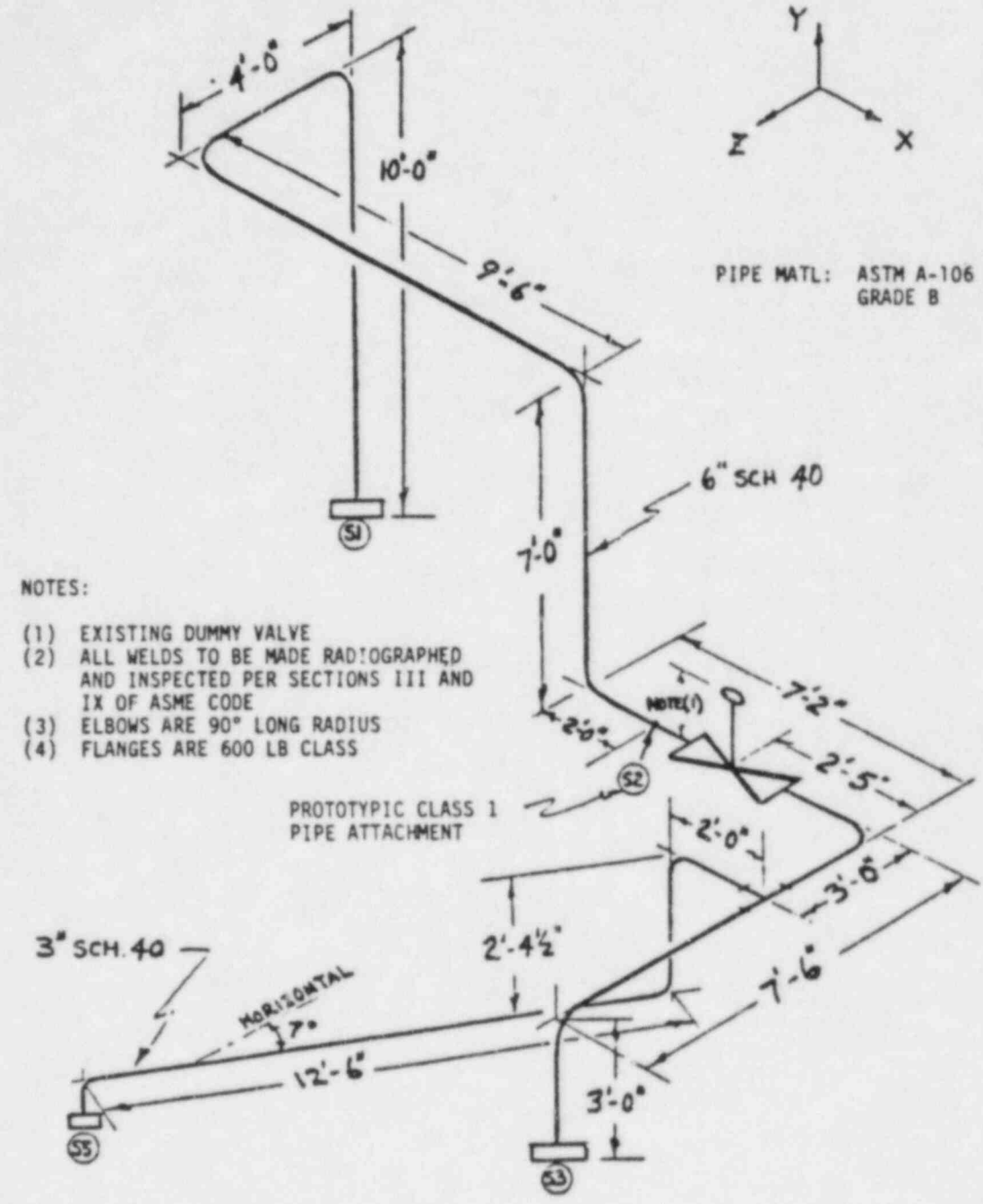

Figure 2 - Schematic Drawing of Test Article for the ETEC Piping Fragility Demonstration Test

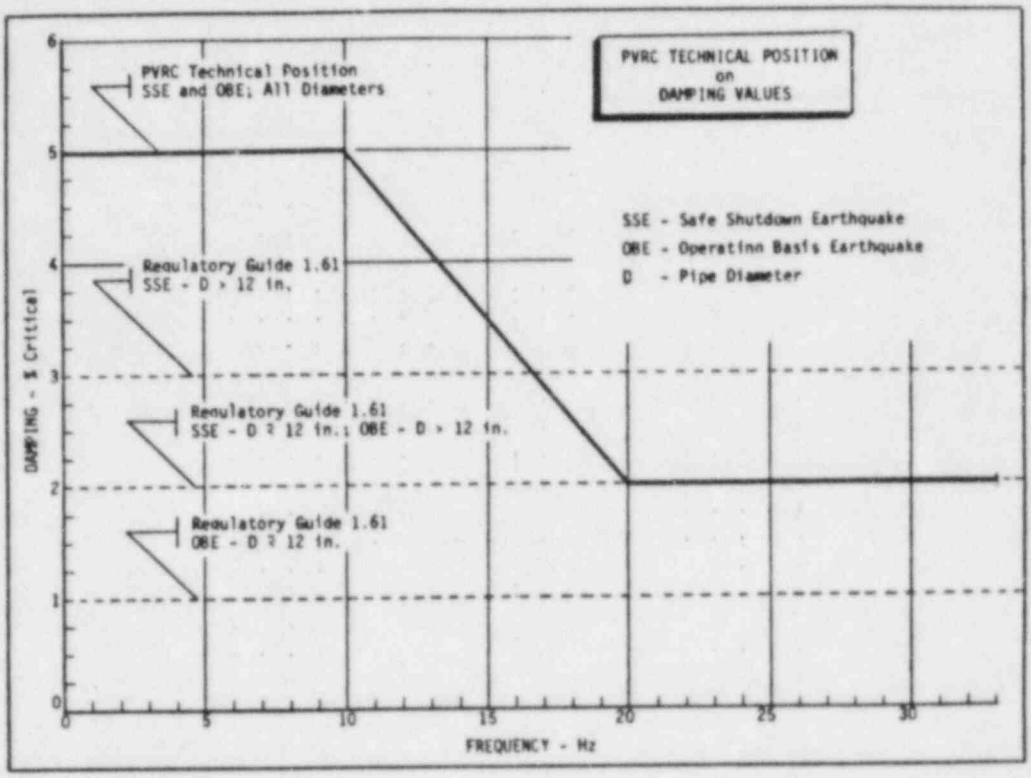

Figure 3 - PVRC Pipe Damping Curve

References

1. NUREG 1061 Volume 1, "Investigation and Evaluation of Stress Corrosion Cracking in Piping of Boiling Water Reactor Plants," August 1984.

2. NUREG 1061 Volume 2, "Evaluation of Seismic Designs - A Review of Seismic Design Requirements for Nuclear Plant Piping," April 1985.

3. NUREG 1061 Volume 3, "Evaluation of Potential for Pipe Breaks, November 1984.

4. NUREG 1061 Volume 4, "Evaluation of Other Dynamic Loads and Load Combinations," December 1984.

5. NUREG 1061 Volume 5, "Summary - Piping Review Committee Conclusions and Recommendations," April 1985.

6. EPRI NP-4210, "Conceptual Study to Develop Revised Dynamic Code Criteria for Nuclear Power Plant Piping," August 1985.

7. Welding Research Council, "Technical Position on Damping Values for Piping--Interim Summary Report," Welding Research Council Bulletin 300, December 1984.

8. "A Survey of Experimentally Determined Damping Values in Nuclear Power Plants", Idaho National Engineering Laboratory, NUREG/CR-2406, November 1981.

9. "Parameters That Influence Damping in Nuclear Power Plant Piping Systems", Idaho National Engineering Laboratory, NUREG/CR-3022, November 1982.

10. "Impact on Changes in Damping and Spectrum Peak Broadening on the Seismic Response of Piping Systems," Lawrence Livermore National Laboratory, UCRL-53491, NUREG/CR-3526, March 1984.

11. "Reliability Analysis of Stiff Versus Flexible Piping," Lawrence Livermore National Laboratory, NUREG/CR-3718, March 1984.

12. "Response Margins of the Dynamic Analysis of Piping Systems", NUREG/CR-3996, October 1984.

13. "Alternate Procedures for Seismic Analysis of Multiply Supported Piping Systems", Brookhaven National Laboratory, NUREG/CR-3811, August 1984.

14. Welding Research Council, Bulletin 297, "Local Stresses in Cylindrical Shells Due to External Loadings on Nozzles - Supplement to WRC Bulletin No. 107," August 1984.

PIPE DAMPING[1]

A. G. Ware
EG&G Idaho, Inc.
Idaho National Engineering Laboratory (INEL)

Studies are being conducted at the Idaho National Engineering Laboratory to determine whether an increase in the damping values used in seismic structural analyses of nuclear piping systems is justified. Increasing the allowable damping would allow fewer piping supports which could lead to safer, more reliable, and less costly piping systems. Test data from available literature were examined to determine the important parameters contributing to piping system damping, and each was investigated in separate-effects tests. From the combined results a world pipe damping data bank was established and multiple regression analyses performed to assess the relative contributions of the various parameters. The program is being extended to determine damping applicable to higher frequency (33 to 100 Hz) fluid-induced loadings. The goals of the program are to establish a methodology for predicting piping system damping and to recommend revised guidelines for the damping values to be included in analyses.

INTRODUCTION

One of the parameters which the structural analyst routinely uses in the dynamic seismic analysis of nuclear power plant piping systems is the structural damping. The damping values are prescribed for the analyst, according to the pipe size and the earthquake level, in Regulatory Guide (RG) 1.61 [1] issued by the U.S. Atomic Energy Commission (AEC), predecessor of the present U.S. Nuclear Regulatory Commission (NRC). At the time of issue of RG 1.61 (1973), the AEC had gathered the best available experimental data on piping system damping values and the opinions of leading experts in the field to establish a set of values which would be easy for the analyst to use and which would be conservative. These values (1 to 3% of critical damping) are generally conservative in that piping system motions are over-predicted so that the resulting calculated stresses are high enough to ensure the system is adequately supported for seismic motions.

---

[1] Work supported by the U.S. Nuclear Regulatory Commission, Office of Nuclear Regulatory Research, under Interagency Agreement DOE 40-550-75 with the U.S. Department of Energy.

Over the years since the issue of RG 1.61, nuclear power plant piping has been designed as relatively stiff systems, employing many seismic supports, to keep the combined stresses due to earthquakes plus other loads below allowable values. These stiff systems are unduly restrained from thermal growth, leading to a greater susceptibility to thermal cracking of the pipe wall due to fatigue. In addition, many systems are supported by snubbers which resist sudden high acceleration seismic motions, but which allow slow thermal movements without resistance. These snubbers are sometimes unreliable, are costly to purchase and install, and require a maintenance program throughout their plant life.

It has been widely recognized that piping systems have a great deal of design margin for dynamic loads. Therefore, a program has been developed by EG&G Idaho, Inc. and the NRC to examine damping values and determine the possibility of revising the present guidelines to reflect current "best estimate" values.

A majority of tests used to establish damping values have been conducted on actual power plant piping systems or on laboratory models of these systems. These systems were fairly complicated and many variables were present which could tend to mask the nature of the damping in the system. In addition, the primary purpose of most of these tests was not to determine the system damping; thus the values of the various parameters needed to assess the contribution of each were not recorded. The scatter in the data is considerable, due to a great extent to the fact that low amplitudes of vibration were used in the tests.

INEL PROGRAM

The pipe damping study program developed at the INEL is directed towards establishing best-estimate values for use in dynamic structural analyses. In order to accomplish this, the available literature on piping system damping was reviewed, the parameters influencing damping were identified, and a program of laboratory separate-effects tests is being carried out. Gaining insights into the physical phenomena causing energy dissipation is a significant step in acquiring the ability to predict damping for a particular set of piping system parameters. This in turn will allow new guidelines to be recommended which will have a solid technical basis.

The INEL program began by examining the damping data available in the published literature [2]. The amount of test data was sparse, there was a great deal of scatter in the results, and significant parameters required to assess the factors influencing damping often were not reported. However, by a qualitative evaluation of the data, the following parameters were identified as being most highly correlated with damping [3]:

1. Supports
2. Amplitude
3. Modal Frequency
4. Insulation.

Subsequently, a test program was developed to examine each of these parameters in more detail. In addition, other potential effects such as pipe size, geometry, pressure, type of excitation, and method of damping calculation are being investigated. The first tests conducted at the INEL were straight sections of 3-inch and 8-inch pipe, approximately 33 feet in length. From these tests, important insights were obtained with respect to the influence of pipe supports and amplitude [4]. In a follow-up test a 5-inch pipe with four elbows is being tested to obtain additional information on the identified parameters. Cooperative testing with other organizations has also been undertaken [5].

The damping test results collected to date have been placed in a world-wide data bank at the INEL. To store as much relevant information as possible and to encourage researchers to record and report the values of parameters which would be of interest to users of the data bank, a standardized form has been developed. This form has been distributed globally to the leading researchers in the field, and their resulting contributions are being cataloged into the data bank. Using this data, multiple regression analyses have been performed in an attempt to quantify the parametric effects. Unfortunately, due primarily to the data scatter and the lack of information on several relevant parameters, only frequency was identified as highly correlated with damping. Both frequency and damping are generally reported for a test and thus the data for these two variables was the most extensive. The regression analysis showed frequency was inversely proportional to damping, especially below 20 Hz. When damping was removed as a variable and replaced by mode number, the regression analysis showed damping was also inversely related to mode number. In addition the damping increased as the piping system length to number of supports ratio decreased. Based partially on the results of a previous regression analyses, a Task Group on Damping of the Pressure Vessel Research Committee (PVRC) recommended the revised damping shown in Figure 1 as an interim position. This curve has been adopted for ad hoc use by the NRC and has been approved as Code Case N-411 of the ASME Boiler and Pressure Vessel Code. The INEL regression analyses used a more extensive data base that was available at the time of the original PVRC recommendations, and confirmed the results of the original PVRC analysis.

PARAMETERS INFLUENCING DAMPING

Based on the literature survey, separate-effects tests, the regression analyses, and intuition, the mechanisms for energy dissipation have been evaluated and explanations for the test results have been developed. A low damping level is inherent in any piping system due to a small material damping and dispersion of energy (radiation damping) through the supports to the environment. This accounts for perhaps less than 1% of critical damping. More major contributions to energy dissipation are the interaction of the supports with the piping through friction and impacting, through material hysteresis damping in the pipe at higher amplitudes (and possibly also in the supports), and through friction between the pipe and its insulation. Each of these effects will be discussed individually.

Supports/Modal Frequency

The regression analyses and visual inspection of the data sets showed that in many (but not all) cases, the damping and modal frequency were inversely proportional. Figure 2 is a curve of a typical data set with this relation. This relation has been questioned by several piping system experts as having no physical basis. Indeed modal frequency itself is not a parameter which can dissipate energy such as can friction, radiation, or impacting; but is merely a function of the geometry and material of the piping system. It is, however, generally measured and reported with each damping value which accounts for its abundance in the data base. In order to assist in resolving this question, the test results from other parameters were examined.

From tests of various types of supports [4], two basic types of energy dissipation are apparent. The first is friction such as between the springs and their housings in spring hangers or in the internal mechanisms of constant force hangers. This friction manifests itself at small strain amplitudes as shown in Figure 3 which is indicative of Coulomb (dry) friction. At higher strain levels the damping becomes fairly constant. The second energy dissipation mechanism of supports is impacting such as occurs in snubbers (both in internal gaps and in connections), rigid struts, and rod hangers. At low amplitudes the weight of the pipe keeps it from exercising the gap in the rod hanger. Once lift-off occurs impact damping takes place within the eye of the rod. At low amplitudes the size of the gap and the relative magnitudes of the gap and the motion within the gap affect damping. Overall, these effects lead to a wide variety of possibilities than can occur at low vibration levels and can change with only a slight pertubation of vibration amplitude. This accounts for much of the scatter in the data, especially the very low strain level data in which hammer taps are the source of the vibration. This makes damping almost impossible to predict at low amplitudes and extrapolation of this data to higher amplitudes is cautioned. However, this does not present as much of a problem as first imagined, since the designer is really looking for damping at OBE and SSE levels, not at very small stress levels.

The INEL tests also proved the relationship of the modes and the energy dissipating supports was an important factor in determining piping system damping. Those modes which interact directly with a support causing frictional or impact energy losses result in high damping. For example, for a straight section of pipe supported only at the ends, the damping was calculated to be less than 1% of critical. When a rod hanger was added at the center, the two lowest modes were an antisymmetric mode in which each half of the pipe pivoted about the rod hanger, and a symmetric mode in which both halves moved in the same direction. In the antisymmetric mode there was minimal interaction between the pipe and the rod hanger; however, for the symmetric mode there was considerable impacting in the eye of the rod. Damping increased to approximately 5% of critical for the second (symmetric) mode but remained less than 1% for the first mode. When a large bolt was used between the pipe clamp and the eye of the rod hanger, eliminating the clearance, the damping returned to less than 1% of critical

for the symmetric mode. When the amplitude was increased, the impacting and damping were also increased for the symmetric mode with a gap while damping still remained unchanged for the antisymmetric mode. These phenomena help explain the frequency effect. Now although this experiment consisted of a contrived laboratory piping geometry where the mode/support relation was such that the damping was smaller in the lower mode due to impacting in the gap, this is not generally the case in nuclear plant piping systems. In a typical geometry, the lower modes of a piping system have a greater probability of interacting with energy dissipating supports than the higher modes in which most of the motion occurs away from supports. Furthermore, the displacements are higher for the lower modes causing greater friction and impacting losses. Thus the regression analysis finding that, in general, damping is inversely proportional to modal frequency is really a manifestation of pipe-support interaction. There will of course be a few cases in which the geometry of the system is such that the lower modes' relation to the supports does not promote increased energy dissipation. This explains why in some cases researchers have not observed a frequency effect.

Amplitude

The discussion on supports/frequency above explained the variations in damping that could occur at low strain amplitudes and why this type behavior would be difficult to predict. However, once strain levels rise above 100 to 200 με, the damping trend becomes easier to characterize. From the 100/200 με to 800/1000 με range the damping is fairly constant and is induced primarily by the supports. At the upper end of this range a threshold is reached in which damping increases with increasing strain amplitude. This threshold coincides approximately with the end of the proportional strain range (Hookes law applies) where the beginning of plastic action begins. Data in the high strain plastic range is sparse since the test usually renders the pipe unsuitable for further use. Obviously, only laboratory tests have been conducted at high strains.

Figure 4 shows the damping trend at high strain amplitudes. These tests were all of straight piping sections with no typical supports. Thus only material damping is present. If supports were added, even greater damping might be present from the impact effects and material hysteresis in the supports themselves. An important point to note is that from above a threshold strain, damping increases almost linearly to 10-12% of critical at 2000 με which is often quoted as the yield strain of a material. From the data it appears that at large strains, the damping will increase to a considerable value. Consequently, the forces required to make the pipe deform further must become very large, and a resonance buildup of amplitude is severly inhibited. It is thus doubtful that pipe failure could occur due to inertial bending caused by seismic excitation. Now, the basic characteristic of an ASME Boiler and Pressure Vessel Code primary stress is that it is not self-limiting, whereas the increased damping at large strain amplitudes limits the inertia bending stresses in pipe sections. Therefore, the plastic stresses caused by low cycle seismic effects might

in this sense be considered ASME secondary stresses. Of course the stress amplitude range and fatigue usage remain important, and line-mounted equipment such as valves must be adequately supported.

More high strain data is needed to fill in the gaps in knowledge of damping behavior in this region. Of particular importance is the effect bends/elbows and/or supports would have on high strain damping. One such test on a 5-inch system is presently being conducted at the INEL.

Insulation

Insulation produces two effects on the piping system. It adds mass and it dissipates energy by slippage against the piping. Intuitively, the larger the mass of insulation, the greater the frictional force resisting dynamic slippage between the pipe and insulation and thus higher energy dissipation. A few studies have been conducted in Japan and Germany which have concluded that insulation increases damping. By far the most comprehensive program evaluating the effect of insulation on damping has been by the Westinghouse Hanford Energy Development Laboratory (HEDL) which has focused on LMFBR type insulation. The typical LMFBR insulation ratio (IR), which is the weight of the insulation divided by the total weight of the piping system, is much larger than for light water reactor (LWR) piping systems. The HEDL study concluded that damping increased with increasing IR. A comparison of damping test results for uninsulated and insulated (IR=0.07 calcium silicate) conditions on a 5-inch piping system is currently being conducted at the INEL.

CONCLUSION

A program of testing and data evaluation is being carried out at the INEL to understand the physical nature of piping system damping and to recommend changes to current allowable values use in dynamic analyses. To most accurately predict piping system damping would require a computer code which would account for the piping geometry, location and type of supports, interaction of each mode with supports, and strain amplitude. This would be an interactive process which would be too complicated and costly to fully carry out at present. A simpler method is required. The PVRC curve in Figure 1 is a first step in removing some of the conservatism in piping analysis. The frequency effect of this curve takes into account the increased interaction with supports at the lower modes. With the knowledge gained to date, a better model which contains more parameters that influence piping system damping will be able to be proposed through the INEL program. With continued research, each subsequent iteration of the model can possibly produce more accurate prediction methods.

REFERENCES

[1] U.S. Atomic Energy Commission, "Damping Values for Seismic Design of Nuclear Power Plants," Regulatory Guide 1.61, October 1973.

[2] A. G. Ware, A Survey of Experimentally Determined Damping Values in Nuclear Power Plant Piping Systems, NUREG/CR-2406, EGG-2143, EG&G Idaho, Inc., November 1981.

[3] A. G. Ware, Parameters that Influence Damping in Nuclear Power Plant Piping Systems, NUREG/CR-3022, EGG-2232, EG&G Idaho, Inc., November 1982.

[4] A. G. Ware and G. L. Thinnes, Damping Results for Straight Sections of 3-in. and 8-in. Unpressurized Pipes, NUREG/CR-3722, EGG-2305, EG&G Idaho, Inc., April 1984.

[5] J. G. Arendts, A. G. Ware, Tests to Determine How Support Type and Excitation Source Influence Pipe Damping, NUREG/CR-3942, EGG-2337, EG&G Idaho, Inc., September 1984.

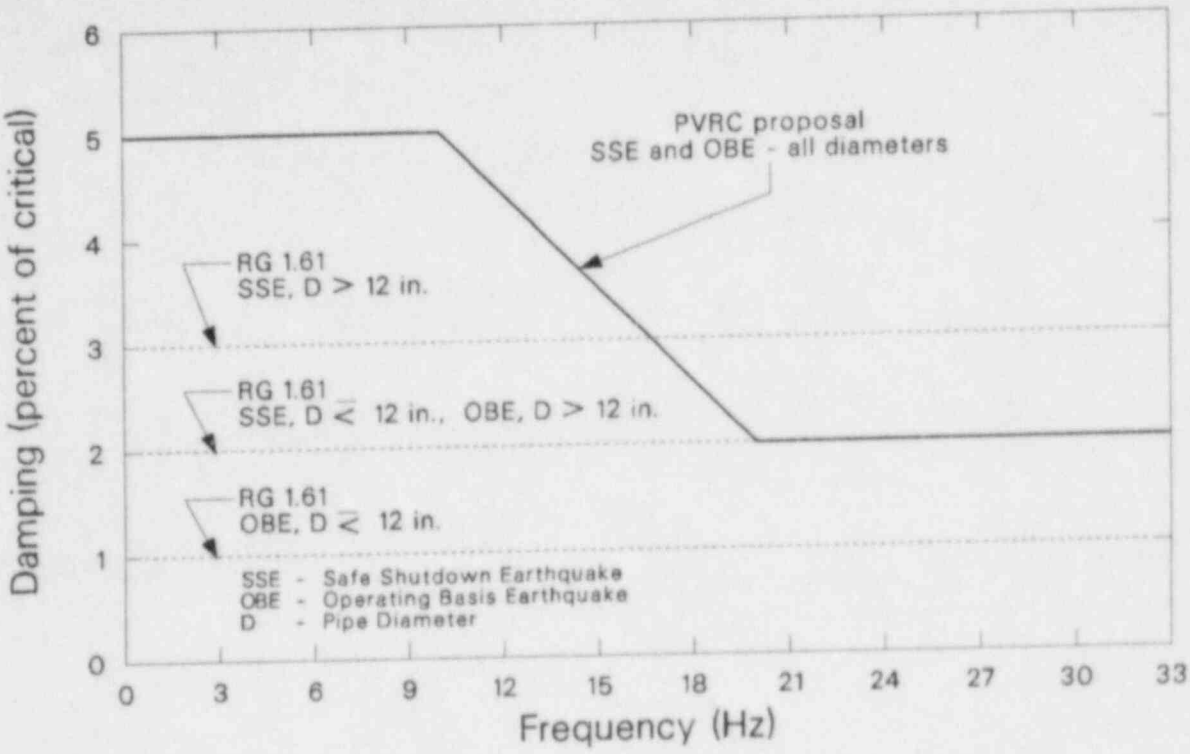

Figure 1. PVRC damping.

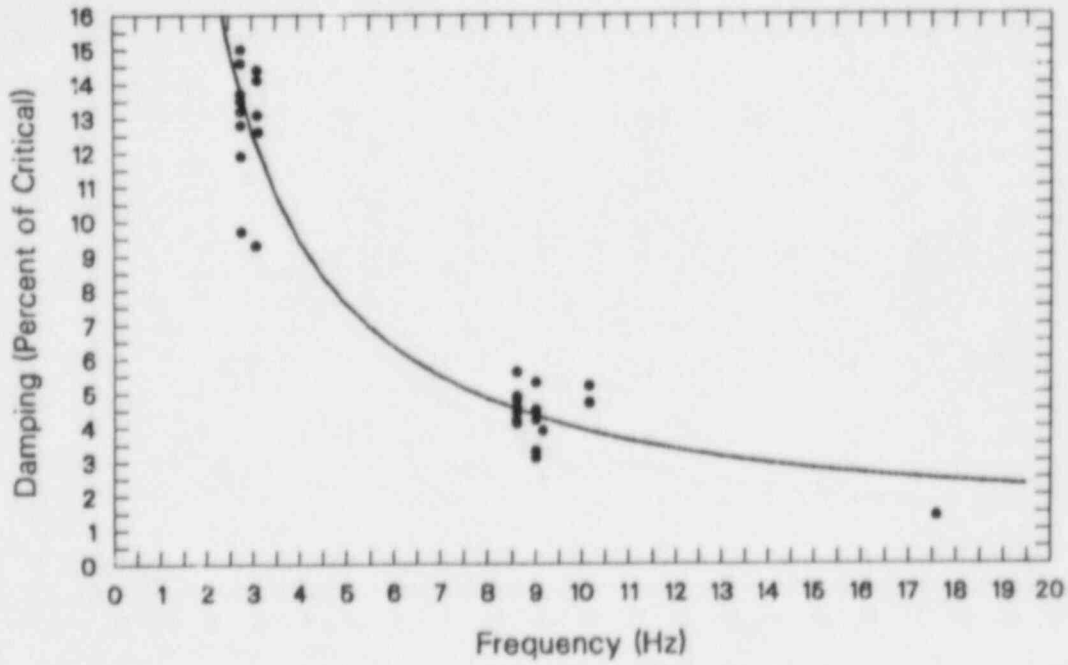

Figure 2. Typical frequency dependent data.

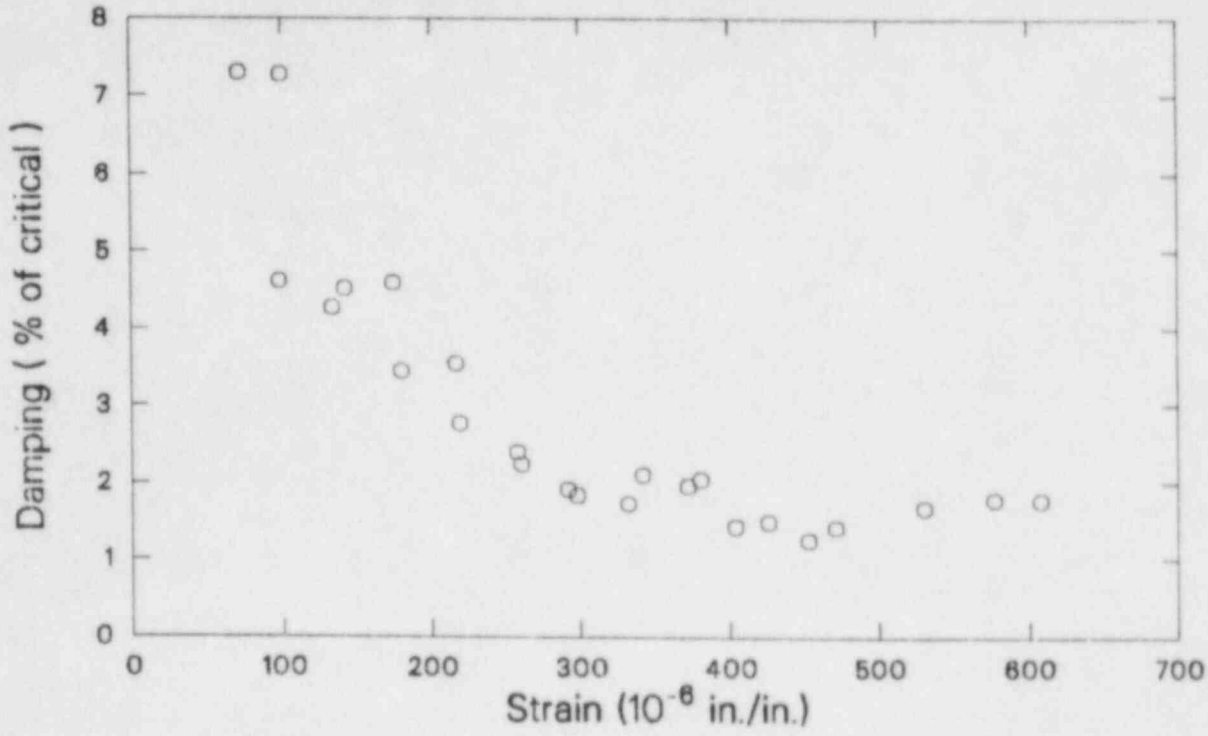

Figure 3. Low strain damping trends.

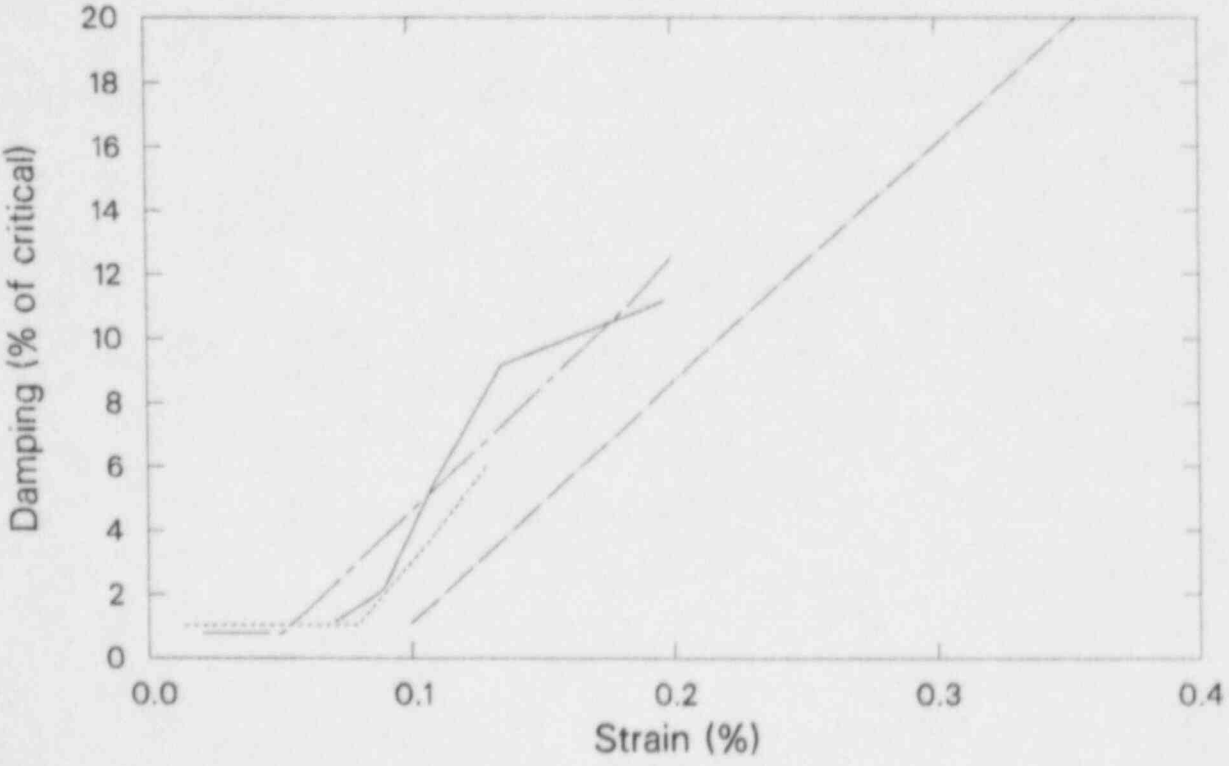

Figure 4. High strain damping trends.

BNL PIPING RESEARCH

P. Bezler, M. Subudhi, and Y.K. Wang and S. Shteyngart
Brookhaven National Laboaratory

Abstract

Brookhaven National Laboratory (BNL) has assisted in the development of methods to evaluate the analysis methods used by industry to qualify nuclear power piping. Through FY 1985 these efforts were conducted under the Mechanical Piping Benchmarks project while current and future efforts will be performed under the Combination Procedures for Piping project. Under these projects BNL has developed analytical benchmark problems for piping systems evaluated using uniform or independent support motion response spectrum methods, investigated the adequacy and limitations of linear piping analysis methods by comparison to test results and evaluated and developed criteria for new and alternate methods of analysis. A summary description of the status of these efforts is provided.

1. INTRODUCTION

The Structural Analysis Division of the Department of Nuclear Energy at the Brookhaven National Laboratory (BNL) has and continues to perform various research tasks relating to piping analysis for the U.S. Nuclear Regulatory Commission (USNRC). Until the current period the BNL efforts were funded under the Mechanical Piping Benchmarks Project monitored by J. O'Brien of the USNRC. The current and future efforts are funded under the project entitled, "Combination Procedures for Piping Response Spectra Analysis monitored by D. Guzy of the USNRC.

The BNL research efforts may be broadly characterized into three areas; the development of benchmark problems and solutions suitable for the verification of applicant piping analysis methods, the investigation of the adequacy of linear analysis methods by the comparison of analysis and test results for piping (Physical Benchmarking) and the evaluation of new and alternate methods for the dynamic analysis of piping systems. At present, the benchmarking efforts, both analytical and physical, have ceased, each having satisfied the funded project goals under the Mechanical Piping Benchmarks project. The investigation of new and alternate analysis methods continues under the second project. A summary description of the three research areas follows.

Work performed under the auspices of the U.S. Nuclear Regulatory Commission.

2. PHYSICAL BENCHMARK PROBLEMS

The benchmark problems and solutions developed to verify applicant piping analysis methods are published in the Piping Benchmark Problems Report Series [1,2]. Although it was anticipated that there would be five volumes in the report series, only the first two volumes have been issued to date. In the current period the second volume [2] of the series entitled, "Piping Benchmark Problems, Dynamic Analysis, Independent Support Motion, Response Spectrum Method", was issued. In the report, four benchmark problems and solutions developed for verifying the adequacy of computer programs used for the dynamic analysis and design of elastic piping systems by the independent support motion (ISM), response spectrum method are presented. The dynamic loading is represented by distinct sets of support excitation spectra assumed to be induced by non-uniform excitation in three spatial directions. Complete input descriptions for each problem are provided and the solutions include predicted natural frequencies, participation factors, nodal displacements and element forces for independent support excitation and also for uniform envelope spectrum excitation. Solutions to the associated anchor point pseudo-static displacements are not included.

All solutions were developed using the finite element code PSAFE2 [3]. In each solution combination over group contributions was performed first, followed by SRSS interspatial combination, followed by SRSS intermodal combination without the consideration of closely spaced frequencies. For the ISM solutions both absolute and SRSS combination between support group contributions were considered where a support group was defined as all supports exhibiting the same motion. Figure 1 shows the finite element grid for the third benchmark problem which involved 54 pipe elements and four distinct support groups.

3. Physical Benchmarks

The basic premise of the physical benchmarking effort is that the relative accuracy of computational methods can be gauged by the direct comparison of physical test results to the analytical predictions of those results. In the effort a total of six evaluations were performed involving simple and complex laboratory tested systems and actual power plant systems tested in situ. In all cases the evaluations were performed after the test programs, conducted by others, were completed. Each evaluation, except one, was performed blind with only the measured inputs provided at the time of analysis and the measured response data made available for comparison after the analyses were complete. After evaluation no attempts to improve the results with refined analyses was undertaken.

A description of each of the piping systems evaluated, with a summary of the key results, is provided in Table 1. Detailed descriptions of each evaluation are provided in References 4-7 while examples of typical results are shown in Figures 2-4 and Table 2.

A sketch of the Main Pipeline [7] is shown in Figure 2. The system was totally supported and excited by actuators located at positions S1 through S4. For the test simulated the actuators imposed nearly in phase, seismic like excitation of the system in the X coordinate direction. The measured and computed natural frequencies for the system are shown in Table 2. A review of this data indicates that the correspondence was good and this level of agreement for frequencies was typical in the evaluations. An example of good agreement between the predicted and measured acceleration response for an interior point is shown in Figure 3. The figure shows predicted and measured time history traces of the acceleration in the X coordinate direction of a point in the vicinity of the valve. An example of poor agreement between predicted and measured response is shown in Figure 4. These are the accelerations in the Z coordinate direction of a point located on the uppermost horizontal run. Good agreement for responses in the direction of excitation X direction, and poor agreement for responses in the unexcited directions was typical for this evaluations. The poor correspondence for the unexcited directions was attributed to the failure to monitor and therefore simulate in the analysis the input motions in the directions orthogonal to the actuators.

In summary, the linear analysis methods were found to provide reasonable estimates of system response. The estimates for system natural frequencies were good while the estimates for displacements and accelerations ranged from poor to good. For a near linear system and using conservative estimates for system damping good correlation of response traces and acceptable estimates of response peaks can be expected. Using realistic estimates of uniform system damping large underestimates of peak response components were observed and deviations of 100% or greater should be expected.

4. Alternate Analysis Methods

Standard practice to qualify piping for dynamic events is to perform a response spectrum analysis of the system assuming uniform excitation of all supports to the envelope spectrum level coupled with a conservative estiamte of the additional responses associated with differential support point movement [8]. For systems subjected to multiple independent support motions a modified response spectrum procedure which allows the use of separate response spectra for each support group seems more appropriate. To assist the USNRC in its evaluation of the Independent Support Motion (ISM) response spectrum method BNL undertook an evaluation of ISM methods and the associated computation of anchor movement (pseudo-static) response. The evaluation was performed under the Mechanical Piping Benchmarks project and involved a consideration of systems exhibiting uniform damping only. An extension of the evaluation for systems exhibiting frequency dependent (PVRC) damping is currently being performed under the project monitored by D. Guzy.

To predict the dynamic component of response a response spectrum method which allows the use of independent spectra sets for each support or group of supports was evaluated. In this method a response parameter is predicted as a function of each support group for each mode and each direction of excitation.

To obtain the total dynamic response a combination over groups, modes and directions must be performed. In this evaluation the square root of the sum of the squares (SRSS) combination over directions and SRSS combination with clustering for closely spaced modes were accepted for the combination over directions and modes. For the combination over groups algebraic (methods 1 and 2), SRSS (Methods 3-8) and absolute (methods 9-14) combination were considered. Further all sequences of performing these combinations were considered. In all fourteen different combination strategies, methods 1-14 were evaluated for the computation of the dynamic component of response.

To predict the SAM component of response five procedures were evaluated. Four of these were based on the use of absolute peak support displacement data. These methods differed in the manner in which the supports were grouped to account for the unknown phasing between supports. The grouping assumptions considered were random phasing (method 2), grouping by global direction (method 3), grouping by attachment point (method 4) and grouping by elevation (method 5). Within each group support effects were summed algebraically. Between groups both SRSS and absolute summation were considered. The remaining method evaluated (method 1) was based on sampling the support point displacement time history records. Since in this method support point phasing information is retained, no grouping assumptions were made.

To compute the total component of response, both SRSS and absolute combination between the dynamic and SAM components were considered. The response parameters computed included pipe displacements, accelerations, support forces and resultant moments. At each stage the predicted response estimates were compared to response estimates developed using ISM time history methods which were assumed to represent the true response. The relative approach of each predicted value to the time history result was expressed as a degree of exceedance given by Predicted-TH/TH (TH = time history).

The evaluations were performed for five different piping-structure problems. The salient characteristics for each problem are summarized in Table 3. To provide a statistical basis to the study the evaluations for two of the problems, the AFW model and the RHR model, were performed for thirty-three different seismic events. For these the time history results were provided by an alternate NRC contractor.

All study results are summarized in tabular form. Each table lists the time history estimate as well as the response estimate for each calculational option and parameter studied. For the two problems involving thirty-three seismic events the pertinent results are summarized in figure form. Figures 3 and 4 show these results for resultant moments in the RHR problem. Figure 3 corresponds to the dynamic component while Figure 4 corresponds to the SAM component. Each figure shows the mean (data point) $\pm$ one standard deviation (line extent) for the parameter over the thirty-three seismic events. The figures show the results only for those elements which establish the lower bound of degree of exceedance (define the minimum level of conservatism). A comprehensive presentation of the results is provided in Reference 9.

At the completion of the study the following recommendations were advanced:

Dynamic Component of Response

The independent support motion response spectrum method should be certified as acceptable for the evaluation of the dynamic component of response.

SRSS combination between support group contributions should be adopted in the independent support motion response spectrum analysis.

Pseudo-Static Component of Response

For displacements, pipe moments and support forces:

Method 5 (grouping by elevations) with absolute combination between groups should be used for preliminary design.

Method 4 (grouping by attachment points) with absolute combination between groups should be used for final design.

For accelerations:

Absolute combination between support groups should be adopted.

Combined Response

SRSS combination between the dynamic and static components of the response should be adopted.

As mentioned, BNL is currently extending the evaluation of ISM methods to consider the effect of PVRC damping. Pending tasks also include the evaluation of proposed modal combination methods accounting for closely spaced modes, frequency dependent effects and an investigation of the impact of correlation between inputs on the combination rules recommended for the ISM method.

5. REFERENCES

1. Bezler, P., Hartzman, M. and Reich, M., "Piping Benchmark Problems, Dynamic Analysis Uniform Support Motion Response Spectrum Method", NUREG/CR-1677, Vol. 1, August 1970.

2. Bezler, P., Subudhi, M. and Hartzman, M., "Piping Benchmark Problems, Dynamic Analysis Independent Support Motion Response Spectrum Method", NUREG/CR-1677, Vol. II, August 1985.

3. Subudhi, M. and Bezler, P., "PSAFE - Piping Analysis Program - User's Manual - Version 1981", Informal Report, July 1981.

4. Bezler, P., Subudhi, M. and Shteyngart, S., "In Situ and Laboratory Benchmarking of Computer Codes Used for Dynamic Response Predictions of Nuclear Reactor Piping", NUREG/CR-3340, May 1983.

5. Bezler, P. and Subudhi, M., "Corroboration of Heissdampfreaktor Reactor Recirculation Loop Piping Investigations", BNL-NUREG-31732, August 1982.

6. Bezler, P., Subudhi, M. and Shteyngart, S., "Physical Benchmark Evaluation, Extended Z-Bend", BNL-NUREG-34354, February 1984.

7. Bezler, P., Subudhi, M., Shteyngart, S. and Wang, Y.K., "Conclusion and Summary Report on Physical Benchmarking of Piping Systems", NUREG/CR-4291, June 1985.

8. U.S. Nuclear Regulatory Commission, "Dynamic Testing and Analysis of Systems, Components and Equipment", Standard Review Plan, NUREG-0800, Section 3.9.2.

9. Subudhi, M., Bezler, P., Wang, Y.K. and Alforque, R., "Alternate Procedures for the Seismic Analysis of Multiply Supported Piping Systems", NUREG/CR-3811, May 1984.

Table 1
Physical Benchmark Evaluations

System	System Description	Input Excitation	Comments and Results
Z Bend	Planar configuration of 4" pipe supported from and excited by three hydraulic actuators	Laboratory tested with independent seismic excitations of each actuator	Results good except in vicinity of central actuator. Poor results here attributed to existence of a clearance gap at central actuator
Indian Point Rigid Strut Configuration	Segment of boiler feed system of shutdown Indian Pt. Unit 1 power plant. 8 in, sch 80 pipe approx. 100 ft. long supported with rigid struts	In situ, snap back test	Results poor. Correlation good for maximum responses, poor everywhere else. Poor results attributed to the approximations used to model supports
HDR-URL Piping	Recirculation loop of shutdown Heissdampfreactor. 450 and 350 mm piping with two pumps and four valves	In situ explosive, 5 Kg blast in near field	Results poor. Correlation good for peak responses. Poor results attributed to the use of linear analysis methods to model a system with strongly nonlinear support elements
Extended Z Bend	Z Bend configuration redesigned to eliminate all clearance gaps	Laboratory tested with independent seismic excitations of each actuator	Results fair. Estimates of displacements good. Estimates of accelerations ranged from good to poor.

Table 1 (Cont'd)
Physical Benchmark Evaluations

System	System Description	Input Excitation	Comments and Results
Main Pipeline	Three-dimensional configuration of 8" and 6" pipe supported from 4 hydraulic actuators located at ends and two interior points	Laboratory tested with independent seismic excitations of each actuator	Results fair. Better for displacements and accelerations in direction of excitation. Peak responses underestimated. Deviations attributed to boundary element effects.
Main Pipeline with Branches	As above with two 3" lines branched from main line. Supported from 4 end point and one interior point hydraulic actuators.	Laboratory tested with independent seismic excitations of each actuator	Results fair/poor. Correlation for response in directions orthogonal to excitation poor. Peak responses underestimated. Poor correlation attributed to failure to monitor and therefore simulate dominant inputs.

TABLE 2

Predicted and Measured Natural Frequencies for Main Pipeline.

Mode No.	Predicted Hz	Measured Hz
1	4.45	4.62
2	7.24	7.11
3	9.08	9.16
4	11.45	11.66
5	13.79	13.54
6	18.01	17.71
7	18.77	18.53
8	20.46	23.94
9	25.21	25.87
10	26.72	28.06

Table 3 Model Parameters

Model	Structure	No. of Equations	Pipe Size	Pipes Frequencies 1st, 2nd	No. of Support Groups	No. of Seismic Events	No. of Modes Used	No. of Moments	No. of Support Forces	No. of Disp./Accel. Parameters
RHR	Zion (3D)	423	8", 12"	3.86, 8.11	9	33	18	22	15	17 x 3
AFW	Zion (3D)	945	3", 16"	2.86, 3.76	15	33	37	23	28	21 x 3
Z-Bend	ANCO Test (3D)	204	4"	8.67, 17.42	3	1	10	39	16	34 x 3
BM 1	PWR (3D)	336	2", 6"	5.05, 14.63	5	1	15	55	32	56 x 3
BM 2	BWR (Stick)	336	2", 6"	5.05, 14.63	4	1	15	55	32	56 x 3
BM 3	Test Reactor	228	3", 4", 8"	2.91, 4.39	2	1	23	37	30	38 x 3

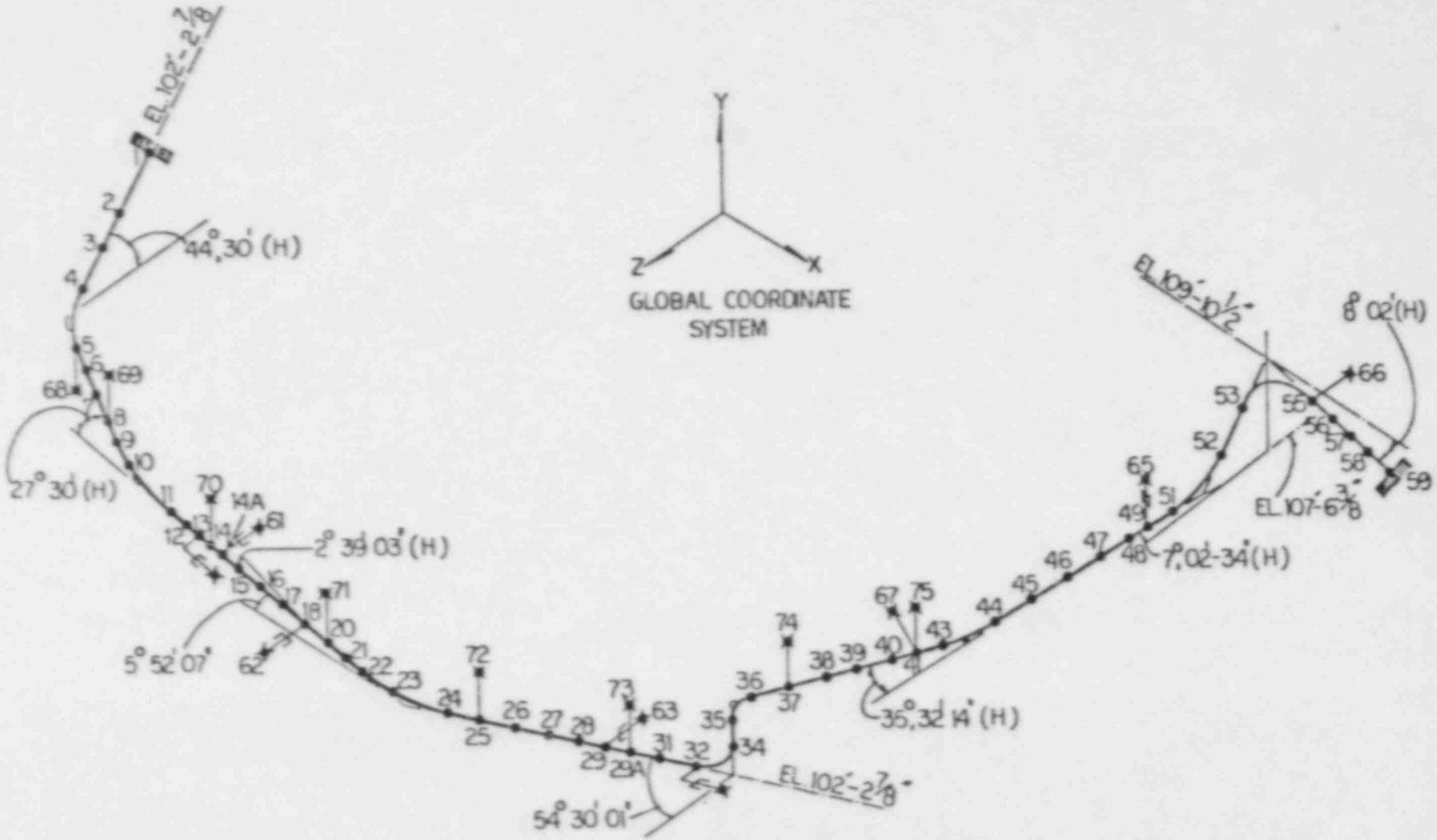

BENCHMARK PROBLEM NO. 3

Figure 1

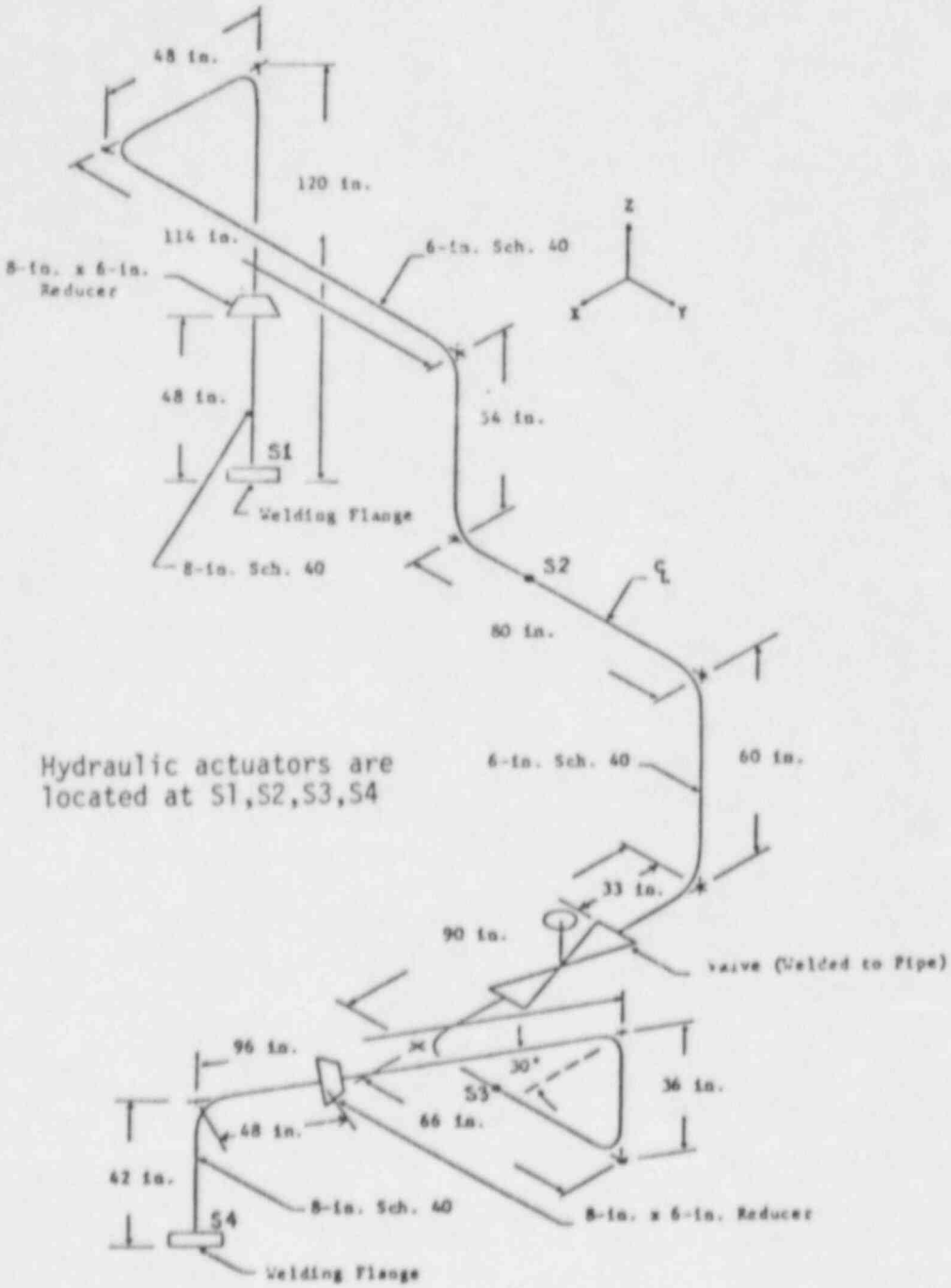

Fig. 2 Main Pipeline

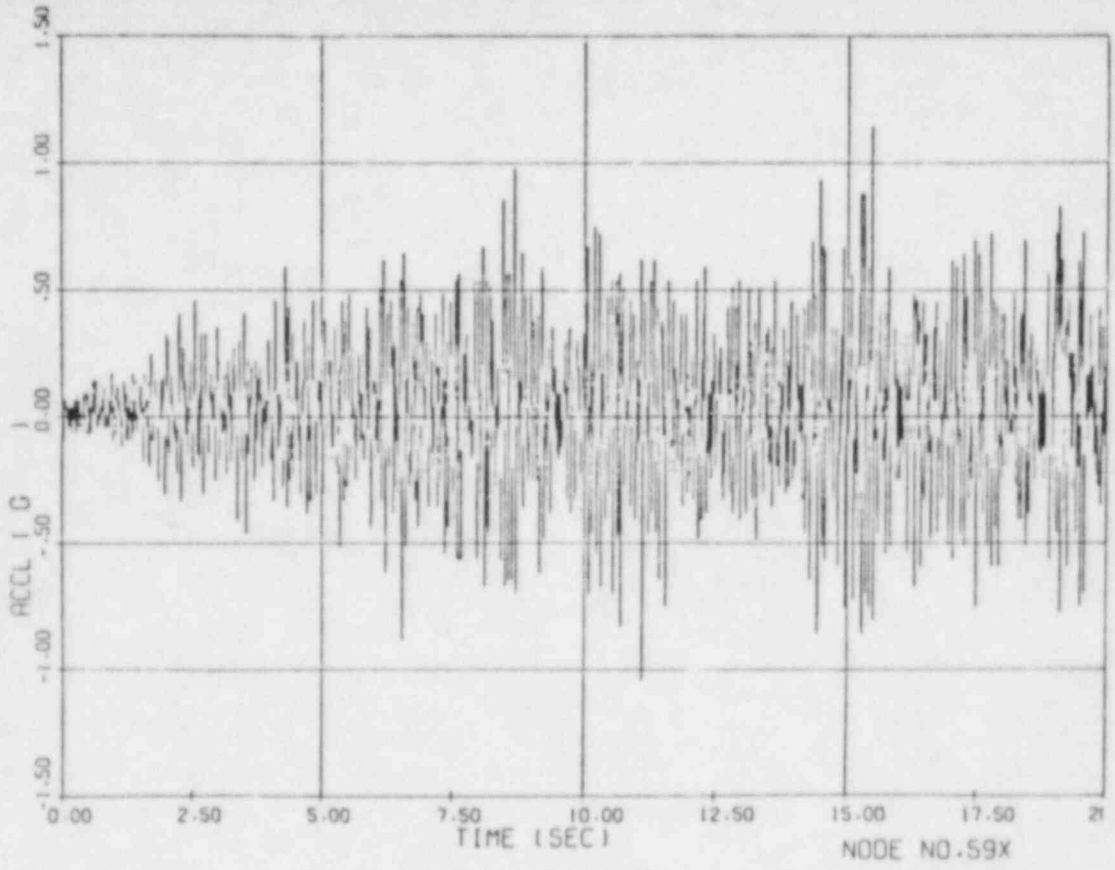

Experimental

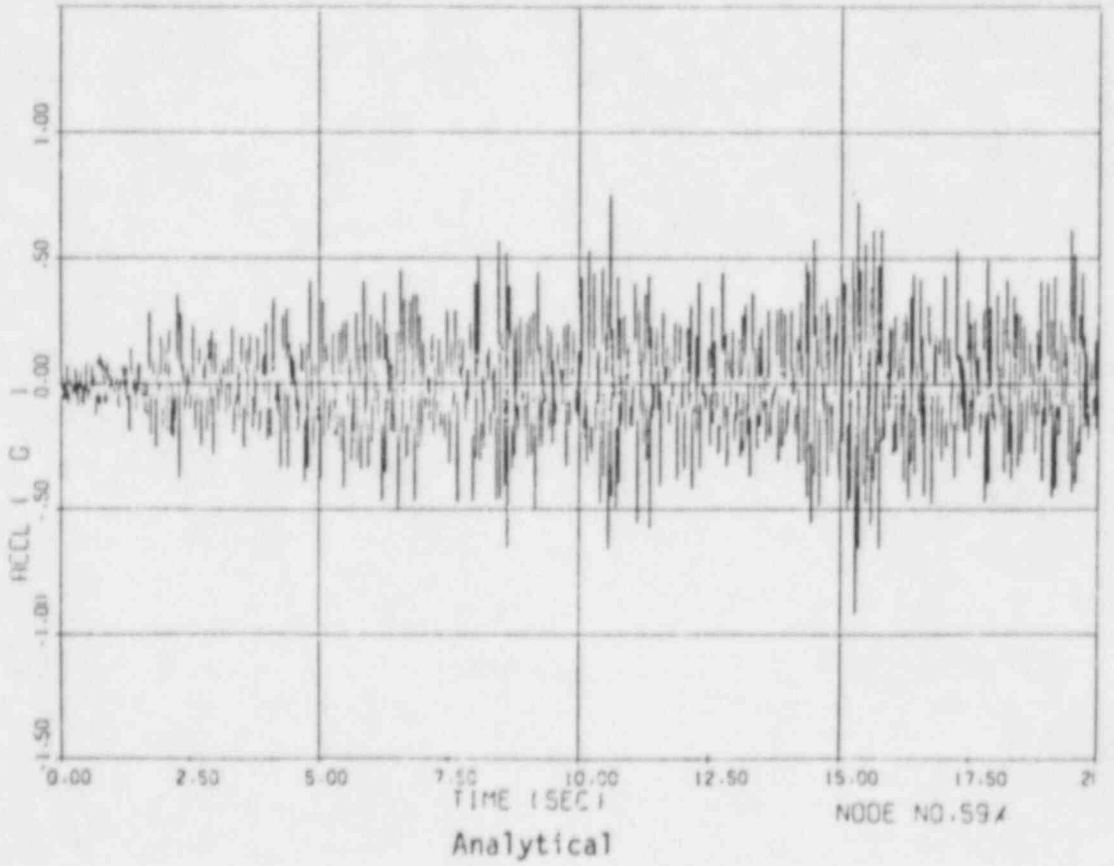

Analytical

Fig. 3 Acceleration Response, Main Pipeline Node No. 59X

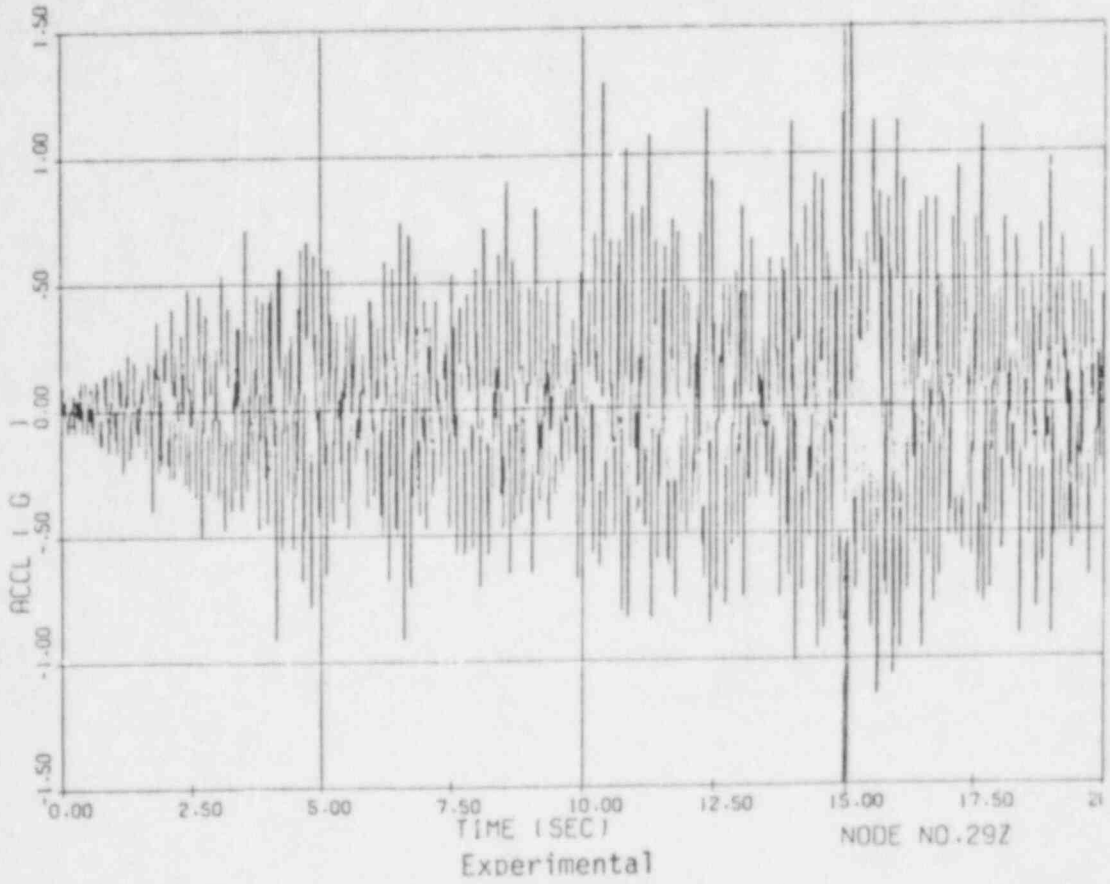

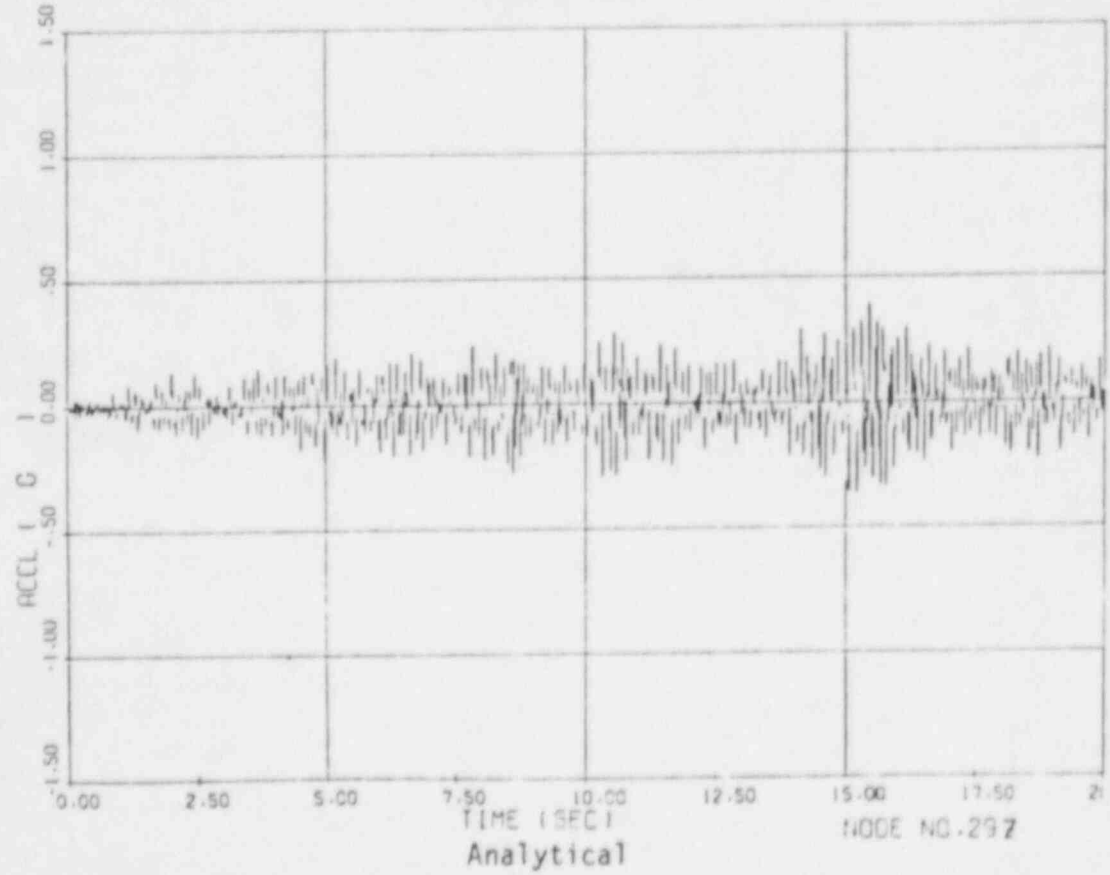

Fig. 4 Acceleration Response, Main Pipeline Node No. 29Z

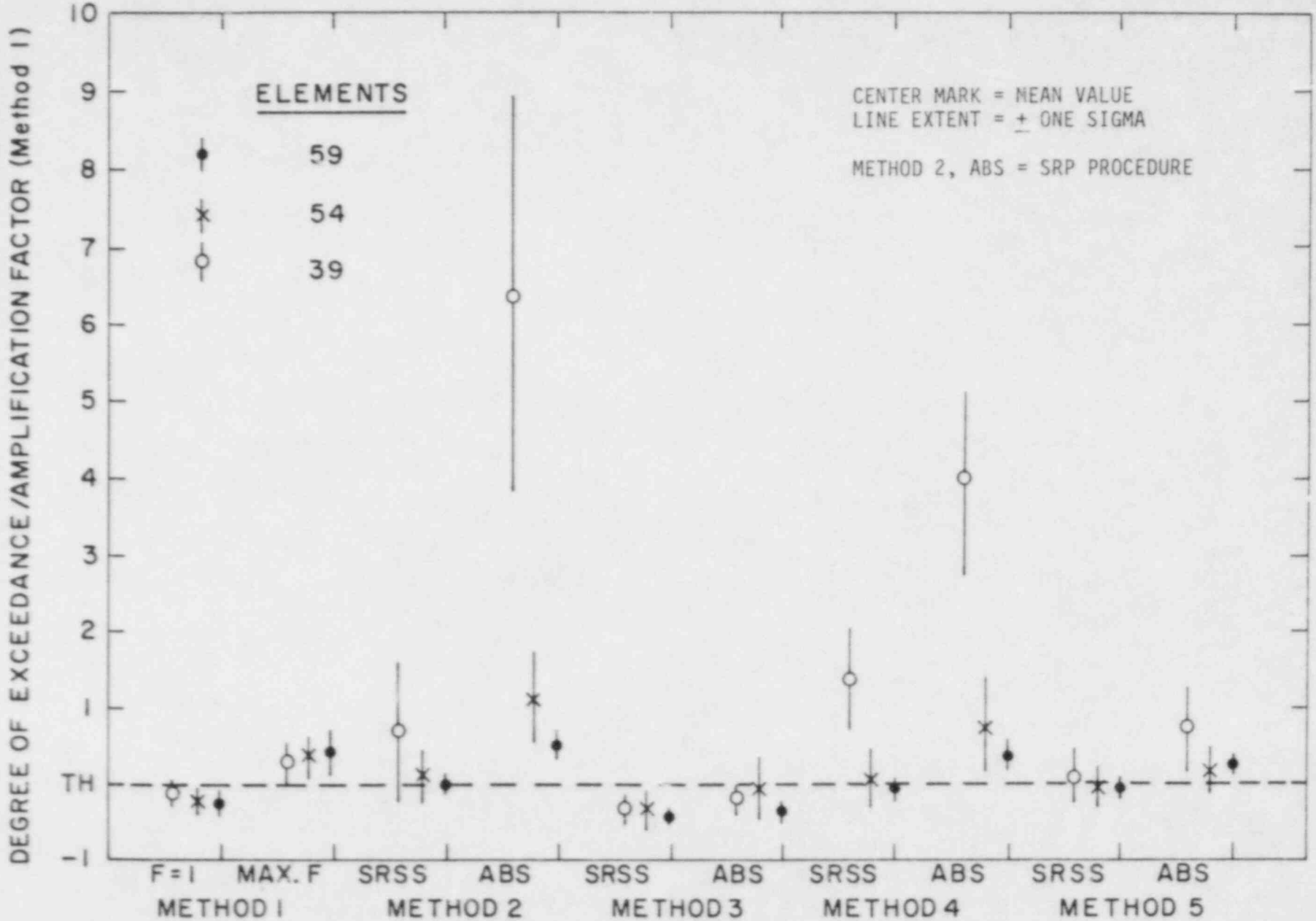

Figure 5 - Static Pipe Resultant Moment Responses for RHR Model

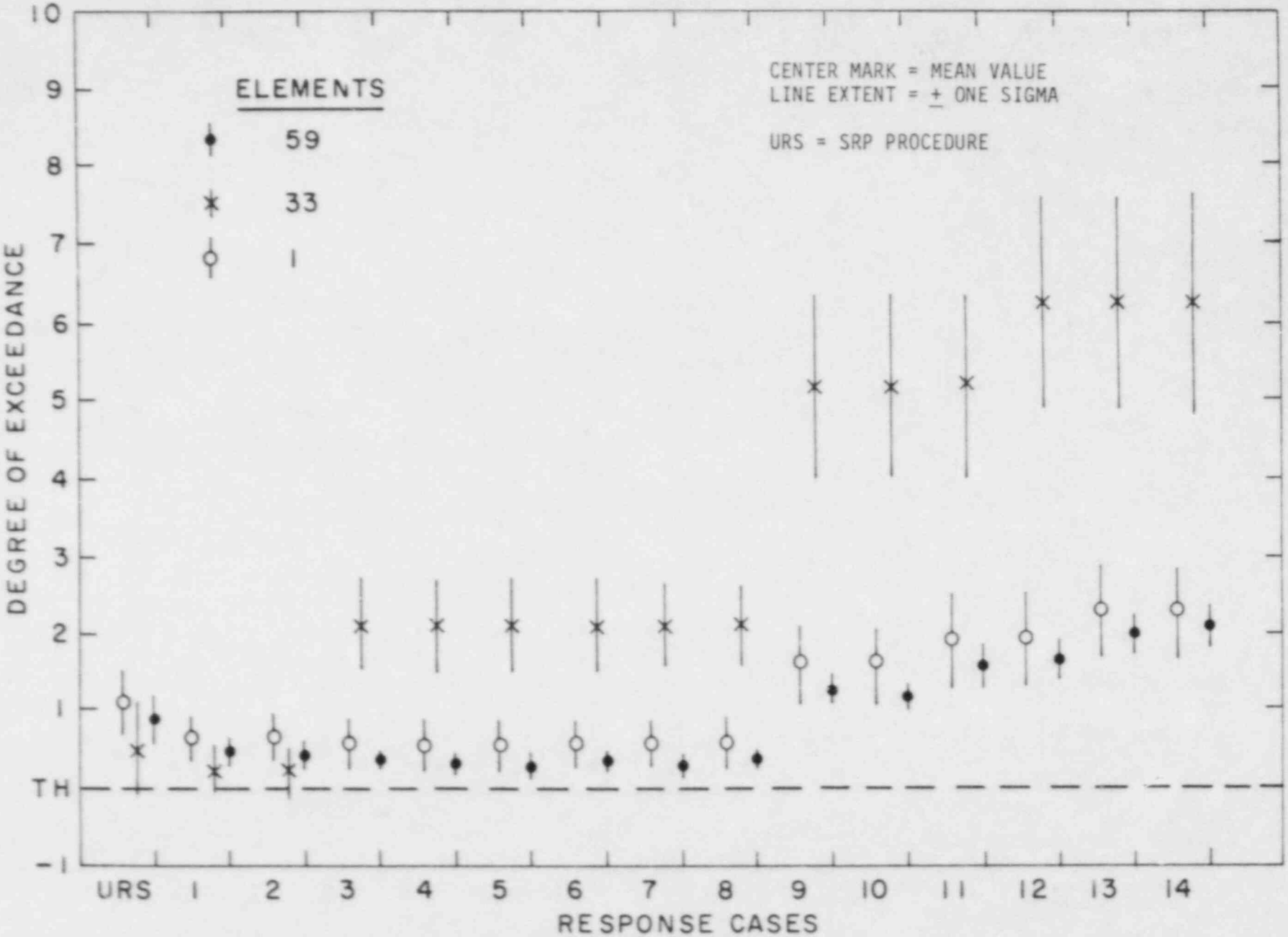

Figure 6 - Dynamic Pipe Resultant Moment Responses for RHR Model

PIPE RUPTURES IN BWR PLANTS*

G. Holman, T. Lo, and C. K. Chou

Lawrence Livermore National Laboratory
University of California
P. O. Box 808, Livermore, California 94550

ABSTRACT

The U. S. Nuclear Regulatory Commission is reevaluating current design criteria for light water reactor plants that require postulation of a double-ended guillotine break (DEGB) in reactor coolant piping. In support of this reevaluation, the Lawrence Livermore National Laboratory has estimated the probability of occurrence of a DEGB, and has assessed the effect that earthquakes have on DEGB. The results of prior LLNL evaluations indicated that the probability of DEGB is very low in PWR reactor coolant loop piping, suggesting that reactor coolant loop DEGB could be eliminated as a basis for plant design. This report describes a probabilistic evaluation of recirculation, main steam, and feedwater piping in boiling water reactor plants. As in the earlier PWR evaluations, two causes of pipe break are considered: pipe fracture due to the growth of cracks at welded joints ("direct" DEGB) and pipe rupture caused by the seismically-induced failure of heavy component supports ("indirect" DEGB). The probability of direct DEGB was estimated using a probabilistic fracture mechanics model. The probability of indirect DEGB was estimated by convolving seismic hazard and heavy component support fragility. Two additional factors not applicable to PWR reactor coolant loop piping -- intergranular stress corrosion cracking and pipe support fragility -- were considered in the BWR study. The results of this study indicate that the probability of DEGB is very low for all three piping systems, except for recirculation piping when IGSCC is a factor in which case IGSCC dominates the probability of failure.

1. Introduction

The Lawrence Livermore National Laboratory (LLNL), through its Nuclear Systems Safety Program, has performed probabilistic reliability analyses of PWR and BWR reactor coolant piping for the NRC Office of Nuclear Regulatory Research. Specifically, LLNL has estimated the probability of a double-ended guillotine break (DEGB) in the reactor coolant loop piping of PWR plants, and in the main steam, feedwater, and recirculation piping of BWR plants. For these piping systems, the results of these investigations provide NRC with one technical basis on which to:

(1) reevaluate the current general design requirement that DEGB be assumed in the design of nuclear power plant structures, systems, and components against the effects of postulated pipe breaks.

---

* "This work was supported by the United States Nuclear Regulatory Commission under a Memorandum of Understanding with the United States Department of Energy."

(2) determine if the earthquake could induce the DEGB and thus reevaluate the current design requirement that pipe break loads be combined with those resulting from a safety shutdown earthquake (SSE).

(3) make licensing decisions concerning the replacement, upgrading, or redesign of piping systems, or addressing such issues as the need for pipe whip restraints on reactor coolant piping.

In estimating the probability of DEGB, LLNL considers two causes of pipe break; pipe fracture due to the growth of cracks at welded joints ("direct" DEGB) and pipe rupture indirectly caused by the seismically-induced failure of critical supports or equipment ("indirect" DEGB).

Although these investigations have been limited to the specific piping systems mentioned earlier, the techniques used to assess piping reliability are sufficiently general that they could be conveniently applied to other piping systems with little or no modification.

2. General Approach

Generic evaluations of reactor coolant loop piping have been completed for PWR nuclear steam supply systems manufactured by Westinghouse, Combustion Engineering, and Babcock & Wilcox. In these evaluations, LLNL performed the following:

(1) estimated the probability of direct DEGB taking into account such contributing factors as the initial size (depth and length) of pre-existing fabrication flaws, pipe stresses due to normal operation and sudden extreme loads (such as earthquakes), the crack growth characteristics of pipe materials, and the capability to detect cracks or to detect a leak if a crack were to penetrate the pipe wall. To accomplish this LLNL developed a probabilistic fracture mechanics model using Monte Carlo simulation techniques, implemented in the PRAISE (Piping Reliability Analysis Including Seismic Events) computer code.

(2) estimated the probability of indirect DEGB by identifying critical supports or equipment whose failure could result in pipe break, determining the seismic "fragility" (relationship between seismic response and probability of failure) of each, and then combining this result with the probability that an earthquake occurs producing a certain level of excitation ("seismic hazard").

(3) for both causes of DEGB, performed sensitivity studies to identify key parameters affecting the probability of pipe break.

(4) for both causes of DEGB, performed uncertainty studies to quantify how uncertainties in input data affect the uncertainty in the final estimated probability of pipe break.

The results of these evaluations consistently indicated that the probability of a DEGB in PWR reactor coolant loop piping is extremely small, about 10^{-7} events per reactor-year from indirect causes, and less than 10^{-10} events per reactor-year from direct causes. It

was also found that thermal stresses dominated the probability of direct DEGB, and that earthquakes contributed only negligibly. These results suggest that the DEGB design requirement -- and with it related design issues such as coupling of DEGB and SSE loads, asymmetric blowdown and the need to install pipe whip restraints -- warrants a reevaluation for PWR reactor coolant loop piping. Details of these investigations have been extensively documents elsewhere [1,2,3,4] and will not be discussed here except as they relate to the BWR study.

The objectives and approach of the BWR study have been essentially the same except that different dominant failure mechanisms were added. LLNL has so far limited its investigation to Mark I plants, which have recirculation piping particularly susceptible to the effects of intergranular stress corrosion cracking (IGSCC). A detailed pilot study based on the Brunswick plant operated by Carolina Power & Light has been completed, the results of which will be discussed here, as well as preliminary evaluations of certain other Mark I plants.

3. Double-Ended Guillotine Break Caused by Crack Growth

The probability of "direct" DEGB in reactor coolant piping is estimated using a probabilistic fracture mechanics model implemented in the PRAISE computer code and its associated pre- and post-processing routines. Details of this model have been presented elsewhere [5,6] and will not be repeated here, but can be summarized as follows.

For a given weld joint in a piping system, the leak or break probability is estimated using a Monte Carlo simulation technique. Each replication of the simulation -- and a typical simulation may include many thousand replications -- begins with a pre-existing flaw having initial length and depth randomly selected from appropriate distributions. These distributions in turn relate the probability of crack existence. Fatigue crack growth is then calculated using a Paris growth model, to which are applied stresses associated with normal operating conditions and postulated seismic events. The influence of such factors as non-destructive examination (NDE) and leak detection is also considered through the inclusion of appropriate statistical distributions (e.g., probability of crack non-detection as a function of crack size). Leak occurs when a crack grows through the pipe wall, break when failure criteria based on net section stress (for austenitic materials) or tearing modulus (for carbon steels) are exceeded.

Completing all replications for a given weld joint and tabulating those cracks that cause failure yields the failure probability as a function of time at that weld. If only pre-existing cracks are considered, then "stratified sampling" can be applied to assure that initial crack samples are selected only from those sizes that can potentially cause pipe break. Through this technique, very low failure probabilities (less than one in a million) can be reliably estimated from only a few thousand replications of the Monte Carlo simulation.

After the failure probabilities at all weld joints in a piping system have been estimated, a "systems analysis" combines these results with the non-conditional crack existence probability (a function of total volume, of weld material) and seismic hazard (which relates the occurrence rates of earthquakes as a function of peak ground acceleration) to obtain the non-conditional probabilities of leak and DEGB.

This was the basic approach followed in our evaluations of PWR reactor coolant loop piping. Two additional factors, however, make the evaluation of BWR reactor coolant piping, particularly recirculation loop piping, more complex. The first of these is the potential effect that failure of "intermediate" pipe supports and supports for light loop components (e.g., recirculation pumps) could have on the probability of direct DEGB. The second is intergranular stress corrosion cracking (IGSCC). IGSCC may affect not only the growth of pre-existing cracks but also cause new cracks to initiate after plant operation has begun, which must be considered in addition to pre-existing fabrication flaws.

Effect of Intermediate Support Failure on DEGB Probability

The potential effect of intermediate support failure on estimating the probability of direct DEGB is two-fold:

(1) support failure would redistribute applied stresses at weld joints, in turn affecting crack growth rates as well as the failure criteria used to define when pipe break occurs.

(2) accounting for stress redistribution would require an individual PRAISE evaluation for each support failure scenario, dramatically increasing the computational effort involved. For example, even if only four supports were addressed, sixteen separate PRAISE runs would be required to cover all possible combinations and permutations of support failure.

Reactor coolant loops in PWR plants typically have small length-to-diameter ratios and, because of their stiffness, are supported solely by the major loop components (reactor pressure vessel, reactor coolant pumps, and steam generators); therefore, no additional supports are needed. However, recirculation loop piping in BWR plants is longer and smaller-diameter (typically 12 to 26 inches), and requires additional support from sprint- or constant-load hangers. This piping may also have numerous snubbers to reduce stresses in the event that an earthquake occurs. Each recirculation loop at Brunswick, for example, has a snubber pair each on the inlet and outlet lines, as well as a snubber tripiet at the top and at the bottom of the recirculation pump.

Our evaluations of indirect DEGB (i.e., support reliability) in PWR reactor coolant loop piping were based on the assumption that failure of a heavy component (e.g., steam generator) support conditionally led to pipe break. This assumption was regarded as conservative (in reality a pipe would likely experience severe inelastic deformation before actually breaking) but nevertheless resulted in very low DEGB probabilities. To have assumed that failure of a snubber or a constant-load support would similarly cause a DEGB in BWR recirculation piping would have been unreasonably conservative; therefore, a more detailed approach had to be developed to investigate the effect of support failure on the probability of direct DEGB.

We first divided the recirculation loop snubbers into four groups (inlet line, outlet line, top and bottom of the recirculation pump) and estimated the seismic "fragility" (probability of failure as a function of seismic response) of each; the failure of spring or constant-load hangers was not considered because seismic loads on these support types would be very low compared to those on the snubbers. We then identified each possible

combination of support failure, including that in which no failure at all occurred, and performed a stress analysis for each to determine how stresses were redistributed. Finally, using modified versions of the standard pre- and post-processing routines for PRAISE, we performed sensitivity calculations to determine the effect of support failure on DEGB probability. These routines are normally used respectively to develop the stratified sampling space used by PRAISE (see Ref. 5 for details) and to perform the "systems analysis" described above, and execute much faster than PRAISE itself. Improved computational efficiency comes at the expense of accuracy in the probabilistic results; however, because we were addressing only relative effects in these sensitivity calculations, we concluded that the simplified analyses were sufficient for our purposes.

Using the generic seismic hazard curves that we had developed as part of our evaluation of PWR plants east of the Rocky Mountains, we investigated the effect that seismically-induced snubber failure had on the probability of direct DEGB. Our generic hazard curves relate the probability of occurrence of peak ground accelerations up to five times that of the SSE at a given plant site (0.16g at Brunswick). In our sensitivity study, we truncated these curves at maximum values of PGA ranging from one to five times the SSE, and then estimated the probability of direct DEGB for each. The results of these sensitivity calculations indicated the following:

- based on the generic hazard curves, snubber failure has a negligible effect on the probability of direct DEGB if the hazard curves are truncated at twice the SSE or less. Above this level, the effect of snubber failure is non-negligible; however, the extremely low frequency of earthquakes greater than the SSE keeps the overall failure probability low.

- for this particular snubber design, "failure" occurs when a relief valve opens; snubber function is recovered when the load drops off. Permanent failure of the snubber would occur only at much higher loads, implying that the earthquake levels above are conservative.

From the results of this sensitivity study we concluded that failure of intermediate supports could be neglected in our later detailed PRAISE evaluations.

Intergranular Stress Corrosion Cracking

Recirculation piping in older BWR plants, particularly those plants characterized by the General Electric Mark I containment design, has been found in recent years to be susceptible to intergranular stress corrosion cracking. Stress corrosion cracking occurs in stainless steel piping (in this case, Type 304) when the dual conditions of "sensitization" -- material properties conducive to IGSCC that result from prolonged exposure to high temperatures during welding -- and applied loads are met. IGSCC is important not only as it affects the growth of existing cracks, but more so because it causes new cracks to initiate after plant operation has begun.

Earlier versions of PRAISE included the effect IGSCC on pre-existing cracks through a simple relationship between growth rate and the stress intensity factor at the crack front; crack initiation was not modeled at all. This model was not applied in our PWR evaluations because operating experience has indicated that IGSCC is not a problem in PWR reactor coolant loop piping.

As part of our BWR study we developed an advanced IGSCC model for the PRAISE code. This model is semi-empirical in nature, and is based on experimental and field data compiled from several sources. Using probabilistic techniques, the model addresses the following IGSCC phenomena:

- o crack initiation, including the effects of environment, applied loads, and material type (i.e., sensitization). Crack location, time of initiation, and velocity upon initiation are all defined by appropriate distributions based on experimental data.

- o crack growth rate, including effects of environment, applied loads, and material type.

- o multiple cracks. Because our earlier evaluations were based on pre-existing flaws only, each Monte Carlo replication included one crack only. Inclusion of crack initiation requires that multiple cracks be considered during each replication.

- o crack linking. Treating multiple cracks requires that their potential linkage into larger cracks be considered. This is done using linkage criteria specified in Section XI of the ASME Boiler and Pressure Vessel Code.

- o residual stresses. Steady-state pipe loads due to welding residual stresses are considered an addition to fatigue loads.

Crack growth rates and times-to-initiation are correlated against "damage parameters" which consolidate the separate influences of several individual parameters. These include:

- o environment, specifically coolant temperature and dissolved oxygen content.

- o applied loads, including both constant and variable loads to account for steady-state operation and plant loading or unloading, respectively.

- o material sensitization.

Figures 1 and 2 show, respectively, times-to-initiation and crack growth rates for Type 304 stainless steel. The solid curved lines in Fig. 2 show crack growth rates predicted by the earlier IGSCC model in PRAISE for oxygen concentrations of 0.2 ppm (typical during plant operation) and 8 ppm (typical during startup); the relatively close agreement implies that the earlier model gave reasonable crack growth rates despite its much simpler approach.

The damage parameters in the current model were based on the results of both constant-load (CL) and constant extension rate (CERT) IGSCC tests. Many other factors were considered during initial model development, but were later excluded from consideration either because they were judged to be of secondary influence for 304SS, or because suitable operating data was not available to exercise them in a plant-specific evaluation. Although the present model was developed for Type 304 stainless steel, the correlation scheme is sufficiently generic that it can be adapted for other materials. We are in fact currently modifying the model to include Type 316NG stainless steel, in order to compare the reliability of piping fabricated from this IGSCC-resistant material with that of Type 304 piping.

Residual stresses are treated as a random variable in the Monte Carlo simulation. Distributions of residual stress as a function of distance from the inner pipe wall were developed from experimental data for three categories of nominal pipe diameter. For large lines (20 to 26 inches), residual stresses took the form of a damped cosine through the wall as based on data collected by General Electric and Argonne National Laboratory (see Fig. 3). The nominal tensile stress at the inner pipe wall is about 40 ksi. For intermediate-diameter (10 to 20 inches) and small-diameter (less than 10 inches) lines, a linear distribution was assumed through the pipe wall with respective inside wall stresses of 9.3 ksi and 24.4 ksi.

The model was benchmarked by comparing predicted leak rates under nominal BWR applied load conditions against actual leak and crack indication data made available to us by the NRC Office of Nuclear Reactor Regulation (NRR). During benchmarking we quickly ascertained that residual stress was the parameter most influencing the predicted leak rates, and we therefore opted to "tune" the model on this basis. A variety of schemes were considered before we settled on adjusting the stress magnitude (using a multiplication factor) to bring the model into agreement with the field data. Figures 4 and 5, respectively, compare predicted leak rates and number of NDE indications greater than 10 and 50 percent of wall thickness with the corresponding field data for various adjustment factors. As these figures show, surprisingly large reduction factors had to be applied to bring the model into line with the field data, suggesting that factors other than residual stress may be more influential than we first concluded.

Probability of Direct DEGB

We applied this model in a pilot study to estimate probabilities of leak and DEGB for the Brunswick BWR plant. During development of the IGSCC model, we found that its complexity greatly increased computer time requirements for its execution. Two factors were predominantly responsible for this:

- if only pre-existing cracks are considered (as was the case in our PWR evaluations), each Monte Carlo replication tracks the growth of a single crack. Because the IGSCC model includes crack initiation, up to 40 cracks per replication (depending on pipe size) are possible.

- because multiple cracks are allowed during each replication, the possibility of crack linking cannot be disregarded. Since all cracks must be tracked throughout the entire calculation, regardless of size, stratified sampling cannot be used. This increases the number of replications required to generate a reliable Monte Carlo probability.

For example, the assessment of one PWR reactor coolant loop (typically about 15 welds), including the systems analysis, had required about one CPU hour of computer time (on a CDC 7600 machine) based on 10,000 replications. By comparison, the current model requires up to three hours of CPU time to generate a DEGB probability for one weld only.

Because older recirculation loops may have up to 60 welds, it was clearly impractical to calculate weld-by-weld DEGB probabilities. Instead, we grouped the welds in the Brunswick recirculation piping, taking those welds with the highest applied

loads in each group. We then estimated the leak and DEGB probabilities at each of these representative welds and performed a systems analysis assuming that these leak and DEGB probabilities applied to all welds in the respective group. These weld-by-weld probabilities and the resultant system probabilities are presented in Table 1 for both leak and DEGB. These results apply to the existing recirculation piping at Brunswick. A replacement configuration, fabricated from Type 316NG and including fewer welds (eliminating, for example, the recirculation pump bypass piping), has been proposed for the Brunswick plant. For purposes of comparison, Table 1 includes the number of replacement welds in each pipe group.

Table 2 and 3 present, respectively, probabilities of DEGB and leak for both configurations of recirculation piping without IGSCC, as well as for one feedwater and two main steam lines. The two main steam lines "A" and "B" differ slightly in length, and are mirror images of the "C" and "D" lines, which were not evaluated separately. These tables show that in the absence of IGSCC, leak and break probabilities are both on the same order as those for PWR reactor coolant loop piping. Furthermore, if IGSCC is not a factor, thermal fatigue is the primary cause of direct DEGB. As for PWR reactor coolant loop piping, earthquakes contribute only negligibly to the probability of direct DEGB.

4. Double-Ended Guillotine Break Indirectly Induced by Earthquakes

If earthquakes and DEGB are considered as purely random events, the probability of their simultaneous occurrence is negligibly low. However, if an earthquake could cause DEGB, then the probability of simultaneous occurrence would be significantly higher. Our study of direct DEGB concluded that earthquakes were not a significant contributor to this failure mode. However, another way in which DEGB could occur would be for an earthquake to cause the failure of component supports or other equipment whose failure in turn would cause a reactor coolant pipe to break. Evaluating the probability of indirect DEGB involves the following four steps:

(1) identify "critical" components whose failure could induce a DEGB. For each component, estimate the conservatism and the uncertainty in the calculated structural responses for various loading conditions, such as dead weight, thermal expansion, pressure, and seismic loads. In our PWR evaluations, we identified as critical components the reactor pressure vessel supports, the steam generator supports, and the reactor coolant pump supports. A BWR, of course, has no steam generators and the failure of coolant pump supports was considered as part of the direct DEGB evaluation. Therefore, the only critical components that we considered in our Brunswick indirect DEGB evaluation were those making up the reactor support structure.

(2) for each critical component, develop a fragility description for each failure mode. The fragility of a component may be based on several factors (see Table 4). Each fragility description relates the probability of structural failure conditioned on the occurrence of an earthquake of given peak ground acceleration.

(3) calculate the overall "plant level" fragility to account for all significant failure modes and the associated fragility descriptions.

(4) calculate the non-conditional probability of indirect DEGB by convolving the plant level fragility with an appropriate description of seismic hazard. Seismic hazard relates the probability of occurrence of an earthquake exceeding a given level of peak ground acceleration.

Typical descriptions of seismic hazard are shown in Fig. 5. For Brunswick, we found that the probability of indirect DEGB was about 2×10^{-8} events per reactor-year, with a 90th-percentile value (confidence limit) of 5×10^{-7} per reactor year. It was found that the star stabilizer at the top of the RPV, which restrains the RPV against lateral motion in the event of an earthquake, was the primary contributor to failure.

5. Summary and Discussion

We have completed a pilot evaluation of leak and DEGB probability in the recirculation, main steam, and feedwater piping of the Brunswick Mark I BWR plant. Although we have followed the same general approach for BWR plants as we did for PWR plants, two additional factors have required consideration in our direct DEGB evaluation:

- the potential failure of intermediate pipe supports and supports for light loop components (PWR reactor coolant loop piping is supported solely by loop components).

- intergranular stress corrosion cracking (IGSCC) in recirculation loop piping.

Support Failure

Failure of intermediate pipe supports (e.g., hangers, snubbers) would redistribute the applied stresses at weld joints and therefore change crack growth rates. We developed a method of incorporating support fragility into the probabilistic fracture mechanics evaluation, and used it to investigate the effect of support failure on the probability of direct DEGB for our reference "pilot" plant. After identifying support failure scenarios, we calculated the pipe stresses for each. We then performed sensitivity analyses which indicated that the probability of DEGB due to hanger and snubber failure was about the same (about 10^{-8} events per reactor year) as that of indirect DEGB due to the failure of the reactor pressure vessel support structure. We concluded that we could neglect support failure in our subsequent direct DEGB evaluations.

Intergranular Stress Corrosion Cracking

To evaluate the effect of intergranular stress corrosion cracking on the probability of DEGB in BWR recirculation piping, we incorporated an advanced IGSCC model into our PRAISE computer code. This model probabilistically simulates crack initiation (number, time, location, velocity) and the growth of initiated and pre-existing cracks. Unlike our earlier PWR evaluations, in which each replication of the Monte Carlo simulation only considered a single pre-existing crack, the IGSCC evaluations allow the simultaneous growth and potential linkage of multiple cracks. Crack growth rates and times-to-initiation are based on experimental data correlated against "damage parameters" which consolidate the effects of coolant environment (temperature and dissolved oxygen content), material type (including the effect of weld sensitization on time-to-initiation), applied loads, and residual stress. The constitutive relationships that define the damage parameters are generic in form, but contain terms which vary

according to the particular material being considered. The specific features of this model were selected for Type 304 stainless steel. A large number of IGSCC-related factors other than those eventually included in the model were also considered and excluded from consideration.

Applying this model in our Brunswick pilot study, we estimated the leak and DEGB probabilities in the present recirculation piping (both loops combined) to be about 0.68/py and 9.0×10^{-4}/py, respectively, when IGSCC is present. Note that these results imply about one leak for each plant-year of operation. Field observations, however, indicate that the actual occurrence rate is closer to one in every ten plant-years of operations, leading us to conclude that our predicted leak probabilities are between one and two orders of magnitude high. We cannot, of course, similarly compare our DEGB results against field observations, but our extensive past evaluations of PWR primary coolant piping have consistently indicated that plant-to-plant variations in DEGB probability follow the same general trend as those in the leak probability. Therefore, we believe that the DEGB probabilities estimated for the Brunswick recirculation loop piping are similarly high when IGSCC is taken into account.

In our PWR evaluations, order-of-magnitude variations in DEGB probability were not of particular concern to us because even after extensive sensitivity and uncertainty studies, the results were still extremely low. For example, that the best-estimate probability of direct DEGB in Westinghouse plants east of the Rocky Mountains was about 10^{-12} events per plant year, with a 90th-percentile "upper bound" about two orders of magnitude higher. Despite this difference, the basic regulatory implication -- that direct DEGB is an extremely unlikely event -- remains unchanged. By contrast, however, the difference between a 10^{-3}/py and a 10^{-5}/py DEGB probability has a potentially far more serious effect on how the safety of BWR recirculation loop piping is perceived. We therefore believe it essential to take a second look at the basic premises of our IGSCC model to better distinguish real physical behavior from modeling conservatisms. This work is currently in progress, with expected completion in mid-1986.

From our evaluations to date we can conclude that IGSCC clearly dominates the probability of direct DEGB in recirculation piping fabricated from Type 304 stainless steel. Residual stresses appear to be the dominate factor influencing the number of cracks initiated and, to a lesser degree, their growth rates. Probabilities of direct DEGB in the main steam and feedwater piping are similar to those estimated for PWR reactor coolant loop piping. Thermal stresses dominate the probability of direct DEGB; earthquakes contribute only negligibly. In the absence of IGSCC, these results also hold true for recirculation piping. This result implies that if IGSCC can be satisfactorily mitigated (for example through use of IGSCC-resistant materials), then reactor coolant piping DEGB could be eliminated as a design basis for BWR plants as is currently being done through rulemaking actions related to PWR reactor coolant loop piping.

REFERENCES

1. G. Holman, "Double-Ended Breaks in Reactor Primary Piping", Lawrence Livermore National Laboratory, Report UCRL-91731 (October 1984). Presented at the 12th Water Reactor Safety Research Information Meeting, Gaithersburg, Maryland, October 22-26, 1984.

2. Probability of Pipe Failure in the Reactor Coolant Loops of Westinghouse PWR Plants, Lawrence Livermore National Laboratory, Report UCID-19988, NUREG/CR-3660, Vols. 1-4 (1984).

3. Probability of Pipe Failure in the Reactor Coolant Loops of Combustions Engineering PWR Plants, Lawrence Livermore National Laboratory, Report UCRL-53500, NUREG/CR-3663, Vols. 1-3 (1984).

4. Probability of Pipe Failure in the Reactor Coolant Loops of Babcock & Wilcox PWR Plants, Lawrence Livermore National Laboratory, Report UCRL-53644, NUREG/CR-4290, Vols. 1-2 (1985).

5. D. Harris, et al., Probabilistic Fracture Mechanics Models Developed for Piping Reliability Assessment in Light Water Reactors, Lawrence Livermore National Laboratory, Report UCRL-15490, NUREG/CR-2301 (April 1982).

6. T. Lo, et al., "Failure Probability of PWR Reactor Coolant Loop Piping," Lawrence Livermore National Laboratory, Report UCRL-86249 (February 1984).

Table 1. Probability of direct DEGB, Brunswick recirculation piping (current loop configuration)

Weld Group	Diameter (in)	Welds/Loop[1]	P[Leak][2]	P[DEGB][2]
Suction	26	10 (11)	5.3e-6 (5.3e-3)	1.3e-6 (1.3e-5)
Discharge	26	6 (5)	9.0e-4 (5.4e-3)	5.0e-5 (3.0e-4)
Header	20	5 (2)	3.2e-3 (1.6e-2)	5.0e-6 (2.5e-5)
Riser	12	20 (12)	1.2e-2 (2.3e-1)	4.0e-6 (8.0e-5)
Bypass	3	10 (0)	8.9e-3 (8.8e-2)	3.0e-6 (3.0e-5)
Total, both loops (with IGSCC)		102	6.8e-1/py	9.0e-4/py
Total, both loops (w/o IGSCC)		102	3.6e-7/py	7.7e-12/py

Notes:

(1) Value in parentheses is number of welds in proposed replacement configuration.

(2) Events per weld-year. Value in parentheses is events per plant-year for weld group considered.

Table 2. Probability of direct DEGB, no IGSCC (events/py)

Piping System	Confidence limit		
	10%	50%	90%
Recirculation (current)	1.3e-16	1.8e-13	2.5e-10
Recirculation (proposed)	n/a	3.8e-12	n/a
Main Steam "A"	5.0e-15	2.5e-13	1.5e-10
Main Steam "B"	n/a	1.6e-12	n/a
Feedwater	1.1e-14	1.3e-12	1.5e-9

Table 3. Probability of leak, no IGSCC (events/py)

Piping System	Confidence limit		
	10%	50%	90%
Recirculation (current)	1.5e-8	1.0e-6	1.0e-5
Recirculation (proposed)	n/a	1.8e-7	n/a
Main Steam "A"	8.3e-9	8.8e-8	1.1e-5
Main Steam "B"	n/a	7.0e-8	n/a
Feedwater	4.3e-9	5.0e-7	2.5e-5

Table 4. Parameters considered in developing component fragilities

Structural Response
o Ground spectrum used for design
o Structural damping
o Site characteristics (rock or soil, shear wave velocity, thicknesses of different strata)
o Fundamental frequency of internal structure if uncoupled analysis was performed
o Interface spectra for NSSS points of connection to structure if uncoupled analysis was performed
o Input ground spectra resulting from synthetic time history applied to structural model
NSSS Response
o Method of analysis (time history or response spectrum, etc.)
o Modeling of NSSS and structure (coupled or uncoupled)
o NSSS system damping
o NSSS fundamental frequency or frequency range
o If uncoupled analysis was performed, whether envelope or multi-support spectra were used

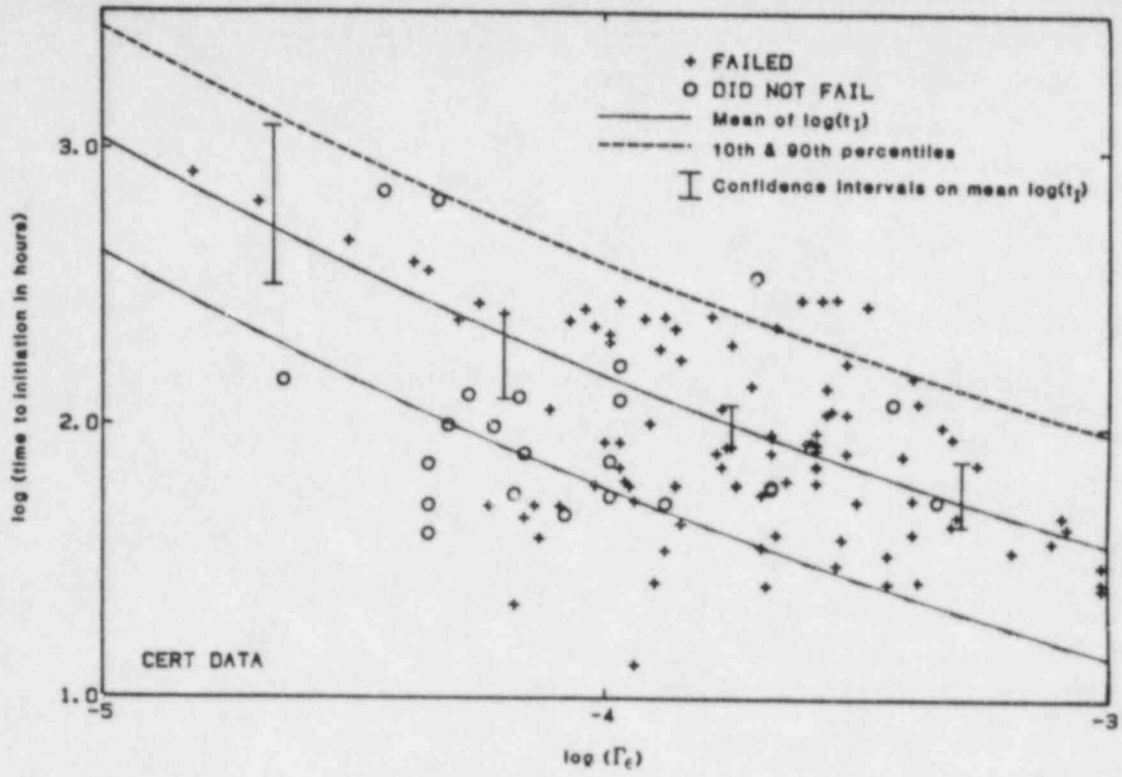

Fig. 1. Time-to-initiation for IGSCC cracks as a function of damage parameter, plant loading/unloading.

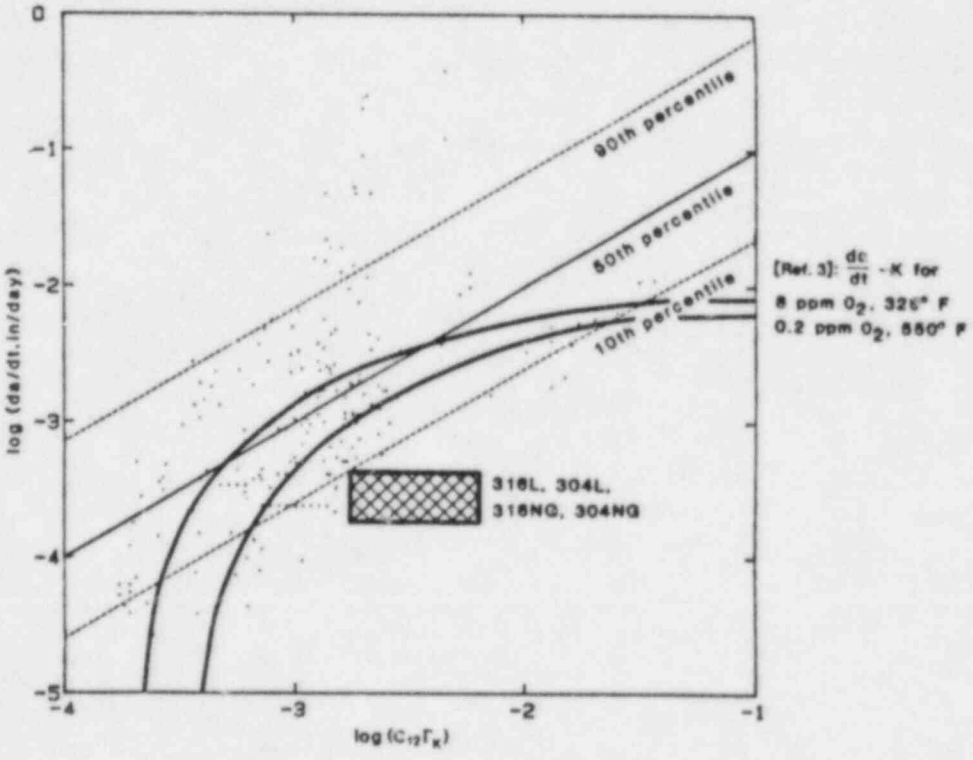

Fig. 2. IGSCC crack growth rate as a function of damage parameter, steady-state operation. The solid lines represent crack growth rates predicted by the earlier IGSCC model in PRAISE.

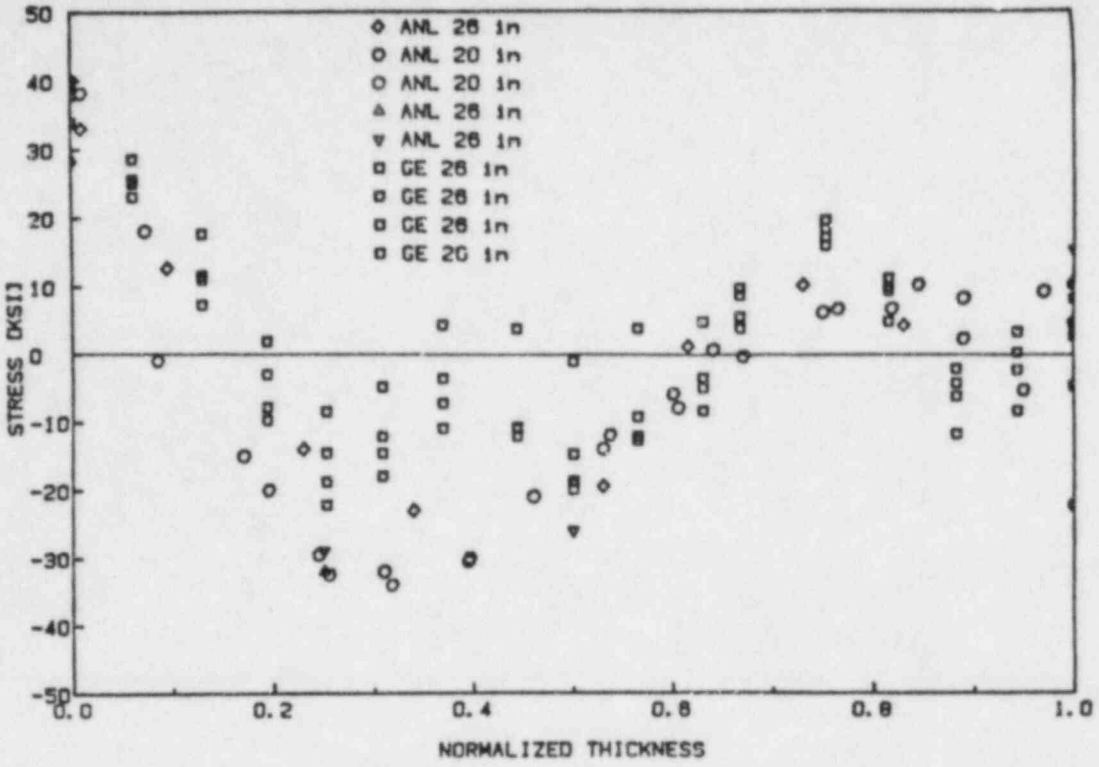

Fig. 3. Residual stress data for large-diameter (20 to 26 inches) piping as a function of distance from the inner wall.

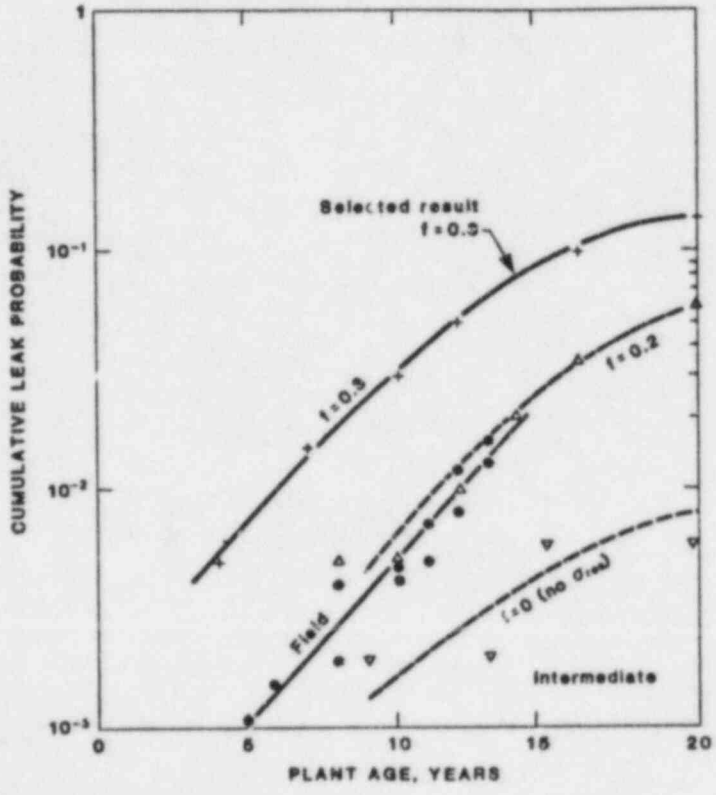

Fig. 4. Comparison of leak probabilities derived from field data with leak probabilities estimated by PRAISE for various values of residual stress adjustment factor.

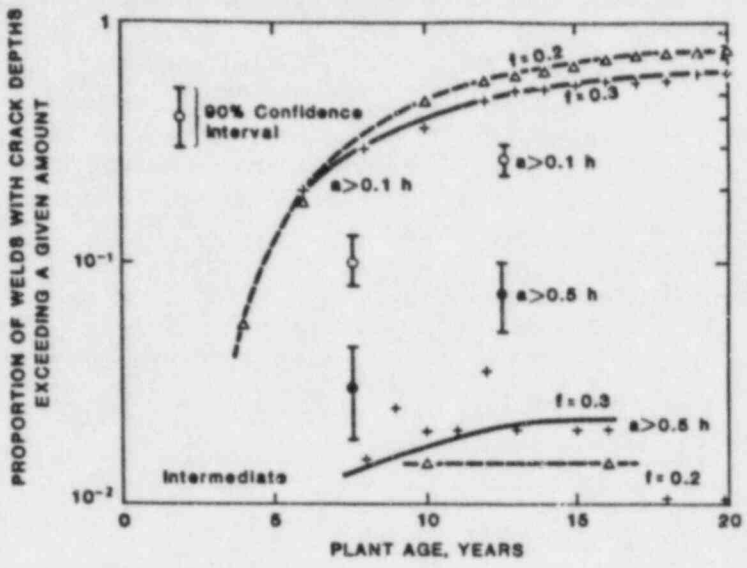

Fig. 5. Comparison of crack indications derived from field data with PRAISE results for various values of residual stress adjustment factor.

Valve Performance Testing

N. M. Jeanmougin
Energy Technology Engineering Center

ABSTRACT

The Valve Performance Test Program addresses current requirements for testing of pressure isolation valves (PIVs) in water reactors. The program is aimed at evaluating the existing leak rate limits for PIVs and the Section XI correlation for extrapolating leak rates between the test and operating conditions. The use of acoustic emission monitoring will be evaluated as an alternative method for assessing the sealing capability of these valves. In addition, motor operator signature testing will be evaluated as a method for assessing gate valve operability. Currently three check valves, ranging in size from a nominal four inch diameter to twelve inch diameter, are being tested. No significant valve deterioration has resulted from a program of life cycling the valves. Future efforts will focus on loosened internals testing of the check valves and life cycle testing of the gate valves.

PRESSURE ISOLATION VALVES: REGULATORY REQUIREMENTS

Pressure isolation valves (PIVs) isolate the high pressure primary reactor coolant system from any connected lower pressure piping systems. PIVs must be periodically leak tested in accordance with Section XI of the ASME Boiler & Pressure Vessel Code. The acceptable leak rate across the PIVs is defined in the technical specification for each light water plant. Until recently, the technical specifications for most plants set the maximum leak rate for each PIV as one gallon per minute (gpm), with the exception of Event V valves. The Committee to Review Generic Requirements has recently approved a change which would allow a leakage rate of one half gpm per inch of nominal valve size, but no more than five gpm on any valve. Leakage through PIVs is monitored and limited for two safety reasons. First, the overall leak rate from the high pressure system to the low pressure system must not exceed the low pressure system's pressure relief and radiological processing capabilities. Second, leak rates are monitored to detect imminent failure of the valves to serve as a pressure barrier.

The monitoring of leak rate trends, as called for in the ASME Code, is expected to provide an indication of accelerated valve deterioration. Therefore, leak rate trends should provide an assurance of valve performance which is at least as reliable as the flat one gpm leak rate allowance.

Modification of the allowable leak rate for individual PIVs will not effect the plant technical specification for overall allowable leakage from the reactor coolant system. This will ensure that the plant pressure relief and radiological processing systems will not be overtaxed.

The NRC had a study prepared by EGG on leak test requirements for PIV's.[1] As part of this study, a survey was conducted of nine plants to obtain information about actual in-plant experience with leak rate testing of PIVs. It was concluded that allowable leak rate criteria, such as the criteria described above based on nominal valve size, should be adopted. The study also indicated that current utility practice is to conduct PIV leak tests at reduced pressure and to extrapolate to leak rates at normal operating pressure (2235 psig) using the correlation given in Section XI of the ASME Code. This correlation is based on a ratio of the differential pressure across the valve during normal operation to the differential pressure across the valve during the leak test raised to the one half power. Analysis of the survey data indicated that this correlation might be erroneous. In November of 1983, NRC requested proposals for a Valve Performance Test Program to "validate the theoretical work performed during the survey of the nine utilities, to evaluate the effectiveness of valve leakage as an indicator of valve degradation, and to examine other valve parameters and their effects on valve operability."

VALVE PERFORMANCE TEST PROGRAM

The objectives of the Valve Performance Test Program, currently being conducted at the Energy Technology Engineering Center (ETEC) are to:

1. Provide recommendations regarding the present technical specification allowable leak rates, and the ASME Code Section XI method for correlating leak rates at test and operating pressure differentials.

2. Evaluate the use of valve leakage as an indicator of valve degradation.

3. Evaluate motor signature monitoring as a means of assessing valve operability, including stroke timing, packing tightness, and torque switch settings.

4. Evaluate acoustic emission techniques for detecting, quantifying, and trending valve leakage.

Test Articles

In order to meet these objectives, ETEC purchased six test articles--three check valves and three gate valves. The valves are typical of those used in LWRs for the purpose of primary system pressure isolation. All six valves were purchased from utilities who had obtained them for nuclear units which were cancelled subsequent to valve fabrication or from units which had surplus valves. The majority of the valves are ASME Section III, Class 1 valves. The Class 2 valves are of the same design as the Class 1 valves and thus are equally representative. The Class 2 valves, however, do not have the same quality assurance/verification documentation as Class 1 valves. A description of the individual test articales is given below:

1. 4-in. 1512 lb, swing check valve, buttweld ends, 316 SS body, ASME Section III, Class 1, manufactured by Nuclear Valve Division, Borg-Warner Corp.

2. 12-in. 1512 lb, swing check valve, buttweld ends, 316 SS body, ASME Section III, Class 1, manufactured by Nuclear Valve Division, Borg-Warner Corp.

3. 6-in. 1500 lb, swing check valve, buttweld ends, 304 SS body, ASME Section III, Class 2, manufactured by Atwood & Morrill Co.

4. 4-in. 1525 lb, gate valve, buttweld ends, 316 SS body, flexible disc, electric motor operated (Limitorque). ASME Section III, Class 2, manufactured by Westinghouse (W-EMD).

5. 10-in. 1525 lb, gate valve, buttweld ends, 316 SS body, flexible wedge disc, electric motor operated (Limitorque). ASME Section III, Class 1, manufactured by Westinghouse (W-EMD).

6. 4-in. 1600 lb, gate valve, buttweld ends, 316 SS body, double disc-parallel seat, electic motor operated (Limitorque), ASME Section III, Class 1, manufactured by ACF Industries, W-K-M Valve Division, Model M-I-OPG POW-R-SEAL.

All valves are new and unused, and were stored, packaged, and shipped in accordance with ANSI/ASME N45.2.2 requirements. All drawing, manuals, and quality records avilable to the utilities for each valve were included as part of the valve order.

Check Valve Testing: Original Program Plan

The method of degrading the test article valves to be representative of PIVs in LWRs is a key issue for the Valve Performance Program. A program of dry and wet cycling of the valves to simulate the cycling, and thus the valve seat wear, that an average PIV undergoes during its life was developed. A survey of nine nuclear power plants was made to identify how many cycles a PIV would see in an average plant application. Ten dry cycles and two hundred wet cycles were determined to be reasonable. A series of leak tests were planned to measure valve leakage prior to the start of the test program, following the ten dry cycles, after the first fifty wet cycles, and following completion of the wet cycling. This approach was developed to gain information on the effectiveness of valve leakage as an indication of valve degradation. The leak tests would be conducted at a variety of temperature and pressure conditions, as specified in Table 1. These data would be used to evaluate the Section XI correlation for extrapolating leak rates at test conditions to leak rates at nominal plant operating conditions.

Another mechanism which has been identified as a major cause of check valve failure is loosened internals. This condition results when the nut which secures the disc to the clapper becomes loose, see Figure 1. This condition could be caused by the stud impacting the valve body during cycling. A

Table 1: Leak Text Matrix

Ident No.	Inlet T (F)	Inlet P (psig)	Outlet P (psig)
1	Amb	50	Atm
2	Amb	150	Atm
3	Amb	250	Atm
4	Amb	350	Atm
5	Amb	700	Atm
6	Amb	1100	Atm
7	Amb	2250	Atm
8	300	2250	2200
9	300	2250	1550
10	300	2250	1150
11	450	2250	2200
12	450	2250	1550
13	450	2250	1150
14	550	2250	2200
15	550	2250	1550
16	550	2250	1150
17	550	2250	1092
18	550	2250	1046
19	550	2250	1000
20	550	2250	1150

FIGURE 1. TYPICAL CHECK VALVE INTERNALS

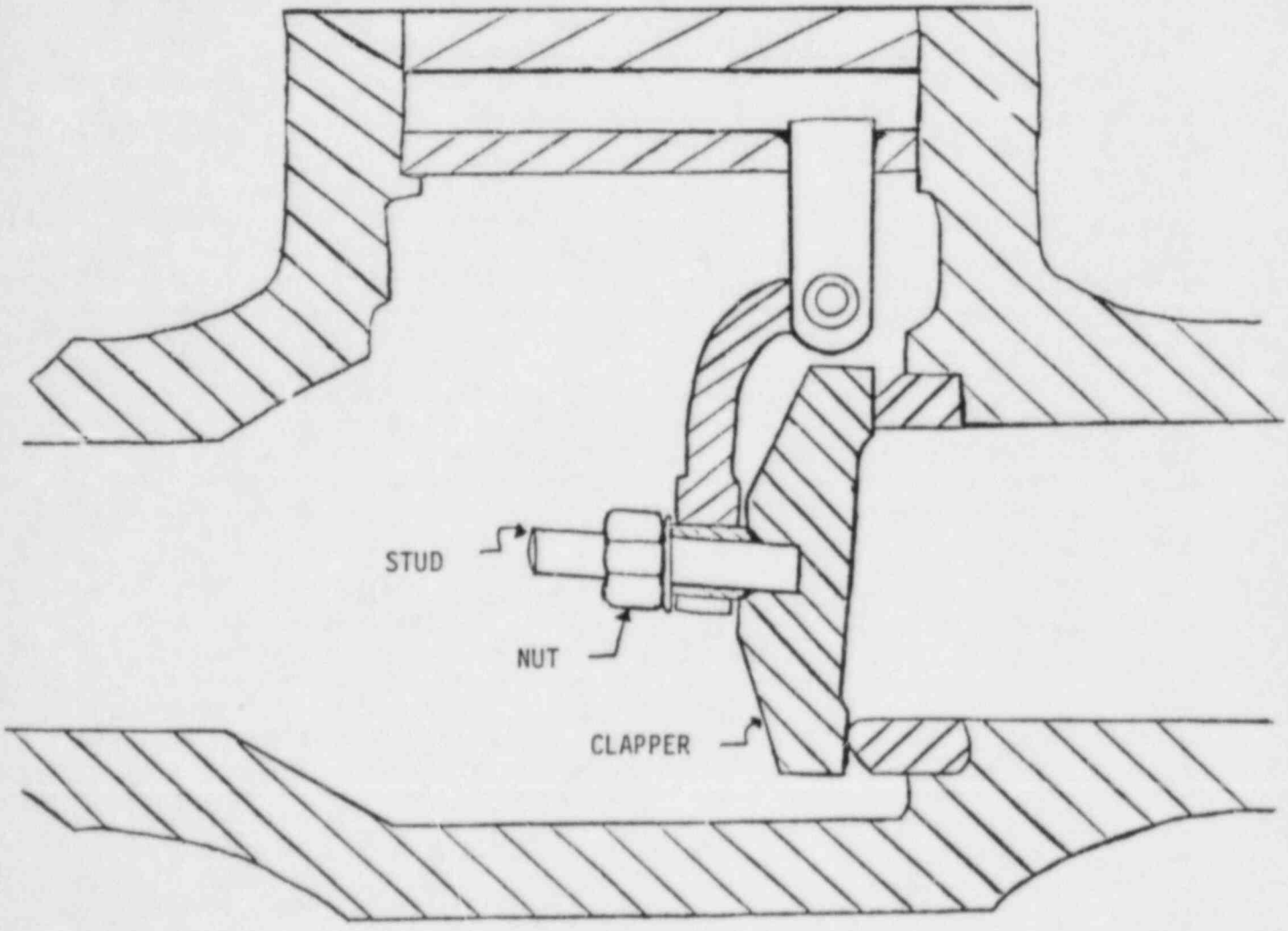

portion of the program is devoted specifically to examining the effect of loosened internals. That is, whether valve leak rate tests are effective in detecting this form of check valve degradation. The loosened internals tests originally were to be performed only on the four inch check valve.

Check Valve Test Results to Date

The four inch check valve has been subjected to ten dry cycles, fifty wet cycles (conducted at 250 F and 2250 psid), and one hundred and fifty additional wet cycles. Leak tests at various temperature and pressure conditions were conducted with the valve in the as-received condition and following each period of valve cycling. The baseline leak tests showed very small leak rates, on the order of 10E-5 lb/sec. Following the dry cycles the valve exhibited no measureable leak rate, perhaps indicating that the valve seating surfaces had "worn in". After wet cycling the valve leak rate was again in the measureable region, but was still very low, on the order of 10E-5 lb/sec. At these very low leak rates, there was no meaningful correlation between leak rate and either differential pressure or temperature. The only discernible effect of differential pressure was seen at low differential pressures. The leak rate was highest at these conditions indicating that the low differential pressures did not provide enough force to properly seat the valve.

The six inch check valve was leak tested in the as-received condition, dry cycled ten times and again leak tested. The results were similar to the four inch check valve tests. The six inch valve had a very small leak rate in the as-received condition and the leak rate following the dry cycling was not measureable.

The twelve inch check valve was not cycled, but baseline leak tests were conducted. The leak rates for the twelve inch valve in the as-received condition were roughly the same as they were for the four and six inch valves, on the order of 10E-6 lb/sec. Thus, the leak rate across each of the three valves in the as-received condition met typical technical specfications for new PIVs.

Based on the four and six inch check valve testing described above, ETEC, with the approval of the NRC, decided to modify the plan for check valve testing. Life cycling of the valves was not causing significant degradation of the valve seat. Although this is an interesting result, it was decided that the test program objectives could be better met by investigating the effect of other check valve degradation mechanisms. The first mechanism which was examined was erosion or wire drawing caused by flashing across the PIV. The survey of utilities indicated that some PIVs are installed in locations where the pressure and temperature conditions would result in flashing across the valve for extended periods of time. Average conditions for these valves was determined to be approximately 1500 psid at 550 F. The ETEC test facility was then put into a hot shutdown mode and these conditions were established across all three check valves for a two month period. The facility was not staffed with operators during this time but periodic leak test measurements were made.

A power loss was experienced at the facility during this time resulting in a loss of pressure differential across the valves. After the pressure differential was re-established, the leak rate across the four inch valve was noted to have suddenly increased, to approximately one liter per hour (10E-3 lb/sec). Although this leak rate is orders of magnitude greater than the previously measured leak rates, it is still much lower than the one gpm currently allowed for most PIVs. As the increase in leak rate occur suddenly after the valves were cycled due to the loss of the differential pressure, the increase may be due to impurities lodged between the seating surfaces. The leak rate across the four inch valve has been roughly constant throughout the long term flashing test. No increase in leak rate across the six or twelve inch check valves has been measured since the start of the long term flashing test. This portion of the program is now being concluded.

Acoustic Emission Monitoring

Acoustic emission data was gathered during the valve cycling, during the leak tests, and it is now being gathered on the four inch check valve during the long term flashing test. To maximize the benefit of the acoustic emission (AE) monitoring, AE equipment supplied by Argonne National Lab (ANL), Oak Ridge National Lab (ORNL), and the Naval Ship Research & Development Center are being used in addition to the ETEC equipment.

The Naval Ship Research & Development Center equipment is portable equipment which must be manually operated, therefore it has not been used as extensively as the other equipment. The ANL, ORNL, and ETEC equipment each consist of two sensors, one mounted on the valve body and one mounted on the upstream piping. These sensors are read automatically by the facility Data Acquisition System.

Future Check Valve Testing

The life cycling and erosion testing of the check valves conducted during fiscal year 1985 has produced minimal valve damage. The seating surface damage which would be expected to result from erosion and wear is not the type of damage likely to produce imminent accelerated deterioration or possible failure of the check valves. However, loosened internals could result in possible failure of the check valve to operate or to adequately isolate the primary coolant system; and loosened internals has been identified as a major check valve failure mechanism. Therefore, fiscal year 1986 check valve testing will focus on loosened internals testing. The loosened internals portion of the Valve Performance Test Program is being enlarged to encompass at least two of the check valve test articles rather than simply the four inch valve.

The loosened internals testing will consist of breaking the weld between the nut and the stud identified in Figure 1. The nut will then be backed off a specified number of rotations and locked in place with a backing nut. If there is inadequate room for a backing nut, the nut will be tack welded in place. The valve will be cycled five times and leak tests will be conducted. The process of cycling and leak testing will be repeated twice. The goal of the additional cycles and leak tests is to determine whether a check valve

with loosened internals seats in a repeatable manner.

The sequence of tasks described above will be done for three different loosened conditions for each check valve. The nut will be backed off as far as possible for the third loosened condition.

The check valves installed in many LWRs, and the check valves used in this test program, are self-centering. It is possible that the leak rate across these valves may not significantly increase even though the integrity of the valve internals is compromised. Therefore, the acoustic emission equipment will be monitored during the valve cycling as well as during the leak tests. The AE equipment supplied by ETEC will be readjusted to monitor the signal frequencies which occur during valve cycling. This will enable evaluation of the feasiblity of using techniques, other than valve leak rate monitoring, to detect valve degradation.

Gate Valve Testing

The gate valves will be tested following the completion of the check valve testing. The gate valve program will consist of a series of dry and wet cycling interspersed with leak rate testing at various temperature and pressure conditions. This program is identical to the program originally planned for the check valves. The gate valve seating surfaces should substain more damage during cycling because their operators provide a higher seating force. Wear damage of this type has been identified by ORNL as a major cause of valve leakage in motor operated valves.[2] As a part of their work on nuclear power plant aging, ORNL made a study of motor-operated valve failures. This study showed that the primary reported failure mode was a failure to change position caused by problems with the motor operator. Most of the reported failures of the valves themselves were failures to pass the required leak rate tests. Wear or foreign material on the valve seat were identified as the major causes of the leakage.

The acoustic emission equipment described for the check valve testing will also be used during the gate valve leak rate testing. In addition, motor operator signature tests will be conducted. ETEC is working with ORNL in defining the motor operator signature tests. Current plans call for the motor operator signature tests to be conducted on a four inch gate valve and the ten inch gate valve. The following parameters will be monitored:

1. Stem velocity
2. Stem strain
3. Vibration
4. Motor current
5. Torque switch angular position
6. Torque sutich open/close status
7. Limit switch open/close status

The instrumentation will be installed and the valves stem packing gland nuts will be adjusted to manufacturer's specifications at the beginning of the life cycling/leak rate testing program. Upon completion of the life cycle testing,

the stem packing gland nuts will be loosened and later tightened specified amounts beyond the manufacturer's specifications. The valves will be cycled at various temperatures and differential pressures at each condition.

The purpose of the motor operator signature tests is to identify methods of surveillance which are effective in detecting significant aging and service wear effects and deterioration of valve operability prior to loss of safety function.

Conclusions & Recommendations

It is too early in the program to form firm conclusions or recommendations with regard to the objectives of the Valve Performance Program. However some conclusions and some interesting areas which may deserve further investigation can be discerned based on the data gathered to date.

1. The utilities should be careful to ensure that they conduct leak rate testing at differential pressures which are adequate to ensure the valve is seated. Leak rate testing which is conducted at very low differential pressures will tend to give overly conservative results and may result in the utility performing unnecessary maintenance.

2. Life cycling of check valves, in the absence of other degradation mechanisms, did not result in significant degradation of the valve seating surface.

3. Flashing, or wire drawing, across the check valves appears to have resulted in damage to the four inch check valve seating surface. The type and degree of damage will be determined during post-test visual examination.

4. Additional testing to identify the conditions and mechanisms which cause valve degradation would increase the understanding of what types of surveillance or inservice testing are effective in identifying imminent accelerated valve deterioration or possible valve failure.

References

1. Livingston, R.A.,"Inservice Leak Testing of Primary Pressure Isolation Valves," EGG-NTAP-6175,FIN A6367, February 1983.

2. Eissenberg, D.M., et al,"Aging and Service Wear of Electric Motor-Operated Valves Used in Engineering Safety-Feature Systems of Nuclear Power Plants," NUREC/CR-4234, (ORNL-6170/V1), Volume 1, June 1985.

THE SEISMIC CATEGORY I STRUCTURES PROGRAM

by

Joel G. Bennett
Wade E. Dunwoody
Charles R. Farrar
Los Alamos National Laboratory
Los Alamos, New Mexico 87545

ABSTRACT

With the use of different size scale models, the Seismic Category I Structures Program has demonstrated consistent results for measured values of stiffness at working loads. Furthermore, the values are well below the theoretical stiffnesses calculated from an uncracked strength-of-materials approach. The scale model structures, which are also models of each other, have demonstrated scalability between models. The current effort is to demonstrate that the use of microconcrete and other modeling effects do not introduce significant distortions that could drastically change conclusions regarding prototype behavior for these very stiff, shear-dominated structures. Working closely with the technical review group (TRG) for this program, structures have been designed and tests have been planned that will help to resolve issues surrounding the use of microconcrete scale models.

INTRODUCTION

The Seismic Category I Structures Program is being carried out at the Los Alamos National Laboratory under sponsorship of the U.S. NRC, Office of Nuclear Regulatory Research, and has the objective of investigating the structural dynamic response of Seismic Category I reinforced concrete sturctures (exclusive of containment) that are subjected to seismic loads beyond their design basis.

Specific program objectives are as follows:

1. Develop experimental data for determining the sensitivity of structural behavior (acceleration, displacement, frequency, structural stiffness, etc.), in the elastic and inelastic ranges, of noncontainment Category I structures to variations in configuration and earthquake loading.

2. Identify the sensitivity of floor response spectra changes to the variations selected in No. 1.

3. Develop a way of representing damping in the inelastic range. Demonstrate how this representation of damping changes when going from the elastic through the inelastic ranges, relating the sensitivity of these changes to the variations selected in No. 1.

4. Develop experimental data to verify ductility factors used in conjunction with deterministic and probabilistic analyses.

5. Develop experimental data that will enable others to validate computer programs used to predict the behavior of noncontainment Category I structures in the elastic and inelastic ranges.

The predominate feature of the typical structure under investigation is that shear rather than flexure is dominant, that is the ratio of displacement values calculated from terms identified with shear deformation to the values contributed from bending deformation is one or greater; thus these buildings are called "shear wall" structures.

Results from the Seismic Category I Structures Program through the end of FY84 (September 1984) were described at this conference last year.[1] This paper will describe current program emphasis to determine the credibility of previous
experimental work and future program direction.

STIFFNESS DIFFERENCE AND SCALABILITY ISSUE

The experimental program plan was developed with the foreknowledge that scale model testing of reinforced concrete structures is a somewhat controversial issue in the U.S. civil engineering community, particularly when the structures are loaded into the inelastic range. The similitude requirements for our models were carefully considered and discussed in detail in Ref. 2. The experimental plan incorporated both static and seismic testing-to-failure of scale model Category I box-like structures as well as tests on isolated shear walls. The isolated shear wall tests were carried out first; they were then followed by static and seismic tests on one and two-story box-like structures. To verify that the scaling relationships could be used to translate test results to different models and prototypical structures, two 1/30-scale and one 1/10-scale models of a two-story Diesel Generator Building structure were seismically tested. The first 1/30-scale model structure was tested to aid in the development of the test program for the 1/10-scale structure. After the 1/10-scale model tests, the second 1/30-scale model was tested in a manner similar to the 1/10-scale model.

Fig. 1 compares data taken from tests on a 1/30-scale model Diesel Generator Building (30-12-2) and one 1/10-scale model (CERL No. 2). When the measured first-mode frequency is normalized by the frequency scale factor, N_f, and the peak acceleration is normalized by the acceleration scale factor, $N_{\ddot{y}}$, the data can all be plotted on the same curve. In this notation, the scale factor indicates the ratio of the prototype to the model. In addition, the models had the appropriate added masses, and the base motion was properly frequency scaled so that the 1/30-scale structure is a true 1/3-scale model of the 1/10-scale structure while both structures are models of the assumed prototype. When the data are illustrated as in Fig. 1, the prototype behavior is shown directly, while the individual model data require knowledge of the scale factors (1/30 scale: N_f = 1/11.8, $N_{\ddot{y}}$ = 1/4.6 and 1/10 scale: N_f = 1/6.8, $N_{\ddot{y}}$ = 1/4.6).

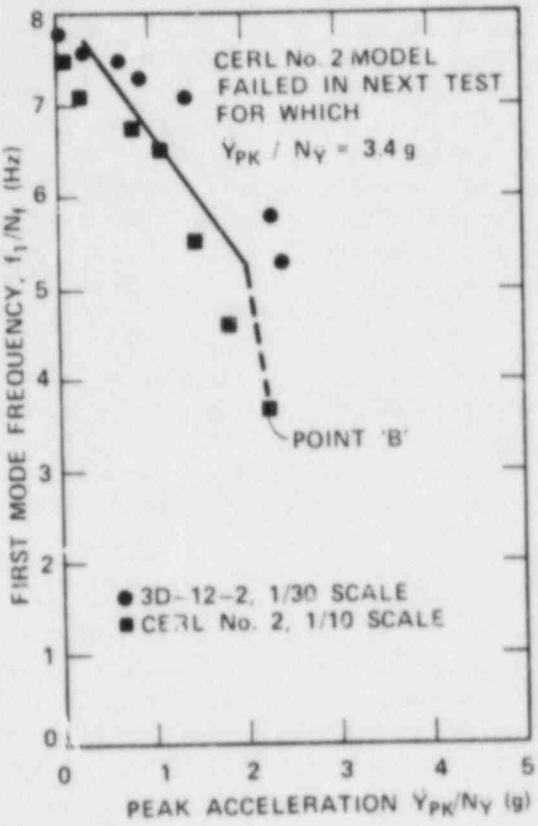

NOTES:

FOR 1/30 SCALE, $N_f = 1/12.2$, $N_y = 1/4.95$

FOR 1/10 SCALE, $N_f = 1/7.04$, $N_y = 1/4.95$

EXAMPLE:

AT POINT 'B' CERL TEST No. 2

$f_{1_{PROT.}} = 25 \times 1/7.04 = 3.6$ Hz

$\ddot{Y}_{PK_{PROT.}} = 11.3 \times 1/4.95 = 2.3$ g

Fig. 1. Data illustrating the first mode frequency shift as the model structures were progressively damaged by increasing peak seismic base accelerations.

Clearly, the scalability of the results from seismic testing the two different sized models is demonstrated, but because both models are made of micro-concrete with simulated rebar, scalability to the prototype structure is still an issue. In addition, both static and dynamic tests using isolated shear walls and box-like structures indicate that the stiffness is significantly less than the stiffness computed assuming an uncracked concrete cross section.

The lower than expected initial stiffness is further addressed in Fig. 2. This figure illustrates the secant stiffness plotted against the concrete modulus, E_c. The secant stiffness was taken at 50% of the ultimate load (measured from experimental results) normalized by the structure's theoretical value calculated from an uncracked cross-section strength-of-materials approach. The concrete modulus was obtained from the equation $E_c = 57000 \sqrt{f'_c}$ as recommended in ACI 349 for normal weight concrete. With the exception of a single point (a "wet" test in an aging study) the data consistently show that calculated stiffnesses are down by a factor of 3 to 4 at this load level. Similar differences have been reported in certain papers in the literature. On the other hand, values reduced by 20% or less have also been indicated in the literature.

The point marked "Sozen" was deduced from Ref. 3 and should be explained. The initial stiffness found from a pluck test on the model in Ref. 3 was almost the theoretical value. The point shown on Fig. 2 is the stiffness of the structure as found after subjecting it to a 1/4-g seismic excitation. The point marked "Unemura" was taken from the figures of Ref. 4 using the same method we have used on our data.

Early in the life of this program, a Technical Review Group (TRG) consisting of nationally recognized seismic and concrete experts on nuclear civil structures was established to both review the progress and make recommendations regarding the technical directions of the program. The recommendations of this group have been evaluated in light of the needs of the USNRC and, where possible, have been carefully integrated into the program.

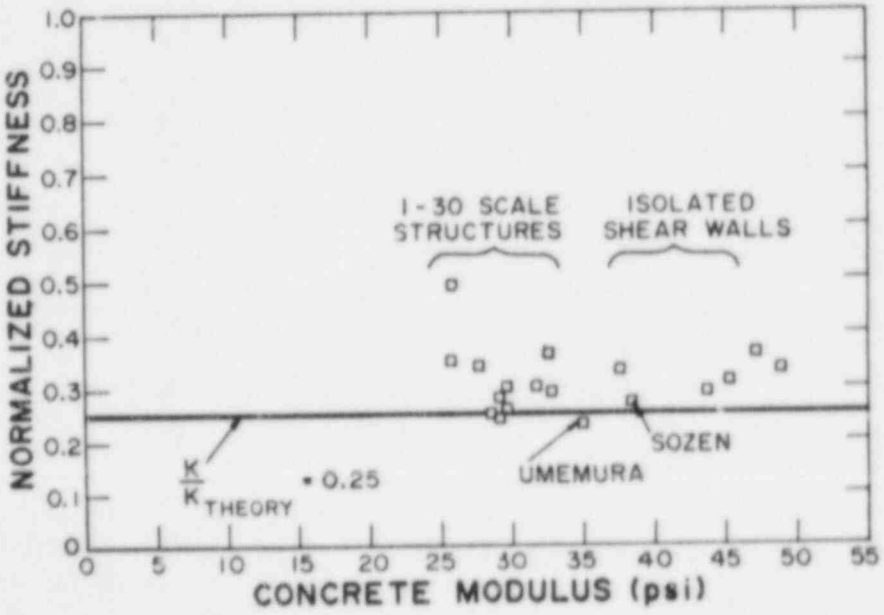

Fig. 2. Normalized stiffnesses versus concrete modulus from this program and other literature values.

During their review of the data through FY84, the TRG pointed out the following:

1. Design of prototype nuclear plant structures is normally based on an uncracked cross-section strength-of-materials approach that may or may not use a "stiffness reduction factor" for the concrete; however if one is used, it is never as large as 4.

2. Although the structures themselves appear to have adequate reserve margin (even if the stiffness is only 25% of the theoretical), any piping and attached equipment will have been designed using incorrect floor response spectra.

3. Given that a nuclear plant structure designed to have a natural frequency of about 30 Hz really has a natural frequency of 15 Hz (corresponding to a reduction in stiffness of 4), and allowing further that the natural frequency will decrease because of degrading stiffness, the natural frequency of the structure may shift well down into the frequency range for which an earthquake's energy content is the largest. This will result in increased amplification in the floor response spectra at lower frequencies, and this fact potentially has significant impact on the equipment and piping design response spectra and equipment and piping margins of safety.

Note that all three points are related to the difference between measured and calculated stiffnesses of these structures.

Having made these observations, several questions now arise. Does our previous experimental data taken on microconcrete models represent data that would be observed on prototype structures? What is the appropriate value of the stiffness that should be used in design and for component response spectra computations in these structures? Should it be a function of load level? Have the equipment and piping in existing buildings been designed to incorrect response spectra?

Thus, the primary program emphasis at this time is to assure credibility of previous experimental work by beginning to resolve the "stiffness difference" issue. The Technical Review Group (TRG) for this program believes that this important issue must be addressed before the program objectives can be accomplished.

To address these stiffness-related concerns, it was agreed that a series of credibility experiments will be carried out using both large and small-scale structures. For the large-scale structure, the TRG set limitations on the design parameters. Their recommended "ideal" structural characteristics, in order of decreasing priority, are as follows:

1. provide a maximum predicted bending and shear-mode natural frequency $\leq$ 30 Hz

2. use a wall thickness $\geq$ 4 in.

3. use a height-to-depth ratio of shear wall ≤ 1

4. use actual No. 3 rebar for reinforcing

5. use realistic material for aggregate

6. use 0.1 to 1% steel (0.3% each face, each direction ideally)

7. use water-blasted construction joints to assure good aggregate frictional interlock.

It was further agreed that the best plan would be to build two of these structures as nearly identical as possible. To compare the results from these tests with previously obtained data, one model should be tested quasistatically and cyclically to failure, and the second model should be test dynamically.

Following these recommendations and other TRG suggestions, and after analyzing a number of potential designs, the structure shown in Fig. 3 was proposed

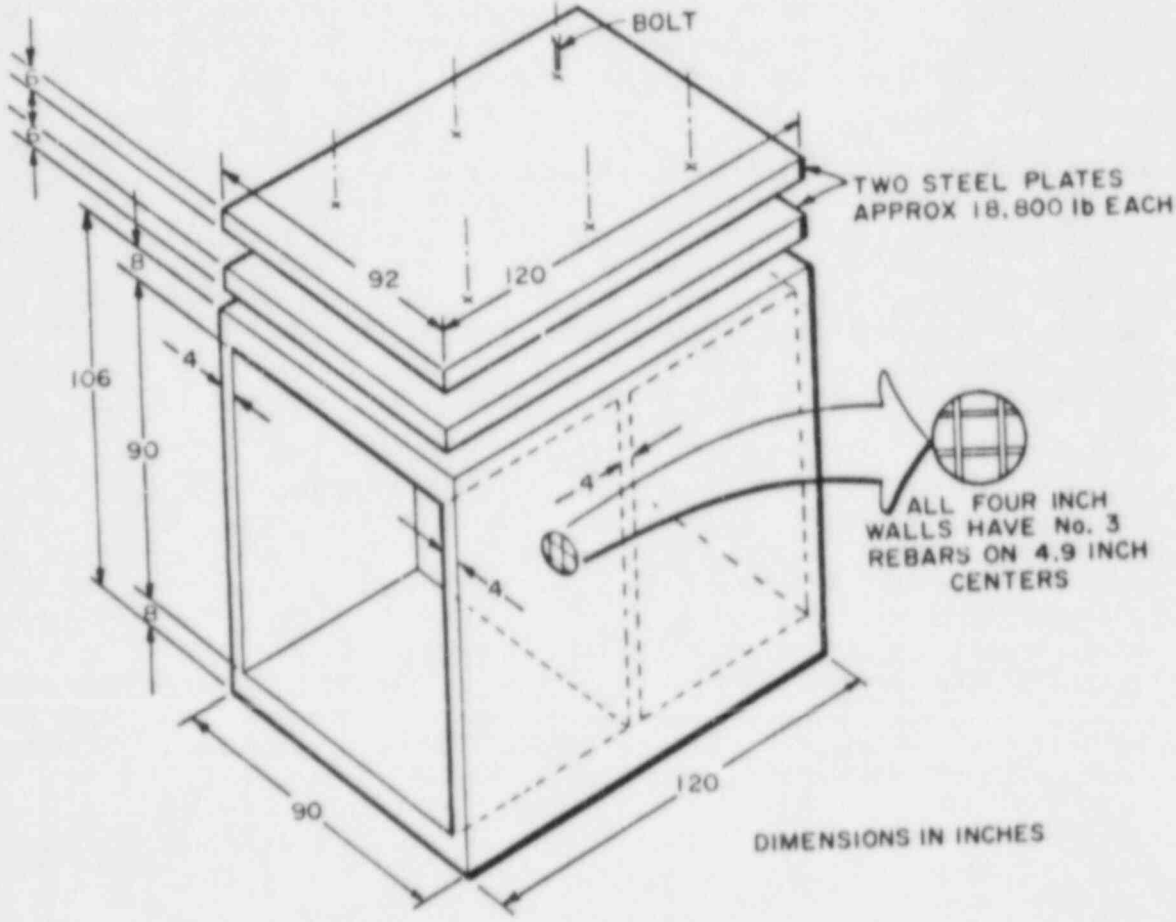

Fig. 3. TRG structural test model.

to both the TRG and NRC as being a test structure fulfilling the design requirements. Table I gives some of the details of this structure. After resolving a number of questions relating to the details and the potential response (dealing with out of plane bending of walls, torsion, etc.,) of the structure, the decision was made to construct and test this particular configuration and its models.

TABLE I
COMPUTED CHARACTERISTICS OF THE TRG MODEL STRUCTURE

$I_{uncracked\ transformed\ section}$	= 2.06×10^6 in.^{4}
A-effective shear	= 379 in.^{2}
Area total	= 1288 in.^{2}
Total uncracked bending stiffness	= 2.5×10^7 lb/in.
Shear stiffness	= 5.3×10^6 lb/in.
Total stiffness	= 4.2×10^6 lb/in.
Max dead weight normal stress	= 42 psi
Max shear stress in flange at 5 g due to assumed 5% torsion (approx.)	= 35 psi
Total concrete	6 cubic yards
Total added weight	37,000 lb.
Total weight	61,000 lb.

Treating the TRG structure of Fig. 3 as the "prototype," the plan was to first construct 1/4-scale Case-I type models from microconcrete. In a Case I model, the mass is scaled by the length scale cubed. All gravitational effects are distorted (they are too low) by a factor of the length scale. For example, normal dead weight stresses are 10 psi in a 1/4-scale model instead of 40 psi, but both values are small compared to the cracking strength of the concrete. Overturning moment due to gravity is low by 4, but the overturning moment due to the inertia force is scaled correctly (and is usually orders of magnitude larger than that due to gravity alone.) In general, for this model as with the other models used in this program, the magnitude of the distortions and their effects are understood and are deemed to be acceptable. The major exception is the scaling effects associated with the use of microconcrete.

THE ONE-QUARTER-SCALE MODELS

The purpose of the 1/4-scale models is as follows: first, by applying the same principles of analysis and design and construction practices as have been applied in our previous work, we will attempt to demonstrate the scalability of the results to the prototype TRG model. Second, conclusions (based on calculations) concerning the model and prototype torsional response, individual wall frequencies, out-of-plane bending, and other features that affect the response of the large TRG structure can be confirmed on an inexpensive test structure. Third, instrumentation and other data acquisition requirements can be worked out in advance of the larger scale tests. As an example, a good analytical model may have to treat the shear stiffness before and after cracking quite differently, and instrumentation to separate overall shear distortion from overall bending distortion on the large model in the static loading case has been proposed. This instrumentation has been designed and checked

on the small model. Also, low load-level testing (modal and static) is a new feature for this program, which in the past has been concerned with working load levels. Methods and details for this type of testing have been worked out using the small models.

The two 1/4-scale models have been completed, and testing of the second model is in progress with testing of the first being complete.

The 1/4-scale models were constructed of microconcrete using our previous construction experience. A double row of 1/4-inch hail screen reinforcing simulating 0.56% steel in each direction was placed on the centerline of each end wall and the shear wall. The top and bottom slabs were heavily reinforced with No. 3 bars. Properties of the first model's reinforcing and the microconcrete are given in Table II.

TABLE II
MATERIAL PROPERTIES FOR TRG MODEL I

Concrete

E = (measured at $\sigma - \varepsilon$ origin) = 3.18×10^6 psi

f'_c = (compressive strength) = 3769 psi

f_t = (split tensile test strength) = 513 psi

E'_c = $57000 \sqrt{f'_c}$ = 3.5×10^6 psi

Steel - Bilinear Properties - 0.6% Both Directions

E	=	25.6×10^6 psi
Yield Strength	=	42.7 KSI
Ultimate Strength	=	53.1 KSI
Elongation at Failure	=	0.04
Diameter	=	0.042 in.

TESTING PROGRAM

The testing program for this model consisted of a series of very low load-level modal and static tests followed by increasingly severe random and simulated seismic testing to failure. The low load-level testing were all "bare" model tests (no added mass), and the random and seismic tests were conducted with 575 lb. of added weight as is appropriate for a 1/4-scale model of the large 30-Hz TRG structure.

DETERMINATION OF INITIAL STIFFNESS

The primary purpose of all low-level tests was to compare the so-called "undamaged" stiffness or virgin model stiffness to the theoretical values. A model shear-bending stiffness was deduced from all modal and low-level static tests, and these values are given below in Table III. The consistency of the values between the static (direct measurement) and dynamic (indirect measurement) methods is obviously good.

Table IV presents the results of all calculated values using both the strength-of-materials approach and a finite element calculation, and the three various estimates for the concrete modulus, $E_c = 3 \times 10^6$ psi (design value), $E_c = 3.18 \times 10^6$ psi (strain-gage measured value), and $E_c = 3.5 \times 10^6$ psi (ACI Method, $E_c = 57000\sqrt{f'_c}$). Clearly, the measured values of the stiffness at low levels are within 70-90% of theoretical values.

WORKING LOAD LEVEL TESTS

Following the low-load level testing, the model was subjected to a random and seismic load test plan similar to the test plan used to test all previous models. First, bare model tests were carried out with 0.5-g random base excitation followed by a seismic input that varied from 0.5-g nominal to 1-g nominal. These bare model tests were used to characterize the "undamaged" stiffness at a higher load level than those used in the modal and low-level static tests. These tests indicated a reduction in stiffness over the low-load level value of about 24%. Next, weights (575 lb) were added to the model to fulfill similitude requirements for a 1/4-scale model of the large TRG structure. The initial tests in this configuration were used to calculated the working load stiffness as in previous models and indicated a stiffness of 441200 lb/in, approximately 38% of the value that would be calculated by an uncracked strength-of-materials approach. This value is consistent with values reported in all of our previous tests on the 3-D structures. Figure 4 illustrates this point which shows the normalized measured stiffness reported from previous tests and this current model test structure, when it was subjected to the same testing procedure as in the previous tests on the 3-D test structures.

TABLE III
MEASURED VALUES OF INITIAL STIFFNESS

	Stiffness x 10^6 lb/in
Static or Direct Measurements	
Dial gage data	0.915
Noncontact gage data	0.695
All static data	0.752
Dynamic or Indirect Measurements	
Free-free modal Test 1	0.775
Free-free modal Test 2	0.707
Fixed-free modal test	0.802
Average value from all data	0.774

TABLE IV
CALCULATED VALUES OF STIFFNESS

Method and Assumptions	Stiffness x 10^6 psi
Strength-of-Materials Approach	
E_c = 3.00 x 10^6 psi	1.09
E_c = 3.18 x 10^6 psi	1.15
E_c = 3.50 x 10^6 psi	1.27
Finite Element Method	
E_c = 3.00 x 10^6 psi	0.860
E_c = 3.18 x 10^6 psi	0.910
E_c = 3.50 x 10^6 psi	1.00

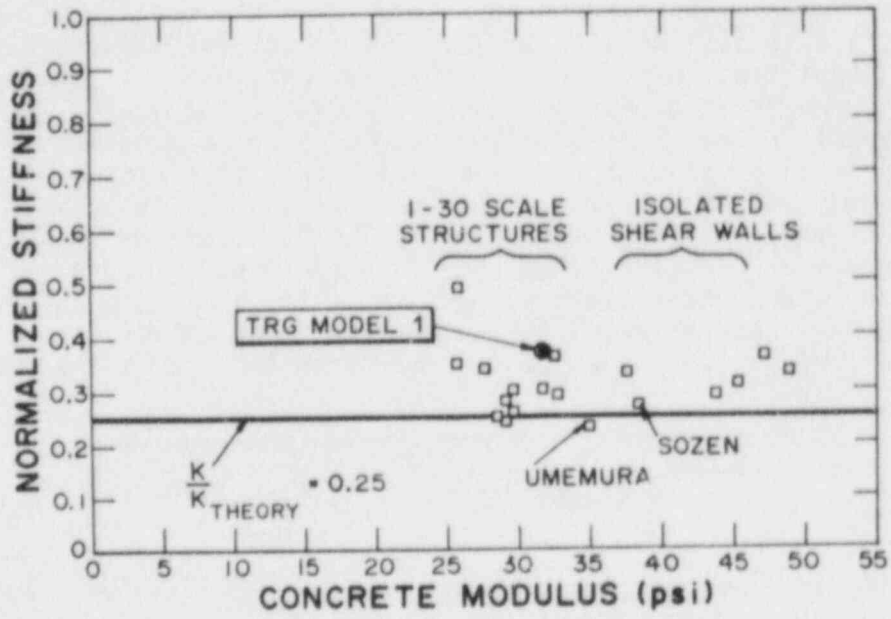

Fig. 4. Normalized stiffnesses versus concrete modulus from this program and others, and showing the 1/4 scale TRG model after being subjected to 1/2 g seismic test.

To date, we believe the TRG series of tests will be valuable in resolving the modeling and reduced stiffness issue. The most important tests in this regard will be the tests of the large models, which are scheduled to begin in November and December.

FUTURE EXPERIMENTS

Following the resolution of the stiffness difference issue, a limited number of tests will be carried out to meet program objectives and aid in benchmarking the analytical model development. If settlement of the scalability and stiffness difference issues allows, these tests will be carried out on one-inch-thick wall concrete models. A statistician, knowledgeable in experimental design, will be used to comment on the test configurations recommended and to assure that the controlled variables (i.e., number of floors, wall arrangement, etc.) and uncontrolled variables (i.e., concrete strength) are incorporated into a cost-effective test matrix to meet program objectives.

One further effort will be investigated and possibly initiated. The program management has noted instances in the shock and vibration literature of researchers measuring and reporting natural frequencies and mode shapes of very large reinforced concrete structures. This developing technology will be investigated and the possibility of performing such a test on a full-scale Category I shear wall structure evaluated. If a suitable structure can be found, such a test combined with analytical modeling could be used as a final confirmation of the as-built stiffness of prototype structures.

REFERENCES

1. Endebrock, E. G., Dove, R. C., and Anderson, C. A., "Seismic Category I Structures Program," Proceedings of the 12th Water Reactor Safety Research Information Meeting, October 22, 1984, Washington, D.C.

2. Dove, R. C., "Scale Modeling of Reinforced Concrete Category I Structures Subjected to Dynamic Loading," Los Alamos National Laboratory report, in press.

3. Sozen, Mete A., "A Note on Nonlinear Seismic Response of Reinforced Concrete Structures with Low Initial Periods," Section 4 of the informal proceedings of the EPRI/NRC Workshop on Nuclear Power Plant Re-evaluation for Earthquakes Larger than SSE, October 15-17, 1984, San Francisco, CA.

4. Umemura, H., Aoyama, H., Ito, M., and Josokawa, Y., "Aseismic Characteristics on RC Box and Cylinder Walls," unknown publication source supplied by Cheng, F. Y., Los Alamos National Laboratory consultant. The data cited is taken from the figures.

Component Fragilities - Data Collection, Analysis and Interpretation

K.K. Bandyopadhyay and C.H. Hofmayer
Brookhaven National Laboratory
Upton, New York 11973

Abstract

As part of the component fragility research program sponsored by the U.S. Nuclear Regulatory Commission, BNL is involved in establishing seismic fragility levels for various nuclear power plant equipment with emphasis on electrical equipment, by identifying, collecting and analyzing existing test data from various sources. With cooperation from utilities, major reactor suppliers, testing laboratories, A/E firms and equipment manufacturers, to date, BNL has reviewed approximately seventy test reports to collect fragility or high level test data for switchgears, motor control centers and similar electrical cabinets, valve actuators and numerous electrical and control devices, e.g., switches, transmitters, potentiometers, indicators, relays, etc., of various manufacturers and models. Through a cooperative agreement, BNL has also obtained test data from EPRI/ANCO. An analysis of the collected data reveals that fragility levels can best be described by a group of curves corresponding to various failure modes. The lower bound curve indicates the initiation of malfunctioning or structural damage, whereas the upper bound curve corresponds to overall failure of the equipment based on known failure modes occurring separately or interactively. For some components, the upper and lower bound fragility levels are observed to vary appreciably depending upon the manufacturers and models. For some devices, testing even at the shake table vibration limit does not exhibit any failure. Failure of a relay is observed to be a frequent cause of failure of an electrical panel or a system. An extensive amount of additional fragility or high level test data exists. If completely collected and properly analyzed, the entire data bank is expected to greatly reduce the need for additional testing to establish fragility levels for most equipment.

1. INTRODUCTION

Safety related electrical and mechanical equipment for nuclear power plants is seismically qualified by proof testing or analysis whereby the equipment function is demonstrated for a plant specific earthquake excitation level or for an excitation level which envelops the requirements of multiple plants. Although this qualification approach meets the requirements of a plant or a group of plants, it has an inherent limitation in that the

Work performed under the auspices of the U.S. Nuclear Regulatory Commission.

qualification data may not reveal the equipment capacity level and failure modes. In the United States, this limitation has never been felt so acutely as in recent years primarily due to two reasons.

First, the possibility of earthquakes greater than the design basis is being considered for many nuclear plants, especially for eastern U.S. plants. This would require reassessment of the existing qualification results in the light of a higher excitation level. However, extrapolation of proof or generic qualification data to new requirements often raises additional concerns rather than resolving the original problems.

The second reason stems from the Probabilistic Risk Assessments (PRAs) being performed on new and existing plants to evaluate their overall safety. PRA's have indicated that seismic events are a non-trivial contributor to overall plant-induced risk to the public and that the seismic behavior of safety related equipment plays an important role in the risk assessment. In order to include in a realistic manner the behavior of equipment in the PRA studies, the seismic fragility levels of such equipment are needed. To this end, usually a qualitative estimate of fragility levels is made based primarily upon engineering judgment and extrapolation of qualification data. Nevertheless, the existing proof or generic qualification results again fail to satisfactorily meet this need.

Although the emphasis in the past has been on proof or generic qualification, numerous tests have been performed at very high seismic levels which approach the capacity of the tested equipment. Some fragility testing has also been conducted in the process of development and evolution of the product. Such testing has been performed by a wide variety of organizations utilizing various methods and vibration inputs; but little has been done to present the results in a systematic fashion to meet current needs as mentioned above.

To meet these needs, the United States Nuclear Regulatory Commission (USNRC) has embarked on a research program to define the seismic fragility levels of safety related electrical and mechanical equipment. Obviously, testing all equipment under this program is not practical from a financial point of view. However, as indicated earlier, it has also been recognized that a certain amount of high level test results exists in various names and forms, that can clearly be utilized to establish seismic fragility of such equipment. Therefore, it has been judged that prior to undertaking an expensive fragility test program, the availability of existing fragility data will be explored. This approach will either outright eliminate the necessity of testing some equipment for which adequate fragility test data exist already, or minimize the testing expense by reducing the gap between the real fragility level and the starting vibration input for a new fragility test.

As part of this component fragility research program sponsored by the USNRC, Brookhaven National Laboratory (BNL) is involved in establishing seismic fragility levels for various equipment by identifying, collecting and subsequently analyzing capacity and fragility test data from various sources.

2. BNL's RESEARCH SCOPE

The scope of BNL's research program includes the following activities:

- Initiate cooperation with domestic and foreign institutions to: (a) establish lines of communication with vendors, owners and testing laboratories to determine availability of already existing component fragility data; (b) negotiate the transfer of existing component fragility data to BNL and (c) host a workshop on component fragility.

- Assemble, analyze and interpret available fragility data for mechanical and electrical equipment important to safety.

- Compare results with component fragilities used in current PRA and seismic margin studies and recommend improvements where possible.

This program is being coordinated with Lawrence Livermore National Laboratory (LLNL) which is developing a scheme for prioritizing components for fragility testing and demonstrating by test a procedure for performing component fragility tests.

The combined efforts of BNL and LLNL represent Phase I of the NRC Component Fragility Program. Phase II of the program may be devoted to the planning, performance and evaluation of comprehensive component fragility tests and supporting analyses, or alternatively may include significantly greater data collection activities. Phase I will provide assurance that any testing performed during Phase II will not duplicate any already existing and useable data. Obviously, the more useable data that is uncovered during Phase I will minimize the need for a large testing program during Phase II.

3. SUMMARY OF ACTIVITIES

As part of the research program, BNL has contacted various equipment manufacturers, testing laboratories, utilities, reactor suppliers and Architect-Engineer (A/E) firms to obtain information on existing component capacity data to establish fragility levels for generic classes of equipment. In the process of developing and/or qualifying their product, these organizations sometimes have capacity level test results of some equipment. Many of these organizations have responded favorably to support BNL's program and provided fragility level or related test data of some equipment. This year the effort has concentrated primarily on electrical equipment since according to present views these are the dominant risk contributors. To date, more than seventy different test reports have been reviewed to collect fragility or high level test data for switchgears, motor control centers and similar electrical cabinets, and numerous electrical and control devices, e.g., switches, transmitters, potentiometers, indicators, relays, etc., of various manufacturers and models. A summary of the collected test data is provided in Table 1. Some of the collected test data indicate testing to the capacity of the shake table with little or no structural damage or malfunction of the equipment. A summary of the collected data is being stored in a computer data base, a sample copy of which is shown in Table 2.

Through a cooperative agreement, BNL is also acquiring data from an industry-based seismic qualification data collection program sponsored by the Electric Power Research Institute and conducted by ANCO Engineers, Inc. The data format shown in Table 2 was originally developed for this program and has been adapted for use in the BNL program to facilitate the exchange of information.

In June 1985, BNL hosted a Workshop on Seismic and Dynamic Fragility of Nuclear Power Plant Components. The workshop participants included representatives of nuclear power plant utilities, major reactor suppliers, USNRC, A/E firms, testing laboratories, equipment manufacturers and suppliers, and seismic consultants. The workshop provided a forum for exchanging concepts, information and experiences on the fragility of electrical, control and mechanical equipment used in nuclear power plants when subjected to seismic and other dynamic environments. The exchange was partly in the form of contributed papers and partly through discussions by the participants. The importance of establishing seismic fragility levels of safety related equipment was upheld in the workshop and the participants expressed their willingness to support the fragility research program by sharing their experience and information. The workshop identified many past and present fragility testing programs and methods to compile, analyze and use fragility data. It highlighted the fact that there are considerable existing data within the industry which if compiled and evaluated could yield better estimates as to how well nuclear power plant components will operate in the event of an earthquake. Twenty-two oral presentations were made during the six workshop sessions. The written contributions that correspond to each presentation were published in August 1985 in NUREG-CP-0700, "Proceedings of the Workshop on Seismic and Dynamic Fragility of Nuclear Power Plant Components".

Current efforts are concentrating on documenting and evaluating the data already collected. The approach used in the evaluation and examples of the findings are described in Section 4. The results of all studies to date will be fully discussed in BNL's Phase I report, expected to be published by December 1985.

4. EVALUATION OF COLLECTED DATA

The data from various sources for an equipment family are assembled together in order to assess its seismic behavior. Test response spectra are used to compare and evaluate the performance of an equipment. As expected, with the increase in the response spectra level, the equipment is observed to exhibit various malfunctions or structural damage. Thus, from testing of one specimen with gradual increase in the test input, a number of response spectra curves are obtained corresponding to various failure modes. Depending upon the use of the equipment some types of malfunctioning or partial structural damage may not be considered to incapacitate the equipment. Consequently, the response spectra level corresponding to such malfunction or damage cannot be termed as the fragility level for that particular application. Therefore,

instead of assigning one curve as the fragility level, a number of curves are presented identifying the associated anomalies observed for each response spectra level so that the user can select the appropriate fragility level of the component by considering its specific application. Thus, the fragility of an equipment is described by a group of response spectra curves corresponding to various failure modes. The lower bound curve indicates initiation of malfunctioning or structural damage; whereas, the upper bound curve corresponds to overall failure of the equipment occurring separately or interactively.

Once the fragility of a component is thus established by a set of curves for one particular model of a manufacturer, another set of such response spectra curves is prepared for a second model of the same manufacturer and compared with the first. This way fragility of an equipment produced by one vendor is defined for all their models. Fragility of the same generic equipment manufactured by other companies is similarly obtained. At this point, the relative fragility levels of the products from various manufacturers are compared. If the levels are comparable, all the curves are assembled into one set and designated as the fragility level, or more precisely, the fragility region, of the particular generic equipment. In case appreciable differences in the fragility levels are observed for products of one or more manufacturers, fragility levels of such products are separately presented.

The upper and lower fragility curves discussed above are based upon the data so far collected for the equipment. For some equipment, a wide spectrum of products manufactured in this country is included in the analysis. The fragility curves presented for such equipment are believed to properly represent their generic capacity levels. For other equipment, this year it was not possible to collect data from all major manufacturers for all their models. Consequently, the fragility region is presented based upon these limited data and is subject to revision, either increase or decrease in the level, pending further data acquisition. The extent of the data collected this year compared to that needed to cover the entire spectrum of a component and the extent to which the presented fragility curves reflect the generic behavior of the component are discussed in the BNL Phase I report for individual equipment. The extent of further data needed for an equipment is also described in the Phase I report with specific reference of numbers of manufacturers and/or models covered in this year's program.

It has been observed that some components were tested to high levels, often to the capacity level of the shake table, but exhibited little or no structural damage or malfunction. Test response spectra levels of such equipment are expected to be used mainly in two different ways depending on the nature of the equipment and its support. If the equipment is generically mounted on a floor slab or a seismically rigid support, then the test response presented in the BNL analysis might be high enough for all practical purposes so that the real fragility levels of this type of equipment need not be established. Consequently, they can be excluded from any future fragility test program. On the other hand, if the component is usually mounted on a flexible

support (e.g., an electrical device in a motor control center) and the component when tested individually withstood vibration input to the shake table limit without exhibiting any anomalies, then the fragility data should be sought in the test data of the assembly (e.g., motor control center). If fragility testing is required for such components, the possibility of undue fatigue failure by shaking at lower levels as well as the testing cost can be substantially reduced by starting with the high level test response presented in the BNL analysis.

Following the guidelines discussed above, the test data collected from various sources are analyzed, and presented by equipment family basis, e.g., switchgear, motor control center, etc. A description of the equipment, typical mounting conditions and failure modes is also included in each section. Fragility data of some devices (e.g., relays) are presented separately although such devices might have been contained in an assembly test presented separately by the assembly name (e.g., a motor control center). Analysis of one such equipment, namely, switchgear is included in this paper as an example of fragility test data. Test results for terminal boards are also included in this paper to illustrate high level test data. Other components are analyzed following an identical procedure. The results will be incorporated in the BNL Phase I report.

4.1 Switchgear (Example of Fragility Test Data)

Equipment Description:

The switchgear is an electrical equipment. A Class 1E switchgear is used to provide and control the power supply to various safety-related equipment in a plant. A switchgear unit, called a vertical section or a line-up, is enclosed on all sides and top with (steel) sheet metal except for ventilation openings and inspection windows. A typical unit contains primary circuit switching or interrupting devices, or both, with buses, connections and auxiliary devices, e.g., relays, transducers, current transformers, potential transformers, etc. The heavy power breakers are typically mounted on guide rails at the base. Access to the interior of the switchgear enclosure is provided by doors or removeable covers. In application, a number (2-12) of such vertical sections are installed side-by-side to form a switchgear assembly.

A switchgear could be metal-clad (i.e., cables are segregated from the bus) or could be metal-enclosed (i.e., cables are not segregated). Depending on the need, it could supply a low voltage (e.g., 600V) or a medium voltage (e.g., 5KV, 15KV). The power breaker can carry as high as 3000 amp and the rating could be as high as 1000 MVA.

In the field, a switchgear assembly could either be bolted or welded to the floor. The size and weight of the equipment vary with the breaker size and capacity (MVA) rating. One typical vertical section of a 15KV, 500MVA switchgear assembly measures about 91" deep x 36" wide x 90" high and weighs about 2700 lbs.

Test Description:

For qualification and fragility purposes, the manufacturers and users have traditionally tested a switchgear assembly comprising of one, two or three vertical sections with related control and protective devices in them. The test results are extended to multiple line-ups by analysis. Some manufacturers have used dynamic analysis method and validated the mathematical model by test results. Devices are sometimes separately tested and input response is compared to the vibration level at the device locations.

Test data have been collected for switchgear manufactured by four major companies. The data cover both the low voltage and medium voltage switchgears and several models of each kind. For most tests random multifrequency biaxial vibration inputs were used. One manufacturer used single frequency sine heat testing. The test specimens were either welded or bolted to the test table. At least on one occasion, the same specimen was first tested with bolts and then with welds. Of the mounting configurations, the bolted one exhibited higher response amplication.

Test Results:

Test results are presented in the form of test response spectra (TRS) corresponding to various failure modes as mentioned earlier. The shake table TRS are the response of the table at the equipment base. They indicate the severity of the vibrating input. The response curves are plotted for a damping value of 2% of the critical damping. Although the BNL Phase I report will address responses in all three orthogonal directions, in this paper only the response in the front-back (FB) direction is presented. The results are discussed in the following paragraphs.

Figure 1 shows the TRS curves for a medium voltage switchgear specimen as the vibration input was gradually increased during the tests. The specimen was welded to the shake table and subjected to 30-second duration biaxial multi-frequency random motion in each test. Two simultaneous, but independent, random signals were used as the excitation to produce phase-incoherent horizontal and vertical motions. The resulting table motion was analyzed by a response spectrum analyzer by the testing laboratory. Some of these TRS curves are presented in Fig. 1.

The test specimen is a three-frame medium-voltage metal-clad switchgear and exhibited the first natural frequency in the range of 8-10 Hz. A total of forty-five electrical devices was contained in the specimen assembly. Electrical channels were used to ascertain electrical continuity, current/voltage levels, spurious operation, contact chatter, timing of relay operation, etc. before, during and after the seismic excitation. The oscillograph recorders contained galvanometers capable of detecting a discontinuity of 0.5 millisecond or greater. The specimen was tested for both electrical conditions, namely, static operation (breakers closed) and dynamic operation

(breakers closed-tripped-closed). A syncronous check relay, an auxiliary relay and a power breaker were observed chattering (>0.5 ms) all through the tests. A ground overcurrent relay indicated change-of-state in almost all tests in FB direction.

Curve 1A shows the TRS level corresponding to the electrical static condition for a ZPA value of 2.1g and peak of 5.7g at 16-20 Hz. Two auxiliary relays, two overcurrent relays, an under voltage relay, a synchronous check relay, a distance relay and a power breaker indicated chattering ($\geq$0.5 ms). Chattering of the power breaker at the very low test voltage should not pose any problem for use in medium voltage.

Curve 1B is the next test with a slight increase in the ZPA level (ZPA = 2.3 g) although the curve dips below 1A at some frequencies. This test is also for static breaker condition. Two overcurrent relays were observed to undergo change-of-state in addition to the similar chattering occurred for curve 1A.

The next random test was performed almost with the same vibration input (the TRS plot is not shown in Fig. 1). At this point, corners of a "distance relay" were torn. In order to increase the natural frequency of door panels where many devices were mounted, the door frame was stiffened with horizontal angle stiffeners. The frequency shifted from 8 to 11 Hz at these locations.

Curve 1C in Fig. 1 corresponds to the level with the minimum electrical disturbance for static breaker condition. Addition of the stiffeners limited the chattering to five devices only (compared to eight for curve 1A). This test did not indicate any change-of-state problem as observed in earlier tests. This curve shows a ZPA of 2.3g with a peak of 7.4g at 25 Hz and another peak of 6.5g at 12.5 Hz.

At almost the same input level, as in curve 1C, the breaker was tested for the electrical dynamic condition. An overcurrent relay was observed not to operate.

The vibration input was further increased to produce curve 1D with a ZPA value of 3.4g and a peak of about 8.9g at 20 Hz. For most frequency range the response exceeded 7.0g. For the breaker closed position, seven devices were detected to chatter and the same ground overcurrent relay changed state. Tests were repeated at the same vibration input level with dynamic breaker conditions. In one test, momentary short circuit was noticed and in another test, the same overcurrent relays was observed not to operate.

The last two FB/V tests were performed with the door stiffeners removed to produce TRS comparable to the levels of curves 1A and 1B and keeping the breaker in the electrically dynamic condition. A number of relays were observed to malfunction (e.g., shorted or did not operate).

A total of nineteen random vibration tests were performed in the FB/V direction at various levels not all of which are shown in Fig. 1. Twenty-one additional tests were performed in the SS/V direction during which the mounting weld was observed broken and a circuit breaker position rod slipped behind the switch operating lever. The corresponding curves are not shown in Fig. 1.

Thus, Fig. 1 depicts various malfunction levels for one specimen of a particular manufacturer. The same model was tested in a different test program with some variations of the devices especially with one heavier breaker. Two TRS, one for static and another for dynamic condition of the breaker, are presented in Fig. 2.

Curve 2A in Fig. 2 corresponds to the static breaker position. It shows a ZPA of 2.65g with a peak of about 8.3g at 20 Hz and another peak of 7.4g at 6.3 Hz. The breaker slipped during the run, nine devices chattered and two other devices (switch and relay) experienced change-of-state.

The ZPA level was further increased to 3.5g for the same specimen as shown in curve 2B corresponding to dynamic breaker condition. The specimen was first bolted and then welded. The bolted configuration exhibited higher amplification. The mounting weld broke and the specimen became loose on the shake table. Numerous electrical malfunctions followed indicating an upper-bound fragility for this specimen.

Curve 2C in Fig. 2 was also for the same model of the same manufacturer but with further heavier units. The three-frame assembly contained fifty-five devices and was welded to the shake table. In the total of twenty-one random tests, out of which twelve were in the FB/V direction, the specimen experienced various damages and/or malfunction with increase in vibration inputs, e.g., the fuse blocks came out, position indicator light broke, shutter arm roller came off, breaker did not trip and under voltage relay did not reset until fuse blocks were installed, etc.

Curve 2D in Fig. 2 is the same curve as 1D in Fig. 1 and is repeated for comparison.

Curve 2E in Fig. 2 shows the TRS of another medium-voltage switchgear model manufactured by the same company. This FB curve corresponds to the breaker dynamic condition and shows a ZPA level of 3.0g with a peak of about 6.9g at 12.5 Hz. This model has a lower MVA rating and weighs and measures appreciably less than the previous one. The fundamental frequency is in the range of 8-10 Hz. The three-frame specimen was welded on the shaker table. Chattering of four devices including two switches was observed during the tests. A total of sixty-one tests were performed on the specimen including thirty-one in the FB/V direction.

Fig. 3 represents the TRS from three major manufacturers for their various models. Curves 3A and 3AA show the respective lower and upper bound enveloping curves for one manufacturer obtained from Fig. 1 and Fig. 2. Curve 3B represents the lower bound of a second manufacturer. Curve 3CC is the upper bound reported by a third manufacturer. The curves presented in this figure are incomplete and may be revised upon analysis of additional test data.

Failure Modes:

The malfunction and damage observed during the above described switchgear tests can be summarized as follows:

a) Chattering of relays and switches
b) Change-of-state of switches and relays
c) Tearing of device enclosure plate at connection
d) Inoperability of relays and switches
e) Damage of indicating lights
f) Tearing of switchgear enclosure plate
g) Tripping of power circuit breakers
h) Failure of breakers to respond to remote control
i) Sliding of fuse blocks
j) Crack of switchgear mounting weld

4.2 Terminal Board (Example of High Level Test Data)

Six different models from five major manufacturers were mounted on a rigid text fixture and shaken to the capacity of a triaxial table. The specimens were vibrationally aged with 50%, 60%, 70%, 80% and 90% of the capacity input prior to the full capacity level test. Electrical continuity was monitored. No malfunction or damage was reported. Figure 4 shows the TRS plot enveloping both horizontal components analyzed at 2% damping.

5. OBSERVATIONS, EXPERIENCE AND PROBLEMS

As a result of the efforts to date, it has been found that a large amount of fragility level data exists in the industry, especially with the manufacturers who conducted tests in the process of developing and improving their equipment. This information, if it can be made completely available, will greatly enhance the fragility data base and dramatically reduce the need and cost of future fragility testing. However, most of these data are confidential and proprietary in nature. This type of information may only be obtained with proper assurance to the data source not to disclose any proprietary test data. BNL has demonstrated their ability to provide such assurance, and various source organizations have expressed their willingness to participate in the fragility program.

For some equipment, there are a number of manufacturers and a large number of models of each manufacturer. Again, different models might have been tested by different test laboratories using different test methods and vibration inputs. Thus, one has to be extremely cautious in establishing a fragility level for a generic family of equipment from a wide spectrum of component and test information.

It has been observed that some of the devices that exhibited malfunction and/or damage were separately tested to high vibration levels by their manufacturers or different organizations although no malfunction was reported in such separate tests. Analysis of the test data indicates that individual device tests did not simulate the proper frequency content and/or amplitude that the device would otherwise experience when installed in an assembly cabinet.

BNL's study increasingly indicates that for most electrical equipment the seismic capacity of an equipment is limited by the functional capability of relays and sometimes switches. Similar studies by the Seismic Qualification Utility Group and the Electric Power Research Institute also reveal that the malfunction of relays is the major factor in determination of seismic ruggedness of an electrical equipment. An identical view was repeatedly expressed during the Component Fragility Workshop, namely, that the study of relays should receive the top priority in a component fragility research program.

However, a complete understanding of relays is not easily gained due to its large family size, varied design patterns, inherent behavioral complexity when subject to seismic vibration and, above all, its interaction with the system it is located in. The study of relays is complex, and deserves special attention before its seismic fragility can be fully understood. Unfortunately, it would be enormously expensive to conduct a new test program enveloping the wide spectrum of models and parameters in order to achieve modest and meaningful fragility information. Fortunately, a vast amount of relay fragility test results are available that could effectively reduce the scope of the test program necessary to resolve this issue.

6. CONCLUSIONS

It has been found that many organizations hold component fragility information. This information is difficult to obtain due to proprietary constraints; however, some organizations are willing to release these data provided they are properly protected and utilized as part of a generic data base.

The efforts to date have been successful in obtaining useful fragility data and it is expected that these efforts will minimize any testing that may be needed in the future. An extensive amount of data is still available which should be collected and fully assessed before further consideration is given to implementing a large testing program. Special attention should be given to collecting and fully evaluating all available data concerning relays.

An understanding of the equipment along with its operation and failure modes plays an important role in fragility determination. Fragility is basically a complex phenomenon controlled by numerous parameters attributable to both the equipment and the environment. The idealization of an equipment by a simpler unit or transforming it to a simplified structural model may underestimate the role of some fragility parameters, especially in the case of complex electrical and control equipment. Fragility should be understood in its proper perspective accepting the equipment as an entity. For example, test results of devices should be used with caution when not tested with the assembly. In summary, a proper analysis of the collected data is extremely important in derivation of reliable fragility curves.

ACKNOWLEDGEMENT

This work is being performed under the auspices of the Division of Engineering Technology, Office of Nuclear Regulatory Research, U.S. Nuclear Regulatory Commission. The authors wish to express their special thanks to Dr. John A. O'Brien, NRC Project Manager, for his continued support and guidance throughout the course of this program. The authors also sincerely acknowledge the cooperation of the organizations and the individuals who participated in the BNL program providing valuable fragility data.

NOTICE

The findings and opinions expressed in this paper are those of the authors and do not necessarily refect the views of the U.S. Nuclear Regulatory Commission or the organization of the authors.

TABLE 1
Summary of Collected Test Data

Equipment	Number of Manufacturers	Number of Reports
Switchgear	4	11
Motor Control Center	4	6
Other Electrical and Control Panels	4	12
Transformer (small)	6	6
Relay	4	10
Switch and Contactor	4	11
Electrical Penetration and Conductor Seal Assemblies	1	5
Other Electrical and Control Devices, e.g., Transmitter, Potentiometer, Indicators, etc.	3	15
Mechanical Equipment and Accessories, e.g., Operator	3	4

TABLE 2

NRC/BNL - EPRI/ANCO Equipment Data Base

Equipment Descriptor File

FORM ID:	BNL.SWGR001
GENERIC CLASS:	Switchgear
SPECIFIC EQUIP TYPE:	Medium voltage metal-clad 3-frame cabinet
MANUFACT STANDARDS:	Not available
MANUFACTURER/MODEL:	*
SIZE LxWxH (INCHES):	108x98(D)x90
WEIGHT (LBS):	11,500
CG (INCHES):	Not available
SOURCE OF INFO:	BNL
TEST ORGANIZATION:	*
TEST PLAN:	*
TEST REPORT:	*
ENVIRON QUAL:	Not available
TEST DATE:	8-25-77
INPUT DIRECTION:	Independent bi-axial
EQUIP TEST ORIEN:	FB,SS
TEST TYPE:	Random multi-frequency, 45 sec duration, more than 5-OBE and 3-SSE
FUNCTION MONITORED:	Electrical continuity, current/voltage levels, spurious operation, contact chatter timing of relay operation, etc. before, during and after tests in three electrical conditions: a) static operation - breaker closed, b) static operation - breaker open and c) dynamic operation.
ACCEPT CRITERIA:	No electrical malfunction, no gross structural failure. Record relay chatter.
EXCEPTIONS:	Fuse blocks came out, position indicator lights broke, shutter arm roller came off, breaker did not trip and under voltage relay did not reset until fuse blocks were reinstalled, lockout relays were in tripped condition during 2 SSE tests
RESONANT SEARCH:	FB 7.5 hz, SS 12 hz, V 60 hz
TEST MOUNTING.	Cabinet on shake table
BOLT DESCRIP:	Not applicable
WELD DESCRIP:	1/2 inch long fillet weld - 10 places
BASE/FRAME DAMAGE	3 base welds broke, base frame buckled
APPEND SIMULATED:	Not available
NO. OF SUBCOMP:	55
NO. OF TRS:	3
COMMENTS:	Breaker-retaining brackets 3-inch long 2x2x3/16 angle were added to alleviate inadequate racking roller engagement. This design change was implemented in 1977.

* Concealed information.

TABLE 2 (Cont'd)

NRC/BNL - EPRI/ANCO Equipment Data Base

Subcomponent Descriptor File

FORM ID:	BNL.SWG001
NO. SUBCOMPONENTS:	55
GENERAL SUBCOMP TYPE:	Electrical devices
SPECIF SUBCOMP TYPE:	Relay, Power Breaker, Switch, Transducer
MANUFACT STANDARDS:	Not available
MANUFACTURER/MODEL:	*
SIZE LxWxH (INCHES):	Not available
WEIGHT (LBS):	Not available
LOCATION (ELEV-INCHES):	Various
MOUNTING TYPE:	Screws, details not available

TRS File

FORM ID: BNL.SWGR001			
TRS TYPE:	SSE	SSE	SSE
TRS DIRECTION:	FB	SS	V
TRS LOCATION:	Base	Base	Base
TRS DAMPING:	2%	2%	2%
1.0 HZ:	0.7g	0.7g	0.5g
2.0 HZ:	2.4g	2.3g	1.9g
3.2 HZ:	4.2g	4.2g	4.0g
4.0 HZ:	6.0g	5.9g	5.5g
5.0 HZ:	6.8g	5.6g	6.9g
6.3 HZ:	6.4g	5.6g	6.4g
8.0 HZ:	6.0g	5.6g	6.8g
10.0 HZ:	6.2g	6.0g	5.8g
12.5 HZ:	7.0g	6.5g	6.0g
16.0 HZ:	6.5g	8.0g	6.4g
20.0 HZ:	7.5g	9.5g	7.5g
31.5 HZ:	4.0g	4.0g	6.0g
PK1/HZ:	7.5g @ 20.0	9.5g @ 20.0	8.5g @ 25.0
PK2/HZ:	7.0g @ 12.5	5.9g @ 4.0	6.9g @ 5.0
ZPA:	2.3g	2.6g	2.8g

* Concealed information.

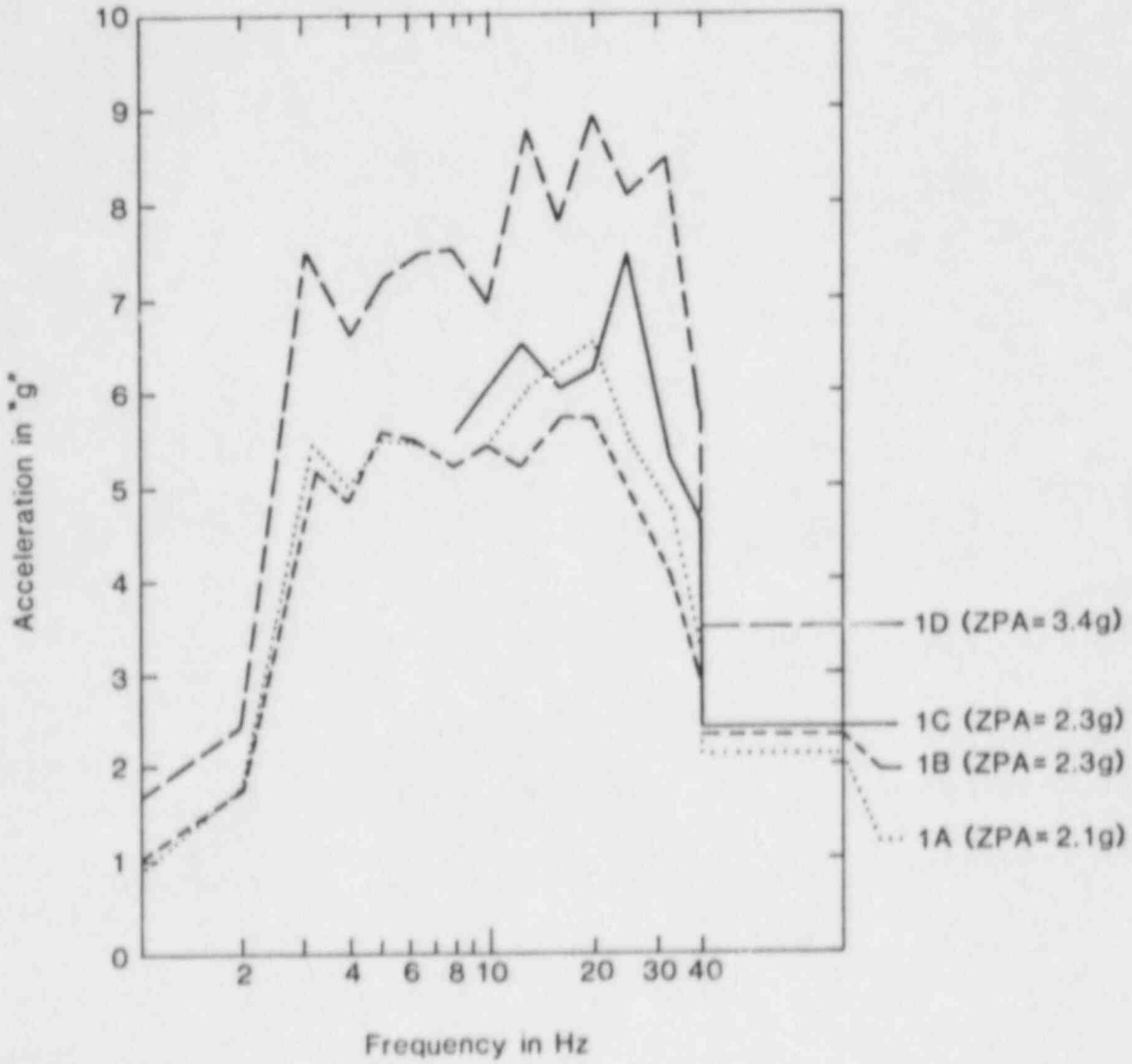

Fig. 1 Front-to-Back TRS at 2% Damping
Medium-Voltage Switchgear
Specimen Subjected to Various Vibration Levels

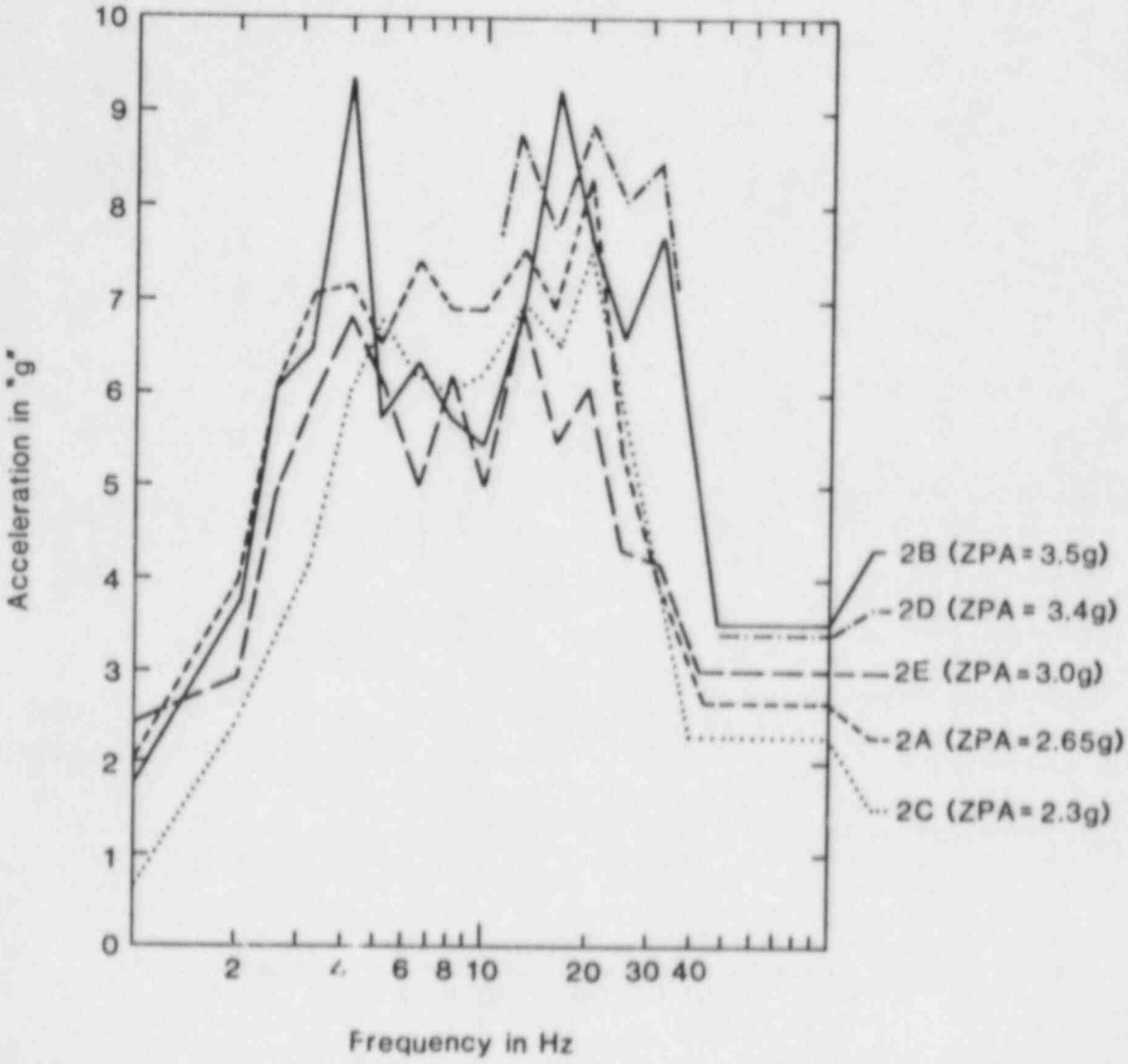

Fig. 2 Front-to-Back TRS at 2% Damping
Medium-Voltage Switchgear
Various Models from One Manufacturer

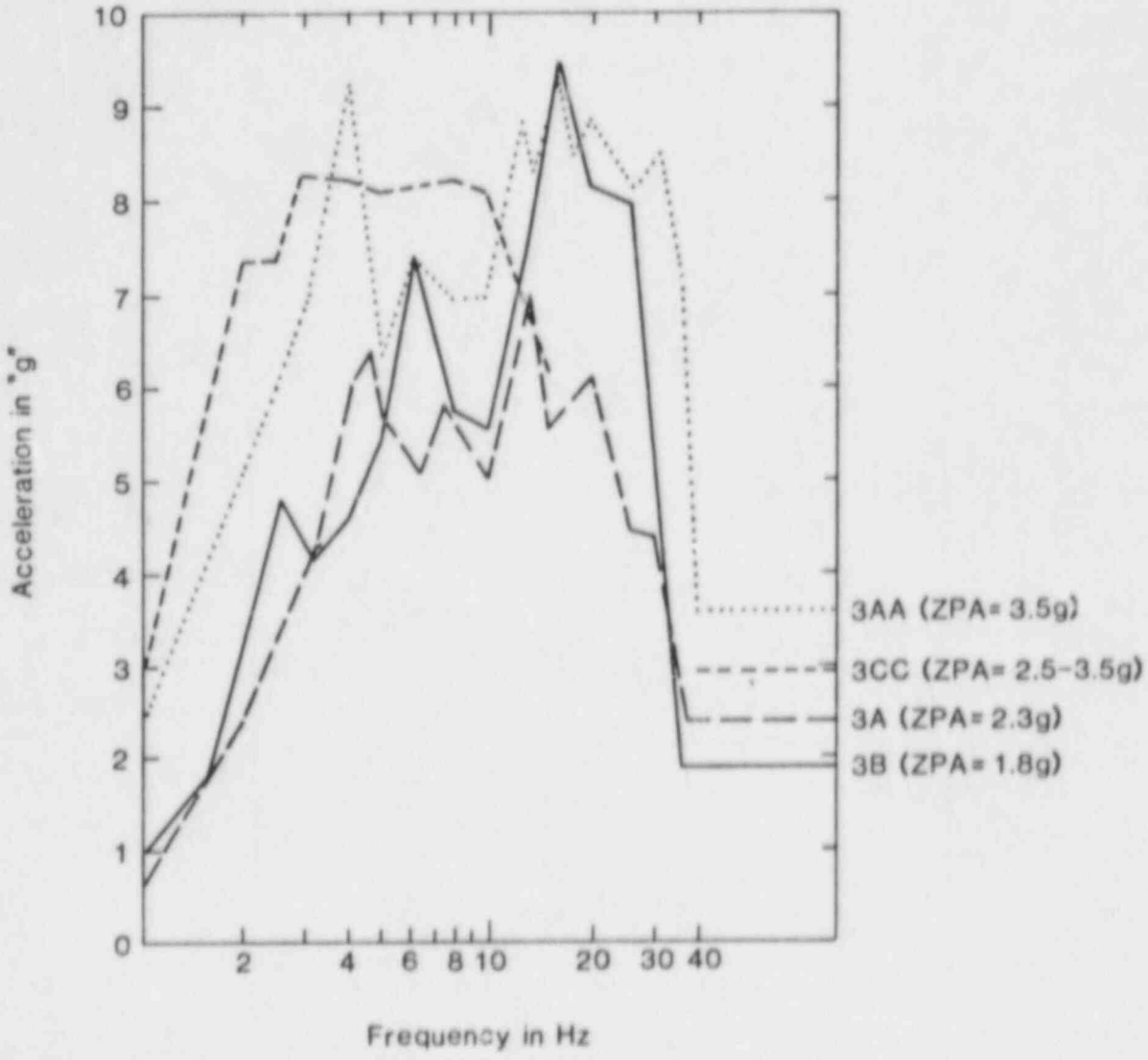

Fig. 3 Front-to-Back TRS at 2% Damping
Medium-Voltage Switchgear
Various Models from Three Manufacturers
(incomplete data)

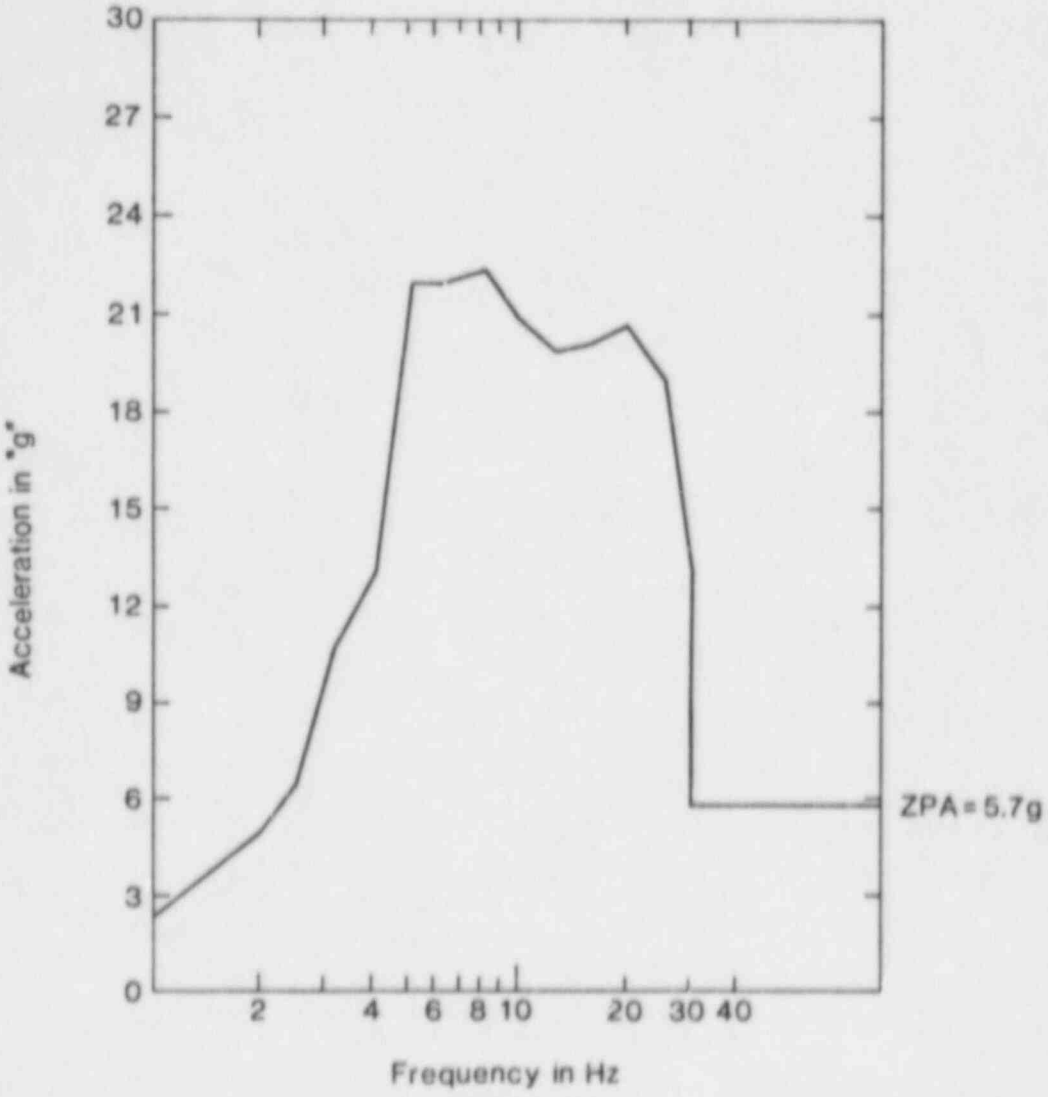

Fig. 4 Horizontal TRS at 2% Damping
Terminal Boards: Six Models from Five Manufacturers

Heissdampfreaktor Phase II Vibration Tests

Lothar Malcher, Kernforschungszentrum Karlsruhe,
HDR Project, FRG

Helmut Steinhilber, Fraunhofer Institut für Betriebsfestigkeit (LBF), Darmstadt, FRG

Chris Kot, Argonne National Laboratory
Argonne, Illinois, USA

1. INTRODUCTION

In the second phase of the earthquake investigations at the Heissdampfreaktor (HDR), FRG, high level shaker tests will be performed in June 1986. The purpose of these tests, supported by the German and U.S. Governments, is to investigate full scale structural response involving significant concrete and soil strains as well as strong indirect excitation of vessels, pipes and other mechanical equipment.

The vibrator, designed by ANCO Engineers, is a "coast- down" shaker, whose two eccentric masses of up to 40 tons, each on a common shaft, are brought up to speed in balanced condition. Unbalancing will take place after decoupling from the drive system and the shaker will then coast down through the building's resonances. Acceleations of 4 - 5 m/s^2 and corresponding displacements of $\pm$ 7 cm are expected in the fundamental rocking mode of the HDR building at 1 - 1.4 Hz.

In designing the shaker, extensive computer simulations of the dynamic behavior of the coupled shaker/HDR building system as well as safety calculations were carried out to evaluate the

load carrying capacity of the HDR building. This has resulted in a number of new findings over and above those contained in the presentation given at the 12th WRSRIM in OCtober 1984, which will be covered in this report.

2. FINAL DESIGN OF THE SHAKER

2.1 Shaker Frame

The design of the frame has been thoroughly changed over the original shaker design (cf. Fig. 1). This modification of the frame was necessitated by the problem of local load introduction and anchorage In the original design, the load was to be introduced into the HDR working platform through four buttresses. As a consequence of the softness of the frame, the global overturning moment of the rotating unbalanced masses would have resulted in a local instantaneous load on the floor in the region of the buttresses, which could not have been accommodated by that part of the structure. As a consequence, the shaker frame had to be stiffened in such a way that no such local moments can occur.

This resulted in the design shown in Fig. 2, with a square frame stiffened by diagonal ties. This frame is attached to anchor plates 4 cm thick which, in turn, are bolted to the floor by some 200 dowels for transmission of the horizontal forces (Fig. 3). Prestressed tie rods ("suspenders") at the four corners of the frame serve to introduce the tensile forces resulting from the global overturning moment into the load bearing walls approximately two meters below the floor (Fig. 4).

2.2 Eccentric Masses

Fig. 5 shows the design of the unbalance masses of the shaker. The total eccentricity of the shaker can be varied between 4000

and 145,200 kgm by a total of two sets of nine plates each of 100 and 180 mm thickness respectively, which are attached to the base plates of the shaker arms (see Fig. 6). Each steel plate is 1.70 m high. Its width has been dimensioned so that the two unbalance masses will just contact each other at an angle of 60° between the shaker arms.

2.3 Central Shaft, Shaker Arms, Drive

The two shaker arms are positioned on a shaft supported in the top and the bottom of the frame, one arm being permanently connected to the shaft, while the other arm is hinged to the shaft by means of an eccentric support. In the balanced condition, the movable shaker arm is immobilized in its position by fixing device (explosive bolt) to allow the desired starting frequency to be reached easily. When this frequency has been reached, the bolt is blown out and the driving system is decoupled. The energy of rotation of the movable shaker arm hinged to the eccentric support is used to bring the two shaker arms together and in this way produce the desired unbalance condition of the shaker arms.

Fig. 7 shows a schematic model of this setup as used in the simulation calculations, and a plan view of the design. The centrifugal force acting on the unbalance mass of the movable arm produces a moment in the position sketched here, which accelerates this mass in the direction towards the driven arm as soon as the explosive bolt in place during startup is blown out when the test starting frequency has been reached.

When the two shaker arms meet, the coupling mechanism must accomodate the collision impulse resulting from the difference in velocities of the two shaker arms. The collision impact is reduced by additional spring elements with progressive characteristics.

The shaker unit is driven by hydraulic motors supplied from a hydraulic system. Two electric motors of 220 kW each are used to drive the hydraulic pumps.

3. TEST PLAN

The SHAG test group will be carried ou in two steps:

Step one will be devoted to trials of the experimental setup in order to demonstrate its functioning capability and safety. This step will be called functional tests below and is planned for January 1986.

In these functional tests, the shaker will be operated in the unbalanced and balanced conditions, cf. Fig. 8. The trial runs in the balanced condition mainly serve for the verification of estimated parameters of traveling resistance:

- air drag,
- bearing friction,
- inertia of the system.

In the functional demonstration tests conducted in the unbalanced condition, the HDR will be loaded in the same way as in the main test, but at a lower load level. Obviously, the response behavior of the reactor during the functional tests will be logged by the central data acquisition system and these measured data will be used to verify the safety calculations and will serve as a basis of extrapolation for the main tests.

In Fig. 9, the force and frequency range of the unbalanced functional tests are compared to the force and frequency range of the main tests.

During these main tests it is intended to reach the highest possible loading without global structural failure of the building. Pretest calculations using linear and non-linear methods are performed not only for the maximum load case but for all test load cases. Selected acceleration and strain measurements serve to compare predictions and reality after each test to continuously update the remaining safety margin for the next test run. Fig. 10 + 11 show the actual test matrix for the main tests.

An important part of these tests is dedicated to a comparison of the behavior of stiff versus flexible piping systems. One selected piping, the VKL-System (Fig. 12), will be tested with three different support systems under equal loading conditions and at two different temperature and pressure levels.

Furthermore, NRC is planning to install a valve into the VKL-piping to perform operability tests during strong vibrations (cf. Fig. 12).

4. MEASURING SETUP

The measurements are to allow the load produced by the shaker to be traced up to the individual components selected in the HDR reactor building, the operations and processing building, and in the adjacent VAK plant. For this purpose,

- forces
- accelerations,
- velocities,
- displacements,
- strains,

will be measured for the duration of the experiment at specific points of the

- test setup,
- reactor building (internal structures, steel containment, outer containment),
- pipes and vessels inside the containment
- safety related points outside the HDR (see above).

These data will be recorded and output by the Central Data Acquisition System (ZMA). The measuring points are selected in such a way that both the excitation quantities and the vibration responses, stresses and boundary conditions of the structures under investigation will be considered.

Fig. 13 presents a rough overview of the type and scope of instruments to be used in the main tests.

For the functional tests, a selection of 85 of these measuring transducers will be instrumented.

The selection was made in the light of the following aspects:

- Better data should be made available on the air drag, bearing friction and other parameters dependent on the shaker, which are of importance in precalculating the experiments.

- Measurement of the vibration responses inside the HDR, in the office building, in the adjacent VAK power plant, and of strains at highly stressed points in the steel containment and the foundation is to allow a preliminary evaluation and calibration to be made of the safety calculations.

5. STATUS OF TEST PREPARATIONS, TIME SCHEDULE

The central shaker unit (shaft with the shaker arms) and the hydraulic driving system have already been delivered to the HDR plant. The shaker frame is under construction in Germany and will be delivered in November. The unbalance masses have been

fabricated and their weights set. The anchor plates will be installed in November. Installation of the shaker in the HDR plant will begin on January, 1986. The functional tests will be carried out in late Janauary 1986. The main experiments will be conducted as scheduled, in June 1986.

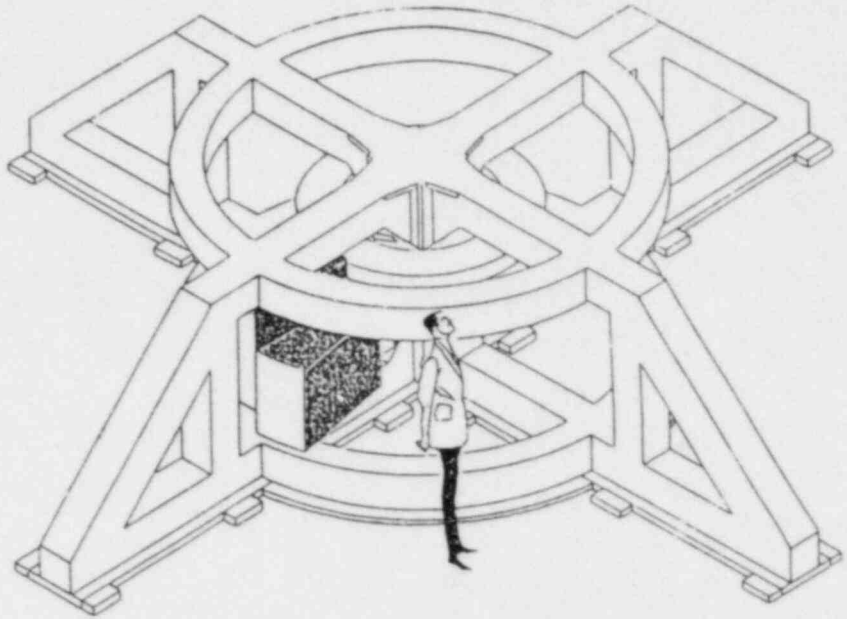

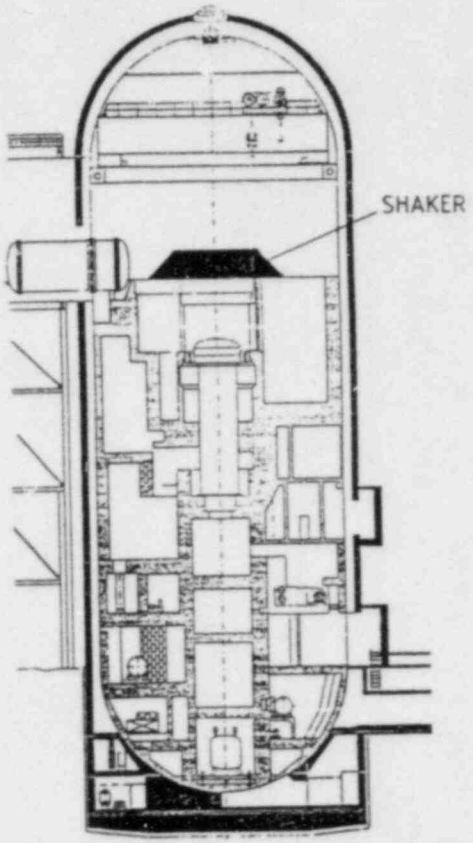

KfK

ANCO MK16 ECCENTRIC MASS VIBR. (ORIG. DES.) FIG. 1

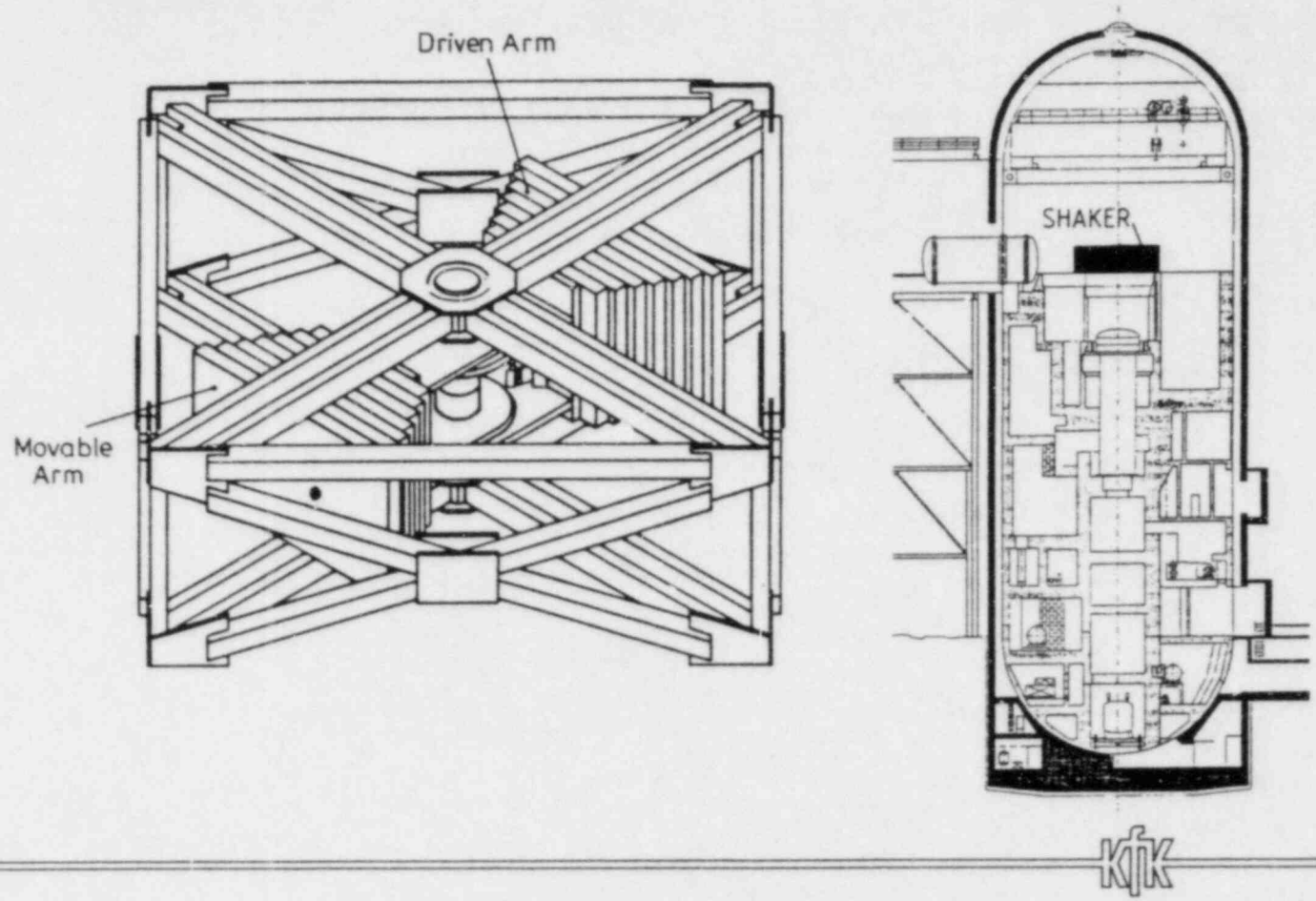

KfK

ANCO MK16 SHAKER (FINAL DESIGN)

FIG. 2

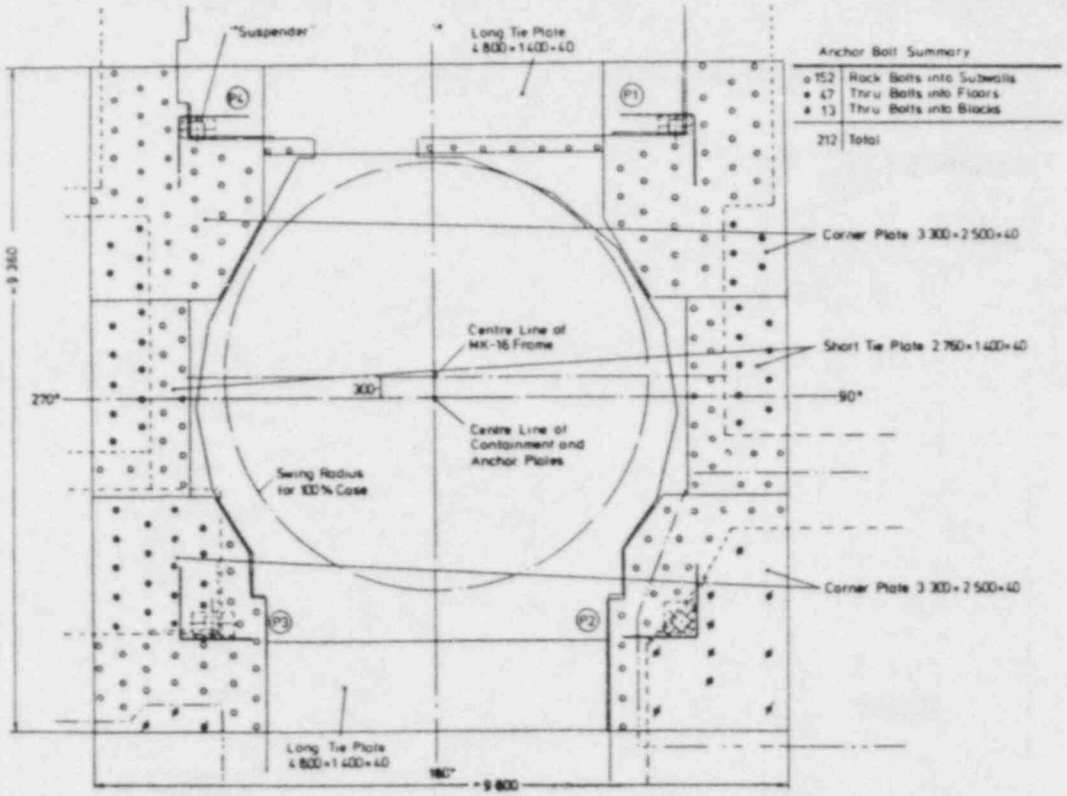

MK16 SHAKER ANCHORAGE

FIG. 3

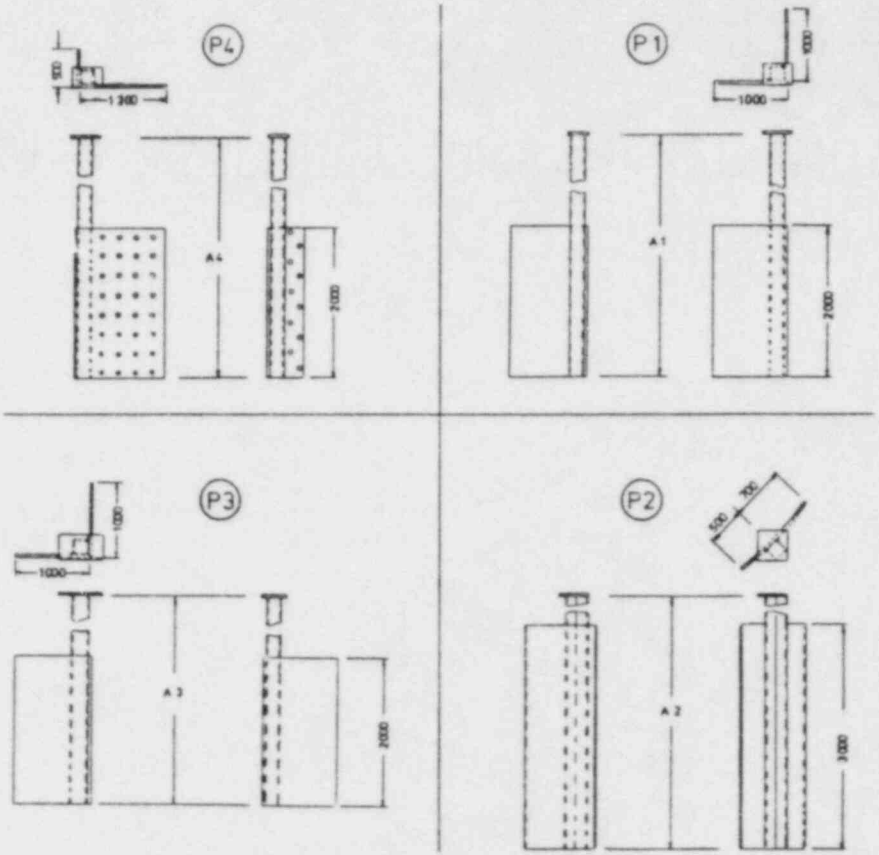

SUSPENDERS DESIGN

FIG. 4

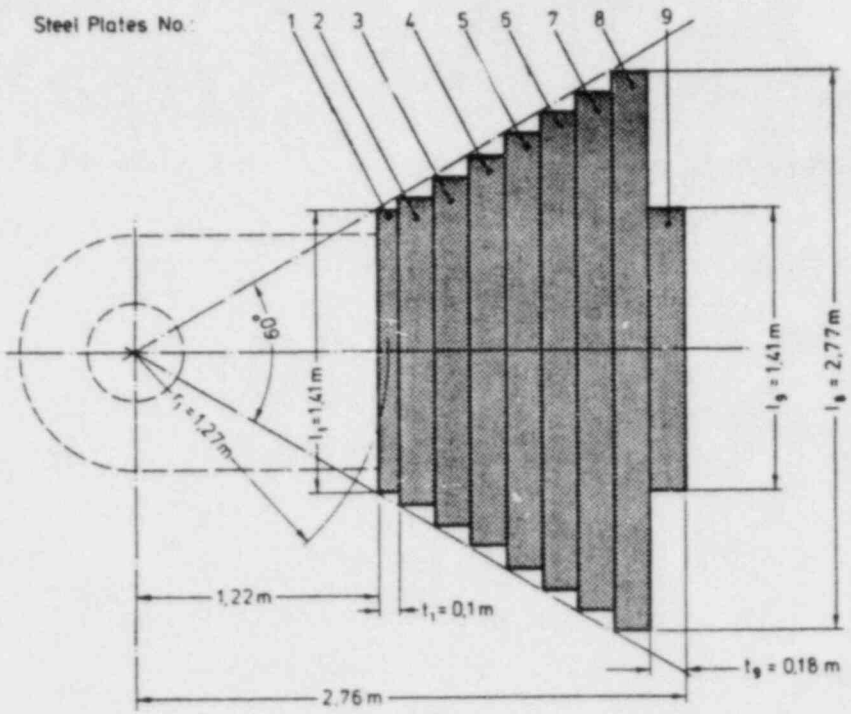

KfK

ECCENTRIC MASS ASSEMBLY (ONE SHAKER ARM) FIG. 5

Steel Plates No.	1	2	3	4	5	6	7	8	9
Thickness t_i in mm	100	180	180	180	180	180	180	180	180
Length l_i in mm	1 408	1 523	1 731	1 939	2 147	2 354	2 562	2 770	1 411
Mass m_i in kg	1 879	3 658	4 158	4 658	5 157	5 655	6 154	6 654	3 389
Radius r_i in mm	1 269	1 409	1 589	1 769	1 949	2 129	2 309	2 489	2 669
Eccentricity Contribution of both Arms in kgm[+)]	4 200	8 600	11 000	14 200	18 000	18 000	23 800	33 200	10 200
Total Eccentricity of both Arms in kgm[+)]	8 200	16 800	27 800	42 000	60 000	78 000	101 800	135 000	145 200

All Steel Plate widths 1 700 mm

[+)] ANCO - Telex 12.7.1985

KfK

OVERVIEW ON SHAKER ECCENTRICITIES FIG. 6

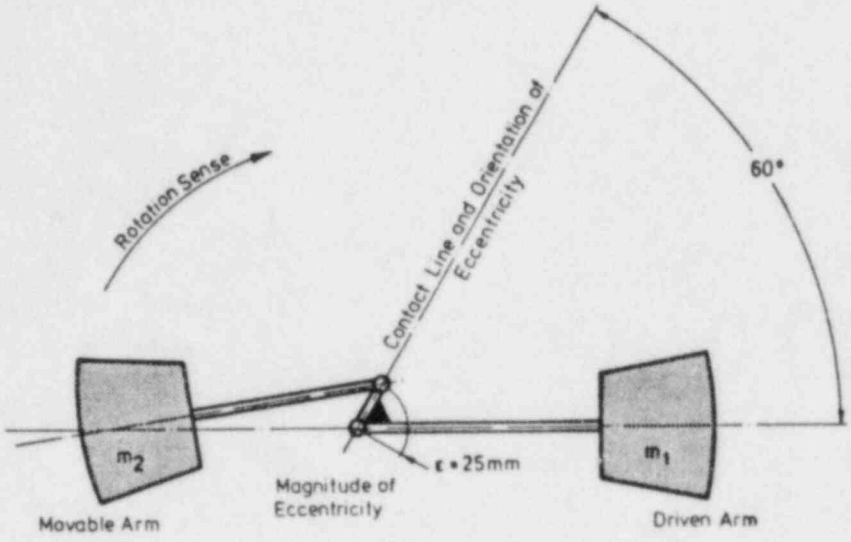

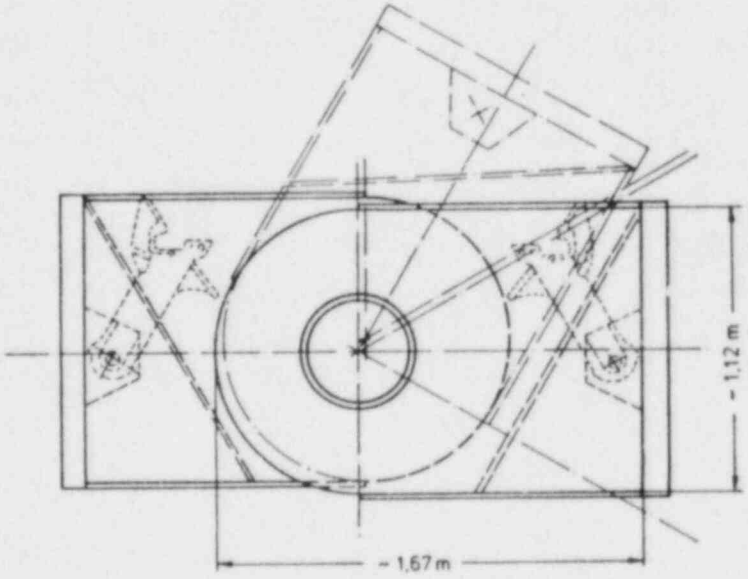

CENTRAL HUB ASSEMBLY FIG. 7

Test Run No.	Shaker Configuration	max. Shaker Force in kN	Mass		Shaker Eccentricity in kgm	Starting Frequency in Hz	Remarks
			Total in kg	Remarks			
T 40.01	balanced	-	8 070	only Arms	4 000 *)	8,0	
T 40.02	unbalanced	3 198	8 070	only Arms	4 000	4,5	
T 40.03	balanced	-	19 144	1.+2.Steel Plates	16 800 *)	4,0	
T 40.04	unbalanced	2 149	19 144	1.+2.Steel Plates	16 800	1,8	
T 40.05	balanced	-	90 794	1.-9.Steel Plates	145 200 *)	0,2 / 0,5	max. Mass

*) Shaker Eccentricity Corresponding to Unbalanced Shaker Configuration

KfK

TEST MATRIX FUNCTIONALITY TESTS FIG. 8

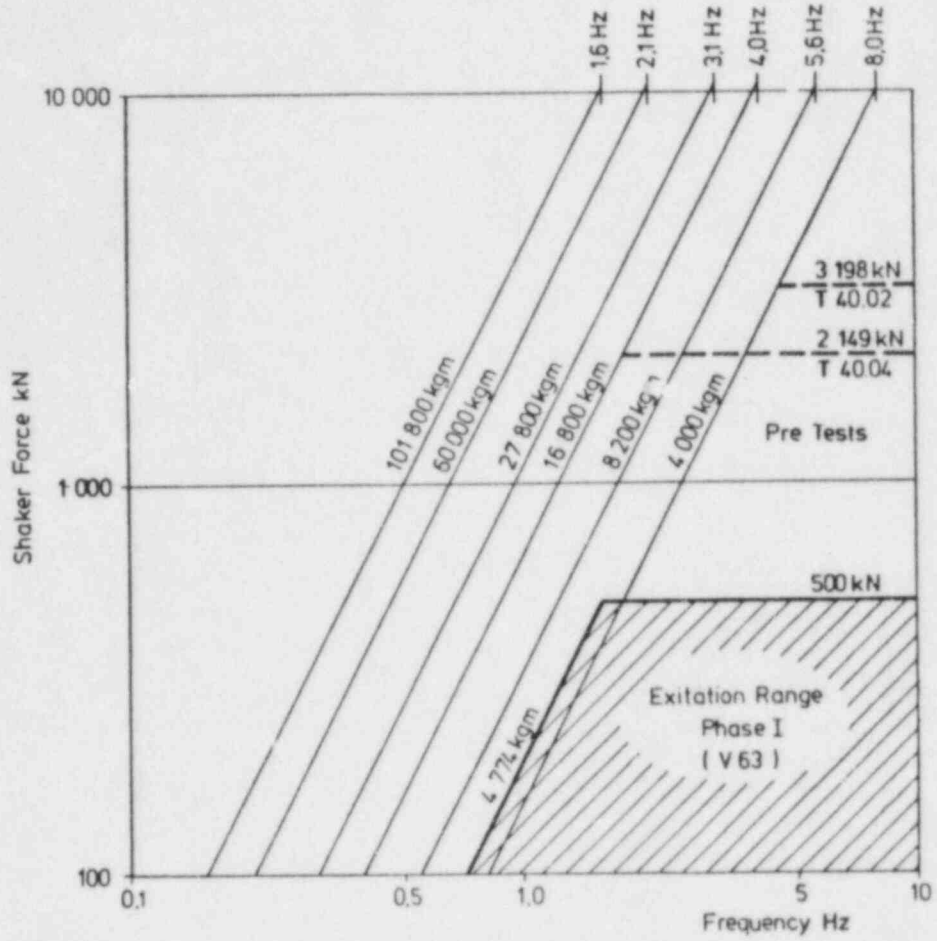

FORCE/FREQUENCY FUNCT. TESTS FIG. 9

Run No. T 40.	System Conditions		Shaker Eccentricity kgm	Starting Frequency Hz	Max. Force kN
	Temp.	Conf.+)			
11	20°	1	4 000	6.0	5 700
12			4 000	8.0	10 100
13			8 200	5.6	10 150
14			16 800	4.0	10 600
15	20°	1	27 800	2.1	4 840
16	20°	1	60 000	2.1	10 450
17			101 800	1.6	10 300
18	20°	1	27 800	3.1	10 550
19	285°	1	8 200	5.6	10 150
20			16 800	4.0	10 600

+) Configuration 1 : German Design of Supports

KfK

TEST MATRIX MAIN TESTS (PART1) FIG.10

Run No. T 40.	System Conditions		Shaker Eccentricity kgm	Starting Frequency Hz	Max. Force kN
	Temp.	Conf.+)			
21	20°	2	8 200	5.6	10 150
22			16 800	4.0	10 600
23	285°	2	8 200	5.6	10 150
24			16 800	4.0	10 600
31	20°	3	8 200	5.6	10 150
32			16 800	4.0	10 600
33	285°	3	8 200	5.6	10 150
34			16 800	4.0	10 600

+) Configuration 2 : NRC - Design of Supports
3 : Weak Supports

KfK

TEST MATRIX MAIN TESTS (PART2) FIG. 11

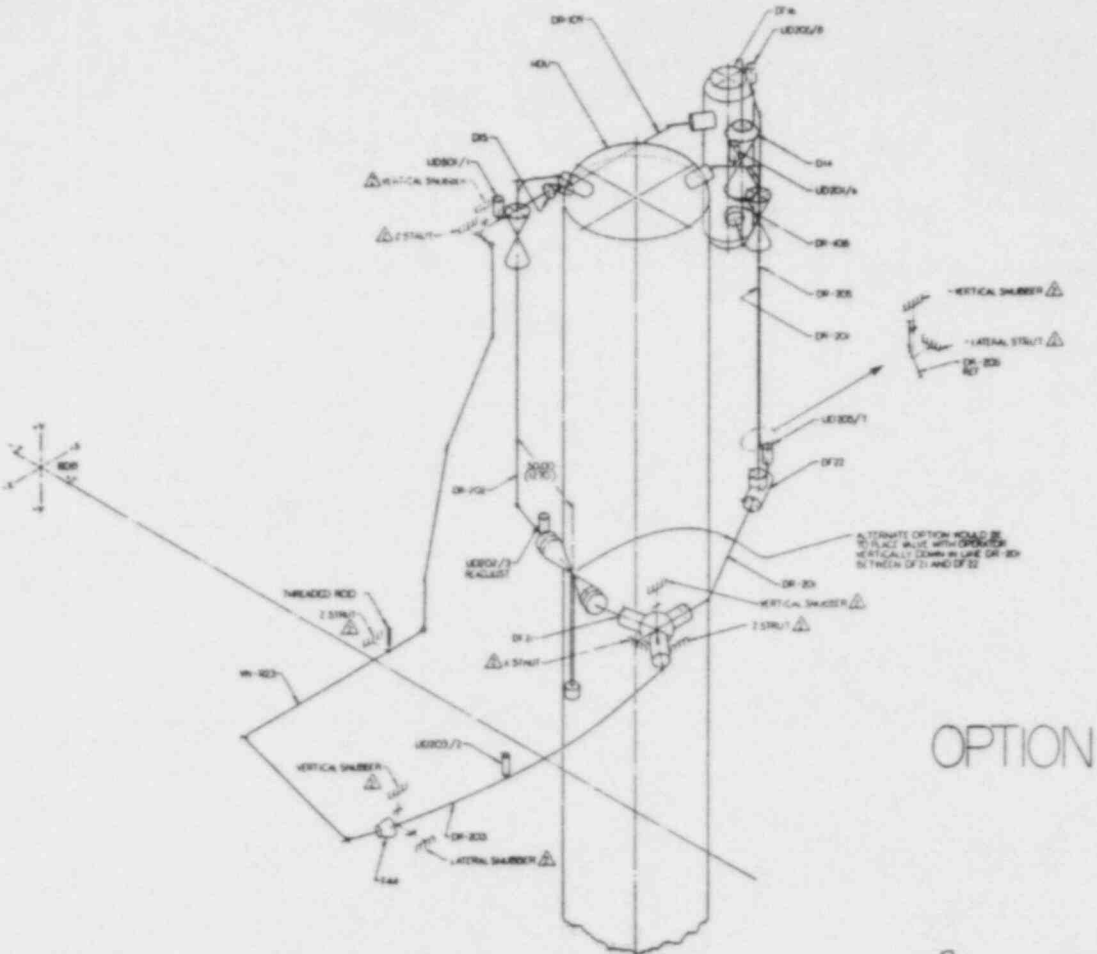

VKL SYSTEM WITH USNRC VALVE

Fig12

STRUCTURE \ TRANSDUCER TYPE	ACCELERATION	DISPLACEMENT	STRAIN	FORCE	PORE WATER PRESSURE	INTERFACE GAGES	ALL TRANSDUCERS
REACTOR BUILDING	36	12	50	12	-	-	110
RPV + CORE BARREL	8	8	20	10	-	-	46
PDL	12	11	10	2	-	-	35
HDU / VKL	12	12	20	6	-	-	50
RESONANCE PLATFORM	10	8	20	12	-	-	50
ALL OTHER COMPONENTS	20	10	20	-	-	-	50
SOIL NEAR FIELD	12	-	-	-	6	2	36
SOIL FAR FIELD	16	-	-	-	-	-	
HDR OFFICE BUILDING	12	-	-	-	-	-	12
VAK AND OTHER NEIGHBOUR FACIL.	8	-	-	-	-	-	-
ALL STRUCTURES	146	61	140	42	6	2	397

OVERVIEW ON INSTRUMENTATION EFFORT FIG. 13

BWR RISK ASSESSMENT*

by

T. Y. Chuang, D. L. Bernreuter, J. C. Chen
G. E. Cummings, D. A. Lappa, J. J. Johnson, J. E. Wells
Lawrence Livermore National Laboratory

Abstract

The simplified seismic risk methodology developed in the U. S. NRC Seismic Safety Margins Research Program (SSMRP) was demonstrated by its application to the Zion nuclear power plant, a pressurized water reactor (PWR). A detailed model of Zion, including systems analysis models (initiating events, event trees, and fault trees), SSI and structure models, and piping models, was developed and used in assessing the seismic risk of the Zion nuclear power plant, a PWR. The simplified seismic risk methodology is being applied to the LaSalle County Station nuclear power plant, a boiling water reactor (BWR), in order to further demonstrate its applicability, and to provide a basis for comparing the seismic risk from PWRs and BWRs.

1. Introduction

The Seismic Safety Margins Research Program (SSMRP) (1) was a multi-year program conducted by the Lawrence Livermore National Laboratory (LLNL) and funded by the U. S. Nuclear Regulatory Commission (NRC). Its goal was to develop a complete, fully coupled analysis procedure (including methods and computer codes) for estimating the risk of a seismically induced radioactive release from a commercial nuclear power plant. The analysis procedure is based upon a state-of-the-art evaluation of the current seismic analysis and design process and explicitly accounts for uncertainties inherent in such a process.

The seismic risk methodology developed in the SSMRP was demonstrated by its application to the Zion nuclear power plant (2), a pressurized water reactor (PWR). A detailed model of Zion, including systems analysis models (initiating events, event trees, and fault trees), SSI and structure models, and piping models, was developed and analyzed. At the request of the U. S. NRC, LLNL has developed a simplified seismic risk assessment methodology (3). The purpose of this methodology is to reduce cost while adequately assessing the seismic risk from a nuclear power plant. The simplified methodology was used to assess the seismic risk from the Zion nuclear power plant. These results were then compared with the results from the detailed analysis. It was found that the simplified method generally provides more conservative results than the detailed one. To demonstrate its applicability, and to provide a basis of comparison of seismic risk between a PWR and a BWR when analyzed with comparable methodology and assumptions, a seismic risk analysis is being performed on the LaSalle County Station.

*This work was supported by the U. S. Nuclear Regulatory Commission under a Memorandum of Understanding with the U. S. Department of Energy.

A brief methodology overview of seismic risk analysis is presented in Section 2. Section 3 describes the LaSalle County Station. The development of the seismic input for the LaSalle site is described in Section 4. It briefly delineates the methodology used to develop the hazard curves as well as the results, the LaSalle hazard curves. Section 5 discusses the seismic responses of structures and components. Three aspects of seismic responses are discussed: median level response, variability of response and correlation of response. The structure and component fragilities are described in Section 6. Fragilities were developed for all structural elements in the critical structures. Component fragilities were treated in two ways: LaSalle specific fragilities were derived for major components (e.g., reactor pressure vessel, pumps and etc.) and generic fragilities were used for other components. Section 7 presents a limited investigation of the effects of hydrodynamic loads on the seismic risk. The plant logic models are described in Section 8. Two sets of fault trees were generated. One is a simple set of fault trees while the other is more detailed and complete. Comparison of the results using these two sets will be made. Section 9 delineates the seismic risk quantification. Finally, conclusions of this study are presented in Section 10.

2. Methodology Overview

Seismic risk analysis can be considered in five steps: seismic hazard characterization (seismic hazard curve, frequency characteristics of the motion); seismic response of structures and components; structure and component failure descriptions; plant logic models (fault trees and event trees); and probabilistic failure and release calculations.

Key elements of the LaSalle simplified seismic risk analysis are to:

- Develop the systems models (e.g., event and fault trees)
- Benchmark best estimate seismic response of structures, components, and piping systems with design values for the purposes of specifying median responses in the seismic risk calculations
- Develop the seismic hazard at the LaSalle site including the effect of local site conditions
- Develop building and component fragilities for important structures and components
- Investigate the effects of hydrodynamic loads on seismic risk
- Estimate the seismically induced core melt frequency.

3. LaSalle County Station

LaSalle County Station is located in the agricultural area of Brookfield Township, LaSalle County, Illinois. It is approximately 55 direct-line miles southwest of Chicago and 20 miles west of Dresden power station. The station utilizes two single-cycle forced-circulation boiling water reactors, each rated at 3293 MWt and designed for 3434 MWt. The gross electric output of each unit is 1122 MWe; the net output is 1078 MWe from each General Electric (GE) turbine-generator. The nuclear steam supply system (NSSS) supplier was GE (Nuclear Energy Division).

The containment design employs the BWR Mark II concept of over-under pressure suppression with multiple downcomers connecting the reactor drywell to the water-filled pressure suppression chamber. The primary containment is a steel-lined, post-tensioned,

concrete enclosure, housing the reactor and the suppression pool. This primary containment is entirely enclosed in the reinforced concrete reactor building which is the secondary containment structure. The power generation complex includes several contiguous buildings-two reactor buildings, an auxiliary building (housing the control room), the turbine building, diesel-generator buildings, the radwaste building, the service building, and the off-gas building.

4. Seismic Input

The methodology used to develop the hazard curves (the probability of exceeding any given level of peak ground acceleration, PGA) is based on the methodology and data given in (4). Descriptions of the zonation, seismicity and choice of ground motion model are based on the opinions of eleven seismicity experts and five ground motion experts. These expert opinions were used to supplement the available data. One of the important features of the methodology is to identify and assess the uncertainty in all the parameters of the analysis, and propagate that uncertainty using a Monte Carlo simulation approach. The parameters used in the simulations are described by probability distributions. The zonation maps and the ground motion models have discrete probability distributions. All other variables have continuous probability distributions.

The one major departure from the methodology described in (4) was in the way local site conditions were taken into account. In (4), three types of approaches are used to incorporate the local site effect. The first approach is to make no correction for site type. The second approach is to use only a simple soil or rock classification for a site and apply a simple constant correction factor for each site category. The third approach is to apply a set of generic site correction factors to the category of a site. The generic site correction factors were obtained with 1-D wave propagation analysis. Eight site categories were developed based on the available site parameters of eastern U.S. power plant sites. The ground motion panel experts then provided weights for the three approaches.

In this study the time histories of motion used in the structural analysis for the LaSalle structures were developed in the following manner. First, hazard curves were developed at a hypothetical rock outcrop at the LaSalle site using the approach discussed above and based on the models given in (4). Secondly, strictly speaking, a set of event specific spectra (2), should have been developed for the LaSalle site. However, in keeping with the simplified methods approach, we used the two sets of rock outcrop time histories developed for the Zion site based on the argument that the LaSalle site is reasonably close to the Zion site, thus the distribution of earthquakes contributing to the hazard would be similar for the two sites. Finally, to correct for the local soil conditions, these rock outcrop time histories are then propagated through the LaSalle soil column as discussed below in Section 5 to get the time histories used in the SSI analysis. It should be noted that these time histories have the appropriate duration for distribution of earthquakes occurring near the LaSalle site. The duration of the earthquake varies from 5 to 18 seconds.

The hazard curves developed for the LaSalle site are for a hypothetical rock outcrop at the site. A Monte Carlo numerical simulation techniques were applied to account for uncertainty. A total of 2750 simulations were used. Each simulation gives one hazard curve. Figure 1 shows the resultant 15th, 50th and 85th constant percentile hazard curves based on the 2750 simulated hazard curves. It also shows the median and

range of the actual computed values of the PGA at the top of the soil column at the LaSalle site at the 0.2g and 0.6g rock outcrop PGA levels. The site specific values for the LaSalle site generally show a deamplification at the 0.6g PGA rock outcrop level. This is because the soil column at the LaSalle site is very soft and exhibits a large nonlinear effect at the higher PGA levels leading to a deamplification of the computed PGA.

5. Seismic Response of Structures and Components

For each level of earthquake described by the seismic hazard curve, three aspects of seismic response are necessary to perform the seismic risk analysis: median level (or best estimate) response, variability of response, and correlation of responses. Seismic responses are required for all structures and components contained in the plant logic models. These responses together with fragilities allow for the calculation of seismically induced failure probabilities. The three aspects of seismic response are discussed:

- Median level response: the median level response given an earthquake occurrence is needed. In general, this median level response differs from the design values because, in the latter case, design analysis procedures, parameter selection, and qualification procedures are conservatively biased.

- Variability of response: variability in seismic response resulting from variations in the earthquake excitation, the physical properties of the soil/structure/piping system, and our ability to model them must be acknowledged and included in the seismic risk analysis to permit calculation of probability of component failure and core melt frequency.

- Correlation of response: tendency for pairs of responses to have simultaneously high or low values results from two sources -- the level of the earthquake and the dynamic characteristics of the system. The level of the earthquake affects correlation since a large earthquake (large peak acceleration) may cause all response to be large, whereas, a small earthquake produces the opposite effect. The second source of correlation is due to system response itself. For example, floors within a structure may all experience high values of response simultaneously due to the dynamic characteristics of the structure itself.

Three approaches to developing median level responses are possible: re-calculation using best-estimate methods and parameters such as was done in the SSMRP; scaling of design responses to account for conservatisms introduced in their development; and a combination of the two preceding approaches, i.e., a limited amount of re-calculation of the response using best-estimate methods and parameters and a use of scale factors applied to the design responses. The latter case is being applied to the LaSalle seismic risk assessment.

The basic strategy for developing median level responses was to perform selected probabilistic response analyses of the LaSalle structures for two ranges of earthquakes -- a lower level earthquake and a higher level earthquake henceforth called Acceleration Range 1 and 2, respectively. Results of the analyses gave probability distributions on two types of response -- in-structure forces and moments to be used in the fragility evaluation of the structures themselves; and in-structure response spectra at equipment

and component locations for their fragility evaluation. Two acceleration levels were considered to permit interpolation for other earthquakes of different peak accelerations. Each element of the probabilistic response analysis is discussed:

- Seismic hazard. The seismic hazard for the LaSalle site is specified on a rock outcrop due to the presence of a shallow soil layer (approximately 170 ft.) overlying the stiff bedrock. Local site amplification was taken into account explicitly as described below. Specifying the seismic hazard for the purpose of the seismic risk assessment entailed specifying the hazard curve — the probability of occurrence of an earthquake of given peak ground acceleration, and the frequency characteristics of the motion — an ensemble of acceleration time histories (three components per earthquake simulation) on the rock outcrop.

- Local site amplification. Using equivalent linear viscoelastic soil properties developed as a function of earthquake excitation level and the assumption of vertically propagating waves, earthquake motions on the soil surface were developed for response prediction. This representation of local site amplification is a source of modeling uncertainty. Mean response spectra on the soil free surface for Acceleration Range 1 are shown in Fig. 2.

- Soil-structure interaction (SSI) parameters. The soil configuration and low strain soil properties were established based on the boring logs and soil reports for the LaSalle site. Nominal soil properties as a function of excitation level were estimated from a series of SHAKE analyses (5) using rock outcrop motion as input and material property variations vs. strain relations developed by the geotechnical engineer for the utility. SSI parameters (foundation impedances and scattering matrices) were developed for the important LaSalle buildings and the CLASSI programs (6). The LaSalle structure analyzed in detail is a single complex structure which contains the reactor building, the auxiliary building, the turbine building, the off-gas filter building, the service building, and the diesel generator buildings. An average embedment of approximately 51 ft. was treated in developing the SSI parameters.

- Structure model. Structure models developed by the utility and used in the design seismic analysis were used in the probabilistic response analyses. Fixed-base eigensystems for the horizontal and vertical models were developed by the utility for use in the analyses. The SMACS methodology (7) of the SSMRP was used here. SSI is treated by the substructure approach.

- Response analyses. SMACS analyses were performed on the LaSalle structure complex including the effects of SSI. SMACS links together seismic input, SSI, structure response, and piping system and component response. All aspects except piping system responses which were calibrated by using design values (3), were calculated — component response was determined from in-structure response spectra. Variability is treated in SMACS. For the LaSalle SMACS analyses, variability due to randomness only was treated. 48 in-structure response spectra were calculated for equipment and component failure assessment. 145 structure forces and moments were calculated for structure failure assessment.

Median responses were calculated directly for the two acceleration ranges or scaled from the design results based on scale factors developed here or in previous studies. Variability and correlation of responses were assigned based on previous studies and recorded data.

Median in-structure response spectra provided the response input for the probabilistic failure calculations of components. In some instances, the LaSalle SSE design response spectra were overplotted with these in-structure spectra for comparison purposes. One difficulty in interpreting the comparisons of median response spectra of Acceleration Range 1 and 2 and the design spectra is a lack of correlation of the design free-field ground motion and that of Acceleration Range 1 and/or 2. The LaSalle seismic design criteria specify the design ground motion at foundation level (44 feet below the surface) and no free surface response spectra are available. The LaSalle seismic hazard for this study was defined on a hypothetical rock outcrop and local site amplification was treated explicitly. Hence, no direct comparison of free-field ground motion can easily be made. The median peak ground acceleration (PGA) of Acceleration Ranges 1 and 2 are approximately 0.2g and 0.35g, respectively. Neither of these correspond to the design PGA of 0.2g at foundation level. Frequency content of the free surface motion for this study and the design are likely to be quite different. Recognizing the difficulty in comparing the results, one still observes that the design spectra are generally conservative compared to median response spectra for Acceleration Range 1 and, in some frequency ranges, notably above 2 Hz., very conservative. Comparing the design spectra with those of Acceleration Range 2, the latter frequently exceeds the former at low frequencies but the design spectra are generally very conservative in the high frequency range. Figure 3 shows a typical comparison.

6. Structure and Component Fragilities

The development of structure fragilities proceeded as follows. A review of the seismic design analysis results and development of a preliminary set of structure element capacities initiated the task. Simultaneously, a preliminary SMACS analysis was performed for a single earthquake simulation at near the SSE level to provide a basis of comparison with the design results. Having reviewed the design analysis results and structure model, changes in the structure model to better capture the expected behavior of the structure were recommended and incorporated into the SMACS analysis. Additional preliminary SMACS analyses were performed, loads generated, and an assessment of the model modification made. The initial model changes led to limited load redistribution and motivated a second set of model changes which were incorporated into the SMACS model and again evaluated. The result was the best-estimate structure model. 145 structure forces and moments at two excitation levels were obtained from the SMACS analyses and used in the fragility development. A comparison of the capacities of the structural elements with the SMACS generated median loads shows very large ratios for Acceleration Ranges 1 and 2 which makes it highly unlikely that structural failure will occur for any excitation level considered in the hazard curve, i.e., structural element failure will have very low probabilities of occurrence.

Component fragilities were developed for major LaSalle components identified as important in terms of systems behavior and risk. Examples are items such as: reactor pressure vessel, reactor internals, recirculation pump, diesel generators, pumps (HPCS, RCIC, RHR, RHR, SW), batteries, switchgear, SBLC pump & tank, suction strainer (HPCS, RCIC, LPCS, RHR), and etc. LaSalle specific design reports and equipment

qualification data were used as the principal basis for fragility assessment. Median level responses were used in the fragility assessment as generated from the SMACS analyses. A comparison of median response for Acceleration Ranges 1 and 2 with the capacities of components considered here shows large margins and that the failure probabilities of these components due to seismic events will likely be quite small.

7. Hydrodynamic Loads

In a seismic risk analysis of a BWR, it is necessary to consider the combined effects of seismic loads and one or more hydrodynamic load since seismic events can potentially induce hydrodynamic events (safety relief valve (SRV) discharge, pool swell, condensation oscillation, and chugging). For LaSalle, we evaluated which of these loads were likely to occur simultaneously with an earthquake and developed a probabilistic approach for combination of the seismic and hydrodynamic responses. The approach was applied to the combination of seismic and SRV discharge responses. Based on the results of several case studies, simple combination rules for obtaining the median and the logarithmic standard deviation of the combined responses from the median and logarithmic standard deviation of the individual responses were developed. The seismic risk analysis is performed for the combined seismic and SRV events.

The need for combining hydrodynamic load responses with seismic response depends on the relative magnitudes of the individual responses, the time-phasing of the loads, and the conditional probability of the hydrodynamic load being induced by earthquakes. Based on the screening criteria developed for this study, only certain SRV load responses and, possibly, condensation oscillation load responses need be combined with seismic responses.

The SRV loading was considered in detail. Note, the SRV-all is the dominant case for vertical response and SRV-asymmetric is dominant for horizontal response. Our efforts focused on the effect of the hydrodynamic loads on equipment function rather than stress related failures of ductile components and structures. It was judged that the high frequency nature of the loads would have negligible effect on stress to failure of ductile components. Hence, we focused on equipment response as characterized by in-structure response spectra. Two sets of information formed the basis for estimating median SRV responses — the in-structure design response spectra and the results of limited in-plant tests. From the in-plant test results, in-structure design response spectra were reduced to an estimated median response level. The logarithmic standard deviation of the SRV loading was estimated to be 0.3.

The median combined response (seismic and SRV) may be obtained approximately by the SRSS combination of the median maximum responses of the individual values. This rule was evaluated for a number of cases using the time history response due to seismic and that due to SRV. The logarithmic standard deviation of the combined response is expressed as a function of the median and logarithmic standard deviations of the individual maximum responses. These rules were used to combine the seismic responses for each acceleration level of the seismic hazard curve with the SRV responses for the seismic risk analysis. Qualitatively, the effect of SRV loading on the combined seismic and SRV response was small for the components of interest.

8. Plant Logic Models

The accident sequences in the LaSalle analysis were identified using event trees (8). Two sets of event trees were used. One set was developed by the Risk Methodology Integration Evaluation Program (RMIEP) (9). The other set is more simple and was developed at LLNL.

Fault tree analysis (10) was used to define the failure paths in the accident sequences. For LaSalle two sets of fault trees were also generated. One is a simple set (9 systems) while the other is more detailed and complete (23 systems). The simple set of fault trees were developed by LLNL independently from the detailed set of fault trees generated by the RMIEP. Two sets of fault trees were generated so that a comparison between them could be made. This comparison will indicate whether or not highly detailed fault trees are warranted for a simplified seismic risk analysis.

RMIEP fault trees were generated for all the major safety systems at LaSalle and included the support systems, such as electric power and component cooling water. Consequently, the trees are quite large, involving thousands of gates and events. To make the problem manageable, the fault trees were probabilistically culled to obtain the minimal cut sets.

The system fault tree minimal cut sets were combined according to the event tree logic to give Boolean expressions for each accident sequence. Each accident sequence was culled so that it contained no more than 5000 minimal cut sets. This was done to accommodate the risk quantification process.

The initiating event definitions are the remaining elements of the plant logic model. Because of pipe and component failures, the probability of an initiating event occurring during a seismic event is increased over that of an event containing only random failures. All the initiating events developed by the RMIEP were studied and their relationship to the seismic problem assessed. Based on that study, the appropriate pipe and component failures were used to define initiating event minimal cut sets.

9. Seismic Risk Quantification

The quantification of seismically induced failure probabilities and core melt frequency are accomplished in the computer program SEISIM (11). SEISIM computes the failure probabilities taking into account the dependence between basic events. SEISIM does this by computing the multi-normal integral whose integrand is specified by the means, standard deviations, and correlations of responses and fragilities.

In addition to computing core melt frequency, SEISIM also performs an importance analysis whose objective is to find the initiating events, components, accident sequences, etc., that most influence the results. Results from the importance analysis are used to focus attention on key contributors to seismic risk.

10. Conclusion

A seismic risk assessment using the simplified methodology developed in the SSMRP is being conducted on the LaSalle County Station, a BWR. Both simple and detailed plant logic models will be evaluated. So far, our results indicate low seismic responses of plant structures and components. This is at least partly due to the soft soil at the LaSalle site which attenuates the earthquake motion. These low responses coupled with seismic capacities of structural elements and components suggest low probabilities of seismically induced failure.

References

(1) Smith, P. D., R. G. Dong, D. L. Bernreuter, M. P. Bohn, T. Y. Chuang, G. E. Cummings, J. J. Johnson, R. W. Mensing, and J. E. Wells, "Seismic Safety Margins Research - Phase I Final Report," Lawrence Livermore National Laboratory, Livermore, California, UCRL-53021, NUREG/CR-2015, Vols. 1-10, 1981.

(2) Bohn, M. P., L. C. Shieh, J. E. Wells, L. C. Cover, D. L. Bernreuter, J. C. Chen, J. J. Johnson, S. E. Bumpus, R. W. Mensing, W. J. O'Connell, and D. A. Lappa, "Applications of the SSMRP Methodology to the Seismic Risk at the Zion Nuclear Power Plant," Lawrence Livermore National Laboratory, Livermore, California, UCRL-53483, NUREG/CR-3428, 1984.

(3) Shieh, L. C., J. J. Johnson, J. E. Wells, J. C. Chen, and P. D. Smith, "Simplified Seismic Probabilistic Risk Assessment: Procedures and Limitations," Lawrence Livermore National Laboratory, Livermore, California, UCID-20468, NUREG/CR-4331, 1985.

(4) Bernreuter, D. L., J. B. Savy, R. W. Mensing, J. C. Chen, and B. C. Davis, "Seismic Hazard Characterization of the Eastern United States, Vol. 1: Methodology and Results for Ten Sites and Vol 2: Questionnaires," Lawrence Livermore National Laboratory, Livermore, California, UCID-20421, 1985.

(5) Schnabel, P. B., J. Lysmer, and H. B. Seed, "SHAKE--A Computer Program for Earthquake Response Analysis of Horizontally Layered Sites," Earthquake Engineering Research Center, University of California, Berkeley, California, EERC 72-12, 1972.

(6) Wong, H. L. and J. E. Luco, "Soil-Structure Interaction: A Linear Continuum Mechanics Approach (CLASSI)," Dept. of Civil Engineering, University of Southern California, Los Angeles, California, CE 79-03, 1980.

(7) Johnson, J. J., G. L. Goudreau, S. E. Bumpus, and O. R. Maslenikov, "SSMRP Phase I Final Report - SMACS - Seismic Methodology Analysis Chain with Statistics (Project VIII)," Lawrence Livermore National Laboratory, Livermore, California, UCRL-53021, Vol. 9, NUREG/CR-2015, Vol. 9, 1981.

(8) "PRA Procedures Guide", U. S. Nuclear Regulatory Commission, NUREG/CR-2300, Vol. 1, 1983.

(9) Kolb, G. J., D. J. Alpert, D. L. Berry, R. G. Easterling, F. E. Haslain, J. W. Hickman, J. L. Sprung, D. W. Stack, M. W. McCann, J. W. Reed, and K. G. Murphy, "Risk Methods Integration and Evaluation Program Plan", Sandia National Laboratories, Albuquerque, New Mexico, 1984.

(10) Barlow, R. E. and Lambert, H. E., "Introduction to Fault Tree Analysis", Reliability and Fault Tree Analysis, SIAM, Philadelphia, Pennsylvania, 1985.

(11) Wells, J. E., "SEISIM: A Probabilistic Risk Assessment Tool Used in Evaluating Seismic Risk," Proceedings of the Conference on Seismic Risk and Heavy Industrial Facilities, San Francisco, California, 1983.

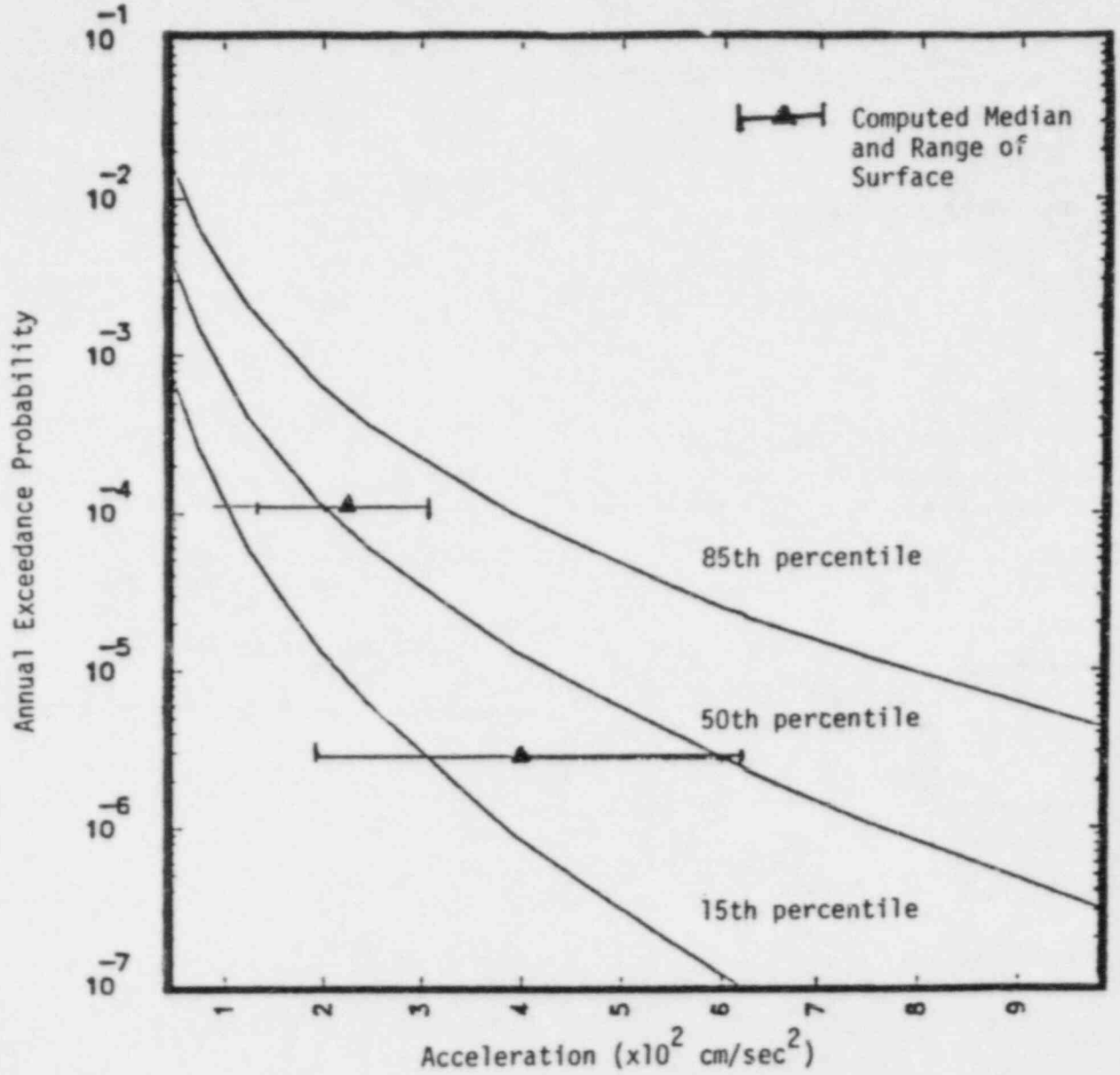

Fig. 1 LaSalle Hazard Curve at a Hypothetical Rock Outcrop

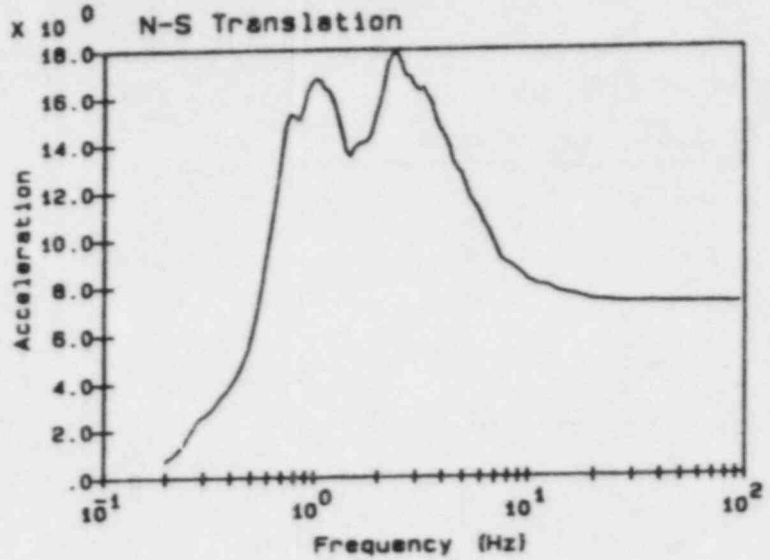

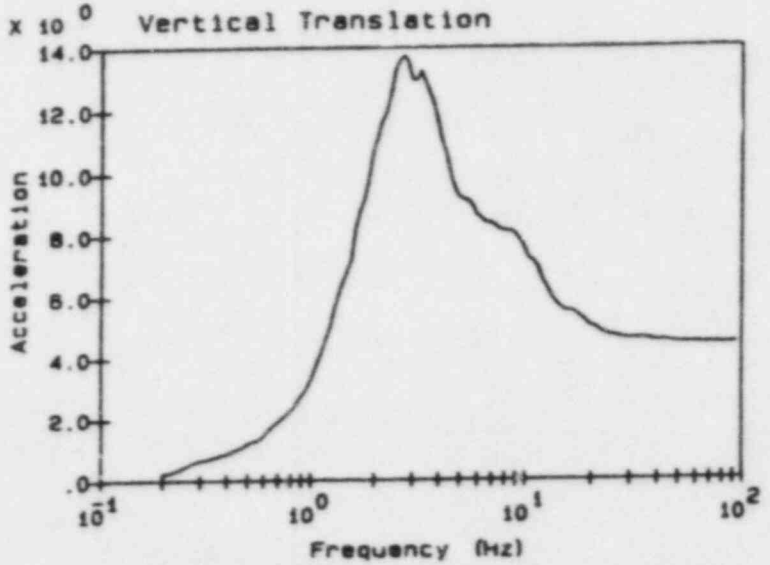

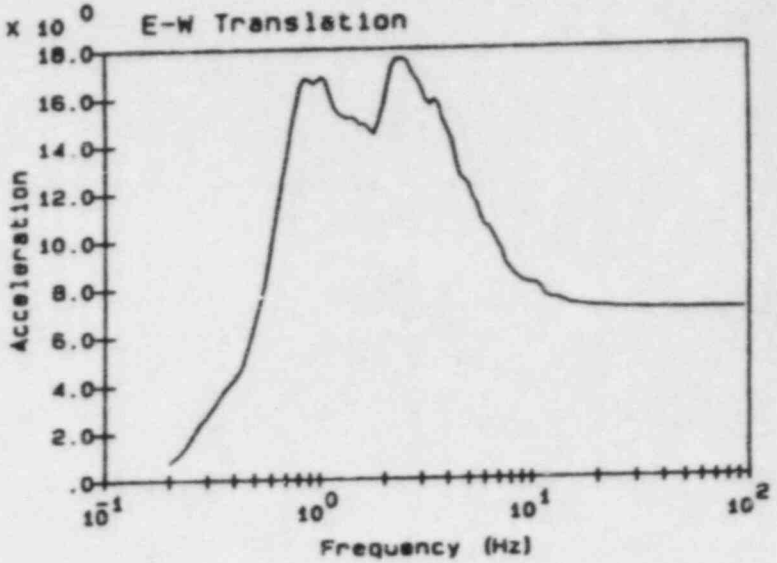

Notes:

Freefield Motion

All accelerations in units of ft/sec2.

All spectra calculated at 5.0% damping.

Fig. 2 Mean Free-Field Ground Response Spectra on Soil Free Surface, El. 710', Acceleration Range 1.

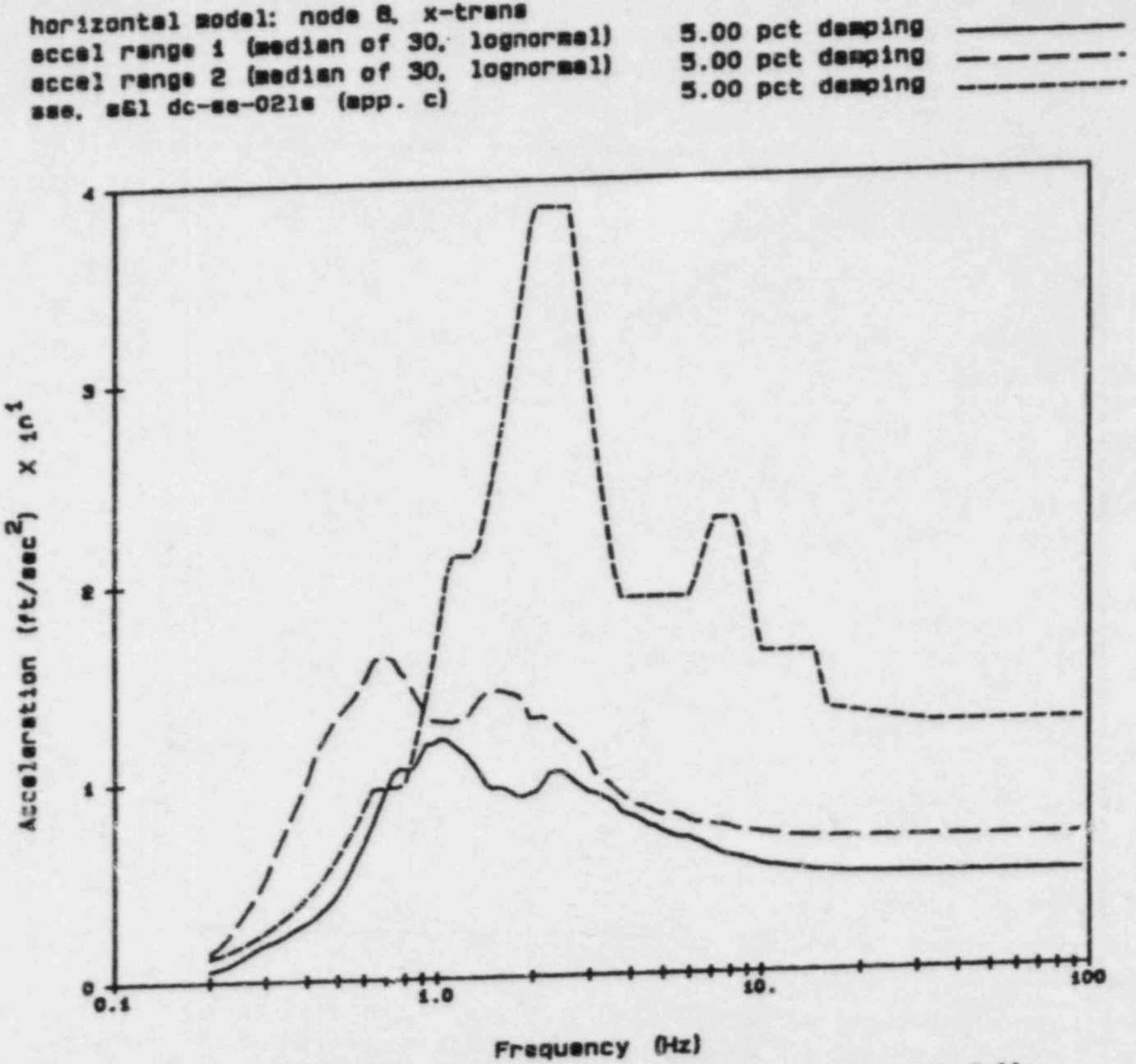

Fig. 3 Comparison of In-Structure Response Spectra at Top of LaSalle Structure Complex, Median Acceleration Range 1 vs. Median Acceleration Range 2 vs. SSE Design, (a) N-S Direction

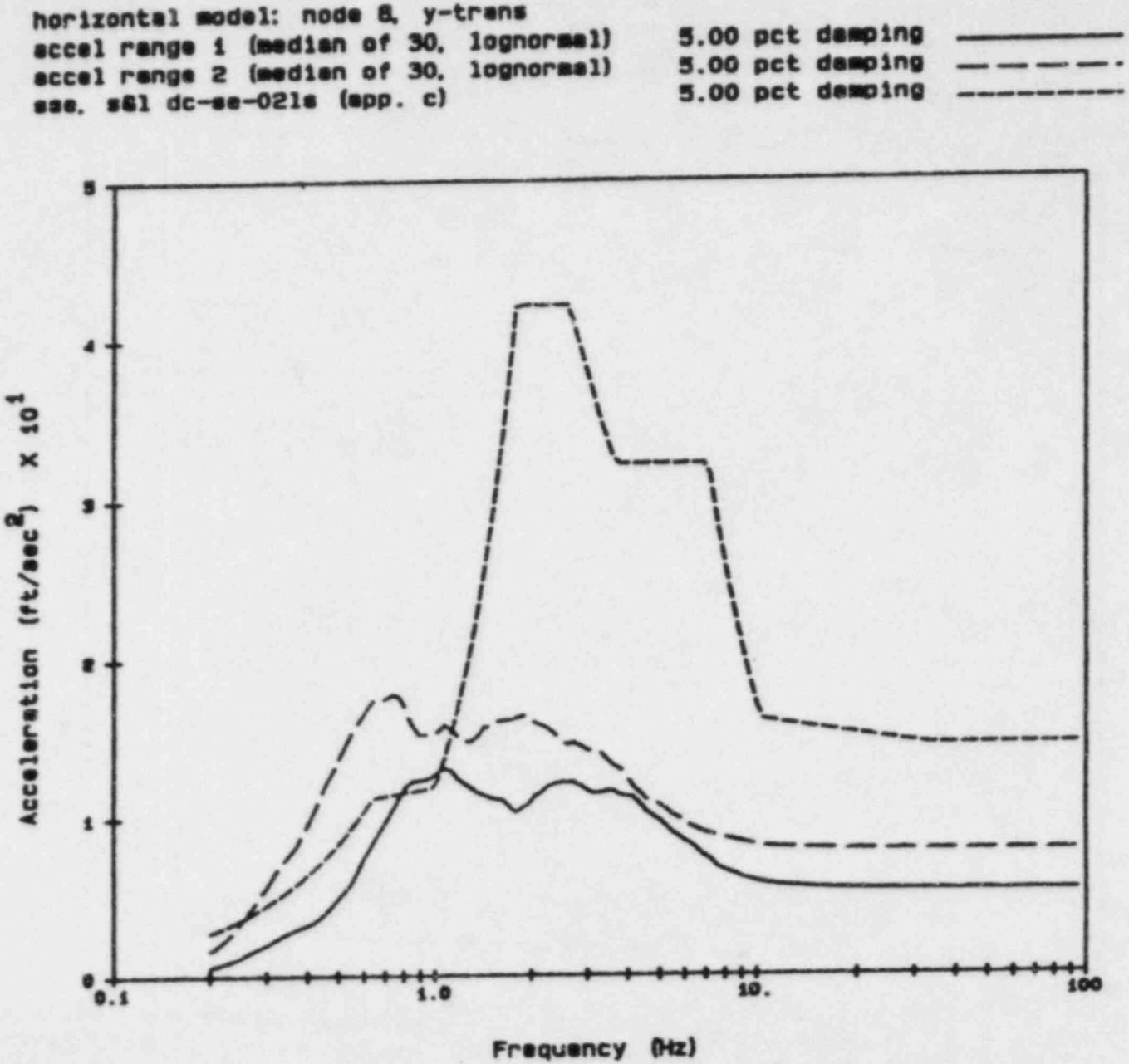

Fig. 3(b) E-W Direction

BWR RISK ASSESSMENT

BY:

T. Y. CHUANG, D. L. BERNREUTER, J. C. CHEN, G. E. CUMMINGS
D. A. LAPPA, J. J. JOHNSON AND J. E. WELLS

PRESENTED BY:

G. E. CUMMINGS
NUCLEAR SYSTEMS SAFETY PROGRAM
LAWRENCE LIVERMORE NATIONAL LABORATORY

PRESENTED TO:

13TH WATER REACTOR SAFETY RESEARCH INFORMATION MEETING
GAITHERSBURG, MARYLAND

OCTOBER 23, 1985

S85-152

THIS PRESENTATION WILL COVER SIX TOPICS

- PROJECT OBJECTIVES
- METHODOLOGY
- SEISMIC HAZARD
- STRUCTURE AND COMPONENT RESPONSES
- STRUCTURE AND COMPONENT FRAGILITIES
- PROBABILISTIC FAILURE AND RELEASE CALCULATIONS

THERE ARE TWO MAJOR OBJECTIVES FOR THE BWR SEISMIC RISK ASSESSMENT PROJECT

- PERFORM A BENCHMARKING SEISMIC RISK ANALYSIS OF A BWR (LASALLE) USING SIMPLIFIED METHODS BASED ON RESULTS FROM THE SEISMIC SAFETY MARGINS RESEARCH PROGRAM (SSMRP)

- IDENTIFY ANY MAJOR GENERIC DIFFERENCES IN SEISMIC RISK BETWEEN A PWR AND A BWR

nssp
NUCLEAR SYSTEMS SAFETY PROGRAM
S85-135

THERE ARE FIVE STEPS IN A SEISMIC RISK ASSESSMENT

1. SEISMIC HAZARD CHARACTERIZATION
   (SEISMIC HAZARD CURVE, FREQUENCY CHARACTERISTICS OF MOTION)

2. SEISMIC RESPONSE OF STRUCTURES AND COMPONENTS
   (BEST ESTIMATES OR MEDIANS, VARIABILITY, CORRELATION)

3. STRUCTURE AND COMPONENT FAILURE DESCRIPTIONS

4. PLANT LOGIC MODELS
   (FAULT TREES, EVENT TREES)

5. PROBABILISTIC FAILURE AND RELEASE CALCULATIONS

THE FIVE STEPS MAY BE SHOWN SCHEMATICALLY

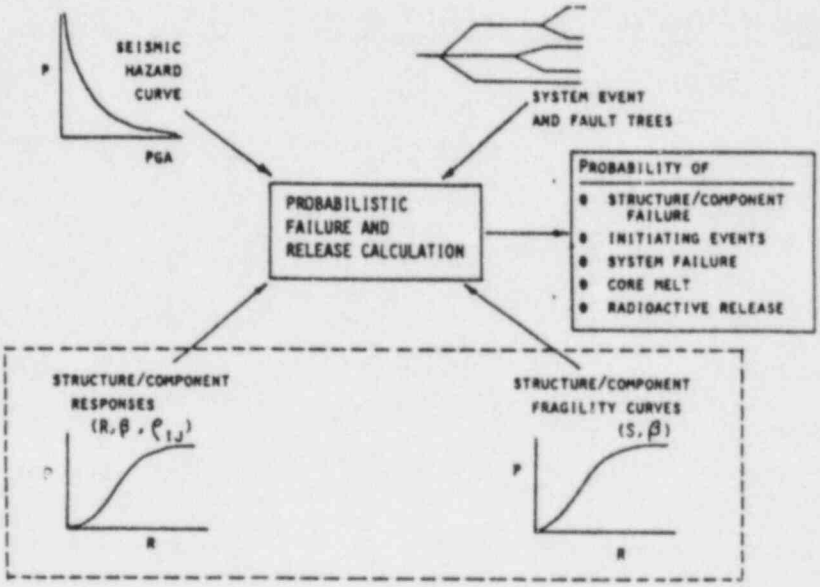

nssp
NUCLEAR SYSTEMS SAFETY PROGRAM

S85-135

STEP 1

THE SEISMIC HAZARD FOR THE LASALLE SITE WAS COMPUTED USING CURRENT METHODS DEVELOPED FOR NRC

- ZONATION AND SEISMICITY MODELS DEVELOPED FROM INPUT FROM ELEVEN EXPERTS
- GROUND MOTION MODELS SELECTED BY A PANEL OF FIVE GROUND MOTION EXPERTS
- A COMPLETE UNCERTAINTY ANALYSIS PERFORMED USING A MONTE CARLO SIMULATION APPROACH
- TWO SETS OF TIME HISTORIES (0.2G AND 0.6G) WERE DEVELOPED WITH THE APPROPRIATE DISTRIBUTION OF MAGNITUDES, DISTANCES AND DURATIONS
- TIME HISTORIES CORRECTED FOR THE LOCAL SOIL COLUMN

nssp
NUCLEAR SYSTEMS SAFETY PROGRAM

S85-152

WE HAVE DEVELOPED CONSTANT PERCENTILE HAZARD CURVES

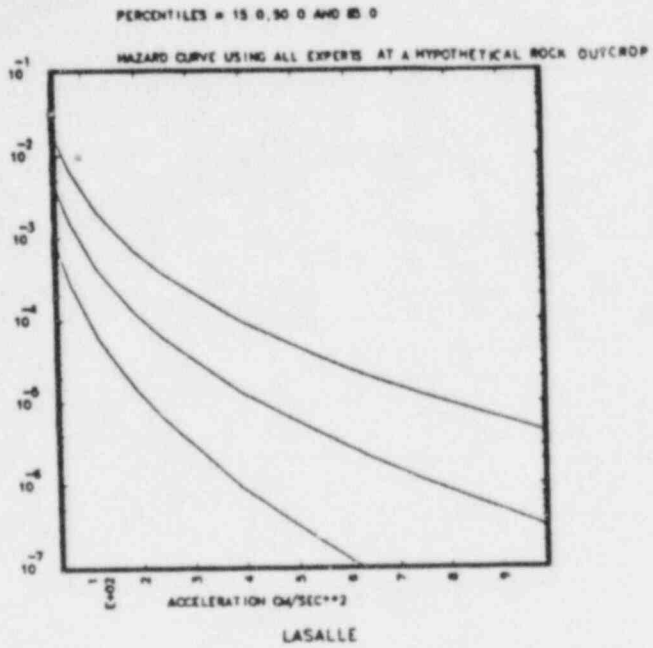

nssp
NUCLEAR SYSTEMS SAFETY PROGRAM

S85-135

[STEP 2]

THE OBJECTIVE OF THE RESPONSE STEP IS TO DETERMINE THE SEISMIC RESPONSE OF STRUCTURES AND COMPONENTS

RESPONSES MUST BE CALCULATED FOR

- ALL BASIC EVENTS INCLUDED IN FAULT TREE EVALUATION (PUMP FAILS, PIPE RUPTURES, VALVE FAILS TO OPEN, ...)
- INITIATING EVENT PROBABILITY CALCULATIONS

THE RESPONSES MUST BE

- COMPATIBLE WITH FRAGILITY DESCRIPTIONS
- ESTIMATED FOR THE RANGE OF EARTHQUAKES AT THE SITE
- BEST ESTIMATE CALCULATIONS

CALCULATIONS WERE PERFORMED ON THE LASALLE STRUCTURES TO ESTIMATE MEDIAN LEVEL RESPONSES AT TWO EARTHQUAKE LEVELS USING THE SSMRP COMPUTER CODE SMACS

- SEISMIC HAZARD CURVE IS DEFINED ON THE HYPOTHETICAL ROCK OUTCROP AND DISCRETIZED FOR INTEGRATION PURPOSES

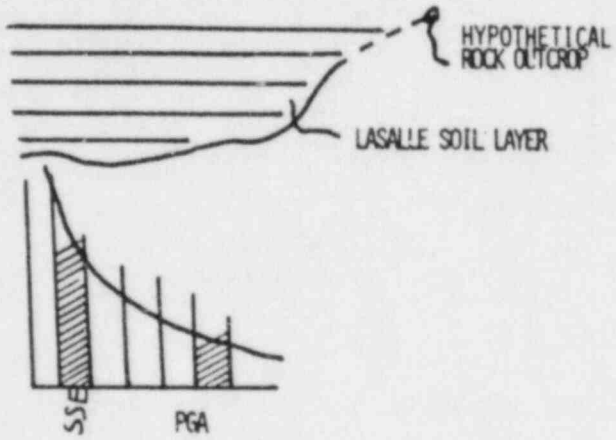

- TWO DISCRETIZATION INTERVALS WERE TREATED EXPLICITLY
  0.18 - 0.27G AND 0.58 - 0.73G

nssp
NUCLEAR SYSTEMS SAFETY PROGRAM

CALCULATIONS WERE PERFORMED ON THE LASALLE STRUCTURES TO ESTIMATE MEDIAN LEVEL RESPONSES AT TWO EARTHQUAKE LEVELS USING THE SSMRP COMPUTER CODE SMACS (CONTINUED)

- SMACS ANALYSES WERE PERFORMED
  - -- EARTHQUAKE ACCELERATION TIME HISTORIES DEFINED ON ROCK OUTCROP
  - -- LOCAL SITE AMPLIFICATION MODELED
  - -- STRUCTURE MODELS WERE THE LASALLE DESIGN MODELS
  - -- PROBABILISTIC RESPONSES WERE CALCULATED
    - STRUCTURE ELEMENT FORCES AND MOMENTS FOR FRAGILITY ASSESSMENT OF STRUCTURAL MEMBERS
    - IN-STRUCTURE RESPONSE SPECTRA FOR FRAGILITY ASSESSMENT OF LASALLE COMPONENTS
- MEDIAN LEVEL RESPONSES FOR EARTHQUAKES OUTSIDE THE TWO RANGES WERE EXTRAPOLATED FROM THE CALCULATED VALUES
- BEST ESTIMATE SAFETY RELIEF VALVE DISCHARGE RESPONSES WERE COMBINED WITH SEISMIC TO YIELD TOTAL RESPONSE
- PIPING AND VALVE MEDIAN LEVEL RESPONSES WERE CALIBRATED BY USING DESIGN VALUES

LA SALLE STRUCTURAL MODELS WERE USED IN THE SMACS ANALYSES

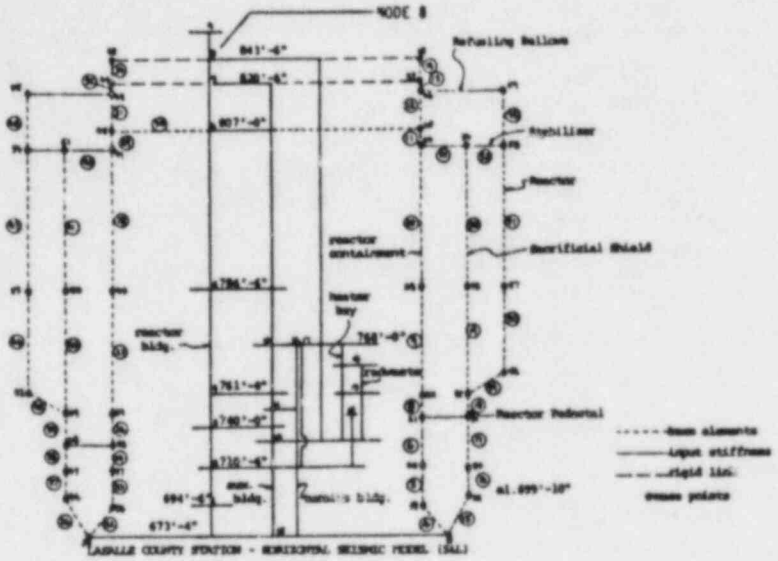

nssp
NUCLEAR SYSTEMS SAFETY PROGRAM
S85-152

DESIGN RESPONSE SPECTRA GENERALLY SHOW SIGNIFICANT CONSERVATISM WHEN COMPARED TO MEDIAN RESPONSE SPECTRA FOR ACCELERATION RANGES 1 AND 2

843' ELEVATION IN REACTOR BUILDING - N-S DIRECTION
ACCELERATION RANGE 1 ———— (.18 - .27G, .2G MEDIAN)
ACCELERATION RANGE 2 — — — (.58 - .73G, .6G MEDIAN)

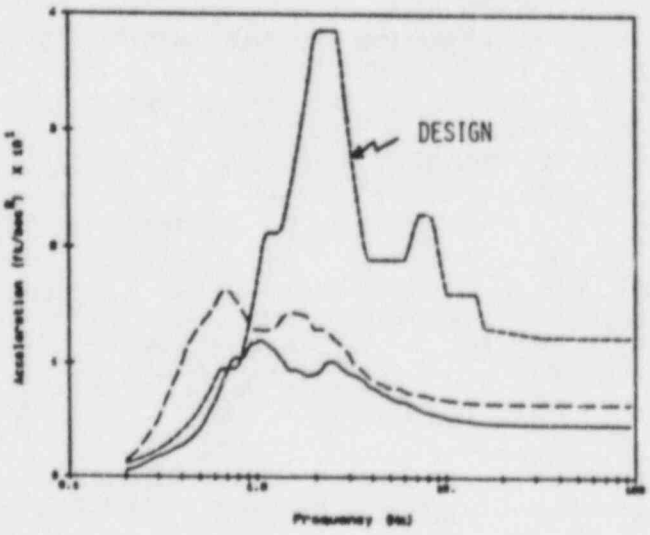

S85-152

THIS CONSERVATISM IS DUE TO:

- SITE SPECIFIC SEISMIC INPUT VS. VALUES USED IN DESIGN
- DEGRADATION OF SOIL PROPERTIES WITH EXCITATION LEVEL WHICH SHIFTS FREQUENCIES TO LOWER VALUES

nssp
NUCLEAR SYSTEMS SAFETY PROGRAM

S85-135

STEP 3

STRUCTURE FRAGILITIES WERE DEVELOPED FOR ALL STRUCTURAL ELEMENTS

- ASSESS OVERALL STRUCTURAL FAILURE
- ASSESS LOCAL FAILURE OF STRUCTURAL MEMBERS CAUSING EQUIPMENT FAILURE
- FRAGILITY DESCRIPTIONS WERE IN TERMS OF CALCULATED LOCAL RESPONSE (SHEARS AND MOMENTS)
- EFFECTS OF THE MAGNITUDE OF EARTHQUAKES AND NONLINEAR BEHAVIOR BEFORE FAILURE WERE TAKEN INTO ACCOUNT

FRAGILITIES WERE DEVELOPED FOR ALL STRUCTURAL ELEMENTS IN THE CRITICAL LASALLE STRUCTURES

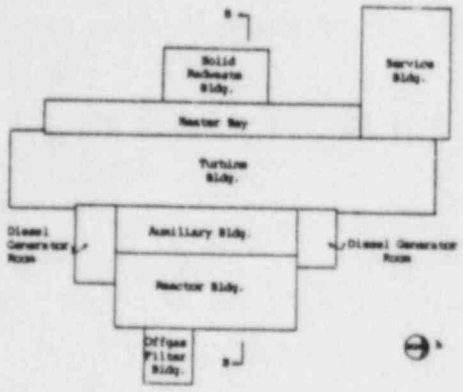

Plan View of LaSalle County Station Units 1 and 2

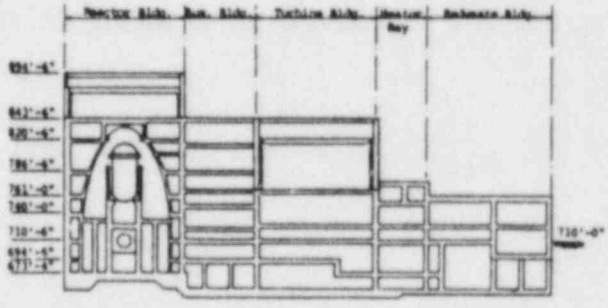

EAST-WEST SECTION (A-A)
TURBINE BUILDING

nssp
NUCLEAR SYSTEMS SAFETY PROGRAM
S85-135

COMPONENT FRAGILITIES WERE TREATED IN TWO WAYS

- LASALLE SPECIFIC FRAGILITIES WERE DERIVED FOR MAJOR COMPONENTS (27)
  - BASED ON LASALLE DESIGN AND QUALIFICATION DATA
    E.G., PUMPS (RECIRC, HPCS, RCIC, LPCS, ETC.), REACTOR VESSEL, ETC.

GENERIC FRAGILITIES WERE USED FOR OTHER COMPONENTS (31 CATEGORIES)

S85-152

STEP 4

TWO SETS OF FAULT TREES WERE GENERATED

	"SIMPLE"	"DETAILED"
BASIC EVENTS	853	3378
NUMBER OF SYSTEMS	9	23

nssp
NUCLEAR SYSTEMS SAFETY PROGRAM

S85-152

SIMPLIFIED SEISMIC RISK METHODOLOGY IS BEING USED

- MEDIAN RESPONSES USED
- RANDOM UNCERTAINTIES ONLY
- CORRELATIONS BASED ON ZION ANALYSIS

S85-152
STEP 5

THE SSMRP COMPUTER CODE SEISIM IS BEING USED TO COMPUTE CORE MELT AND RELEASE PROBABILITIES

- HANDLES CORRECTLY THE DEPENDENCE BETWEEN BASIC EVENTS IN A CUT SET
- PERFORMS IMPORTANCE AND SENSITIVITY ANALYSES
- ALLOWS FOR MULTIPLE RISK WEIGHTING SCHEMES

S85-135

CONCLUSION

- A SEISMIC RISK ASSESSMENT USING THE SSMRP SIMPLIFIED METHOD IS BEING CONDUCTED ON A BWR (LASALLE)
- BOTH SIMPLE AND DETAILED PLANT LOGIC MODELS ARE BEING EVALUATED
- ANALYSIS WILL BE COMPLETED DURING THE NEXT YEAR
- SO FAR OUR RESULTS INDICATE A LOW SEISMIC RESPONSE AT LEAST PARTLY BECAUSE OF THE SOFT SOIL AT THE LASALLE SITE

Progress on Qualification Testing Methodology Study of Electric Cables

S.Okada, Y.Kusama, M.Ito, T.Yagi, M.Yoshikawa, K.Yoshida, N.Tamura, W.Kawakami
Japan Atomic Energy Research Institute (JAERI), Takasaki Radiation Chemistry Research Establishment

ABSTRACT

Degradation behavior of mechanical and electrical properties of cable materials such as ethylene-propylene rubbers(EPR) and chloro-sulfonated polyethylenes(Hypalon) was investigated in various LOCA-simulating environments. The LOCA exposures in combined environments of radiation and steam/chemical spray i.e. simultaneous tests were performed for four cases: short term (about 1 week) exposures at a high dose rate (about 10 kGy/h) up to 1.5MGy in air-free and air-containing steam, and long term (about 3 months) exposures at a low dose rate (0.6kGy/h) up to 1.4MGy in air-free and air-containing steam. Sequential exposures i.e. irradiations followed by steam/chemical spray exposures were also carried out. In the sequential tests, the irradiations were performed under such various conditions as at a high dose rate (about 10kGy/h) and a low dose rate (about 1kGy/h) at room temperature in air; at an intermediate dose rate (5kGy/h) at 70°C in air; at an intermediate dose rate (4.2kGy/h) at room temperature in pressurized oxygen (0.5MPa). The effects of the steam temperature (120 to 160°C) and the air partial pressure (0 to 0.5MPa) in the steam/chemical spray exposure after the irradiation were investigated as well. Comparison between the degradations in the simultaneous and the sequential tests showed that the various cases of the simultaneous LOCA exposures will be well simulated by the sequential tests in which the conditions of the irradiation and the steam are selected suitably to cause the same extent of the degradations as in the simultaneous environments.

1.INTRODUCTION

Safety-related electric cables in nuclear power plants are required to function even if they should be subjected to a postulated design basis event such as a loss-of-coolant accident (LOCA) at the end of their intended service life. In a LOCA the cables are assumed to be exposed to combined stresses of radiation, high temperature steam, spray and, under certain

circumstances, air. The condition of the stresses, such as the exposure time or dose rate, is expected to depend upon the plant type and the accident scale. In almost cases of the electric cable qualification in Japanese plants, however, the cables are tested by such a method as irradiation followed by steam/spray exposure i.e. sequential method in short term (about one week for each of the irradiation and the steam/spray exposure) tests. Therefore, it has been one of the most important subjects in the testing methodology study to assure the validity of the short term sequential test by finding adequate conditions to simulate the long or short term combined stresses.

We performed short term (about 1 week) and long term (about 3 months) tests of electric cable materials such as ethylene-propylene rubber (EPR) and chloro-sulfonated polyethylene (Hypalon) in combined environments of the irradiation and the steam/chemical spray exposure i.e. the tests by simultaneous method for both cases of containing and not containing air in the steam. The test conditions are assumed to correspond to various types of LOCA. Mechanical and electrical property degradations in the simultaneous tests were compared with those in the sequential tests in which the conditions of the irradiation and the steam exposure were systematically altered in order to find suitable conditions to cause the same extent of the degradations as in the simultaneous environments.

2.EXPERIMENTAL

2-1.Materials

Sheet samples of ethylene-propylene rubbers (EPR's) and chloro-sulfonated polyethylenes (Hypalons) were investigated. The thickness of the samples was about 1mm. The dumbbell-shaped samples and the sheets of 8cmX8cm were used for a tensile test and electrical property measurements, respectively. They include materials formulated for cables of general use and for fire-retardant safety-related cables used in nuclear power plants as listed below.

SAMPLE NAME	SPECIFICATION
HYPALON-A	STANDARD (BASE POLYMER: HYPALON 40)
HYPALON-B	STANDARD (BASE POLYMER: HYPALON 40)
HYPALON-C	UNSPECIFIED (for reactor use)
HYPALON-D	UNSPECIFIED (for reactor use)
EPR-A	STANDARD (BASF POLYMER: NODEL 1040)
EPR-B	UNSPECIFIED (for reactor use)
EPR-C	UNSPECIFIED (for reactor use)

2-2.LOCA Simulation

2-2-1.Simultaneous Method

The LOCA exposures in combined environments of radiation and steam/chemical spray were performed for four cases (Sim-A,B,C,D) shown in TABLE-1 by using a LOCA-simulating test chamber SEAMATE-II[1-4]. They are assumed to correspond to the following various cases of LOCA: short term accident where most of the radiation energy is deposited in the earlier stage and the removal of heat and radiation sources from a primary containment vessel is effective in the post-accident stage; long term accident where the radiation sources and heat reside for a long time; a case where air in the containment vessel is substituted in normal operation or is almost entirely purged at the accident; another case where the air is not entirely purged.

Quantity and formation of the chemical spray were according to IEEE Std.323[5]. The spray was introduced during all the period of the tests. The time versus temperature profile used in the experiments is shown in FIG.-1, which has been applied to Japanese PWR plant qualification based on IEEE Std.323 appendix. Not only the exposures according to the profile but also those at constant temperature of 120°C were carried out. The temperature conditions of the former and the latter will be described such as "(Profile)" and "(120°C)" respectively hereafter all through this paper. Although the temperature 120°C may be too high in the long term cases (Sim-B and Sim-D) compared with a practical assumption on long duration accidents, it was adopted for comparison between the short and the long term cases from the viewpoint of dose rate effects. Therefore, the cases Sim-B and Sim-D may be considered to be extreme cases.

In cases Sim-C and Sim-D, air was introduced into the steam so that the pressure in the test chamber was 0.05MPa higher than the saturated steam pressure at the temperature tested, which will be described as 0.05MPa air partial pressure hereafter. The quantity of the air corresponds to an oxygen content of about 5% in the containment atmosphere during LOCA at 120°C.

2-2-2.Sequential Method

The LOCA-simulating sequential exposures i.e. irradiation, which will be called pre-irradiation hereafter, followed by steam/chemical spray were carried out for four cases (Seq-a,b,c,d) listed in TABLE-2 by using the same apparatus as the simultaneous exposures. In cases Seq-a and Seq-b the samples were irradiated at a high dose rate (about 10kGy/h) i.e. under a condition where oxygen supply into the sample is assumed to be not enough to catch up with radical formation by the irradiation, whereas in cases Seq-c and Seq-d the irradiations were performed

under such conditions as the oxygen is expected to be supplied sufficiently to oxidize almost throughout the samples. In cases Seq-a and Seq-c the steam in the steam/chemical spray exposure after the pre-irradiation did not contain air, which is called saturated or air-free steam hereafter, while in cases Seq-b and Seq-d the steam contained air. Effect of the air content on the degradations was examined in case Seq-b in the range of the air partial pressure from 0.05 to 0.5MPa. On the other hand, the steam/spray exposure was performed for only one case of the air partial pressure of 0.05MPa in case Seq-d. The steam/spray exposures according to the PWR LOCA profile, which are indicated by "P" in TABLE-2, as well as those at constant temperatures were carried out in cases Seq-a and Seq-b, where the temperature dependence of the degradations was investigated in the range from 120 to 160°C. The conditions of the temperature profile and the spray were the same as in the simultaneous exposures. The pre-irradiations and the steam/spray exposures in case Seq-c and Seq-d are partly undergoing at the present stage of the experiment.

The samples pre-conditioned under such a condition as thermal aging at 121°C for 7days followed by 0.5MGy irradiation at about 10kGy/h were also exposed to the above simultaneous and sequential LOCA-simulating environments. However, these results are not referred in this paper in order to simplify the explanation. No important difference by the pre-conditioning was found in comparisons either between the simultaneous and the sequential methods or among Sim-A,B,C,D and among Seq-a,b (The pre-conditioning has not been examined in Seq-c,d.).

2-3.Measurement

Tensile strength (Tb) and elongation (Eb) at break were measured by using an Instron tension tester (type 1130) with a crosshead speed of 500mm/min. Volume resistivity at 1 minute after the start of the 500V D.C. impression was measured by a high resistance meter and a resistivity cell (Yokogawa-Hewlet-Packard 4329A and 16008A). Dielectric properties such as dielectric loss factor were measured by an Ando Electric TR-1C wide range dielectric loss measurement system. All the measurements were performed at room temperature 2 weeks or more after the LOCA exposures, when the properties were expected to be stable. The purpose of the measurements was to compare the influences of the various LOCA-simulating environments on the material property changes. Practical safety-related aspects i.e. results of electrical resistance measurement during the LOCA simulations and voltage-endurance tests in water immediately after the exposures were partly referred in the previous work[6] and will be reported in the future.

3.RESULTS AND DISCUSSION

3-1.Simultaneous LOCA Simulation

3-1-1.Hypalon:Mechanical Property

In FIG.-2 is shown a typical degradation behavior of mechanical properties of the Hypalons, where Eb, Tb, Ebo and Tbo are elongation at break (%), tensile strength at break (MPa), and their original values, respectively. Degradation levels at 1.5MGy for cases Sim-A and Sim-C and those at 1.4MGy for cases Sim-B and Sim-D are determined as drawn in the figure.

[Comparison between Sim-A,B(air-free) and Sim-C,D(air-containing)]

In the air-free environments, the elongation degrades as a hyperbolic function, whereas it degrades exponentially in the air-containing exposures. By using a numerical analysis the authors have found that the order of decay, n, in the following equation is near 2 for the former and near 1 for the latter:

$$-dEb/dt = KEb^{n},$$

where t is time or dose, and K is the decay constant of the elongation degradation in the combined environments of radiation and steam. The difference is supposed to be due to the predominant chemical reactions i.e. cross-linking predominates in the air-free exposure while oxidation scission is a predominant reaction in the air-containing environment[7].

Therefore, the elongation degradation in the air-containing environment is smaller than in the air-free one at the earlier stage of the exposure whereas it degrades more in the former than in the latter at the end ultimately as shown between Sim-A and Sim-C. The tensile strength also degrades more in the air-containing cases, as is obvious from comparison between Sim-A and Sim-C and that between Sim-B and Sim-D.

[Comparison between Sim-A,C(short term) and Sim-B,D(long term)]

The mechanical properties degrade more in the long term exposure (Sim-B) than in the short term one (Sim-A) even where the steam does not contain air. The difference is assumed to be due to additional thermal degradation independent of radiation-induced reactions because, as mentioned afterwards, little difference is found between these two cases in the EPR's which are generally considered to be more resistant against heat than Hypalons. Such a thermal effect of the Hypalons may be called "long term effect" although it could be one of "dose rate effects" in a wide sense of the word.

There is a remarkable difference between the long term (Sim-D) and the short term (Sim-C) exposures in case of the air-containing steam. This may be interpreted by other aspects of

the dose rate effect in addition to the above thermal effect. At higher dose rates oxygen supply diffusing from the surface of the sample does not catch up with radiation-induced radical formation, which causes an oxidation concentration gradient inside the sample i.e. the oxidation scission occurs predominantly near the surface whereas the cross-linking predominates in the vicinity of the inside center[8-11]. Moreover, even if the oxygen supply is sufficient due to high temperature, the radical formation is too fast at higher dose rates to provide enough time with the consequent oxidation reactions, resulting in one of the dose rate effects[12].

3-1-2.EPR:Mechanical and Electrical Property

Typical examples of the degradation behavior in the mechanical properties and electrical resistance (volume resistivity ρ ; original value ρ_0) are shown in FIG.-3 and FIG.-4 respectively.

[Comparison between Sim-A,B(air-free) and Sim-C,D(air-containing)]
The mechanical behavior of the EPR's is entirely similar to the Hypalons in comparison between the air-free and the air-containing environments. It should be noted that the air remarkably affects the electrical property.

[Comparison between Sim-A,C(short term) and Sim-B,D(long term)]
In the air-free environments, there exists no difference between the short term (Sim-A) and the long term (Sim-B) exposures in the elongation degradation. Though there is a little difference in the strength and also in the electrical property, which was observed in the other samples (EPR-A and EPR-C) than this example, the long term effect is not so remarkable as the mechanical properties of the Hypalons.

In the air-containing environments, on the contrary, the degradation in the long term exposure (Sim-D) is notable both in the mechanical and the electrical properties compared with the short term one (Sim-C) as well as the other exposures. It is suggested that the remarkable degradation is associated with the dose rate effects on the oxidation described in the previous subsection.

3-1-3.Summary on the Simultaneous LOCA Simulation

A summary on the order of the degradation, the predominant reactions and the long term or the dose rate effect in the simultaneous exposures is shown in TABLE-3.

3-2.Sequential LOCA Simulation

3-2-1.Integrity Phase

There may be different phases or grades required for the safety of the electric cables at the accident, which will be determined by the property concerned. We define the phases, which will be called integrity phases hereafter, as below, and discuss sequential LOCA simulations which are expected to be applicable to cause the same extent of the degradation as the four cases of the simultaneous LOCA-simulating environments for each integrity phase.

PHASE-1:Sheath Mechanical Property

Only mechanical properties of sheath (jacketing) materials are required to keep the integrity. This point of view is based upon an experimental experience that the insulation resistance was satisfactory to apply the rated voltage and current on the cable during each simultaneous LOCA test due to a protection effect of the sheath material on the insulator[6] as far as the sheath was not broken.

PHASE-2:Core Electrical Property

Only electrical properties of core (insulation) materials are required to maintain the integrity. Here it is considered that the cable could operate safely only if the electrical insulation is sufficient even when the sheath was broken.

PHASE-3:Core Electrical and Mechanical Properties

Mechanical as well as electrical properties of core materials are required to keep the integrity. In this point of view is taken into account a possibility of cracking of the insulator by such a mechanical shock as seismic which would break the electrical insulation.

PHASE-4:Sheath Mechanical and Core Electrical and Mechanical Properties

Not only electrical and mechanical properties of core materials but also mechanical ones of sheath materials are required to maintain the integrity. This includes a concept of multiple protection.

3-2-2.Simulation of Sim-A(short term, air-free) by Sequential Method

[PHASE-1]

In FIG.-5 is shown a typical example of the mechanical property degradation behavior during the pre-irradiation at about 10kGy/h at room temperature in air on the left hand and during the consequent steam/chemical spray exposures of Seq-a (Profile & 120°C) and Seq-b (Profile & 120°C; air partial pressure 0.05MPa)

on the right hand. The degradation levels of the simultaneous exposure at 1.5MGy are also drawn in the figures with the standard deviation. It is obvious that the mechanical properties of the Hypalon are degraded by both Seq-a and Seq-b exposures to the same extent as or much more than Sim-A. Although the Seq-a exposure is preferable for the simulation of Sim-A because there exists little effect of oxygen in the pre-irradiation due to the high dose rate and no additional oxidation in the steam exposure, the Seq-b exposure could be also applicable from a phenomenalistic viewpoint.

[PHASE-2]

FIG.-6 shows a typical electric resistance change of the EPR's by Seq-a and Seq-b. It should be noted that the Seq-a exposure at 120°C does not cause any degradation. The authors have found that the insulation degradation of EPR's is caused by introduced and retained water molecules inside the material by some radio-chemical reactions in such a simultaneous environment as Sim-A, which results in increase of the dielectric loss at the lower frequency range as shown in FIG.-7[13]. The lower dielectric loss of the Seq-a at the lower frequency range suggests that the water molecules are not so much introduced as the simultaneous one. When the steam contains air in the sequential exposure (Seq-b), on the contrary, the oxygen in the steam may take part in the introducing of water molecules, which causes increase of the dielectric loss at the lower frequency range and decrease of the insulation resistance as shown in FIG.-7 and FIG.-6. Therefore, the Seq-b exposure is preferable for the simulation of Sim-A in spite of a difference that oxygen does not concern the degradation in Sim-A but does affect the insulation in Seq-b.

[PHASE-3]

The mechanical degradation behavior of the EPR's is similar to the Hypalons as shown in FIG.-8. Taking the electrical property degradation into account, the Seq-b exposure is considered to be suitable for the simulation of Sim-A.

[PHASE-4]

The above discussions indicate that the Seq-b exposure is applicable to satisfy the conditions required for all the properties.

3-2-3.Simulation of Sim-B(long term, air-free) by Sequential Method

[PHASE-1]

As already mentioned in the previous section, the Hypalons show a long term effect even in the air-free environments i.e. the mechanical degradation is greater in Sim-B (long term) than in Sim-A (short term), which is assumed to be due to additional

thermal degradation. The additional degradation can be provided by elevating the steam temperature instead of prolonging the exposure time in the Seq-a exposure as shown in FIG.-9.

[PHASE-2]

There is only a little long term effect on the electrical degradation of the EPR's in the air-free environments. Therefore the Seq-b exposure is available for the simulation of Sim-B as well as Sim-A. However, the Seq-a exposure is also applicable only if the steam temperature is elevated because the insulation resistance decreases by the Seq-a exposure at 140 °C and 160 °C to the same extent as or much more than in Sim-B as shown in FIG.-10. It is remarkable that the resistance degrades so much at the elevated temperature in spite of no decrease observed at 120°C. It is assumed that the higher temperature may activate water molecule motion penetrating into the material.

The higher temperature Seq-a exposure is preferable compared with Seq-b from the viewpoint that oxygen is not or less concerned with the degradation both in Sim-B and Seq-a.

[PHASE-3]

FIG.-11 shows that the Seq-a exposure at 120°C brings about enough degradation to simulate Sim-B, as far as only the mechanical properties of the EPR's are concerned, because of little long term effect in the air-free environments. However, the higher temperature Seq-a exposure is preferable for the simulation of Sim-B taking the electrical property into account, although the Seq-b exposure is also available by the same reasons as pointed out in PHASE-2.

[PHASE-4]

The higher temperature Seq-a exposure is most applicable for the simulation of Sim-B.

3-2-4.Simulation of Sim-C(short term, air-containing) by Sequential Method

[PHASE-1]

As mentioned before, oxidation scission predominates in Sim-C. To simulate the environment, therefore, it is necessary to perform the sequential test under an oxidation condition both in the pre-irradiation and the consequent steam exposure or in either of the two. In FIG.-12 are shown typical mechanical degradations of the Hypalons in the Seq-b exposures, where the steam contains oxygen instead of less oxidation in the pre-irradiation due to the higher dose rate, at various temperatures. Though the mechanical properties are not degrade sufficiently to simulate Sim-C by the Seq-b exposure at 120 °C, the higher temperature causes enough degradation. It was also found that the degradation is stimulated to the same extent as or much more

than in Sim-C by increasing the air partial pressure up to 0.5MPa instead of elevating the temperature.

[PHASE-2]

The Seq-b exposure brings about sufficient electrical degradation even at 120°C or the profiled temperature in the EPR's formulated for reactor use (EPR-B and EPR-C) as shown in FIG.-13. As regards EPR-A for general use, however, such a sufficient degradation was not observed even at elevated temperature up to 160°C. These results may be interpreted by whether the material contains frame-retardant additives or not. Therefore, the Seq-b exposure (120 °C & Profile) could be applicable for the simulation of Sim-C as far as EPR's for reactor use are concerned.

[PHASE-3]

As shown in FIG.-14, the tensile strength degradation of EPR-B in the Seq-b exposure approaches to the level of Sim-C retaining a little difference at the higher temperature while the elongation degrades at within 120°C to 160°C sufficiently for the simulation of Sim-C. In this way, it was observed that either of the elongation or the strength of EPR-A and EPR-B is not degraded completely to the sufficient level even by the higher temperature Seq-b exposure whereas both of the two properties of EPR-C are degraded to the same extent as Sim-C.

On the other hand, the mechanical properties of all the EPR's were found to degrade remarkably when the air partial pressure in the steam was increased up to 0.5MPa in the Seq-b exposure. However, the increased air content does not always cause the sufficient electrical resistance decrease, as shown in FIG.-15. In this example the resistance degradation is smaller at larger air partial pressure if more than 0.05MPa. The result is unexpected. Although it is assumed that excess oxygen molecules may take part in some additional oxidation decomposition resulting in the remarkable mechanical degradation on one hand and in the suppression of the resistance decrease by removing electrically sensitive species on the other hand, a further investigation will be expected for the details. Therefore, the Seq-b exposure with increased air partial pressure in the steam may not be recommended at the present stage of the investigation.

From the above results, it is supposed that the Seq-b exposure at the elevated temperature is approximately applicable for the simulation of Sim-C. For a strict simulation, however, other sequential methods such as Seq-c or Seq-d will be referred.

[PHASE-4]

The conclusion is the same as PHASE-3.

3-2-5.Simulation of Sim-D(long term, air-containing) by Sequential Method

[PHASE-1]

The elongation of the Hypalons is degraded by the Seq-b exposure at 160°C to a sufficient level for the simulation of Sim-D whereas the tensile strength is not degraded sufficiently as shown in FIG.-16. As already mentioned, the oxidation degradation is remarkable in Sim-D due to the long term or dose rate effects compared with Sim-C. Therefore, it is suggested that sufficient oxygen supply is necessary not only in the steam exposure as Seq-b but also in the preceding pre-irradiation. FIG.-16 also shows the degradation in Seq-c exposures at 120 °C after the pre-irradiations at a low dose rate (about 1kGy/h) at room temperature in air and at a higher dose rate (5kGy/h) but at 70 °C in air as well as in a Seq-d exposure at 120°C after pre-irradiation of the same condition as the former of the above two. These irradiations were performed for the materials to be sufficiently oxidized already at the stage of the pre-irradiation. Experiments on the pre-irradiation in pressurized oxygen,which is also supposed to cause the sufficient oxidation, and the Seq-c and Seq-d exposures at elevated temperature after these sufficiently oxidative irradiations are now in progress or are planned to carry out. Since the Seq-b exposure at 160 °C causes a considerable degradation in spite of the high dose rate pre-irradiation, the Seq-d exposure which combines the sufficiently oxidative pre-irradiation with the air-containing steam exposure at elevated temperature is expected to be promising for the simulation of Sim-D.

[PHASE-2]

FIG.-17 shows a typical degradation behavior of the electrical resistance of the EPR's in the same exposures as described above. It is notable that the resistance decreases considerably already at the stage of the pre-irradiation in cases of the sufficiently oxidative irradiations and that, especially in the air-free steam exposure at 120 °C following the pre-irradiation at 70°C, it degrades much more approaching to the level of Sim-D in spite of lower temperature and no oxygen in the steam. This suggests that the Seq-d exposure at elevated temperature after such a pre-irradiation may cause the same or further extent of the degradation compared with Sim-D.

[PHASE-3]

As regards the mechanical properties of the EPR's, the same possibility as pointed out for the electrical property may be suggested by FIG.-18.

[PHASE-4]

The sufficiently oxidative pre-irradiation followed by the air-containing steam exposure at elevated temperature (Seq-d) is possibly expected to be applicable for the simulation of Sim-D.

Especially the pre-irradiation at 70°C is promising from the viewpoint of the electrical degradation behavior and because of short time and simple device required. Practically the steam temperature of the sequential exposure might be not necessarily elevated so high because Sim-D is an extreme case adopted for comparisons as mentioned earlier in this paper. The condition will be determined by more realistic postulate on a long term accident in an air-containing environment.

4.CONCLUSION

The various cases of the simultaneous LOCA exposures will be well simulated by the sequential tests in which the conditions of the irradiation and the steam are selected suitably to cause the same extent of the degradations as in the simultaneous environments, as indicated in TABLE-4.

REFERENCES

[1]S.Tanaka, Y.Nakase, Y.Kusama, M.Ito, S.Okada, K.Yoshida, "Engineering data of SEAMATE-II, 1. Rapid heating test", JAERI-M 9361 (1981)

[2]S.Tanaka, Y.Nakase, S.Okada, M.Ito, Y.Kusama, K.Yoshida, "Engineering data of SEAMATE-II, 2. Test on the characteristics of temperature regulation in the pressure vessel", JAERI-M 9699 (1981)

[3]S.Okada, Y.Nakase, Y.Kasahara, S.Tanaka, M.Ito, Y.Kusama, K.Yoshida, "Constitution and performance of the electrical loading system in Simulated Environmental Apparatus for Material Testing II (SEAMATE-II)", JAERI-M 9706 (1981)

[4]K.Yoshida, Y.Nakase, S.Okada, M.Ito, Y.Kusama, S.Tanaka, Y.Kasahara, S.Machi, Radiat. Phys. Chem. Vol.18, No.3-4, pp689-700 (1981)

[5]IEEE Std. 323-1974, "IEEE Standard for Qualifying Class 1E Equipment for Nuclear Power Generating Stations", IEEE Inc., New York (1974)

[6]M.Ito, Y.Kusama, T.Yagi, S.Okada, M.Yoshikawa, K.Yoshida, "Progress on qualification testing methodology study of electric cables", Proceedings of the U.S. Nuclear Regulatory Commission NUREG/CP-0058, No.5, pp351-371 (1985)

[7]S.Okada, Y.Kusama, M.Ito, T.Yagi, M.Yoshikawa, K.Yoshida, "Kinetic analysis on insulating materials degradation in LOCA-simulating environments", EIM-82-111, IEEJ Discussion Meeting on Electric Insulating Materials (1982)

[8]T.Seguchi, S.Hashimoto, W.Kawakami, I.Kuriyama, JAERI-M 7315 (1977)

[9]T.Seguchi, S.Hashimoto, K.Arakawa, N.Hayakawa, W.Kawakami, I.Kuriyama, Radiat. Phys. Chem., 17, 195 (1981)

[10]T.Seguchi, K.Yoshida, IEEJ Meeting on Insulation Materials, EIM-82-113 (1982)

[11]T.Seguchi, N.Hayakawa, S.Okada, Proceedings of Int. Symp. on Ageing in Tests of Safety Equipment for Nuclear Power Plants, pp100-108 (Paris, May 1984)

[12]K.Arakawa, T.Seguchi, Y.Watanabe, N.Hayakawa, I.Kuriyama, S.Machi, J. Polym. Sci., Polym. Chem. Ed. 19, 2123 (1981)

[13]S.Okada, M.Yoshikawa, M.Ito, Y.Kusama, T.Yagi, K.Yoshida, "Effects of LOCA-simulating environments on electric property change of insulating materials", IEEJ Meeting on Insulation Materials, EIM-82-109 (1982)

[TABLE-1] Test conditions of simultaneous LOCA exposures

CASE	TEST PERIOD	DOSE RATE (kGy/h)	DOSE (MGy)	AIR PARTIAL PRESSURE IN STEAM (MPa)
Sim-A	~ 1 Week	~ 10	up to 1.5	0
Sim-B	~ 3 Months	0.6	up to 1.4	0
Sim-C	~ 1 Week	~ 10	up to 1.5	0.05
Sim-D	~ 3 Months	0.6	up to 1.4	0.05

TEMPERATURE PROFILE : PWR LOCA PROFILE & 120℃ CONSTANT

[TABLE-2] Test conditions of sequential LOCA exposures

CASE	PRE-IRRADIATION	STEAM/SPRAY EXPOSURE
Seq-a	High Dose Rate (~10 kGy/h) at room temperature in air	Saturated Steam (P; 120℃; 140℃; 160℃)
Seq-b		Air-containing Steam (air 0.05MPa: P, 120℃, 140℃, 160℃) (air 0.13MPa,120℃; 0.25MPa,120℃; 0.5MPa,P & 120℃)
Seq-c	・Low Dose Rate (~1.0 kGy/h) at room temperature in air ・Intermediate Dose Rate (5.0 kGy/h) at 70℃ in air ・Intermediate Dose Rate (4.2 kGy/h) at room temperature in pressurized oxygen (0.5MPa)	Saturated Steam (120℃)
Seq-d		Air-containing Steam (120℃, air 0.05MPa)
	DOSE: up to 1.5MGy	P: PWR LOCA temperature profile

[TABLE-3] Summary of degradation behavior in various simultaneous LOCA exposures

CASE	Predominant Reaction	OXIDATION	LONG TERM EFFECT (DOSE RATE EFFECT)
Sim-A	CROSS-LINKING	NO	----------
Sim-B	CROSS-LINKING	NO	HYPALON: YES (Additional Thermal Degradation) EPR: NO
Sim-C	SCISSION	YES	----------
Sim-D	SCISSION	YES (Remarkable)	HYPALON & EPR: YES (Additional Thermal Degradation + Sufficient Oxygen Supply + Sufficient Time for Oxidation Reactions)

-DEGRADATION-
Sim-D>Sim-B>Sim-C>Sim-A (HYPALON MECHANICAL)
Sim-D>>Sim-C>=Sim-B>=Sim-A (EPR MECHANICAL and ELECTRICAL)

[TABLE-4] Integrity phases of cables and corresponding applicable sequential LOCA simulations for various accident cases.

ACCIDENT CASE (SIMULTANEOUS)	APPLICABLE SIMULATION (SEQUENTIAL)			
	PHASE-1 Sheath Mech. (SM)	PHASE-2 Core Elec. (CE)	PHASE-3 CE+CoreMech. (CM)	PHASE-4 SM + CE + CM
Sim-A (Short term, Air-free)	Seq-a	Seq-b	Seq-b	Seq-b
Sim-B (Long term, Air-containing)	Seq-a (elevated temp.)	Seq-a (elevated temp.)	Seq-a (elevated temp.)	Seq-a (elevated temp.)
Sim-C (Short term, Air-containing)	Seq-b (elevated temp.)	Seq-b(*) (elevated temp.)	Seq-b(*) (elevated temp.)	Seq-b(*) (elevated temp.)
Sim-D (Long term, Air-containing)	Seq-d(**) (elevated temp.)	Seq-d(**) (elevated temp.)	Seq-d(**) (elevated temp.)	Seq-d(**) (elevated temp.)

*: a little different from Sim-C
**: promising (The experiments are in progress.)

[FIG.-1] Time versus temperature profile for simultaneous and sequential LOCA simulations. (X: total exposure time)

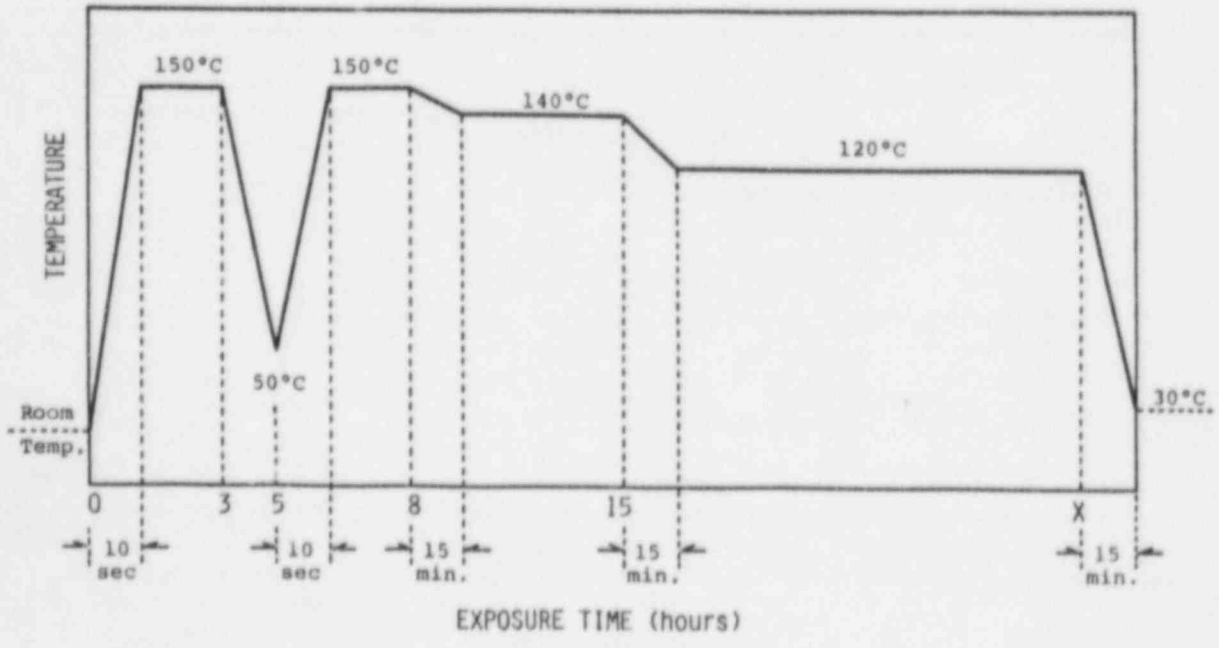

[FIG.-2] A typical degradation behavior of mechanical properties of the Hypalons in various simultaneous LOCA-simulating exposures and the ultimate degradation levels (Hypalon-C).
○:Sim-A, △:Sim-B, □:Sim-C, ◇:Sim-D
open mark: 120℃, closed mark: Profile

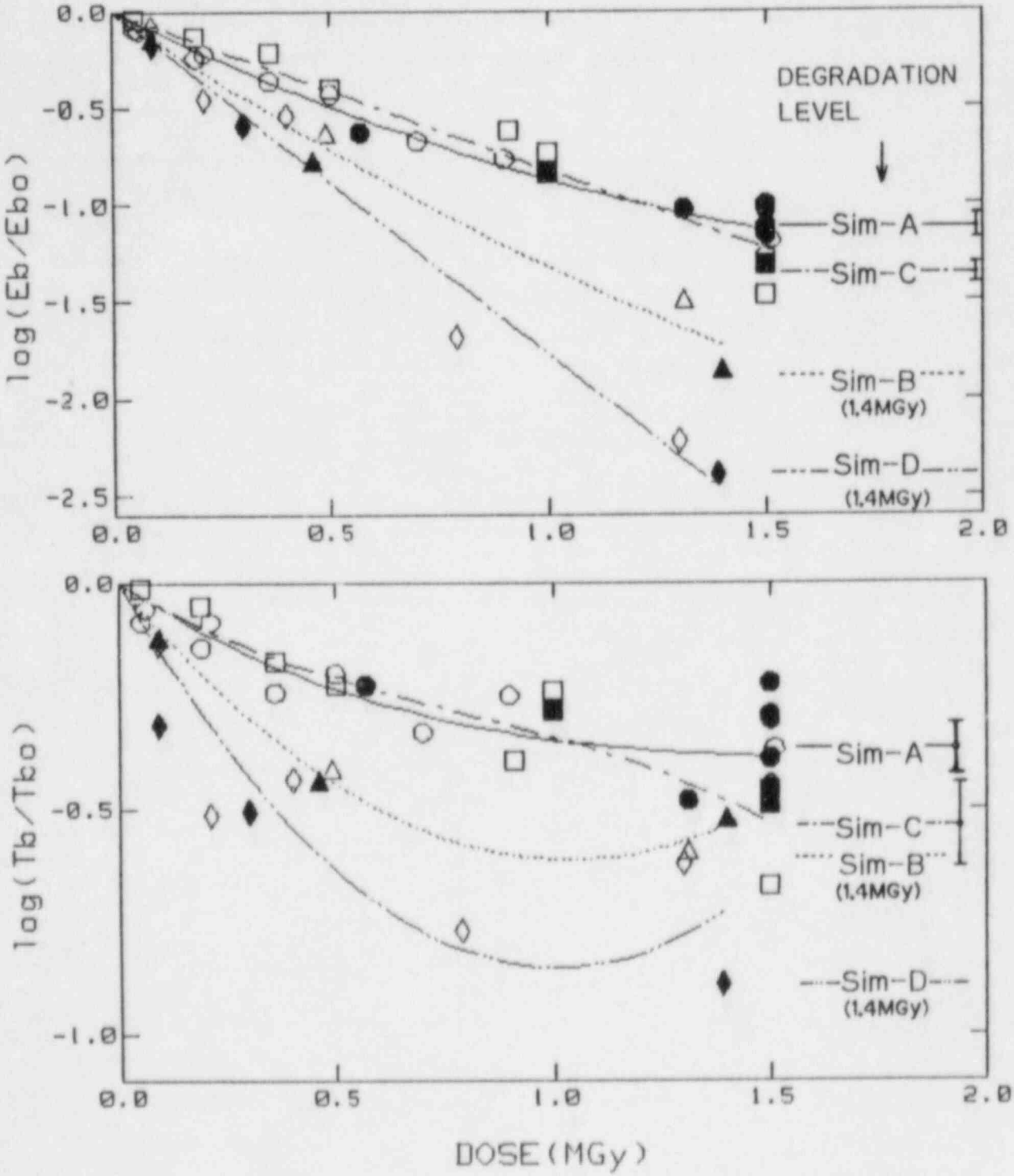

[FIG.-3] A typical degradation behavior of mechanical properties of the EPR's in various simultaneous LOCA-simulating exposures and the ultimate degradation levels (EPR-C).
(The symbols are the same as in FIG.-2.)

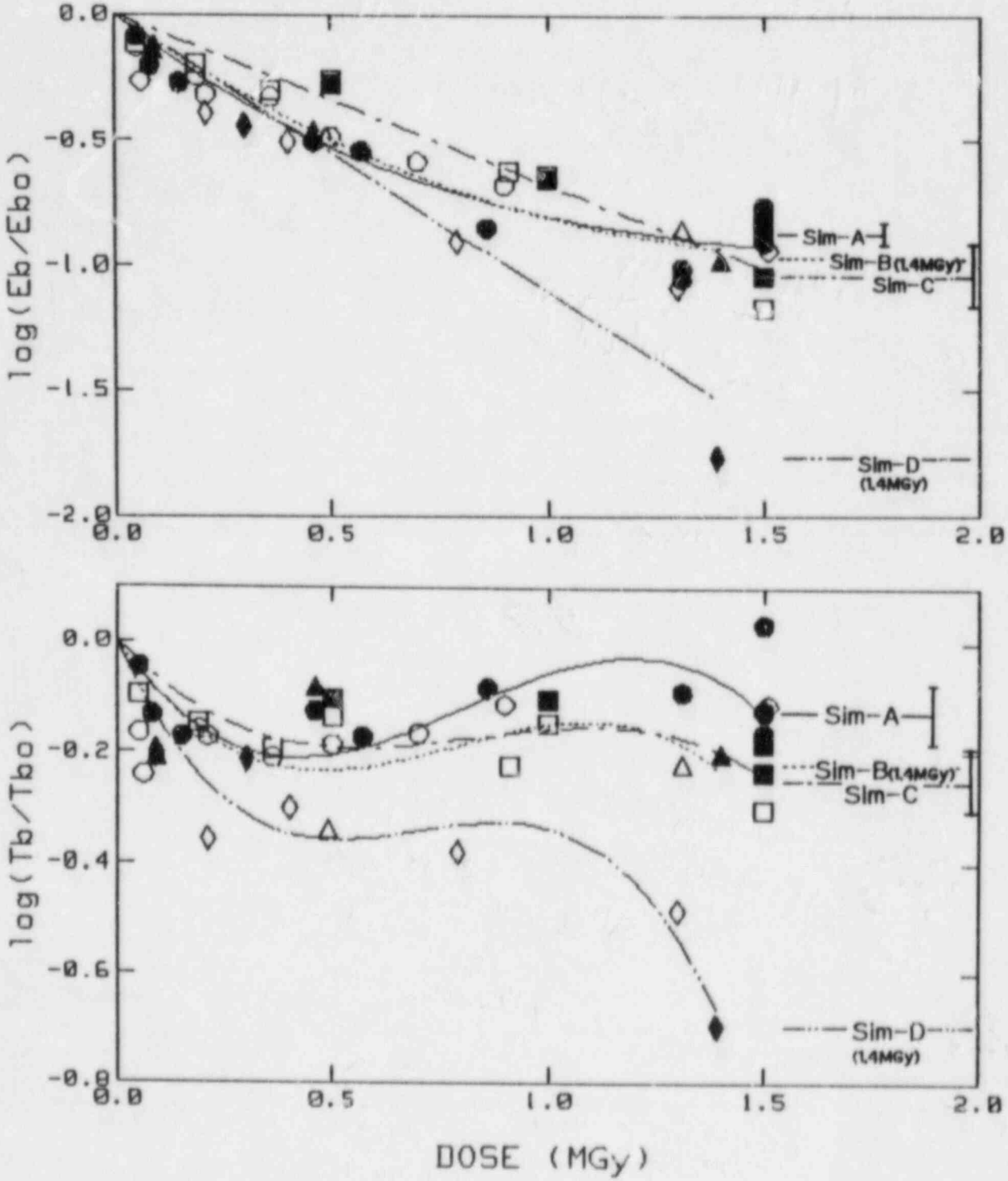

[FIG.-4] A typical degradation behavior of electrical resistance of the EPR's in various simultaneous LOCA-simulating exposures and the ultimate degradation levels (EPR-B).
(The symbols are the same as in FIG.-2.)

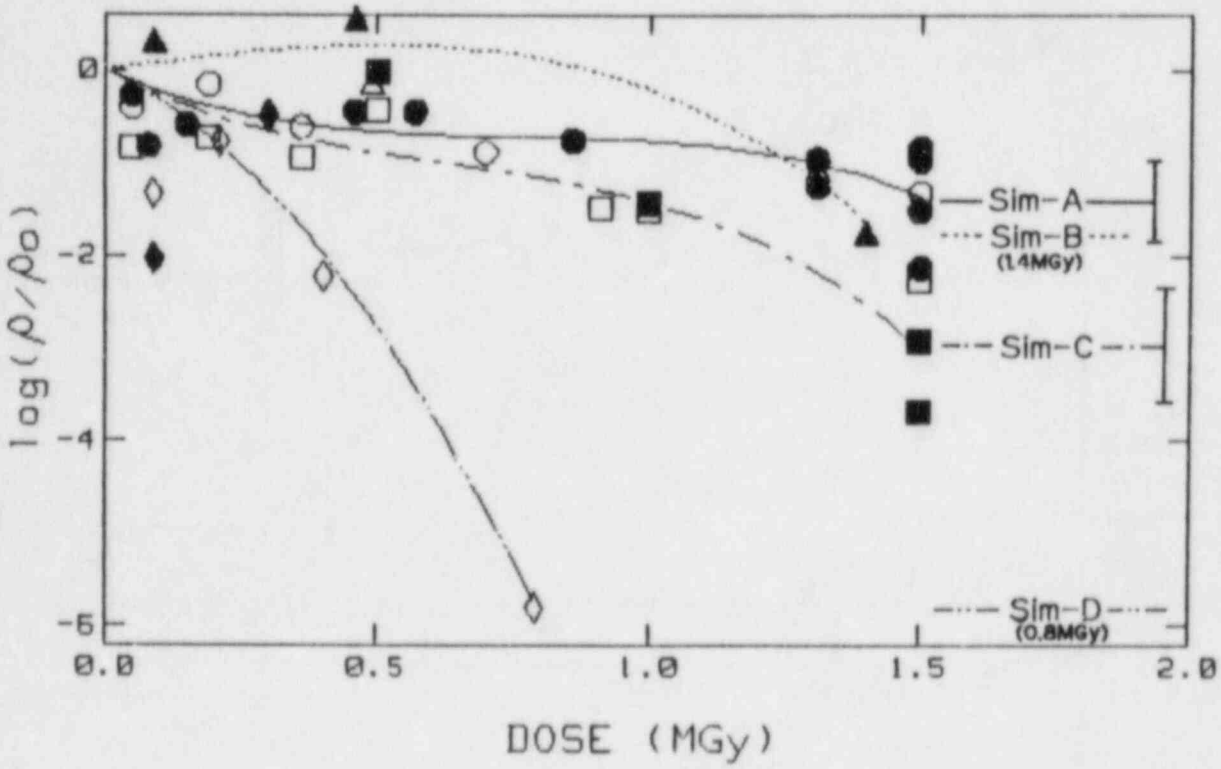

End of Figures for Simultaneous Methods

[FIG.-5] A typical degradation behavior of mechanical properties of the Hypalons during the pre-irradiation at about 10kGy/h in air at room temperature and the consequent steam/chemical spray exposures of Seq-a (○:120℃, ●:Profile) and Seq-b (□:120℃, ■:Profile ;air partial pressure 0.05MPa), together with the degradation level of Sim-A for comparison (Hypalon-A).

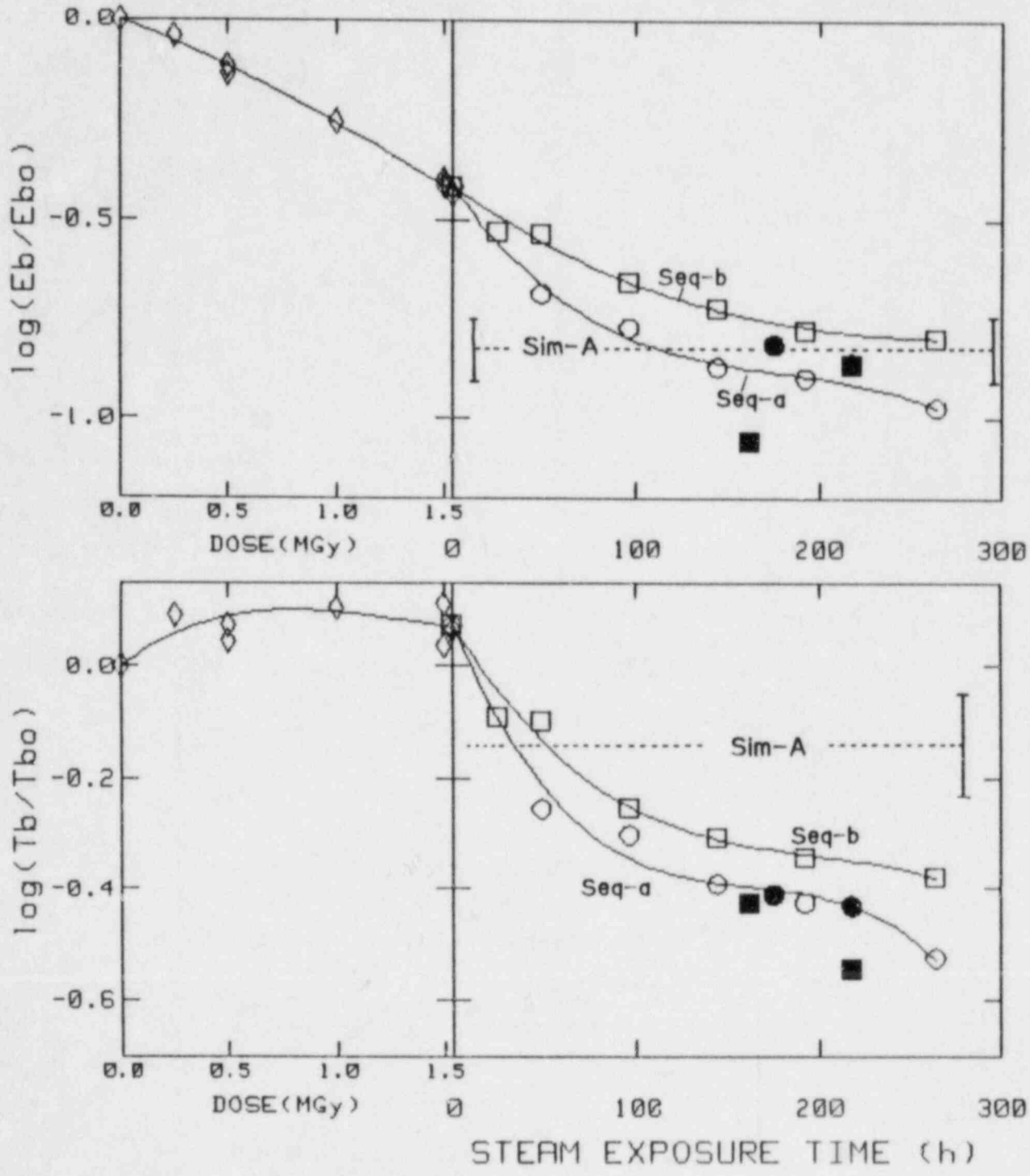

[FIG.-6] A typical degradation behavior of electrical resistance of the EPR's during the pre-irradiation at about 10kGy/h in air at room temperature and the consequent steam/chemical spray exposures of Seq-a (○:120℃, ●:Profile) and Seq-b (□:120℃, ■:Profile ;air partial pressure 0.05MPa), together with the degradation level of Sim-A for comparison (EPR-B).

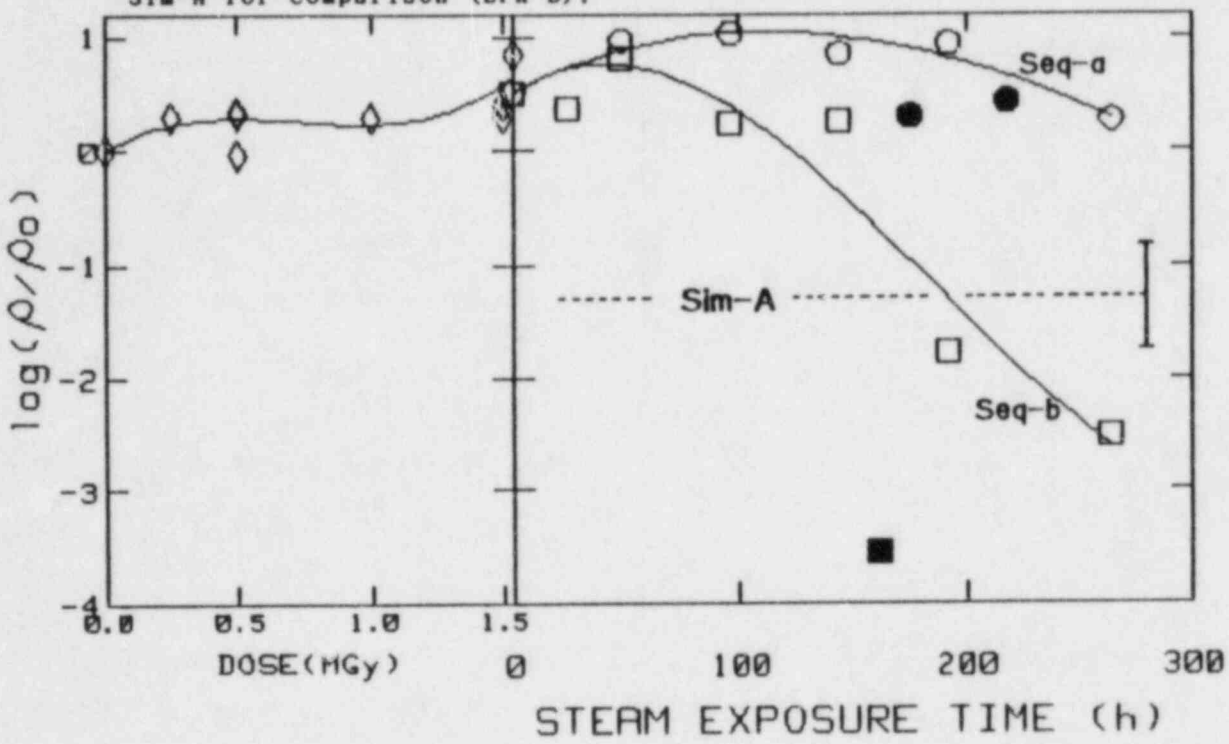

[FIG.-7] Frequency dependence of dielectric loss factor of EPR-B exposed to various LOCA-simulating environments.

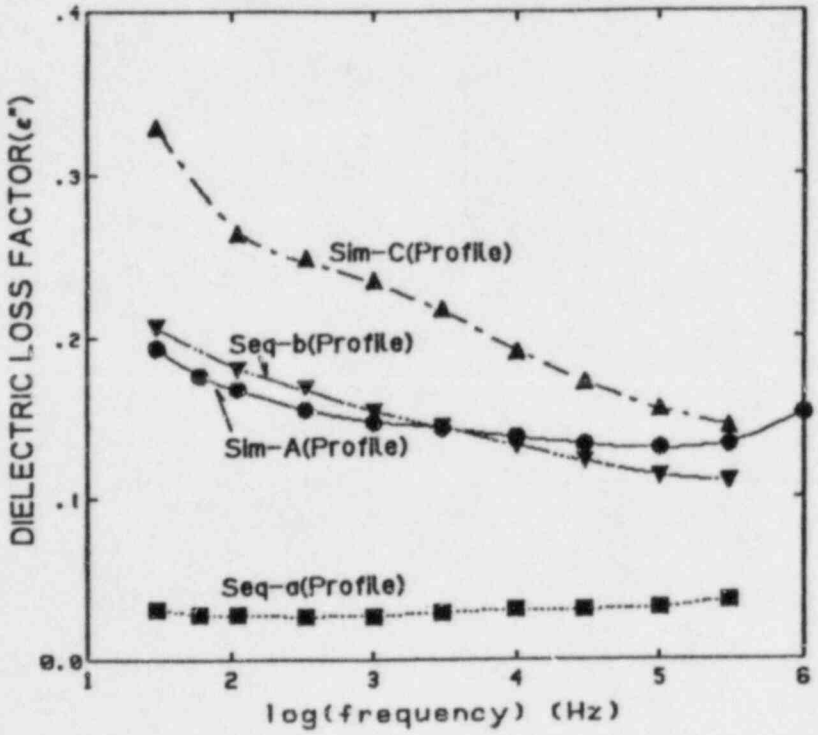

[FIG.-8] A typical degradation behavior of mechanical properties of the EPR's during the pre-irradiation at about 10kGy/h in air at room temperature and the consequent steam/chemical spray exposures of Seq-a (○:120℃, ●:Profile) and Seq-b (□:120℃, ■:Profile ;air partial pressure 0.05MPa), together with the degradation level of Sim-A for comparison (EPR-B).

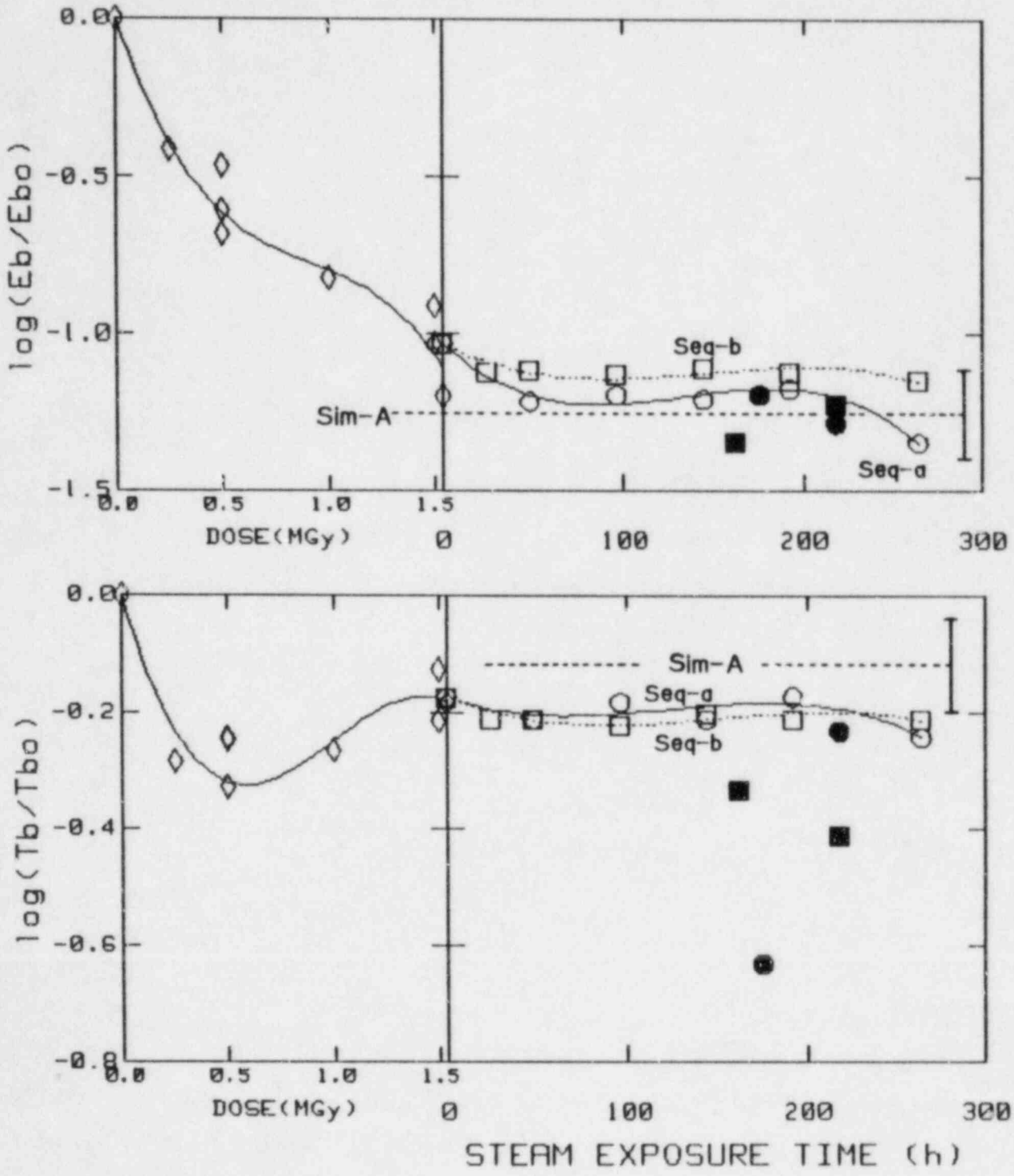

[FIG.-9] A typical degradation behavior of mechanical properties of the Hypalons during the pre-irradiation at about 10kGy/h in air at room temperature and the consequent steam/chemical spray exposures of Seq-a (○:120℃, △:140℃, □:160℃), together with the degradation level of Sim-B for comparison (Hypalon-D).

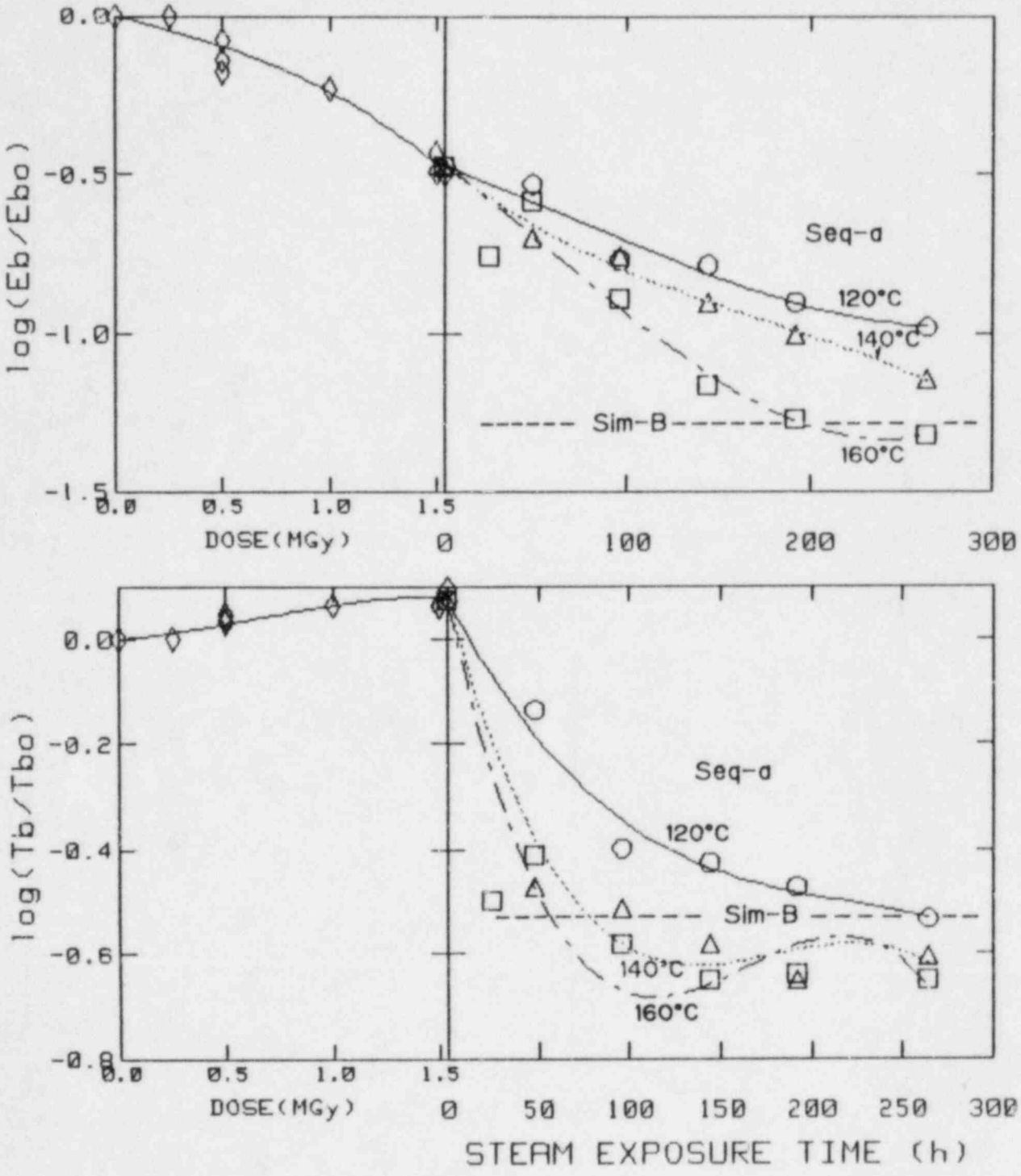

[FIG.-10] A typical degradation behavior of electrical resistance of the EPR's during the pre-irradiation at about 10kGy/h in air at room temperature and the consequent steam/chemical spray exposures of Seq-a (○:120℃, △:140℃, □:160℃), together with the degradation level of Sim-B for comparison (EPR-B).

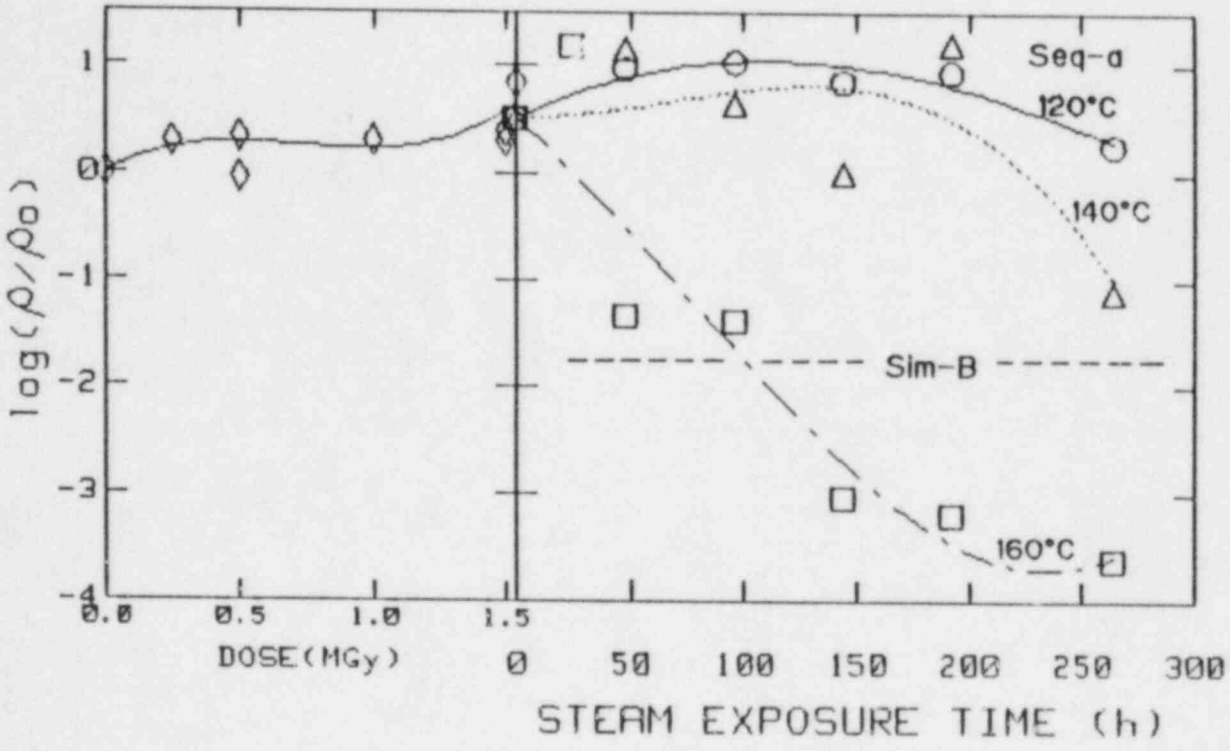

[FIG.-11] A typical degradation behavior of mechanical properties of the EPR's during the pre-irradiation at about 10kGy/h in air at room temperature and the consequent steam/chemical spray exposures of Seq-a (○:120℃, △:140℃, □:160℃), together with the degradation level of Sim-B for comparison (EPR-B).

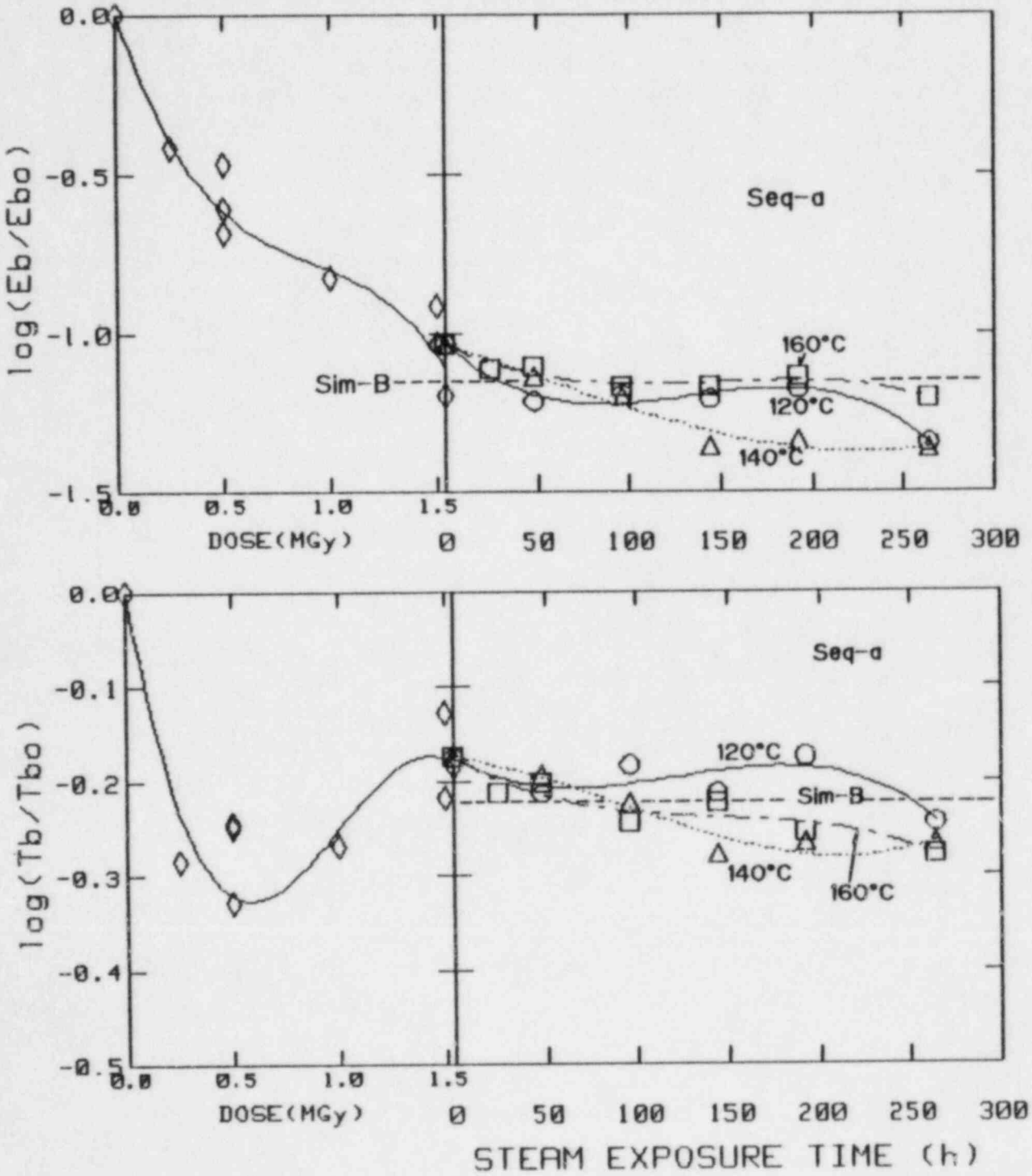

[FIG.-12] A typical degradation behavior of mechanical properties of the Hypalons during the pre-irradiation at about 10kGy/h in air at room temperature and the consequent steam/chemical spray exposures of Seq-b (●:Profile, ◑:120℃, ▲:140℃, ◧:160℃ ;air partial pressure 0.05MPa), together with the degradation level of Sim-C for comparison (Hypalon-C).

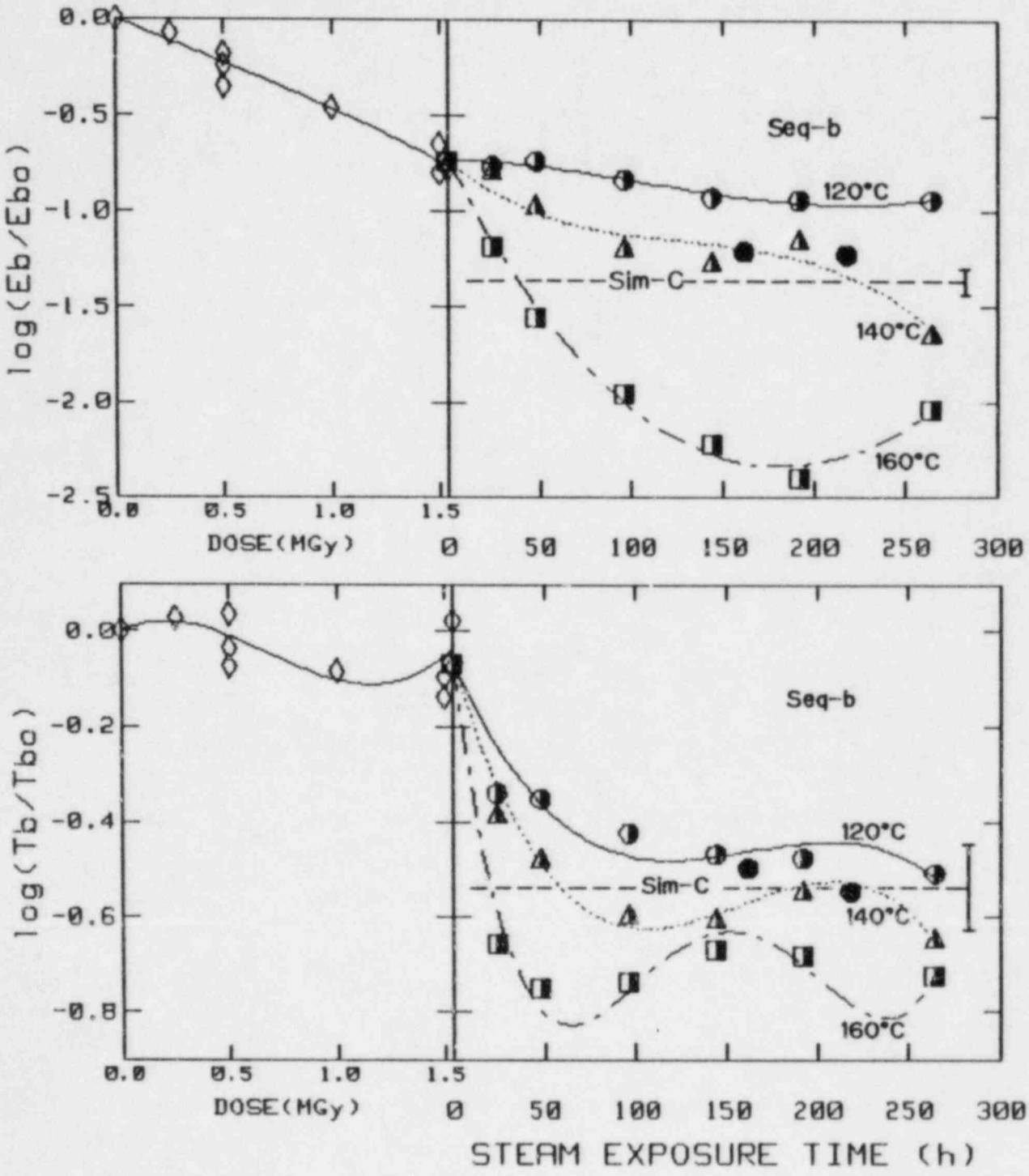

[FIG.-13] A typical degradation behavior of electrical resistance of the EPR's during the pre-irradiation at about 10kGy/h in air at room temperature and the consequent steam/chemical spray exposures of Seq-b (●:Profile, ◑:120℃, ▲:140℃, ◨:160℃ ;air partial pressure 0.05MPa), together with the degradation level of Sim-C for comparison (EPR-B).

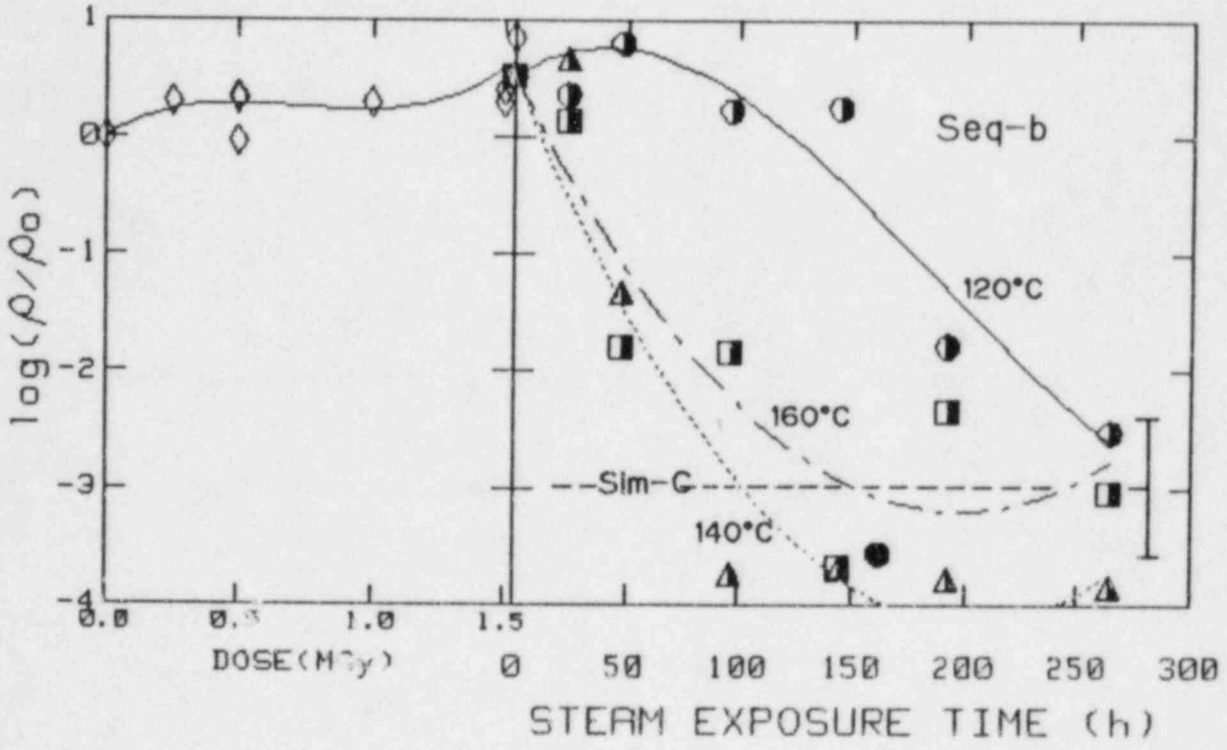

[FIG.-14] A typical degradation behavior of mechanical properties of the EPR's during the pre-irradiation at about 10kGy/h in air at room temperature and the consequent steam/chemical spray exposures of Seq-b (●:Profile, ◑:120℃, ▲:140℃, ◨:160℃ ;air partial pressure 0.05MPa), together with the degradation level of Sim-C for comparison (EPR-B).

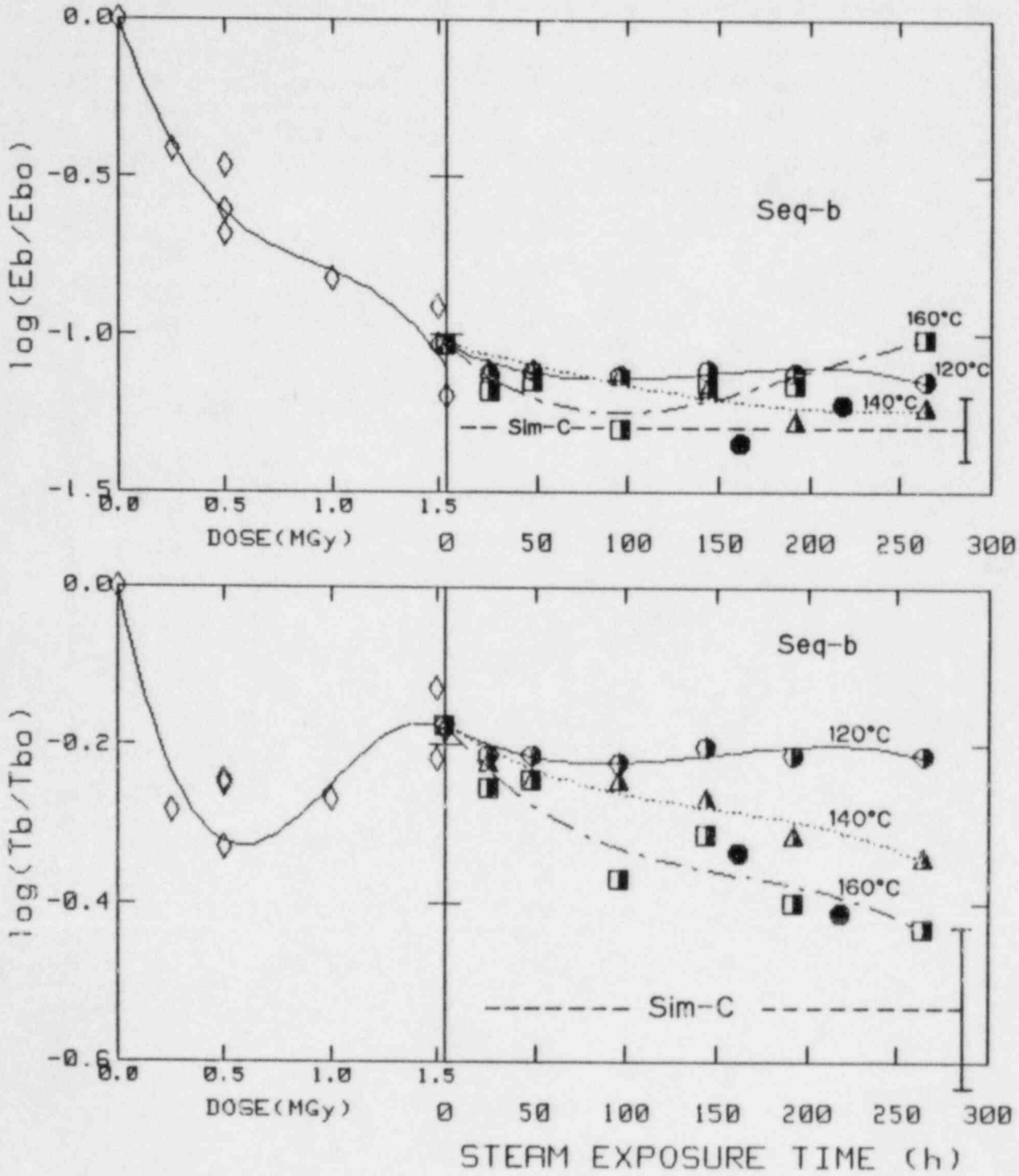

[FIG.-15] Degradation behavior of electrical resistance of EPR-B during the pre-irradiation at about 10kGy/h in air at room temperature and the consequent steam/chemical spray exposures at 120℃ with various air partial pressures in the steam, together with the degradation level of Sim-C for comparison .

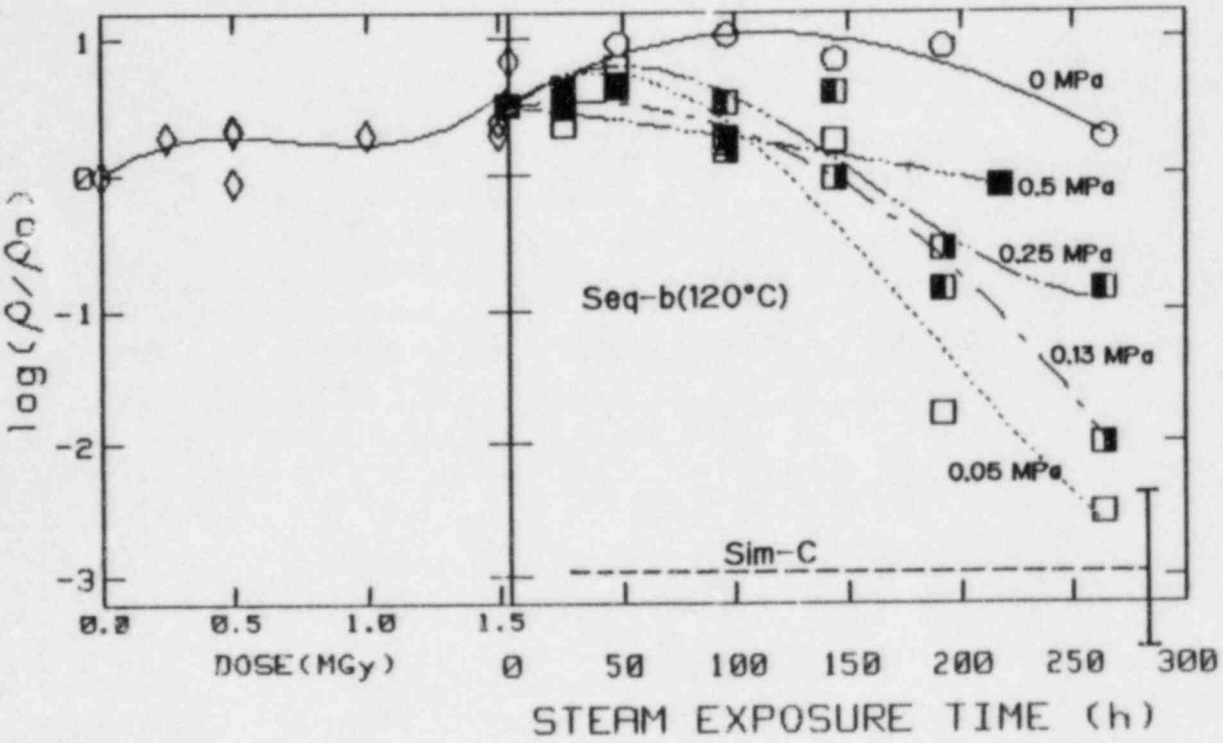

[FIG.-16] A typical degradation behavior of mechanical properties of the Hypalons during a high dose rate pre-irradiation and sufficiently oxidative ones and during the consequent steam/chemical spray exposures, together with the degradation level of Sim-D for comparison (Hypalon-C).

◇:pre-irradiation at ~10kGy/h in air at room temp. → ◆:Seq-b(160℃)
△:pre-irradiation at ~1kGY/h in air at room temp. → ▲:Seq-c(120℃)
→ ▲:Seq-d(120℃)
□:pre-irradiation at 5kGy/h in air at 70℃ → ■:Seq-c(120℃)

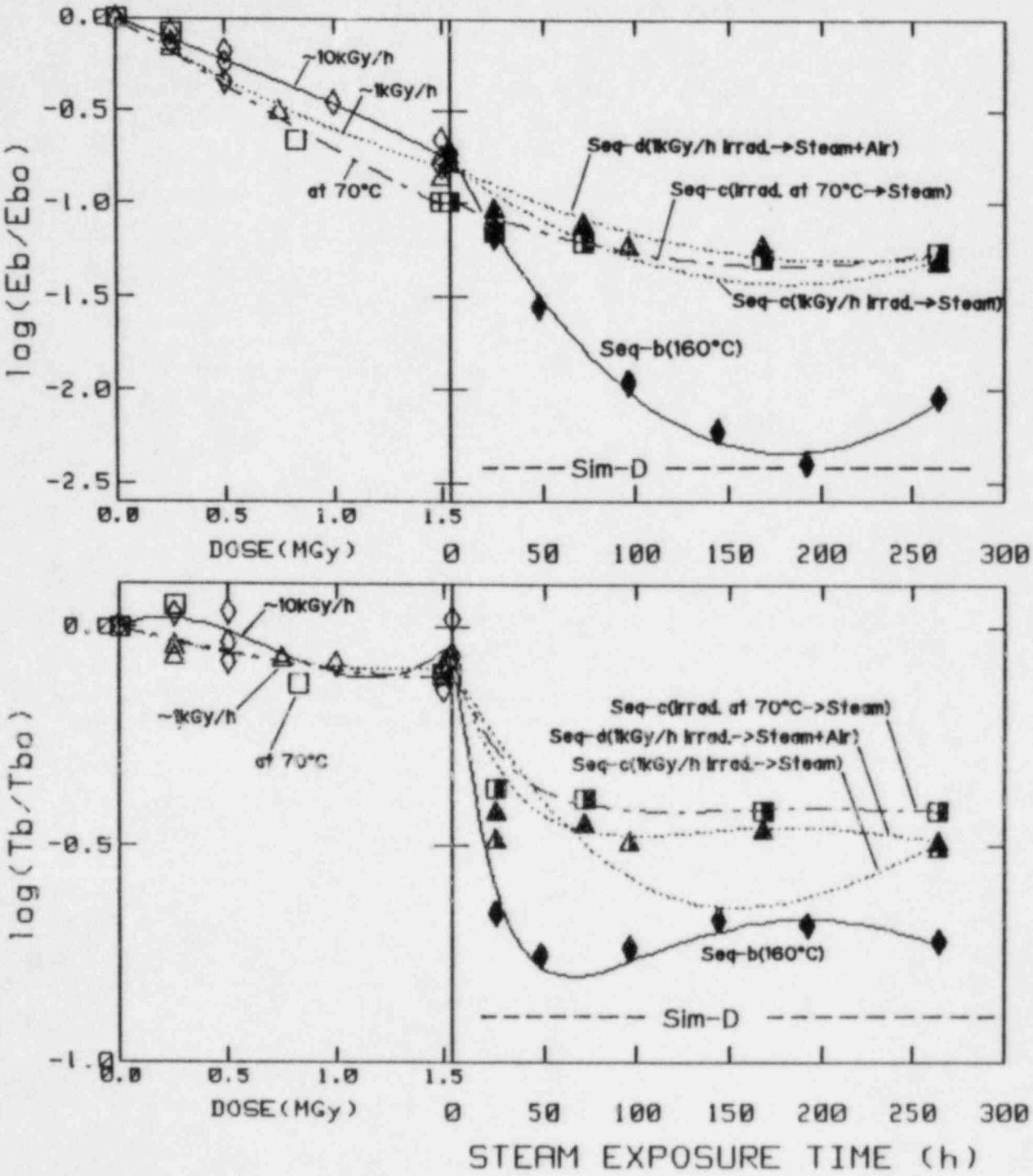

[FIG.-17] A typical degradation behavior of electrical resistance of the EPR's during a high dose rate pre-irradiation and sufficiently oxidative ones and during the consequent steam/chemical spray exposures, together with the degradation level of Sim-D for comparison (EPR-C).
(The symbols are the same as in FIG.-16.)

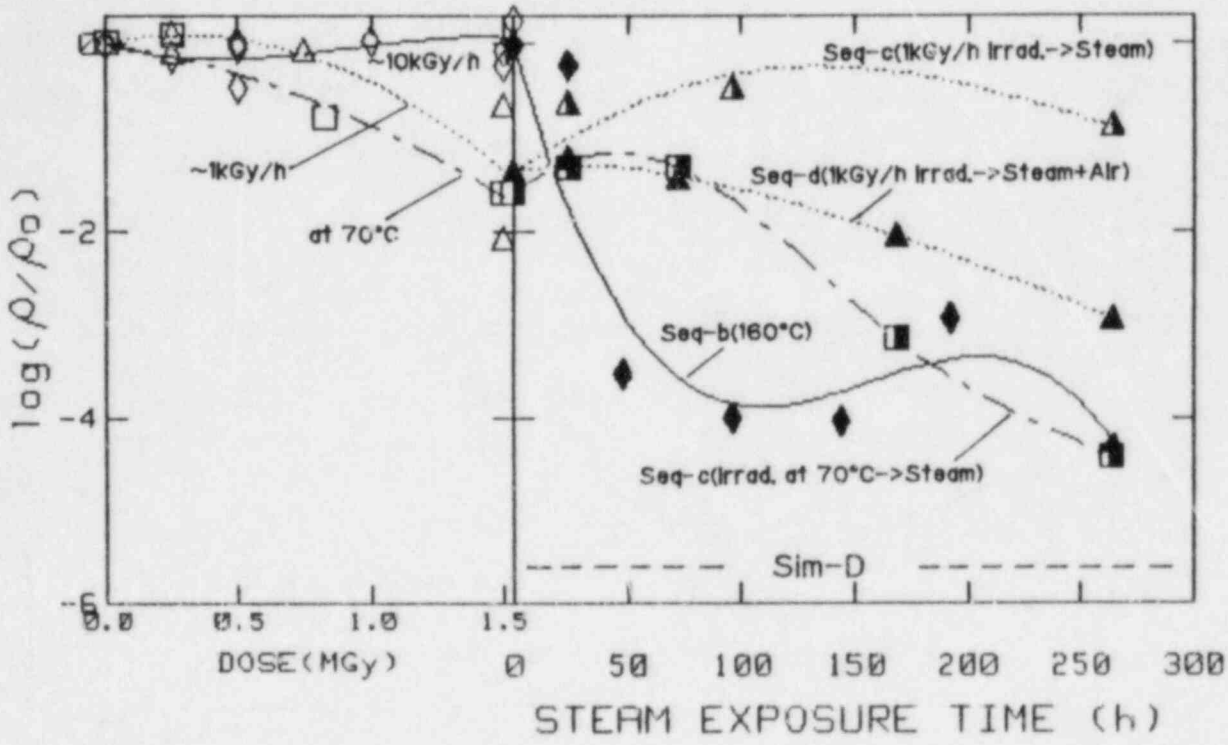

[FIG.-18] A typical degradation behavior of mechanical properties of the EPR's during a high dose rate pre-irradiation and sufficiently oxidative ones and during the consequent steam/chemical spray exposures, together with the degradation level of Sim-D for comparison (EPR-C).
(The symbols are the same as in FIG.-16.)

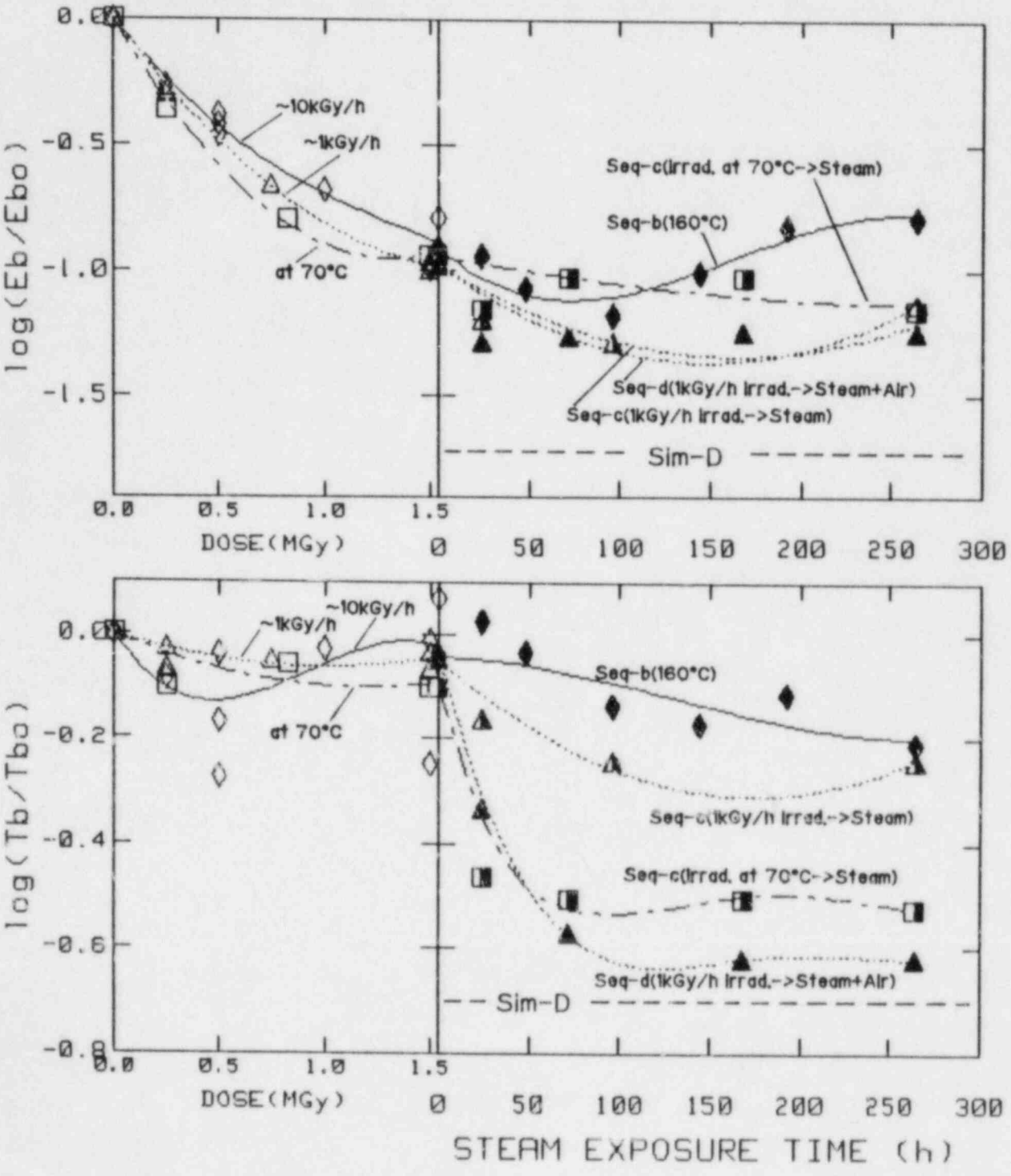

SAND85-1712C

EQUIPMENT QUALIFICATION AND SURVIVABILITY RESEARCH AT SANDIA NATIONAL LABORATORIES*

Lloyd L. Bonzon
Sandia National Laboratories, Albuquerque

Abstract

Since its inception in 1975, the Qualification Testing Evaluation (QTE) Program has been concerned with several broad issues in safety-related equipment qualification. These concerns encompass both aging simulation methods as well as accident simulation methods. Much of the effort is concerned with combined environments, especially radiation in combination with other environments including oxygen, temperature, mechanical stress, and accident thermodynamic environments like pressure/temperature/chemical spray. The Electrical Penetrations Assemblies (EPA) Program is specifically concerned with the survival (i.e., leak-rate integrity) of such assemblies under severe accident conditions. A brief discussion of several current and planned projects illustrate the scope of these NRC-sponsored efforts.

EPA Program

Introduction

The goal of this Program[1] is to evaluate the leak-rate integrity of electrical penetration assemblies, under severe accident conditions (i.e., beyond design basis accidents); the program supports the overall containment integrity evaluation efforts sponsored by the NRC. Based on a previous study,[2] EPAs representing the three remaining U.S. manufacturers have been, or will be, subjected to three representative severe accident profiles.

The EPAs and test profiles selected were based on plant usage and potential for leakage (shown in Table 1).

The EPA plant and profile matches were finally selected as:

- D. G. O'Brien EPA (modular) in a PWR environment

* This paper was supported by the U.S. Nuclear Regulatory Commission, Office of Reactor Safety Research, as part of the Qualification Testing Evaluation (QTE) Program (FIN #A-1051) and the Electrical Penetration Assemblies (EPA) Program (FIN #A-1364) being conducted by Sandia National Laboratories, under Interagency Agreement DOE-40-550-75.

- Westinghouse EPA (modular) in a MK III BWR environment

- Conax EPAs (canister and modular) in a MK I BWR environment

All purchases were made for the most severe environment for which the EPA was qualified and in accordance with applicable standards (e.g., IEEE 317-1976 and 323-1974). But, it must be emphasized that these are not qualification tests; these severe accident environments are generally more severe than qualification tests. Moreover, our emphasis is leak integrity with only a secondary interest in electrical functionability.

TABLE 1
Potential for Leakage

	D. G. O'Brien	Westinghouse	Conax
Organic seals and gaskets		X	X
Elastomer O-rings on header plates	X	X	X
Designs for low pressure capability	X		

D. B. O'Brien EPA Test

The first test has recently been completed.[3] A D. G. O'Brien EPA was subjected to a simulated (large-PWR) severe accident with peak pressure of 155 psia at 361°F (saturated steam); radiation and thermal aging was a part of the test program (200 Mrad and 135°C for 168 hours). The steam test included a slow ramp to full pressure over a 12-hour period, then held for 9 1/2 days, with a slow (12-hour) ramp down to check for contraction leakage. These are significant overtests to obtain engineering data.

Although evaluations continue, there were no detectable leaks through the EPA during the steam pressurized portions, including none through the header plate O-ring seals. As a significant secondary issue, the electrical properties of the EPA degraded over the first 2 days to the point that all modules measured less than 10^6 ohms to ground at 50 volts, and 5 out of the 8 circuits allowed (at least) 1/2 amp leakage currents to ground after 10 days. Figures 1 and 2 show representative results.

Future Tests

Tests of a Westinghouse EPA are currently under way. It will be subjected to a simulated (Mark III, BWR) severe accident with a peak pressure of 75 psia at 400°F (superheated steam). Planning is under way for the third test in this series that will involve a Conax EPA subjected to a simulated (Mark I,

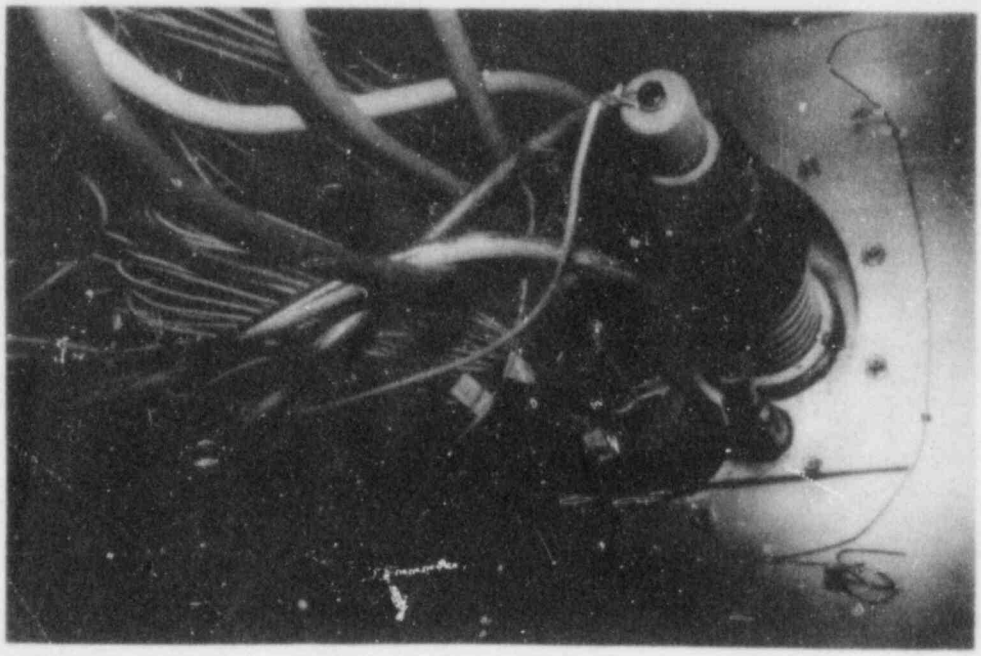

Figure 1: Posttest view of the penetration connector assemblies and cabling.

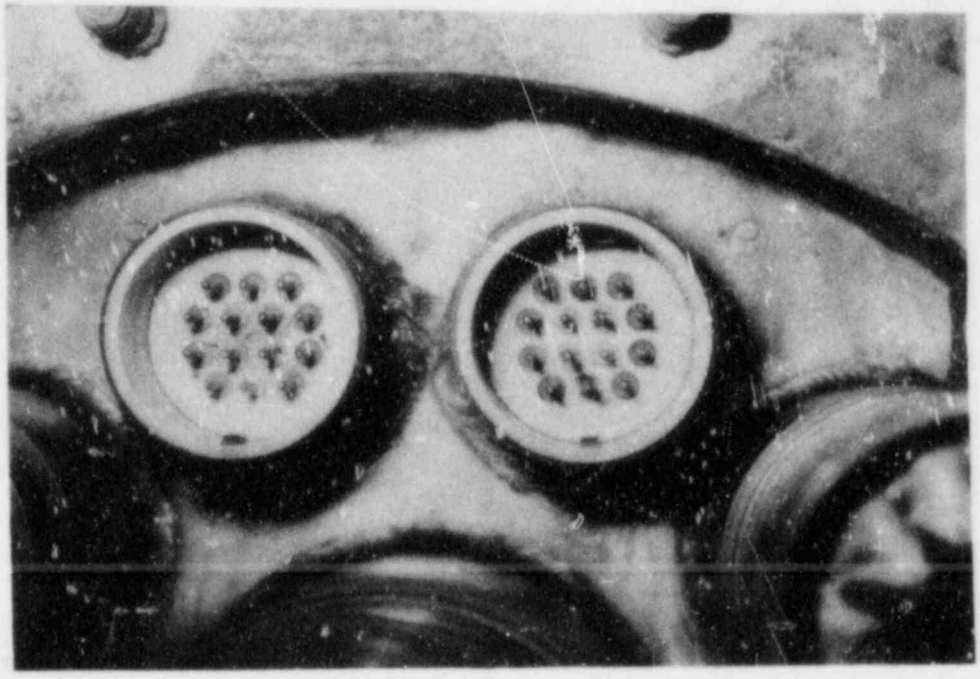

Figure 2: Posttest view of the multi-pin connectors, leakage current "tracks" are visible.

BWR) severe accident with the most extreme environments, 135 psia and 700°F (superheated steam).

QTE Program

This overall Program[4] effort has four major objectives:

- to obtain data needed for confirmation of the suitability of current standards and regulatory guides for Class 1E safety-related equipment
- to obtain data that will provide improved technical bases for modifications of these standards and guides where appropriate
- to establish data-based and standardized test methodologies for equipment qualification programs
- to support the NRC licensing process with qualification expertise and test capabilities

The Program is issues oriented covering the major areas of: (1) methods for simulating aging conditions, (2) methods for simulating accident conditions, and (3) special topics. Table 2 summarizes these issues. To illustrate recent developments, several selected activities will be described in the following section, covering the broad areas of aging and accident methods research. It is essential that the interested reader refer to the References to get the details of the experimental method and results; it is not possible to provide that detail here.

Aging Research: Materials Degradation, Modeling and Techniques

Sandia researchers have published numerous reports[5-9] on material degradation as a function of dose, dose-rate, combined (radiation plus thermal) environments, sequential and simultaneous aging. More recent activities have concentrated on modeling techniques for dose-rate effects so that the extrapolation from accelerated-aging can be made to actual use conditions.[10] This is an excellent example of applications-oriented NRC-sponsored research and is illustrated in Figures 3 and 4.

Figure 3 shows a seeming miscellaneous collection of dose-rate at various temperatures data leading to a specific Dose to Equivalent Damage (DED), here chosen as a 60% change in elongation. Using the models developed in Reference 10, the data shift smoothly as shown in Figure 4 and now extrapolations to use conditions can be made. This "predictive" capability is a major advance in the state-of-the art of accelerated aging.

Another benefit of this work has been the development of several, simple techniques to determine the uniformity of material degradation.[9] These techniques include the use of density gradient columns, microhardness profiling, and metallographic polishing.[6,11,12] In particular, density profiling is a simple technique but can quickly identify degradation heterogeneities that may be an artifact of the choice of accelerated aging parameters. Figure 5 shows an example, with time and temperature as

TABLE 2

Technical Issues Related to Methods for Simulating Aging Conditions

- Realistic Ambient Environments
- Validity of Arrhenius Method
- Dose Rate Effects
- Simultaneous/Sequential Exposures
- Mechanical Stress Effects
- Oxygen Effects
- Humidity Effects
- Analytical and Experimental Techniques for Correlation
- Comparison of Artificially and Naturally Aged Equipment

Technical Issues Related to Methods for Simulating Accident Conditions

- Simultaneous/Sequential Exposures
- Superheated/Saturated Steam Effects
- Thermal Shock and Steam Impingement
- Dose-Rate Effects
- Beta/Gamma Radiation Effects
- Oxygen Effects
- Chemical Spray Effects
- Acceleration of Postaccident Environments
- Sensitivity of Accident Simulations to Aging Methods
- Hydrogen Burn Influence on Accident Simulation Methods
- Submergence Simulation

Special Topics Related to Equipment Qualification

- Statistical/Fragility Concepts Versus Margin
- TMI-2 Experiences
- Evaluation of Qualification Procedures for Specific Equipment Types
- RG 1.97 Requirements
- Fiberoptics Radiation and Qualification Issues
- Realistic Accident Radiation Environments and Calculational Models
- Criteria for Selecting Simulation Methods
- Review of Standards and Guides
- Battery Aging Methods
- Radiation Damage Thresholds

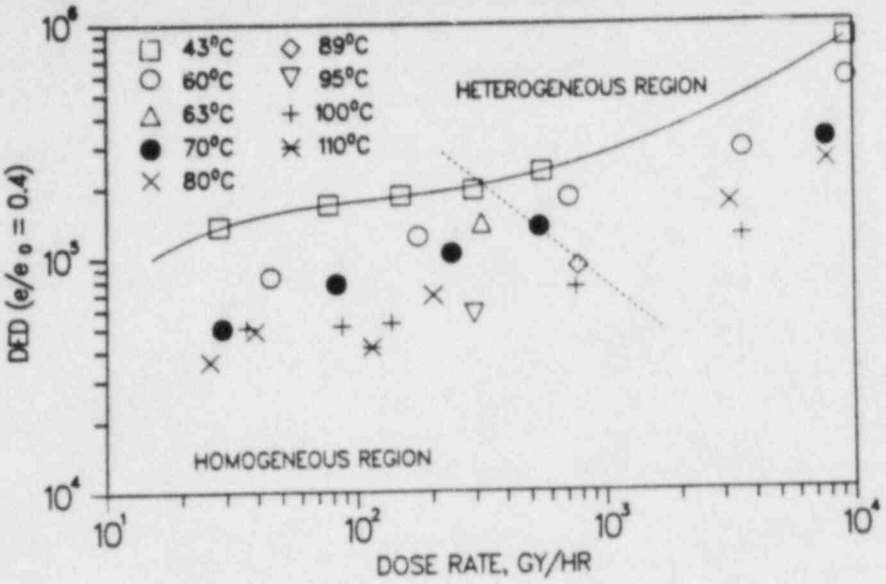

Figure 3: Radiation dose required for the elongation of PVC to decay to 40 percent of its unaged value at various dose rates and temperatures. To highlight the complicated dose-rate effects, a solid curve is drawn through the 43°C data. The dashed curve separates the homogeneous aging region from the heterogeneous aging region.

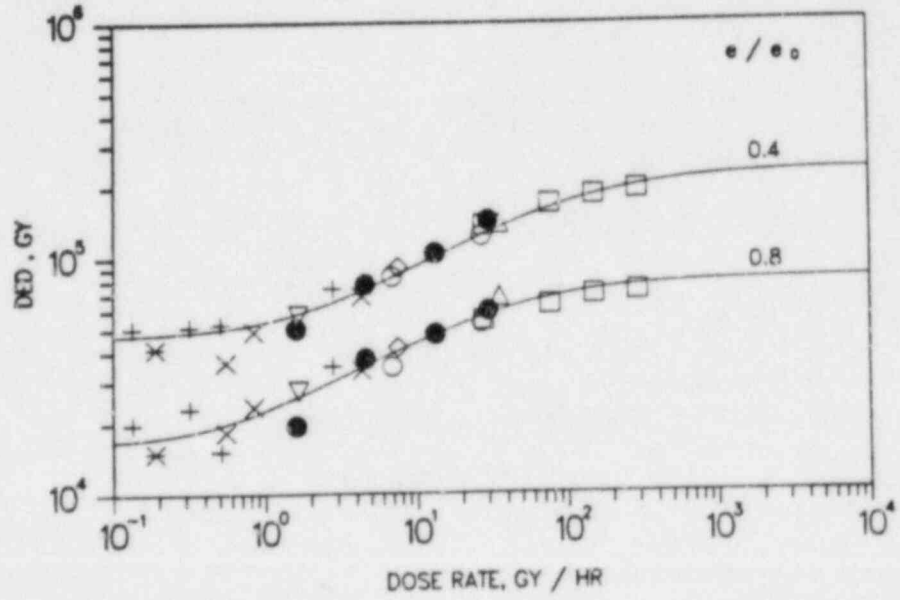

Figure 4: Upper data represents the homogeneous PVC data ($e/e_0 = 0.4$) shifted to a reference temperature of 43°C, using the models in Reference 10. The solid curve represents the theoretical fit to the shifted data. Lower data and curve are for $e/e_0 = 0.8$ data.

parameters; it clearly shows that oxygen cannot diffuse to the interior (middle) of the sample rapidly enough to compensate for the high temperatures used and hence the material density increases at the exposed surfaces.

Some new work has been initiated in the area of combined dose (dose-rate), temperature, and mechanical stress on seals and gaskets. Also, based on an earlier study of electronics aging,[13] electronic pieceparts are being studied by varying several parameters: component type, dose, dose-rate, temperature, and voltage bias.

Aging Research: Batteries

A project involving the seismic-fragility of nuclear station batteries has several objectives:

- To determine actual failure modes and thresholds, primarily using naturally-aged cells.
- To select the dominant aging mechanism(s) through this testing experience, other test experience, and expert evaluations.
- To compare/correlate the response of naturally-aged cells and cells aged by the accelerated methods described in IEEE Std. 535-1979 and compare dominant failure modes in both cases.

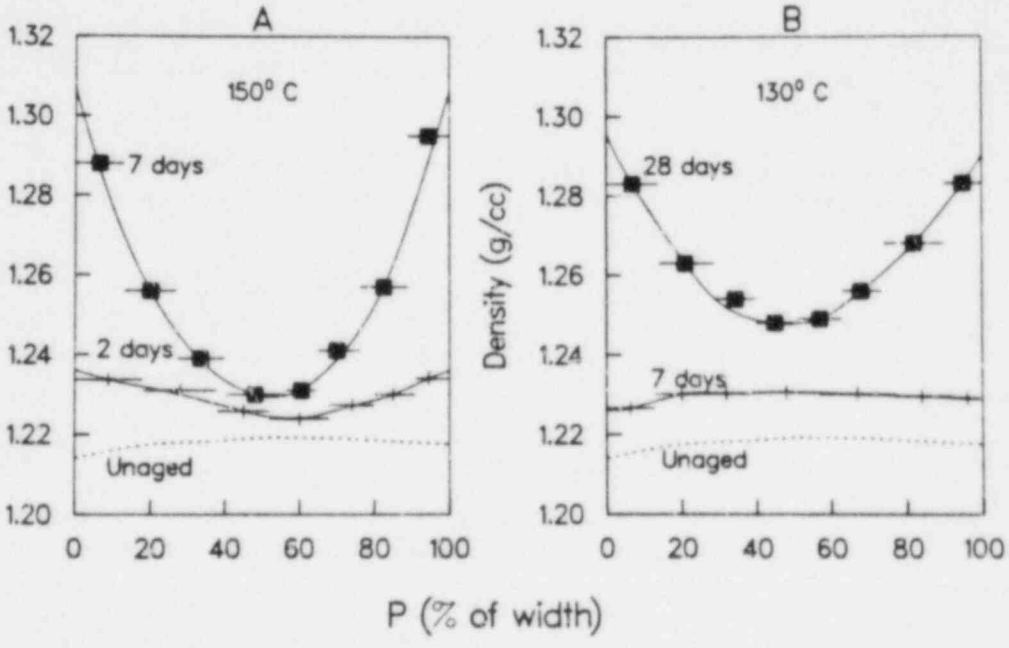

Figure 5: Density profiles for the nitrile rubber material heat aged in air. A: aging at 150°C. B: aging at 130°C.

- To determine appropriate aging methodologies for the dominant mechanism(s).

- To demonstrate the methodologies by a specific demonstration test program.

- To make final recommendations of the appropriate accelerated-aging methodology(ies) for nuclear station batteries.

We were fortunate in obtaining naturally-aged batteries from several nuclear power stations which represented all three major manufacturers: Gould NCX-2250, 12-years service; Exide FHC-19, 10-years service; C&D LCU-13, 10-years service. In addition, 27-year old Exide EMP-13 cells were available from Shippingport. Seismic-fragility tests have been conducted on these and reported.[14-17] It must be emphasized, however, that these tests were done to severe acceleration levels involving repeated severe motion; they are not directly comparable to qualification tests. In one case, the cells were destroyed because of complete breakage at the positive bus bar and terminal post interface. There was also loss of electrical discharge capacity capability in many cells. A detailed age-degradation report is being prepared which includes teardown evaluations. Some preliminary conclusions include:

1. The batteries, in general, were very durable considering the repeated, high-level seismic fragility tests imposed. (These are not qualification tests!)

2. Embrittlement and/or cracking of positive buses was aided by corrosion along large grain boundaries in all cell types tested. Fine grained material remained ductile.

3. Formation of brittle bus material is a significant aging effect which can lead to abrupt failure during a seismic event or reduced capacity after the event.

4. Excessive sulphation leading to plate hardening and expansion is also an aging effect of significance, but of less importance than the formation of brittle materials, as it reduces postseismic discharge capacity and increases self-discharge.

5. There is evidence that overcharging is a significant aging mechanism.

New cells, of the same type, were also obtained. Baseline seismic-fragility tests were run on some cells for comparisons, and detailed evaluations are being conducted.

Some new cells were also aged using the IEEE-535 suggested methods. Seismic-fragility tests were run on these in mid-September 1985. The failure modes were very different than for the naturally-aged cells. Besides jar cracking (in some cases, total destruction), first looks at the (accelerated-aged) plates showed them to be in very bad condition, see Figure 6. Analyses and reporting continues. The results from these two aging

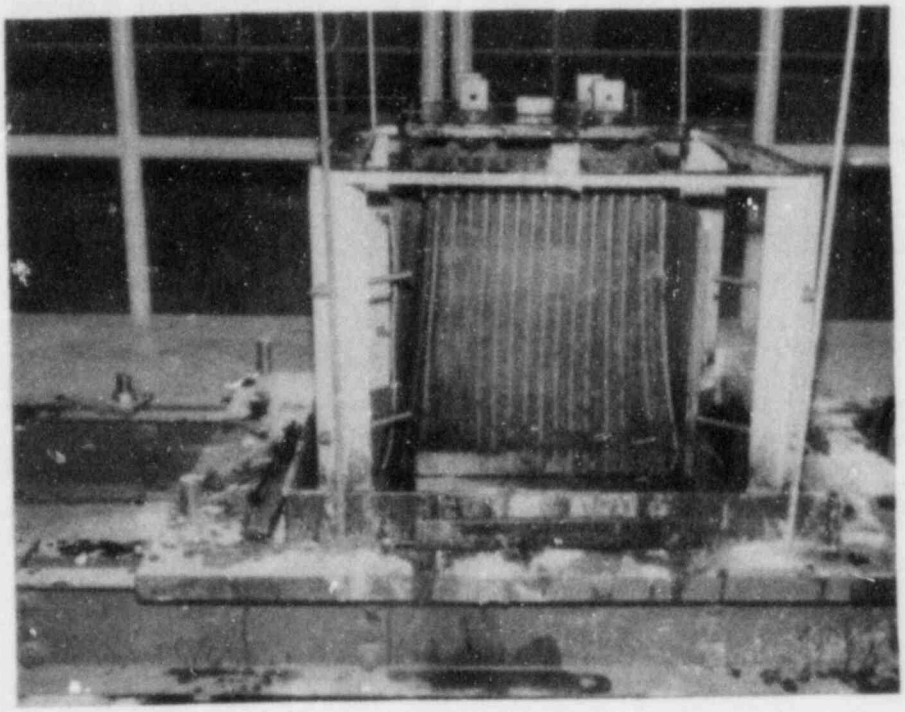

Figure 6: Results of seismic-fragility tests of an artificially-aged (12-years per IEEE-535) NCX-2250 cell.

methods will be evaluated in order to establish the relevance and applicability of accelerated aging methods.

Accident Research: Adequacy of Radiation Simulators

In evaluating the adequacy of radiation simulators, the concern is for the accident situation: high dose rates, large total doses, gamma and beta radiations, and combined accident environments. Particularly, the presence of beta radiation complicates the testing of material and equipment specimens. Electron-irradiation charge-breakdown experiments were previously done on rubber insulation materials;[18] charge breakdown was not apparent using "real" conditions (but was observed during experiments in vacuum). Currently the simulator-adequacy evaluation activity involves comparison of beta and gamma effects on material degradations to determine a gamma-equivalent test approach; this work is being done jointly with French researchers.

In the joint U.S./French project we are attempting to determine the photon dose required to import damage equivalent to that resulting from beta radiation on selected organic materials; this is being done in three phases, (1) dosimetry and facility normalization, (2) gamma and beta materials irradiations, and (3) synergistic effects of mixed radiation fields. Phase 1

has just been completed and the Phase-2 Screening tests are just being initiated; these include several test parameters:

Specimens	-	1-mm and 2-mm thick EPR
Exposures	-	beta and Co-60 gamma
	-	0, 15, and 50 Mrad
	-	0.3, 1, and 2 Mrad/hr
Beta energies	-	0.5, 1.0 Mev

Accident Research: LOCA Tests

Combined-environments accident testing has been done, and continues. The importance of oxygen during accident simulations has been observed and reported.[19] Enhanced degradation of materials in simultaneous (radiation plus accident thermodynamic) profiles has also been observed and reported.[20] The "sensitivity" of material degradation to the choice of aging and accident simulation methods has just been completed and reported.[21]

This latter effort is especially interesting because it provides the start for a data base from which a generic test sequence that is "conservative" for all materials can be selected. Eighteen U.S. and French materials were exposed to a wide variety of aging and accident simulation techniques:

- Accident simulations were performed both sequentially and simultaneously.
- Accident steam exposures were performed both with and without air.
- Irradiations were performed both at 28°C (R28) and 70°C (R70).
- Sequential aging exposures were performed using two sequences: T→R and R→T.

Table 3 shows the qualitative conclusion for each material type. In summary, we were able to conclude that:

- R→T aging was generally more conservative than T→R aging.
- Material classification and chemical composition had an important influence on test results.
- LOCA(air) exposures were generally more degrading than LOCA(nitrogen) exposures, but not universally so.

For all of the materials of our data base, the following qualitative conclusion applies:

> A R70→T aging simulation followed by a R70→LOCA(air) accident simulation would be appropriate.

TABLE 3

Qualitative Conclusions for Each Class of Material
Joint U.S./French Program

Material Class	Appropriate Sequential Qualification Procedures
Cross-linked Polyolefins	
XLPO 1	Any sequential simulation
XLPO 2	Any sequential simulation
PRC (82I1)	Any aging sequence followed by R70 → LOCA(air) accident simulation
Ethylene Propylene Rubbers	
EPDM (82I2)	A R → T aging sequence followed by any accident simulation
EPDM(82I9)	A R → T aging sequence followed by a R70→LOCA(air) accident simulation
EPR (82H4)	Any sequential simulation
EPR 1	A R → T aging sequence followed by a R70 → LOCA(air) accident simulation
EPR 2	A R70 → T, or T → R70 aging sequence followed by R70 → LOCA(air) accident simulation
TEFZEL	
TEFZEL 1	Elevated temperature irradiations for sequential aging and accident exposures
TEFZEL 2	R70 → T aging sequence followed by an accident simulation
Chlorosulfonated Polyethylene	
HYPALON (82G10)	Any sequential simulation
CSPE	R70 → T aging sequence followed by an accident simulation
O-Ring Materials	Any sequential simulation
Connector Materials	
PPS (82H6)	Any sequential simulation
Polydiallylphtalate (82H5)	Any aging simulation followed by the R28 → LOCA(air) or R70 → LOCA(air) accident simulations
VAMAC	Any sequential simulation
CPE	R70 → T aging technique followed by any accident simulation

Very recently,[22] tests of cables in superheated-steam conditions was completed. The impetus for the effort was to repeat earlier tests[20] of EPR cables which were done in saturated-steam (consequently at higher pressure).

Figure 7 shows the response of the most severely degraded cable. But as shown in Figure 8, the response of EPR cables in superheated-steam closely paralleled the previous saturated-steam test results. The preliminary results are:

1. Single conductors and multiconductors behaved differently for aged EPR D lot 1 cables. This suggests that qualifying single conductors may not be appropriate to qualify multiconductors.

2. Since the same results were found using superheated-steam as were found using saturated-steam conditions, the superheat parameter appears to have little effect. It only delays the failure of the cables slightly.

3. EPR D lot 1 was certified to LOCA requirements, but failed the test. EPR D lot 2, although not certified, passed the test. Two possible explanations for this result are (1) some change in material and/or processing occurred between lot 1 and lot 2 and/or (2) there was insufficient quality control.

4. Since only one product (aged multiconductor EPR D lot 1 cable) had low IR values and large leakage currents, the differences between the electrical degradation of single and multiconductor cables does not appear to be generic to all cables.

Major Planned Activities

We expect a major test emphasis in FY-86, and numerous tests and test planning are currently underway. To provide an overview, Table 4 is a summary of these plans. Of course, test results and sponsor needs will affect the activities actually accomplished.

Summary

The USNRC concerns for data-based equipment qualification methods and equipment integrity information are being addressed in the QTE and EPA Programs. The results presented in this paper illustrate the most recent, and planned, activities. In summary:

- Significant research has been conducted and documented.
- Results have impacted the regulation and licensing process.
- Several new areas of investigation are underway or planned.
- The program represents a coordinated issues-oriented effort.
- Issues resolutions are well underway.

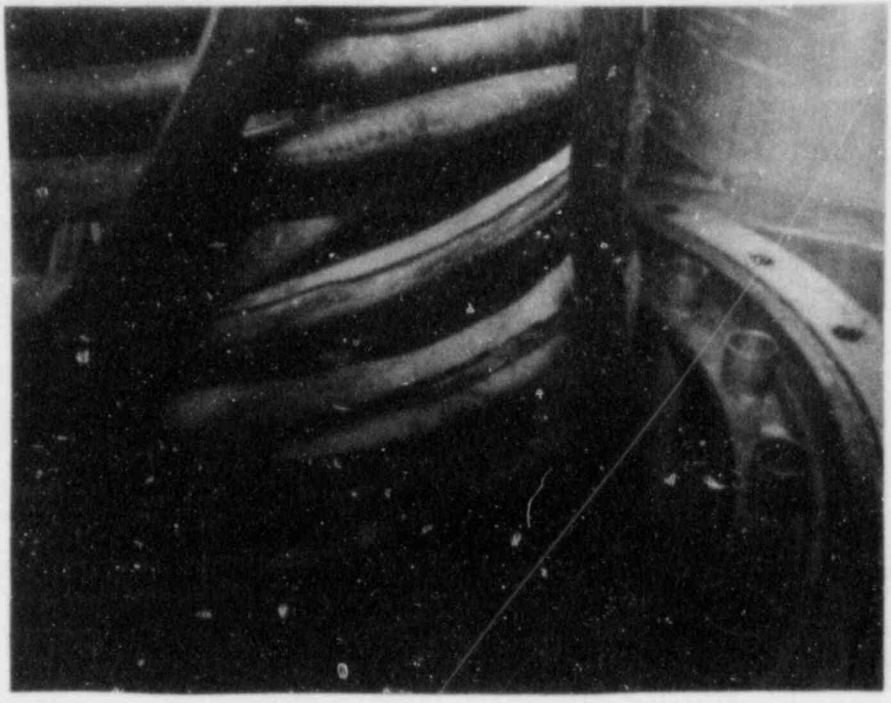

Figure 7: Posttest photo showing the responses of EPRD, Lot 1 multiconductor cable, after a simultaneous superheated-steam test.

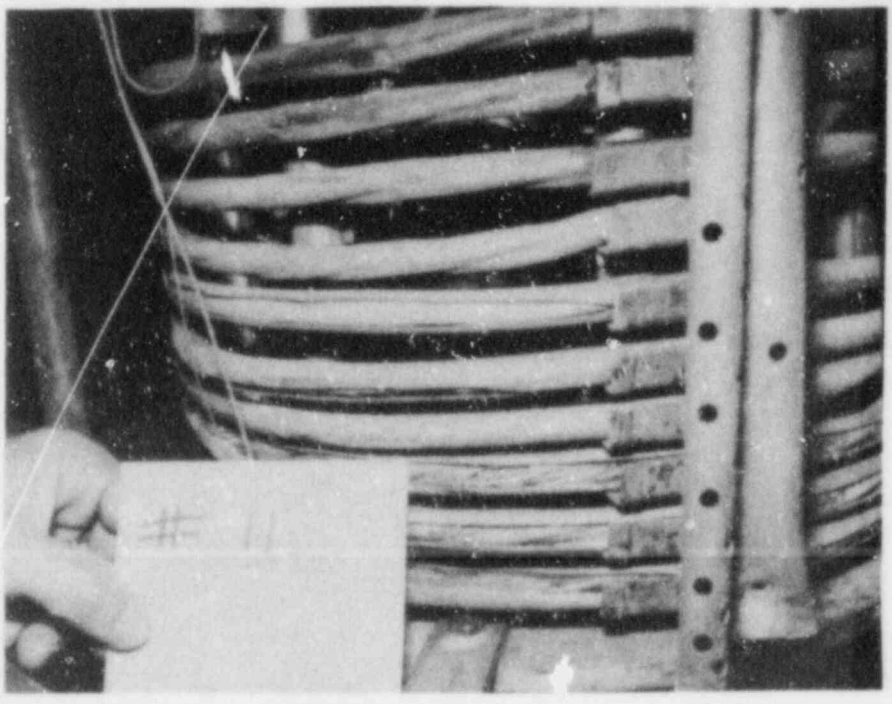

Figure 8: Posttest photo showing the responses of EPRD, Lot 1 multiconductor cable, after a simultaneous saturated-steam test.

TABLE 4
Major Planned Activities

Aging Research

- General materials evaluations
- Seals/gaskets, including mechanical stress
- Thermal-Arrhenius validity
- U.S./Japan oxygen overpressure research
- Battery aging methods
- Acquire ambient-aged equipment for evaluation (Ambient plant environments)
- Electronics aging evaluations

Accident Radiation Environments Research

- Joint U.S./French beta/gamma equivalence
- Sandia program on beta effects (materials and equipment)
- Impact of Source Term research
- Calculational models for dose/rates to safety-related equipment

Accident Research

- Radiation monitor tests
- Coaxial/triaxial cable tests
- Oxygen overpressure effects on cables/materials
- Post-DBE acceleration tests on materials/cables and selected equipment
- Long-term aging and LOCA tests on cables
- Sealing systems (moisture ingress) tests
- Transmitter tests
- Integral systems tests
- Evaluation of impact of TMI-2 research on EQ methods

Planning

- Complete Issues Resolution topical report
- Update long-range research plan
- Summary report of significant foreign research.

References

1. F. V. Thome, Results of Leak-Rate Testing of Electrical Penetration Assemblies under Severe Accident Conditions, SAND84-1496A. Presented at the 8th International SMIRT Conference, Brussels, August 19-23, 1985.

2. W. A. Sebrell, The Potential for Containment Leak Paths Through Electrical Penetration Assemblies Under Severe Accident Conditions, SAND83-0538, NUREG/CR-3234, July 1983.

3. Quick-Look Report on Test for Evaluating Leak Behavior of a D. G. O'Brien EPA under Severe Accident Conditions, July 12, 1985. Letter F. V. Thome (SNL) to W. S. Farmer (NRC).

4. Sandia Laboratories Staff, Status Report on Equipment Qualification Issues Research and Resolution, SAND85-1309, NUREG/CR-4301. To be published.

5. L. L. Bonzon, K. T. Gillen and E. A. Salazar, Qualification Testing Evaluation Program Light Water Reactor Safety Research Quarterly Report, October-December 1978, SAND79-0761, NUREG/CR-0813, June 1979.

6. R. L. Clough, K. T. Gillen, and C. A. Quintana, Heterogeneous Oxidative Degradation in Irradiated Polymers, SAND83-2493, NUREG/CR-3643, April 1984.

7. R. L. Clough and K. T. Gillen, Investigation of Cable Deterioration Inside Reactor Containment, Nuclear Technology, Vol. 59, November 1982, pp. 344-354.

8. R. L. Clough and K. T. Gillen, Complex Radiation Degradation Behavior of PVC Materials Under Accelerated Aging Conditions, SAND82-1414, NUREG/CR-3151, July 1983.

9. R. L. Clough, et al, Accelerated-Aging Tests for Predicting Radiation Degradation of Organic Materials, SAND83-0798J, Nuclear Safety, Vol. 25, No. 2, March-April 1984, pp. 238-254.

10. K. T. Gillen and R. L. Clough, General Extrapolation Model for an Important Chemical Dose-Rate Effect, SAND84-1948, NUREG/CR-4008, December 1984.

11. R. L. Clough and K. T. Gillen, Techniques for Studying Heterogeneous Degradation in Polymers, SAND83-2171. Presented at the American Chemical Society Symposium on Polymer Degradation, St. Louis, Missouri, April 8-13, 1984.

12. K. T. Gillen, R. L. Clough, and N. J. Dhooge, Density Profiling of Polymers, SAND85-0795J, March 1985. To be published in Polymer.

13. R. T. Johnson, F. V. Thome, and C. M. Craft, A Survey of the State-of-the-Art in Aging of Electronics with Application to Nuclear Power Plant Instrumentation, SAND82-2559, NUREG/CR-3156, April 1983.

14. L. L. Bonzon and D. B. Hente, Test Series 1: Seismic-Fragility Tests of Naturally-Aged Class 1E Gould NCX-2250 Battery Cells, SAND84-1737, NUREG/CR-3923, September 1984.

15. L. L. Bonzon and D. B. Hente, Test Series 2: Seismic-Fragility Tests of Naturally-Aged Class 1E Exide FHC-19 Battery Cells, SAND84-2628, NUREG/CR-4095, March 1985.

16. L. L. Bonzon and D. B. Hente, Test Series 3: Seismic-Fragility Tests of Naturally-Aged Class 1E C&D LCU-13 Battery Cells, SAND84-2629, NUREG/CR-4096, March 1985.

17. L. L. Bonzon and D. B. Hente, Test Series 4: Seismic-Fragility Tests of Naturally-Aged Exide EMP-13 Battery Cells, SAND84-2630, NUREG/CR-4097, March 1985.

18. W. H. Buckalew, F. J. Wyant, and G. J. Lockwood, Response of Rubber Insulation Materials to Monoenergetic Electron Irradiations, SAND83-2098, NUREG/CR-3532, November 1983.

19. K. T. Gillen, et al, Loss of Coolant Accident (LOCA) Simulation Tests on Polymers: The Importance of Including Oxygen, SAND82-1071, NUREG/CR-2763, July 1982.

20. L. D. Bustard, The Effect of LOCA Simulation Procedures on Ethylene Propylene Rubber's Mechanical and Electrical Properties, SAND83-1258, NUREG/CR-3538, November 1983.

21. L. D. Bustard, et al, The Effect of Alternative Aging and Accident Simulations on Polymer Properties, SAND84-2291, NUREG/CR-4091, May 1985.

22. Quick-Look Report on Superheated-Steam Cable Tests, October 17, 1985. Letter P. R. Bennett (SNL) to W. S. Farmer(NRC).

Fire Protection and Hydrogen Burn Equipment Survival Research

D. L. Berry

Sandia National Laboratories

ABSTRACT

A discussion is presented of the Fire Protection and Hydrogen Burn Equipment Survival Research Programs at Sandia National Laboratories, with emphasis on the experimental efforts completed in FY85 to characterize fires and fire damage and to understand equipment response to hydrogen burns. The results of fire characterization tests, electrical cabinet fire tests, large-scale enclosure fire tests, and cable and relay damage threshold tests are described. The results of hydrogen burn simulation tests of cable, solenoid valves, and pressure transmitters are also described, including testing using both realistic heat flux conditions and heat fluxes beyond those anticipated during an actual hydrogen burn. Plans for FY86 analysis and testing are summarized.

INTRODUCTION

The Fire Protection and Hydrogen Burn Equipment Survival research programs at Sandia National Laboratories involve both testing and analyses. Each program has followed separate yet parallel paths for assessing the likelihood that equipment will survive either a fire or a hydrogen burn accident environment. To do this, both programs have strived to characterize their respective accident conditions and to test the survivability of equipment to these conditions. For fire protection research, work has been aimed at supporting licensing and probabilistic analysis needs for data relevant to nuclear power plant situations. For hydrogen burn research, work has been aimed at performing experiments and analyses to support past and pending licensing decisions which require an understanding of equipment thermal response and survival in a hydrogen burn. Because of the obvious environmental similarities that exist between fire and hydrogen burn equipment survival, research for these programs is being performed at Sandia within one division using some of the same facilities and analysis techniques.

FIRE PROTECTION RESEARCH

The objectives of the Sandia Fire Protection Research Program have changed over the years since its inception in 1975.

During its initial phases, emphasis was placed on performing tests which would confirm the adequacy of a variety of fire protection measures that were being proposed or implemented as regulations. The results of this work yielded insights into the adequacy of fire protection measures being used in nuclear power plants, with a summary of the major findings given in Reference 1. Examples of conclusions derived from this work include:

1. Fire retardant cable insulation, coatings, cable tray covers, or solid bottom cable trays reduce fire severity.

2. Even qualified cabling or cabling protected with coatings can be ignited, burned, or damaged.

3. Water, CO_2, and Halon suppression systems eventually extinguish fires, even those that involve deep seated burning conditions.

4. Gaseous suppression agents permit temperatures in rooms to remain high and water produces severe moisture environments which could damage equipment.

5. Penetration seals to prevent the spread of fire may fail if they have cracks as a result of installation or maintenance operations.

6. Hot gas layers can cause damage to equipment or cabling that is spatially separated from a source fire.

In recent years the fire protection research program has shifted from a program in which the adequacy of specialized fire protection measures is confirmed through testing to a program aimed at providing the analytical tools and data base necessary for judging the residual risk of fire to the overall safety of power plants. The need for this new emphasis was highlighted by the findings of numerous probabilistic risk assessments (PRA's) that have indicated that the core melt frequency estimated for fire represents a significant portion of the overall core melt frequency attributable to other accident scenarios. Although in most cases, steps have been taken to reduce these estimates by eliminating the specific sequences that contributed to them, the fact remains that several different assessments of fire risk indicate that fire may represent a significant threat to power plant safety and in some cases may represent a threat that exceeds accident scenarios traditionally assumed to be dominant (e.g. seismic).

Unfortunately, though, fire risk assessments have been forced to base assumptions and analyses on a marginal understanding of fire phenomena and the effect of fire environments on the

operability of safety equipment in nuclear power plants. In some cases these assumptions appear to have a conservative basis, while in other cases the analyses may have overlooked some of the impacts of fire. Several important examples of where fire risk assessments have been forced to make unsubstantiated assumptions involve the effectiveness of ventilation systems to control smoke movement during fires, the ability of manual fire fighting teams to perform in the confines of a power plant, the detrimental effects of suppression actuation or invertant suppression actuation, the vulnerability of safety equipment to fire environments, and the susceptibility of control rooms or remote shutdown areas to cabinet fires. Although Sandia has done or is planning to do work in each of these areas, only those areas investigated in FY85 will be discussed here. This will be done in the context of the steps and data base needs of a fire risk assessment.

Fire PRA's

In general, fire risk assessments involve four major steps which are intended to yield a quantitative estimate of the frequency of core melt attributable to fires of various types in a nuclear power plant. The four steps involve:

1. Selection of plant areas for analysis;

2. Selection of ignition probabilities and fire scenarios;

3. Calculation of expected fire environments;

4. Assessment of component damage resulting from the fire environments.

Except for the first task, which is based upon a systems analysis of required safety operations in a nuclear power plant, all steps of the fire risk assessment require data and analysis tools unique to fire. The tasks outlined in the NRC fire protection research program plan, Reference 2, are aimed at gathering required data on potential fire sources, ensuing fire environments, and equipment response in support of performing steps two through four of a fire risk assessment.

Fire Characterization

Fire environment models available for performing fire probabilistic risk assessments are unable, using current technology, to accurately predict the burning characteristics of source fires. As a result, these models generally rely upon fire characterization input of source fires as described by heat release rates and combustion product release rates. The

objective of the fire characterization task is to determine the rates of heat and combustion product release during open burning for a variety of transient and insitu fuels found in nuclear power plants. To date work has concentrated on trash fires, liquid pool fires, and electrical cabinet fires involving cable insulation. In the future, testing involving cable trays as source fires for fire models will be performed. To date, a variety of parameters including fuel configuration, fuel quantity, rates of burning and fuel type have been investigated. Over twenty-four (24) heat release rate tests on various types and sizes of fuels have been completed, with approximately 15 full-scale cabinet fire burn tests using IEEE-383 qualified or unqualified cabling also being performed.

The facility used to perform these tests is shown in Figure 1. As configured, the facility controls the amount of air available for burning by a forced ventilation system, and it monitors the combustion products released by the fire to yield rates of heat release as a function of oxygen consumption and carbon dioxide and carbon monoxide production. In addition, a variety of thermocouples, calorimeters, radiometers, and flow measuring devices are installed for each of the tests. For the cabinet tests, approximately 120 channels of data were recorded. Load cell information giving mass release rates was measured to compare with the oxygen consumption measurements to yield an estimated smoke production rate in terms of unburned pyrolyzates.

As an initial calibration of the facility, burner tests were performed using calibrated burners to yield a comparison of the measured heat release rate to the theoretical heat release rate based upon the mass of fuel burned. Figure 2 shows the comparison of these results for unsmoothed mass loss rate data. It can be seen that a favorable comparison exists, taking into account an approximate 2 minute delay time in the response of the gas analysis equipment. For each of the source fire burns, heat release rates and some temperature measurements were made. Figure 3 shows a typical example of the results obtained for a trash fire involving a thirty gallon plastic trash can of the type found in some nuclear power plants. It can be seen here that the peak heat release rate during this fire was ~ 110 kilowatts.

The cabinet fire characterization effort represented a more extensive test scheme. A major objective of this effort was to gather information on the way cabinet fires may be expected to burn to serve as input into full-scale room testing using a control room mock up. In order to perform these tests, it was necessary to establish the test parameters to be investigated. This was done by performing a number of surveys of nuclear

power plants, architectural engineers, and nuclear steam supply system vendors to establish typical ranges of cabinet sizes, fuel loads, construction materials, and cabinet configurations for testing.

The initial test series involved vertical cabinets, using both qualified and unqualified cable, with an ignition source based upon discussions with NRC inspectors and observations by Sandia personnel during visits to power plants. The ignition source consisted of a plastic bucket with a box of cleaning tissues and a quart of acetone in a plastic bottle. This source was chosen because it had been observed in actual power plants, and it represents what we believe to be a credible ignition source.

Figure 4 shows the results of one of the cabinet tests involving a vertical cabinet with a fuel load of unqualified cable, together with the ignition source of a plastic bucket, cleaning tissues, and acetone. As can be seen from the test sequence photos, the fire involving unqualified cable developed very quickly. For this test, heat release rate measurements gave a peak value of ~ 1000 kilowatts. A similar sequence is shown in Figure 5 for qualified cable in the same configuration as that in Figure 4 for unqualified cable. In this case it can be seen that the degree of burning within the cabinet was limited to the initial cable bundles exposed to the source fire. For this case, the peak heat release rate was measured to be only ~ 57 kilowatts. In two later tests, the results shown in Figures 4 and 5 were reinvestigated using benchboard style cabinets. However, in an effort to achieve an even more realistic ignition scenario, the benchboard test using unqualified cable used an electric ignition source of approximately 100 watts concentrated at a screw in a terminal block. This simulated a high resistance point of over heating. Figure 6 shows the results of this test, indicating clearly that an electrically ignited fire is possible and can grow quickly and achieve a large heat release rate in unqualified cable. Efforts to electrically ignite qualified cable using the same scheme have been unsuccessful. Figure 7 shows the details of the electrical ignition source used to start the fire in Figure 6. The results of the qualified cable benchboard test are not yet available.

On the basis of test findings to date involving cabinet fires a number of conclusions can be reached. First, it appears that for qualified cable the intensity of a cabinet fire is low enough as to pose no appreciable threat to adjacent cabinets or to other equipment around a cabinet in terms of high temperatures. Second, for unqualified cable fires in cabinets, the thermal effects of the fire on equipment within the room containing the cabinet are not severe, however the potential appears to exist for igniting other unqualified cable in

cabinets adjacent to a burning cabinet as a result of heat transfer between walls separating the cabinets. Third, for both qualified and unqualified cable, the amount of smoke produced during cable fires appears to be large enough to obscure the vision of operators and fire fighting teams within a short time after the start of the fire.

The validity of these conclusions is being examined further in testing underway at Factory Mutual Research Corporation, sponsored by Sandia for the NRC as part of the enclosure fire environment testing being conducted there.

Enclosure Fire Environment Testing

For a fire probabilistic analysis, the timing of fire scenarios and the resulting environments must be calculated using room fire models. With information on the strength of source fires from fire characterization testing, room fire models can be used to calculate the temperatures and in some cases smoke concentrations that result throughout a room from a fire of a given magnitude. To date, only a few fire models have been used or proposed for use in nuclear power plant fire PRA's. Unfortunately, however, each of these models lacks an adequate data base for validation and benchmarking. As a result, questions often arise regarding the validity of the models and the accuracy of their predictions.

The objective of the enclosure fire test effort is to provide a quantitative data base on the environments resulting from fires involving fuels, room configurations, and ventilation conditions found in nuclear power plants. To do this work, Sandia surveyed a large number of facilities in the United States that could perform full-scale room testing. As a result of this survey and a subsequent contracting effort, Factory Mutual Research Corporation was chosen to perform tests in a room that is 60' x 40' x 20' high with an extensive instrumentation array of about 300 channels. The room selected for the testing was based upon our surveys of typical room sizes in nuclear power plants and represents the largest test effort of its kind ever conducted.

To date, the first seventeen tests in Phase I of the enclosure test effort have been completed with the remaining six tests in Phase I currently being performed. Figure 8 shows the control room mock up configuration being used for the last six tests of Phase I. Besides the extensive instrumentation provided in these tests, a variety of other capabilities have been planned for and incorporated as part of this test program. These include the capability to vary the ventilation rate between 1 and 10 room changes per hour, the capability to lower the ceiling height from 20 feet to 14 feet using a false ceiling, and the capability to subdivide the room into a smaller room to investigate the effects of smoke movement from room to room.

From the tests completed to date, a few observations can be made. First, it appears that for fires as large as 2000 kilowatts, the thermal environments in large rooms are not severe enough to cause flash-over conditions or even autoignition of other combustibles. In contrast to this however, it appears that smoke production and its distribution throughout large rooms poses a severe problem in the form of obscuring virtually all visibility within a short time. During one test using a 500 kilowatt propylene burner which produced a sooty smoke similar to that observed from cable insulation, the test room became obscured to eye level within about three (3) minutes, and within five (5) minutes, the smoke level descended to the floor obscuring even 1000 watt light bulbs located only 20 feet from an observation window. This condition occurred despite the fact that the room was being ventilated at a rate of 8000 cubic feet per minute or 10 exchanges per hour. The full significance of this observation must await data reduction of light obscuration measurements and subsequent testing involving actual cables in cabinets and in cable trays.

Equipment Damage Threshold Testing

In order to make an assessment of the possibility and probability of fire-induced component damage which might jeopardize plant safety, component fragility data must be available. To date, most fire probabilistic assessments have limited their scope to the failure of electrical cabling under conditions estimated to be autoignition temperatures of the cable. In one case, consideration was given to the failure of cabling at temperatures below autoignition conditions. However, relevant data to support this analysis was not available.

The objective of the component failure threshold test effort is to obtain data relevant to nuclear power plant components for their damage potential and failure thresholds under fire environment conditions. To do this, several classes of components have been screened on the basis of their functional intolerance to fire, their damage proneness, and their safety significance. Some of the top ranking components have been tested under actual fire conditions and simulated fire conditions using a test chamber. The purpose of performing experiments in a test chamber is to ensure reproducible fire environments involving controlled convective and radiative heating, water sprays, high humidities, smoke particulates, and corrosive vapors.

To date, tests have been performed on qualified and unqualified cables and control relays. The cables selected were the same as those used during previous tests by Sandia, including the 20 foot separation tests performed by Underwriters Laboratories

for Sandia in 1983 (Ref. 3). For the cable tests and relay tests the chamber shown in Figure 9 was used to produce a variety of transient temperature conditions in which the temperature of the walls of the chamber and convective air entering the chamber was ramped to correspond to conditions measured during the 20 foot fire tests and other transient tests. The relays used in the test effort were of the same manufacturer and model type as those used in the LaSalle Nuclear Power Plant which is being studied as part of the Risk Methodology Integration and Evaluation Program PRA.

For the cables, a variety of observations were made as a result of the test effort. These are illustrated in Figures 10 and 11. For both qualified and unqualified cable as illustrated in Figure 10, it was found that cabling having ends terminating within the test chamber electrically failed earlier than those cases where the corresponding cable had ends outside of the test chamber. This observation leads to the conclusion that in order to appropriately account for the failure thresholds of cabling under fire conditions, the installation conditions of the cabling, including its termination within a room of interest, needs to be considered. In Figure 11 another effect is noticeable which can influence the susceptibility of cables to fire damage. In this figure it can be seen that cable damage was experienced as a result of convective heat transfer in certain areas of the test chamber having a high velocity corresponding to the velocities measured during the 20 foot fire tests. Where velocities were not as high, yet temperatures were the same as those in high velocity regions of the chamber, cable damage was not observed. This dependence of failure of cabling on convective heat transfer raises questions about the use of radiative heat testing for determining the failure thresholds of cable. Because of the dependence of heat transfer on the velocity of air, a factor of two to four in heat transfer rate can be caused by the flow of hot gases from a fire. Other findings of the cable damage testing effort are presented in Ref. 4.

For the control relays tested, it was found that the operability of the relays, under high temperature conditions exceeded manufacturers estimates. In one case a relay continued to operate until temperatures reached 400°C in the test chamber, well beyond the temperature threshold at which one would expect relay failure. Figures 12 and 13 show the temperature profile and the resulting relay damage for one of the relays tested.

Future component test efforts will concentrate on the damageability of components under other fire environment conditions including high humidities, sprays, and corrosive vapors. During actual fire testing, it was found that a

significant amount of hydrochloric acid can be produced by the smoke from chloride containing cables. In addition, during suppression activities, water may be sprayed directly on cabling or components that have not been damaged by thermal effects. Further, high humidity conditions resulting from suppression activities, together with corrosive vapors containing hydrogen chloride have been observed in actual fires to produce severe corrosive damage to components. The degree to which cables or components that have survived high temperatures, may be jeopardized by moisture or corrosive environments is now being investigated as part of chamber simulation tests and full-scale tests at Factory Mutual Research Corporation.

HYDROGEN BURN SURVIVAL RESEARCH

The Hydrogen Burn Equipment Survival Program has two primary objectives. The first is to develop an understanding of the performance or modes of failure of safety-related equipment when subjected to the environments resulting from hydrogen combustion in a reactor containment building. The second is to develop analytical means of predicting the response of safety-related equipment to a hydrogen burn environment. After an initial effort in FY81 and 82 to identify safety-related components in use in nuclear power plants which may be subjected to hydrogen burn environments, work began in FY83 to develop a simulation scheme for testing equipment under the heat flux conditions resulting from a hydrogen burn using the Sandia Central Receiver Test Facility. In addition to this, a computer program (called HYLER), used to calculate hydrogen burn environments, was developed and analyses were performed of the data generated during the Electric Power Research Institute (EPRI) large-scale hydrogen burn tests at the Nevada Test Site (NTS). All of this work was aimed at gathering a better understanding of the damageability of safety components to a hydrogen burn environment and to support NRC's rule making activities regarding large dry containments, ice condenser containments, subatmospheric containments, and BWR MARK III containments. More recently, work at Sandia is shifting to address questions regarding standing flame environment conditions in BWR containments.

In FY85, two series of hydrogen burn simulation tests were conducted. The first was a simulation of a thirteen volume percent hydrogen deflagration from the EPRI-NTS test series. During the simulation test series, Class 1E pressure transmitters and electrical cables were subjected to the heat flux pulse of an EPRI-NTS test. A second series of hydrogen burn simulation tests involved endurance testing to study the durability of new and thermally aged Class 1E cables and pressure transmitters. Starting with a base pulse representative of a hydrogen burn in a large dry containment

resulting from a 75% metal water reaction, test specimens were exposed to increasingly severe heat flux pulses until a pulse of three times the base pulse was used. In addition to these experiments, analytical efforts to characterize the hydrogen burn environment and resulting response of equipment were performed using the HECTR computer code to characterize the environment resulting from the TMI-2 hydrogen burn. (The HECTR code is similar to HYBER except that HECTR can use multiple burn compartments, while HYBER uses only a single compartment). Also, an indepth analysis of the data from 21 of the EPRI-NTS hydrogen burn tests was performed. Finally, a calculation was performed using HECTR to estimate the surface temperature of equipment in an ice condenser containment during hydrogen burns resulting from several severe accident sequences. For purposes of the current discussion, however, only the results of the two hydrogen burn simulation test series of equipment will be reviewed.

NTS Simulated Equipment Testing

In order to augment results obtained from the hydrogen burn equipment survival tests performed by EPRI at the Nevada Test Site, a series of tests was conducted at the Sandia National Laboratories Central Receiver Test Facility (CRTF). The CRTF tests simulated a 13 volume percent burn from the EPRI-NTS series and involved test specimens of safety-related equipment and cables which were the same as or very similar to those used in the EPRI series. The specimens selected for the CRTF tests were a Barton pressure transmitter, an ASCO solenoid valve, Okolon cable, Rockbestos cable, and Brand Rex cable. All of the specimens exposed to the simulated hydrogen burn heat flux were in unaged condition and all performed their design function during exposure to the simulated burn. Each cable was connected in series with a resistance and received an applied potential of 10 volts DC. The solenoid valve was pressurized to 30 psig and tested in both the actuated and unactuated positions. After testing it was cycled to check for possible sticking. The pressure transmitter was pressurized to 750 psig (its operating span was 0-1000 psig). The transmitter output signal, some internal voltages, and the temperature of its case and several internal electronic components were monitored during the tests. The results of these tests are reported in Reference 5.

The average total and average radiant heat fluxes to which test specimens were subjected were determined using the data reduction routine SMOKE. The convective heat flux was taken to be the difference between the total and radiative heat fluxes. Using methods described in Reference 6, a solar flux profile equivalent to the sum of the incident radiative and convective fluxes was calculated for each of the sample types tested. The calculated solar profiles account for differences in infrared hydrogen burn and solar CRTF spectral responses of the

individual test specimens. The heliostats (mirrors) of the CRTF were then selected to generate the calculated solar flux profile. The heat flux profile used in testing black electric cables is shown in Figure 14, while similar profiles were developed for the transmitter and solenoid valve. The pressure component of the EPRI-NTS test environment was not tested because components at the CRTF could not be pressurized while receiving the solar flux. However, prior to exposure to the simulated hydrogen burn fluxes, the solenoid valve and pressure transmitter were preheated to temperatures near the preburn gas temperature of the NTS. (i.e approximately 156°F.) The preheating was done using one or two heliostats as required. The preheating was done slowly so that thermal gradients in the test specimen were minimized. Cable samples were preheated differently because of their low heat capacity. Cables warmed very rapidly even under the flux of a single heliostat. They also cooled rapidly when the shutter was closed in front of them. As a result, cables were "preheated" by holding the peak flux on the test bay for one second longer at the start of the burn simulation. The results of this showed that the issue of cable preheating is mute, because the temperature of cables immediately becomes dominated by cable ignition upon exposure to the hydrogen burn heat flux. It was the heat from the cable combustion which drove the initial temperature of the cable samples high.

As a result of the tests a number of observations were made. First, at heat fluxes comparable to those in the EPRI-NTS P20 test, a spontaneous ignition of cable jacket material can occur. Although this ignition caused the outer jackets of several cable samples to blister and crack, it was found that in virtually all cases the interior conductors of the cable remained intact and maintained their insulation resistance properties. Figure 15 shows the surface damage experienced by one of the cable types tested. The second conclusion reached from the testing is that exposure in several tests brought only slight changes in the calibration of the Barton pressure transmitter. The significance of these small changes are dependent upon the use of the instrument but correspond to about 2 1/2% of the full-scale reading when the applied pressure was 1000 psig. This insensitivity to the heat flux environment is consistent with the very slight thermal changes experienced by the interior of the Barton pressure transmitter as illustrated in Figure 16. The third conclusion reached from the tests is that temperature changes measured for the solenoid valve and pressure transmitter indicate that temperatures sufficient to damage these pieces of equipment were not reached during the CRTF tests and probably were not reached during the NTS P20 Tests.

In summary these tests demonstrate the durability of the multiconductor cables, solenoid valve, and transmitter when subjected to heat flux pulses having high peak fluxes and time decay characteristics similar to those resulting from hydrogen burn in large scale tests. Based on the best available information for comparison, (e.g. close-up photographs from the P20 cable samples and temperature data for the Barton transmitter potentiometer bracket), the NTS simulation tests conducted at the Sandia CRTF reasonably simulated the EPRI-NTS P20 thermal flux environments.

Endurance Testing of Equipment

The analytical and experimental efforts to date to investigate the survival of equipment during hydrogen burn conditions have limitations. The computer codes use lumped parameters which predict volume averages and not local conditions. The thermal models of equipment are simple and at best predict only approximate thermal and not operational equipment responses. Finally, the experimental results of hydrogen burns in vessels which are not the actual sizes and configurations of containment buildings represent conditions that are not easily extrapolated to containment buildings because of uncertainties in the understanding of volume and configuration effects.

In order to address these uncertainties, a series of equipment tests was conducted at the Sandia National Laboratories CRTF. Specimens of nuclear qualified Brand Rex three conductor cable and Barton Model 763 pressure transmitters were subjected to simulated hydrogen burns at increasing heat flux levels and their temperature response and performance were monitored. The cables were tested in both artificially thermally aged and unaged conditions. The test specimens were first exposed to a base heat flux pulse that conservatively simulated a deflagration resulting from a 75% core metal-water reaction in a reactor housed in a large dry containment building. After the base pulse several successive pulses were applied at heat flux levels which increased in increments of 50% of the base heat flux pulse. The heat flux levels of the final pulse were 300% of those of the base pulse. Similar to the test described in the previous section of this paper, the cables were electrically powered during exposure to the heat flux pulses and monitored for short circuits and open circuits. For the pressure transmitter, temperatures inside and outside the transmitter were monitored during the test and post-test calibration tests were made. Reference 7 reports the complete test effort and findings of the test.

In summary, it was found during the tests that with only one exception, the cable samples displayed no significant insulation or degradation in post exposure testing and second,

both unaged and thermally aged Barton Model 763 pressure transmitters withstood the heat flux pulses and continued to deliver a signal corresponding to the applied pressure. Exposure to the severe heat flux pulses produced only small changes in the transmitter calibration. This point is illustrated by the relatively small temperature changes experienced inside and on the rear of the Barton transmitter as shown in Figure 17. It can be seen from this figure in comparison to Figure 16, that the thermal inertia of the Barton transmitters prevents even heat fluxes three times those expected from a 75% metal water-reaction from causing significant changes in the thermal environment within the transmitter.

CURRENT AND FUTURE RESEARCH PLANS

The Fire Protection and Hydrogen Burn Equipment Survival Research Programs at Sandia National Laboratories in the past have involved both testing and analysis. Some of the past activities in these programs has been reported here. In FY86 the fire protection program will complete much of its test activities, including evaluation of the damaging effects of suppression and corrosive environments resulting from fires on cable and equipment and a study of the effects of control room fires on the survival of control room equipment and the ability of operators to maintain plant control. Beyond FY86, issues concerning the effectiveness of HVAC systems for controlling smoke during fires, the effectiveness of manual fire fighting teams, and the interrelationship of seismic events and fires are planned for analysis. In the hydrogen burn survival research program, plans for FY86 include further analyses of the environments associated with hydrogen deflagrations in large dry and subatmospheric containments, analyses of the thermal environments associated with standing flames in boiling water reactors, and testing of equipment to standing flame thermal environments.

REFERENCES

1. D. A. Dube, Fire Protection Research Program for the U.S. Nuclear Regulatory Commission 1975-1981, SAND82-0431, NUREG/CR-2607, Sandia National Laboratories (April 1983).

2. A Datta, Nuclear Power Plant Fire Protection Research Program, NUREG-1148, U.S. Nuclear Regulatory Commission (July 1985).

3. D. D. Cline, W. A. von Riesemann, J. M. Chavez, Investigation of Twenty-Foot Separation Distance as a Fire Protection Method as Specified in 10CFR50, Appendix R, SAND83-0306, NUREG/CR-3192, Sandia National Laboratories (October 1983).

4. W. T. Wheelis, Transient Cable Damageability Results, Phase I Quick Look Report, Sandia National Laboratories (July 1985).

5. V. J Dandini, J. J. Aragon, Simulation of an EPRI-Nevada Test Site (NTS) Hydrogen Burn Test at the Central Receiver Test Facility, SAND85-0205, NUREG/CR-4146, Sandia National Laboratories (June 1985).

6. V. J. Dandini, J. J. Aragon, Testing of Safety-Related Nuclear Power Plant Equipment at the Central Receiver Test Facility, SAND83-1960, NUREG/CR03776, Sandia National Laboratories (July 1984).

7. V. J. Dandini, Testing of Nuclear Qualified Cables and Pressure Transmitters in Simulated Hydrogen Deflagrations To Determine Survival Margins and Sensitivities, SAND85-1481, NUREG/CR-4324, Sandia National Laboratories (November 1985 - estimated).

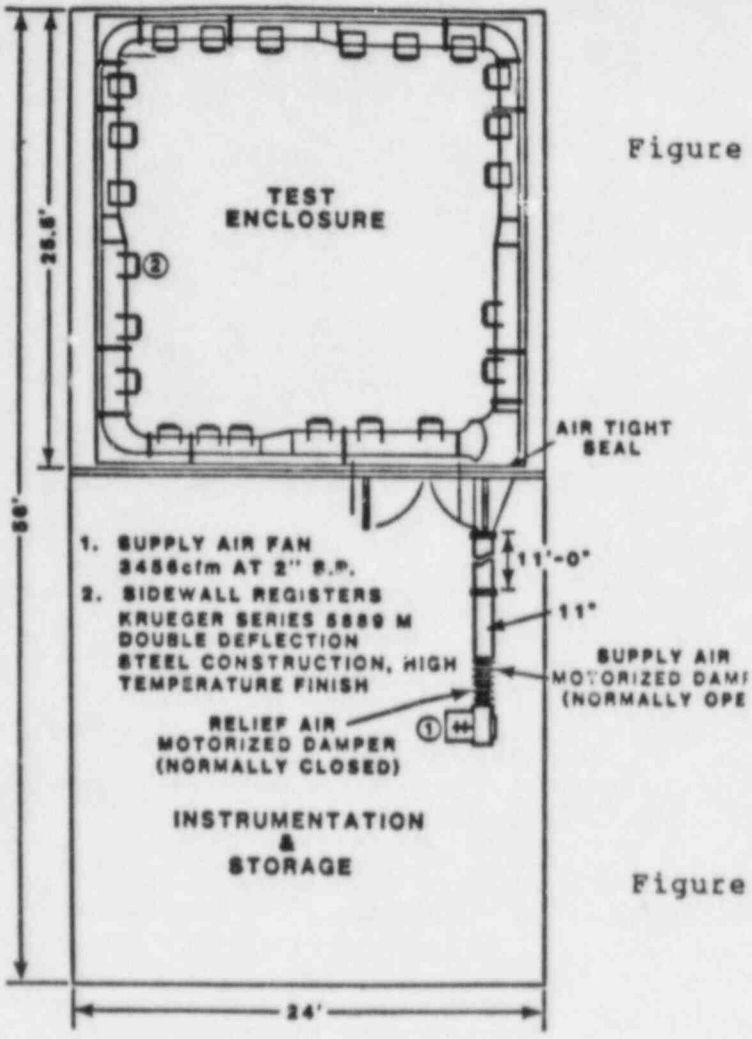

Figure 1: Plan View of Sandia National Laboratory Burn Room Facility

Figure 2: Comparison of Heat Release Rate Measurements Using Oxygen Consumption and Mass Balance

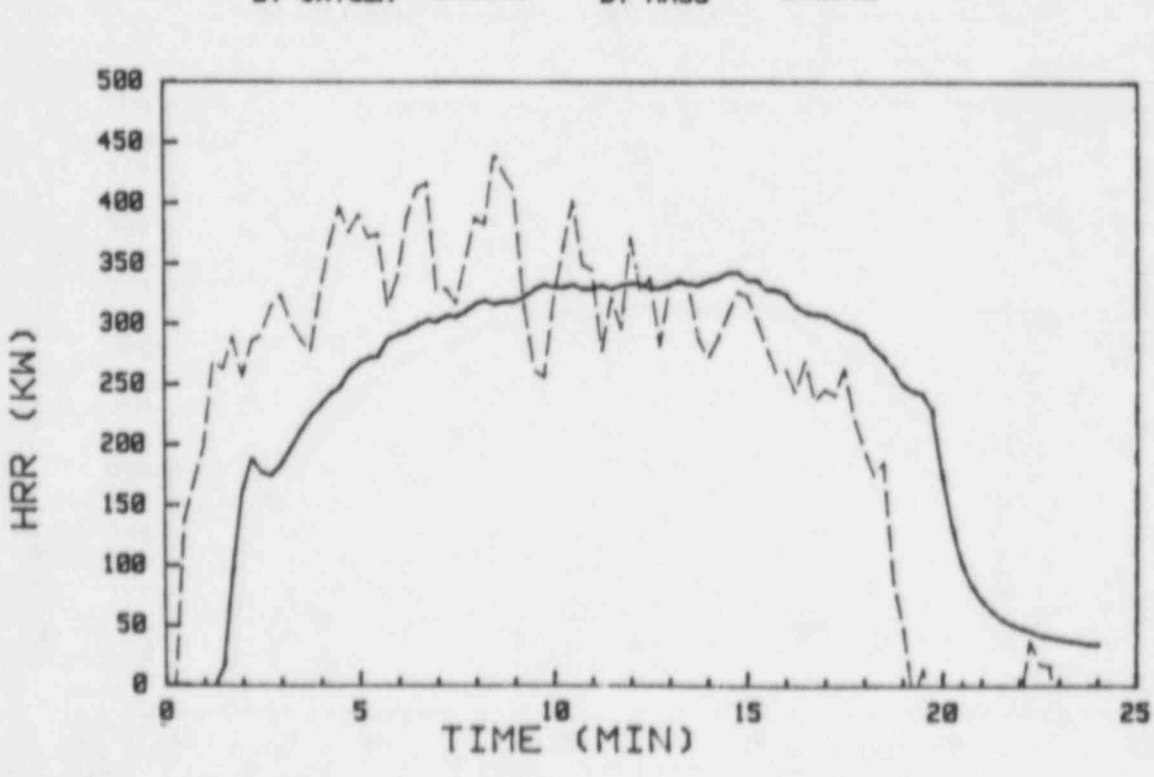

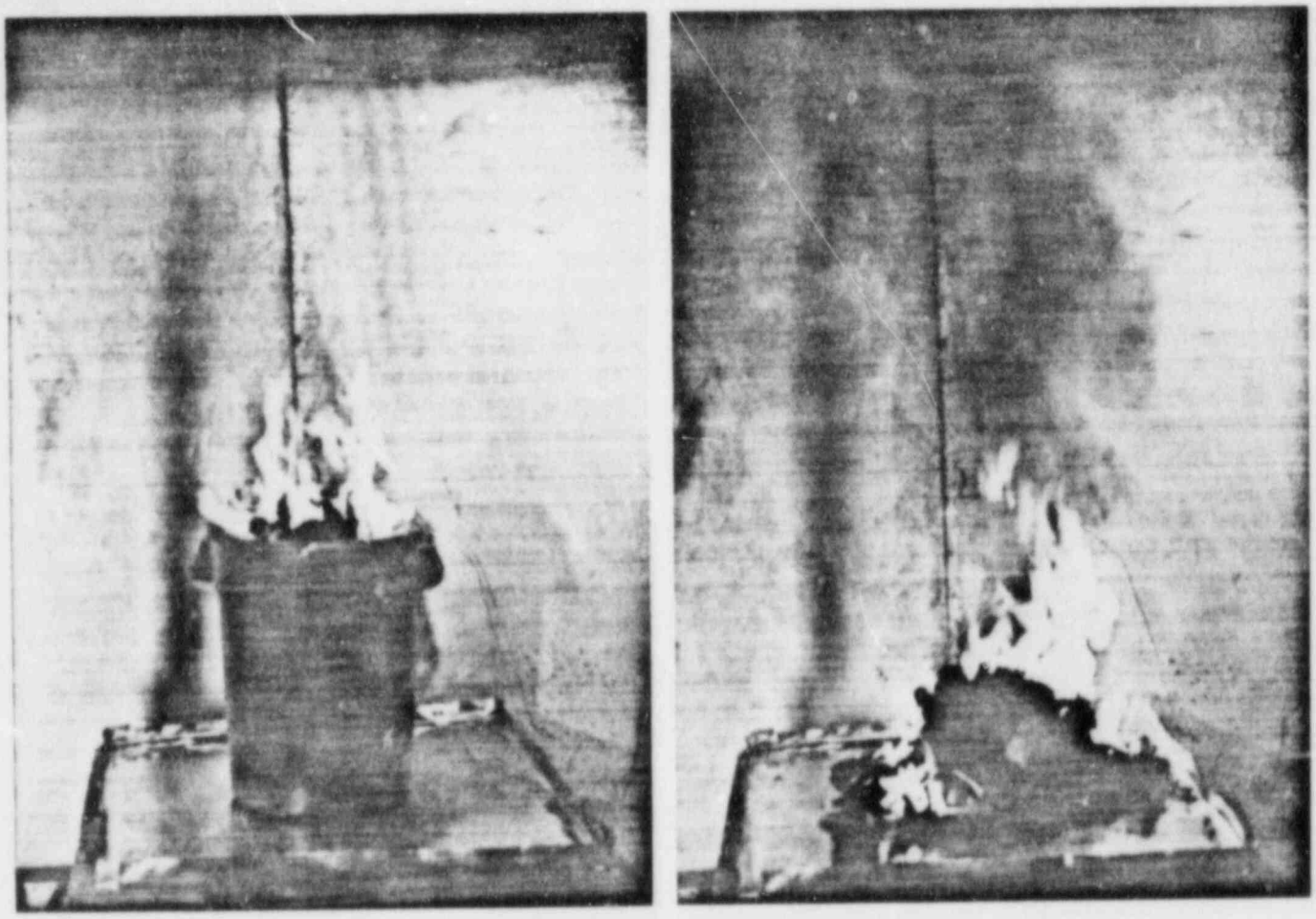

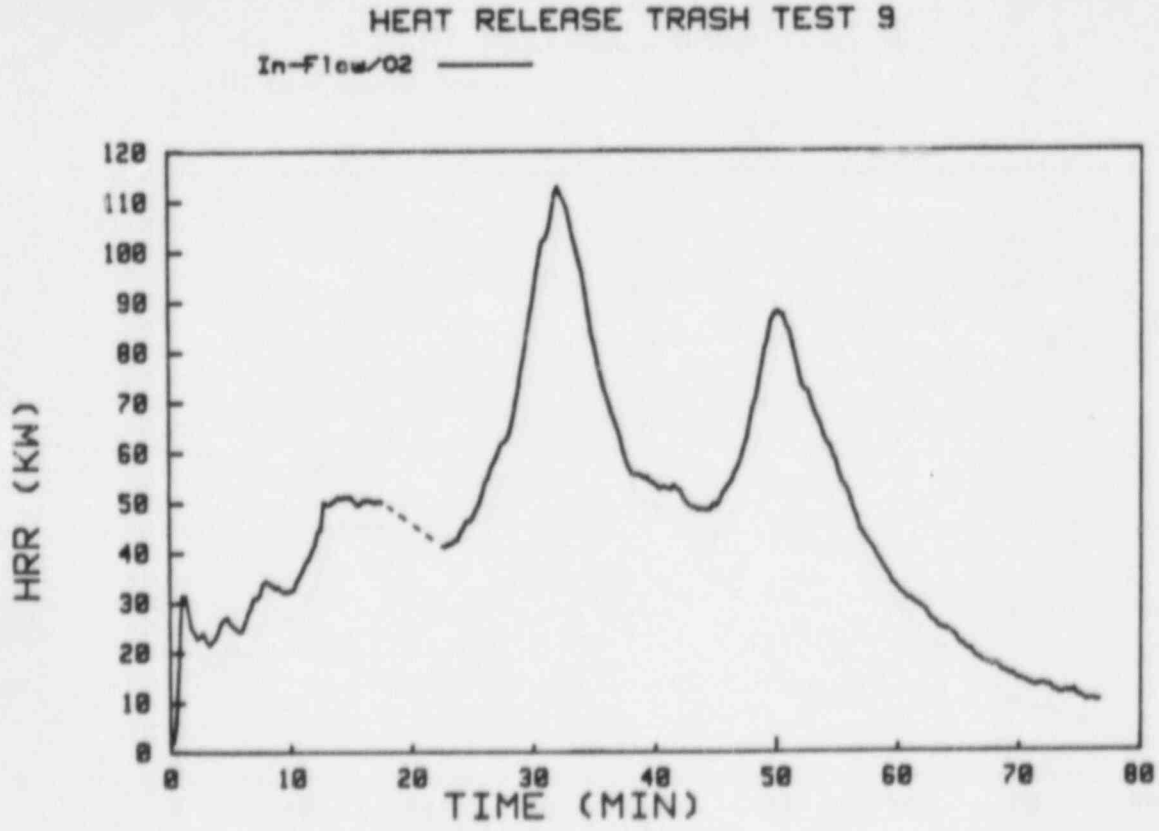

Figure 3: Fire Characterization Heat Release Rate and Photos for 30 Gallon Trash Can Test

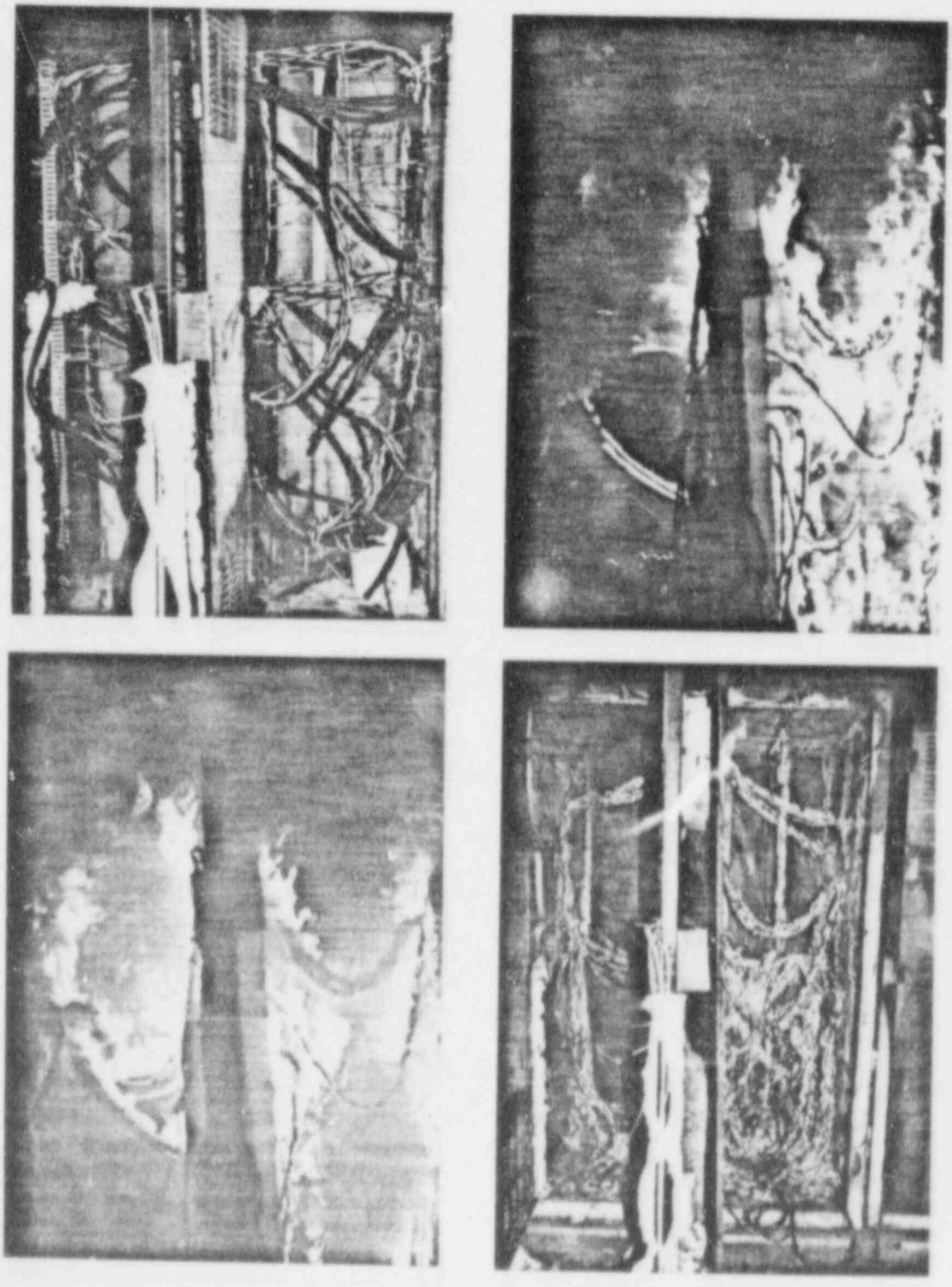

FIGURE 4: VERTICAL CABINET FIRE TEST
FUEL LOAD ~ 1,000,000 BTU
UNQUALIFIED PVC CABLE

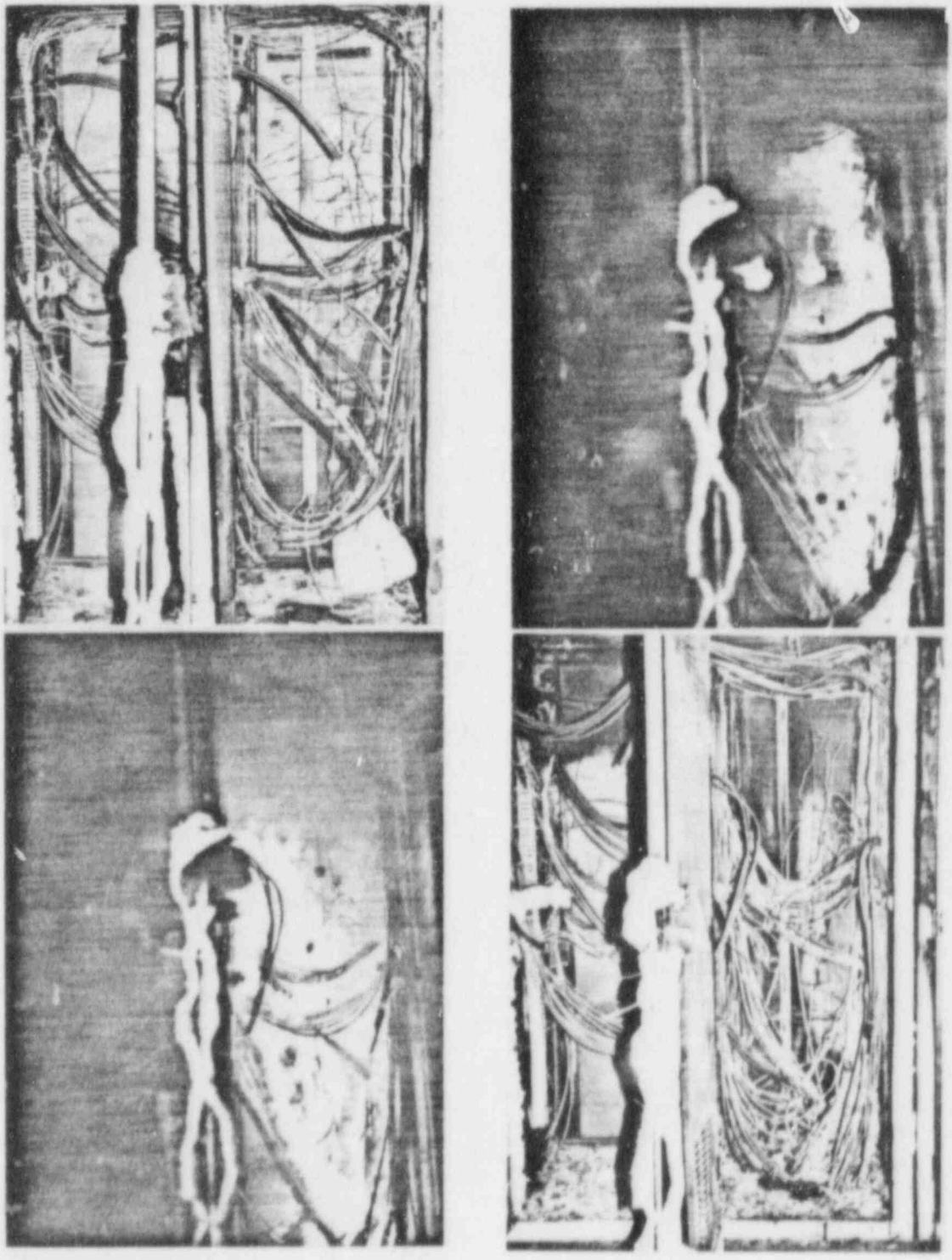

FIGURE 5: VERTICAL CABINET FIRE TEST
FUEL LOAD ~ 1,000,000 BTU
QUALIFIED POLYETHYLENE CABLE

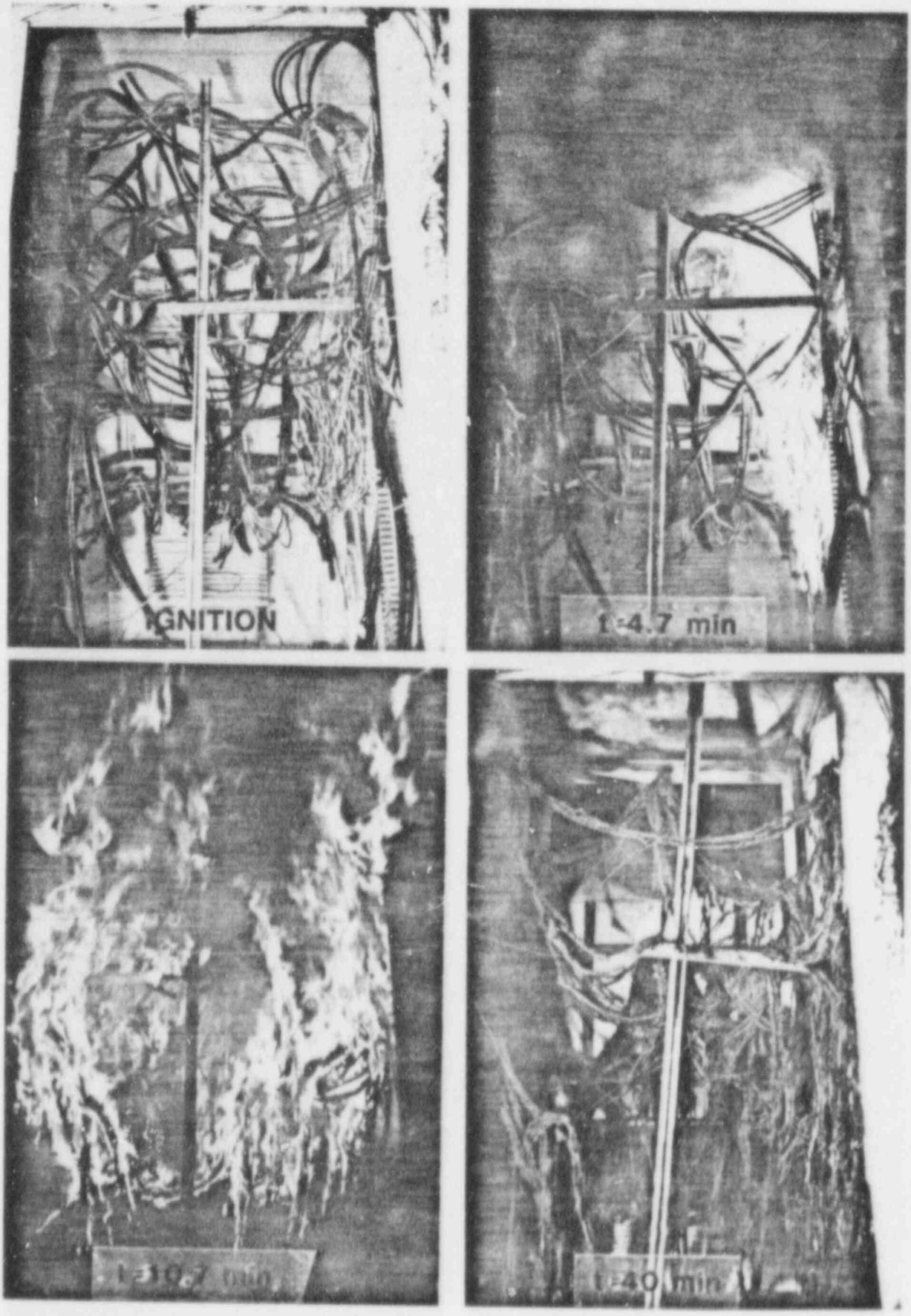

FIGURE 6: BENCHBOARD CABINET FIRE TEST
FUEL LOAD ~ 1,500,000 BTU
UNQUALIFIED PVC CABLE

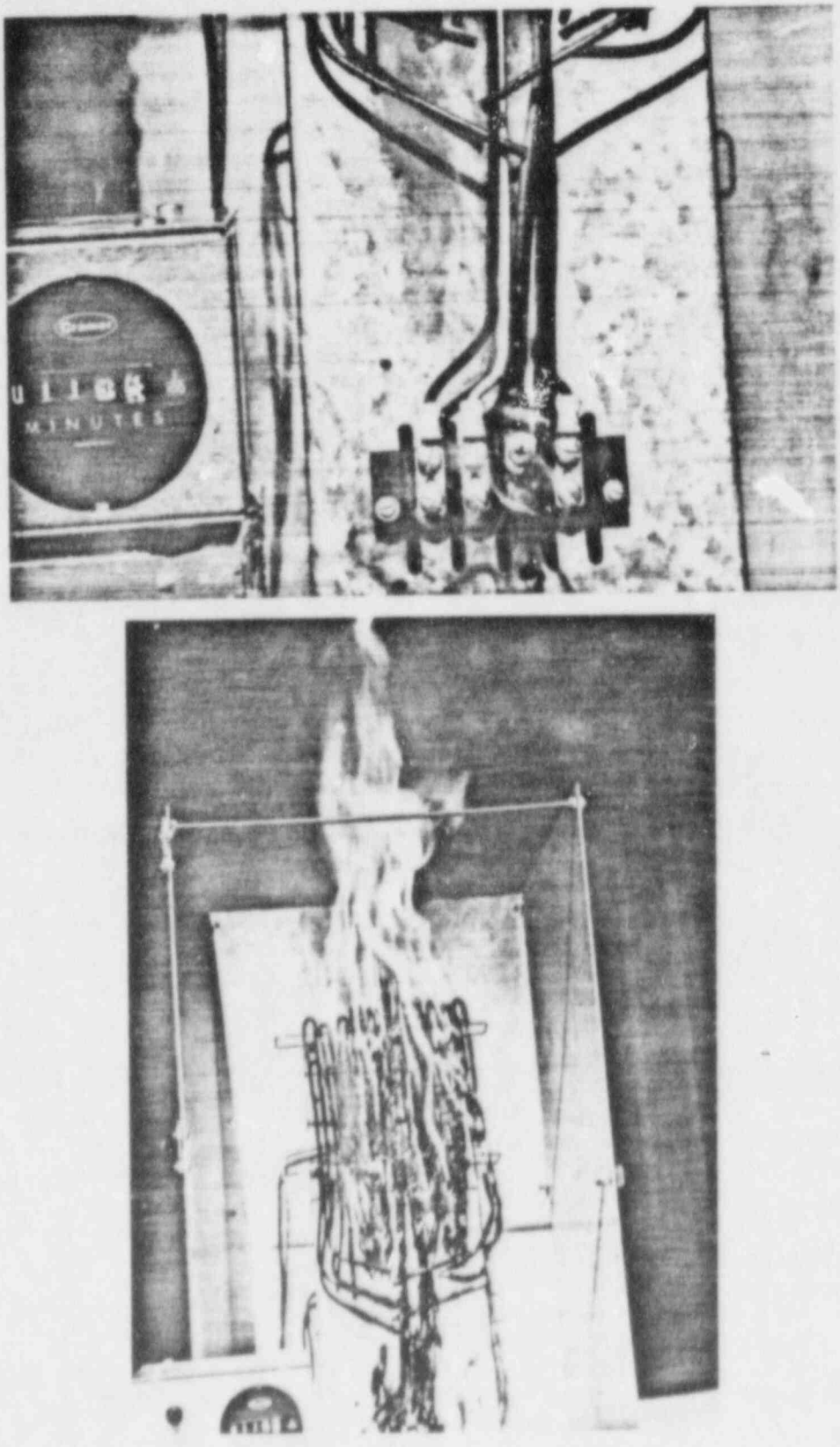

Figure 7: Electrical Initiation Terminal Block and Resulting Source Fire

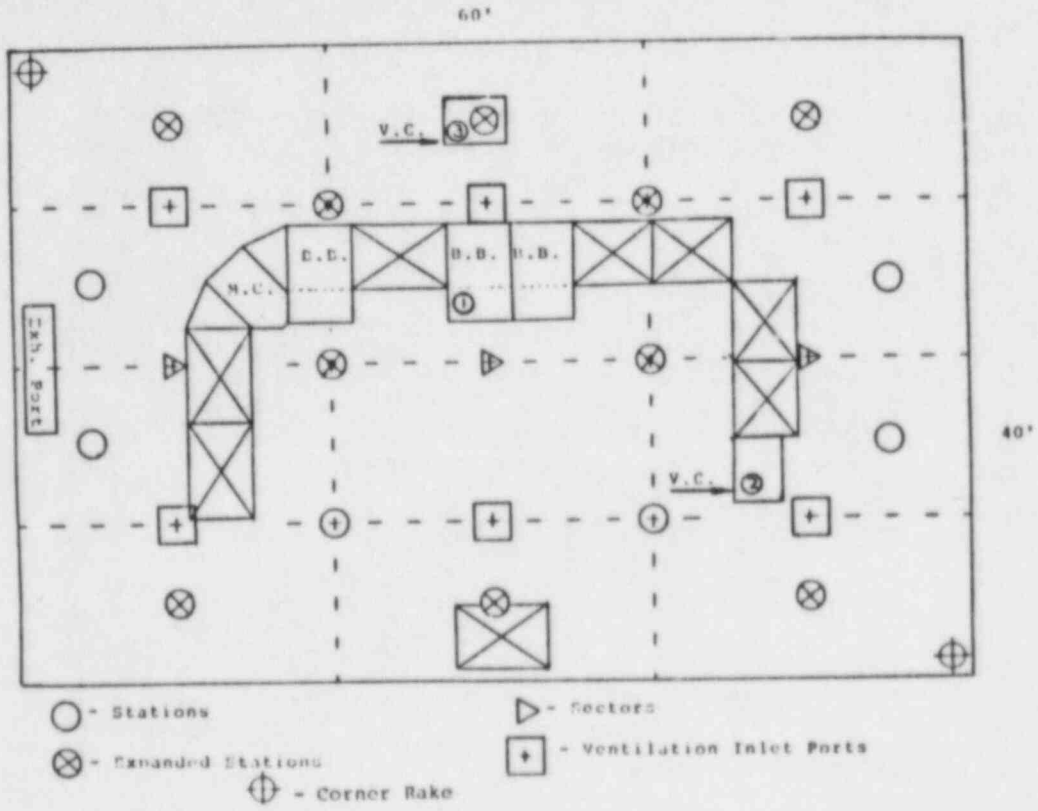

Figure 8: Plan View of Control Room Mockup

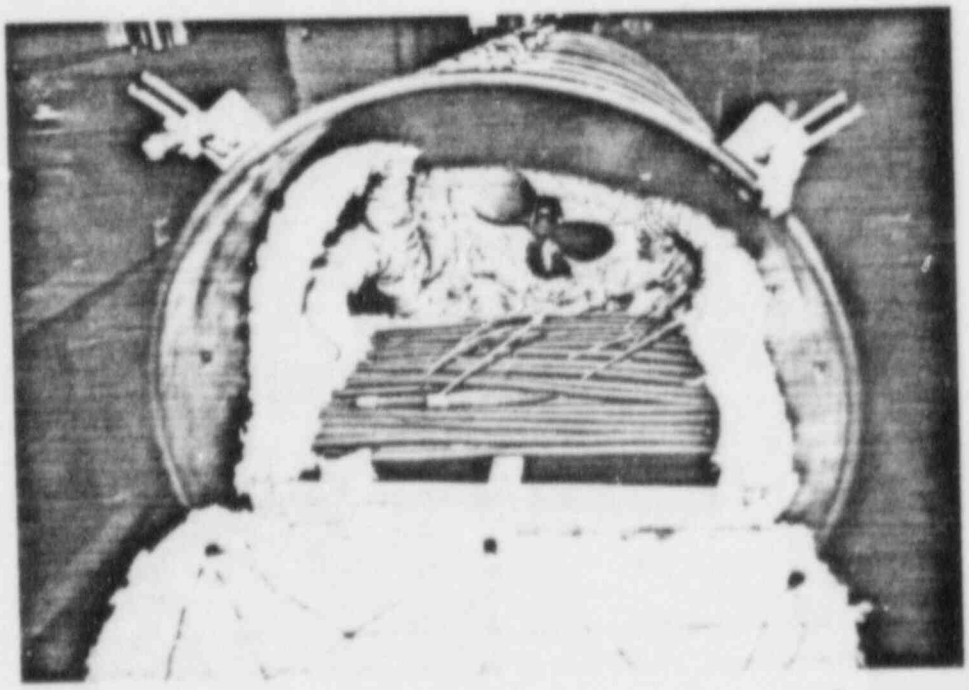

Figure 9: Test Chamber for Cable and Relay Fire Simulation Testing

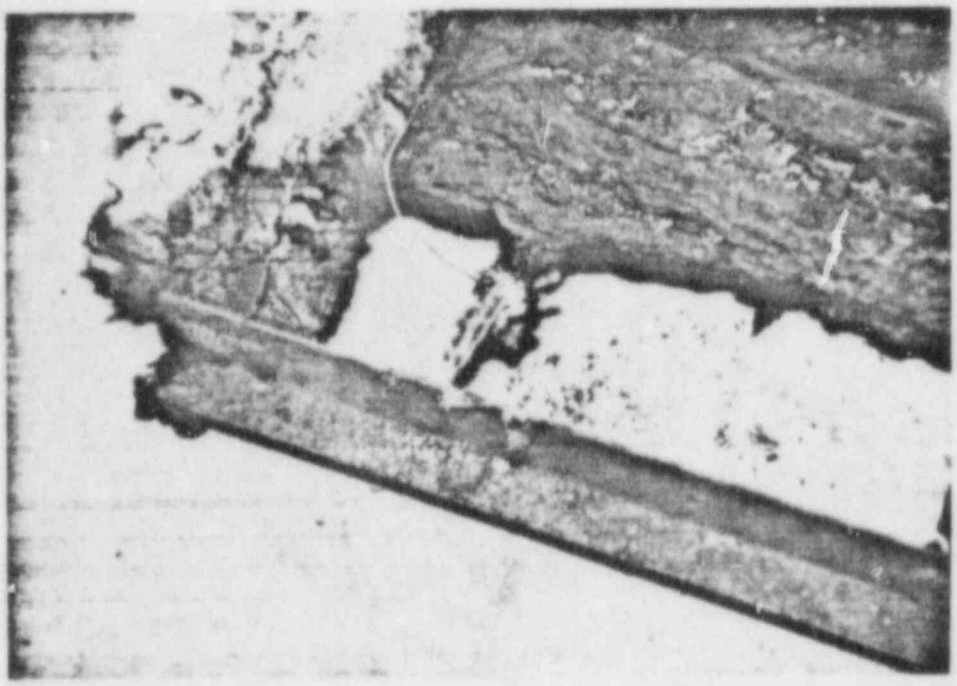

Figure: 10: Damage to Cable Terminations
Causing Electrical Failure

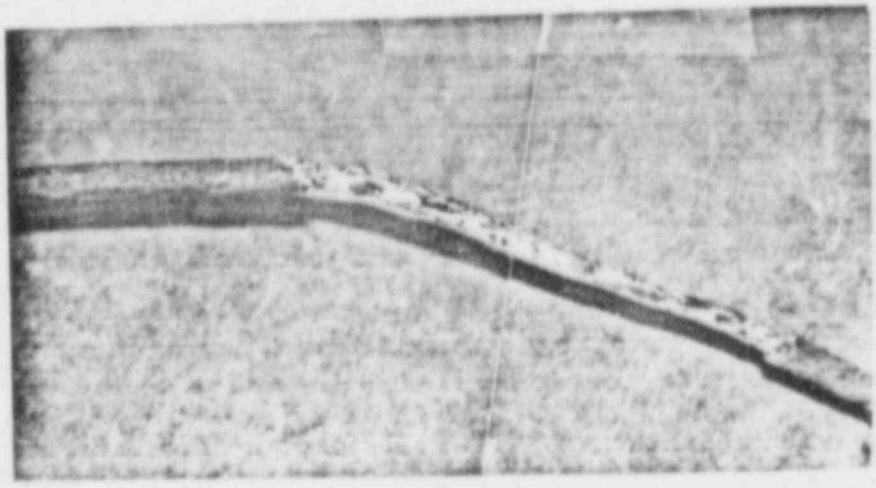

Figure 11: Preferential Cable Damage
Caused by Convective Heating

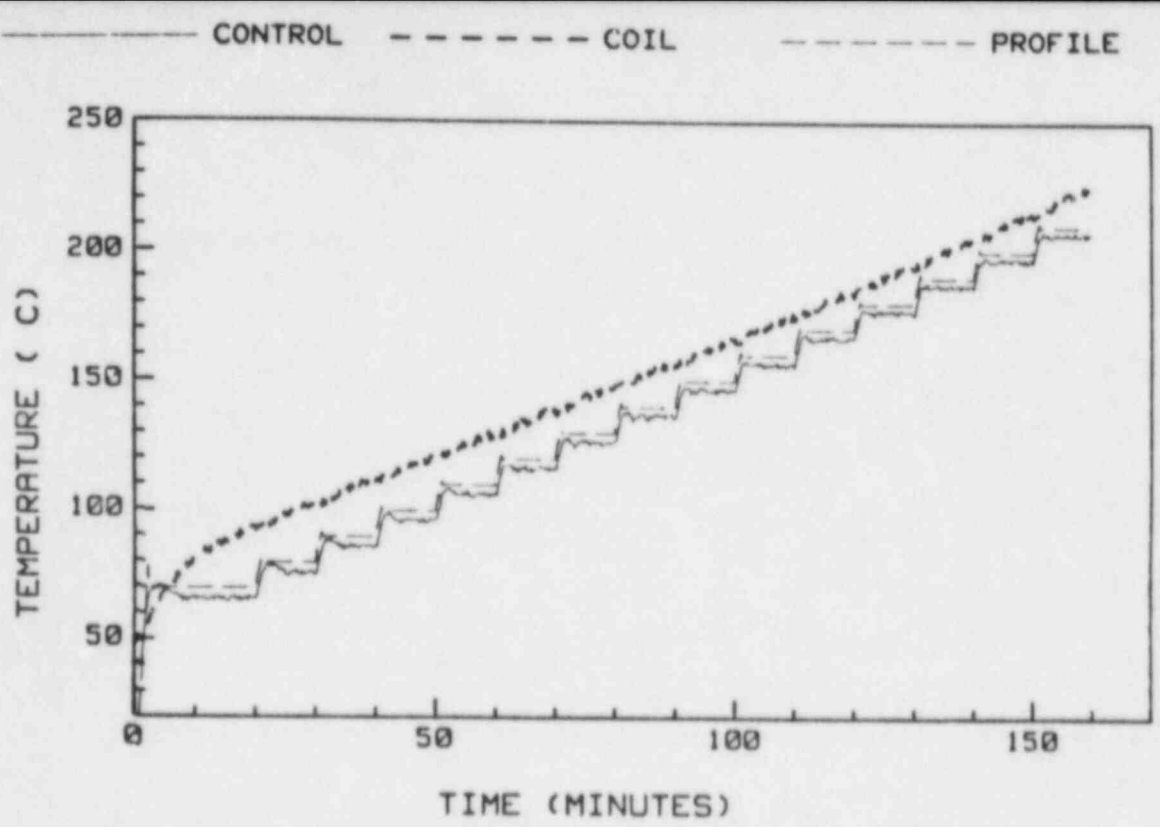

Figure 12: Temperature Profile Used for Agastat GPI Relay Fire Fragility Test

Figure 13: Damage Sustained By Relay During Fire Environment Simulation Test

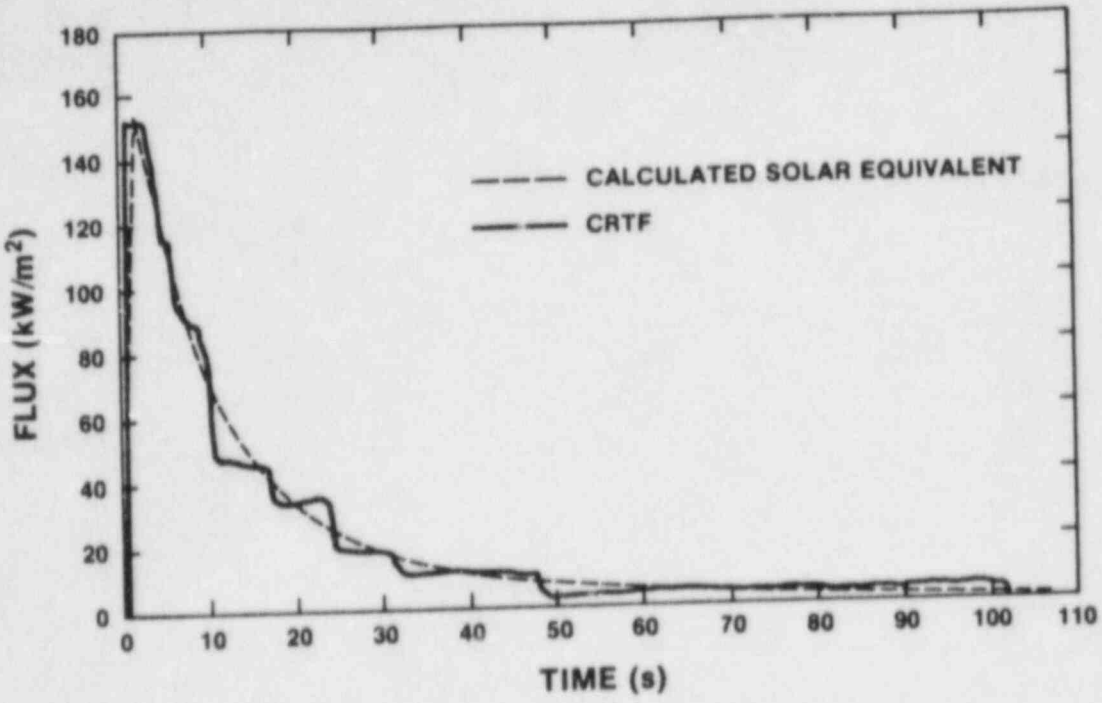

Figure 14: Flux Profile Used at CRTF for Cable and Transmitter Tests

Figure 15: Surface Damage Experienced by Typical Cable Sample

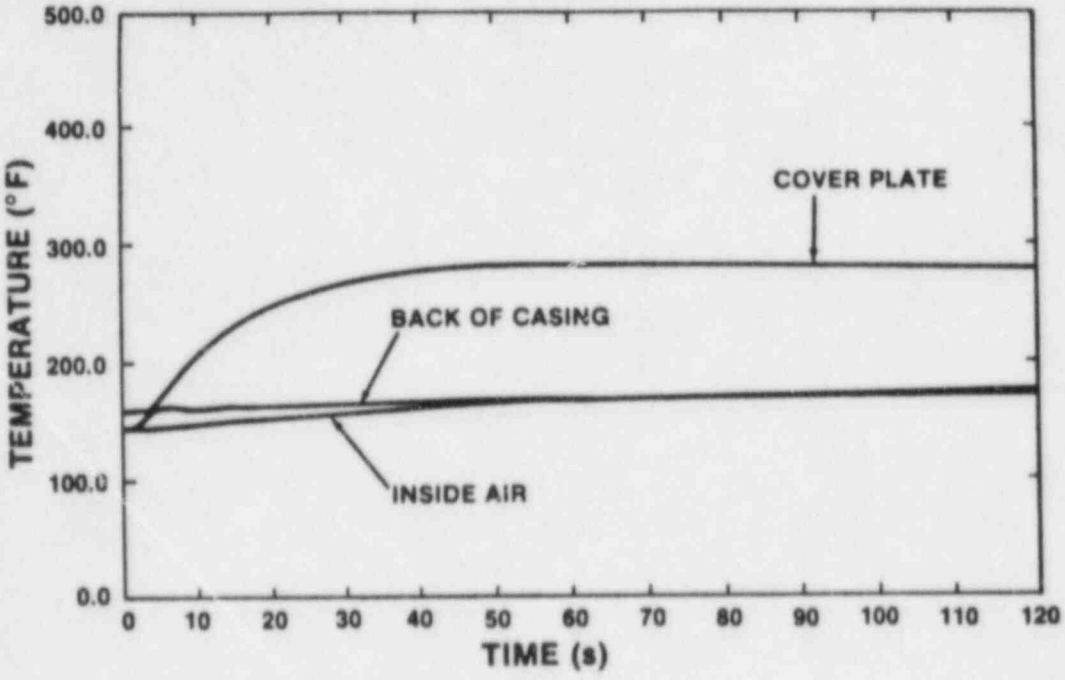

Figure 16: Transmitter Temperatures at Figure 14 Exposure Flux

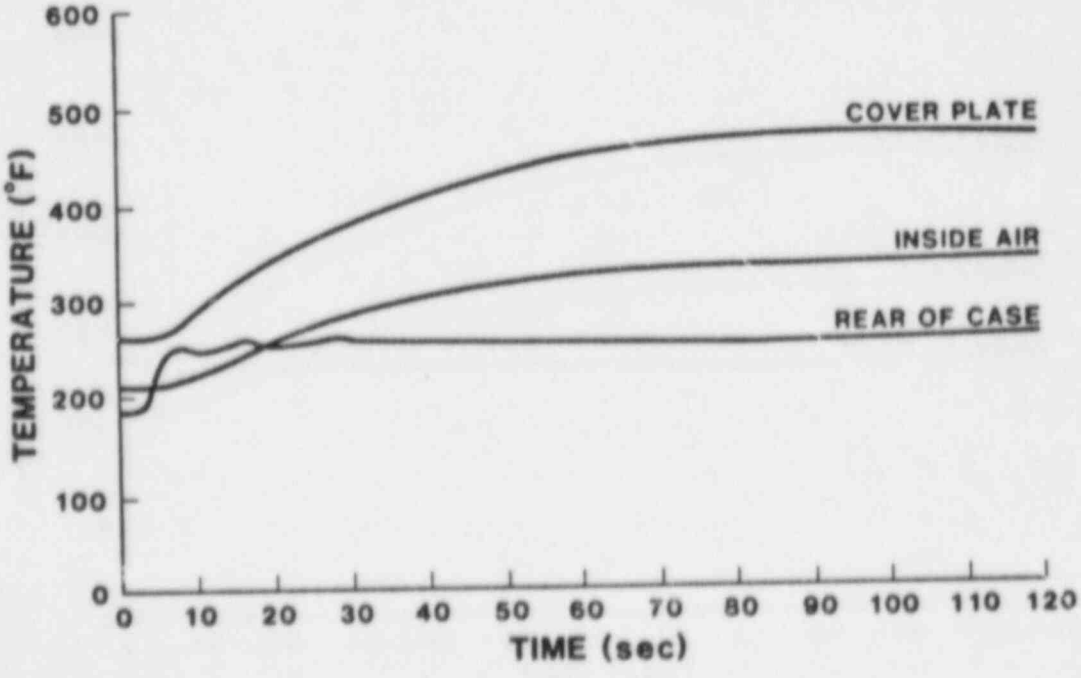

Figure 17: Transmitter Temperatures at 3 x Exposure Flux

ENVIRONMENTAL AND DYNAMIC QUALIFICATION OF EQUIPMENT RESEARCH AT THE IDAHO NATIONAL ENGINEERING LABORATORY

R. C. Hill
Idaho National Engineering Laboratory
EG&G Idaho, Inc.

ABSTRACT

A description of the Equipment Qualification Program at the Idaho National Engineering Laboratory (INEL) is presented. Current projects include research into reactor coolant pump seal behavior under station blackout conditions. The results of this project have shown that failure of elastomeric seals can be anticipated when seal cooling is interrupted.

Valve research, emphasizing behavior in simulated seismic and accident conditions, is in progress with significant testing completed on containment purge and vent valves. Experimentally based techniques are described for predicting, from limited test data, the torque necessary to close butterfly valves.

Other tasks include research into the adequacy of qualification standards, with respect to the simulation of vibrational environments experienced in actual service.

Equipment qualification research is being conducted by the Idaho National Engineering Laboratory to investigate the acceptance criteria, requirements, and methodologies for the dynamic (including seismic) and environmental qualification of mechanical equipment, and for the dynamic (including seismic) qualification of electrical equipment. This paper presents a summary of results obtained to date for: reactor coolant pump shaft seal research; valve research, with emphasis on containment isolation valves; dynamic margin relationship to equipment qualification; and dynamic research that assesses the effect of phenomena such as flow-induced vibration, in-structure generated motion, and plant vibration on equipment response.

Reactor Coolant Pump Shaft Seals

Failure of reactor coolant pump shaft seals under station blackout conditions could lead to a significant loss of primary coolant. Of particular concern is the influence of increasing primary coolant temperature on non-metallic elements of the seals during station blackout conditions when the cooling to the seals is interrupted. To assess the possible degradation effects of prolonged high temperature (approximately 550°F) on the non-metallic elements, extrusion tests were performed using experimental apparatus. This apparatus simulated the non-metallic O-ring seal elements of a three-stage hybrid (hydrostatic-hydrodynamic combination) seal depicted in Figure 1. This type of seal is used in some domestic main coolant pumps. Tests were also performed in a blowdown fixture to assess the effect of seal

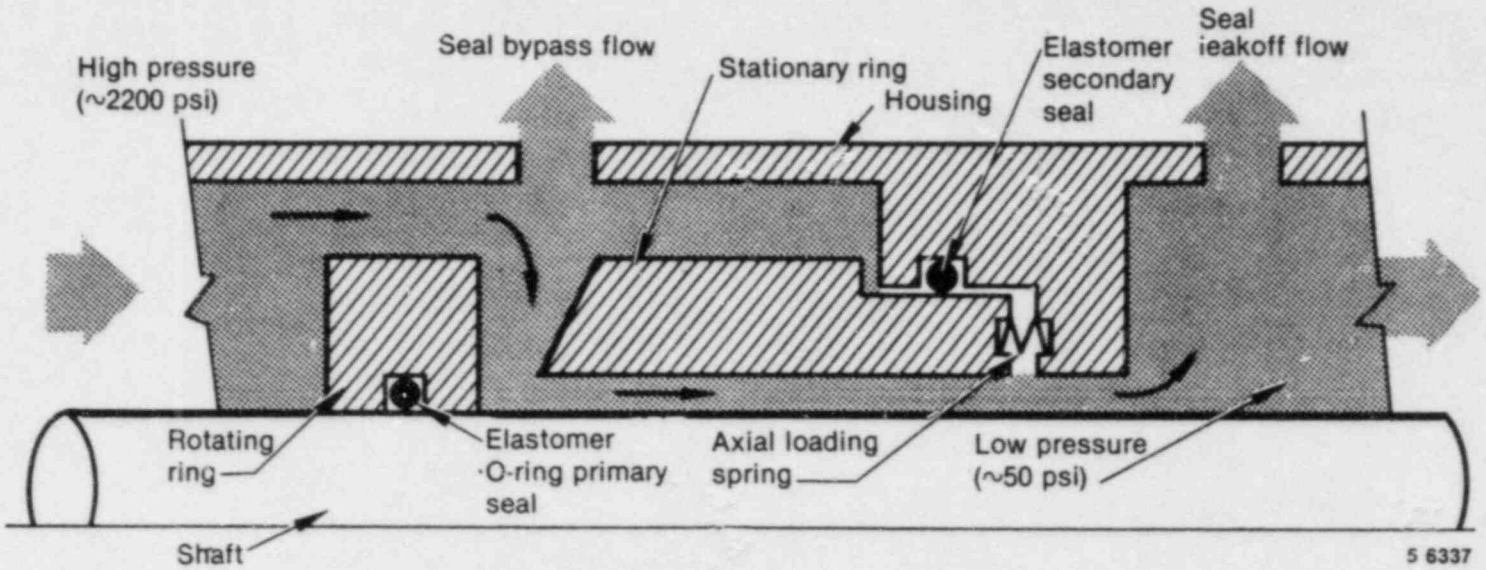

Figure 1. Schematic of a pump hybrid shaft seal.

coolant flashing to steam between the faces of the hydrostatic seals. The experimental program, its results and conclusions are documented in Reference 1.

O-Ring Extrusion Tests

O-rings fabricated from ethylene-propylene E515-80 were subjected to extrusion tests in a fixture which simulated the seal geometry surrounding O-rings (Figure 2). Temperatures varied from 520 to 580°F and pressures varied from 800 to 2400 psi. The clearance between the O-ring and the metal surface varied from 1.5 to 34 mils. The test O-rings were 1.17 in. inside diameter compared to the 8 in. fullscale O-rings used in the seals. The O-ring thickness, however, was fullscale, 0.139 in. Table 1 summarizes the results and corresponding conditions for the O-ring extrusion tests. Those tests concluded that ethylene propylene E515-80 is likely to blowout under the conditions predicted for station blackout. Extrusion tests of O-rings, using a second ethylene propylene designated E740-75, were also conducted. This material demonstrated a superior resistance to high temperature extrusion. During some of these tests, the E740-75 O-rings were backed with TF828-217 tetralon 720 channel seals. In these cases, severe extrusion of the channel seal occurred. For small gaps (approximately 0.010 in.), the extruded material prevented subsequent sealing by the O-ring and blowout occurred. At larger gaps (0.013-0.018 in.), the tetralon extrusion was sufficient to allow O-ring sealing corresponding to cases which evaluated only the O-ring.

Blowdown Tests

Water blowdown tests were also conducted during which the water flashed to steam between simulated hydrostatic seal faces (Figure 3). The tests were conducted on two hydrostatic seal models depicted in Figure 4, with seal face outer diameters of 2-7/8 and 4-3/4 in. As depicted in Figure 3, a back pressure was applied to the outboard seal rings to force them towards the inner seal rings. The pressure at the seal was approximately 1000 psi. The back pressures were chosen to give face seal loadings typical of those experienced in an operating pump. The seals were designed and fabricated to approximate the leakage per circumference through full size pump seals of 11 $in.^3/s$ at 2200 psig and 130°F. To achieve this flow rate, the seal rings were lapped to provide a 0.00046 and 0.00054 inch gap convergence (taper) across the smaller and larger face seals respectively. Adequacy of the taper was verified through flow tests with water at 113°F.

Two-phase seal tests were performed to assess overall face seal behavior. While these were primarily scoping tests, the results did indicate that seal instability-oscillation (with a corresponding increase in flow through the seal) may occur within the range of fluid conditions anticipated when seal cooling is lost.

Additional research has been initiated to improve understanding of the importance of various parameters to seal stability. Other research currently underway includes an investigation into the effects of elastomer extrusion on frictional loading within the face seal assembly. The added loading is expected to impact stability.

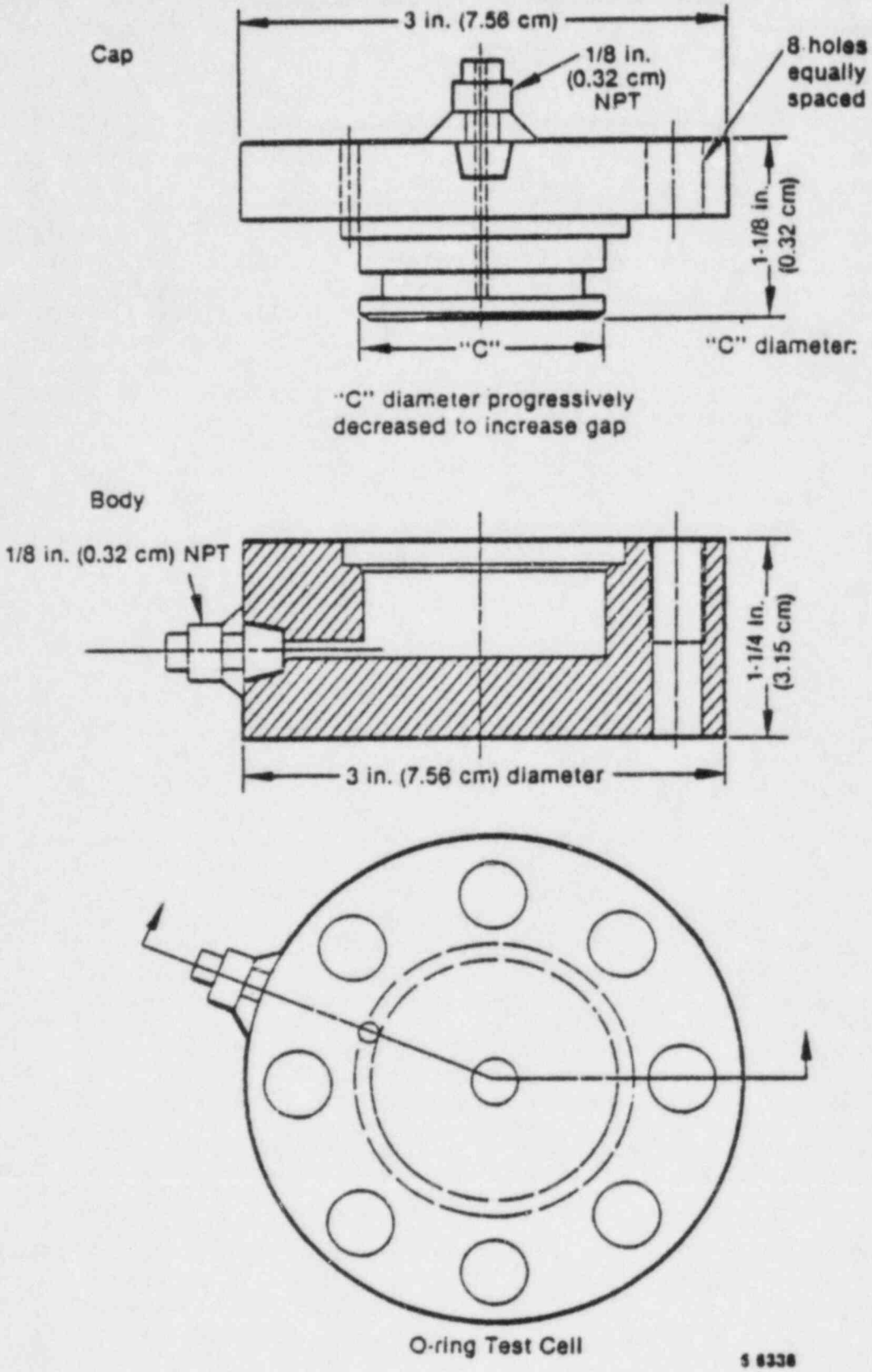

Figure 2. O-ring test fixture.

TABLE 1. RESULTS OF EXTRUSION TESTS FOR E515-80 O-RINGS

Temperature (°F)	Gap (inches)	Pressure Differential (psi)	Time to Blowout (hours)
580	0.0015	1600	--[a]
560	0.0015	1600	3
560	0.0015	2400	6
560	0.0015	2400	2.8
560	0.0015	2400	2
550	0.0015	1200	--[a]
550	0.0015	1200	--[a]
550	0.0015	1200	--[a]
550	0.0015	1600	--[a]
550	0.0015	1800	2.3
550	0.0015	2000	1.5
550	0.0027	1200	--[a]
550	0.0027	1600	--[a]
550	0.0027	1800	--[a]
550	0.0027	2000	--[a]
550	0.0027	2200	--[a]
550	0.0027	2400	--[a]
550	0.0048	1000	--[a]
550	0.0048	1200	--[a]
550	0.0048	1600	1.5
550	0.0048	1800	1.8
550	0.0065	800	5.5
550	0.0065	1000	2.5
520	0.0027	2200	--[a]
520	0.0027	2400	--[a]
520	0.0048	1600	--[a]
520	0.0048	1800	2.5
520	0.0065	800	--[a]
520	0.0065	1000	3.5
550	0.009	800	6
520	0.009	800	17

a. There was no failure during the 18 h test.

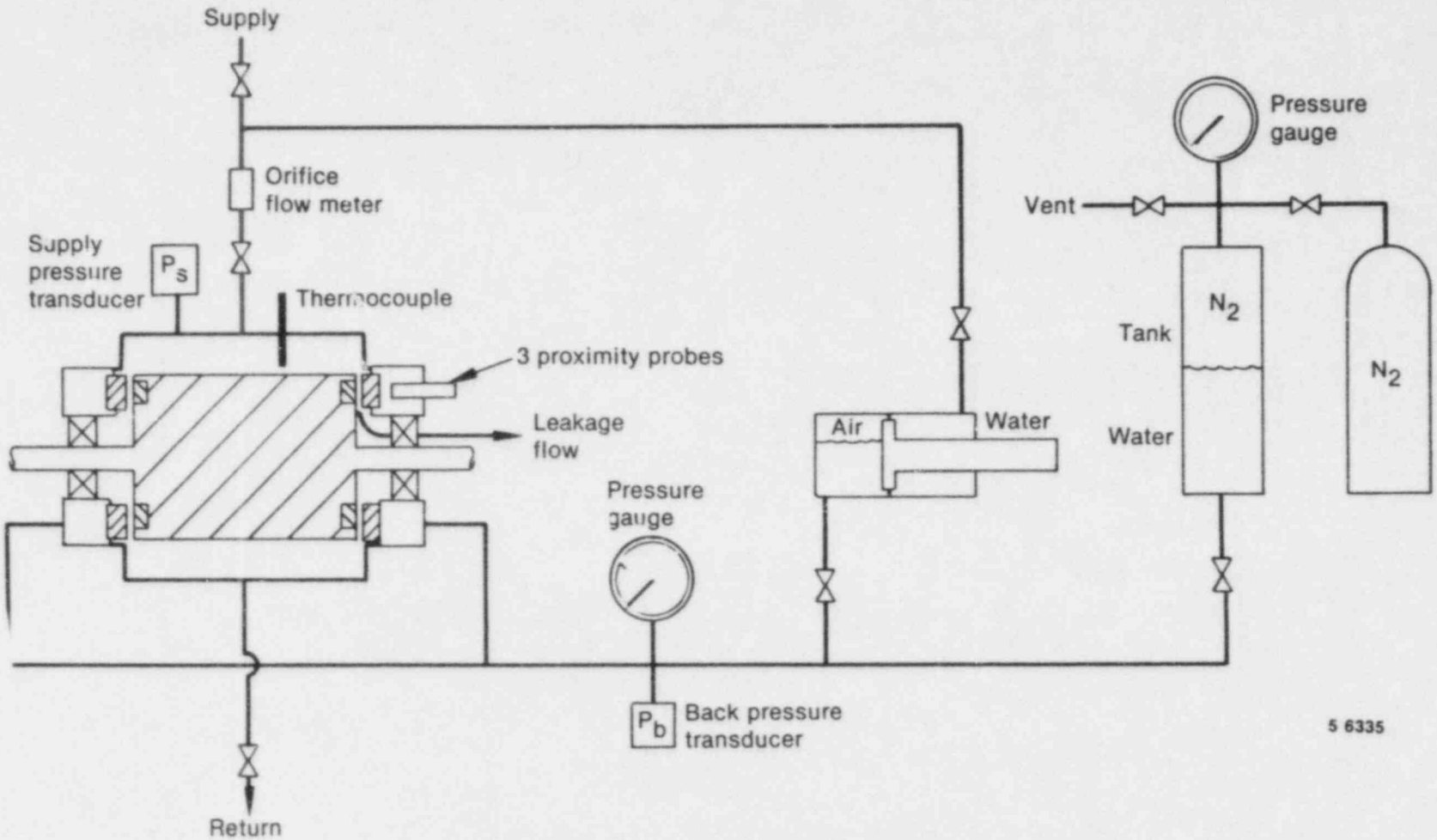

Figure 3. Schematic of a seal blowdown test system.

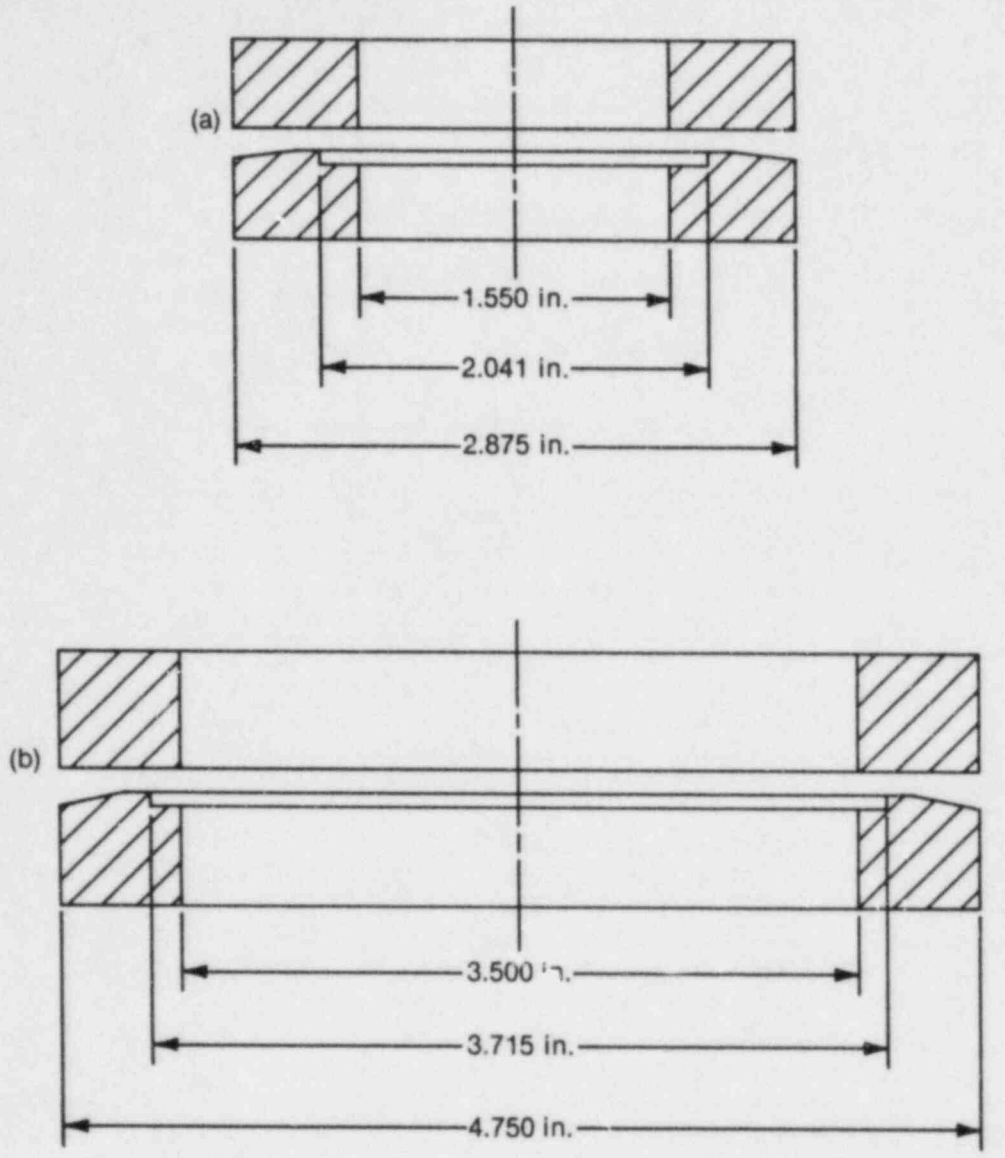

Figure 4. Diagrams of seal rings: (a) 2 7/8 inch OD rings, (b) 4 3/4 inch OD rings.

Valve Research

Containment integrity is most likely to be compromised during an accident by failure of one of the many penetrations rather than by failure of the structure. A technical basis is required to predict the effect of accident conditions on the operability and leak integrity of containment isolation system (CIS) valves, which include containment purge and vent valves. The purposes of the valve research are to identify loads and acceptable methods for qualifying specific types of CIS valves to withstand design basis loads; and to characterize the behavior of selected CIS valves under accident conditions.

Purge Valves

An experimental program was conducted to test butterfly valves typical of those used in containment purge and vent systems. This was done in order to improve understanding of valve operator torque requirements. Three valves were obtained (two 8-in. and one 24-in.), from two of the three manufacturers most commonly used by utilities. The 24-in. valves and one of the 8-in. valves were manufactured by the same company and were chosen to provide data on the validity of extrapolating torque requirements from a small (tested) valve to a larger valve. The other valve was deliberately chosen from another manufacturer to provide information relative to different designs of the same rominal pipe size. The valves were all ANSI 150 lb offset disc types and (compared to other butterfly valves) typically require higher operating torque due to the fluid dynamic loading on the thick disc.

The valves were installed in a duct system with either a straight inlet geometry or with a nearby upstream elbow (Figures 5 and 6). This permitted the measurement of the effect of a flow disturbance. In addition, the valves were installed with the curved (shaft) face of the disc facing upstream first, and then downstream. Figures 7 and 8 show basic valve configurations. Measurement of the torque required to close the valve, as a function of disc position, was taken with nitrogen flowing through the valve. Constant inlet pressure was maintained for each test run. This sequence was repeated for inlet pressures from 5 to 60 psig. The experiments, associated results, and conclusions are documented in Reference 2.

One of the prime equipment qualification issues addressed by these experiments is the issue of extrapolation of smaller valve performance to large valve performance, to ensure that the valve torque requirements are within the capability of the valve operator. Based upon the analysis of the experimental data, several conclusions regarding the feasibility of and conditions for extrapolation were developed:

- Maximum torque requirements are a linear function of static pressure upstream from the valve. This result is at some variance with the currently accepted practice of assuming the operating torque is proportional to the pressure drop across the valve.

- Extrapolation to bound torque requirements is feasible if the scale-model valve is reasonably scaled to the larger valve with respect to disc shape, aspect ratio (disc thickness to diameter ratio), and ratio of disc size to nominal bore size.

- Extrapolation of torque requirements is conservative when the torque measurements used for the larger valve extrapolation are obtained with the scale-model valve installed in a position such that the disc shaft is upstream (curved face of the disc is upstream). The extrapolations, multiplying by the ratio of valve disc diameters cubed, is not conservative with the curved face of the disc downstream.

- Extrapolation is feasible when the inlet pressure of the scale-model valve is equal to or greater than the maximum inlet pressure of the larger valve.

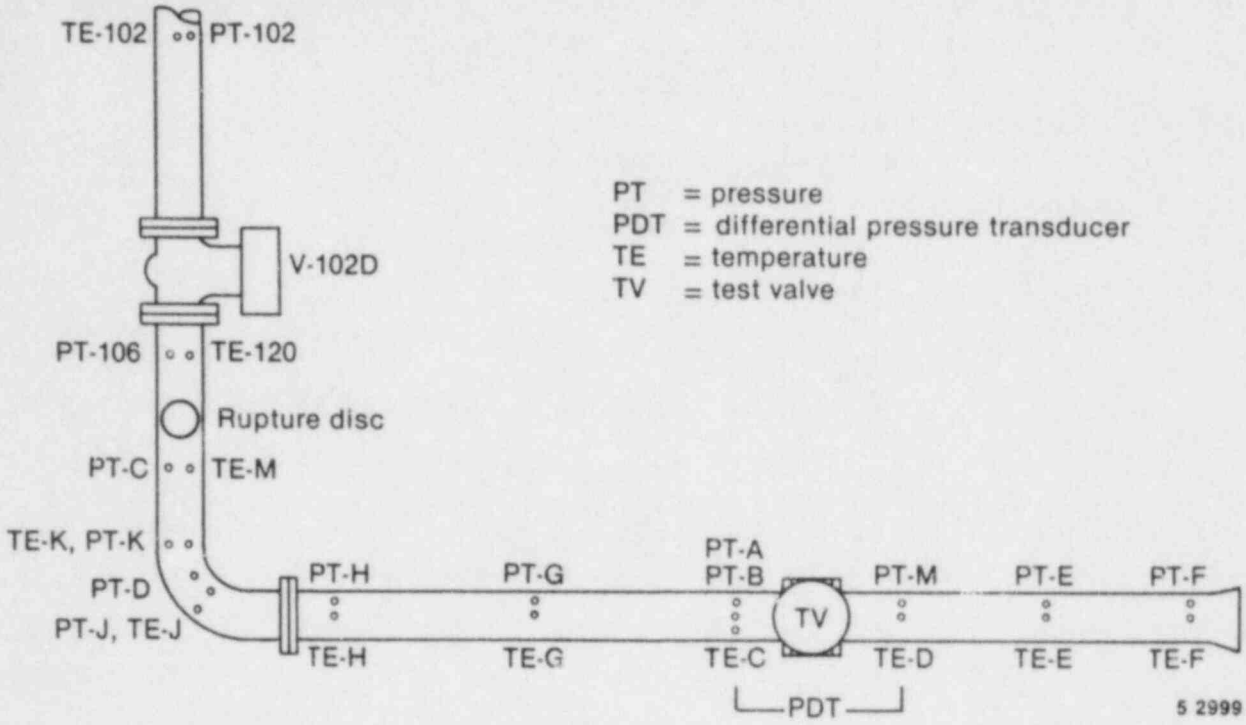

Figure 5. Typical installation, nominal inlet flow test section.

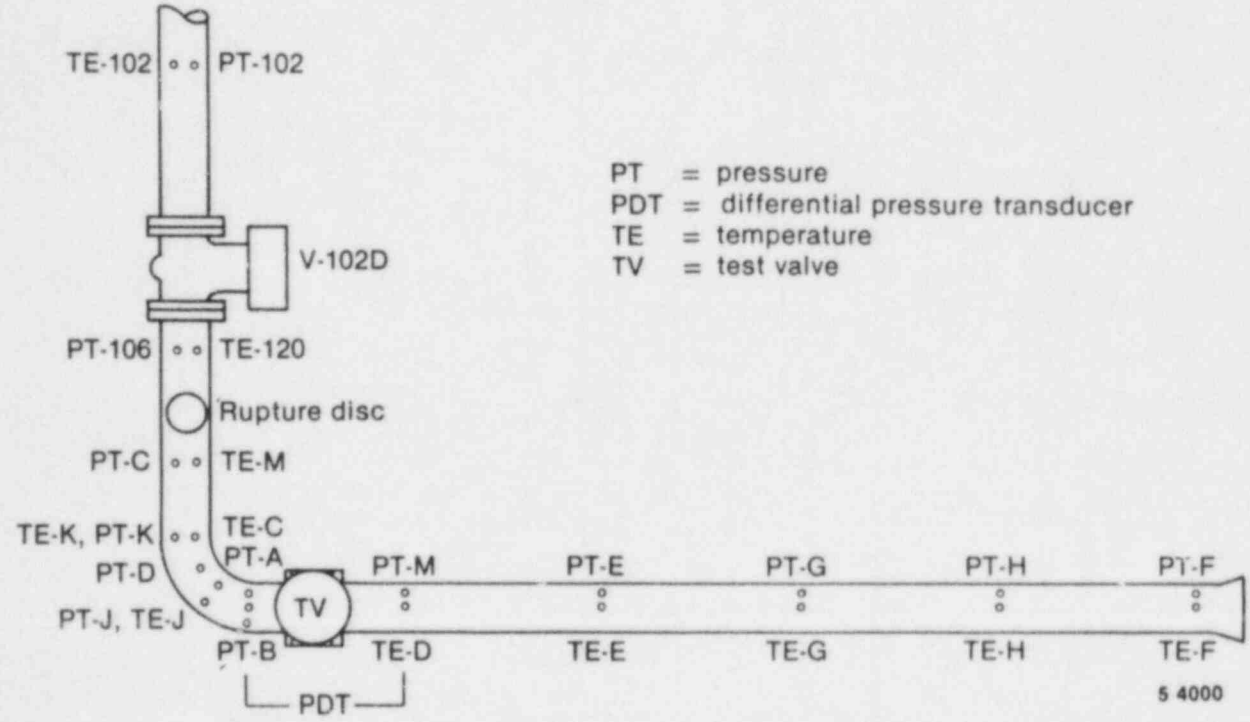

Figure 6. Typical installation, nonuniform inlet flow configuration.

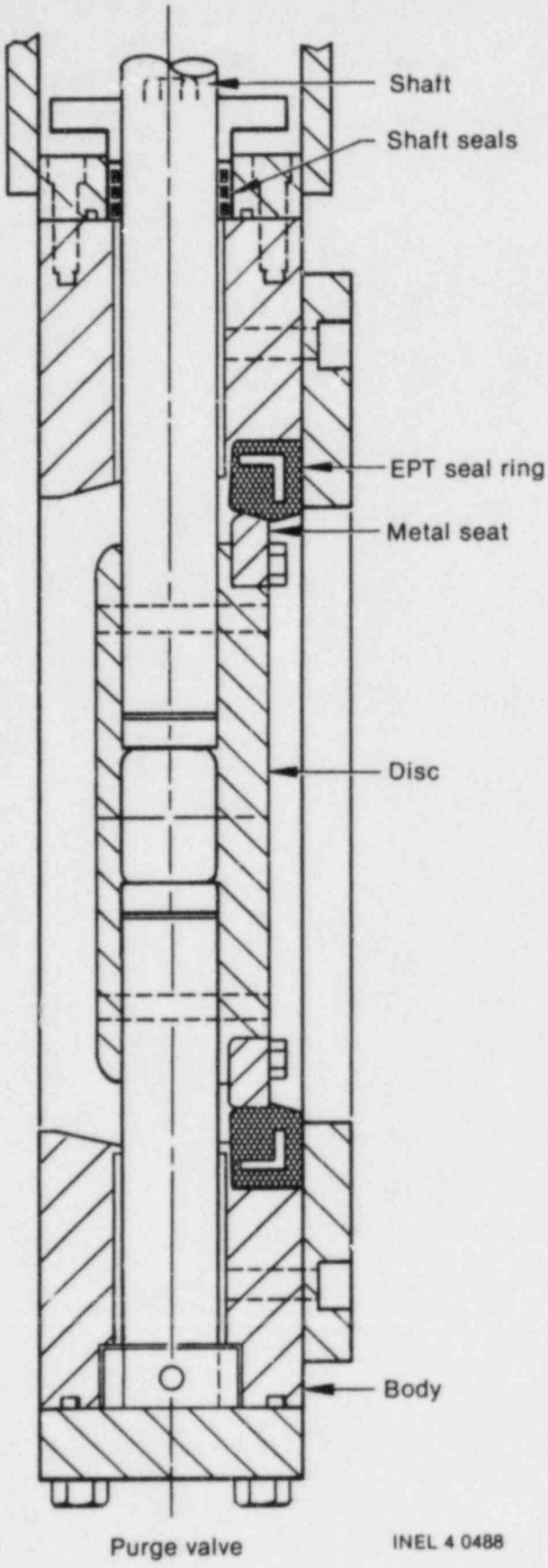

Figure 7. Purge Valve No. 1.

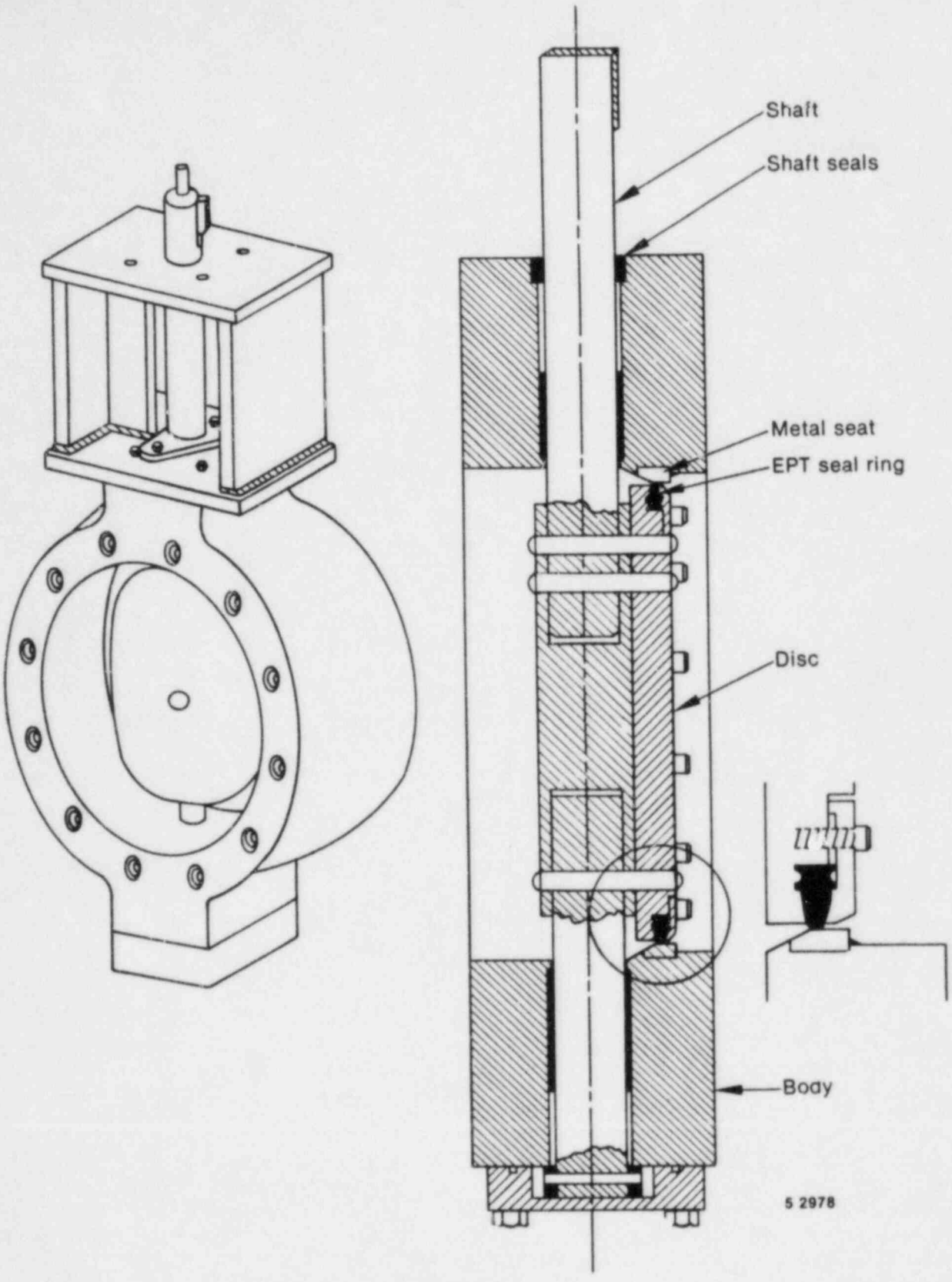

Figure 8. Purge Valve Nos. 2 and 3.

- Conservative torque requirements can be extrapolated when one of the following expressions is used for extrapolating the scale-model valve results.

$$LVT_T = \frac{LVD^3}{SVD^3} SVT_d - LVT_b \quad (1)$$

or

$$LVT_T = \frac{LVD^3}{SVD^3} (SVT_T + SVT_b) - LVT_b \quad (2)$$

where

LVD = Large valve diameter

LVT = Large valve torque

SVD = Small valve diameter

SVT = Small valve torque

b = Bearing

d = Dynamic

T = Total (Bearing and Dynamic).

- Nonuniform inlet flow to the larger valve, due to the upstream presence of an elbow, may be conservatively accounted for by multiplying the nominal or straight inlet predictions by 1.5. Application of this value would require validation prior to use for other upstream disturbances.

- The extrapolation range is limited and it is recommended that the candidate valve basic inside diameter be within 50% to 200% of the test valve.

CIS Valves

The purge valve experimental conclusions will be augmented by data from additional CIS experiments which have been planned and will be conducted in the near future.

The CIS experiments will assess the behavior of typical containment penetration piping assemblies in seismic and accident environments. The systems to be tested consist of: the containment wall penetration; isolation valves on each side of the wall; and sufficient piping and supports to provide typical loads on the penetration and valves. Three systems will be tested: an 8-in. schedule 40 piping assembly with butterfly valves; an 8-in. schedule 40 piping assembly with gate valves; and a 2-in. schedule 160 piping assembly with globe valves. The specific systems were chosen to

represent: containment vent and purge systems, which communicate directly from containment to atmosphere; containment spray systems, required to mitigate the effect of a LOCA on containment loading; and the many small bore containment penetrations for support systems. The test configurations were based on an extensive review of existing piping geometries that exist in operating utilities. Parameters of special interest, in addition to pipe size and valve type, were: distances from the containment wall to the isolation valves, distances between components and supports, location and direction of bends and elbows, and support locations and orientations. Figure 9 shows a representative test configuration.

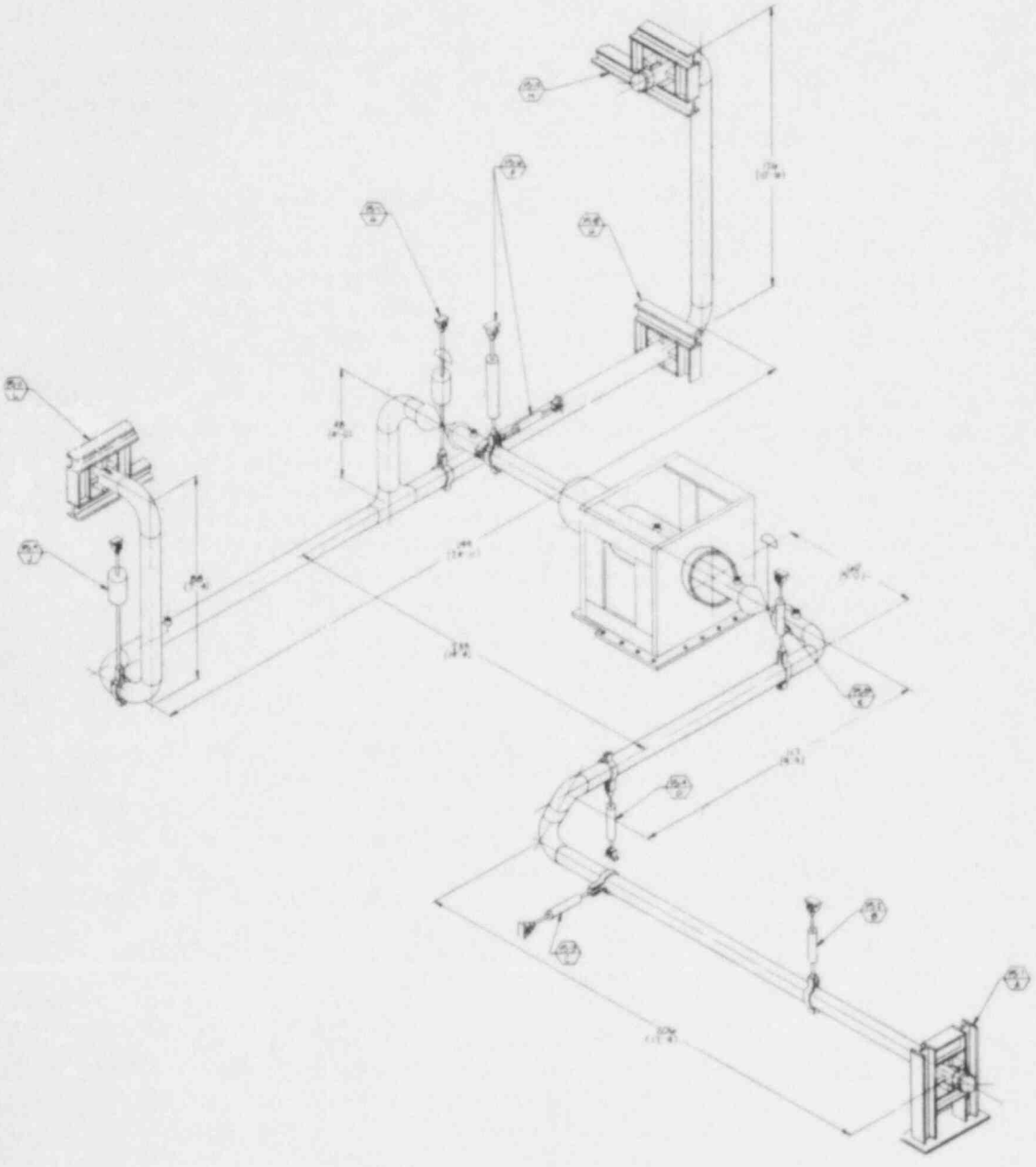

5 4828

Figure 9. Typical 8 inch CIS piping system.

As in the case of system selection, seismic and accident load characteristics were based on extensive reviews of existing safety documentation applicable to operating nuclear power plants. Both seismic and accident loads have been specified to represent typical containment responses; the specified loads envelope about 80% of the plants studied. All types of containment designs were included in the study of predicted responses.

Testing will be performed in two completely separate phases. For the dynamic (operating basis earthquake and safe shutdown earthquake) testing, the piping assemblies will be mounted in a large test fixture and excited by hydraulic actuators to the specified excitation spectrum. The fixture, fabricated from 14-inch square steel tubing, measures approximately 25 feet by 15 feet by 8 feet high and weights 15,000 lb. During the simulated seismic motion, extensive piping system strain and acceleration data will be taken for later comparison to analytical predictions. Valve operating torques and leakage measurements will be obtained to emperically determine the effect of seismic motion on valve operability.

The second phase of the CIS experiments will simulate accident conditions ranging from design basis loss-of-coolant accident conditions (pressure of 60 psig and temperature of 280°F) to severe accident conditions (pressure of 120 psig and a temperature of 350°F). The same test piping assemblies used for dynamic testing will be used during this phase of the program. The experiments will consist of an input motion of the piping penetration, simulating containment wall motion, while all piping supports and hangers are anchored to fixed points on the test fixture or test facility floor. Input deflections at the penetration are controlled through a hydraulic ram and, for some experiments, exceed 5 inches of travel. Extensive piping system yielding and probable failure of some piping supports is predicted. During the gradual motion of the penetration, the valves will be cycled to measure operator torque requirements; periodic seat leakage measurements will also be taken. Those portions of the test piping that represent inside containment systems will be heated to the time-dependent temperatures predicted for a design basis or severe accident.

HDR Valve Experiments

The purge valve and CIS valve experiments have been designed to assess valve behavior under closely controlled input excitation conditions. To further assess the effects of dynamic loads on valves installed in a complex pipe system (Figure 10), dynamic experimental measurements will be obtained from a valve installed in a piping system which is part of the Federal Republic of Germany Heissdampfreaktor (HDR) decommissioned experimental reactor facility. For this experiment, piping excitation will be provided through building motion caused by a very large coastdown shaker mounted on the operating floor of the facility.

The HDR provides two significant differences from the CIS valve research described above. First, the piping is designed as a "hot" system; that is, one specifically designed to accommodate thermal expansion. Secondly, the system will be operating (flowing hot water) during the simulated seismic event. As in the case of the CIS testing, valve operating torques will be measured to determine the effects of dynamic excitation to

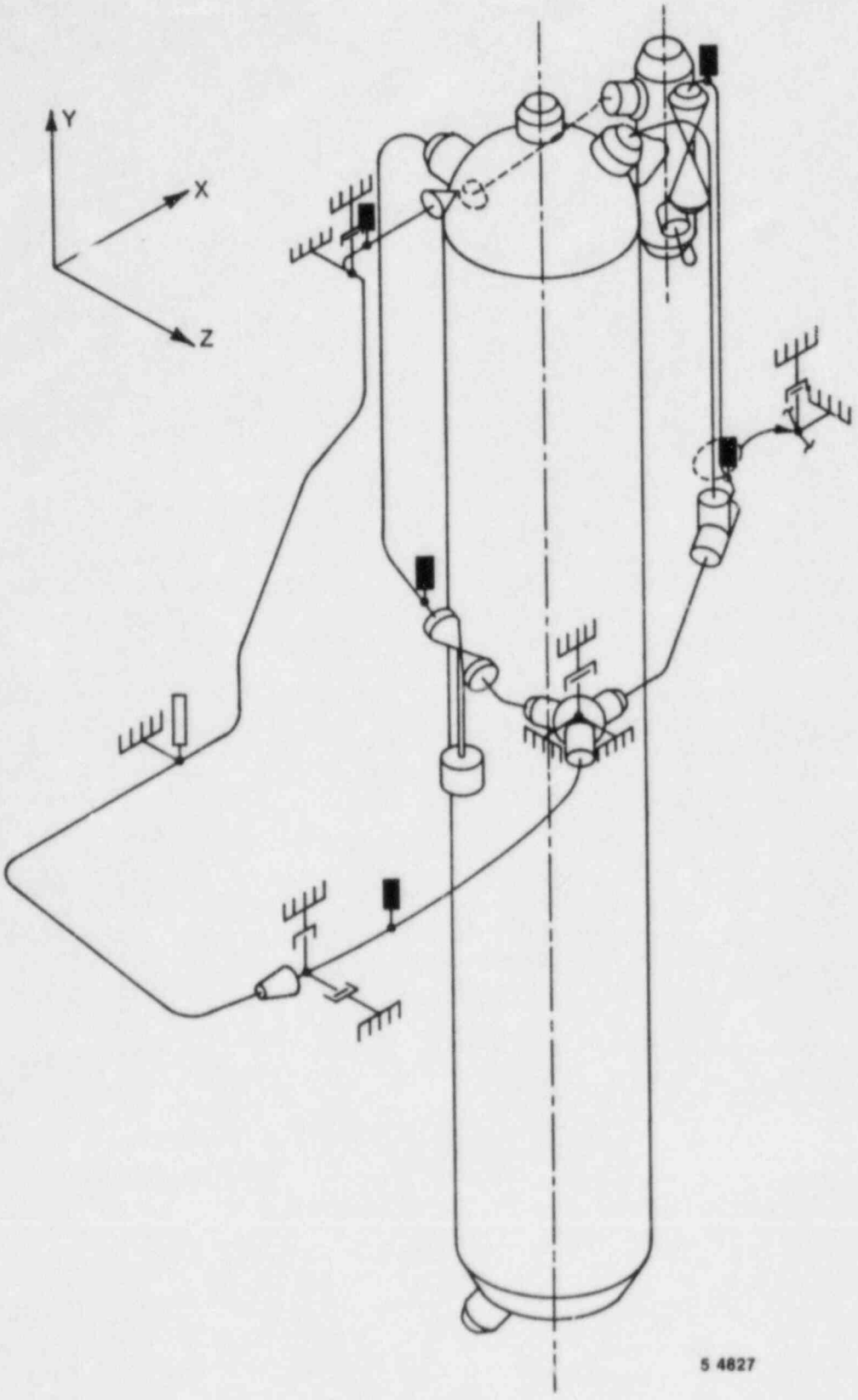

Figure 10. VKL system.

the system. Based on extensive strain and acceleration measurements taken throughout the system, a comparison of predicted to actual piping response will also be made.

Dynamic Research

The equipment qualification research at EG&G Idaho/INEL is also investigating several topics directly related to dynamic qualification criteria, requirements, and methodologies.

Research is being conducted to develop methods that can be used to establish dynamic load qualification margins for mechanical and electrical equipment. The methods will assist in the establishment of test equivalency guidelines and data transfer methods such that existing data obtained by different techniques can be used to qualify various categories of equipment. The methods will be used to quantify margins in new and operating equipment.

Research is also being conducted to evaluate current qualification methods for safety injection pumps which intermittently operate. Specifically, the influence of normal operating loads, including system vibration on pump performance, will be investigated. The objective of the research is to determine whether or not normal operating loads are being properly simulated in current pump qualification procedures.

In addition, research is in progress to evaluate the need to include frequencies above the seismic range in current qualification procedures. Research is currently being done to: define conditions under which equipment can be excited by frequencies in the 50-200 Hz range; define sensitive components; and develop and validate guidelines for qualifying equipment for the higher frequencies.

The program is also initiating research which will identify equipment susceptible to flow-induced vibration, characterize the vibration most detrimental to the equipment, and develop and validate necessary procedures to account for the flow-induced vibration loading.

REFERENCES

1. C. A. Kittmer, et al., Reactor Coolant Pump Shaft Seal Behavior During Station Blackout, NUREG/CR-4077, April 1985.

2. R. Steele and J. C. Watkins, Containment Purge and Vent Valve Test Program Final Report, NUREG/CR-4141, September 1985.

MATERIALS ASPECTS OF BWR PLANT LIFE EXTENSION

B.M. Gordon and G.M. Gordon
General Electric Company
175 Curtner Avenue, M/C 785
San Jose, California 95125

ABSTRACT

Considerable experience with plant equipment performance in nuclear power stations has indicated that the principal factors limiting the life of BWRs and PWRs are materials related. Specifically, for LWRs it is known that these materials issues generally include parameters related to stress corrosion cracking, corrosion fatigue, wear and radiation embrittlement. Not only do these parameters affect and limit the actual useful design life of plant components but also affect the plant's operating availability. In all these cases, the elimination or control of one or more of these critical parameters should improve the plants availability and significantly extend the useful service life.

In the present paper, research performed to address the intergranular stress corrosion cracking (IGSCC) area is described. Specific emphasis is placed on Type 304 stainless steel which has suffered IGSCC in piping in the heat-affected-zones (HAZs) adjacent to the welds in the BWR primary system. Research has developed and qualified a number of techniques which address the three necessary conditions for IGSCC in BWRs: (1) sensitized microstructure, i.e., chromium depletion at the grain boundaries during welding; (2) over yield tensile stress; and (3) oxygenated (200 ppb) high temperature (288°C) water.

Another potential life-limiting IGSCC phenomenon for certain components, irradiation assisted stress corrosion cracking (IASCC) of stainless steel exposed to a high neutron flux, is also discussed. Unlike the IGSCC, IASCC results in intergranular cracking of annealed material at low stress. Fortunately, preliminary research has indicated that some of the techniques utilized for IGSCC control in piping as well as new controlled impurity level stainless steel alloys may reduce the future potential IASCC concern to an insignificant level.

1.0 INTRODUCTION

The first major occurrence of IGSCC of welded Type 304 stainless steel piping occurred in late 1974. All of these IGSCC incidents were identified in small diameter [< 25.4 cm (10 in.)] lines. Since that time, numerous cracks have been found in large diameter piping systems [71.1 cm (28 in.)]. Although these cracking incidents are not safety related, they do impact availability, operating costs, man-Rem exposure for inspection and repair, and anticipated design life. To achieve the goal of extended life, a series of development and qualification programs, co-sponsored by General Electric and the Electric Power Research Institute (EPRI), were initiated to solve the cracking issue by attacking one or more of the three necessary factors for IGSCC in the BWR, i.e., (1) sensitized microstructure; (2) over yield tensile stresses; and (3) high temperature (288°C) oxygenated (200 ppb) water.[1] An additional potential life limiting concern involves the IGSCC of highly irradiated non-sensitized stainless steel. It appears that this concern can also be addressed by a materials and/or environmental approach.

2.0 MITIGATION OF INTERGRANULAR STRESS CORROSION CRACKING OF BWR PIPING

2.1 Materials Solutions

2.1.1 Type 316 Nuclear Grade and Type 304 Nuclear Grade Stainless Steel

An alternate material program was performed to identify and qualify alternate piping materials which would be suitable for BWR piping systems. This strategy addresses the materials/sensitization factor of IGSCC and, in particular, identifies materials which are more resistant to sensitization kinetics as a result of welding or other thermal mechanical treatments.

It is well known that decreasing the carbon content of the stainless steel would retard the kinetics of sensitization.(2-3) Molybdenum also accomplishes the same objective.(4) Therefore, changing the composition of Type 304 stainless steel by lowering the carbon to that of Type 304L stainless steel and adding molybdenum to that of Type 316L stainless steel will synergistically increase the alloy's resistance to the sensitization reaction. However, Type 316 Nuclear Grade and Type 304 Nuclear Grade stainless steel is designed to provide extra margin.

Instead of the 0.03 w/o carbon maximum of the L-grade stainless steels, the Nuclear Grades are characterized by a maximum carbon content 0.020 w/o. The second important composition modification of Type 304NG and Type 316NG is the specification of 0.060 to 0.100 w/o nitrogen to recover the decrease in alloy strength by the reduction of the carbon content. The L-grade stainless steels differ from the Nuclear Grades in nitrogen specification in that a limit of 0.100 w/o nitrogen is allowed. Table 1 presents the composition limits of the Nuclear Grade and reference materials.

A time-temperature sensitization diagram of the relative sensitization kinetics of Type 304, 316 and 316L stainless steel is presented in Figure 1. The "nose" of the time-temperature sensitization curve is about a factor of 30 in time greater for Type 316L as compared to Type 304 stainless steel. Alternatively, about 150 minutes are available for cooling past 700°C (1290°F) within the heat-affected zone of a Type 316L stainless steel weld. In general, this cooling time is slower than a normal air cooling rate, and, therefore, the threat of weld sensitization of Type 316L stainless steel is essentially nil. Evidence of molybdenum causing greatly reduced rates of sensitization is also shown in Figure 1.

To qualify the Nuclear Grade alloys, a four-year extensive laboratory program was conducted at GE as co-sponsored by EPRI. A unique testing technique using full-size pipe tests was utilized. The results of these accelerated tests in high oxygen (8 ppm O_2) high conductivity (~1 μS/cm) water at 288°C (550°F) of welded reference Type 304 stainless steel for comparison to Type 316, 316L, 304L, 304NG, 316NG, CF3, and 347 stainless steel indicated that resistance to IGSCC of the alloys not only increases as carbon content decreases, but also as nitrogen and manganese content increase.

For the Nuclear Grade materials, pipe tests have shown that factors of improvement (FOI) over Type 304 stainless steel performance can be expected to be 50-100 times in normal BWR operation. The necessary FOI for 40-year service life is 20. Accordingly, the replacement of Type 304 stainless steel piping with Type 316 Nuclear Grade will provide substantial resistance to IGSCC over the life of an extended life plant.

No stress corrosion cracking occurrences have been reported for uncreviced/non-cold worked Types 316NG, 304NG, 316L and 304L stainless steel piping used for many years in operating BWRs. While field experience is rather limited, these materials have accumulated over 7000 weld-years of operation (as of September 1985). Further, no evidence of field cracking has been reported in any Type 304 stainless steel heats containing less than 0.043% carbon. This again demonstrates that significant margin is gained by reducing carbon to a maximum of 0.02% for the Nuclear Grades.

2.1.2 Solution Heat Treatment

The elimination of weld sensitized regions can reduce the likelihood of IGSCC in Type 304 stainless steel. The solution heat treatment (SHT) process redissolves the chromium carbides, eliminates chromium depletion around previously sensitized grain boundaries, and eliminates cold work and weld residual stress in the pipe. Operating plant experience supports the use of SHT as a remedy. No instances of IGSCC in stainless steel piping systems have been reported in solution heat treated or mill annealed material. Rare instances of cracking associated with excessive cold work, and/or crevices, or areas sensitized by processes other than welding are the only examples of piping IGCSS incidents not related to weld HAZs.

Although no unusual welding controls are employed during welding, after welding operation, the entire pipe segment is solution annealed at 1038 to 1148°C (1900 to 2100°F) for 15 minutes per 2.54 cm (in.) of thickness but not less than 15 minutes nor more than 1 hour regardless of thickness, followed by quenching in circulating water to a temperature below 204°C (400°F).

Solution heat treatment is limited to those weld joints fabricated in the shop where heat treatment facilities are available, by dimensional tolerance considerations, by size constraints of the vendor facilities (furnace and quench tank), and by cooling rate requirements (dead end legs).

2.1.3 Corrosion Resistant Cladding

This remedy reduces the risk of IGSCC by utilizing the IGSCC resistance inherent in duplex weld metals.(5) Although carbide precipitation observed in the HAZ inside surface is also present in the weld metal, the nature of the duplex (austenitic-ferritic) structure of the weld metal provides resistance to IGSCC in the BWR. In fact, IGSCC propagating from the weld HAZ are blunted when they reach the weld metal.

Corrosion-resistant cladding can be of two basic configurations, depending on the possibility of solution heat treatment of the clad spool pieces. The two basic configurations -- solution heat treated and nonsolution heat treated -- are possible. These two configurations have been referred to as shop and field CRC, respectively. In the shop CRC case, a region of cladding is first applied to the inside diameter away from the weld end. This cladding (minimum ferrite level at 8%) is then solution heat treated with the spool piece to eliminate the slightly sensitized region adjacent to the clad ring. After solution heat treatment, the remaining cladding is applied out to the weld end. This non-solution heat treated cladding will retain its full ferrite content and serve as the protective cover for the HAZ created by the final pipe weld. Because this process eliminates all traces of exposed sensitization, it is preferred over the field CRC option whenever solution heat treatment is possible. When application prohibits solution heat treatment of the clad weld ends, field CRC may be used. In this case, the weld metal is applied to the inside surface of the pipe in a one-step process, leaving a slightly sensitized region at the end of the clad ring. This sensitization, which results from application of the cladding, is not through-wall, is slight compared to that produced by the groove weld and is away from the maximum tensile stress.

2.1.4 Weld Overlay

Prior to any discussion on weld overlay is presented, it is important to note that the weld overlay repair technique is not a fully qualified long-term mitigation technique for IGSCC. Currently the NRC allows two fuel cycles operation ($\sim$ 36 months) with a weld overlay. Recent testing suggests that a minimum of 7 fuel cycles ($\sim$ 126 months of operation) would be acceptable for weld overlay.

Although weld overlay technique is similar to CRC in that it uses layers of IGSCC-resistant duplex weld metal, the most critical difference is that the layer of weld metal is placed on the OD of the pipe and is used to prevent a crack from penetrating through the wall. The weld overlay also serves as a structural reinforcement to restore the original piping safety margins. Another critical effect of the weld overlay is that it produces a favorable (compressive) residual stress pattern which retards or arrests crack growth.

The weld overlay technique has the potential for being a rather cost effective life extension technique as compared to other repair techniques which require draining of the system. It also does not require accurate sizing of crack depths as would be necessary in some tensile stress mitigation techniques since no structural credit is taken for the original piping.

2.2 Tensile Stress Solutions

2.2.1 Heat Sink Welding

The heat sink welding (HSW) program was designed to develop and qualify procedures that would reduce the sensitization produced on the inside surface of welded pipe, and reduce or change the state of surface residual welding stresses from tension to compression. This approach can be used in shop or field applications. HSW basically involves water cooling the inside surface of the pipe during all weld passes subsequent to the root pass or first two layers.

Residual stresses on laboratory Type 304 stainless steel butt welds were measured using strain gages. Measurements revealed that in a variety of pipe sizes, the inside surface tensile surface residual stress is reduced substantially or changed from tension to compression as a result of this approach. Figure 2 shows these results for pipe sizes of 5.1, 10.1, 20.3 and 30.5 cm (2, 4, 8 and 12 in.) diameters.(6) Axial and circumferential stresses were measured at 3 mm (0.12 in.) from the fusion line and were, in all cases, zero or compressive for both spray cooling and running water. Without the HSW process, stresses as high as 393 MPa (57 Ksi) were recorded. Similar benefits have been measured on 50.8 cm (20 in.) diameter piping.

Heat sink welding, as mentioned above, has a secondary benefit in that it reduces the time-at-temperature for sensitization due to the presence of the cooling water heat sink. This factor is illustrated in Figure 3, where the time-at-temperature for a reference and HSW are plotted. In the case of the HSW, the integrated area over the sensitization line of 400°C (750°F) is significantly reduced.

2.2.2 Induction Heating Stress Improvement

The Induction Heating Stress Improvement (IHSI) technique reduces the typical high tensile stress present on the pipe inside diameter (ID) HAZ surface compressive stress. This process involves induction heating of the outer pipe surface of completed girth welds, while simultaneously cooling the inside surface with flowing water (Figure 4). Thermal expansion caused by the

induction coil heating plastically yields the outside surface in compression, while the cool inside surface plastically yields in tension. After cooldown, contraction of the pipe outside diameter (OD) causes the stress state to reverse, leaving the ID in compression and the OD in tension.

The IHSI qualification process has demonstrated the following factors (7):

1. ISHI reduces typical high tensile inside surface residual stresses to compressive stresses as shown in Figure 5.

2. IHSI does not increase the degree of sensitization of the HAZ.

3. Plant loads do not erradicate the induced compressive stress.

4. Outside induced surface tensile stresses do not affect pipe stress analysis or fatigue life.

5. IHSI produces compressive stress at the tip of pre-existing cracks and crack extension does not occur in the process itself.

It is important to note that present NRC guidelines suggest that IHSI be not applied to piping with pre-existing cracks greater than 10% through-wall.

2.2.3 Last Pass Heat Sink Welding

Analytical studies on heat sink welding revealed that the last pass by the welding torch during the process has the highest contribution to induced compressive residual stress. Thus it could be possible to return to previously untreated weld, mechanically remove the weld crown and perform a new last pass weld while cooling the inside surface. While last pass heat sink welding (LPHSW) has its roots in HSW, the process is actually more similar to IHSI in that the heat is progressively supplied around the pipe during LPHSW by a torch as opposed to IHSI where the heat is simultaneously supplied around the pipe by an induction coil.

The results of the program revealed that LPHSW will produce a highly compressive residual stress on the pipe ID in the HAZ region for various pipe diameters. An analysis also predicted that the residual stresses would be compressive to $\sim$ 35% throughwall and that the last weld pass does control the final residual stress state. Subsequent strain gage measurements verified that the stresses were compressive up to 50% throughwall. $MgCl_2$ tests verified that the LPHSW process does produce residual stresses uniformly around the pipe circumference, and stress relief strain gage techniques verified that the axial stress was compressive [-206.8 MPa (-30 ksi)].

IGSCC improvement was evaluated using full-size environmental pipe tests to determine a factor of IGSCC improvement data using 10.2 cm (4 in.) diameter specimens. Conventional welding practice was used to manufacture the baseline welds. The qualified LPHSW processes were then used to produce compressive residual stresses in the welds in four pipes. Pipe tests were then performed at

stresses above yield, in a high oxygen (8 ppm) high temperature (288°C, 550°F) water environment.

The pipe test results are plotted with reference data in Figure 6. At the end of the program period, the pipes had been on test over 5500 hours, demonstrating a factor of >5.5 and >6.5 improvement, respectively, at the two test stresses [193.7 and 211 MPa (28.1 and 30.6 ksi)]. This factor of improvement approaches that determined for IHSI. This data is encouraging in that it establishes that the LPHSW processed welds had highly compressive residual stresses. If this were not true, the applied stress would have shaken down the residual stresses leading to IGSCC failure.

2.3 Environmental Solution - Hydrogen Water Chemistry

The recirculating coolant in a BWR is high-purity neutral pH water containing typically 200 ppb (ppb = µg/ℓ) radiolytically produced dissolved oxygen with stoichiometric amounts of dissolved hydrogen ∿ 25 ppb). Laboratory and field results clearly indicated that this level of oxygen is sufficient to serve as the chemical driving force for IGSCC. If it were possible to reduce this necessary factor for IGSCC below some threshold level, the likelihood of IGSCC could be reduced. It was therefore necessary to identify this threshold level and determine a means of accomplishing this level in a BWR.

Numerous laboratory studies have indicated that susceptibility to IGSCC in stainless steels diminishes with decreasing oxygen content of the water below 200 ppb.(9) However, the first objective of testing was to determine the threshold oxygen level below which IGSCC will not occur on sensitized Type 304 stainless steel. To accomplish this objective, a series of straining electrode tests (SETs) were performed. The tests were performed on an extremely susceptible heat of Type 304 stainless. This test indicated that at a corrosion potential of -230 mV IGSCC does not occur which is equivalent to approximately 20 ppb oxygen.

The candidate additives to the BWR environment which could reduce the dissolved oxygen content below this threshold 20 ppb level included ammonia, hydrazine, morpholine, various combinations of the three and hydrogen. Hydrogen was the most suitable additive as based on initial laboratory investigations, overall systems analysis and economic analysis.

Initially, a short term HWC demonstration was performed at Commonwealth Edison Company's (CECo's) Dresden 2 plant in 1982.(10) This six-week study revealed that hydrogen additions to the feedwater reduces the dissolved oxygen content and electrochemical potential of Type 304 stainless steel below the threshold level for cracking.(11) In-reactor constant extension rate technique (CERTs) tests on furnace sensitized Type 304 stainless steel and SA533B low alloy steel also revealed complete mitigation of stress corrosion cracking. During Dresden-2's full time operation on HWC, which initiated in April 1983, additional in-reactor CERT tests were performed. Table 2 presents results of all the in-reactor CERTs plus some of the confirming laboratory CERT tests. It is important to note that even a precracked CERT specimen showed no signs of

crack propagation in the in-reactor HWC environment (Test 8). This result was confirmed by other laboratory studies.

Crack growth data versus real time on a precracked furnace sensitized Type 304 stainless compact tension specimen is currently being obtained at Dresden-2 using the reversing DC electrical potential monitoring (EPM) technique.(12) The compact tension specimen was precracked in the laboratory in the nominal 220 ppb O_2 environment as was the Test 8 CERT described above, and then shipped to Dresden-2 for testing. The K_1 level for the specimen bounds that of some known cracks at Dresden-2 (27.5 MPa$\sqrt{m}$, 25 ksi$\sqrt{in}$). The results of this test revealed an approximate crack growth rate of 3.8×10^{-12} m/s (5.4×10^{-7} in/hr) excluding the effects of reactor scrams while the crack growth obtained at the same K_1 obtained in the laboratory in the nominal environment is approximately 1.5×10^{-10} m/s (2.2×10^{-5} in/hr). Mid-cycle and end-cycle in-service-inspection at known pipe cracks at Dresden-2 also showed no sign of crack growth during hydrogen injection.

The laboratory HWC materials program, which is co-sponsored by EPRI and GE, is characterized by an extensive test matrix.(13) The testing techniques utilized in the program include full-size pipe tests, fracture mechanics studies, electrochemical investigations, constant extension rate tests (CERT), straining electrode tests (SET), constant load tests, bent beam tests, fatigue testing, cyclic crack growth studies, general, galvanic and crevice corrosion investigations, corrosion oxide analyses, etc.

The results of the laboratory HWC program indicated the following:

1. For Type 304 stainless steel welded pipe with deep IGSCC, the subsequent exposure to HWC environment would result in the arrest of these cracks with no additional intergranular propagation even at stress levels of twice the ASME Code allowable (i.e., 2 S_m).

2. Factors-of-improvement based on crack initiation data for the HWC environment are at least 25X the nominal environment.

3. Under constant loading conditions, no measurable crack growth was detected for furnace-sensitized Type 304 stainless steel, furnace-sensitized Type 316 Nuclear Grade stainless steel, SA508 Cl.2 low alloy steel and SA333 Gr. 6 carbon steel in the HWC environment. In the nominal environment, measurable crack growth is observed at significantly lower stress intensities on furnace-sensitized Type 304 stainless steel and is observed on SA106-B carbon steel. No crack growth is noted in the low alloy and Type 316 Nuclear Grade stainless steel in the nominal environment, (Tables 3 and 4).

4. The cyclic crack propagation rates for furnace-sensitized Type 304 stainless steel, SA508-C1-2 low alloy steel and SA333 Gr. 6 carbon steel tested at 0.74 cycles per hour were 3, 7 and 20 times lower in the HWC environment, respectively, as compared to the nominal BWR environment. Tests at higher frequencies (7.5 cph) showed even greater improvement (Table 5).

5. The fracture morphology produced under constant or cyclic loading of furnace-sensitized Type 304 stainless steel in the 200 ppb O_2 reference environment is completely intergranular, while HWC produces a transgranular mode of fracture, thus indicating the total mitigation of IGSCC in HWC. The transgranular cracking of this material has no engineering significance.

6. No detrimental effects such as hydrogen embrittlement have been found for high strength materials such as Alloy 600, Alloy X-750 and martensitic stainless steels in the HWC environment.

7. The general corrosion rate of Types 304 and 316L stainless steel is extremely low in either the HWC or reference environment. Although the general corrosion rate of Alloy 600 are significantly reduced in the HWC environment, there is an initial acceleration in general corrosion rates of carbon and low alloy steel. However, the long term carbon and low alloy steel general corrosion rate appears to be similar to that obtained in the normal BWR environment.

3.0 IRRADIATION ASSISTED STRESS CORROSION CRACKING (IASCC)

The IGSCC discussed in Section 2.0 was the result of the simultaneous interaction of sensitized stainless steel, i.e., chromium depletion at the grain boundaries, high tensile stresses (weld residual, pressure and thermal) and oxygenated high temperature water. The mechanism of irradiation assisted stress corrosion cracking (IASCC) appears to involve the simultaneous interaction of highly irradiated annealed material with diffusion of impurities (S, Si, P) to the grain boundaries, lower stress (fabrication, irradiation creep) and high temperature oxygenated water with short lived oxidizing species (H_2O_2), gamma and neutron flux. It is extremely important to note that IASCC does not require chromium depletion sensitization or high tensile stresses to produce failures.

During the early history of the BWR (1960's), Type 304 stainless steel was utilized as a fuel cladding material. Since this highly stressed material suffered extensive cracking, the Type 304 stainless steel was replaced with Zircaloy-2. It is believed that this instance of cracking was the first indication that annealed Type 304 stainless steel could suffer IGSCC in the BWR environment. Since this type of intergranular cracking was produced in non-sensitized, highly stressed, highly irradiated components, this form of IGSCC is referred to as IASCC.

Recently, neutron source holders, control blade absorber tubes, and nuclear instrument tube holders have cracked in the BWR environment. Tables 6 and 7 present a summary of field IASCC experience for the era prior to 1980 and post 1980, respectively. It is obvious that the trend for this type of cracking is increasing and the tensile stress necessary to produce cracking is low. It is also important to note that PWR's as well as non-GE BWRs have also experienced this type of corrosion phenomenon.

The results of the field IASCC experience suggest the following:

1. Dynamic strain or high stresses produced IASCC in most early cases.

2. More recent results indicate that the stress threshold for IASCC may be lower than initially believed.

3. No field IASCC has been observed at a fluence of $\leq 5 \times 10^{20}$ NVT (>MeV).

4. Cracks may occur at lower stresses for higher fluences.

5. Although cracking instances may often be sporadic, a significant number of components have cracked.

Obviously, the major concern of IASCC is not so much the cracking of replaceable components such as control blades and instrument tube holders, but rather the potential for cracking of major internal BWR components such as the shroud and top guide. To evaluate this potential, GE has constructed an extensive hot-cell test facility.

To simulate the highly oxidizing conditions in the core, CERT tests were performed on irradiated annealed Type 304 stainless steels at different levels of fluence. The IASCC phenomenon was reproduced and the results indicate the observed field IASCC threshold is consistent with the laboratory CERT tests.

Table 8 presents a listing of the highest fluence BWR components. All these components are characterized by end of life fluences which put them at risk for IASCC. In particular, the top guide has the highest fluence of all the major structural components. The peak fluence for the top guide is approximately 10^{22} for earlier BWRs with long fuel. The top guide also has a rather steep flux gradient between its bottom and top surfaces as well as from the center to periphery.

Fortunately, the same environmental solution for the IGSCC of piping (HWC) appears promising for this potential issue. Table 9 presents the results of CERT tests on commercial purity annealed Type 304 stainless steel in high oxygen (32 ppm) environment simulating the highly oxidizing regions in the core and HWC. The differences in SCC response is dramatic. The highly oxidizing environment produced a fracture surface with 99% IGSCC while the HWC produced ductile failure. The reason for this significant disparity may be explained by the electrochemical potential (ECP) of Type 304 stainless steel which is significantly more oxidizing in the core region than in the recirculation piping system. HWC by lowering the ECP appears to be a promising method of mitigation for IASCC.

The second promising technique for mitigating IASCC is the use of high-purity materials containing controlled amounts of impurities such as sulfur, phosphorous and silicon.(14) This mitigation technique is based on the highly successful in-reactor performance of high purity Type 348 stainless steel at the La Crosse BWR. Commercial-purity materials with the nominal levels of S, P, Si installed at the La Crosse BWR suffered IASCC. Other support for the implementation of high-purity materials is based on laboratory studies on unirradiated

stainless steel where the presence of these specific impurities increased the IGSCC susceptibility.(15) Work is continuing in this area.

4.0 DISCUSSION

All of the several qualified IGSCC mitigation methods summarized in Table 10 should result in life extension of BWR piping systems. These mitigation techniques attack one or two of the necessary factors for IGSCC. Some of the techniques such as IHSI, LPSHW, Weld Overlay and HWC can be readily applied to an operating BWR without the necessity of draining of the piping system. In addition, HWC offers the potential for "blanket" protection where other materials/stress fixes can not be implemented. It also has the potential for mitigating IASCC. The implementation of these IGSCC mitigation methods to BWRs should increase its availability factor and level of reliability. Further, the application of one or more of these IGSCC mitigation techniques may offer the potential for extending the life of the BWR piping systems beyond the current 40 year design life.

For example, full scale pipe test have indicated that properly processed Type 316 Nuclear Grade and Type 304 Nuclear Grade stainless steel should not suffer IGSCC in over 100 years of nominal BWR service. The application of HWC to an operating BWR, such as has occurred at Dresden-2 since 1983, suggests that not only can IGSCC initiation be prevented in the field, but pre-existing cracks should be arrested or grow at greatly retarded rate.

Another important factor is that the piping IGSCC mitigation techniques are qualified and are being implemented now. Since numerous BWR utilities have applied one or more of these techniques to their piping systems, the operational data base for these mitigation methods is increasing daily. Dresden-2 has operated for over 2 years on HWC with no serious difficulties. A number of utilities have also replaced their recirculation piping systems with newly designed Type 316 Nuclear Grade stainless steel systems with 40% fewer welds.

In the area of IASCC, two methods appear promising for mitigating this infrequently occurring phenomenon, that is, HWC and high purity materials. An extensive effort is underway to improve our understanding of IASCC.

5.0 CONCLUSIONS

The results of extensive in-reactor and laboratory tests suggest the following conclusions concerning the mitigation of IGSCC in BWR piping systems and IASCC in reactor internals and their impact on future BWR performance.

1. The IGSCC of BWR piping is understood and its risk can be significantly reduced by a number of qualified mitigation techniques.

2. A new "blanket" protection technique for IGSCC and potentially IASCC, hydrogen water chemistry, has been implemented in a domestic BWR for over two years of successful operation.

3. Materials cracking contribution to BWR plant unavailability will decrease in the future.

4. The potential for extending the design life of BWR piping systems and other components appears promising.

6.0 REFERENCES

1. Klepfer, H.H., NEDO-21000-1, 75NED35, July 1975.

2. Tedmon, C.S., Jour. Elect. Soc., 118, 1971.

3. Strawstrom, C. and M. Hillert, JISI, 207, 77, 1969.

4. Cihal, V., Corrosion-Traitements-Protection-Finition, 18, 1970.

5. Alexander, J., EPRI, NP-2671-LD, October 1982.

6. Imai, K. et al, "Mitigation of Inside Surface Residual Stress of Type 304 Stainless Steel Pipe Welds by Running Warter Cooling Method," Third Inter. Conf. of Welding in Nuclear Engineering, Dusseldorf, West Germany, November 28, 1978.

7. Offer, H.P., EPRI NP-3375, November 1983.

8. Horn, R.M., "Last Pass Heat Sink Welding," EPRI NP-3479-LD, March 1984.

9. Indig, M.E. and A.R. McIlree, Corrosion, 35, 1979.

10. Burley, E.L., "Oxygen Suppression in Boiling Water Reactors - Phase 2 Final Report," DOE/ET/34203-47, NEDC-23856-7, October 1982.

11. Gordon, B.M., "Mitigation of Stress Corrosion Cracking Through Suppression of Radiolytic Oxygen," Proceedings of the International Symposium on Environmental Degradation of Materials in Nuclear Power Systems - Water Reactors, NACE, Houston, 1984.

12. Prater, T.A., W.R. Catlin and L.F. Coffin, "Surface Crack Growth in High Temperature Water," 83CRD277, December 1983.

13. Gordon, B.M., "Laboratory Studies of Materials Performance in Hydrogen Water Chemistry," paper presented at EPRI Seminar on BWR Corrosion, Chemistry and Radiation Control, Palo Alto, CA, October 1984.

14. Jacobs, A.J. and G.P. Wozadlo, "Irradiation-Assisted Stress Corrosion Cracking as a Factor in Nuclear Power Plant Aging", paper presented at the International Conference on Nuclear Power Plant Aging, Availability Factor and Reliability Analysis, San Diego, CA., July 8-12, 1985.

15. Duncan, R.N., "Stainless Steel Failure Investigation Program", Final Summary Report, General Electric Company Report No. GEAP-5530 (1968)

TABLE 1

CHEMICAL COMPOSITION LIMITS AND RANGES
NUCLEAR GRADE STAINLESS STEELS AND REFERENCE MATERIALS

Alloy	C max	Mn max	Si max	P max	S max	Cr	Ni	Mo	N
304NG	0.020	2.00	1.00	0.045	0.030	18.00-20.00	8.00-12.00	--	0.060-0.100
316NG	0.020	2.00	1.00	0.045	0.030	16.00-18.00	10.00-14.00	2.00-3.00	0.060-0.100
304	0.08	2.00	1.00	0.045	0.030	18.00-20.00	8.00-12.00	--	--
304L	0.030	2.00	1.00	0.045	0.030	18.00-20.00	8.00-12.00	--	0.100 Max
316	0.08	2.00	1.00	0.045	0.030	16.00-18.00	10.00-14.00	2.00-3.00	--
316L	0.030	2.00	1.00	0.045	0.030	16.00-18.00	10.00-14.00	2.00-3.00	0.100 Max
347	0.08	2.00	1.00	0.045	0.030	17.00-19.00	9.00-13.00	--	--
CF3	0.030	1.50	2.00	0.04	0.04	17.0 -21.0	8.0 - 12.0	--	

TABLE 2

RESULTS OF DRESDEN-2 AND LABORATORY HWC CERT TESTS

	Material	Test Location	O_2 (ppb)	K[1] (μS/cm)	Time To Failure(h)	Time Off HWC(h)	Elongation %	Result
1)	FS[2] T-304	D-2	268	0.29	108	0	12	70% IGSCC
2)	FS T-304	D-2	40	0.37	143	2	20	35% IGSCC
3)	FS T-304	D-2	<20	0.29	>297[4]	4	38[5]	DF[3]
4)	FS T-304	D-2	5-20	0.29	208	5	NM	DF
5)	FS T-304	D-2	5-23	0.17	181	15	NM	Minor IGSCC along gauge
6)	FS T-304	D-2	3-30	0.13	396	36	45	DF
7)	FS T-304	D-2	7-19	0.09	400[7]	25	46	DF
8)	FS T-304PC[6]	D-2	12-20	0.09	301	7	40	No IGSCC Extension
9)	FS T-304	VNC[8]	195	<0.1	156	NA[9]	17	85% IGSCC
10)	FS T-304	VNC	15	<0.1	262[10]	0	NA	DF
11)	SA 533B	D-2	150-280	0.29	37	NA	12	40% TGSCC
12)	SA 533B	D-2	5-20	0.29	63	0	24	DF
13)	SA 533B	VNC	200	<0.1	43	NA	11	40% TGSCC
14)	SA 533B	VNC	12	<0.1	60[11]	0	22	DF
15)	SA 508-2[12]	D-2	12-18	0.08	52	0	NM	DF
16)	SA 508-2	VNC	50	<1	44	0	29	DF
17)	SA 106B	D-2	8-14	0.12	94	2	NA	DF
18)	SA 106B	VNC	50	<1	40	0	29	DF

1) K = Conductivity
2) FS = Furnace Sensitized 621°C (1150°F)/24 hr
3) DF = Ductile Fracture
4) Thermal Overload Ended Test
5) NM = Not Measured to Date
6) PC = Precracked in 200 ppb O_2
7) Plus 67 Hours Precracking (368 hr total)
8) VNC = Vallecitos Nuclear Center
9) Not Applicable, i.e., not a HWC Test
10) Extension rate was 3 mils/h for SA 533, SA 508-2, SA 106B and 1 mil/h for Type 304 Stainless Steel
11) Motor Failure, Specimen Fractured Manually
12) Creviced

Table 3. SCC Crack Growth Test Results in HWC

HWC (20 ± 15 ppb O_2, 125 ± 25 ppb H_2, <0.2 μS/cm)

Material	Growth Rate	Stress Intensity
FS Type 304	No Growth	$K \leq 31.2$ MPa $\sqrt{m}$ (28.4 ksi $\sqrt{in.}$)
FS Type 316 NG	No Growth	$K \leq 30.1$ MPa $\sqrt{m}$ (27.4 ksi $\sqrt{in.}$)
SA 508-2	No Growth	$K \leq 50.9$ MPa $\sqrt{m}$ (46.3 ksi $\sqrt{in.}$)
SA 333-6	No Growth	$K \leq 44.8$ MPa $\sqrt{m}$ (40.3 ksi $\sqrt{in.}$)

Table 4. SCC Crack Growth Test in 200 ppb Oxygen Water

Material	Growth Rate	Stress Intensity
FS Type 304	$8.9X10^{-8}$ mm ($3.5X10^{-9}$ in.)/sec.	K=17.3 MPa $\sqrt{m}$ (15.7 ksi $\sqrt{in.}$)
FS Type 316 NG	No Growth	$K \leq 26.7$ MPa $\sqrt{m}$ (24.3 ksi $\sqrt{in.}$)
SA 508-2	Incipient Growth	K=49.1 MPa $\sqrt{m}$ (44.7 ksi $\sqrt{in.}$)
SA 106-B	$1.4X10^{-7}$ mm ($5.2X10^{-9}$ in.)/sec.	K=44.0 MPa $\sqrt{m}$ (40.0 ksi $\sqrt{in.}$)

TABLE 5

FATIGUE CRACK GROWTH TEST RESULTS

Material	Cyclic Frequency (cph)	Environment	Stress Intensity MPa $\sqrt{m}$ (ksi $\sqrt{in.}$)	Crack Growth Rate mm/cycle ($\times 10^{-5}$)	Crack Growth Rate (in./cycle) ($\times 10^{-5}$)	Factor of Improvement
FS Type 304	0.74	HWC	30.9 (28.1)	69	(2.7)	∿ 3
		200 ppb O_2	30.3 (27.6)	254	(10)	----
	7.5	HWC	31.3 (28.5)	16	(0.63)	∿ 3
		200 ppb O_2	25.8 (23.5)	50	(2.0)	----
SA 508-2	0.74	HWC	34.1 (31.0)	7.6	(0.3)	∿ 7
		200 ppb O_2	37.6 (34.2)	50.8	(2.0)	----
	7.5	HWC	33.8 (30.8)	1.7	(0.07)	∿ 450
		200 ppb O_2	33.7 (30.7)	760	(30)	----
SA 333-6	0.74	HWC	30.4 (27.7)	5.6	(0.22)	∿ 20
		200 ppb O_2	30.6 (27.8)	109	(4.3)	----
	7.5	HWC	24.2 (22.0)	0.33	(0.013)	∿1000
		200 ppb O_2	23.7 (21.6)	333	(13)	----

* Since no control test for Type 316 Nuclear Grade was performed, no comparison can be made in this table.

TABLE 6

SUMMARY OF FIELD IASCC EXPERIENCE UP TO 1980

Component	Fluence (N/cm^2)	Source of Stress
Fuel Cladding	$5x10^{20}$-$2x10^{21}$	o Fabrication o Fuel Cladding Interaction
Neutron Source Holders	10^{21}-10^{22}	o Welding o Beryllium Swelling After Initial Crevice Attack
Control Rod Absorbers Tubes	$5x10^{20}$-$3x10^{21}$	o B_4C Swelling
Fuel Bundle Cap Screws	10^{21}-10^{22} (Estimated)	o Fabrication and/or Assembly
Rivets in Control Rod Follower	$5x10^{20}$	o Unknown

TABLE 7

SUMMARY OF POST 1980 IASCC FIELD EXPERIENCE

Component	Fluence (N/cm^2)	Source of Stress
Plate Type Control Blade	$2x10^{21}$	B_4C Swelling
IRM/SRM Dry Tubes	$\sim 1x10^{22}$	Fabrication

TABLE 8

HIGHEST FLUENCE BWR COMPONENTS

Component	Estimated End of Life Fluence
Shroud	$\sim 1 \times 10^{21}$ NVT
Top Guide	$\sim 1 \times 10^{22}$ NVT (Peak)
Control Blade Sheath	$\sim 5 \times 10^{21}$ NVT
SRM/IRM	$> 1 \times 10^{22}$ NVT

TABLE 9

HOT CELL CERT RESULTS ON
IRRADIATED TYPE 304 STAINLESS STEEL

Environment	Fluence	Results
32 ppm O_2	2×10^{21} NVT (>1 MEV)	99% IGSCC
HWC	2×10^{21} NVT (>1 MEV)	Ductile

TABLE 10

SUMMARY OF IGSCC MITIGATION TECHNIQUE

Mitigation Technique (qualification Year)	Affected SCC Parameter			Potential Implementation by Plant Status			
	Material	Stress	Environment	Operating Plants: Retrofit	Operating Plants: Repair	Plants Under Construction	Future Plants
Nuclear Grade Alloys (1978)	X				X	X	X
SHT (1978)	XP[1]	XS[2]				X	
CRC (1978)	X				X	X	
Weld Overlay[3]	XP	XS			X		
HSW (1978)	XS	XP			X	X	
IHSI (1978)		X		X	X	X	
LPHSW (1983)		X		X	X	X	
HWC (1983)[4]			X	X		X	X

(1) XP = primary benefit area.
(2) XS = secondary benefit area.
(3) Undergoing final qualification testing.
(4) Laboratory qualification completed in 1983, final in-reactor qualification underway.

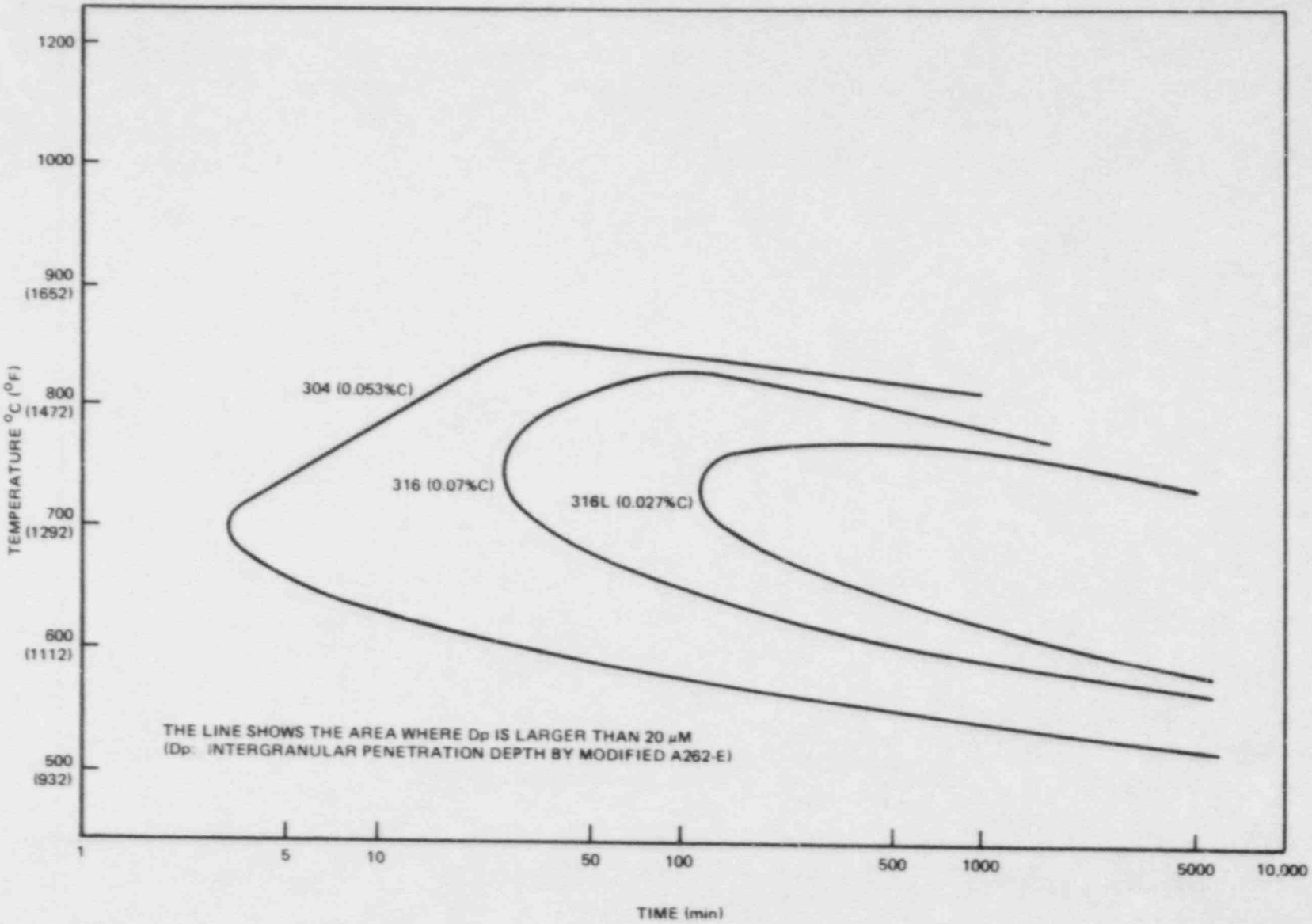

Figure 1. Time-Temperature Sensitization Diagrams of Type 316 and 316L Compared with Type 304

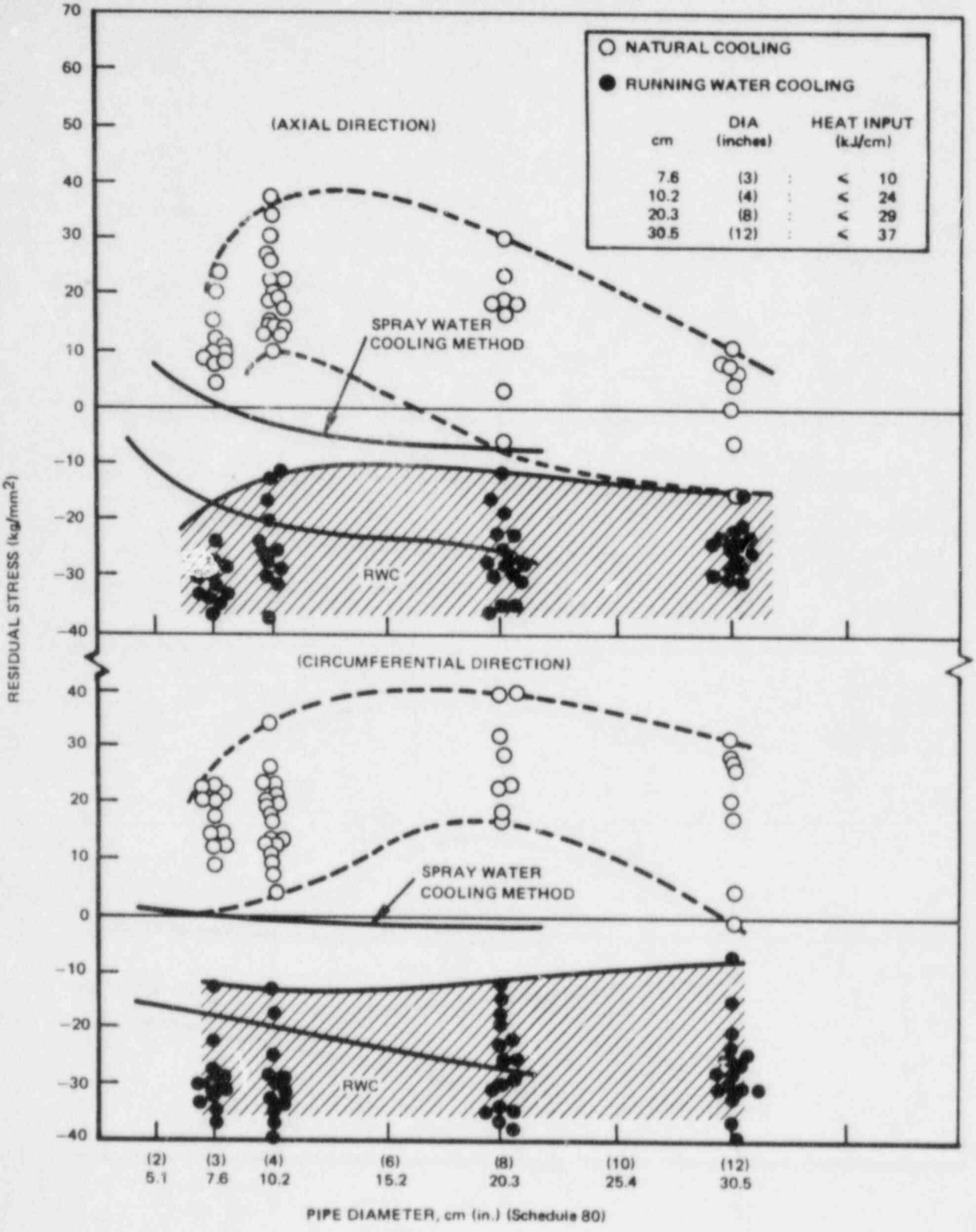

Figure 2. Effect of Welding Conditions on Residual Stress on the Inside Surface in HAZ of Welded Pipe. [7.6 cm (3 in.): GTAW, Other Sizes: SMAW]

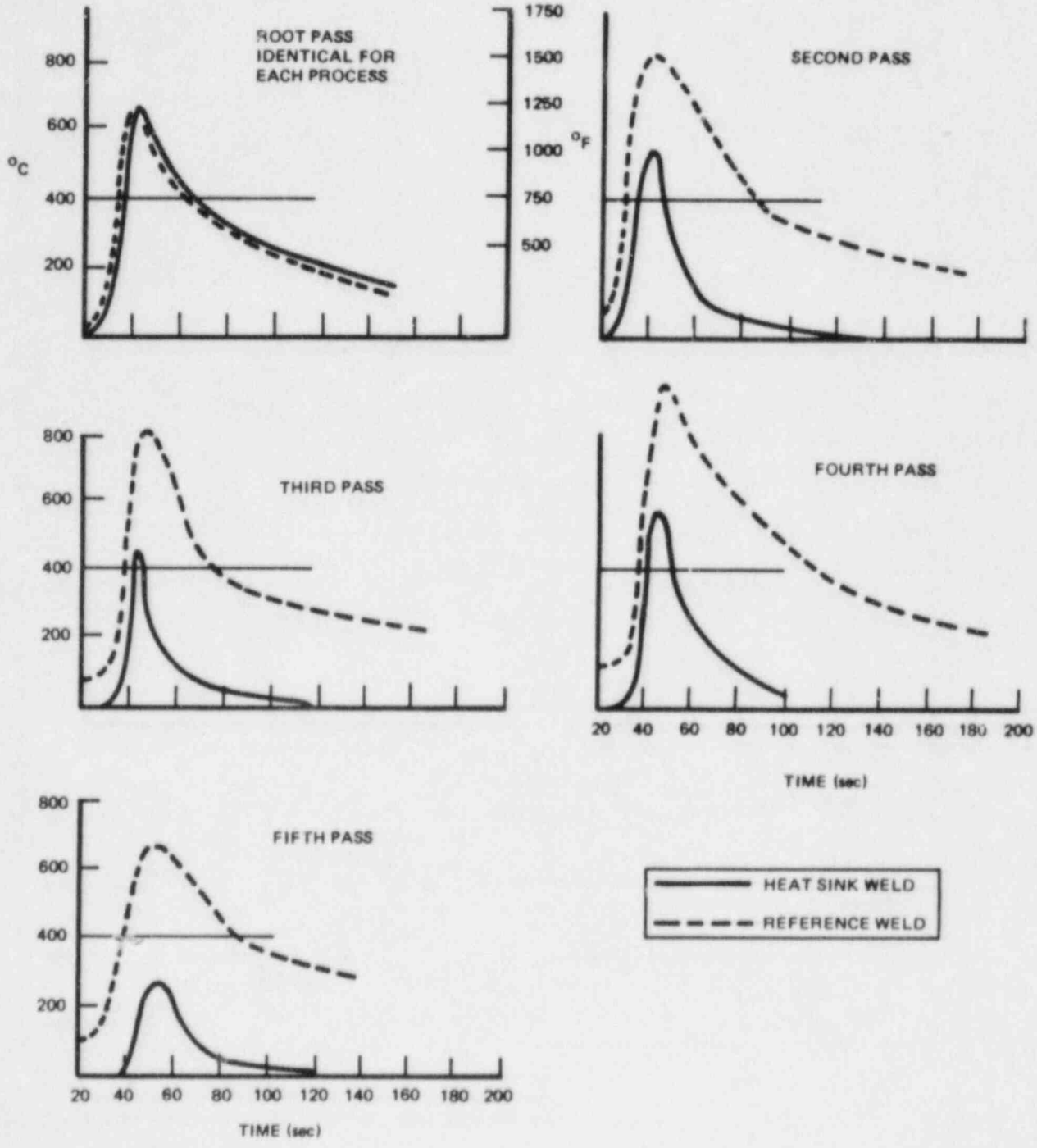

Figure 3. Time at Temperature Comparison of a Reference and Heat Sink Weld

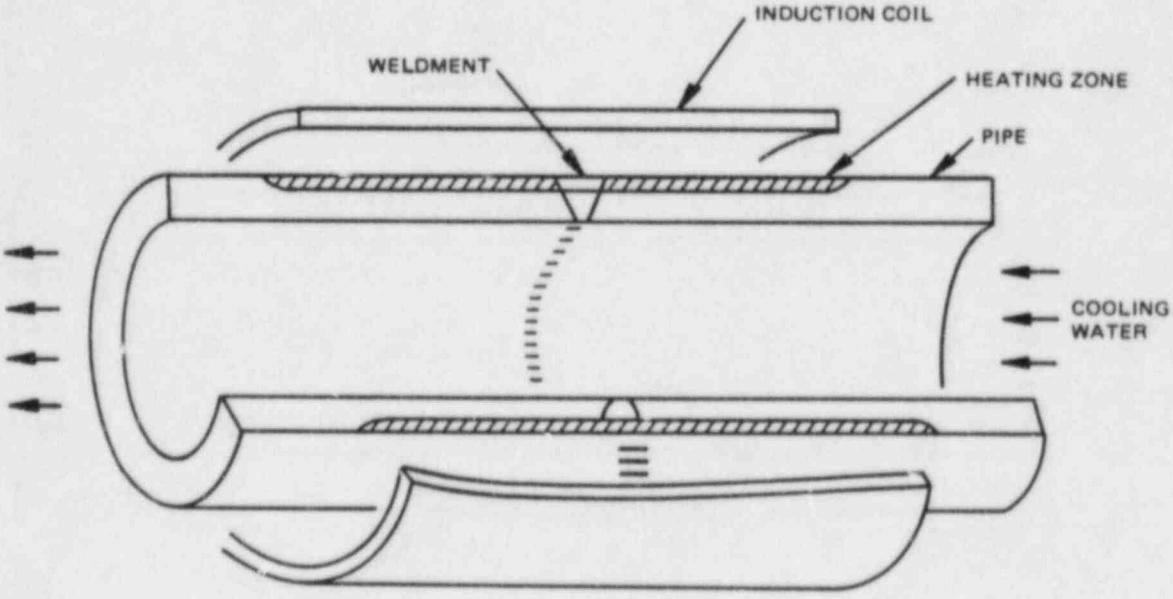

Figure 4. Outline of Heating and Cooling Process

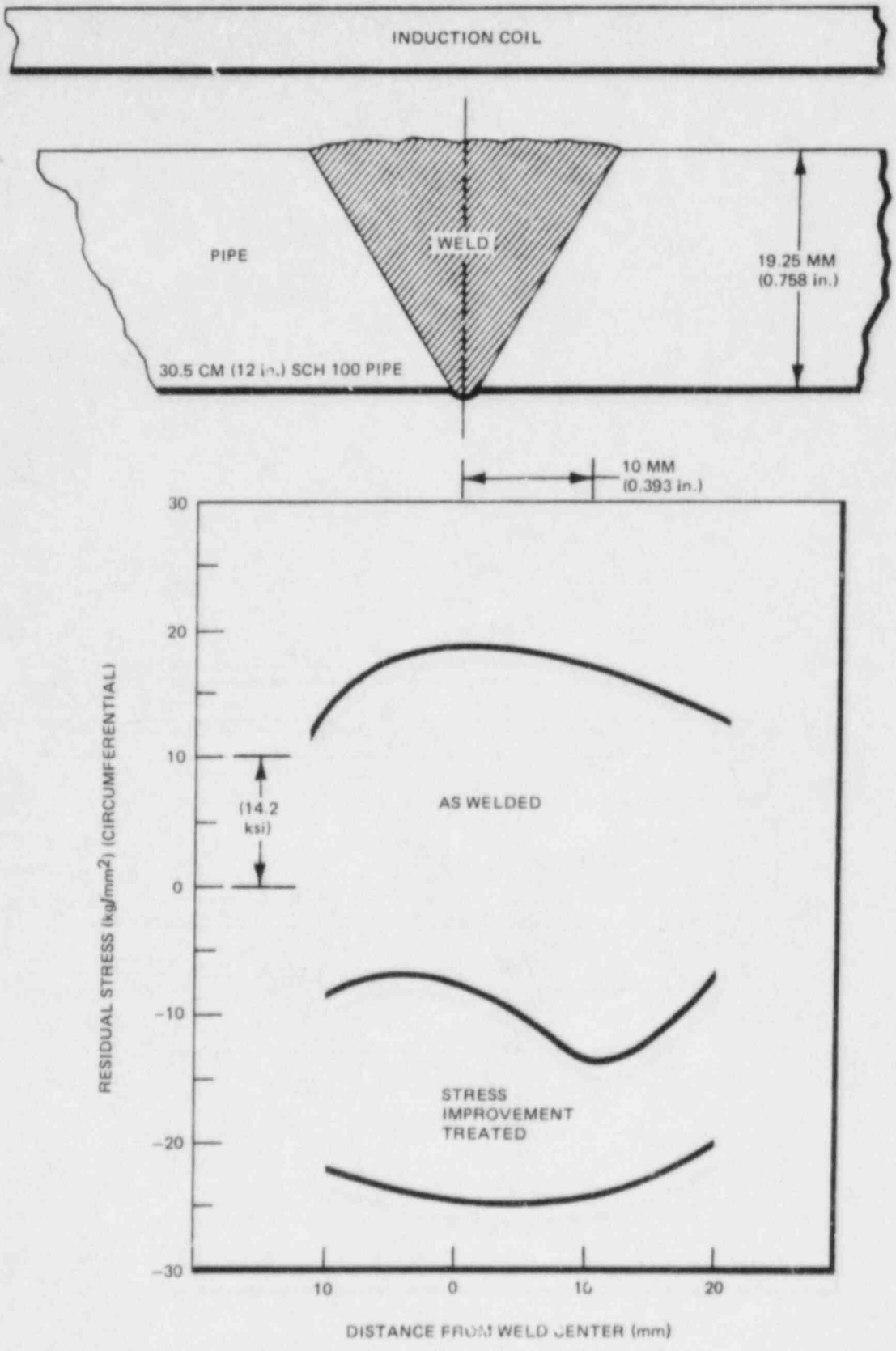

Figure 5. Residual Stress Comparison for IHSI

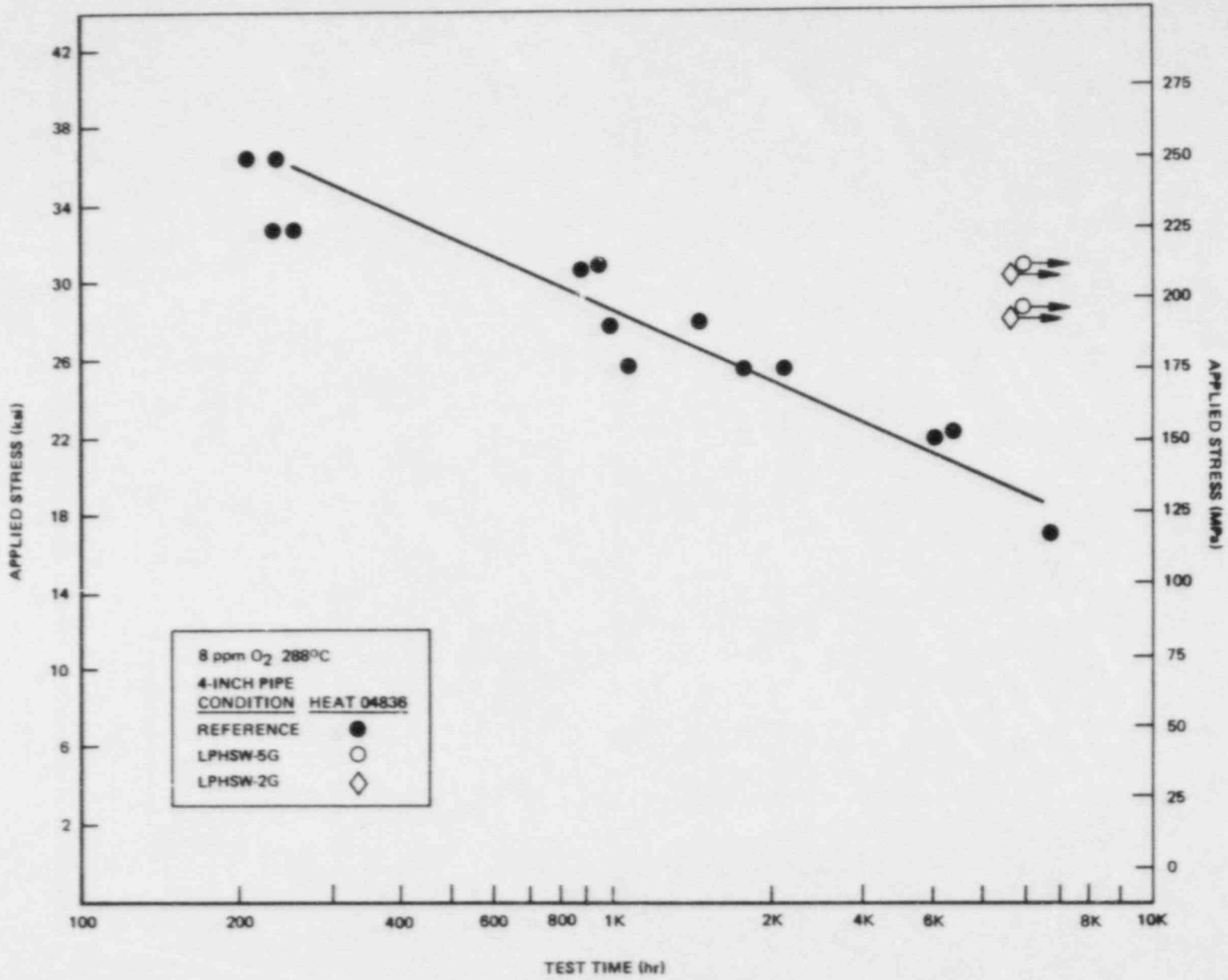

Figure 6. Comparison of LPHSW Pipe Tests with Reference Pipe Tests

THE MEASUREMENT OF EQUIPMENT DEGRADATION

Gary J. Toman

Franklin Research Center
Division of Arvin/Calspan
20th and Race Streets
Philadelphia, PA 19103

Abstract

All equipment deteriorates with time due to many stresses that act on any piece of equipment whether it is being stored, used, or lying dormant. Knowledge of the level and rate of deterioration is desirable to allow repair or replacement of equipment prior to failure or loss of adequate functional capability. Many of the traditional testing and surveillance techniques measure parameters of functional interest, but do not provide information relating to the actual deterioration that has occurred. This paper provides examples of techniques that may be used to evaluate indicators of deterioration and gives an example of evaluation of multiple types of data for a complex piece of equipment.

INTRODUCTION

All equipment degrades with time. From the time of manufacture to the time of removal from service, equipment is subjected to stresses that cause deterioration and wear. The stress may be expected or unexpected and may not have been considered and accounted for in the design and application of the equipment. If all stresses acting on a piece of equipment were known and measured continuously and a model existed for evaluation of the effects of the stresses, the deterioration of the equipment could be accurately assessed at any time. However, in most practical cases, all of the stresses are not fully identified, and an adequate deterioration model does not exist.

Since a precise theoretical model does not exist for accurately determining the level of deterioration, continuous or periodic measurement of the effects of deterioration is desirable for equipment that can affect the safety or operation of a nuclear plant. While qualified lifetimes have been established for safety-related equipment, the large uncertainty in existing models for accelerated aging, such as the Arrhenius thermal degradation model, the high probability of unexpected stresses occurring before or after installation of the equipment, and variations in the manufacture of the equipment combine so that the true life of any piece of equipment is not fully known. The actual life may be shorter or longer than that indicated by the qualification program. The equipment may be in service too long, thereby jeopardizing safety. Or, it may be replaced too soon, resulting in unnecessary replacement costs. In either case, a means of determining the level of deterioration is desirable.

MEASUREMENT OF DETERIORATION-INDICATING PARAMETERS

To assess equipment deterioration, a set of parameters which will indicate the level of deterioration must be determined, measured, and evaluated so that the ability of the equipment to continue to function can be estimated. The set of parameters may vary from one to very many, depending on the device being evaluated and the level of sophistication of our knowledge of the device and our test methods.

Figure 1 [1] provides a theoretical representation of the deterioration of functional capability with time. The solid curve represents functional capability. The dashed curves represent the values of equipment parameters that also degrade with time. The dashed curve to the right of the functional capability curve decays at a later time than the functional curve. Therefore, it is an unacceptable parameter to monitor since the function could be impaired before the indicator changed significantly. The dashed curve to the left of the functional capability curve represents an acceptable indicator since it changes in advance of the change in functional capability.

Many of the parameters presently used to measure nuclear plant equipment are unacceptable for estimating deterioration. This does not mean that they should be discontinued: they may provide data for other purposes. However, these tests often indicate significant changes in function only after serious deterioration has occurred. For example, the tests most often per- formed on electrical cable relate to the electrical characteristics of the insulation system. These tests relate to one key functional characteristic of the cable: the ability to insulate two or more different potential gradients from one another. However, for the present types of organically insulated cables used in nuclear plants, the electrical characteristics would probably not change until significant deterioration of the insulation system had occurred. This level of deterioration could be such that the insulation would not be able to withstand the environments associated with design basis events. As the cable degrades, the mechanical properties of the cable deteriorate first. Most often, the insulation hardens and eventually cracks. If electrical measurements are taken in a dry environment, no significant change of insulation resistance may occur, even when the insulation cracks, since dry air is a good insulator and other cables in the same cable tray may further insulate the deteriorated cable. However, if steam or spray were to impinge upon the insulation, it might fail and allow short circuits. Therefore, it would be desirable to measure the mechanical parameters of the cable insulation to determine the level of deterioration. Unfortunately at present, mechanical tests, such as elongation-at-break, are destructive in nature and are not easily implemented.

CONSTRAINTS FOR HARSH ENVIRONMENT EQUIPMENT

Those pieces of safety-related equipment that may be exposed to a harsh environment in a nuclear plant must be able to withstand an accident environment any time during their qualified life and remain capable of performing their safety function. In Figure 2 [1], the stresses acting on a device over time and the accumulated deterioration are shown. For harsh environment equipment, the ratio of normal environment deterioration (O-A) to the accident environment deterioration (A-B) is not well documented. In many cases, the normal life deterioration is expected to be less than the deterioration caused by the accident. Therefore, for harsh environment equipment, the change in condition during normal life may be very small and difficult to measure. Since only a small amount of deterioration may be allowed before the ability to withstand an accident environment is jeopardized, the criteria for acceptable and unacceptable deterioration must be revised. For example, in non-nuclear applications, a nearly total loss of resilience in gasket material for electrical compartments may be acceptable. However, in nuclear applications, partial loss of resilience coupled with deterioration from accident environments may result in contamination of electrical components with steam and chemical spray.

PRACTICAL DEGRADATION MEASUREMENT CONCEPTS

Ideally, degradation monitoring techniques should be:

- nondisruptive
- noninvasive
- repeatable
- accurate
- cost-effective

and should yield data that are comparable to a known deterioration reference.

Ideally, techniques should be nondisruptive. Interruption of operation should be minimized, since disconnection of wiring and piping equipment may result in a high probability of failure upon reconnection. The result of an

improper reconnection could be a loss or deterioration of functional capability, which is unacceptable. In addition, disassembly and reassembly is costly. Degradation measurement techniques should not require disconnection unless they are combined with other requirements.

The technique should also be noninvasive. It should avoid the need for opening of cavities or the disassembly or major modification of equipment. Again, disassembly and reassembly of equipment may be costly and may be performed improperly.

It should be recognized that while noninvasive and nondisruptive diagnostic measurements are desirable, they are not necessarily possible in all cases. An example of possible noninvasive, nondisruptive degradation measurements is that of tests for coil integrity on relays and solenoids. An example of a semi-nondisruptive test would be the measurement of transient and steady state currents. While at present such tests would require disconnection of coil leads, the test could be made nondisruptive by using the fuse clip associated with the coil for making the tests. A probe that would be inserted into the fuse clip could be used, which would require only removal of the fuse and would not require lifting of leads. A fully nondisruptive test method could entail use of infrared pyrometry or infrared photography for measurement of coil temperatures. An extremely hot coil could indicate breakdown of the insulation and impending failure. Another potential test method is that of measuring radio noise generated upon deenergization or energization of the coil. Radio noise detection techniques are used on high voltage equipment but are not commonly used on low voltage equipment.

Repeatability and accuracy of measurements are very important because degradation monitoring is a long-term process. Measurements may be taken at yearly or longer intervals; therefore, the procedure and equipment to be used must be precisely defined. Even methods using continuous monitoring will need precise techniques and procedures. The interpretation of the results should be clear-cut and require a minimum of judgment. The test technician or engineer should not have to rely on judgment or extensive experience to arrive at a conclusion. Since it is desirable to be able to measure low levels of deterioration, the accuracy of the test method and test equipment will be important. Noise in the test data may completely obscure the deterioration

information. All test methods for deterioration measurement should be cost-effective. In some cases, deterioration evaluation will be necessary regardless of cost because the equipment is safety-related, but ultimately it should be performed when it is cost-effective and yields results that improve operation and reduce costs to the plant.

APPLICATION OF DEGRADATION MONITORING TO A COMPLEX SYSTEM

A diesel engine and the associated generator for a nuclear plant are a complex interactive system. To monitor the condition of the system, multiple parameters must be evaluated. The diesel engine has a starting system, fuel supply system, lubrication system, cooling system, and many built-in monitoring devices. For the purpose of diesel engine monitoring, many sensors and sensor ports already exist. However, some of these sensors will have to be upgraded in type and quality, e.g., pressure switches may have to be replaced by transmitters. Since the diesel generator is complex, automated integration and analysis of the monitored data will be necessary to provide indication of present condition and impending problems. List 1 provides some of the parameters that should be included in a monitoring system. It should be noted that the diesel generator itself is a good transducer, and analysis of the voltage wave shape should provide data about misfiring and unbalance of the diesel system.

While the list of data to be monitored appears long, the complexity of the diesel and its importance should allow cost-effective use of an extensive monitoring system. List 2 shows the calculated diesel performance and condition measures that may be calculated from the monitored parameters. A dedicated computerized system could be used to monitor the condition of the diesel generator. Such a system would be comprised of sensors, a multiplexer, a timing and synchronizing circuit, a dynamic signal processor, a static signal processor, a computer, and display devices [2]. The inputs from the diesel monitoring devices would be analyzed and processed, results recorded, and alarms generated, as appropriate. Since the monitoring system for a diesel generator is complex, to make it work properly, algorithms must be devised that will allow the computer to analyze trends in data and to compare data and information to predefined limits. The development of the algorithms and the

LIST 1. MONITORABLE DIESEL PARAMETERS

- Temperature (exhaust ports, oil, fuel, intake air)
- Pressures (ambient air, intake manifold after turbocharger, lubricating oil, fuel, cooling water)
- Vibration (rocker box [valve] cover, engine block)
- Flow (fuel supply, fuel return, blowby, engine oil, air-intake)
- Crank shaft position (degrees)
- Shaft speed
- Electrical output (power, frequency, phase angle variation)

LIST 2. CALCULATED DIESEL PERFORMANCE/CONDITION MEASURES*

- Specific fuel consumption
- Coolant temperature rise
- Fuel temperature rise
- Blower pressure rise
- Blower performance
- Turbocharger performance
- Intercooler temperature
- Overall efficiency,
- Speed/instantaneous velocity performance
- Power fluctuations
- Turbocharger efficiencies
- Crankcase blowby flow rate
- Cylinder performances (comparison)
- Lube system performance
- Cooling system performance
- Water pump condition

*Measured parameters should be corrected to standard reference conditions.

limit criteria is probably the most expensive portion of the whole system. At least one project is presently underway to define the requirements for such an algorithm [3].

DETERIORATION REFERENCE DATA

As a minimum, an end of qualified life criterion is needed to evaluate the level of deterioration of a device; however, a deterioration data reference graph would be preferable. With such a plot, estimates of remaining and useful life could be estimated. To be able to develop an end of qualified life criterion, a relatively simple system may be employed. The device would be analyzed to determine the appropriate parameters to monitor. Baseline measurements would be made on a newly manufactured item. Then, the aging simulation that was performed during the qualification program for the device would be reperformed. Following the aging simulation, measurements would then be taken to determine the level of deterioration that has occurred. From these measurements, the end of life criterion would be developed. If a device had not deteriorated to the criterion level during normal service, it would be acceptable for an accident service condition. However, upon reaching the criterion level, the device would have to be replaced, since it no longer would be capable of performing continued normal service while retaining accident service capability.

The criteria that are derived from duplication of accelerated aging may have some uncertainty involved. For example, the true acceleration achieved by simulated aging is really a wide range rather than a fixed ratio.

To develop a reference plot for deterioration, a similar process would be performed; however, the aging simulation would be performed incrementally with deterioration measurements performed after each increment. A further refinement would be to take measurements of equipment condition from like equipment at plants of different ages. These could be plotted along with the results from the aging simulation to verify the adequacy of the aging simulation model and to further refine the data. It is recognized that this is no easy task in light of equipment and environmental variations.

CONCLUSIONS

Useful measurement techniques are possible to estimate deterioration. Unfortunately, few are in readily usable formats. Many of the functional tests presently performed are not suitable. The development of noninvasive, nondisruptive tests is possible for many devices. For some devices, such as diesel generators, integration of deterioration monitoring detection or indication devices into the equipment is quite possible. Development of criteria for end of qualified life limits is also possible, as is the development of deterioration reference plots. These criteria may be further refined through the use of data gathered from similar equipment of various ages in existing power plants.

REFERENCES

1. S. Ahmed, S. P. Carfagno, and G. J. Toman, "Inspection, Surveillance, and Monitoring of Electrical Equipment Inside Containment of Nuclear Power Plants - With Application to Electrical Cables," Oak Ridge National Laboratory for the U.S. Nuclear Regulatory Commission, NUREG/CR-4257, ORNL/Sub/83-28915/2, August 1985.

2. R. R. Holden, "Condition Monitoring Techniques for Electromechanical Equipment Used in Air Force Ground C^3I Systems," Rome Air Development Center, Report No. RADC-TR-83-180, August 1983.

3. R. H. Badgley, "A Knowledge Based System Approach to Improve Marine Diesel Engine Condition Assessment," Marine Engine Development, SP-625 Government/Industry Meeting Exposition, Society of Automotive Engineers, Warrendale, PA, May 1985.

Figure 1. Use of Functional Indicators for Condition Monitoring [1]

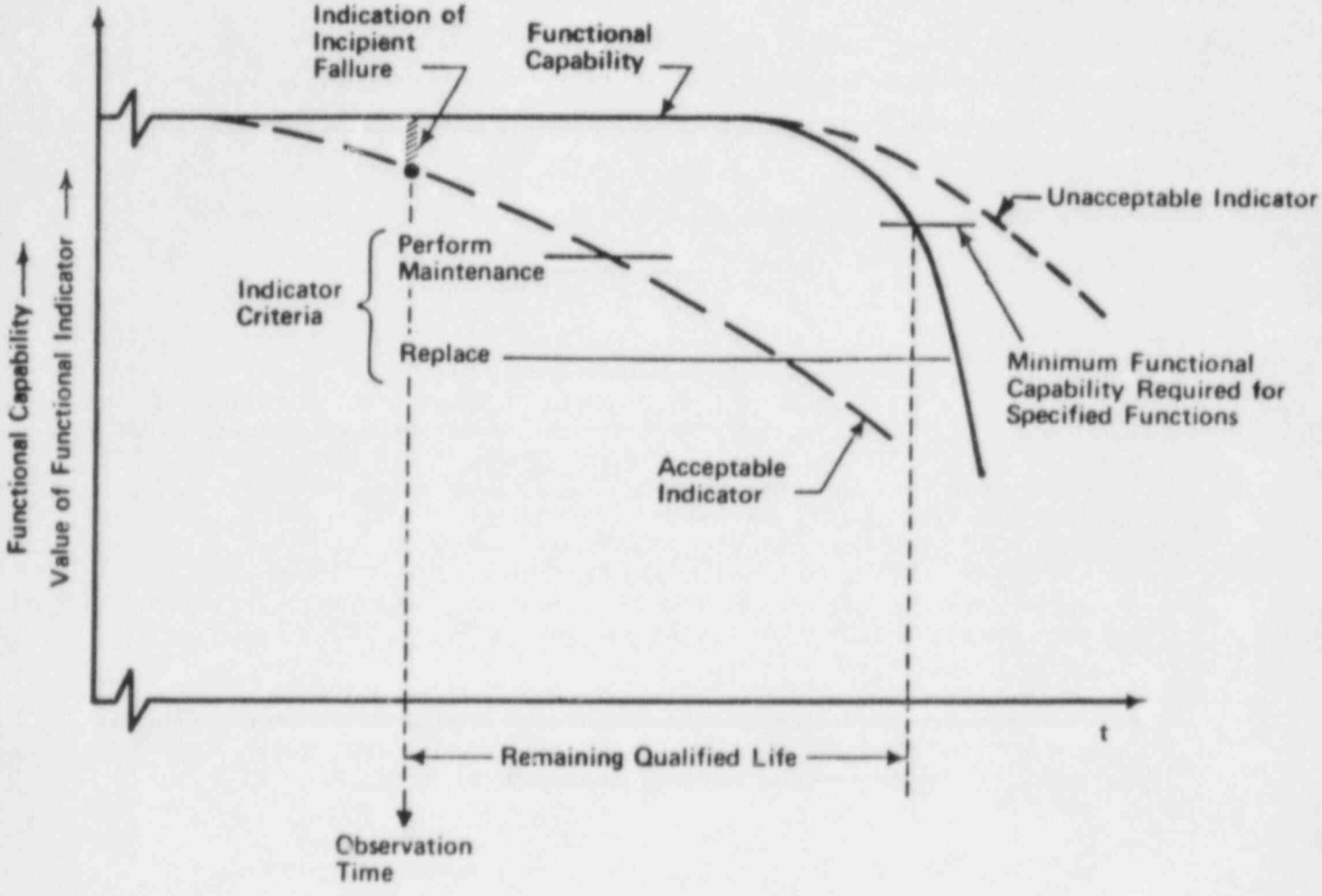

Figure 2. Accumulated Deterioration Related to Service and Design Basis Event (DBE) Stresses (Seismic, LOCA, MSLB) [1]

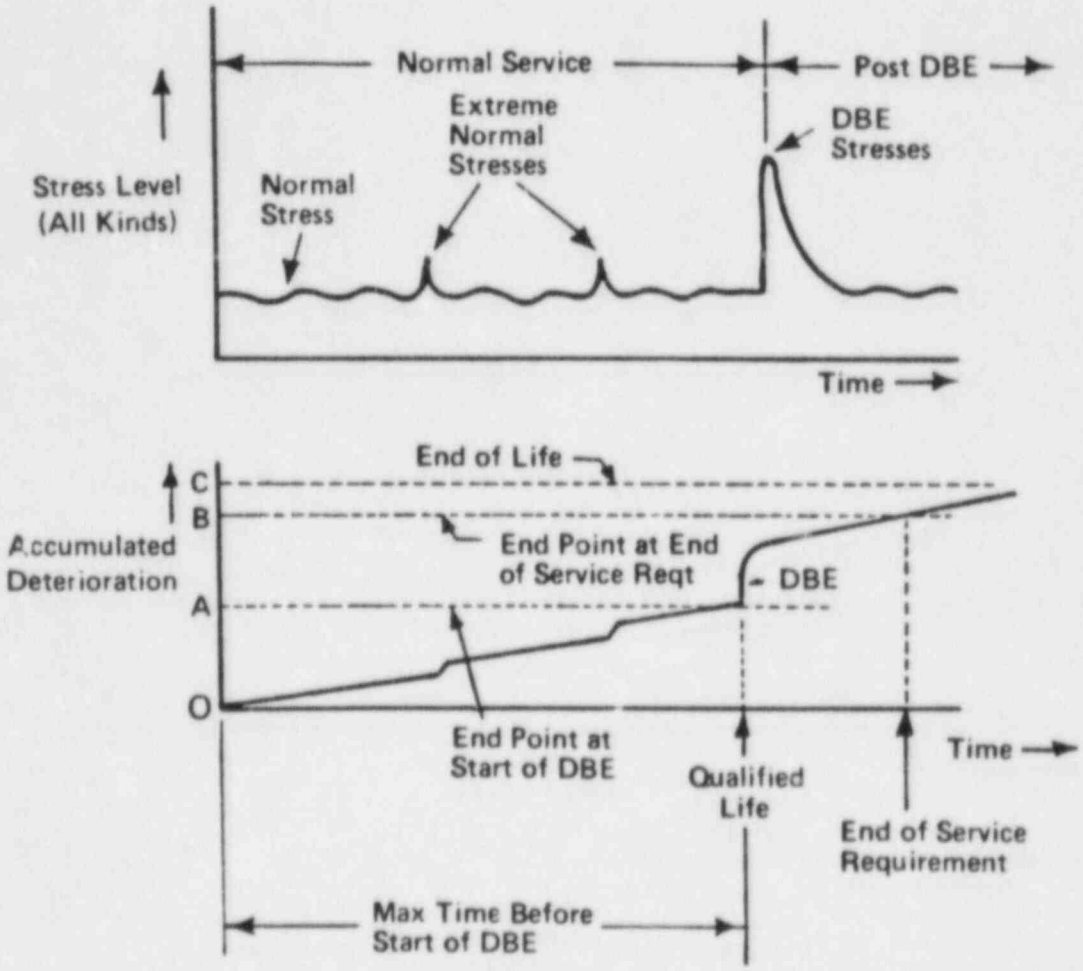

AN APPROACH TO EVALUATE THE SAFETY AND RISK IMPLICATIONS OF AGING

W. E. Vesely

Battelle's Columbus Laboratories
505 King Avenue
Columbus, Ohio 43201-2693

Arguments are made that to most directly evaluate the regulatory and research impacts of aging, the risk impacts of aging need to be directly quantified. An approach is presented to quantify the risks of aging using available data and present information. Both the relative effects of aging and the absolute time dependent effects are evaluated in the approach. The uncertainties associated with the results are also evaluated to show the maximum risk impacts of aging and to indicate where research can be directed to most effectively reduce the uncertainties.

INTRODUCTION

From a regulatory perspective, the importance of any aging which occurs at a nuclear power plant is directly tied to the risk and safety implications which arise from the aging. Aging is important if there are significant safety and risk implications and unimportant if there are no significant safety and risk implications.

An issue is whether from a risk and safety standpoint aging is a current problem or whether it can be an actual future problem. There are certainly evidences of component aging in current data but there are generally no direct implications on system unavailability increases or risk increases. Current probabilistic risk analyses (PRAs) and safety analyses do not evaluate the effects of aging. Some aging and sensitivity analyses have been performed but these only show how risks could change if input failure probabilities are assumed to change by some hypothetical amount.

In order to determine the risk and safety implications of aging phenomena, the aging phenomena which have been observed and which are projected to occur need to be translated into explicit risk and safety implications. Current PRAs and safety assessments do not show the explicit effects of aging because the current approaches do not, and were not meant to, explicitly consider aging. Aging, for example, could be causing significant risk effects which would not be identified by current PRA approaches and applications because of their limitations in this area.

Furthermore, the traditional time dependent approaches which utilize detailed time histories of failures to make inferences on aging are not applicable with available data (1), (2), (3). The FRANTIC II computer

code (4) has been developed to evaluate the risk effects of specific types of aging, however, the inputs required for FRANTIC II are generally not obtainable from available data.

Consequently, we believe that what is needed is a project whose objective is to quantify the risks of aging using to the maximum extent data that are available and information that can be presently obtained. By quantifying the risks of aging, that information and research will be focused upon which is key in relating aging characteristics to risk impacts.

Because of the present lack of knowledge, there can be large uncertainties associated with quantified estimates of the risk impacts due to aging. However, the uncertainties show the ramifications of our present state of knowledge. The upper bounds on the risks show how large the aging impacts can be with the information presently available. The dominant contributors to the aging uncertainties show where research can be directed to most effectively reduce the uncertainties.

RISK EVALUATIONS OF AGING PHENOMENA PROJECT

A project plan has been developed to address the problems of explicitly quantifying the risk effects of aging. The project has been named the Risk Evaluations of Aging Project or the REAP Project for short. The general objective of the REAP Project is to quantify the risk effects of aging. To accomplish this objective in a timely and logical manner, REAP has the following sub-objectives.

1. To quantify the relative contributions of aging mechanisms and aging causes to system unavailability. This will provide important insights in a short time frame and will help guide further research.

2. To develop models and approaches to quantify to varying degrees of accuracy and detail the time dependent risk effects of aging. This will provide models which in the near term will quantify the gross risk effects of aging and in the longer term will provide more detailed quantification for selected important areas.

3. To apply the developed time dependent models and approaches to systems and plants to quantify the risk and risk uncertainty effects from aging. This will identify the present and projected size of aging risk effects, the important contributors to aging risks, the size of aging risk uncertainties, and the important contributors to aging risk uncertainties. In the near term the approaches will be demonstrated on selected areas, and in the longer term comprehensive plant models will be evaluated.

The above sub-objectives are consistent with the broader objectives of the Nuclear Plant Aging Research (NPAR) Program (5) which include (1) identifying where in the plant and when in the plant's lifetime aging of components and systems is a risk and safety concern, and (2) identifying specific components and systems for which detailed engineering studies need to be performed on aging effects because of their potential risk and safety importance.

REAP OUTPUTS

It is planned that in the first phase of the REAP Project, relative contributions of aging to system unavailability will be evaluated, and time dependent models and approaches will be developed. The time dependent models and approaches will be demonstrated on selected components and systems. Aging related data will also be assembled and reviewed. In the second phase, comprehensive plant models will be evaluated for projected aging risk impacts to identify areas of regulatory and research importance. Models and data will also be extended for selected important areas.

Results will be produced on the risk implications of aging at different levels from component reliability effects to plant risk effects throughout the REAP Project. A high priority of the Project is to produce timely results to the NPAR Program to provide information for regulatory and research programs. Table 1 outlines the outputs which are planned to be obtained in the first phase from REAP. To provide the outputs in a timely manner and to be as efficient as possible, the REAP Project will utilize, to the maximum extent, already available models, data, and analyses. The evaluations of the relative effects of aging on system unavailability will utilize the data already collected in the NPAR Program and the Root Cause Data Program conducted by the Division of Risk Analysis and Operation (DRAO). The development of approaches and software to evaluate the risk effects of aging will modify and extend the approaches used in the FRANTIC II code. The evaluations of relative and time dependent aging effects will utilize the available plant fault tree and event tree models developed in the Accident Sequence Evaluation Program (ASEP) conducted by the DRAO.

REAP TASKS

The task definition and flow chart for the first phase of the REAP Project is shown in Table 2. During the first phase, three activities are planned to be carried out:

1. Evaluation of the Relative Effects of Component Aging on Component and System Unavailability

2. Development of Component Aging Reliability Models

3. Development of Approaches and Software to Evaluate the Plant Risks of Aging.

Table 1. Risk Evaluations of Aging Phenomena: First Phase Program Outputs

Outputs	Regulatory and Research Utility
1. Relative contributions of aging mechanisms and causes to component unavailability and system unavailability.	Relative percentages of component and system unavailability due to aging mechanisms will identify those areas where aging is an important contributor and can have large risk effects not shown by current analyses.
2. Quantitative models to evaluate the time dependent effects of aging on component reliability.	The models will include parsimonious models which do not require detailed, time dependent histories but can quantify the gross effects of aging. All the models will be able to be used in PRAs to evaluate time dependent risk effects of aging.
3. Quantitative approaches and software to evaluate the time dependent effects of aging on plant risks.	Approaches and software will be developed to quantify the time dependent effects of aging on system unavailability, safety function unavailability, accident sequence frequency, core melt frequency, and public health risks. The approaches will be able to utilize existing PRA fault tree models, event tree models, and minimal cut sets.
4. Demonstration of time dependent aging effects on system unavailability.	The time dependent impacts of aging on system unavailability will demonstrate the kinds of quantitative projections which can be made using available data and information. The results will show how aging effects can be bounded even with gross data and how the importance of contributors to aging and aging uncertainties can be identified.

Table 2. Risk Evaluations of Aging Phenomena: First Phase Tasks

Activity	Tasks			
1. Evaluation of the relative effects of aging.	Assemble available data.	Select system models to be evaluated.	Assemble algorithms and software to perform evaluations.	Calculate relative contributions of aging.
2. Development of component aging reliability models.	Develop linear damage models.	Develop nonlinear extensions.	Demonstrate models on selected components.	
3. Development of approaches and software to evaluate the plant risks of aging.	Develop linear and nonlinear aging algorithms.	Modify FRANTIC II to incorporate the algorithms.	Demonstrate the approaches in selected systems.	

As part of the modeling and development activities (Activities 2 and 3) specific applications will be carried out to demonstrate the research and regulatory utility of the approaches.

The first activity, Evaluation of the Relative Effects of Component Aging, consists of the following four tasks:

1.1 Assemble failure data. Fractional contributions of aging causes to component failures will be assembled from various data sources to form generic root cause fractions. The data sources will consist of data from the NPAR data projects and the Root Cause Program. Any significant plant specific deviations will be identified. Uncertainties for the root cause fractions will also be initially estimated. Standard PRA data will also be assembled (component failure rates, human error rates, etc.); the ASEP data base will be used as the basic PRA data base.

1.2 Select system models to be evaluated. The ASEP system models will be reviewed to identify the specific plant system models to be utilized. The cut sets for the system models will be identified for actual quantification purposes.

1.3 Assemble algorithms and software to perform evaluations. The root cause fraction approaches developed in the Root Cause Program will be extended to handle individual and joint contributions of different aging causes. The preliminary software developed in the Root Cause Program will be extended to handle the aging contribution calculations.

1.4 Calculate relative contributions of aging. The data, models, and software will be utilized to calculate the relative percentage contributions of aging causes to system unavailability. Initial calculations will be focused on simpler systems using grosser categorizations of aging causes to provide initial results. Figure 1 illustrates one type of relative information that will be obtainable.

The second activity, Development of Component Aging Reliability Models, consists of three tasks:

2.1 Develop linear damage models. Linear damage models will be reviewed and be applied to different aging mechanisms and to specific components. Competing cause analyses will be utilized to model the component failure rate contributions from different competing

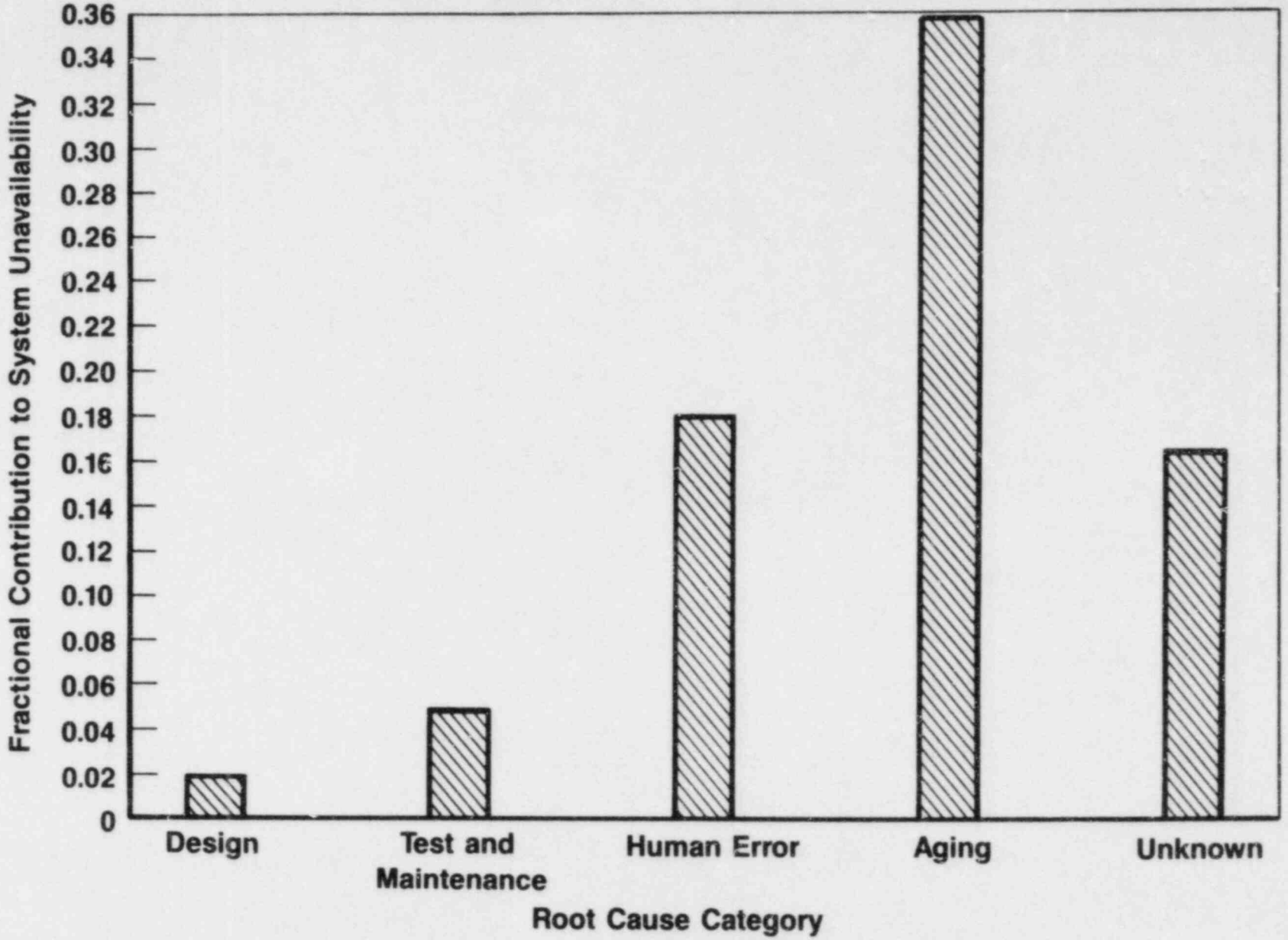

Figure 1. Example of Relative Contributions of Causes to System Unavailability

causes, both aging and non-aging related. Statistical techniques will be identified for estimating the rate of failure rate growth using available data on the relative contribution of aging causes and the average time (or cycles) of exposure to the aging mechanism. The techniques will allow gross bounds and engineering assessments to be utilized.

2.2 Develop nonlinear extensions. The linear damage models will be extended to nonlinear damage models by transforming the exposure time. The nonlinear models will allow the linear models to be statistically tested for their accuracy in representing experience data. Statistical techniques will be identified and developed for parameter estimation and testing.

2.3 Demonstrate the models on selected components. The aging models, particularly the linear aging models, will be demonstrated on specific components to show the time dependent unavailabilities and reliabilities which can be projected from current data and experience. The projections will include bounds and uncertainties to reflect current knowledge. Data requirements will be identified to most effectively improve the projections.

The third activity, Development of Approaches and Software to Evaluate the Plant Risks of Aging, has three tasks:

3.1 Develop linear and nonlinear aging algorithms. The linear damage and nonlinear damage models developed in the second activity will be translated into algorithms which can be incorporated into the FRANTIC II computer code. The specific changes required in FRANTIC II will be identified down to the detail of specific statements in the code which need to be modified.

3.2 Modify FRANTIC II to incorporate the algorithms. The FRANTIC II computer code will be modified to calculate the time dependent contributions from different aging causes using the linear or nonlinear damage models. The modifications will allow only certain components to be modeled as aging or will allow all components to be aging. Time dependent system unavailability, function unavailability, and core melt frequency will be able to be calculated. A user's manual will be developed for the modified code.

3.3 Demonstrate the approaches on selected systems. The modified FRANTIC II code will be utilized on specific system models in ASEP to demonstrate the time dependent

system unavailability projections which can be made using current data and experience. Methods for incorporating uncertainties into the evaluations will be described. Uses of the code to identify risk important areas and dominant contributors to aging and aging uncertainties will be described. Figure 2 illustrates one type of time dependent result that will be obtainable.

REAP INTERFACES

It is planned that the REAP Project will interface with a variety of other programs. First of all, as stated, the REAP Project will interface with the data analyses programs which have been conducted by the NPAR Program in that the data will be utilized in evaluating the risk effects of aging. The outputs from the REAP Project will in turn help to guide the other research activities in the NPAR Program (see the NPAR Program Plan NUREG-1144 for complete details).

With regard to interfaces external to the NPAR Program, as previously indicated, the REAP Project will utilize ASEP models in the plant evaluation of aging effects. The data from the Root Cause Data Program conducted by DRAO will be utilized as an important, additional data input to the evaluations performed in the REAP Project. The outputs from the REAP Project will be input to the Operational Safety Research Program, the Inspection Prioritization Program, and the Probabilistic Evaluation of Technical Specifications Program, all being conducted by DRAO.

A priority of the REAP Project is to communicate the results and regulatory implications to the Office of Nuclear Reactor Regulation (NRR) and the Office of Inspection and Enforcement (IE). Interfaces with the aging work being conducted by the Electric Power Research Institute (EPRI) and the utilities will also be pursued in the REAP Project.

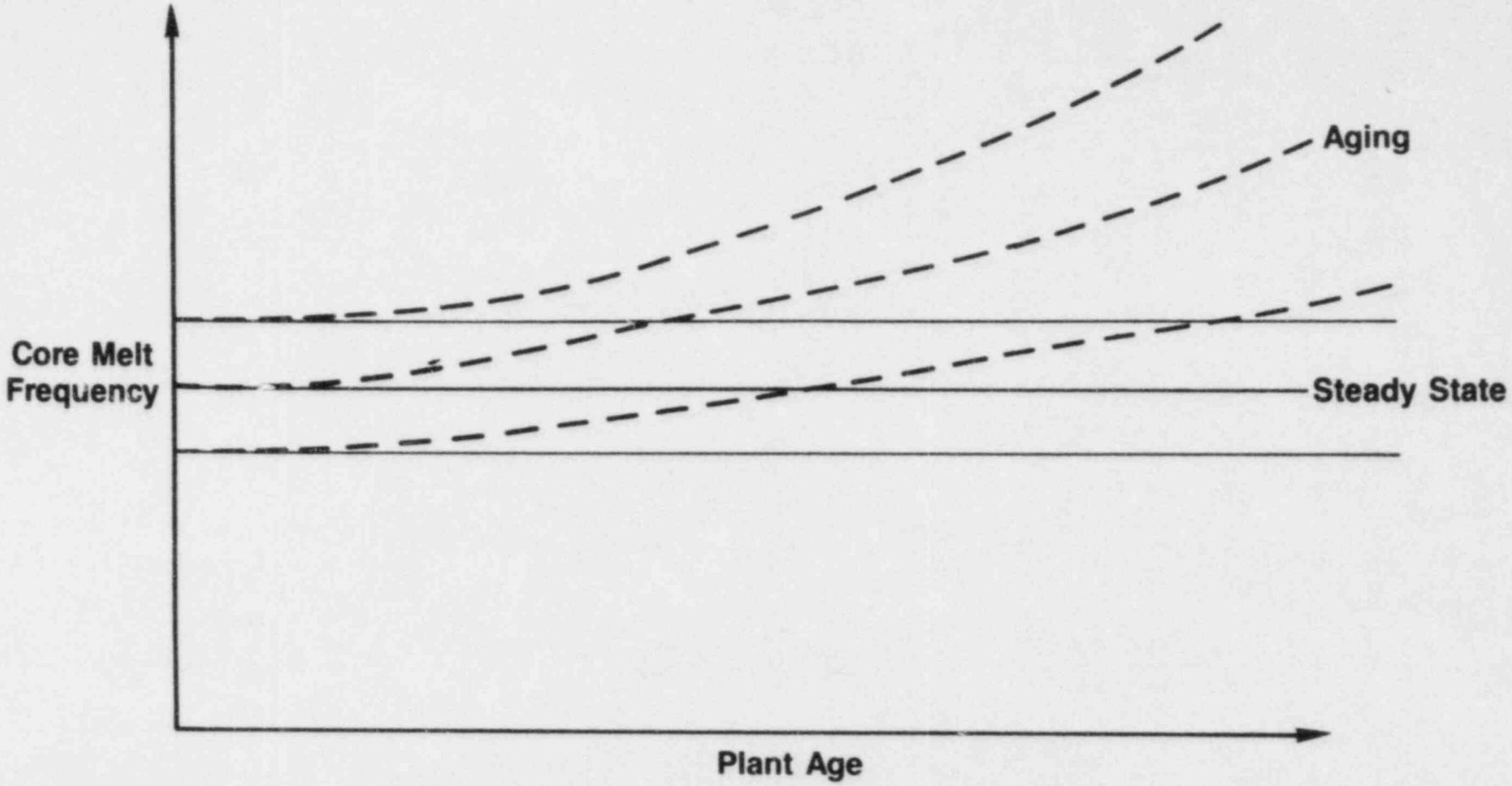

Figure 2. Illustration of Potential Aging Effects on Core Melt Frequency

REFERENCES

1. NUREG/CR-3543, "Survey of Operating Experience from LERS to Identify Aging Trends", January, 1984.

2. NUREG/CR-4156, "Operating Experience and Aging-Seismic Assessment of Electric Motors", Preliminary Report, December, 1984.

3. ORNL Draft Report, "Aging and Service Wear of Electric Motor-Operated Valves Used in Engineered Safety-Feature Systems of Nuclear Power Plants", March, 1985.

4. NUREG/CR-1924, "FRANTIC II - A Computer Code for Time-Dependent Unavailability Analysis", July, 1980.

5. NUREG-1144, "Nuclear Plant Aging Research (NPAR) Program Plan", July, 1985.

6. BCL Draft Report, "PRA Root Cause Evaluations", May, 1985.

IDENTIFICATION AND EVALUATION OF FACILITATION TECHNIQUES FOR DECOMMISSIONING LIGHT WATER POWER REACTORS

Prepared by

Thomas S. LaGuardia, PE

TLG Engineering, Inc.
640 Federal Road
Brookfield, CT 06804

ABSTRACT

This paper describes a study sponsored by the U.S. Nuclear Regulatory Commission to identify practical techniques to facilitate the decommissioning of nuclear power generating facilities. The objectives of these "facilitation techniques" are to reduce public/occupational exposure and/or reduce volumes of radioactive waste generated during the decommissioning process.

The paper presents the possible facilitation techniques identified during the study and discusses the corresponding facilitation of the decommissioning process. Techniques are categorized by their applicability of being implemented during the three stages of power reactor life: design/construction, operation, or decommissioning. Detailed cost-benefit analyses were performed for each technique to determine the anticipated exposure and/or radioactive waste reduction; the estimated cost for implementing each technique was then calculated. Finally, these techniques were ranked by their effectiveness to facilitate the decommissioning process.

This study is a portion of the NRC's evaluation of decommissioning policy and supports the modification of regulations pertaining to the decommissioning process. The findings can be used by the utilities in the planning and establishment of the activities to ensure all objectives of decommissioning will be achieved.

1.0 INTRODUCTION

1.1 BACKGROUND

All electric generating facilities must be retired from service and decommissioned at the end of their operating life. Over the next four decades the operating licenses of 81 U.S. commercial nuclear power plants will expire, leaving the owner utilities with the liability of ultimate disposition. The objective of decommissioning a nuclear power plant is to remove the facility from service in a safe manner while protecting the safety of the public and environment. This decommissioning process may include removal or isolation of radioactive materials so that the site can be released for unrestricted use, either by immediate dismantling of the facility or removal following a storage period. Consequently, decommissioning involves occupational radiation exposure and the generation of radioactive wastes.

The "Draft Generic Environmental Impact Statement on Decommissioning" (Ref. 1) indicated that an important aspect of planning for reactor decommissioning is to consider those techniques that minimize occupational or public exposure and/or radioactive waste volume. The proposed rule, "Decommissioning Criteria for Nuclear Facilities," (Ref. 2) will be followed by an NRC Regulatory Guide to recommend that the utilities identify the techniques they will use to facilitate the decommissioning of their stations at end of life. This study was performed to identify a number of decommissioning facilitation techniques and present them to the industry for consideration.

1.2 OBJECTIVE

The objective of this study is to provide practical recommendations to facilitate decommissioning of commercial light water power reactors by reducing occupational exposure and radioactive waste volume. These facilitation techniques are primarily addressed to decommissioning, but may also be implemented during design/construction or operations if they will ultimately benefit decommissioning. These recommendations identify how the techniques facilitate decommissioning while considering the effect of implementation on plant design, operations, present technology, safety and costs in all phases of power plant life. Attention was given to identifying techniques addressing specific dismantling activities incurring substantial occupational exposure and generating significant quantities of radio-

active waste volume. This study is part of the NRC re-evaluation of decommissioning policy and can be used as partial support for the modification of existing regulations pertaining to the decommissioning process. This study can also be used by utilities in their decommissioning planning to ensure all the objectives of decommissioning will be achieved. This program lists the identified facilitation techniques and methods to be considered in expanding and supplementing existing alternatives in the safe decommissioning of light water commercial power reactors at their end of life.

1.3 SCOPE

The scope of this study was limited to the decommissioning process as currently defined in U.S. NRC Regulatory Guide 1.86, "Termination of Operating Licenses for Nuclear Reactors," (Ref. 3) and consequently only addresses those activities involved in the disposition of the radioactive materials/equipment of a light water reactor facility. Therefore, the investigation does not address such areas as containment demolition or site reconstruction since these are beyond the scope of NRC jurisdiction.

The decommissioning process defined in Regulatory Guide 1.86 addressed four decommissioning alternatives: Prompt Removal/Dismantling, Mothballing, Entombment and Conversion. The recently published Proposed Rule on decommissioning now considers only three major classifications referred to as DECON, ENTOMB and SAFSTOR and defined as follows:

> DECON is the alternative in which the equipment, structures and portions of a facility and site containing radioactive contaminants are removed or decontaminated to a level that permits the property to be released for unrestricted use shortly after cessation of operations.
>
> SAFSTOR is the alternative in which the nuclear facility is placed and maintained in such condition that the nuclear facility can be safely stored and subsequently decontaminated (deferred decontamination) to levels that permit release for unrestricted use.
>
> ENTOMB is the alternative in which radioactive contaminants are encased in a structurally long-lived material, such as concrete. The entombed structure is appropriately maintained and

continued surveillance is carried out until the radioactivity decays to a level permitting unrestricted use of the property. This alternative would be allowable for nuclear facilities contaminated with relatively short-lived radionuclides such that all contaminants would decay to levels permissible for unrestricted use within a period on the order of 100 years.

The facilitation techniques identified in this study are applicable to any of the three decommissioning alternatives. However, the detailed results presented in this paper are for the DECON alternative.

The techniques described herein are applicable to commercial light water power reactors located in the United States. Applicability of these techniques to other nuclear facilities is not within the scope of this study and is not implied, but could be examined.

The basis for evaluation of most of these facilitation techniques is the reference PWR described in NUREG/CR-0130 (Ref. 4) and the reference BWR described in NUREG/CR-0672 (Ref. 5). Detailed evaluation of a technique to a specific nuclear power plant should be determined on a case by case basis using specific plant parameters.

Current practices used in operating power plants to maintain occupational exposures "as low as reasonably achievable (ALARA)" or "Volume Reduction (VR)" methods were considered to be routinely applicable to decommissioning and not included here. The techniques evaluated in this study were judged to be new concepts or logical extensions of existing concepts/methods specifically for decommissioning.

2.0 GENERAL METHODS OF TECHNIQUE IDENTIFICATION AND EVALUATION

This section presents a description of the approach used to identify, evaluate and determine the benefits (exposure and waste volume reduction) presented in the results of the study. It should be noted that the quantitative study results presented herein are specific to the characteristics of the reference PWR and BWR and therefore may not be realized at other than those units. The following methodology is also intended to present an evaluation model to be used for site-specific evaluations of techniques.

2.1 GENERAL METHODOLOGY AND APPROACH

The general method of approach for this study is presented in Figure 2.1-1, "Facilitation Technique Evaluation Program Methodology Flow Diagram." In general, the study involved four sequential phases, including:

- Identification and Categorization of Techniques
- Safety/Feasibility Evaluation of Techniques
- Cost Benefit Analyses
- Rating of Facilitation Techniques

The approach of the study was to focus on those dismantling activities that generated the greatest percentage of occupational exposure and waste generation. Based on these activities, techniques were identified that reduce exposure and/or waste volume when applied to those major activities and/or subactivities.

Lists of major activities for dismantling power reactors associated with the immediate dismantling alternative (DECON) were developed for both pressurized water and boiling water reactor types. These lists were generated from decommissioning activity lists provided in the PWR and BWR NUREG studies. Each activity from these studies was then examined in sufficient detail to identify the sources of occupational exposure and types or general quantities of radwaste being generated. This effort provided a preliminary activity performance baseline and also identified areas where potential techniques could be applied.

Table 2.1-1 (a and b) reiterates those lists of dismantling activities presented in the PWR and BWR studies. Those tables also include both the occupational exposure and waste volume generated during each of the dismantling activities. As seen from those tables, the PWR's major dismantling activity generating the largest

FIGURE 2.1-1

TECHNIQUE EVALUATION METHODOLOGY AND FLOW DIAGRAM

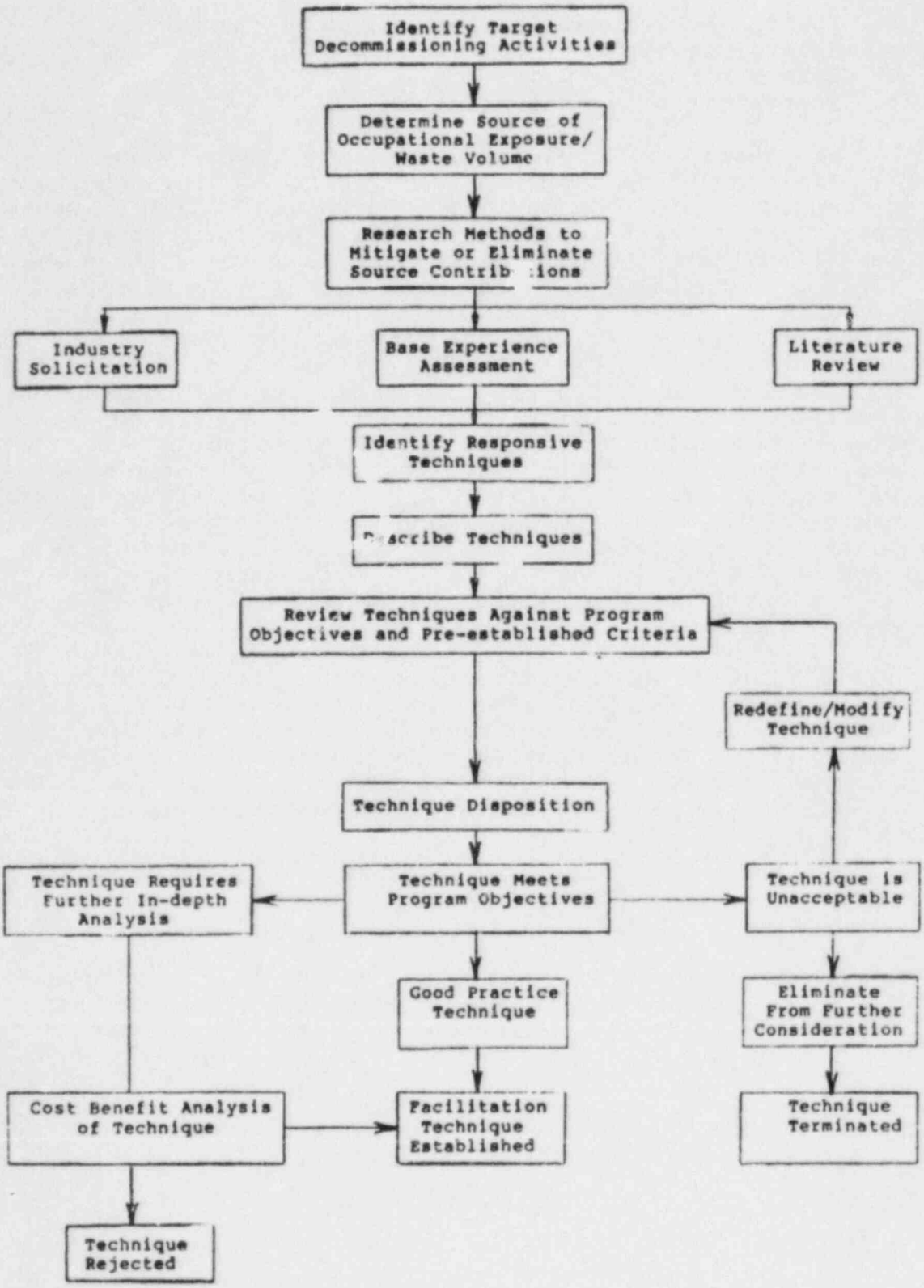

TABLE 2.1-1(a)
PWR DISMANTLING ACTIVITIES: EXPOSURE & WASTE VOLUME

Description	Occupational Radiation Exposure			Radioactive Waste Burial Volume		
	Estimated Total ManRem	% of Total	Ranking	Estimated Volume (ft3)	% of Total	Ranking
REACTOR BUILDING						
Move internals to refueling cavity; segment & load containers	100.4	9.1	3	8,000	1.4	12
Comprehensive predismantling radiation survey	9.0	0.8	17	NI		
Segment RPV and load containers	78.0	7.1	7	7,000	1.3	14
Segment steam generators (4) and prepare for shipment	144.0	13.1	2	21,362	3.5	5
Remove RCS pumps (4) and RCS piping	67.2	6.1	8	7,500	1.2	15
Remove pressurizer, relief tank, and safety injection system	64.8	5.9	9	8,000	1.4	12
Remove HX's and assorted pumps	28.8	2.6	12	400	<0.1	23
Remove contaminated internal structures (bioshield & reactor cavity liner)	81.0	7.3	6	73,600	12.1	3
Remove spray piping and ventilation system	11.5	1.0	16	3,840	0.9	16
Decontaminate remaining internal surfaces	5.8	0.5	23	640	0.1	22
Subtotal	590.5	53.6		132,742	22.8	
AUXILIARY BUILDING						
Remove electrical equipment	1.46	0.1	27	NI		
Decontamination (contact work & internal flushes)	12.6	1.1	15	896	0.1	21
Remove selected building internals & package (plugs/walls/platforms)	1.4	0.1	27	239,300	39.3	1
IX resin, filters removal	23.2	2.1	14	2,315	0.4	18
Remove IX and filters system piping	96.1	8.7	4	1,400	0.2	20
Remove tanks, pumps, and HX's	154.3	14.0	1	33,326	5.5	4
Remove HVAC and fire sprinkler systems and monorails	7.3	0.7	20	109,240	1.7	9
Subtotal	296.3	26.9		287,485	47.2	
FUEL BUILDING						
Remove CVC System	84.7	7.7	5	1,664	0.3	19
Remove condensate holding tank system	7.0	0.6	21	3,584	0.6	17
Remove new fuel storage racks and install electropolishing system	0.9	0.1	29	NI		
Remove boric acid system, tanks, & piping	34.2	3.1	10	12,928	2.1	8
Remove CCW system	4.3	0.4	25	18,176	3.0	6
Remove spent fuel racks, fuel transfer system & peripheral equipment	7.0	0.7	19	14,336	2.4	7
Remove SFP recirculation system, liners, & bldg contaminated concrete	8.0	0.7	18	119,226	19.6	2
Subtotal	146.9	13.3		169,914	28.9	
ANCILLARIES						
Comprehensive plant radiation survey	2.0	0.2	26	NI		
Special radiation surveys	6.3	0.6	22	NI		
RCS & CVCS chemical decontamination	26.4	2.4	13	9400	1.5	10
Decontamination (electropolishing) & disposal (packaging & shipping of contaminated equipment & debris)	4.6	0.4	24	Included above		
Packaging (combustible wastes)	29.2	2.6	11	10,125	1.7	10
Miscellaneous & contaminated concrete	170	15.7	1	369,192	58.3	1
Subtotal	68.5	6.2		19,525	3.2	
TOTAL FOR IMMEDIATE DISMANTLING	1102.2	100.0		609,666	100.0	

- - - - -

NI Not Included

( ) Includes only waste generated by the decontamination process only; equipment waste volumes & exposure given in appropriate systems

TABLE 2.1-1(b)
BWR DISMANTLING ACTIVITIES: EXPOSURE & WASTE VOLUME

Description	Occupational Radiation Exposure			Radioactive Waste Burial Volume		
	Estimated Total ManRem	% of Total	Ranking	Estimated Volume (ft3)	% of Total	Ranking
REACTOR BUILDING/PRIMARY CONTAINMENT						
Install HEPA Filters	3.4	0.2	29	(a)		
Comprehensive Radiation Survey	.5	<0.1	40	(a)		
Remove Dryer and Separator	8.0	0.4	24	5121	0.8	23
Drain Suppression Pool to Radwaste; Water-Jet Clean	2.3	0.1	32	(b)		
Remove & Ship Reactor Vessel Internals	100.5	5.4	8	7593	1.1	21
Drain Reactor Well Pool to Radwaste; Water-Jet Clean	0.3	<0.1	46	(b)		
Chemical Decon Reactor Water Recirculation & cleanup systems	7.1	0.4	25	(c)		
Clean up, Stage, & Shield Hot Spots in Primary Containment	0.154	0.4	23	(a)		
Enlarge Suppression Chamber Access	2.357	0.1	31	(d)		
Remove & Ship Reactor Vessel	32.6	1.8	12	17,693	2.6	14
Remove Primary Containment Piping & Equipment	193.887	10.5	5	50,975	8.8	4
Remove Sacrificial Shield & Radial Beams	79.789	4.3	9	31,889	4.8	7
Remove Contaminated Concrete from Primary Containment	16.439	0.9	17	11,053	1.7	20
Remove HVAC and Electrical Systems from Primary Containment	1.996	0.1	33	14,665	2.2	16
Drain Contaminated Systems to Radwaste	0.252	<0.1	47	(b)		
Chemical Decon Residual Heat Removal, Low- and High-Pressure Core Spray Systems	9.309	0.5	18	(c)		
Remove Reactor Building Piping	272.895	14.8	1	21,224	3.2	12
Drain Dryer and Separator Pool to Radwaste; Water-Jet Clean	0.517	<.1	39	(b)		
Chemical Decom Drain Systems	0.453	<.1	41	1,412	0.2	24
Drain Spent Fuel Pool to Radwaste; Water-Jet Clean	0.546	<.1	38	(b)		
Chemical Decon Fuel Pool Cooling & Cleanup System	0.364	<.1	44	(c)		
Remove Reactor Building Equipment	32.637	1.8	11	12,925	1.9	19
Remove Liners from Spent Fuel Pool, Reactor Well, and Dryer and Separator Pool	8.587	0.5	21	(b) 13,455	2.0	18
Remove Reactor Building Contaminated Concrete	19.274	1.0	15	15,326	2.3	15
Remove HVAC and Electrical Systems from Reactor Building	8.912	0.5	20	22,389	3.3	11
Final Radiation Survey	0.872	<0.1	49	(a)		
Subtotal (c,d)	891			233,728	34.9	
TURBINE GENERATOR BUILDING						
Install HEPA Filters	3.295	0.5	19	(a)		
Comprehensive Radiation Survey	0.199	<0.1	48	(a)		
Clean Up and Stage	0.856	<0.1	36	(a)		
Remove Turbine	8.432	0.5	22	49,252	7.4	5
Drain Contaminated Systems to Radwaste; Water-Jet Clean Condensate Storage Tanks	0.059	<0.1	52	(b)		
Remove Condenser	34.723	1.9	10	64,272	9.6	3
Drain Condenser to Radwaste; Water-Jet Clean	0.818	<0.1	54	1,412	0.2	24
Chemical Decon Drain System	0.326	<0.1	45	(c)		
Remove Piping	104.534	5.7	7	71,888	10.6	2
Remove Equipment	32.283	1.7	13	80,923	12.0	1
Remove Contaminated Concrete	1.938	0.1	34	7,593	1.1	21
Remove HVAC & Electrical Systems	8.425	<0.1	43	26,627	4.0	9
Final Radiation Survey	0.837	<0.1	53	(a)		
Subtotal (c,d)	193			308,667	44.9	
RADWASTE AND CONTROL BUILDING						
Comprehensive Radiation Survey	0.796	<0.1	37	(a)		
General Cleanup	2.368	0.1	30	(a)		
Chemical Decon Drain Systems	0.441	<0.1	42	1,413	0.2	24
Chemical Decon Equipment; Water-Jet Clean	18.824	1.0	15	(c)		
Remove Piping	248.742	13.5	2	18,717	2.8	13
Install Temporary Radwaste System	0.869	<0.1	50	(a)		
Remove Equipment	243.648	13.2	3	44,849	6.7	6
Remove Contaminated Concrete	7.991	<0.4	25	14,267	2.1	17
Remove Miscellaneous Steel Structures	0.888	<0.1	35	1,412	0.2	24
Remove HVAC & Electrical Systems	6.826	0.3	27	30,194	4.5	8
Final Radiation Survey	0.951	<0.1	51	(a)		
Subtotal (c,d)	530			110,852	16.6	
ANCILLARIES						
Operate Radwaste System	20.843	1.1	14	(c)		
Routine Radiation Surveys	6.352	0.3	28	(a)		
Package Dry Solid Wastes	38.881	2.1	11	23,943	3.6	10
Miscellaneous	165	8.9	5	NAP		
Subtotal (c,d)	231	12.5	4	23,943	3.6	
TOTAL FOR IMMEDIATE DISMANTLING	1,845	100.0		669,182	100	

(a) Small amount of waste generated from these activities included in Package dry solid waste activity.
(b) Wet solid waste accounted for in "Chemical Decon Drain Systems" task.
(c) All wet solid waste associated to DECON process is accounted for in "Radwaste/Control Building Remove Equipment" task.
(d) Contaminated concrete included in "Remove Reactor Building Contaminated Concrete" task.

occupational exposure and waste volume was the removal of contaminated concrete (Ancillary category). This activity contributed to approximately 15.7% and 58.3% of the total exposure and radioactive waste burial volume, respectively. For the BWR, the dismantling activity, "Removal of Reactor Building Piping," generated the greatest occupational exposure, while the dismantling activity, "Remove Turbine Building Equipment," generated the largest amount of radioactive waste. These two activities generated approximately 14.8% of occupational exposure and 12.0% of waste burial volume, respectively.

2.2 IDENTIFICATION AND CATEGORIZATION OF TECHNIQUES

Three methods were used to identify potential facilitation techniques. These included soliciting comments from the nuclear industry, performing a literature search and reviewing experience gained in past decommissioning projects.

Questionaires were used to solicit comments from over 250 individuals representing a wide cross-section of nuclear and related industries. These individuals represented major utilities, major architect-engineers, constructors, research and development facilities and consulting organizations within the United States and overseas.

Additional techniques were identified by reviewing specific literature addressing the subject of decommissioning, including government-sponsored reports, published papers, conference proceedings, research reports, actual decommissioning project reports and other related public documents.

Other potential techniques were developed by reviewing past decommissioning programs performed within the industry. One approach was to review planned dismantling activities versus actual dismantling activities in past programs and determine if variations indicated the use of any optimizing methodologies. When data were available, this information provided a reliable source to validate the technique's contribution to facilitate decommissioning.

Techniques identified from these initial investigations could be potentially implemented during any or all stages of plant life including design/construction, operation, and decommissioning.

The initial investigation produced a list of 104 techniques; these were then evaluated further for their feasibility, safety and contribution in reducing dose or waste volume.

2.3 SAFETY/FEASIBILITY EVALUATION OF TECHNIQUES

Each of the identified techniques were evaluated with regard to safety, feasibility and assurance that the objective of each technique was consistent with the goals of the study. Implementing scenarios were developed to maximize the benefits of each technique in reducing exposure and waste generation. This process clarified each technique and provided a baseline for a safety/feasibility review.

Review criteria were formulated to standardize the evaluation of all identified techniques. Table 2.3-1 presents a list of the review criteria and the aspects of each of the review criterion considered in the evaluation. Techniques failing identified safety criteria were not immediately rejected. An evaluation was first performed to determine if corrective action would alleviate or correct the concern, and if so the technique was revised and the evaluation process repeated.

The safety/feasibility review of the technique eliminated the nonviable techniques. An engineering assessment of the remaining techniques was then performed to objectively evaluate the practicality of their implementation.

The guidelines of this engineering assessment were:

- There should be a relatively high potential for implementation of the technique; i.e., the implementing technology should exist, a methodology identified and the applications exist.

- Techniques already recognized as standard industry practice would be consolidated into a general discussion or overview of current practices.

- Techniques identified for a common application would be assessed, with the potential for consolidation and redefinition of the objectives and technique(s).

TABLE 2.3-1
SAFETY/FEASIBILITY REVIEW CRITERIA

	Criteria Factors and Description
1	**Safety** Industrial safety (OSHA), fire, emergency evacuations, toxic/radioactive inhalation
2	**Engineered Safeguards** Protection of safety functions of affected engineered safeguard systems
3	**Seismic Design** (Seismic Category 1) Components, systems and structures must be protected to ensure safe shutdown of the reactor during a design basis earthquake
4	**Pipe Whip Restraints** Engineered safeguard systems must be protected from adjacent high energy (high pressure, temperature) piping in the event of a pipe rupture; pipe whip restraints must not be compromised by facilitation techniques
5	**Redundancy of Components** Engineered safeguard systems using redundant components as backup systems must not be compromised by facilitation techniques
6	**Separation of Components** Engineered safeguard systems located in separate cubicles or in separate parts of the facility must not be compromised by facilitation techniques
7	**Postulated Accidents** Facilitation techniques must not present potential accidents, nor increase the severity of postulated accident scenarios analyzed as part of the plant safety analysis for its operating license
8	**Security** Maintenance of plant security procedures, systems and barriers
9	**Accessibility** Potential interference to perform routine operation, maintenance and repair functions, and performance of preservice and inservice inspections

TABLE 2.3-1
(Continued)

Criteria	Factors	Description
10	**Material Handling**	Clearance interferences, obstructions, reduction in laydown space, material size restrictions, rigging problems and material removal rate reductions
11	**Decontamination**	Loss or reduction in ability to decontaminate structures, systems or components
12	**Durability**	Potential of degradation from radiation, temperature and humidity (normal operation and accidents)
13	**Material Compatibility**	Effect of substitution of materials on corrosion, surface finish, electrical conductivity, flamability and chemical reaction
14	**Portability**	Feasibility for rapid installation and removal to perform maintenance, repair or ultimate removal
15	**Component/Plant Capacity**	Effect on capacity of individual components or of overall plant

Using this safety/feasibility criteria, some of the initial techniques were eliminated for failing to meet an "acceptability criteria." Nineteen of the remaining techniques were then further examined in an attempt to quantify costs and benefits in terms of capital expense, occupational exposure, and waste volume.

2.4 DISPOSITION OF TECHNIQUES

These facilitation techniques were grouped into two categories: those being "Good Practice" techniques and those techniques supported by detailed cost benefit analyses.

Good Practice Facilitation Techniques:

> These techniques provided benefits that could not be quantified because of the generality of the technique. However, engineering judgment indicated that qualitative benefit could be obtained should the technique be implemented.

Facilitation Techniques Requiring Cost Benefit Analysis:

> These techniques required a detailed analysis to determine their viability. A detailed cost benefit analysis provided actual quantitative results, i.e., actual manRem and waste volume reductions.

These latter techniques were examined further using a cost benefit approach including the base case and the facilitation case. By definition, these cases are:

Base Case

> This case represents normal practice and/or techniques used to dismantle a nuclear facility. These base case techniques have been used or assumed in past decommissionings and therefore set a precedent for further application.

Facilitation Technique

> This case represents the application of the facilitation technique to the decommissioning process. These cases are scenarios where the technique is applied to the actual facility decommissioning.

The benefits of the techniques were determined by comparing the results (occupational exposure, waste volume generation) between the two cases.

2.5 RATING OF TECHNIQUES

The techniques were rated by their potential savings and costs associated with those savings. The initial investigation produced a list of 104 potential techniques. Of these, 68 were determined to actually facilitate the decommissioning process. Forty nine were then identified as Good Practice techniques, those not lending themselves to rigorous cost benefit evaluation but providing some benefit in reducing exposure or waste volume. The remaining 19 techniques required that detailed cost benefit analyses be performed to determine and quantify their potential benefits.

Table 2.5-1 presents the results of this study with a list, description and category (Good Practice or Cost Benefit) of all facilitation techniques identified. The cost benefit techniques were further ranked with respect to their contribution in reducing the overall occupational exposure, waste volume and cost.

TABLE 2.5-1

DISPOSITION OF FACILITATION TECHNIQUES FOR DECOMMISSIONING LIGHT WATER POWER REACTORS

Phase/Technique	Description	Good Practice	Cost Benefit
Decommissioning Phase			
Radiological Characterization	...to identify/locate extent of contamination for ALARA planning	*	
Segregation of Waste	...to minimize burial volume by controlled separation	*	
Magnets for Lifting	...to minimize exposure when removing contaminated components	*	
Prior Removal of Clean Components	...to control cross-contamination during dismantling process	*	
Urethane Foam/Spray Fixing	...of contaminated components to reduce exposure	*	
Segmenting under Negative Pressure	...to minimize airborne releases and subsequent contamination	*	
Post-Activity Debriefings	...to reduce exposure be preparing for efficient time management	*	
Mockup Testing/Training	...to reduce exposure during actual dismantling effort	*	
Nuclear Training Center	...to reduce both exposure and waste volume by prior practice	*	
On-Site Radiological Laboratory	...to expedite process of categorizing waste	*	
Mobile Shielded Work Stations	...to minimize exposure during removal activities	*	
Waste Compaction	...of small bore piping, conduit, cable trays		*
Railcar Casks	...for shipment of radwaste to burial ground		*
Homogenized Cask Shipments	...to optimize NSSS packaging for transport/burial		*
Cask Liner Geometry	...to optimize liner geometry/waste configuration		*
End of Life Decontamination	...of primary NSS system		*
Incineration	...of dry active radwaste during dismantling		*
Worker Training	...to reduce exposure during unique dismantling activities	*	*
On-site Decon Facility	...to process small contaminated equipment		*
Explosive Cutting	...of primary piping and components in high radiation areas		*
Intact Removal of Components	...for large contaminated components		*
Barge Shipment	...of all radioactive waste to burial		*
Robots	...for removal of highly activated concrete		*
Operations Phase			
Comprehensive Data Base	...to accurately record plant data necessary for decommissioning	*	
Segregation of Oil Bearing Waste	...to reduce damage to waste handling systems	*	
Maintain Storage Pools	...for future use as segmentation pools during dismantling	*	
Repassivation	...of decontaminated systems/components prior to return to service		*
Incineration	...of dry active waste during plant operation		*
Prepolishing of Components	...to minimize collection of radioactive crud in plant systems		*
Design & Construction Phase			
Construction Scale Models	...for clearances evaluation during removal of contaminated equipment	*	
Remote Sampling/Measuring	...to reduce exposure and improve time efficiency	*	
Sealed Nonporous Insulation	...to reduce contamination and subsequent waste volume	*	
Enclosed Cable Trays	...to reduce cable tray waste volume and incurred removal exposures	*	
Minimize Cable Trays in Contaminated Areas	...to minimize subsequent volume of radwaste	*	
Relocated Motor Control Centers	...to reduce waste by minimizing potential equipment contamination	*	
Sufficient Waste Storage Capacity	...to circumvent critical path items and facilitate waste removal	*	
Bolted Steel Construction	...to reduce exposure by decreasing disassembly time	*	
Quick Disconnect of Components	...to decrease disconnect time by using flanged/bolted connections	*	
Shearable Nuts and Bolts	...to reduce exposure by allowing for remote segmentation	*	
Non-Embedment of Pipes in Concrete	...to reduce removal and dismantling effort	*	
Removable Roof, Wall Panels/Plugs	...to improve access for removal of radioactive components	*	
Access to and into all Tanks	...to allow for decontamination by water lancing or entry	*	
Plant Breathing Air Supply System	...to increase worker efficiency and reduce time and exposures	*	
Pre-Installed Manipulator Structure	...to provide contamination-free access for a portion of reactor removal	*	
Lifting Lugs on Large Components	...to expedite rigging time and reduce exposures	*	
Anchor Points for Lifts	...to reduce exposure time spent rigging for component removal	*	
Tracks for Remote Cutting Devices	...to reduce exposure incurred in dismantling of activated components	*	
Preplaced Core Samples	...to minimize exposures during characterization of activated concrete	*	
Complete Drainage Capacity	...to reduce exposures by eliminating crud traps	*	
Canal Gate	...to segregate reactor cavity and refueling canal for segmentation		*
Comprehensive Data Base	...to accurately record plant data necessary for decommissioning		*
Containment of Liquids	...to minimize spread of contamination	*	*
Preplaced Blast Holes	...for future demolition of bioshield concrete		*
Smooth and Coat Concrete	...to minimize penetration of contamination		*
Substitute/Purify Materials	...to minimize NSSS activation products		*
Modular Biological Shield	...to optimize removal of activated material		*

GP (Good Practice) facilitation techniques, by definition, are activities that, when implemented, will provide positive benefits in reducing either occupational exposures or burial waste volume.

3.0 SUMMARY OF RESULTS

In total, 68 techniques were identified as methods of facilitating reactor decommissioning. The majority of these facilitation techniques were applicable during the design/construction or decommissioning phases of plant life. The actual distribution of techniques between the decommissioning, operations and design/construction stages were 24, 6 and 38, respectively.

3.1 GOOD PRACTICE TECHNIQUES

A majority of the 68 techniques were categorized as Good Practice. Table 3.1-1 presents a compilation of these Good Practice facilitation techniques for each reactor life stage. The Good Practice techiques were accepted based on one or more of the following rationale:

- Technique or generic methodology had been shown successful in past applications at facilitating the decommissioning process with respect to the goals as defined for this program

- Technique had been recommended as a corrective action or as a process enhancement as a result of previous decommissioning programs

- Technique had indisputable potential, the magnitude of the return being dependent upon the extent of application.

Actual benefits (exposure, waste volume and cost reduction) were not determined because of each technique's wide application on a site-specific basis. However, some positive benefit would generally be achieved when applying these techniques to a particular site.

Although actual benefits could not accurately be determined, these techniques were rated using the relative rating system described in earlier. In summary, this relative rating system is delineated as follows:

TABLE 3.1-1

GOOD PRACTICE TECHNIQUE RATINGS

Phase/Technique	Description	Good Practice Ratings			
		Exposure	Waste	Cost	Overall
Decommissioning Phase					
Radiological Characterization	...to identify/locate extent of contamination for ALARA planning	+1	+1	-1	+1
Segregation of Waste	...to minimize burial volume by controlled separation	-1	+1	-1	-1
Magnets for Lifting	...to minimize exposure when removing contaminated components	+1	0	-1	0
Prior Removal of Clean Components	...to control cross-contamination during dismantling process	-1	+1	0	0
Urethane Foam/Spray Fixing	...of contaminated components to reduce exposure	+1	0	0	+1
Segmenting under Negative Pressure	...to minimize airborne releases and subsequent contamination	+1	+1	0	+2
Post-Activity Debriefings	...to reduce exposure be preparing for efficient time management	+1	+1	0	+2
Mockup Testing/Training	...to reduce exposure during actual dismantling effort	+2	0	-1	+1
Nuclear Training Center	...to reduce both exposure and waste volume by prior practice	+1	+1	-2	0
On-Site Radiological Laboratory	...to expedite process of categorizing waste	0	+1	0	+1
Mobile Shielded Work Stations	...to minimize exposure during removal activities	+2	0	-1	+1
Worker Training	...to reduce exposure during unique dismantling activities	+1	+1	-1	+1
Operations Phase					
Comprehensive Data Base	...to accurately record plant data necessary for decommissioning	+1	+1	0	+2
Segregation of Oil Bearing Waste	...to reduce damage to waste handling systems	0	0	0	0
Maintain Storage Pools	...for future use as segmentation pools during dismantling	+1	0	-1	0
Design & Construction Phase					
Construction Scale Models	...for clearances evaluation during removal of contaminated equipment	0	0	-2	-2
Remote Sampling/Measuring	...to reduce exposure and improve time efficiency	+1	0	-1	0
Sealed Nonporous Insulation	...to reduce contamination and subsequent waste volume	+1	+2	-1	+2
Enclosed Cable Trays	...to reduce cable tray waste volume and incurred removal exposures	+1	+1	-1	+1
Minimize Cable Trays in Contaminated Areas	...to minimize subsequent volume of radwaste	+1	+1	0	+2
Relocated Motor Control Centers	...to reduce waste by minimizing potential equipment contamination	+1	+1	0	+2
Sufficient Waste Storage Capacity	...to circumvent critical path items and facilitate waste removal	0	0	+1	+1
Bolted Steel Construction	...to reduce exposure by decreasing disassembly time	+1	0	0	+1
Quick Disconnect of Components	...to decrease disconnect time by using flanged/bolted connections	+2	0	-1	+1
Shearable Nuts and Bolts	...to reduce exposure by allowing for remote segmentation	+1	0	+1	+2
Non-Embedment of Pipes in Concrete	...to reduce removal and dismantling effort	+1	0	+1	+2
Removable Roof, Wall Panels/Plugs	...to improve access for removal of radioactive components	+1	0	0	+1
Access to and into all Tanks	...to allow for decontamination by water lancing or entry	+1	0	0	+1
Plant Breathing Air Supply System	...to increase worker efficiency and reduce time and exposures	+1	0	0	+1
Pre-Installed Manipulator Structure	...to provide contamination-free access for partial reactor removal	+2	0	0	+2
Lifting Lugs on Large Components	...to expedite rigging time and reduce exposures	+1	0	0	+1
Anchor Points for Lifts	...to reduce exposure time spent rigging for component removal	+1	0	0	+1
Tracks for Remote Cutting Devices	...to reduce exposure incurred in dismantling of activated components	2	0	0	+2
Preplaced Core Samples	...to minimize exposures when characterizing activated concrete	1	0	0	+1
Complete Drainage Capacity	...to reduce exposures by eliminating crud traps	1	0	0	+1
Containment of Liquids	...to minimize spread of contamination	1	1	0	+2

Rating	Description
2	Technique provides positive contribution to facilitating decommissioning process by reduction of occupational exposure
1	Technique provides positive contribution to facilitating decommissioning process by reduction of waste burial volume
0	Technique provides no contribution to reducing occupational exposure or waste volume
-1	Technique proides negative benefits to reducing burial volume
-2	Technique, if implemented, would result in increased occupational exposure

3.2 COST BENEFIT ANALYSES

The remaining 19 facilitation techniques were accepted on the basis of detailed cost benefit analyses. Table 3.2-1 presents a compiled summary of the results of each evaluation identifying the net exposure and waste reduction and the cost associated with achieving those reductions. The results presented in this table are based on the scope of the facilitation technique and its applicability to the reference PWR and BWR stations. For each facilitation technique, the following information is provided.

1 Reactor Type

The reactor type identifies either light water PWR or BWR for their applicable results. The "General" classification is assigned when evaluation results are similar for either PWR or BWR within the range of analysis accuracy.

2 Exposure Reduction

The exposure reduction category presents the manRem reduction achieved for a particular technique when applied to the reference reactor type. Note that parentheses ( ) indicate negative exposure reduction (increase in exposure) when implementing the technique.

TABLE 3.2-1

QUANTITATIVE RESULTS OF FACILITATION TECHNIQUES

Technique	Reactor Type	Occupational Exposure Impact: Exposure Reduction (manRem)	Occupational Exposure Impact: % of Event Exposure Reduction (%)	Occupational Exposure Impact: Cost per mR Saved ($)	Occupational Exposure Impact: % of Total Exposure Reduction (%)	Radioactive Waste Volume Impact: Waste Volume Reduction (cu ft)	Radioactive Waste Volume Impact: % of Event Burial Vol. Reduction (%)	Radioactive Waste Volume Impact: Cost per Cubic Foot Saved ($)	Radioactive Waste Volume Impact: % Reduction of Total Burial Vol. (%)
Decommissioning Phase									
Waste Compaction	General	15	61	(86,880)	1.2	40475	68	(32)	6.6
Railcar Casks	PWR	negligible	-	-	<0.1	3080	77	(1894)	0.5
Homogenized Shipments	PWR	<10	<1		<0.1	2380	45	(590)	0.4
	BWR	<10	<1		<0.1	4781	33	35	0.8
Cask Liner Geometry	PWR	(8)	(4)	(115,615)	(0.6)	5580	30	(162)	0.9
End of Life Decon	PWR	3484	89	330	68	(4700)	12	245	(0.8)
	BWR	4453	89	521	66	(11299)	132	205	(1.8)
Incineration	PWR	(1)	(255)	(66,000)	(<0.1)	9170	91	(8)	1.5
	BWR	(2)	(410)	(670,000)	(0.1)	21680	90	(62)	3.6
Decon Facility	General	(21)	100	46,590	(1.7)	7480	90	397	1.2
Explosive Cutting	General	135	33	954	10.6	negligible	<1	-	-
Intact Removal	General	474	83	115	37.3	1398	11	39	0.2
Barge Shipment	PWR	242	53	(16601)	19.0	8437	17	(476)	1.4
	BWR	121	16	2923	6.9	9630	10	37	1.6
Robots	PWR	14	100	7104	1.1	negligible	<1	-	-
	BWR	46	100	2274	2.6	negligible	<1	-	-
Operations Phase									
Repassivation	General	30	20	753	2.4	(83)	(23)	(274)	<0.1
Incineration	General	(2)	(89)	(93,811)	(<0.1)	7239	93	21	1.2
Preoperational Electropolishing	General	17	20	(837)	1.0				
Design & Construction									
Canal Gate	PWR	53	17	(2244)	4.2	620	(4)	(192)	
Liquids Containment	General	<10	10	25,000	10	390	10	135	10
Blast Holes	PWR	72	100	(163)	5.7	negligible	<1	-	-
	BWR	160	100	(164)	9.1	negligible	<1	-	-
Smooth/Coat Concrete	General	(36)	(117)	(5151)	(2.8)	3000	77	(6)	0.5
Substitute/Purify	General	16	6	60340	(1.3)	612	7	1530	0.1
Modular Biological Shield	PWR					11,300	73	(35)	1.9

3 Percent of Event ManRem Exposure

This category represents the percent reduction in manRem exposure.

4 Percent of Total ManRem Exposure

This category represents percent reduction or increase to total manRem exposure incurred during base case dismantling activities. Total base case exposure estimates were taken as 1271 and 1764 manRem, as identified in the reference PWR or BWR studies. These estimates are exclusive of exposure incurred during discharge and shipment of fuel.

5 Cost Per ManRem Saved

This category identifies cost per manRem for implementing a technique to achieve net exposure reduction. Parentheses indicate reduction in cost for the technique used. Costs presented represent all cost elements (labor, materials, packaging, shipping and burial fees) associated with implementing a technique.

6 Volume Reduction

This category identifies the total reduction in radioactive waste burial volume (cu ft). Parentheses indicate increase in burial waste volume.

7 Percent of Event Volume Reduction

This category represents percentage of burial volume reduction achieved over the base case event if the technique is used.

8 Percent of Total Burial Volume

This category represents the percent of reduction in burial volume to the base case burial volume generated during an entire decommissioning project. The total burial volume values of 609,853 and 616,228 cu ft where taken from the reference PWR and BWR studies, respectively.

9 Cost Per Cubic Foot Saved

This category identifies the cost, on a per cubic foot saved basis, to implement a particular technique. The parentheses indicate reduction in cost if the technique were implemented.

The reviewer should keep in mind that the results presented here are specific to the scope of the facilitation technique and the site characteristics of the referenced station. These results will vary on a plant basis and with any change in the scope of technique application. Each of the techniques presented has the potential of providing additional benefits but should be reviewed on a site-specific basis to make that determination.

3.3 RESULTS OF TECHNIQUE RANKING

Detailed cost benefit analysis provided the basis for the ranking of techniques to reduce the overall occupational exposure, waste volume and cost. Table 3.3-1 presents the results of the ranking of all cost benefit techniques.

TABLE 3.3-1

COST BENEFIT TECHNIQUE RANKINGS

Phase/Technique	Description	Good Practice Rankings		
		Exposure	Waste	Cost
Decommissioning Phase				
Waste Compaction	...of small bore piping, conduit, cable trays	6	1	3
Railcar Casks	...for shipment of radwaste to burial ground	8	7	1
Homogenized Cask Shipments	...to optimize NSSS packaging for transport/burial	8	6	6
Cask Liner Geometry	...to optimize liner geometry/waste configuration	10	5	5
End of Life Decontamination	...of primary NSS system	1	11	11
Incineration	...of dry active radwaste during dismantling	9	2	7
On-site Decon Facility	...to process small contaminated equipment	11	4	4
Explosive Cutting	...of primary piping and components in high radiation areas	4	10	8
Intact Removal of Components	...for large contaminated components	2	8	9
Barge Shipment	...of all radioactive waste to burial	3	3	2
Robots	...for removal of highly activated concrete	5	10	10
Operations Phase				
Repassivation	...of decontaminated systems/components prior to return to service	1	2	3
Incineration	...of dry active waste during plant operation	3	1	1
Prepolishing of Components	...to minimize collection of radioactive crud in plant systems	2	3	2
Design & Construction Phase				
Canal Gate	...to segregate reactor cavity and refueling canal for segmentation	2	5	3
Comprehensive Data Base	...to accurately record plant data necessary for decommissioning			
Containment of Liquids	...to minimize spread of contamination	1	5	5
Preplaced Blast Holes	...for future demolition of bioshield concrete	5	2	4
Smooth and Coat Concrete	...to minimize penetration of contamination	3	3	1
Substitute/Purify Materials	...to minimize NSSS activation products	4	1	2
Modular Biological Shield	...to optimize removal of activated material			

4. REFERENCES

1 "Draft Generic Environmental Impact Statement on Decommissioning" (Later)

2 Proposed Rule, "Decommissioning Criteria for Nuclear Facilities," (Later)

3 Regulatory Guide 1.86, "Termination of Operating Licenses for Nuclear Reactors," (Later)

4 R.I. Smith, et al, "Technology Safety and Costs of Decommissioning a Reference Pressurized Water Reactor Power Station," NUREG/CR-0130, June 1978

5 H.D. Oak, et al, "Technology Safety and Costs of Decommissioning a Reference Boiling Water Reactor Power Station," NUREG/CR-0672, June 1980

IMPACTS OF DECONTAMINATION ON SOLIDIFICATION AND WASTE DISPOSAL*

P. L. Piciulo and J. W. Adams

Department of Nuclear Energy
Brookhaven National Laboratory
Upton, New York 11973

ABSTRACT

Brookhaven National Laboratory has carried out a laboratory evaluation of the wet-air oxidation process for destroying chemical decontamination reagents. The data presented indicate that wet-air oxidation can effectively degrade organic complexing agents typically used in chemical decontaminations. Although less than 90% of the available organic carbon was oxidized, more than 95% of the organic reagent was degraded. Additionally, test results are discussed which demonstrate that the decontamination reagent, NS-1, can be solidified in cement. The waste forms prepared had no visible deterioration after 90 days immersion in water.

INTRODUCTION

The Nuclear Regulatory Commission (NRC) is concerned with evaluating the effectiveness and safety of chemical decontamination processes which are being proposed for light-water reactor (LWR) primary systems as a means of reducing occupational exposure and ensuring continued safe operation. The areas of concern being addressed are: the type, volume and toxicity level of the radwaste streams generated by decontamination and their subsequent management at the plant and at the disposal site.

Because of the large amounts of chelates or complexing agents required for a full system decontamination, it is desirable to determine if there are methods which would convert these reagents to more innocuous forms. The objectives of the program at Brookhaven National Laboratory (BNL) are to identify the information and conduct the tests necessary to aid the NRC in making regulatory decisions on the solidification and waste disposal aspects of chemical decontamination processes. In particular, this program focuses on in-plant methods for converting decontamination wastes to more acceptable forms prior to disposal.

---

*Work carried out under the auspices of the U.S. Nuclear Regulatory Commisison.

The BNL program has provided an evaluation of potential decontamination processes, the wastes generated and potential waste management practices.[1] Subsequent laboratory studies[2] have confirmed that incineration and acid digestion are capable of destroying selected decontamination reagents. Further, this work has assessed the solidification of simulated decontamination resin wastes in cement and vinyl ester-styrene.

The laboratory evaluation of processes for destroying decontamination reagents has included wet-air oxidation (WAO). A discussion is given in this paper of data which indicate that wet-air oxidation can effectively degrade the organic complexing agents typically used for chemical decontaminations. Additionally, the results of a limited study on the solidification of NS-1 reagent in cement are presented.

WET-AIR OXIDIATION OF DECONTAMINATION REAGENTS

Wet-air oxidation has been applied to the treatment of several industrial streams.[4] It was claimed that any combustible material that can be maintained in the liquid phase can be oxidized by this process. Wet-air oxidation has also been proposed for management of low-level combustible wastes and alpha-contaminated low-level wastes.[5,6] A limited experimental program[7] was conducted to determine the feasibility of using wet-air oxidation for volume-reducing spent ion-exchange resins prior to disposal.

Wet-air oxidation or pressurized aqueous combustion is a process that involves the oxidation of combustible materials in the presence of liquid. High pressures are employed to maintain the liquid phase. While some work has been reported on batch-type processes,[5,6] the industrial units normally operate with a continuous feed. Recycling the residue and liquid effluent through the process may be advantageous to more complete degradation.

Experimental

The wet-air oxidation of decontamination reagents and ion-exchange resins was carried out in a batch mode using a 2-L Zipperclave supplied by Autoclave Engineers, Inc. A quartz insert was used to isolate the solution from the steel body. The apparatus was equipped with heaters, a cooling coil and a high speed stirrer. Parts on the autoclave head were fitted to allow liquid and gas sampling, and a thermocouple was used to monitor the solution temperature. Further details of the apparatus are given in Reference 3.

Samples of resins equilibrated with organic acids were prepared by mixing a measured quantity of ion-exchange resins with a solution of organic acid (or reagent) such that there was an excess of acid to exchange with the theoretical exchange capacity of resins. IONAC A-365 (Sybron) anion exchange resins were equilibrated with picolinic acid. This resin has a polyacrylic matrix with weak base exchange groups and was used because it is the resin of choice for the LOMI decontamination process reagent which uses picolinic acid. Quantities of the strong base anion exchange resin, IRN-78 (Rohm & Haas), were equilibrated with an excess of ethylenediaminetetraacetic acid

(EDTA), citric acid, oxalic acid and LND 101A reagent. The amount of organic acid (reagent) on the resin/acid samples was determined by measuring the amount of acid in the solution after filtration. The carbon content of the samples was calculated based on the carbon contents of the resins and the acids.

The samples processed consisted of either organic acids, organic ion-exchange resins, or acid/resin mixtures, in one (1) liter of deionized water. Solutions contained either 0.5 or 1.0 percent by weight of material to be processed. Oxygen was used to pressurize the autoclave before heating the system. Typical ranges of operating conditions for processing the acid/resin mixtures were: initial oxygen pressure, 300 to 250 psi; maximum temperature, 210 to 225°C; maximum pressure, 550 to 720 psig; stirrer speed, 800 to 840 rpm; and run time, 5.5 to 6 h.

Aliquots of the processed solutions were collected at the ends of the runs and, in some cases, at different times during the runs. Liquid samples were analyzed for carbon content and, if applicable, the presence of organic acid. A gas sample was collected at the end of the process run time, after the system was cooled to room temperature, and analyzed by gas chromatography for permanent gases (H_2, N_2, O_2, CO_2, CO, and CH_4). Details of the analytical methods have been reported in Reference 3.

Results

A summary of the process results is given in Table 1. The amount of carbon initially present in the sample is based on the mass of the sample processed and the carbon content. Samples of resins and acid/resin mixtures have errors associated with the initial carbon which result from the determination of the carbon content of the samples.[8]

Values of percent organic carbon oxidized are used to monitor the efficiency of the process. These values are based on the amount of organic carbon measured in the process solution as compared with the initial amount of carbon present. All of the carbon in the resins or reagents was considered as organic carbon. Organic carbon remaining in solution after wet-air oxidation may be associated with a fraction of the original organic complexing agent which was not degraded by processing or with other hydrocarbons which were degradation products. If there is insufficient oxygen then hydrolysis can predominate oxidation[4,9] during the wet-oxidation process. The products formed (low molecular weight carboxylic acids such as formic, acetic, propionic, etc.) can resist[5,6,9] further oxidation. Williams[9] and others have indicated that steady concentrations of formic and propionic acids are produced during the oxidation of butyric acid, and that acetic acid concentrations increase. The work done by Clark[5,6] and by Bonnici[7] indicates the production of acetic acid which was somewhat resistant to further oxidation. No detailed analyses were made of the organic chemicals remaining in the process solutions. However, when possible the post WAO samples were analyzed for the presence of the initial acid being processed. Based on the quantity of reagent remaining in solution, the percent reagent destroyed was calculated and the results are also listed in Table 1.

Table 1

WAO Carbon Analyses of Post Run Liquid Samples

Sample	Initial Carbon (mg)	Carbon Remaining[a] Total (mg)	Inorganic (mg)	Organic (mg)	Percent of Organic Carbon Oxidized[b]	Percent of Reagent Degraded[c]
Na_2EDTA	1616	440	280	160	90	>99
Citric Acid(CA)	1875	360	20	340	82	>99
CA/$Fe(NO_3)_3$	1875	496	220	276	85	N.D.
IRN-78	3360±20	1400	N.D.	N.D.	58[d]	N.D.
IRN-78	1781±25	722	185	537	70	N.D.
IONAC A-365	1569±40	743	299	444	71	N.D.
EOC	4968	1972	674	1298	56[f]	99,97,65[e]
Picolinic Acid(PA)	2570	1800	100	1700	34	>99
PA/IONAC A-365(1)	2190±30	1230	402	828	62±2	>99
(2)	2190±30	1227	303	924	58±2	97
(3)	2190±30	1160	325	835	62±2	95
EOC/IRN-78[f] (1)	2360±30	1388	210	1178	50±1	>99,99,94
(2)	2340±30	1011	90	921	61±1	>99,99,92
(3)	2340±30	923	92	831	64±2	>99,99,93
LND 101A/IRN-78(1)	2030±30	733	132	601	70±2	
(2)	2030±30	901	90	811	60±2	
(3)	2030±30	938	103	835	59±2	
Blank	0	10	0	10	N.D.	N.D.

[a]Organic carbon is determined from the difference between total carbon and inorganic carbon. N.D. means not determined.
[b]Percent carbon oxidized is based on organic carbon remaining and the carbon initially present.
[c]Percent degradation is based on the amount of organic acid left in solution compared with that initially present.
[d]Value reported is based on total carbon and carbon available.
[e]Values given are percent destruction of EDTA, OA, and CA, respectively.
[f]Samples contined equimolar amounts (1.55×10^{-3} moles) of EDTA, OA, and CA.

In initial testing, samples of Na_2EDTA and citric acid were processed for about 30 h. These runs were sampled after various times during processing and the data (although limited) suggest that oxidation of the organic carbon occurs relatively quickly and extended processing time does not result in a large increase in the amount of carbon oxidized. Figure 2.1 is a plot of reaction time vs fraction of organic carbon oxidized for the WAO of EDTA and citric acid. After 6.5 h, about 80% of the organic carbon in the EDTA sample was oxidized. An additional 10% of the organic carbon was oxidized after 30 h of processing. Oxidation of organic carbon in citric acid had essentially proceeded to a limiting value after 20 h. The heat was turned off at 28 h and no significant increase in carbon oxidized was observed. The sample collected at 45 h, after the system had returned to room temperature, showed <1% of additional carbon oxidized.

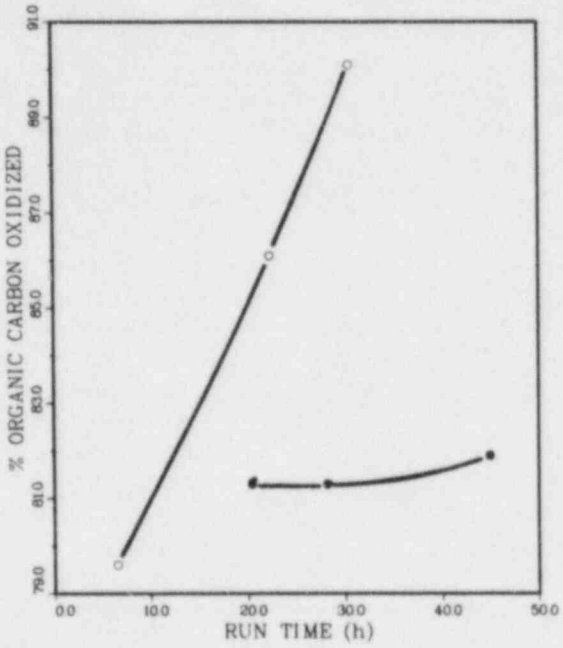

Figure 1. Percent organic carbon oxidized vs run time for the WAO of EDTA (o) and citric acid (•).

A striking difference between the results for EDTA and citric acid is the amount of inorganic carbon detected in the processed solutions (Table 1). Since the disodium salt of EDTA was processed, carbonates and bicarbonates are likely counterions for the remaining sodium present in solution. On the other hand, citric acid contains only C, O, and H, and dissolved CO_2 as carbonic acid may be the likely species to account for the inorganic carbon. The initial amount of Na_2EDTA contains 0.027 moles of sodium which would require an equal number of moles of HCO_3^- or half as many moles of CO_3^{-2} for neutrality. Such quantities from the WAO would result in ≈320 mg and ≈160 mg of inorganic carbon in solution from bicarbonate and carbonate, respectively. The 280 mg of inorganic carbon may be the result of having approximately 75% of the sodium as $NaHCO_3$ and the remaining sodium as Na_2CO_3.

After processing the solutions containing EDTA and citric acid, the samples were analyzed for EDTA and citric acid remaining in solution. The results indicated that >99.9% of the EDTA and 99.8% of the citric acid were destroyed by processing. Other carbon containing species must remain in solution. These can include low molecular weight carboxylic acids such as formic, acetic, propionic, etc.[7,9]

A 1-liter solution of 0.026M citric acid was oxidized for seven hours. The solution also contained $9x10^{-3}$ M ferric nitrate to determine if the presence of iron ions would enhance the amount of citric acid that is degraded. After processing, the final solution was an opaque red and there appeared to be about 85% oxidation of the acid, based on the amount of organic carbon

remaining in solution. The presence of the metallic ion (Fe^{+3}) or perhaps decomposition of nitrate appeared to affect the oxidation. Ion chromatography data are not available for the CA/$Fe(NO_3)_3$ system to compare the amounts of CA left in solution with that determined previously; however, the amount of organic carbon remaining is smaller, indicating some increase in the oxidation of organic carbon.

WAO of the equimolar mixture of EDTA, citric acid and oxalic acid (1.5 weight percent in the simulated waste stream) appears to result in 56% oxidation of the mixture. This result is based on the amount of organic carbon left in solution. Ion chromatography data however, indicate that more than 95% of the EDTA and OA were oxidized compared to ≈65% of the citric acid. The lower percent oxidation of citric acid in the EOC mixture from that observed for CA alone or in CA/$Fe(NO_3)_3$ may be due to the shorter reaction time, the absence of $Fe(NO_3)_3$ or because the sample was a mixture. It is possible that an unidentified product in the WAO process solution may interfere with the ion chromatography analysis for citric acid. A chemical having a retention time similar to that for citric acid would be quantified as citric acid. A high estimate of the amount of citric acid in solution would give a corresponding low estimate of the amount of acid degraded. A complete analysis of the products in the process solution was beyond the scope of this work.

A 5.003-g sample of picolinic acid was processed for more than 6 h. The colorless solution recovered at the end of the run was slightly acid (pH = 6.3). Analysis indicated that only 34% of the organic carbon in the sample was oxidized but more than 99% of the PA was destroyed.

Based on the amount of organic carbon left in solution (Table 1), ion-exchange resins present at 0.5 percent by weight were oxidized ≈70%. No resin beads were observed in the post run solution although some "cloudiness" was noted in the solution. Comparing the two oxidations reported for IRN-78, the amount of resins used varied by a factor of two. If the percent oxidation is estimated from the total carbon remaining, there is no significant change (58% vs 60%). However, based on organic carbon in solution, run 2 showed 70% oxidation of the resins. In this run, a larger amount of oxygen was used.

The oxidation of the IONAC A-365 resins was comparable to that of IRN-78 resins when processed using similar parameters. The post run solutions were yellow in color. The pH of the solutions after processing were ≈4.4 for IRN-78 resins and ≈7.5 for IONAC resins. The oxidation products of the two resin types present different water chemistries after processing. These solutions may have different requirements for successful solidification of the process liquids prior to burial.

Replicate samples of PA/IONAC A-365 processed under similar conditions showed comparable percentages of carbon oxidized. The solutions recovered were pale yellow and neutral to slightly acidic. Small quantities of picolinic acid that were measured in the process solution indicated more than 95% destruction of the acid. Run 1, which was the largest of the three runs, showed >99% destruction of PA. The major differences in process parameters were a higher temperature, higher pressure, and higher stirrer speed.

Oxygen pressure was varied when processing samples of EOC/IRN-78. An increase of 40 psi in oxygen pressure resulted in an increase in the amount of organic carbon oxidized from 50% to more than 60%. Further, there was ≈50% less inorganic carbon remaining in the process solutions of runs with the higher pressure compared with inorganic carbon in EOC/IRN-78(1). Analysis of the process solutions indicated that in all cases, >99% of EDTA, 99% of oxalic acid and about 93% of citric acid initially present in the samples was destroyed.

Three samples of LND-101A/IRN-78 were processed at similar temperatures and pressures but with different stirrer speeds. The resulting process solutions differed in that a pale yellow liquid was recovered from run 1 whereas the other process liquids were darker and contained a fine particulate. The carbon content of the process liquids showed that a greater percentage of organic carbon (70%) was oxidized in the first run than in subsequent runs (≈60%). The last two samples were processed under similar conditions and had similar data for carbon in solution. The major difference among the three runs was the higher stirrer speed of run one. Increased agitation will cause an increase in oxygen transport into the aqueous phase thus promoting oxidation.

A blank run was performed by processing 1-liter of deionized water under typical conditions used to process other samples. The results of the carbon analysis show that ≈10 mg of organic carbon were present at the end of the run. It is possible that the carbon was removed from parts of the apparatus that are difficult to clean between runs (e.g., pressure gauges, tubing), or was admitted to the system as contamination from the O-ring grease (Dow Corning high vacuum grease, which is a silicone lubricant, was used) or from the oxygen feed line. The 10 mg of carbon observed in the total carbon analysis of the solution is equal to between ≈0.5% and 2.8% of the total carbon observed in the WAO runs of reagent samples. This small amount of carbon such as this is not likely to affect either the test being performed or the conclusions drawn.

Analyses of gas samples provide data on the various gas phase species produced during WAO of the simulated decontamination wastes. It was not intended in this work to correlate the carbon in the gas samples with the amount of organic acid destroyed. The analysis was limited to permanent gases (H_2, O_2, N_2, CO, CO_2 and C_1 and C_2 hydrocarbons) by the choice of column used for the gas chromatograph. Thus, there are no data on the presence of nitrogen containing compounds like ammonia, volatile amines, and NO_x species which might be produced on the degradation of anion exchange resins and nitrogen containing organic acids (i.e., EDTA, picolinic acid).

Carbon dioxide was observed, as anticipated, in all samples since it is the expected oxidation product for carbon. The presence of CO, however, indicated that oxidation was not complete. Additionally, the presence of methane and hydrogen suggest that oxidation was not complete. These gases were observed in samples containing IRN-78 anion exchange resins and with citric acid.

Discussion

Based on the WAO process data, the percent oxidation of organic carbon in samples of ion-exchange resins equilibrated with reagents ranged between 50% and 70%. Samples of acids alone showed as much as 90% organic carbon oxidized. Analyses of the process solutions for residual organic acid indicated that nearly all of the original acid present was degraded. Citric acid appeared to be the most difficult acid to degrade of the four tested (EDTA, oxalic acid, citric acid, and picolinic acid).

The limited testing reported here indicates that oxidation is sensitive to the amount of oxygen present (initial pressure) and agitation. Process temperature and operating pressure also had some affect on the efficiency of degrading the materials. Extended processing times did not result in significant increases in the amount of carbon oxidized. The quantity of sample being processed also limits the effectiveness of the treatment. These operating parameters should be considered in the design of a large-scale wet-air oxidiation system.

Complete oxidation of organic carbon was not achieved under the process conditions used here. In particular, samples containing ion-exchange resins showed less than 70% oxidation of organic carbon. Even though the simulated wastes tested were not completely oxidized, wet-air oxidation was effective at degrading the decontamination reagents. Further processing of the waste may not be necessary if degradation of the organic complexing agents is the desired goal. However, the composition of the process solutions may need to be considered when planning the management of these wastes. For example, the presence of organic compounds may cause difficulties in direct solidification of the process liquids.

Based on the organic carbon analysis, process solutions contained organic species other than the original acid. Characterization of the process solutions was beyond the scope of this study, but it is likely that the composition may vary depending on the materials treated and the final degree of oxidation. Other workers[7] have reported that the products of oxidation of ion-exchange resins contained ≈15% low molecular weight carboxylic acid and that acetic acid, a major constituent, was somewhat resistant to further oxidation.

Consideration should be given to the organic acids remaining after wet-air oxidation regarding their potential to enhance radionuclide migration if released to the disposal environment. If the wet-air oxidation process were optimized, it is assumed acetic acid would be the major organic acid remaining. In general, acetate complexes are less stable than metal complexes of EDTA, or picolinic acid. which are used in decontamination reagents. Thus, the presence of acetic acid in the final waste form would be of less significance to the enhancement of radionuclide migration compared with the complexing agents used for decontamination (assuming comparable release of the acids from the waste form). If the decontamination waste was oxidized to an intermediate degree such that the decontamination reagents were degraded but acetic

acid was not the only organic acid that remained, then the composition of the process waste should be evaluated to determine whether the treatment was of value. If oxidation was incomplete, it may be possible to treat the process liquid by filtration and ion-exchange to remove the radioactive species. The nonradioactive liquid presumably containing any complexing agents, could be handled separately from the radioactive waste.

SOLIDIFICATION OF NS-1 REAGENT IN CEMENT

The waste generated by the chemical decontamination of a light water reactor will be disposed of in a shallow land burial site. Disposal of these wastes will be governed by the requirements established in the rule "Land Disposal of Radioactive Waste," 10 CFR Part 61, any future guidance given by the NRC and through site-specific criteria. The regulation establishes a waste classification system for shallow land burial and a set of minimum performance objectives. NRC in the Technical Position on Waste Form provides guidance to waste generators on waste form test methods and results acceptable for demonstrating compliance with the waste stability criteria.

A laboratory evaluation of the capability of methods for solidifying decontamination resin wastes has been performed in order to assess whether they will meet applicable stability criteria. The primary objective of the solidification tests was to determine if cement and vinyl ester-styrene binders are viable agents for immobilizing simulated decontamination resin wastes. Based on current information, both mixed bed resins and anion exchange resins were selected for solidification testing. An acceptable waste form was one that met the requirements in 10 CFR Part 61 and the guidelines given in the Technical Position on Waste Form. Tests for acceptability included a visual inspection for the formation of a free standing monolith, the presence of free liquid, testing of the mechanical stability of the waste form and immersion in water. The details of this work and a discussion of the results can be found in Reference 2.

Work on the solidification of simulated decontamination wastes has been extended to include solidification of a selected liquid waste stream from a concentrated decontamination process. The results of the laboratory-scale tests that were performed are discussed in this section.

Solidification of NS-1 Reagent in Cement

The NS-1 solvent, developed by Dow Chemical Company, is used for decontamination of BWRs. Although designed for use as a "concentrated" reagent, the NS-1 solvent has been used in a diluted form of 10% the original design concentration. Subsystems of various reactors have been treated with either dilute or concentrated NS-1.[10]

The waste stream expected from the use of NS-1 as a "concentrated" reagent was to be concentrated by evaporation of the process solvent. It was planned that the concentrated liquid would be solidified in vinyl

ester-styrene. This was successfully demonstrated, and BNL reported[11] results of physical tests of the waste product.

Alternate methods of waste management can be used for handling the dilute NS-1 solvent. The reagents can be concentrated to a liquid stream, or removed from solution by ion-exchange. Both the concentrated liquid and resin wastes from a NS-1 process have been solidified in cement.[12] Work in the present study was intended to evaluate the direct solidification of dilute NS-1 solvent in cement. Waste composites were prepared and examined for the presence of free liquid, tested for mechanical strength and tested for their ability to withstand immersion in water as recommended in the Technical Position on Waste Form.

A sample of NS-1 solvent was obtained from IT Nuclear Services which is licensed by Dow Chemical Company to apply NS-1. The composition of NS-1 is proprietary. NS-1 is an aqueous solution which in the 100% form contains about 7.5% dissolved solids and has a pH of 3.6. The solvent contains chelates, complexing agents and inorganic salt plus a corrosion inhibitor. BNL received "spent" NS-1 (100%) which had three metallic compounds added to it: 1200 ppm ferric sulfate (or ferric citrate), 600 ppm nickel ammonium sulfate and 30 ppm copper sulfate.

It was believed that a probable waste stream from a NS-1 treatment would have a concentration approximately that of the 100% NS-1. This was based on knowledge that 100% NS-1 solvent can be used at the 10% dilution and then concentrated back to 100% prior to solidification. Further, BNL had a limited quantity of the material available for testing. It was anticipated, based on the results of the resin solidification tests, that pre-treatment by pH adjustment of the waste stream prior to solidification would be advantageous. Portland I cement was chosen for the solidification of NS-1. Details of the solidification are given in Reference 3.

The compressive strengths of the cement forms were measured according to the ASTM C39-80 test method. The average compressive strengths of four NS-1 samples and their controls are given in Table 2. Although the mechanical strengths of the controls were smaller than those of the forms containing NS-1, all forms had compressive strengths larger than the 50 psi recommended in the TP on Waste Form.

Table 2

Compressive Strengths of Cement Composites

Sample	Cure Period (days)	Compressive Strength (psi) pre-immersion	post immersion
NS-1	34	5840±240	6050±560
Control	31	4370±240	4870±100

Four NS-1 composites and three controls were immersed in 1-L of water after a 28-day cure period. After the 90-day immersion test, there was no visible sample deterioration, and the forms had compressive strengths greater than the 50 psi recommended in the TP on Waste Form.

These limited tests demonstrate that NS-1 can be solidified in cement to at least meet the Class A waste form requirements. However, assuming that half of the 7.5% solids in NS-1 are chelating agents then the waste (NS-1 plus water) solidified in these tests contained less than 3% chelating agents. In the field, it may be desirable to concentrate the solvent to a waste stream containing a higher concentration of dissolved solids and thus a higher concentration of organic reagents. Solidification of these wastes may not proceed as it did in the tests reported here. As with the work done on resin wastes, it is expected that variations in the composition of the liquid decontamination waste stream must be taken into account when establishing formulations for solidification.

SUMMARY

Wet-air oxidation appears to be an effective method for degrading simulated decontamination wastes. The process data given in this report show that even though the amount of oxidation of total organic carbon in the acid/resin mixtures ranged between 50 and 70%, there was greater than 92% degradation of the organic reagents. The percent degradation of the organic reagents is based on the quantity of reagent present after processing compared with the initial amount in the sample. It is believed, based on data collected in the ongoing BNL study, that WAO can be comparable to incineration and acid digestion for degrading decontamination wastes. Testing in this program was limited to three simulated waste streams: reagents alone, anion exchange resins and anion exchange resins equilibrated with reagents. For each of the processes evaluated in this study, only limited efforts were made to optimize the process apparatus or operating parameters. It is recommended that waste-specific operating parameters be established if any of these processes are to be used commercially.

The acid/resin mixtures tested in this program were intended to simulate dilute process decontamination wastes. Resin wastes from actual reactor system treatments can include cation exchange resins, metal ions and radionuclides. The presence of these materials in the waste stream may affect the efficiency of degradation by wet-air oxidation. Although it was indicated in earlier studies that transition metal ions may catalyze the oxidation of organic materials (Ca^{+2}, Fe^{+2}, and Mn^{+2} nitrates were used as a catalyst by Clark, W. E.[5]), the presence of iron in processing citric acid had a limited effect. It would be necessary to determine whether a catalyst will increase oxidation of the resins at lower operating temperatures.

The present data suggest that the degradation of each acid can be affected by process parameters such as temperature, pressure, and agitation. Agitation (stirring) and oxygen overpressure did increase the amount of organic carbon oxidized in tests of EOC/IRN-78 and LND-101A/IRN-78. An increase

in process temperature resulted in an increase in the degradation of picolinic acid in samples of PA/IONAC A-365. However, the temperature increase had a corresponding increase in operating pressure which promotes the rate of oxygen transfer into solution. It is not known if an increase in pressure alone would have given a similar result. Analyses of process solutions showed ≈99% degradation of EDTA and oxalic acid, but a somewhat lower percentage degradation was observed for picolinic acid (>95%) and citric acid (≈93%) when processed under similar conditions. Thus, the composition of the waste stream to be processed should be considered when establishing process parameters.

The size of the batch-type processor used in the BNL study limited the sample size that could be treated. Additionally, limitations in the pressurization equipment limited the amount of oxygen in the system. Thus, only samples of 0.5 weight percent of waste-to-water were processed which is below the 2 to 20 weight percent organic matter expected to be treated by WAO. Recycling the process solution or use of a flow system may increase the total degradation of the waste. The design of the WAO reactor must consider the concentration of waste to be processed; in turn, this will affect the effluent streams (off-gas and liquids).

Management of the effluent streams from the WAO process will need to be considered. The process solutions will contain suspended solids, inorganic salts, and can include various inorganic and organic carbon-containing species. Further, the data show that the pH of the liquid stream is dependent upon the material processed. It is anticipated that the volume of the liquid stream would be reduced prior to any further treatment. If this waste stream were to be solidified prior to disposal in shallow land burial, then it should be demonstrated that the subsequent product meets the appropriate requirements of 10 CFR Part 61.

The off-gas stream from the wet-air oxidation of decontamination wastes will contain CO_2, CO, and water vapor. However, methane and hydrogen have been observed and nitrogen-containing gases such as volatile amines and NO_x gases may also be present. Thus, off-gas treatment may be necessary.

Limited tests have demonstrated that a liquid waste stream from a decontamination using NS-1 reagent can be solidified in cement after pre-treatment by pH adjustment. The test reported here was for a single concentration of NS-1 in the waste stream. It is anticipated that the concentration used in this test is low compared to what may be used in full-scale solidifications under field conditions. As with the work done on resin wastes, it is expected that variations in the composition of the liquid decontamination waste stream will have to be considered when establishing process parameters for solidification.

Based on the efforts to date, areas which should be researched in the future include an evaluation of bitumen as a solidification medium for decontamination wastes and the impacts of decontamination wastes on standard containers. The objective of the work is to generate data that will aid NRC in assessing problems that may be encountered with the long-term storage or disposal of decontamination wastes and to evaluate the acceptability of on-site

decontamination waste handling and solidification processes. These experiments would investigate the corrosion or degradation of container materials in contact with decontamination resin wastes and include examination of the effects of irradiation on decontamination wastes which may result in gas generation or the release of liquids. It is believed that the biodegradation of decontamination wastes should be studied, as well as the effects of thermal cycling on solidified wastes. The tests planned are consistent with those recommended by NRC to demonstrate waste form stability.

REFERENCES

1. M. S. Davis, Brookhaven National Laboratory, "The Impact of LWR Decontaminations on Solidifications, Waste Disposal and Associated Occupational Exposure, Annual Report," NUREG/CR-3444, BNL-NUREG-51699, Vol. 1, August 1983.

2. M. S. Davis, Brookhaven National Laboratory, "The Impact of LWR Decontaminations on Solidifications, Waste Disposal and Associated Occupational Exposure, Annual Report," NUREG/CR-3444, BNL-NUREG-51699, Vol. 2, February 1985.

3. P. L. Piciulo, J. W. Adams, and M. S. Davis, "The Impact of LWR Decontaminations on Solidification, Waste Disposal and Associated Occupational Exposure," NUREG/CR-3444, BNL-NUREG-5169, Vol. 3, to be published.

4. Ontario Research Foundation, "Wet Oxidation," ORF-5-48.

5. W. E. Clark, "Status of Pressurized Aqueous Combustion for Burning Solid Wastes Contaminated by Radionuclides," ORNL-TM-3170, October 1970.

6. W. E. Clark and W. C. Ulrich, "Pressurized Aqueous Combustion of Alpha Contaminated Wastes, Final Program Status Report," ORNL-TM-4366, November 1973.

7. P. J. Bonnici and others, "Volume Reduction of Resin Wastes," London Nuclear Limited, LNL-000-G-157, July 1981.

8. B. S. Bowerman and others, Brookhaven National Laboratory, "Decontamination Impacts on Solidification and Waste Disposal, Quarterly Progress Report, July-September 1983," BNL-NUREG-33873, October 1983.

9. P. E. Williams, P. L. Silvestone, and R. R. Hudgens, "Oxidation of Butyric Acid Solutions," Canadian J. of Chemical Engineering 53, 354 (1975).

10. D. E. Harmer, "BWR Decontamination Using NS-1," in Chemical Decontamination of BWRs by J. A. Jones Applied Research Company, Charlotte, NC, 85-WH-22, p. 19-32, 1985.

11. R. E. Barletta and others, Brookhaven National Laboratory, "Physical Tests on Solidified Decontamination Wastes From Dresden Unit 1," NUREG/CR-3165, BNL-NUREG-51648, December 1983.

12. R. Soto, "Management of Chemical Decontamination Wastes," in Chemical Decontamination of BWRs by J. A. Jones Applied Research Company, Charlotte, NC, 85-WH-22, p. 341-363, 1985.

EVALUATION OF NUCLEAR FACILITY DECOMMISSIONING PROJECTS PROGRAM - STATUS

R. L. Miller, P.E.
UNC Nuclear Industries, Decommissioning Programs Department

The Evaluation of Nuclear Facility Decommissioning Projects (ENFDP) program described in this presentation is being undertaken by the U.S. Nuclear Regulatory Commission (NRC) to compile and evaluate the activities of ongoing reactor decommissioning projects. Assessment and evaluation of the methods, impacts, radiation exposures, and costs will provide a basis for evaluating licensees' decommissioning proposals and for future direction and regulation on decommissioning.

Program participants include the U.S. Nuclear Regulatory Commission (NRC) through the Office of Regulatory Research, UNC Nuclear Industries (UNC) through the Decommissioning Programs Department, and nuclear facility licensees.

A computerized data collection system has been developed to store and manipulate relevant data from the nuclear facility decommissioning projects in this study. The decommissioning information included in this data base includes but is not limited to:

- Costs for labor, waste disposal and shipping.
- Radiation exposure and facility dose rates.
- Volume and curie content of generated waste.
- And lessons learned.

Decommissioning projects for which data have been collected include the following:

Research Reactors
- Ames Laboratory Research Reactor
- North Carolina State University Reactor
- Northrop TRIGA Reactor*
- PNL Estimates for Decommissioning a Reference Research Reactor

Test and Demonstration Reactors
- Elk River Demonstration Reactor
- Fermi 1 Demonstration Reactor
- Plum Brook Test Reactor
- Niederaichbach Pressure Tube Reactor*
- PNL estimates for Decommissioning a Reference Test Reactor

Pressurized Water Reactors
- Shippingport Atomic Power Station*
- PNL estimate for Decommissioning a Pressurized Water Reactor
- Data from the Recovery Efforts at Three Mile Island Unit 2*

*Facilities where data collection is ongoing.

Boiling Water Reactors
- Humboldt Bay Unit 3*
- Lingen*
- Gundremmingen*
- PNL Estimates for the Decommissioning of a Reference Boiling Water Reactor

The status of the data collection efforts for the ongoing decommissioning projects for each reactor type is described below.

Research Reactors

Arrangements have been made with Chem-Nuclear Systems, Inc., to provide the desired information related to dismantling the Northrop TRIGA reactor. The dismantlement work was completed during August 1985. Upon completion of our analysis of the data, some preliminary comparison studies for dismantling research reactors can be initiated.

Test and Demonstration Reactors

The Niederaichbach reactor decommissioning project was added to the ENFDP program during FY 1985 and data collection is in the initial phase. Actual dismantling of the facility is still in the engineering/planning phase. The Noell Company of Wuerzburg, FRG is performing the engineering studies and is fabricating the remote tooling for the work. The project is funded by the West German government on a fixed price contract to Noell and will serve as a demonstration project to indicate the capability to completely dismantle a large scale nuclear reactor.

Pressurized Water Reactors

The detailed engineering estimates for dismantling the Shippingport Atomic Power Station (SAPS) have been input into the ENFDP data base. Since actual decommissioning work at SAPS did not start until October of this year very little actual data has been collected. A detailed site radiological survey was performed during FY 1985 and the data is currently being analyzed and prepared for input into the data system.

Data collection continued during FY 1985 for the recovery effort activities at Three Mile Island Unit 2 (TMI-2). Four NUREG documents were published on the status of four major tasks of the project. The documents were:

- Reactor Coolant System and Systems Decontamination
- Reactor Building Decontamination
- Reactor Defueling and Disassembly
- Radioactive Waste and Laundry Shipments

*Facilities where data collection is ongoing.

Boiling Water Reactors

Two West Germany boiling water reactor decommissioning projects, Lingen and Gundremmingen, were added to the ENFDP program during FY 1985. Data collection at the German facilities is in an initial phase and only very basic data has been input into the data system.

Data collection from the Humboldt Bay decommissioning project continued through FY 1985 with a status report published as NUREG/CR-4316, "Status Report Humboldt Bay Power Plant Unit 3 SAFSTOR Decommissioning."

Since all three of the boiling water reactor decommissioning projects are a safe storage mode, it may be possible to initiate some comparisons studies during FY 1986.

Preparation for safe storage at the Humboldt Bay facility is scheduled for completion by December 31, 1985. Preparation for safe storage at both the Lingen and the Gundremmingen facilities is scheduled for completion during 1987.

Summary

The research associated with the ENFDP program continued in the data gathering and analysis phase during FY 1985. Four new facilities were added to the program which should enable us to initiate some comparison studies on research reactor dismantling and BWR safe storage preparation during FY 1986. Pending a favorable outcome of the research reactor studies, additional research reactor decommissioning projects will not be necessary for the program.

LWR Spent Fuel Rod Behavior During Long-Term Dry Fuel Storage Conditions

C. S. Olsen

Idaho National Engineering Laboratory
EG&G Idaho, Inc.

ABSTRACT

A testing program was conducted to investigate the long-term stability of commercial pressurized water reactor (PWR) and boiling water reactor (BWR) spent fuel rods under a variety of possible dry storage conditions. The objective of this project was to provide the Nuclear Regulatory Commission (NRC) with an experimental basis to evaluate the results of short-term, high-temperature tests and to establish a licensing position for long-term, low-temperature (<230°C) spent fuel rod dry storage. A total of nine fuel rods (five BWR and four PWR) were nondestructively examined after interim heating periods, and seven of these fuel rods were destructively examined to determine the degradation of the fuel rods during the long-term, low-temperature dry fuel storage. The results of the nondestructive examinations of all nine fuel rods and the destructive examination of one fuel rod were reported previously. This paper presents detailed results of the destructive examinations of six of the remaining fuel rods, with brief results from the examinations of all the test fuel rods as they pertain to fuel rod behavior during dry spent fuel storage conditions. The results from this program show that U_3O_8, with its significant volume expansion, can still form at temperatures below 250°C and result in fuel rod rupture.

INTRODUCTION

The regulation[1] under which a dry storage license would be granted, 10 CFR 72, requires that fuel cladding must be protected against degradation and gross rupture and that releases to the environment shall be within acceptable limits. These regulations apply to independent spent fuel storage installations, but the Nuclear Waste Policy Act of 1982 requires revision to 10 CFR 72 for spent fuel and high-level radioactive waste storage in a monitored retrievable storage (MRS) installation[2]. These revisions are to establish licensing criteria and include licensing requirements for the long-term storage of spent fuel and high-level radioactive waste in an MRS installation.

In an unlimited air atmosphere, oxidation of UO_2 may occur, with a concurrent volume expansion and rupture of the cladding. The contamination potential may be enhanced by (a) oxidation of the fuel along the grain boundaries, which would release fission gas, (b) fallout of fuel particulate from the rupture; and (c) spallation of the crud from stresses imposed on the cladding by fuel expansion. Similar behavior, although at different rates, may occur with other atmospheres containing impurities, such as an inert atmosphere with air or some other oxidant. Estimates of maximum storage temperatures expected have been made,[3] but information is needed to assess a satisfactory storage temperature with regards to defected rods in an oxidizing environment.

A long-term testing program with nine PWR and BWR fuel rods of commercial design was conducted at the Idaho National Engineering Laboratory (INEL). The objectives of this experimental program were to provide an experimental basis to evaluate the results obtained from high-temperature, short-term laboratory tests and to provide a basis for establishing a licensing position on long-term spent fuel rod dry storage capabilities and requirements. The tests were conducted at temperatures below 230°C and covered a wide range of storage atmospheres, rod types, and cladding conditions. Because the temperature of 250°C was believed to be the temperature above which U_3O_8 forms, resulting in significant fuel swelling and possible cladding rupture[4], 230°C was selected as a conservative upper temperature limit below which fuel oxidation would result in the formation of U_3O_7 but not U_3O_8, resulting in little volume expansion.

Four intact spent fuel rods (two PWR and two BWR) and five intentionally defected spent fuel rods (two PWR and three BWR) were heated in a furnace to simulate temperatures that would be expected to occur during dry storage conditions. During testing, temperatures ranged between 217 and 230°C for different periods of time up to a total of 13,200 h; and the atmosphere surrounding each test rod was either air or an inert mixture of argon and helium. Selected test rods were nondestructively examined at interim times of 2,235, 5,962, and 13,168 h[4-8]. One BWR fuel rod that ruptured was destructively examined[4] and replaced with another defected BWR fuel rod after the second interim examination. During the third interim nondestructive examination, the fifth intentionally defected fuel rod, the three other defected fuel rods, and the remaining four intact fuel rods were examined. Six of the remaining eight fuel rods were selected for a destructive examination[9]. This paper emphasizes the results of these destructive examinations.

The BWR fuel rods were obtained from Peach Bottom Assembly PH462. The burnup of each assembly has not been precisely determined, but the reported average assembly burnups varied between 11,900 MWd/MTU and 12,890 MWd/MTU. The PWR fuel rods were obtained from the H. B. Robinson Assembly B05. The peak burnup was 31,365 MWd/MTU, and the average burnup was 28,025 MWd/MTU.

The testing procedures for this integral testing program and the destructive examinations are presented. The experimental results for the BWR and

PWR fuel rods are presented, followed by a discussion of these results and those from previous examinations. From this discussion, the conclusions are developed.

EXPERIMENTAL PROCEDURE

Four rods (two PWR and two BWR), each containing intentional defects in the form of 0.76-mm-diameter holes at different orientations and axial positions (Table 1), were contained in 1.75-cm ID stainless steel capsules, each of which maintained its own atmosphere (Table 2). Two of the defective rods (one BWR and one PWR) were placed in sealed capsules containing 0.1 MPa of an argon-1% helium mixture. The other two defected rods were placed in capsules which terminated at each end with a series of 2-μm and 15-μm in-line filters open to the cell atmosphere. These filter sizes were based on fuel particle sizes expected from ruptured fuel rods[10]. The intact rods were handled in a similar fashion. One intact rod of each type was placed in a sealed capsule containing 0.1 MPa of an argon-1% helium mixture, and one intact rod of each type was placed in a capsule containing air-1% helium mixture. The leak rate of the sealed capsules was less than 2.5×10^{-7} cm^3/s.

The fuel rods were heated in a shielded, 14-zone, 4.3 m-long clamshell furnace capable of holding the eight encapsulated, unmodified LWR fuel rods (Figure 1). The fuel rod capsules were placed around an instrument train which contained 10 axially distributed thermocouples, and furnace-control thermocouples indicated a ±3°C radial temperature gradient, with the center of the furnace being the hottest.

The furnace temperatures were read and printed on paper tape once an hour with a Fluke data logger. During the last 10 weeks prior to shutting the furnace down for the final nondestructive examination, the data logger was connected to an Apple II[a] personal computer for recording the temperature data on floppy diskettes for subsequent data reduction.

For each furnace campaign, the furnace was brought to temperature over a 12-h period and, other than for power outages, ran continuously until the interim examinations (Figure 2). The furnace was operated at 229°C for 5962 h, and then gradually decreased to 217°C during the next 7206 h.

Peach Bottom rod PH462-E3 was removed from the furnace after 5962 h at 229°C. This rod was replaced with PH462-C5, which was heated for 7206 h at temperatures decreasing from 229 to 217°C. The remaining seven rods were heated for 13,168 h; 5962 h at 229°C and 7206 h at temperatures gradually decreasing from 229 to 217°C. The fuel rod capsules were removed from the furnace on July 13, 1984.

---

a. Trade Mark of Apple Computer Corporation.

Fifteen samples were examined from the Peach Bottom PH462-C5 fuel rod. Eleven of the fifteen samples were from the bottom section where the fuel oxidized at an intentionally induced defect, resulting in cladding strain and a rupture of the cladding over a distance of 1.9 cm. Each of the other two sections from this fuel rod contained an intentionally induced defect. Samples with these defects were used to determine the penetration of the defect into the cladding, the location of the defect with respect to the pellet/pellet interfaces, and the extent of oxidation of the fuel.

Two fuel rods (B05-B8 and PH462-E4) were undefected and heated in a limited air atmosphere. These rods provide a reference for comparison with the fuel and cladding behavior of other defected fuel rods. A transverse section was taken from each of the top two fuel rod sections in areas corresponding to the defect locations in other fuel rods.

For each fuel rod section from rods PH462-D6, B05-G7, and B05-E7, samples containing an intentionally induced defect were used to determine the penetration of the defect through the cladding, the extent of oxidation, and the relation of the defects to the pellet/pellet interfaces. Cladding microhardness measurements were also obtained from selected fuel rod samples.

Fuel samples were taken from selected metallographic sections and selected locations on the sections. These samples were analyzed by X-ray diffraction techniques to determine the oxidation state of the fuel. Detailed examinations are described in a previous publication[9].

Pieces of fuel were extracted from one intact BWR and one intact PWR fuel rod in order to determine the fuel density after irradiation by immersion density measurements[11]. Pore size and size distributions were obtained from photomicrographs of samples at the center, midradius, and edge of the fuel pellets. The pore size and size distribution were obtained with an Omnicon Alpha[a] Image Analyzer using the oversize or cumulative count. With this mode, the number of pores having a maximum horizontal chord larger than a predetermined size was determined.

EXPERIMENTAL RESULTS

BWR Fuel Rods

The general surface condition of the Peach Bottom fuel rods appeared to be unchanged after heating for 13,000 h at temperatures less than 230°C. The fuel rod heated in limited air was similar in appearance to the one heated in argon[7]. The BWR rods did not exhibit much crud deposition on the surface of the cladding.

The outside diameter of the BWR fuel rods varied between 14.25 and 14.27 mm, which is slightly less than the nominal diameter of 14.30 mm. With a cladding wall thickness of 0.96 mm and a nominal pellet diameter of

---

a. Trade Mark of Bausch and Lomb Inc.

12.12 mm[7], the nominal radial gas gap is 125 μm. The fuel cladding gap in the center section of PH462-E4 varied from 27 to 59 μm around the circumference of the cladding, with an average of 40 μm. The nominal as-fabricated gas gap is 150 μm, but the average fuel rod diametrical measurements of 14.25 mm show the gas gap to be 125 μm. The average gap of 40 μm indicates that some fuel swelling from irradiation might have occurred.

The Vicker's diamond pyramidal hardness (DPH) of the BWR cladding ranged from 254 to 268. These values are characteristic of workhardened, stress-relieved zircaloy cladding[12]. The contribution from any irradiation hardening could not be ascertained from these hardness measurements because of the insensitivity of the DPH values in this hardness range.

More porosity lies within the grains at the fuel edge than at the fuel center. Although a few pores are found within the grains at the fuel center, large pores are found in the grain boundaries. Porosities determined from immersion densities from two samples from the top section of PH462-E4 were 4.95% and 3.65%. The porosity determined from a sample from the center section was 5.5%. Based on a manufactured fuel porosity of 5%[13], the BWR fuel had not densified.

The defect at the top of BWR fuel rod PH462-C5 which was heated in unlimited air for 7206 h did not enlarge, because the hole did not penetrate through the wall of the cladding. The defect is located at a pellet/pellet interface, but it only extended 28% into the cladding. X-ray diffraction measurements of a sample of the fuel taken at the midradius indicated that the fuel was UO_2.

The defect in the center section of the fuel rod may have completely penetrated the cladding. The neutron radiograph shows the defect to be located near a large gap in the fuel stack. However, the defect was not located in this sample, probably because of a shift in azimuthal orientation when the hole was drilled.

The fuel was oxidized, as evidenced by the delineation of the grain boundaries in unetched samples. Normally, the fuel must be etched to resolve the grain boundaries; but when the fuel is oxidized, the oxidation occurs along the grain boundaries, delineating the boundaries. For the fuel samples taken in the defect area, the oxidation extended from 2.2 cm above to 3.3 cm below the defect. The apparent porosity of the fuel in the sample with the defect was determined to be 40.9% at the midradius, 40.0% at the fuel center, and 36.4% at the fuel edge. Pull-out of individual grains resulted in dark areas; thus, the above percentages reflect the porosity (about 4 to 5%) and the pull-out of individual grains.

Cracks did not initiate at all defects in the BWR fuel rods; but in unlimited air, a crack was initiated from the intentional defect located at the bottom of BWR fuel rod PH462-C5 (Figure 3). The crack size in PH462-C5 was asymmetrical, extending 8.6 mm up the rod and 10.2 mm down the rod from the initial defect. Its width at the widest point was 1.3 mm. The original

defect, which was 0.76 mm, increased by 0.025 mm neglecting the crack opening. The fuel rod expanded 17% at 90 degrees from the crack and 7% at 30 degrees almost parallel to the crack. The fuel rod deformation was 7.9% at the top of the crack and 6.3% at the bottom of the crack. The deformation of the failed BWR fuel rod was apparently constrained by the fuel rod capsule. The maximum deformation of the fuel rod is 1.73 cm, compared with 1.75 cm inside diameter of the capsule. The fuel rod stuck inside the capsule when the capsule was being unloaded.

About 13 cm of the fuel may be oxidized, as indicated from the neutron radiographs. The pellet/pellet interfaces were still apparent in the neutron radiographs.

The defect is shown in Figure 4. The defect is located within 3 mm of a pellet/pellet interface and has penetrated all the way through the cladding wall. The fuel is mostly oxidized in the fragments developed from fuel cracking.

The typical fuel microstructure of the oxidized fuel is shown in Figure 5. The microstructure indicates that the fuel is more severely oxidized than the samples discussed above because of its dark appearance compared with microstructures of unoxidized fuel. The fuel is not pulled out as in the other samples. The porosity determined by image analysis is 4.7% at the fuel edge and 6.4% at the fuel midradius. Because of the darkness, estimates of the porosity at the pellet center could not be determined.

X-ray diffraction measurements of the sample taken on the same side as the defect indicated U_3O_8 or perhaps $UO_{2.9}^{14}$. The opposite side of the defect indicated UO_2. Because of the lack of resolution with the Debye Scherrer camera, UO_2 may be U_4O_9 or U_3O_7, since the doublets of the distorted cubic structure could not be resolved. The fuel was oxidized from 12.7 cm above the defect to less than 9.2 cm below the defect.

There was a measurable amount of the long-lived isotopes of krypton and xenon released in the capsule containing BWR fuel rod PH462-D6 which was heated in an inert atmosphere for 13000 h. Fission gas release from this rod was also observed during the second nondestructive examination. These gases may have been released from the grain boundaries as the fuel was oxidized.

The leak rate measured at room temperature at the start of the third heating cycle was 5.96×10^{-8} cm^3/s in the capsule containing PH462-D6, and some air leaked into the capsule so that the capsule contained 5.2% nitrogen, 1.38% oxygen, and 0.06% argon. Based upon this composition and a nominal 326 cm^3 capsule volume, 20.3 cm^3 of air leaked into the capsule. During the 7206 h at temperature, the effective leak rate is calculated to be 7.83×10^{-7} cm^3/s.

The top defect was apparently closed, and measurements indicated nominal defect size. The neutron radiograph in the vicinity of the defect shows the fuel to be intact with some minimal longitudinal pellet cracking, but the defect in this section was not located either because of errors in azimuthal

orientation or the defect being too small for detection. The defect should be located at the center of a pellet. Although the fuel was apparently not oxidized, as evidenced by having to etch the fuel to resolve the grain boundaries, X-ray diffraction measurements indicated the presence of U_3O_8. Oxidation was also indicated from X-ray diffraction measurements 3.2 cm above the defect.

Although the fuel rod diameter in PH462-D6 indicated no strain, the middle defect increased in diameter by 0.14 mm, from 0.88 mm measured during the second interim examination to 1.02 mm measured during the third examination. The defect appears to have penetrated the cladding wall, and the neutron radiograph in the defect area indicates fuel oxidation by the large gap in the fuel stack near the defect.

The defect in the center section, shown in Figure 6, is located within 8.2 mm of a pellet/pellet interface. A large gap developed in the fuel stack at the location of the defect. Since this gap was observed in the neutron radiograph, it could not be the result of fuel loss during polishing.

The typical fuel microstructure in the defect area is shown in Figure 7. The grains are relatively free of pores, and the pores lie in the grain boundaries. The apparent porosity determined by image analysis was 16.4% at the fuel midradius and 16.6% at the fuel center. This increase in porosity is attributed to localized fuel pull-out of individual grains. X-ray measurements of three of the samples located at the edge of the fuel indicated only UO_2, but the sample obtained adjacent to the gap in the fuel stack at the center of the pellet indicated some U_3O_8. Fuel oxidation extended 1.9 cm in either direction from the defect, but did not extend as far as 31.8 cm from the defect where a sample was taken.

PWR Fuel Rods

The general surface condition of H. B. Robinson PWR rods appeared to be unchanged after heating for about 13,000 h in limited air. The fuel rod heated in limited air was similar in appearance to that heated in argon. There was little crud deposition on the fuel rod, which had a smooth oxide on the surface.

The measured diameters of the PWR fuel rods were about 10.59 mm, indicating some cladding collapse. The smaller diameter may be attributed to cladding creep during steady-state irradiation in the reactor. These values are comparable to the values measured previously[4,5]. Assuming the nominal preirradiated fuel pellet diameter of 9.3 mm and from the fuel rod measurements, the radial gas gap would be 70 μm. From the metallography, the fuel cladding gap varied from 20 to 34 μm around the circumference of the cladding, indicating some fuel swelling from irradiation.

The Vicker's DPH varied from 247 to 258, with an average of 253. These values represent work-hardened, stress-relieved zircaloy cladding.

From the immersion density of a sample of the irradiated fuel from the top section of rod B05-B8, the porosity was 5.5%; and porosity determined from a sample obtained from the center section was 2.8%. With the 5 to 5.5% porosity in this fuel, about 3% fuel densification has occurred, based upon the as-fabricated density of 92%[13]. The 3% densification (2% in the radial direction) would result in an additional 93 μm radial gas gap, but the cladding creepdown would compensate for some of this gap. Fuel swelling from irradiation could also reduce the gas gap.

The defect in the top section of the PWR fuel rod heated in unlimited air completely penetrated the cladding wall and is located at a pellet/pellet interface. From the neutron radiograph, the fuel was intact in the vicinity of the defect. The large gap in the fuel stack observed in the center section of BWR rod PH462-D6 is not evident in the PWR fuel.

Etching the fuel is not required to reveal the grain boundaries because the fuel is oxidized. However, X-ray diffraction measurements of three fuel samples indicated that the fuel is UO_2, although U_3O_7 may be present. The apparent porosity of this unetched fuel is 37.8% at the fuel edge and 33.5% at the fuel midradius. These large values are due to the fuel pull-out as individual grains. Etching the fuel turns the fuel black except for a few isolated grains which may be unoxidized. The fuel in the sample with the defect appears to be attacked more severely along the fuel edge. The etched fuel at the midradius is not as black as that at the periphery, but there is a large extent of fuel pull-out at this location.

The fuel was oxidized 1.6 cm above the defect and, less extensively, at 30.4 cm below the defect where samples were taken. However, the fuel was oxidized along the pellet/pellet interface and the fuel cracks 30 cm from the defect. Each fuel fragment formed by the cracks is oxidized along the surface, leaving an unoxidized portion in the center.

The defect in the center section of the fuel rod penetrated the cladding wall. The neutron radiograph shows the fuel to be intact in the vicinity of the defect, as with the defect in the top section. The defect is located adjacent to a crack in the fuel, which may act as a path for the migration of air into the fuel rod.

Etching the fuel lightly for 10 s has turned the fuel black, indicating some fuel oxidation. X-ray diffraction measurements indicated the fuel to be UO_2, although the fuel might be U_3O_7.

PWR fuel rod B05-G7 was heated in a capsule containing an inert atmosphere. Prior to the third heating cycle, the cold leak rate was measured to be 1.68×10^{-10} cm^3/s. After the third heating cycle, the capsule contained 5.8% nitrogen and 0.98% oxygen. Based upon this composition and the capsule volume of 326 cm^3, the effective leak rate was 8.67×10^{-7} cm^3/s. The ratio of nitrogen to oxygen is greater than 3.76 for atmospheric air, indicating that some of the oxygen has been consumed in the oxidation of the fuel.

From the visual examination, the defect in the top section did not appear to completely penetrate through the cladding. The neutron radiograph of the fuel rod in the vicinity of the defect shows the fuel to be severely broken up. This fuel fragmentation may be a result of the steady-state irradiation. The defect in the top section was not located, probably because of a shift in azimuthal orientation when the hole was drilled or the defect being too small to be detected. A hole too small seems the more probable cause. The fuel was not found to be oxidized in this section.

The defect in the center section of the rod heated in an inert atmosphere penetrated completely through the cladding. The neutron radiograph of the fuel rod in the vicinity of the defect shows the fuel to be intact. The defect was 0.9 cm from a pellet/pellet interface. The fuel appears oxidized around the periphery of the fuel pellet, as evidenced by the lighter color at the edge. The sample from the center section exhibits more uniform cladding collapse onto the fuel stack than that of the sample from the top section. The fuel/cladding gap varied from 26 to 51 μm around the circumference of the cladding.

In the unetched fuel near the midradius where there is no fuel oxidation, the grain boundaries are not resolved and some porosity is evident, as one would expect. In the oxidized area at the edge of the fuel, the attack on the fuel is evident by the abundance of voids (fuel pullout). However, the grain boundaries are not resolved in the unetched fuel. Upon etching the fuel, the grain structure is resolved, with little attack in the grain boundaries. The porosity was found mainly in the grain boundaries. In the oxidized areas, the oxidized fuel is severely attacked, leaving the individual UO_2 grains. Near the fuel edge (Figure 8), the grain size appears as fine particles.

The sample from the center section 64 cm below the defect exhibits oxidation along the edge of the fuel adjacent to the cladding. The fuel has apparently not oxidized along the pellet cracks or pellet/pellet interface. The fuel/cladding gap varied from 36 to 52 μm around the circumference of the cladding. X-ray diffraction measurements indicated the fuel to be a mixture of UO_2 and U_3O_8.

DISCUSSION

Oxidation of the fuel in both the BWR and PWR fuel rods was extensive. However, the PWR fuel oxidation occurred over large distances from the defect location (up to 65 cm from the defect), while the BWR fuel oxidation was more localized (within 8 to 10 cm of the defect). Similar results of localized oxidation were obtained by Kohli[14] from storage tests with a BWR fuel rod. The radial gap in both PWR and BWR fuel rods varied between 20 and 60 μm; so if one hypothesizes that the radial gap was the path for air transport in the fuel rod, the oxidation behavior should be the same for both fuel rods. The migration paths may be along the fuel cracks in addition to the radial gas gap. However, the cracking patterns in both the PWR and BWR fuel rods are about the same; consequently, the cause of the enhanced gas transport in the PWR fuel rods could not be ascertained. Gas transport studies in PWR

fuel[15] indicate that fuel cracks contribute to the gas transport. The fuel cracks provide a more tortuous path, but evidently gas transport is not inhibited. Unfortunately, no gas transport studies have been made with BWR fuel rods. The densification in PWR fuel but not in BWR fuel may be the source of the differences in the oxidation behavior, but the evidence is inconclusive as to the explanation for the behavior.

Both the BWR and PWR fuel rods had finite leak rates which permitted air to enter the capsules, and the extent of oxidation in those rods with an inert atmosphere were less than in those with unlimited air because of the lower partial pressure of oxygen. After 7206 h at temperature, 22.5 cm^3 of air leaked into the PWR capsule and 20.3 cm^3 of air leaked into the BWR capsule. The leak rates into these capsules account for the air contamination of the inert atmosphere. Because the oxygen content was increasing in the capsules containing the fuel rods, the oxidation rates were slower than the leakage rate into the capsules, as evidenced by the build-up of oxygen.

The oxidation of the PWR fuel rods in unlimited air was not as extensive as that in BWR fuel rods. U_3O_8 was formed in the local oxidation of rods PH462-C5 and -D6, but only minute amounts of U_3O_8 were formed in rod BO5-E7. Since the defect sizes were the same in both rods, the rate of air entering the rods should be the same; but about six times the axial fuel stack length was attacked in the PWR than that of the BWR rod, so the extent of oxidation should be less with the PWR fuel rods.

Although the oxidation of rod PH462-C5 was extensive and microstructure changes could not be readily assessed, the limited oxidation of rod PH462-D6 indicated the attack to be along the grain boundaries. The porosity in rod PH462-E4 and in the unoxidized area of rod PH462-C5 was distributed within the grains and with some porosity in the grain boundaries; the porosity in rod PH462-D6 was mainly in the grain boundaries. Fission gas release observed after the second and third nondestructive examinations occurred as a result of oxidation in the grain boundaries releasing the fission gas contained in the pores. The open porosity in the BWR fuel rod would provide channels for the release of fission gas to the plenum as the oxidation progressed along the grain boundaries.

Of the two BWR fuel rods that ruptured at defects, the ruptures occurred at the extreme ends of the rods rather than in the center. In rod PH462-C5, the rupture occurred at the bottom defect rather than at the center of the rod. The defect at the top of the rod did not penetrate completely through the cladding; therefore, fuel oxidation and cladding rupture did not occur. Rod PH462-E3 ruptured at the defect placed in the top part of the fuel rod[4]. (There was no defect placed in the bottom portion of the fuel rod.) Although the statistics are limited from the small number of rods with defects, the results from the two BWR fuel rods suggest that the location of the defects with respect to the ends of the fuel rods (within about 30 cm) may be more important than the location of the defects with respect to pellet/pellet interfaces. This hypothesis is supported by the results of testing a BWR fuel rod in air[14]. Although this rod had two cladding defects with some

rod deformation at 107 cm and between 200 and 225 cm from the bottom of the rod caused by hydriding after the fuel rod was heated in air, extensive cladding deformation occurred at 366 cm from the bottom of the fuel rod (at the top of the fuel stack) because a hole was drilled into the plenum to aid in the removal of moisture. This hole also allowed air into the plenum, causing fuel oxidation. The location of the defects at pellet/pellet interfaces was thought to be important in the fuel rod behavior[4], but this hypothesis does not appear to be supported by the test results. Also, the unrestricted air transport in PWR fuel rods and the same extent of oxidation at defects located at pellet/pellet interfaces as at defects located away from interfaces in both PWR and BWR fuel rods do not appear to give relevance to the defects located at pellet/pellet interfaces.

The volume expansion arising from the formation of U_3O_8 from UO_2 is 36.4%. For a right-circular cylinder and isotropic expansion, the maximum radial expansion is 25.3%. The radial expansion of rods PH462-E3 and PH462-C5 was about 17%, much less than the maximum amount. Expansion of these rods was constrained by the capsules and limited to 17 to 18%. This constraint may have also limited the crack growth in these fuel rods. The strain at the crack tips was between 6.3 and 7.9% when the fuel rod deformation was 17% as a result of the capsule constraint. If the fuel rod deformation were not constrained, a strain near 25% at the defect would result in perhaps longer cladding cracks for the same strain at crack tips and the same time at temperature.

Fuel rod rupture resulting from the oxidation of UO_2 to form lower density U_3O_8 is a degradation mechanism of concern at the temperatures that are possible in dry storage. As oxygen initially diffuses into the UO_2, the oxygen occupies interstitial positions with a small lattice expansion from the cubic to tetragonal structure with the formation of U_3O_7. The oxygen transport occurs along the grain boundaries, as evidenced by delineation of the grain boundaries in BWR fuel rods at low rates of oxidation. The volume expansion from the formation of U_3O_8 induces such a high stress on each grain that the grains are popped out of the fuel pellet (fuel pullout) if not constrained by the cladding[16]. Although the PWR fuel was oxidized, the fuel pull-out was not as extensive as in the BWR fuel. The PWR fuel was also attacked at the grain boundaries, but the attack does not become apparent until the fuel is etched.

The PWR fuel cracking effectively breaks the pellets into smaller fragments, which then oxidize individually. Although the fuel cracking characteristics in BWR fuel rods apparently do not allow extensive axial migration of air, a similar mechanism may operate on a localized level to accelerate the oxidation toward the center of the fuel pellets.

After the U_3O_7 is formed, the rate of weight gain increases due to the increased oxygen/uranium ratio. This process has been described as a two-phase oxidation in which the accelerated oxidation occurs after an induction period for the formation of U_3O_7 and a postinduction phase involving the formation of U_3O_8. The postinduction period has been characterized with unirradiated materials as the formation of powder when

U_3O_8 is formed. The induction period for irradiated fuel has not been completely verified, but preliminary results indicate that it is shorter than the induction period for nonirradiated fuel. Einziger[4] reported an induction period of up to 1000 h for BWR fuel, but this high value does not appear to be supported by tests with irradiated fuel[17]. The calculations were based upon the oxidation from the fuel edge to the center. The results show that the oxidation occurred by oxidation of each individual fragment of a fuel pellet. The so-called incubation period can be much faster than that indicated by tests with irradiated fuel fragments.

The density changes indicate that parabolic kinetics may be more appropriate than linear kinetics or other mechanisms. The densities (based on theoretical density) increased from 10.96 g/cc for UO_2 to 11.4 g/cc for U_3O_7. These densities result in a slight volume decrease of 2% and a Pilling-Bedworth ratio of 0.98. With a ratio less than 1.0, one may expect linear oxidation kinetics, but a ratio of 0.98 may not be sufficiently less than 1.0 to preclude linear kinetics. As more oxygen is added to the fuel, U_3O_8 forms with a density of 8.35 g/cc. The molar volume expansion is 36.4%, and the Pilling-Bedworth ratio is 1.36, which would indicate a tenacious U_3O_8 film on the U_3O_7 and parabolic kinetics. When kinetic data are obtained for a short period of time and extrapolation is required for long-term effects, it is mandatory to know that the kinetic models are correct for the period of time to be extrapolated.

The oxidation kinetics in terms of the fraction reacted versus time[18] were initially interpreted unsucessfully by the Johnson and Mehl[19] model for recrystallization and grain growth. The exponent varied with the fraction reacted instead of remaining constant. Assuming that the reaction rate at the reacting interface is linear and that the reacting particles are spherical, the fraction reacted, X, is determined in the following expression:

$$(1-X)^{1/3} = kt/r_0 \qquad (1)$$

where k = constant
t = time
r_0 = initial particle radius.

A plot of $(1-X)^{1/3}$ as a function of time would result in a straight-line function. This model also shows that the $(1-X)^{1/3}$ varies inversely with the initial radius of the particle. The data from Harrison et al. were not found to fit this model[20].

Assuming the same spherical particle, but with parabolic kinetics where the interface and the area of the reacting interface move inversely with the thickness of the product, the following function is obtained:

$$2(X)^{2/3} - X^{1/3} = kt/r_0^{\,2}. \qquad (2)$$

For Equation 2, the same approach can be taken as with Equation 1. The function plotted as a function of time would be a straight line, but this

function varies inversely with the square of the initial particle size. The above two expressions reflect a changing reacting surface area with the time of reaction. One could still consider models based upon constant surface area in which the fraction reacted was proportional to time for linear kinetics or proportional to the square root of time for parabolic kinetics. For low-temperature oxidation of UO_2, the appropriate kinetic models are still uncertain.

The metallography of both PWR and BWR fuel indicates that initial oxidation occurs with individual fuel fragments. The oxidation proceeds along the grain boundaries with the formation of U_4O_9 or U_3O_7. At this point, the surface area to be considered is that involved with the grains and not the fuel fragment, so that a model based upon changing surface area is involved with the process. In addition, depending upon fragment size, two kinetic processes may be going on simultaneously; the oxidation of UO_2 to U_3O_7 and the oxidation of U_3O_7 to U_3O_8.

For the relatively short time at temperature (13,000 h), there has been no observable deterioration in the fuel rods from creep rupture or stress corrosion cracking (SCC) except perhaps for rod PH462-E5. Isotopic gamma scanning indicated fuel release from the originally intact fuel rod PH462-E5, which was also confirmed by delayed neutron measurements. This release is indicative of fuel rod failure, but the breach may have been to small to be detected visually since it was not discovered during the visual examination. Tramp fuel (fuel residue on fuel rods during fabrication) may be a source for this contamination, but it was not observed on other intact fuel rods. The breach may have developed during this testing program, but it also could have developed in-reactor.

CONCLUSIONS

A minute amount of fuel was released from the intentionally defected fuel rods, as would be expected from these perforated rods. However, isotopic gamma-scanning indicated fuel release from the intact fuel rod PH462-E5, which was confirmed by delayed neutron measurements. This release is indicative of fuel rod failure, but the breach may have been too small to be detected visually since it was not discovered during the visual examination. The breach may have developed either during in-reactor irradiation or during dry storage testing.

The volumetric expansion associated with the formation of U_3O_8 is 36.4%. The maximum possible expansion in the radial direction is 25.3%. This expansion was not achieved with rods PH462-E3 or -C5, because the capsule containing the fuel rod restricted the expansion.

In BWR fuel, the oxidation was localized and limited to within 8 to 10 cm from the defect. Unlike PWR fuel, the fuel had not densified, the cladding had not exhibited creepdown, and the UO_2 grain size was larger than that of PWR fuel. No cause could be identified for the localized oxidation in BWR fuel.

The gas release for rod PH462-D6 indicated oxidized fuel, which was also supported by the destructive examination. Limited oxidation also occurred with one of the PWR rods heated in an inert atmosphere. Although these capsules were sealed, the capsules still have a measurable leak rate from the mechanical seals that allow air to penetrate the otherwise sealed capsules. The oxidation rate is limited by the partial pressure of oxygen in the capsule. The extent of oxidation was not sufficient after the 13,000-h heating cycle to form U_3O_8 in sufficient quantities to rupture fuel rods with its accompanying expansion. The fuel was oxidized to U_4O_9, or perhaps U_3O_7 with some U_3O_8.

The storage of PWR fuel rods in unlimited air at 229°C has not resulted in fuel rod rupture. The fuel rod heated in an unlimited air atmosphere was oxidized, but not to the extent that BWR rods were and the oxidation extended up to 65 cm away from the defect. The fuel was oxidized to U_3O_7, with a small amount of U_3O_8 in rod B05-E7.

Similar to rod PH462-D6, the PWR fuel rod heated in an inert atmosphere (B05-G7) was also oxidized; but the oxidation was limited by the partial pressure of oxygen. The oxidation rate of PWR fuel is slower than that of BWR fuel.

Even though fuel rods may be stored in an inert atmosphere, cask penetrations will provide leakage paths for air to enter the casks. If the inert gas is not periodically replenished, the oxygen can build up in the cask and oxidize fuel in defected rods. The current tests show that the oxidation rate is less than the rate of leakage, but the oxidation rate would increase with the increase in partial pressure of oxygen as it accumulated.

In both the PWR and BWR fuel rods, oxidation paths were along the gas gap and cracks in the fuel so that the pellets were oxidized by oxidation of the individual pellet fragments. This process enhances the oxidation of the fuel stack over what would be expected from rates determined from out-of-pile tests on fuel fragments and applied to intact fuel pellets. As the fragments are oxidized, the attack is along the grain boundaries, releasing fuel grains in the case of BWR fuel.

A number of different kinetic models for the oxidation of UO_2 have been proposed, but none of them satisfactorily fit the oxidation data because the oxidation kinetics are not really understood. Also, some parameters, such as surface area, are not considered. The kinetic models verified for long periods of time relevant to dry storage will be required to properly evaluate dry storage of nuclear fuel.

The results from this program show that U_3O_8 with its significant expansion characteristics can still form at temperatures below 250°C, resulting in fuel rod rupture. Only U_3O_7, with its low expansion characteristics, was expected to form at a specific temperature below 250°C from which a conservative licensing position could be developed. However, a specific temperature could not be determined for establishing a licensing position. Further studies are required with irradiated BWR and PWR fuel to

determine the oxidation kinetics and mechanisms at temperatures below 250°C for long-term periods simulating dry spent fuel storage conditions. These tests have been particularly useful in providing data with defective fuel rods in an air atmosphere, but the test times were too short and the irradiated fuel rods were perhaps too old to provide much information on potential failure of intact fuel rods during long-term storage.

REFERENCES

1. Code of Federal Regulations, "Licensing Requirements for the Storage of Spent Fuel in an Independent Spent Fuel Storage Installation," Title 10, Part 72; and Radwaste News 1, p. 234 December 1980.

2. Environmental Assessment for 10CFR72, "Licensing Requirements for the Independent Storage of Spent Fuel and High Level Radioactive Waste," NUREG-1092, August 1984.

3. L. D. Blackburn et. al., Maximum Allowable Temperature for Storage of Spent Nuclear Fuel, HEDL-TME 7837, May 1978.

4. R. E. Einziger and J. A. Cook, LWR Spent Fuel Dry Storage Behavior at 229 C, NUREG/CR-3708, HEDL-TME 84-17, July 1984.

5. R. E. Einziger and J. A. Cook, "First Interim Examination of Defected BWR and PWR Rods tested in Unlimited Air at 229°C," Proc. of NRC Workshop on Spent Fuel/Cladding Reaction During Dry Storage, NUREG/CP-0049, August 17-18, 1983.

6. C. S. Olsen, Dry Spent Fuel Storage Test Plan for Final Nondestructive Fuel Rod Examination, NUREG/CR-3921, EGG-2328, July 1984.

7. C. S. Olsen, The Performance of Defected Spent LWR Fuel Rods in Inert Gas and Dry Air Storage Atmospheres, NUREG/CR-4074, EGG-2364 January 1985.

8. C. S. Olsen, Particulate and Gas Release from Light-Water-Reactor (LWR) Fuel Rods Stored in Inert and Dry Air Atmospheres, NUREG/CR-4056, EGG-2359, December 1984.

9. C. S. Olsen, Dry Spent Fuel Storage Test Plan for Destructive Fuel Rod Examinations, NUREG/CR-4084, EGG-2387, January 1985.

10. R. A. Lorenz et al., Fission Product Release from Highly Irradiated LWR Fuel, ORNL/NUREG/TM-287, February 1980.

11. C. S. Olsen, UO_2 Densification in LOFT Fuel, NUREG/CR-1948, EGG-2802, March 1981.

12. D. O. Hobson, The Effect of Thermal Transients on the Hardness of Zircaloy Fuel Cladding, ORNL-NUREG-TM 26, June 1976.

13. R. E. Einziger and R. L. Fish, Characterization of LNWR Spent Fuel Rods Used in the NRC Low-Temperature Whole Rod and Crud Performance Test, NUREG/CR-2871, HEDL-TME 82-27, September 1982.

14. R. Kohli et al., "The Behavior of Breached Boiling Water Reactor Fuel Rods on Long-Term Exposure to Air and Argon at 598 K", Nucl. Tech. 69, 1985, p. 186.

15. S. J. Dagbjartsson et al., Axial Gas Flow In Irradiated PWR Fuel Rods, TREE-NUREG-1158, September 1977.

16. E. R. Gilbert et al., "Oxidation of UO_2 at 150 to 350 C", Presented at the Irradiated Fuel Storage Operating Experience and Development Programs International Workshop, Toronto, Canada, October 17-18, 1984.

17. I. J. Hastings et al., "Postirradiation Behavior of UO_2 Fuel II: Fragments at 175 to 275 C in Air", Nucl. Tech. 68, 1985, p. 40.

18. D. G. Boase and T. T. Vandergraaf, "The Canadian Spent Fuel Storage Canister: Some Materials Aspects," Nucl. Tech. 32, Jaunary 1977, p. 60.

19. W. A. Johnson and R. F. Mehl, "Reaction Kinetics in Processes of Nucleation and Growth", Trans. Am. Inst Mining Met. Engrs. 135, 1939, p. 416.

20. K. T. Harrison et al., "The Kinetics of the Oxidation of Irradiated Uranium Dioxide Spheres in Dry Air", J. Nucl. Mater. 23, 1967, p. 121.

TABLE 1. DEFECT LOCATIONS

	Defect Locations[a]					
	Defect Number 1		Defect Number 2		Defect Number 3	
Fuel Rod	Location (cm)	Orientation (°)	Location (cm)	Orientation (°)	Location (cm)	Orientation (°)
B05-E7	36.8	90	179.1	240	--	--
B05-G7	27.9	200	205.1	0	--	--
PH462-D6	52.1	90	224.8	270	--	--
PH463-C5	66.8	0	236.2	0	401.3	0

a. Measured from the top of the fuel rod.

TABLE 2. FUEL ROD STORAGE CONDITIONS

Reactor Type	Assembly and Rod Number	Capsule Atmosphere	Capsule Pressure (MPa)	Fuel Rod Condition
PWR[a]	B05-G7	Ar/1%-He	0.1	Defected (2 holes)
PWR	B05-E7	Air	0.1	Defected (2 holes)
PWR	B05-08	Ar/1%-He	0.1	Intact
PWR	B05-B8	Air/1%-He	0.1	Intact
BWR[b]	PH462-D6	Ar/1%-He	0.1	Defected (2 holes)
BWR	PH462-E4	Air/1%-He	0.1	Intact
BWR	PH462-E5	Ar/1%-He	0.1	Intact
BWR	PPH462-C5[c]	Air	0.1	Defected (3 holes)

a. PWR is the H. B. Robinson fuel.
b. BWR is the Peach Bottom fuel.
c. After the 2nd furnace campaign, this rod replaced PH462-E3.

Figure 1. Photograph of dry fuel storage furnace.

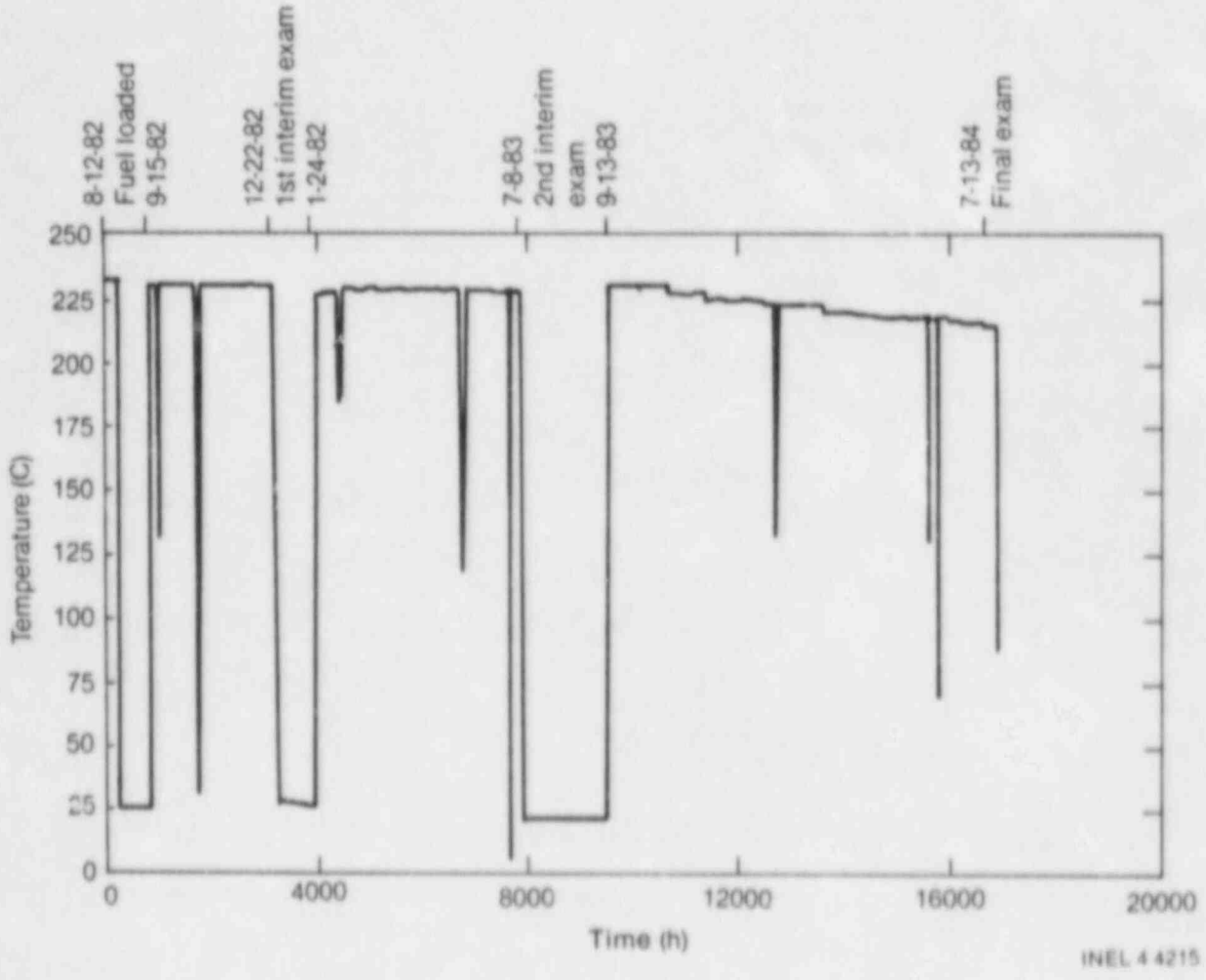

Figure 2. Dry fuel storage temperature history.

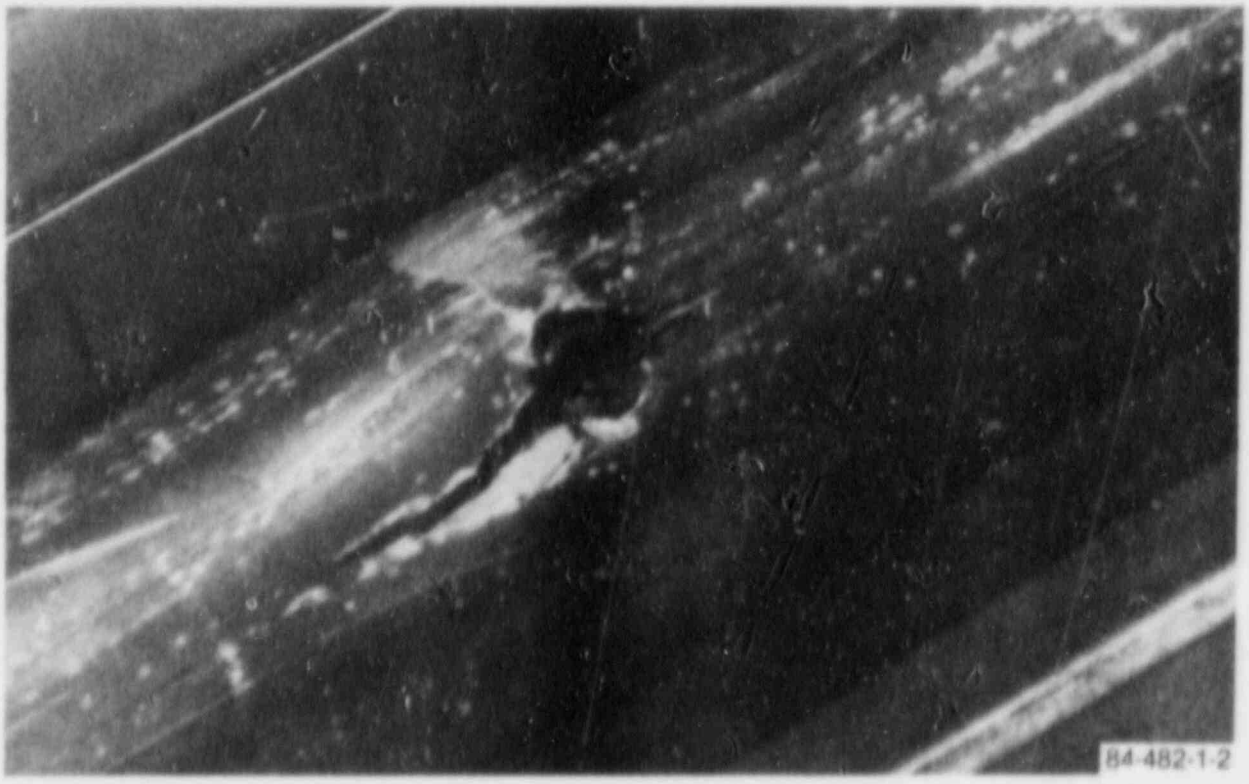

Figure 3. Cladding break in the bottom section of BWR fuel rod PH462-C5.

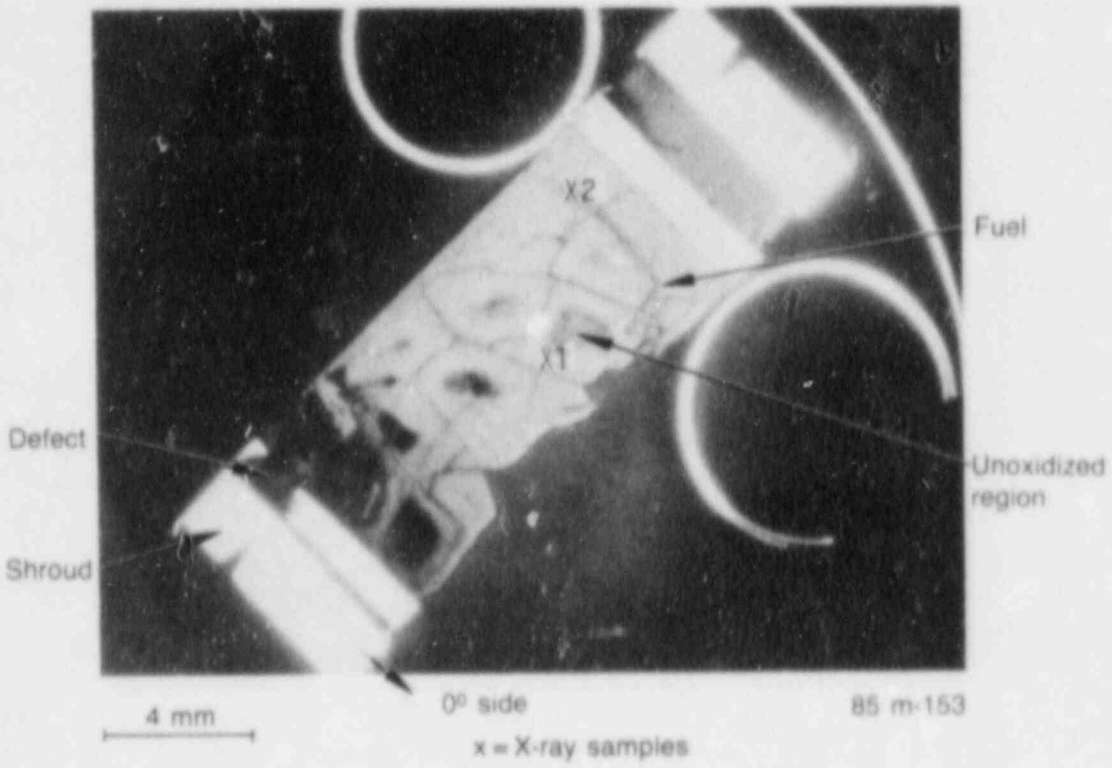

Figure 4. Cross section at defect in bottom section of BWR fuel rod PH462-C5.

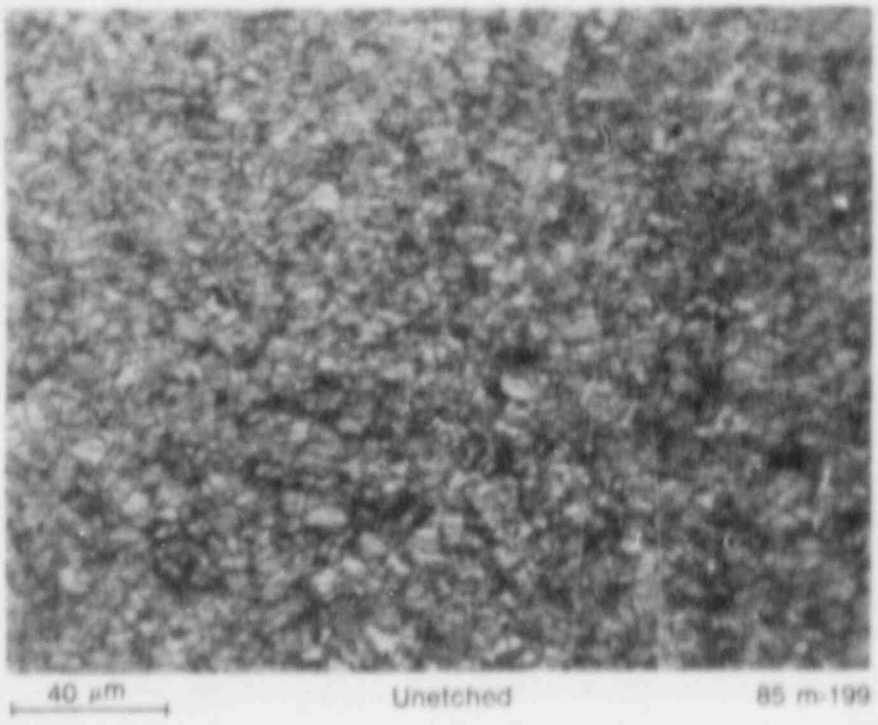

Figure 5. Typical fuel microstructure.

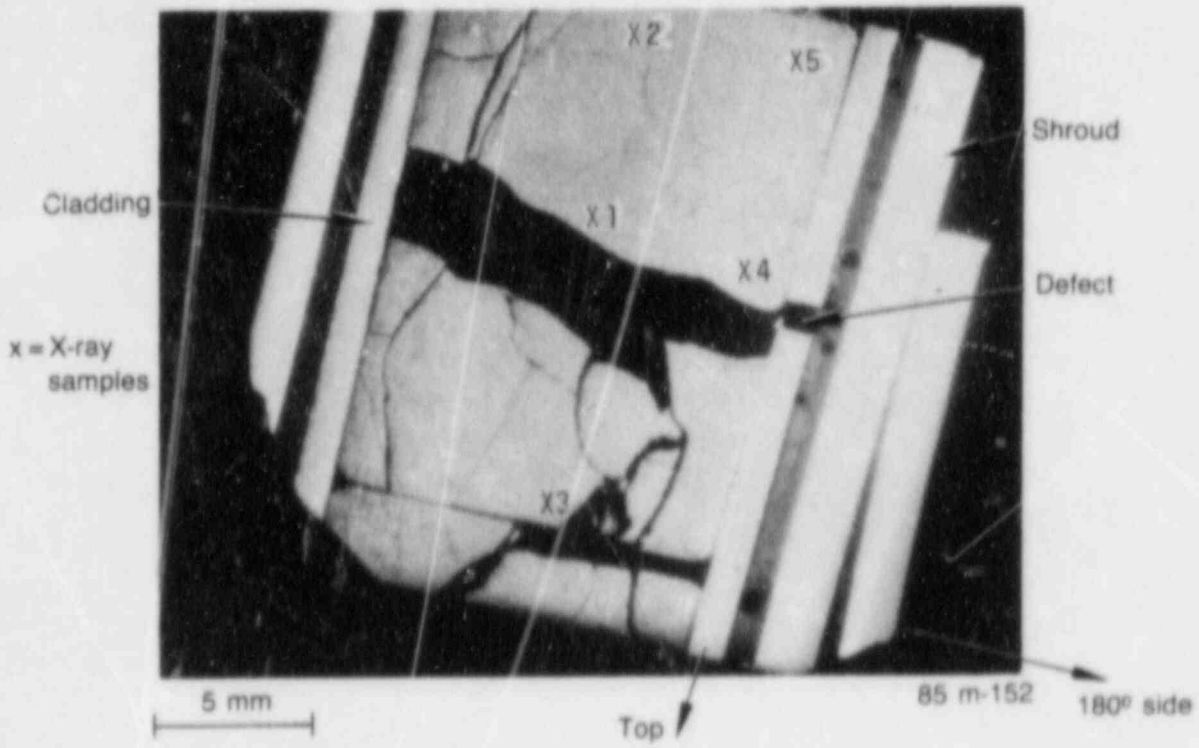

Figure 6. Defect in center section of BWR fuel rod PH462-D5.

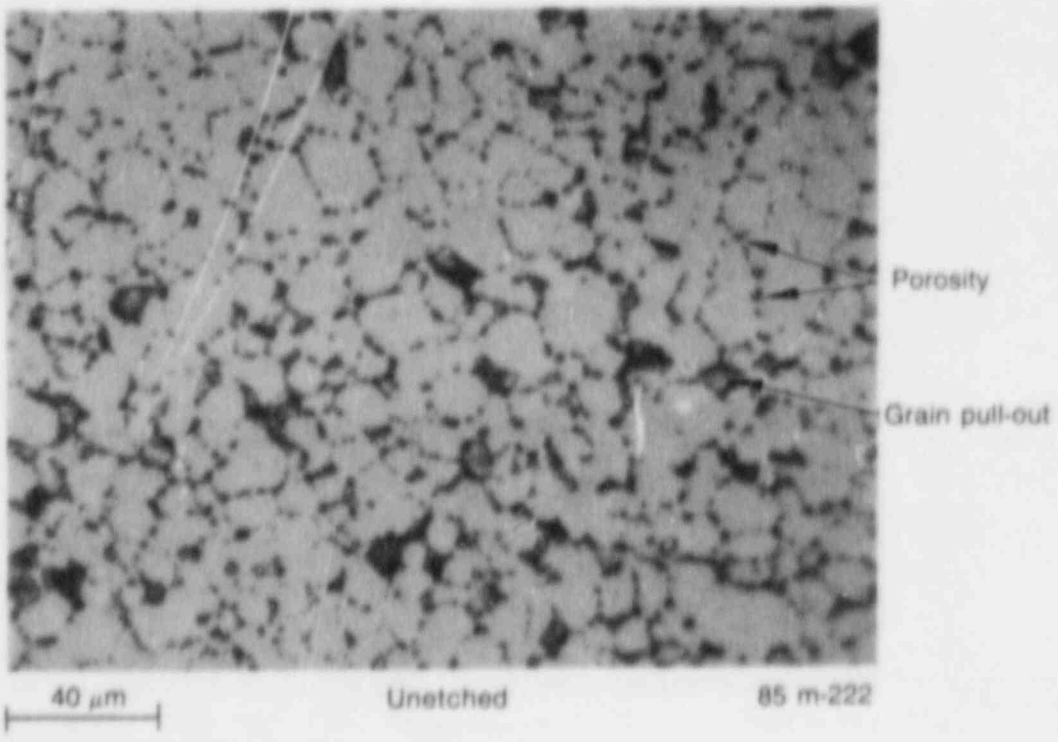

Figure 7. Fuel microstructure at defect in center section of BWR fuel rod PH462-D6.

Figure 8. Oxidized fuel near edge of center section of PWR fuel rod B05-G7.

LESSONS LEARNED FROM A NUREG-0737 REVIEW OF HIGH-RANGE EFFLUENT MONITORS AND SAMPLERS

Andrew P. Hull,

Safety and Environmental Protection Division
Brookhaven National Laboratory, Upton, NY 11973

John R. White,

Emergency Preparedness and Radiological Protection Branch
USNRC Region I, 631 Park Ave.
King of Prussia, PA 19406

ABSTRACT

Shortly after the onset of the accident on 3/28/79 at Unit 2 of the Three Mile Island Nuclear Power Station, the upper range capabilities of its real-time monitors for gaseous, radioiodine and particulate effluents to the atmosphere were exceeded. Subsequently, the NRC required extended range gaseous effluent monitors and an improved capability for the obtaining of frequent samples of radioiodines and particulates at the concentrations that would be anticipated in effluent streams under accident conditions (NUREG-0578, NUREG-0660, NUREG-0737, Items II.F.1-1 + II.F.1-2).

In 1983 an on-site post-implementation review of their installation and operation was initiated by the NRC Region I. The results from nineteen such reviews indicate that the licensees have adopted a variety of approaches to meet the NRC's requirements ranging from the installation of completely new commercial modules to improvised additions to existing monitors and samplers. Some advantages and drawbacks of these various approaches are summarized.

1. INTRODUCTION

As evident from a 1971 survey, concern for the adequacy of the installed effluent monitors at commercial nuclear power reactors preceded the accident at the Three Mile Island Nuclear Power Station (TMI) on March 28, 1979 by almost a decade.[1] Subsequently, criteria for extended range monitors for radiogases, radioiodines and radioparticulates were developed in a follow-up study by Battelle Northwest Laboratories.[2] In 1974 these criteria were incorporated in a proposed ANSI Standard,[3] which was finalized and published in 1978.[4]

In 1977, the U.S. Nuclear Regulatory Commission (NRC) issued Revision 1 to its Regulatory Guide 1.97 which incorporated the criteria of the ANSI standard by reference.[5] At that time, the NRC indicated its intention to implement the guide for all nuclear power plant applications then currently under review and at all operating reactors. The scope for the latter was to be determined by the NRC Staff on a case by case basis.

Only limited progress in this implementation, which had not extended to the TMI reactors, had been made at the time of the TMI accident in 1979. During it and shortly after major fuel cladding damage occurred (at about two hours after its onset), the concentrations of radiogases in the plant effluent stream exceeded the upper range of the installed gaseous effluent monitors.[6] The upper range capability of the installed radioparticulate and radioiodine monitors was also exceeded at about the same time, due to the background from the extraordinary concentration of radiogases. The subsequent retrieval of stack effluent particulate and radioiodine samples for analysis was impeded by the high radiation fields at the location where they were installed.

In its evaluation of this aspect at the accident, the TMI-2 Lessons Learned Task Force observed that at the time of the accident only 20% of the then operating plants had monitors that would have stayed on scale under the TMI accident conditions.[7] They also observed that potential releases from postulated accidents could be several orders of magnitude larger than encountered at TMI. The Task Force recommended the prompt adoption, in its entirety, of the then recently published ANSI Standard on emergency instrumentation, except that they adjudged that real-time monitors for large concentrations of particulates and radioiodines were not practical.

An action plan, incorporating these and other recommendations of the Task Force was subsequently adopted by the Commission in mid-1980.[8] Clarification of the plan, known as NUREG-0737, was provided later in that same year.[9] Its basic requirements with regard to noble gas effluent monitors are contained in its Section II.F.1., Attachment 1, from which Table I is excerpted. The requirements for the sampling and analysis of particulates and radioiodines in plant effluents are contained in Section II.F.1, Attachment 2, from which Table II is excerpted. An implementation date of January 1, 1982 was specified for both II.F.1-1 and II.F.1-2.

Responsibility for the post-implementation review of these selected NUREG-0737 items was assigned by the NRC Office of Inspection and Enforcement to the NRC's regional offices. In mid-1983, the NRC's Region I contracted with the Safety and Environmental Protection Division of Brookhaven National Laboratory for technical assistance in the performance of these reviews. Each has required the identification, acquisition and documentation of the licensee's commitments, clarifications, schedules and orders. A subsequent on-site inspection included physical verification and validation of the installation and operability of equipment, as well as verification of the adequency of the licensee's procedures and of the qualification and training of licensee's personnel.

At the present time, on-site reviews have been completed at the rate of about one per month for nineteen of the twenty licensee sites in Region I, which currently contains a total of twenty-five operating reactors. They are located in four of the New England states: New York, New Jersey, Pennsylvania and Maryland.

II. APPROACH

Before the on-site reviews commenced, the individual elements that should be included in the overall review effort were considered in a Management Oversight and Readiness Tree (MORT). A portion of it is shown in Figure 1.

Following this, a specific set of instructions and/or questions related to each review component was prepared. These included such sub-categories as design, monitoring system, procedures, structures, hardware and support services, readout and recording, personnel and training. An example for the monitoring system is shown in Table III.

III. FINDINGS

A summary of the installed high-range noble gas monitors, according to their location (on-line or off-line), type of detector, and vendor is shown in Table IV. It is evident that the Region I licensees have chosen a variety of approaches to comply with the requirements of Item II.F.1-1. The typical Boiling Water Reactor (BWR) contained either one monitored release point under accident conditions, the unit vent, or a second monitored release point for the standby gas treatment system as shown in Figure 2 (for the Shoreham Nuclear Power Station). The Pressurized Water Reactors (PWR) were more variable from one monitored unit vent and a main steam line monitor found at Millstone 2, to the three monitored vents and steam relief monitor at the Beaver Valley Station, as shown in Figure 3.

Two licensees installed on-line monitors, using ion chambers in or immediately adjacent to stacks or ducts, while seventeen installed off-line monitors. Of the latter, five installed "gas only" high-range monitors as additions to their pre-existing low-range monitors. A schematic of such a monitor which utilizes an ion chamber, is shown in Figure 4. Twelve licensees installed commercially available integrated monitors with modules for both

monitoring and sampling. A block diagram of one (the General Atomics WRGM) is shown in Figure 5 and a view of another (the Kaman KDGM-HR) in Figure 6.

These installations have also incorporated a variety of approaches to the problem of achieving the required full-range sensitivity. Typically, three overlapping-range detectors have been provided, as shown in Figure 7 (for the General Atomics WRGM). In order to achieve the upper limit of 10^5 uCi/cm^3 (^{133}Xe equivalent), most of these monitors are designed so that that a limited volume of gas is viewed by their high-range detectors, compared to that viewed by their mid- or low-range detectors. An example, for the enhanced high-range detector of the Kaman HRH, is shown in Figure 8.

Although Item II.F.1-1 was not specific on calibration of noble gas monitors up to the required upper range, the NRC has provided some guidance.[10] It recognized the problem of the availability of suitable noble gases, i.e. ^{133}Xe, at sufficient concentrations and of their utilization by licensees if they were available. Therefore, the Staff recommended that a one-time "type" calibration in the laboratory over the intended range be performed and that the transfer procedure of ANSI N323-1978 be utilized in conjunction with solid sources at appropriate energies for on-site calibrations.

As suggested by Table V, most of the vendors appear to have performed only a "one point" primary calibration, utilizing ^{133}Xe and ^{85}Kr. They have then performed a number of transfer calibrations with solid sources with a range of activities and energies, such as ^{109}Cd (0.088MeV), ^{139}Ce (0.165 Mev), ^{51}Cr (0.320 MeV), ^{137}Cs (0.662 Mev) and ^{60}Co (1.17 and 1.33 Mev) to establish the energy response and/or range capability of a given detector.

A summary of the sampling arrangements which have been provided to achieve compliance with Item II.F.1-2 and which have been reviewed to date is shown in Table VI. Again, a variety of approaches is evident. Some licensees (including the five who have utilized "gas only" monitors to comply with Item II.F.1-1) installed independent sampling facilities. One licensee wrote emergency sampling procedures which incorporated pre-existing unshielded routine samplers. Five added additional shielded particulate and iodine sample positions which were connected to an existing low-range sample line, while one added a pre-fabricated multiple sample-position module.

Eleven licensees have installed integrated monitor/samplers which contain micro-processor modules that provide for the automatic or remote collection of a sample at one of three individual sample positions, as also shown in Figure 7. Another licensee located its integrated unit in what would be a high-radiation field during post-accident conditions, so elected to create another more remote sampling station. These integrated monitor samplers typically provide for a much reduced flow of a few hundred cm^3/min, as compared to the customary 1-2 cfm provided for low- and mid-range sampling. This is done in order to limit the total amount of activity that would be collected at concentrations which approach the upper design criterion of 100 uCi/cm^3 for the stipulated 30-minute sampling period.

IV. LESSONS LEARNED

A. HIGH-RANGE NOBLE GAS MONITORS

Oversimplifications in the methods for the conversion of the direct indications of the installed gas monitor, typically in cpm or mR/hr, to effluent concentrations and/or rates of release were among the principal shortcomings encountered in the reviews.

As indicated in Table I, the guidance in NUREG-0737, II.F.1-1 states "Design range values may be expressed in ^{133}Xe equivalent values for monitors employing gamma radiation detectors" (as most do). This concept has not been generally understood or employed by vendors or by the reviewed licensees. In some instances, they have employed uninterpreted actual calibration data for ^{133}Xe or ^{85}Kr to establish detector response, without a recognition of their limitations. The former emits low energy photons, with a mean energy of 0.045 MeV per disintegration. Thus, they may be significantly absorbed in the housing or walls of a detector. In contrast, ^{85}Kr is principally a beta emitter, with accompanying bremstrahlung gamma radiations and a 0.51 MeV photon with a yield of only 0.4%. This is apparent from Figure 9, which illustrates the direct response with distance of Eberline's high-range detector to each of these nuclides. When corrected respectively for absorption and bremstrahlung, the true response of this detector is about midway between the two curves, so using one point from either would lead to a factor of two error. An even greater difference in energy response which is presumably related to the same cause, is shown in Figure 10, which is a calculated response for a Victoreen-847 ion chamber installed adjacent to a duct at the TMI-1 Station.

Beyond this, these uninterpreted calibration data have also been employed to calculate release rates (in uCi/sec), without regard to the variable energy response characteristic of the detector on which they are based and in the geometries in which they were installed. This response characteristic may be close to linear with energy, as shown in Figure 11, for the Kaman KDGM-HR, or may be quite non-linear as shown in Figure 12, for the General Atomics WRGM.

All of the reviewed licensees had installed monitors which in principle met the upper range criterion of 10^{-3} uCi/cm^3 (see Table 1). However, only two had calibrated the installed high-range monitors on-site at concentrations approaching 10^{-5} uCi/cm^3. The vendor calibration information supplied by Kaman, as shown in Figure 13, suggested that a test with actual radiogases approaching these concentrations had been performed with ^{133}Xe. However, on the basis of field testing which employed ^{85}Kr it is questionable that this monitor can in fact meet the specified upper range.[11] A similar fall-off at high concentrations was reported by a consultant to a Region I licensee in a field calibration of the high-range detector (SA-9) of the Eberline SPING.

Some licensees recognized the variable energy response of high-range monitors by the provision of corrections in their software for making off-site dose assessments. However, this does not provide guidance for a reactor operator or supervisor who may have to make manual calculations of effluent

release rates before skilled post-accident dose assessors are likely to be available.

As indicated in Table V, three licensees selected the Eberline SPING-4 as a high-range monitor for effluent noble gasses. During the reviews, it was ascertained that the micro-processor of this monitor is not radiation hardened, making it doubtful that it would operate reliably in high-radiation fields. However, in one case the monitor was supplemented by the Eberline SA-10 and SA-9 mid- or high-range detectors, for which the sensitive components were remotely located. When the SPING-4 component of this unit senses high-radiation fields, it is isolated from the sample stream, thus increasing its reliability of function throughout an accident sequence.

In several instances, licensees with installed micro-processer controlled high-range gas monitors were found to have a limited number of plant personnel with sufficient training to be able to retrieve data beyond that routinely displayed. Although this ability is not a requirement, these data could be informative in the event of an accident. The review also revealed that several of these monitors had experienced frequent and/or extended down time of their automatic features, apparently due to the failure of their flow sensors.

Except for those with integrated units which function automatically, provision and/or procedures had not been incorporated by licensees for the isolation and/or purging of their low-level gas monitors, should their range be exceeded. Thus their recovery and availablity would be doubtful following an accident as effluent concentrations declined to within the low-range region.

B. SAMPLING AND ANALYSIS OF PLANT EFFLUENTS

The principal deficiency encountered in the review of arrangements for the sampling of radioiodines and particulates was the inability of licensees to document that their sampling systems could collect representative samples. This is particularly so for those with long sampling lines, in which considerable deposition losses of elemental radioiodines could occur even when they were installed in accordance with the design guidance of ANSI N13.1-1969.

The transmission of elemental iodines through long sampling lines has been measured under controlled conditions in the laboratory by Unrein et al.[12] Their studies suggest that it depends upon the relative rates of deposition and resuspension from their walls. Transmission factors greater than 50% were found for 1" sampling lines at flow rates of 2-3 cfm, for injection periods of several hours. However, these studies did not indicate how long it took to reach equilibrim between deposition and resuspension after an initial injection. Only a small fraction (<1%) of the injected elemental iodine was transmitted through the 1/4" sampling line with a 0.06 cfm flow rate as utilized in the General Atomics WRGM, which is shown schematically in Figure 15.

The NRC's proposed guidance suggests that the closest approximation to representativeness may be achieved at equilibrium, when deposition and re-entrainment or re-suspension are equal. This could be expected to occur most rapidly in a continuously operated system, rather than one in which flow is initiated only upon the occurrence of higher-range concentrations. The Kaman and the Eberline AXM-1 monitors approximate this in that, upon an indication of abnormal gas concentrations, they isokinetically obtain a small local side-stream flow (of a few hundred cm^3/min) from the low-range monitoring/sampling line, in which a much greater flow (1-2 cfm) is maintained.

From the reviews, it has been apparent that most architect/engineers and licensees have been aware of the need for the heat tracing of sampling lines when they are exposed to "outdoor" conditions. However, it was apparent that many of them have not recognized a similar need for the heat tracing of long indoor horizontal sampling lines in which condensation could occur, especially under the high moisture loads of some accident sequences. In a few reviews condensation was found in the sampling medium of sampling positions.

Although IIF.1-2 calls for continuous sampling, the procedures of four licensees called only for the analysis of a grab sample to be collected post-accident over a short period of time (to limit the amount collected to the capability of their laboratory Ge-Li analysis systems), with no indication in their procedures of how they would evaluate the preceding sample to establish the total amount released from the onset of accident conditions.

In six instances, which included the three SPING-4s, the two SAI RAGEMS and one licensee devised installation, the filter assembly for the collection of particulates and iodines was unshielded. None had conducted an analysis to assure that with such an arrangement, the samples could be collected, retained and transported within the GDC-19 dose limits (5 rem whole body and 75 rem to the extremities). It should be noted that by two successive 1/200 dilutions, the RACEMS should collect only relatively low activity samples under all accident conditions.

All of the licensees had Ag-Zeolite collection media available for sampling under accident conditions. Almost all of the installations provided for isokinetic sampling at normal stack flow rates but only a few could maintain it if large deviations from these flows were to occur under accident conditions. Of those that could not, none had developed correction factors, as called for in Item II.F.1-2.

Only a few licensees had developed adequate procedures for the analysis of "hot" samples, in which the collected activity might considerably exceed the upper limit which could be analyzed by their GeLi counting and analysis systems. Although several had established procedures for counting samples with greater than normal activity in a geometry distant from the detector, only a few would be able to cope with an 85-170 Ci sample of radioiodines collected at a concentration of 100 uCi/cm^3 at flow rates of 1-2 cfm for the stipulated 30-minute sampling period.

VI. COMMENTS AND RECOMMENDATIONS

A wide variety of approaches to the monitoring of noble gasses and the sampling of particulates and radioiodines in high concentrations have been encountered in the nineteen reviews which have been conducted over the past two years.

If the monitoring requirements were solely those for the noble gasses, ion chambers would seem the most straightforward detectors, in view of their simplicity, wide range capability, and linear energy response characteristics. However, they are relatively insensitive and therefore require a large volume of contained gas which is difficult to shield from extraneous radiations, as illustrated by Figure 15. The 0.1"-thick steel wall in which this detector is located has a large absorption for low energy photons, such as those from ^{133}Xe, compared to a much smaller absorption of the higher energy photons from shorter-lived noble gases.

The integrated monitoring/sampling devices which incorporate microprocessor data handling and control accomplish the full range requirements of Item II.F-1.1 by routing the flow to more then one detector, each of which is designed to be sensitive to portions of the full range requirement. This permits the isolation of the low-range detector during periods of high concentrations. It also facilitates the routing of flow to a selected shielded filter assembly at the same time. Their ability to store and to provide a history of release rates over time makes them attractive for both routine and accident monitoring. Additionally, the use of a monitor for every-day purposes adds to its reliability for accident monitoring. If not so utilized, they require regular surveillance and maintenance to assure their availability.

To minimize the ambient post-accident radiation fields, most of the post-accident monitors and/or samples are located at considerable distances from the points of effluent release, thus necessitating long sampling lines (typically 1" x 100-250'). This creates a dilemma between the desirability of maintaining a high flow rate in the sample line so as to minimize deposition losses and the desirability of minizing the amount of collected radioactivity on the sampler. It is solved in some monitors, by the provision of a second stage of isokinetic sampling with a probe situated within the high-flow line close to the sampling head, but with a much smaller flow (a few hundred cm^3/min) through the high-concentration sampler. This seems desirable on the grounds of both convenience in handling and analysis and of ALARA considerations.

ACKNOWLEDGEMENTS

The participation in the gathering and interpretation of data in these reviews by John Baum, Alan Kuehner, Edward Lessard, Stephen Musolino, Norman Rohrig and Christopher Weilandics of the staff of the Safety and Environmental Protection Division of Brookhaven National Laboratory and of Marie Miller of the staff of the Emergency Preparedness and Radiological Protection Branch of the USNRC, Region I is gratefully acknowledged.

Appreciation is also appropriate for the typists, Cheryll Christie and Marie Cooney who prepared the text of many revisions of the reports and of this manuscript.

REFERENCES

1. Selby, J.M. and Unruh, C.M., "Technological Consideration in Emergency Instrumentation Preparedness: Phase I - Current Capabilities Survey", BNWL-1552 (Jan. 1971).

2. Selby, J.M. et al, "Technological Considerations in Emergency Instrumentation Preparedness: Phase II-A - Emergency Radiological and Meteorological Instrumentation Criteria for Reactors", BNWL-1635 (May 1972).

3. Wrenn, M.E. (Chair), "Proposed ANSI Standard: Performance Specifications for Reactor Emergency Radiological Monitoring Instrumentation", Final Draft ANSI 413/42 WG6 (Aug. 1974).

4. ANSI, "Performance Specification for Reactor Emergency Radiological Monitoring Instrumentation", ANSI N-320-1978 (Dec 1978).

5. USNRC, "Instrumentation for Light-Water Cooled Nuclear Power Plants to Assess Plant Conditions During and Following an Accident", Reg. Guide 1.97, Rev.1, (Aug 1977).

6. USNRC, "Investigation into the March 28, 1979 Three Mile Accident by the Office of Inspection and Enforcement", NUREG-0600 (July 1979).

7. USNRC, "TMI-2 Lessons Learned Task Force Status Report and Short-Term Recommendations", NUREG-0578 (July 1979).

8. USNRC, "NRC Action Plan Developed as a Result of the TMI-2 Accident", NUREG-0660 (May 1980).

9. USNRC, "Clarification of TMI Action Plan Requirements", NUREG-0737 (Oct. 1980).

10. D.G. Eisenhut, "Proposed Guidance for Calibration and Surveillence Requirements for Equipment Provided to Meet Item II.F.1 Attachments 1, 2, and 3, NUREG-0737" Memorandum to Regional Administrators (Aug. 16, 1982).

11. D. McClure, "Accident Range Monitor Response", HPS Newsletter, 18:6 pg. 7 (1985).

12. P.J. Unrein et al, "Transmission of Radioiodines Through Sampling Lines", Proceedings of the 18th DOE Nuclear Airborne Waste Management and Air Cleaning Conference, CONF-840806, Vol. 1, p. 98-114 (1985).

TABLE I

HIGH-RANGE NOBLE GAS EFFLUENT MONITORS

REQUIREMENT — Capability to detect and measure concentrations of noble gas fission products in plant gaseous effluents during and following an accident. All potential accident release paths shall be monitored.

PURPOSE — To provide the plant operator and emergency planning agencies with information on plant releases of noble gases during and following an accident.

DESIGN BASIS MAXIMUM RANGE

Design range values may be expressed in Xe-133 equivalent values for monitors employing gamma radiation detectors or in microcuries per cubic centimeter of air at standard temperature and pressure (STP) for monitors employing beta radiation detectors (Note: 1R/hr @1 ft = 6.7 Ci Xe-133 equivalent for point source). Calibrations with a higher energy source are acceptable. The decay of radionuclide noble gases after an accident (i.e., the distribution of noble gases changes) should be taken into account.

10^5 uCi/cc — Undiluted containment exhaust gases (e.g., PWR reactor building purge, BWR drywell purge through the standby gas treatment system).

Undiluted PWR condenser air removal system exhaust.

10^4 uCi/cc — Diluted containment exhaust gases (e.g., > 10:1 dilution, as with auxiliary building exhaust air).

BWR reactor building (secondary containment) exhaust air.

PWR secondary containment exhaust air.

10^3 uCi/cc — Buildings with systems containing primary coolant or primary coolant offgases (e.g., PWR auxiliary buildings, BWR turbine buildings).

PWR steam safety valve discharge, atmospheric steam dump valve discharge.

10^2 uCi/cc — Other release points (e.g., radwaste buildings, fuel handling/storage buildings).

TABLE I (continued)

DESIGN CONSIDERATIONS

Off-line monitoring is acceptable for all ranges of noble gas concentrations.

In-line (induct) sensors are acceptable for 10^2 uCi/cc to 10^5 uCi/cc noble gases. For less than 10^2 uCi/cc, off-line monitoring is recommended.

Upsteam filtration (prefiltering to remove radioactive iodines and particulates) is not requ[illegible] however, design should consider all alternatives with respec[illegible]pability to monitor effluents following an accident.

For external mounted monitors (e.g., PWR main steam line), the thickness of the pipe should be taken into account in accounting for low-energy gamma detection.

REDUNDANCY Not required; monitoring the final release point of several discharge inputs is acceptable.

SPECIFICATIONS

(None) Sampling design criteria per ANSI N13.1.

POWER SUPPLY

Vital instrument bus or dependable backup power supply to normal ac.

CALIBRATION

Calibrate monitors using gamma detectors to Xe-133 equivalent (1 R/hr @ 1 Ft = 6.7 Ci Xe-133 equivalent for point source). Calibrate monitors using beta detectors to Sr-90 or similar long-lived beta isotope of at least 0.7 MeV.

DISPLAY Continuous and recording as equivalent Xe-133 concentrations of uCi/cc of actual noble gases.

QUALIFICATION

The instruments shall provide sufficiently accurate responses to perform the intended function in the environment to which they will be exposed during accidents.

From Ref 9

TABLE II

SAMPLING AND ANALYSIS OR MEASUREMENT OF HIGH-RANGE RADIOIODINE AND PARTICULATE EFFLUENTS IN GASEOUS STREAMS

EQUIPMENT — Capability to collect and analyze or measure representative samples of radioactive iodines and particulates in plant gaseous effluents druing and following an accident. The capability to sample and analyze for radioiodine and particulate effluents is not required for PWR secondary main stream safety valve and dump valve discharge lines.

PURPOSE — To determine quantitative release of radioiodines and particulates for dose caiculation and assessment.

DESIGN BASIS SHIELDINC ENVELOPE

10^2 uCi/cc of gaseous radioiodine and particulates, deposited on sampling media; 30 minutes sampling time, average gamma energy (E) of 0.5 MeV.

SAMPLING MEDIA

Iodine > 90% effective absorption for all forms of gaseous iodine.

Particulates > 90% effective retention for .3 micron diameter particles.

SAMPLING CONSIDERATIONS

Representative sampling per ANSI N13.1-1969.

Entrained moisture in effluent stream should not degrade adsorber.

Continuous collection required whenever exhaust flow occurs.

Provisions for limiting occupational dose to personnel incorporated in sampling systems, in sample handling and transport, and in analysis of samples.

ANALYSIS — Design of analytical facilities and preparation of analytical procedures shall consider the design basis sample.

Highly radioactive samples may not be compatible with generally accepted analytical procedures; in such cases, measurements of emissive gamma radiations and the use of shielding and distance factors should be considered in design.

TABLE III

EXAMPLE OF REVIEW GUIDE FOR HIGH-RANGE NOBLE GAS EFFLUENT MONITORS (II.F.1-1)

Monitoring System

A. Are monitors located at all effluent pathways and do they meet the following range requirements?

- containment exhaust, undiluted, 10^{-6} to 10^{5} uCi/cc?
- condenser air removal system exhaust, undiluted, 10^{-6} to 10^{5} uCi/cc?
- auxiliary building and others with systems to contining primary coolant or primary collant offgases, 10^{-6} to 10^{3} uCi/cc?
- steam safety valve discharge*, 10^{-6} to 10^{3} uCi/cc?
- atmospheric steam dump valve discharge*, 10^{-6} to 10^{3} uCi/cc?

* Main steam line monitors located upstream of the valves are acceptable, if considerations have been given to account for low energy gammas.

- radwaste building exhaust, 10^{-6} to 10^{2} uCi/cc?
- fuel handling/storage exhaust, 10^{-6} to 10^{2} uCi/cc?

B. Do the ranges of instruments overlap to cover the entire range of effluent from normal (ALARA) through accident conditions?

C. Are the detectors acceptable?

D. Does the sampling system design conform to ANSI N13.1?

E. Is offline monitoring used for detecting less than 10^{2} uCi/cc? (In-line monitoring is acceptable for 10^{2} uCi/cc to 10^{5} uCi/cc)?

F. Can the system detect and measure compositions of noble gases ranging from fresh to 1-day old with an overall system accuracy of less than 2?

TABLE III (continued)

Verify:

1. that noble gas effluent monitors with an upper range capacity of to 10^5 uCi/cc (Xe-133) are installed,

2. that the range extends from normal conditions (ALARA) to 10^5 uCi/cc (Xe-133),

3. that the system provides continous capability during and following an accident,

4. that a design description of the system identifying the specifications in accordance with Table II.F.1-1 is available,

5. that procedures and calculational methods are established,

6. that instrument ranges will overlap to cover the entire range of effluents, from normal thru accident conditions.

TABLE IV

SUMMARY OF INSTALLED MID- AND HIGH-RANGE NOBLE GAS MONITORS

No.	Range	Detector	Vendor	Model	Operating Mode	Data Processor	Background Subtraction
On-Line							
2	Mid/High	Ion Chamber	(1) GA (1) Victoreen	RD-2A 847	Continuous	No	No
Off-Line							
Gas Only							
1	Mid/High	Plastic	NMC	GA-270	High Alarm	No	No
1	Mid High	GM Ion Chamber	Victoreen Victoreen	847	Continuous	No	No
3	Mid/High	Ion Chamber	Victoreen	847	Continuous	No	No
Integrated Gas Monitors and Particulate-Iodine Samplers							
5	Mid High	Cd-Te Cd-Te	GA	WRCM	High Alarm	Yes	No
3	Mid High	GM GM	Eberline	SPING-4	Continuous	Yes	Yes
2	Mid High	GM GM	Kaman	KGM-HRH	High Alarm	Yes	No
1	Mid/High	Ge-Li	SAI	RAGEMS	Continuous	Yes	NA
1	Mid High	GM GM	Eberline	AXM-1	High Alarm	Yes	Yes

TABLE V

CONCENTRATIONS FOR VENDOR CALIBRATIONS OF II F.1-1 HIGH RANGE MONITORS

	^{133}Xe Concentrations uCi/cm^3	^{85}Kr Concentrations uCi/cm^3
Eberline		
Mid-Range SPING NGD-1 (SA-13)	0.13	0.47
High-Range SPING AXM-1(SA-14)	0.26	1.47
SA-15, SA-9	1.75	9.98
General Atomics		
Mid/High Range-WRCM	0.65	11.1*
Kaman		
High-Range-HRH	$5x10^4$	$1.5x10^5$*

*Based on calibration data supplied by vendor, as inferred for NBS Reference Date.

TABLE VI

SAMPLING AND ANALYSIS OF PLANT EFFLUENTS, II.F.1-2

No.	Range	Vendor	Model	Sample Positions	Shielded	Filter Selection	Remarks
Independent Utility Design							(In each instance)
5	-	-	-	1	Yes		
Vendor Design							
1	-	NRC Ind.	MAP-5	3	Yes	Local/remote control	Timed sample
1	-	Kaman	HRH	1	Yes		
Integrated Units							
4	Mid/High	GA	WRGM	[illegible]	Yes	Local/remote control	Timed sample
3	Mid/High	Eberline	SPING-4	1	No	Fixed	
2	Mid/High	Kaman	KGM-HRH	3	Yes	Automatic (GM Monitor)	Automatically timed sample
3	All	SAI	RAGEMS	1*	Yes	Automatic	
1	Mid/High	Eberline	AXM-1	1	Yes	Fixed (GM Monitor)	

*The remaining licensee to be reviewed has installed this system

Figure 1

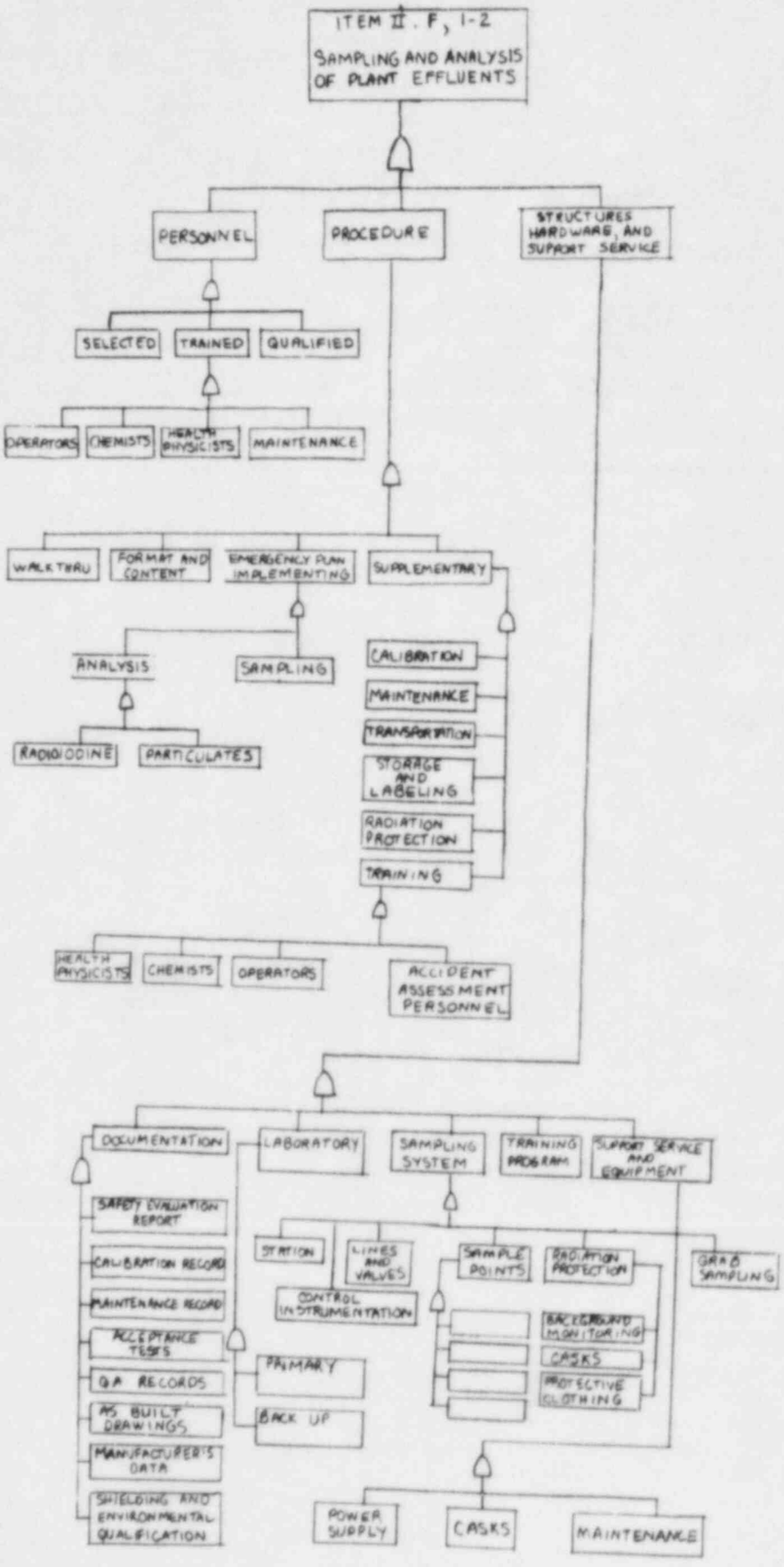
ITEM II. F, 1-2
SAMPLING AND ANALYSIS OF PLANT EFFLUENTS
PERSONNEL
PROCEDURE
STRUCTURES HARDWARE, AND SUPPORT SERVICE
SELECTED
TRAINED
QUALIFIED
OPERATORS
CHEMISTS
HEALTH PHYSICISTS
MAINTENANCE
WALK THRU
FORMAT AND CONTENT
EMERGENCY PLAN IMPLEMENTING
SUPPLEMENTARY
ANALYSIS
SAMPLING
RADIOIODINE
PARTICULATES
CALIBRATION
MAINTENANCE
TRANSPORTATION
STORAGE AND LABELING
RADIATION PROTECTION
TRAINING
HEALTH PHYSICISTS
CHEMISTS
OPERATORS
ACCIDENT ASSESSMENT PERSONNEL
DOCUMENTATION
LABORATORY
SAMPLING SYSTEM
TRAINING PROGRAM
SUPPORT SERVICE AND EQUIPMENT
SAFETY EVALUATION REPORT
CALIBRATION RECORD
MAINTENANCE RECORD
ACCEPTANCE TESTS
QA RECORDS
AS BUILT DRAWINGS
MANUFACTURER'S DATA
SHIELDING AND ENVIRONMENTAL QUALIFICATION
STATION
LINES AND VALVES
CONTROL INSTRUMENTATION
PRIMARY
BACK UP
SAMPLE POINTS
RADIATION PROTECTION
GRAB SAMPLING
BACKGROUND MONITORING
CASKS
PROTECTIVE CLOTHING
POWER SUPPLY
CASKS
MAINTENANCE

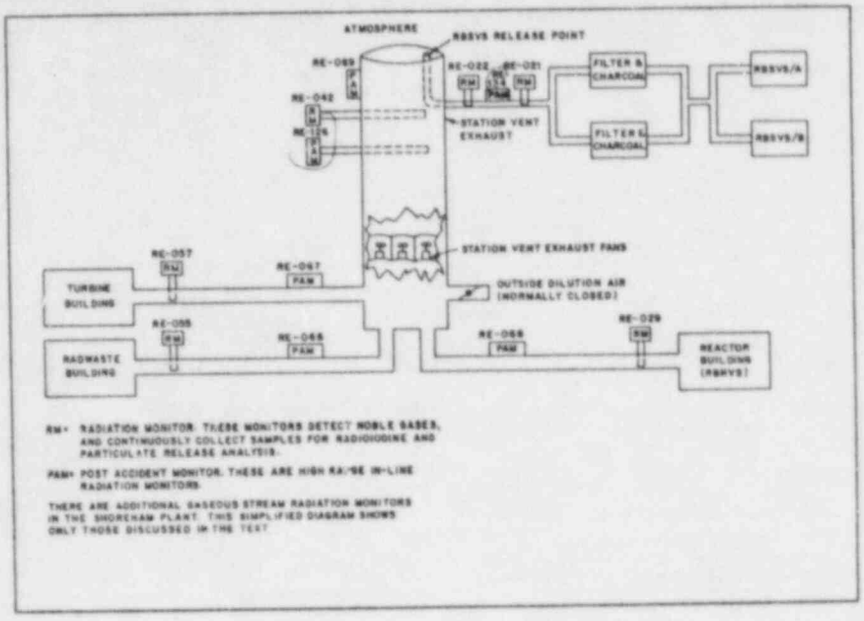

Figure 2. Gaseous effluent radiation monitors.

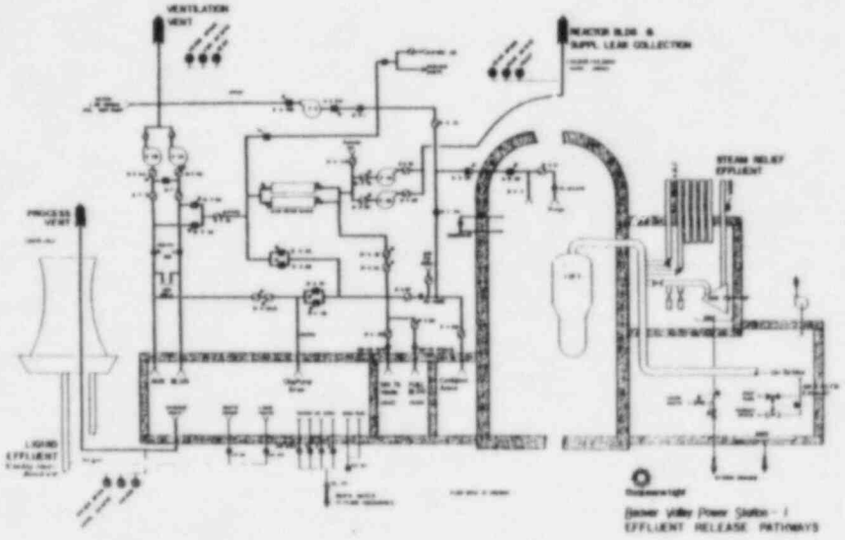

Figure 3. Effluent release pathways.

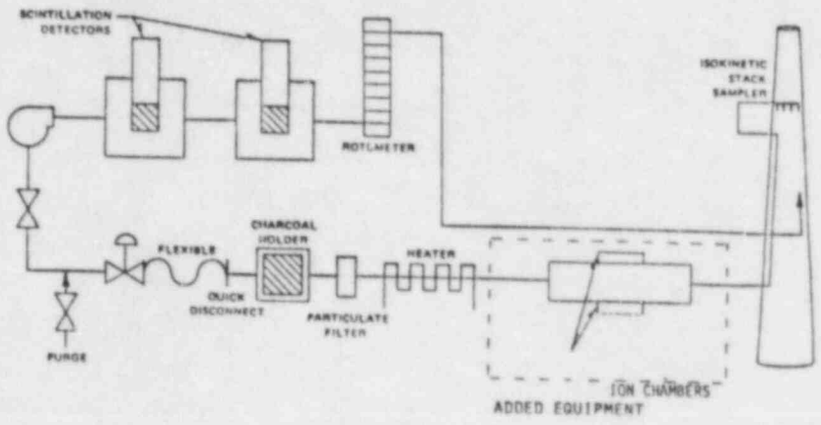

Figure 4. High-range effluent process radiation monitors.

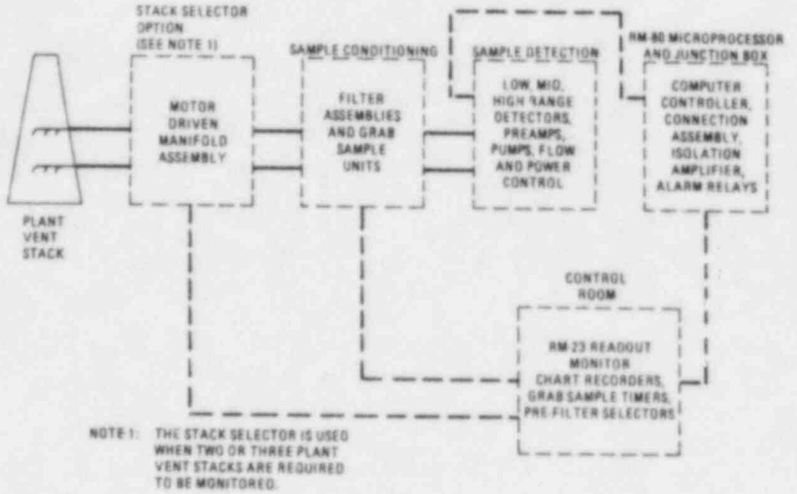

Figure 5. Wide-range gas monitor system block diagram.

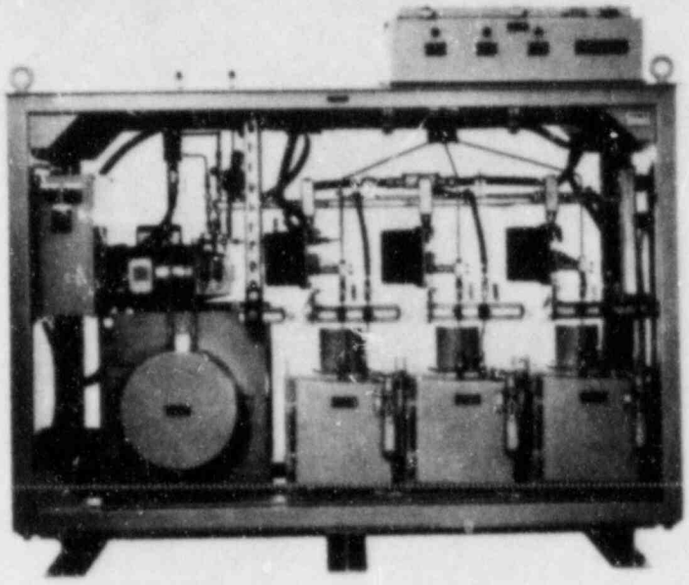

HIGH RANGE

Figure 6. Kaman HRH high-range noble gas monitor and sampler.

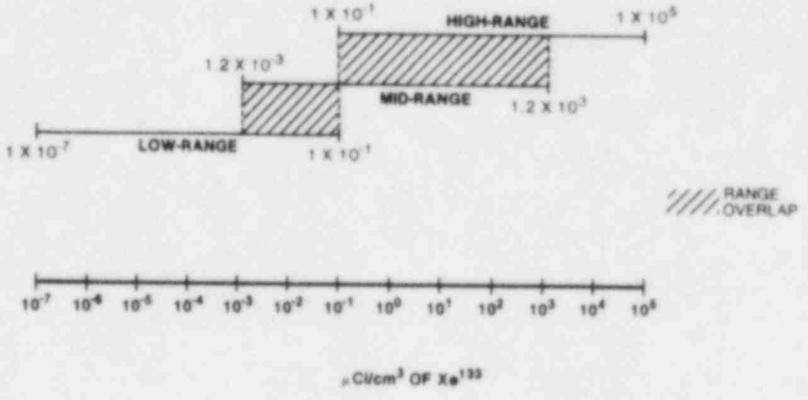

Figure 7. Ranges of General Atomics wide-range gas monitor.

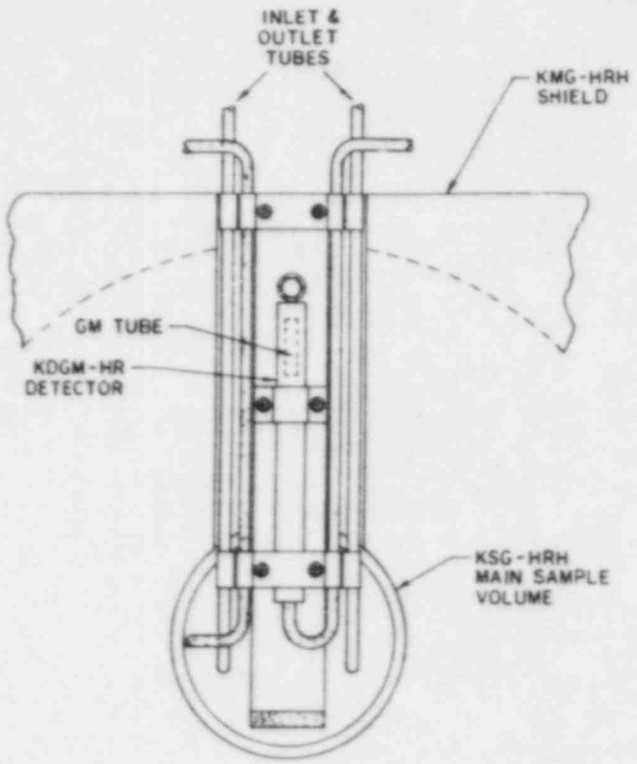

Figure 8. KMG-HRH-Enhanced high-range geometry.

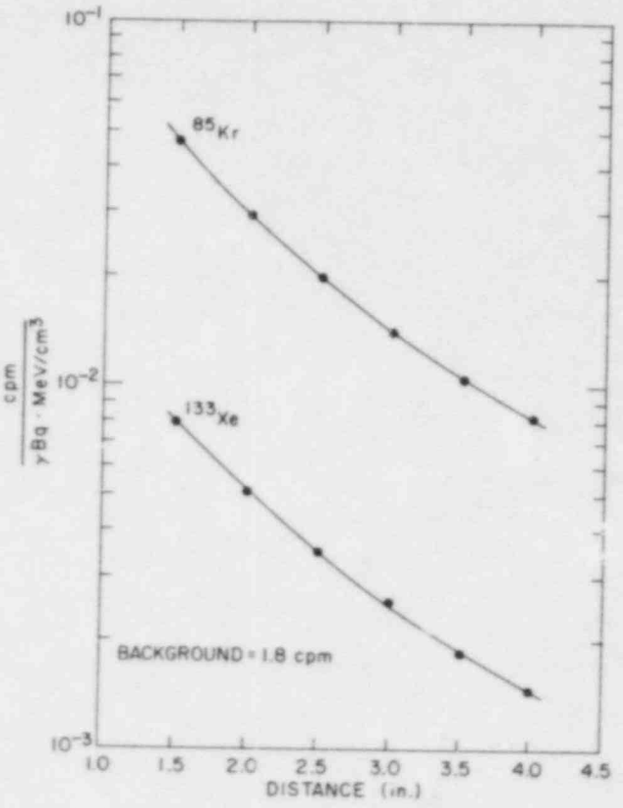

Figure 9. Response of Eberline SA-9 high-range detector to ^{85}Kr and ^{133}Xe.

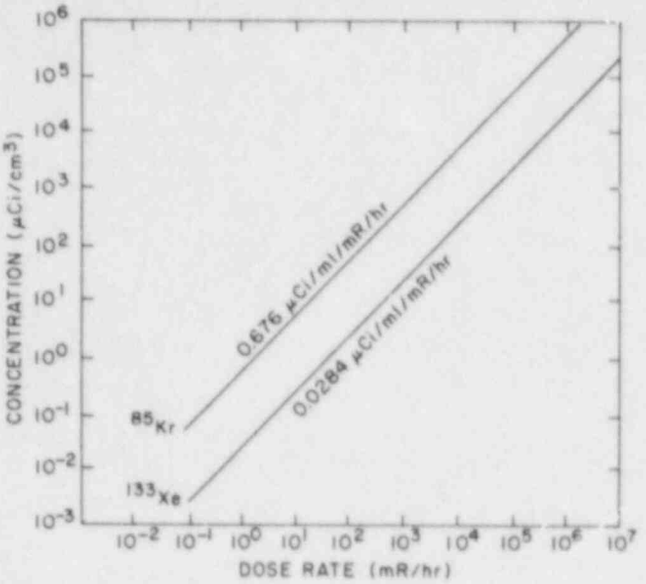

Figure 10. Measured response of a Victoreen Ion Chamber (847-1) installed outboard of a 5" duct and exposed to ^{85}Kr and ^{133}Xe.

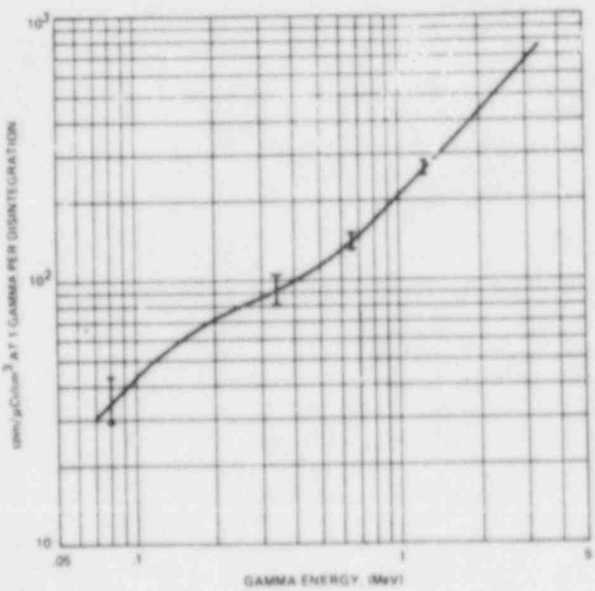

Figure 11. KDGM-HR enhanced detector in KSG-HRH sampler, enhanced high-range position energy dependence characteristic.

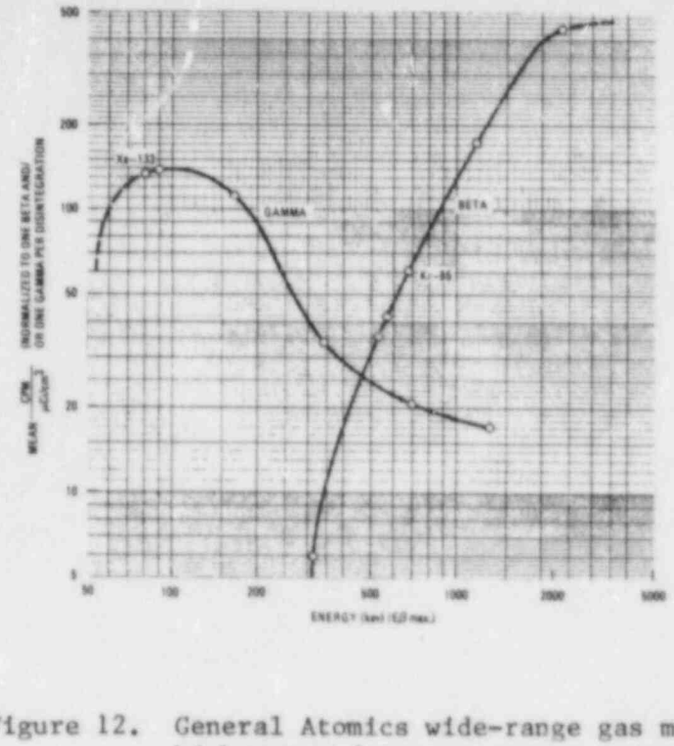

Figure 12. General Atomics wide-range gas monitor RD-72 high-range detector energy response curve.

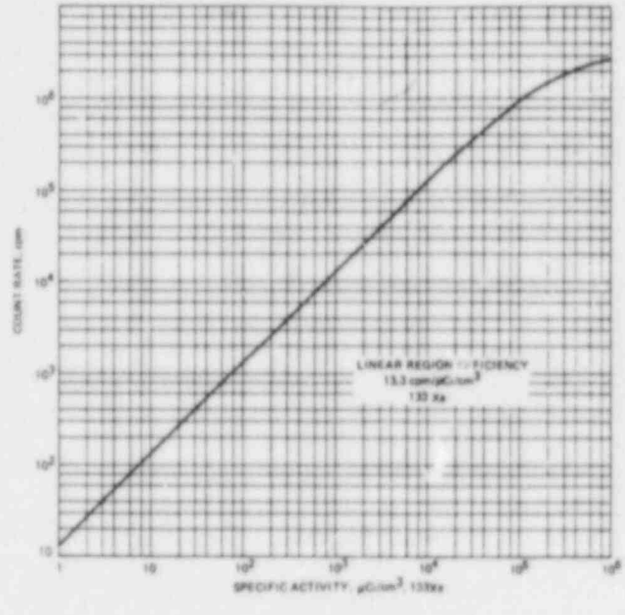

Figure 13. HDGM-HR Enhanced detector in KSG-HRH enhanced high-range position efficiency to Xenon-133.

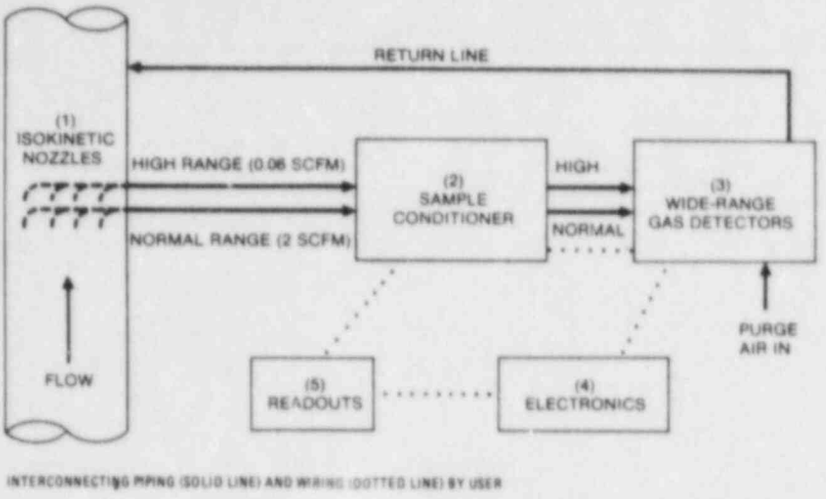

Figure 14. Block diagram, wide-range gas monitor.

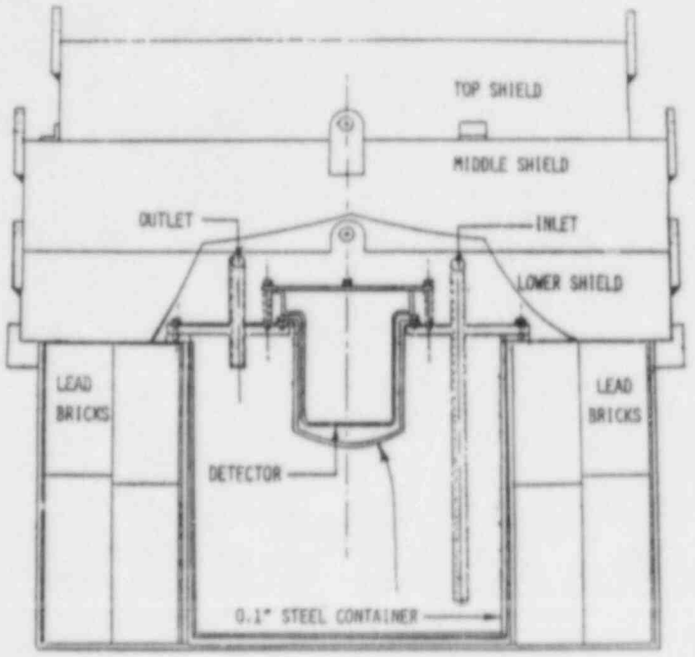

FIgure 15. High-range noble gas monitor.

NRC FORM 335 (2-84) NRCM 1102, 3201, 3202

U.S. NUCLEAR REGULATORY COMMISSION

BIBLIOGRAPHIC DATA SHEET

SEE INSTRUCTIONS ON THE REVERSE

1. REPORT NUMBER (Assigned by TIDC, add Vol. No., if any)

NUREG/CP-0072
Vol. 3

2. TITLE AND SUBTITLE

Proceedings of the Thirteenth Water Reactor Safety Research Information Meeting

3. LEAVE BLANK

4. DATE REPORT COMPLETED

MONTH: January YEAR: 1986

5. AUTHOR(S)

Compiled by Allen J. Weiss, BNL

6. DATE REPORT ISSUED

MONTH: February YEAR: 1986

7. PERFORMING ORGANIZATION NAME AND MAILING ADDRESS (Include Zip Code)

Office of Nuclear Regulatory Research
U. S. Nuclear Regulatory Commission
Washington, D. C. 20555

8. PROJECT/TASK/WORK UNIT NUMBER

9. FIN OR GRANT NUMBER

A-3283

10. SPONSORING ORGANIZATION NAME AND MAILING ADDRESS (Include Zip Code)

Same as Item 7 above

11a. TYPE OF REPORT

Proceedings of conference on safety research

b. PERIOD COVERED (Inclusive dates)

October 22-25, 1985

12. SUPPLEMENTARY NOTES

Proceedings prepared by Brookhaven National Laboratory

13. ABSTRACT (200 words or less)

This six-volume report contains 151 papers out of the 178 that were presented at the Thirteenth Water Reactor Safety Research Information Meeting held at the National Bureau of Standards, Gaithersburg, Maryland, during the week of October 22-25, 1985. The papers are printed in the order of their presentation in each session and describe progress and results of programs in nuclear safety research conducted in this country and abroad. Foreign participation in the meeting included thirty-one papers presented by researchers from Japan, Canada and eight European countries. The titles of the papers and the names of the authors have been updated and may differ from those that appeared in the final program of the meeting.

14. DOCUMENT ANALYSIS - a. KEYWORDS/DESCRIPTORS

reactor safety research
nuclear safety research

b. IDENTIFIERS/OPEN-ENDED TERMS

15. AVAILABILITY STATEMENT

Unlimited

16. SECURITY CLASSIFICATION

(This page) Unclassified

(This report) Unclassified

17. NUMBER OF PAGES

18. PRICE

UNITED STATES
NUCLEAR REGULATORY COMMISSION
WASHINGTON, D.C. 20555